Title

Characterization of the novel coenzyme Q biosynthetic polypeptide Coq11, and other proteins involved in the production and regulation of Q6

Author

Bradley, Michelle Celine

Publication Date

2020

Peer reviewed|Thesis/dissertation

UNIVERSITY OF CALIFORNIA

Los Angeles

Characterization of the novel coenzyme Q biosynthetic polypeptide Coq11, and other proteins involved in the production and regulation of Q_6

A dissertation submitted in partial satisfaction of the

requirements for the degree of Doctor of Philosophy

in Biochemistry, Molecular and Structural Biology

by

Michelle Celine Bradley

2020

ABSTRACT OF THE DISSERTATION

Characterization of the novel coenzyme Q biosynthetic protein Coq11, and other proteins involved in the production and regulation of Q_6

by

Michelle Celine Bradley

Doctor of Philosophy in Biochemistry, Molecular and Structural Biology

University of California, Los Angeles, 2020

Professor Catherine F. Clarke, Chair

Coenzyme Q (ubiquinone or Q_n) is a benzoquinone lipid of varying isoprenoid tail length '*n*', with essential functions within the respiratory electron transport chain and in cellular antioxidant defense. Several Coq polypeptides coordinate to drive the biosynthesis of Q_n at the inner mitochondrial membrane, and are organized into a high-molecular weight complex known as the 'CoQ synthome', Absence of individual Coq enzymes results in decreased content of Q_n and other Coq proteins, in addition to destabilization of the CoQ synthome. Patients with partial defects in Q_{10} biosynthesis suffer from a variety of debilitating diseases. Therefore, the studies outlined here seek to produce a more comprehensive understanding of the Q_n biosynthetic pathway, allowing for more targeted therapeutic strategies. This work employs *Saccharomyces cerevisiae* as a model organism due to the high level of *COQ* gene functional conservation between

yeast and humans. In *S. cerevisiae*, Coq11 was recently identified to associate with members of the CoQ synthome, and was required for efficient *de novo* Q_6 biosynthesis. The function of Coq11 remains uncharacterized.

Chapter 1 provides an overview of the coenzyme Q biosynthetic pathway in both humans and yeast, while highlighting the identification of Coq11 as a novel member of the CoQ synthome. Chapter 2 explores the functional relationship between Coq11 and Coq10, which have evolved as protein fusions in several fungal genomes. Data collected with help from Dr. Roland Stocker's laboratory, Dr. Mario Barros, and Jenny Ngo from Dr. Orian Shirai's laboratory, has demonstrated that the *coq10*Δ mutant respiratory deficiency, sensitivity to lipid peroxidation, and low *de novo* Q_6 biosynthesis is rescued by deletion of *COQ11*. Further, yeast lacking *COQ11* have increased expression of several Coq proteins and a stabilized CoQ synthome. These results indicate that Coq11 may serve as a modulator of Q_6 biosynthesis. Chapter 3 outlines additional experimental characterization towards understanding the role of Coq11 within the Q_6 biosynthetic pathway. With assistance from Dr. Lukas Susac from the laboratory of Professor Juli Feigon, various strategies for Coq11 purification have been documented, with some showing promise for future purification attempts. We have also revealed that Coq11 deletion in combination with deletion of two phenylacrylic acid decarboxylases, Pad1 and Fdc1, fails to effect Q_6 biosynthesis. In collaboration with Dr. Mario Barros, several Coq11 overexpression vectors have been constructed and evaluated for their ability to restore Q_6 biosynthesis in the *coq11*Δ mutant. The data reveal that yeast does not tolerate Coq11 overexpression from the majority of constructs, suggesting that Coq11 is a negative regulator of Q_6 biosynthesis. In Chapter 4, two novel phosphatidylethanolamine methyltransferase deletion mutants, *cho2* and *opi3*, were identified to have significantly higher Q_6 compared to wild type. Dr. Anita Ayer from the Stocker laboratory

conducted a preliminary large-scale screen of the *S. cerevisiae* diploid homozygous knockout library for mutants displaying altered Q_6 content. With help from Dr. Lucía Fernández-del-Río, we confirmed that the *cho2*Δ and *opi3*Δ mutants have increased Q_6 as well as a stabilized CoQ synthome, despite retaining wild-type amounts of Coq proteins. Finally, Appendices I-VIII contain previous publications that detail various aspects of coenzyme Q characterization in several organisms, in addition to a methods paper regarding the detection of protein-protein interaction networks. Together, this work provides novel insights regarding the biosynthesis, cellular functions, and regulation of coenzyme Q.

The dissertation of Michelle Celine Bradley is approved.

Tracy L. Johnson

Joseph A. Loo

Jorge Z. Torres

Catherine F. Clarke, Committee Chair

University of California, Los Angeles

2020

This work is dedicated to my parents, Drs. Patricia & Charles Bradley,

with my gratitude for all they have sacrificed so that I may succeed.

TABLE OF CONTENTS

LIST OF TABLES AND FIGURES

ACKNOWLEDGEMENTS

I have been truly fortunate to have completed my graduate studies under the guidance of Dr. Catherine Clarke. It is particularly rare to find a research mentor that is able to challenge students intellectually while still providing a positive, supportive environment. I am grateful to Cathy for the patience and kindness she has shown me throughout my doctoral program. I could not have asked for a better graduate experience than the one I have had in the Clarke laboratory; Cathy embodies the type of scientist, mentor, and person I aspire to be.

This dissertation contains significant contributions from a group of talented researchers. I am grateful to my thesis committee, Dr. Tracy Johnson, Dr. Joseph Loo, and Dr. Jorge Torres. They have given me instrumental advice regarding research projects and career development. Chapter 2 is a reprint of a published work that appeared in *The Journal of Biological Chemistry* (2020) 295: 6023-6042, and I would like to thank the American Society for Biochemistry and Molecular Biology for permission to use this copyrighted material. I am grateful to all of my co-authors who worked tirelessly towards this publication, including Jenny Ngo who performed the oxygen consumption assays; Dr. Anita Ayer who completed the quantitative PCR analysis of *COQ* genes as well as the evaluation of citrate synthase activity and mitochondrial DNA; and Dr. Mario Barros's work on the *coq10* revertants. For the Coq11 purification studies outlined in Chapter 3, I would like to thank Dr. Lukas Susac who helped establish these constructs and guided the purification work-flow. Preliminary work on the potential of Pad1 and Fdc1 to act as redundant decarboxylases within the Q_6 biosynthetic pathway was done by a former Clarke laboratory member, Dr. Melissa Gulmezian. I am also appreciative of Dr. Mario Barros who provided several Coq11 overexpression constructs. I would like to thank Dr. Anita Ayer for preforming the large-scale screen of the *S. cerevisiae* diploid knockout collection that led to the identification of Cho2

and Opi3 as putative regulators of Q_6 content. A huge thank you to Dr. Lucía Fernández-del-Río for her collaboration on the characterization of *cho2*Δ and *opi3*Δ phenotypes.

Appendix I is a reprint of an article in *Free Radical Biology and Medicine* (2020) 154: 105-118; I would like to thank Elsevier and the primary author Dr. Lucía Fernández-del-Río for permission to use this copyrighted material. Appendix II is a reprint of an article under review in *PLOS ONE* (2020); I would like to thank the primary author Dr. Agape Awad for permission to use this material. Appendix III is a reprint of an article in *Essays in Biochemistry* (2018) 62.3: 361-376; I would like to thank Portland Press and all of the Clarke laboratory co-authors who have contributed, for permission to use this copyrighted material. Appendix IV is a reprint of an article in *The Journal of Lipid Research* (2019) 60:1293-1310; I would like to thank the American Society for Biochemistry and Molecular Biology and the primary author Dr. Hui Tsui for permission to use this copyrighted material. Appendix V is a reprint of an article in *Contact (2019)* 2: 1-14; I would like to thank SAGE Publishing and the primary authors Michel Eisenberg-Bord, Dr. Hui Tsui, and Dr. Lucía Fernández-del-Río, for permission to use this copyrighted material. Appendix VI is a reprint of an article in *BBA Molecular and Cell Biology of Lipids* (2019) 1864: 1226-1234; I would like to thank Elsevier and the primary author Anne Bernert for permission to use this copyrighted material. Appendix VII is a reprint of an article in *The Journal of Biological Chemistry* (2017) 292: 14851-14866; I would like to thank the American Society for Biochemistry and Molecular Biology and the primary authors Dr. Agape Awad and Dr. Srivats Venkataramanan, for permission to use this copyrighted material. Finally, Appendix VIII is a reprint of an article in *Journal of Visualized Experiments:JoVE* (2016) 118: 54870; I would like to thank MyJove Corp for permission to use this copyrighted material. All work is supported by the National Science Foundation Grant MCB-1330803 to Dr. Catherine Clarke, the National Institutes of Health Grant

T32 GM 008496 to Michelle Bradley, and the Whitcome Predoctoral Fellowship to Michelle Bradley.

I also want to recognize and extend thanks to my colleagues in the UCLA Department of Chemistry and Biochemistry. Former Clarke laboratory members Dr. Hui Tsui and Dr. Anish Nag provided invaluable guidance on experiments and taught me important skills that I have incorporated into all of my projects. To the current Clarke laboratory members, Dr. Lucía Fernández-del-Río and Dr. Agape Awad, I thank you for making our laboratory a place of hard-work and laughter. I am grateful for the perfect combination of mentorship and friendship you have both afforded me. I would like to thank Dr. William Silkworth who was always available to assist me with instruments, or simply for a chat. Following my third-year midstream seminar, Dr. Lukas Susac sacrificed his time to teach me protein purification techniques. He is one of the most talented scientists I have ever had the pleasure of working alongside, and I will be forever grateful for his friendship. Above all, the members of the Torres laboratory have given me the gift of unwavering companionship during my time at UCLA. I now appreciate that during stressful times in the laboratory, nothing can make my day better like conversation with my fellow graduate students. I want to express my deepest thanks to the undergraduate students, Krista Yang, Hope Ibarra, Liliana Zar, and Cassandra Bradley, I have mentored during my time in graduate school, for their profound dedication to the projects. I would like to give a special acknowledgement to the undergraduate student I have mentored for the past three and a half years, Krista Yang. The hours we have spent working in the laboratory together will always hold a distinct place in my heart. Krista has proven her unparalleled work-ethic time and time again, yet it is her kindness and camaraderie that I will remember most; I am excited to see what the future holds for such a promising young scientist.

Finally, I want to thank my friends and family, who are some of the most important people in my life. I want to extend my thanks to my best friend and roommate of nine-years, Amanda Molinari, for always listening. I would like to thank my boyfriend Colin Shipley, for reading and editing nearly every piece of writing I completed during graduate school, and giving me the support I needed during difficult times. To my brother and sisters, Christopher, Victoria, and Cassandra: I cannot imagine a more competitive yet loving environment to grow-up in. In unique ways, you have each motivated me to follow my dreams without taking myself too seriously. My mom and dad, Drs. Patricia and Charles Bradley, have inspired me in all aspects of my life. Thank you for giving me everything I could need and more. I am not able to express in words how grateful I am to have such incredible parents. Soon there will be three Drs. Bradley!

VITA

2013-2015	Undergraduate Research Assistant Department of Chemistry and Biochemistry Colgate University Hamilton, NY
2014	Undergraduate Research Assistant National Institutes of Health, National Cancer Institute Bethesda, MD
2015	B.A. Biochemistry, Minor Political Science Colgate University Hamilton, NY
2015-2020	Graduate Research Assistant and Teaching Assistant Department of Chemistry and Biochemistry University of California, Los Angeles Los Angeles, CA
2016-2018	Cellular and Molecular Biology Training Award Fellow University of California, Los Angeles Los Angeles, CA
2018	Excellence in Second Year Academics and Research Award Department of Chemistry and Biochemistry University of California, Los Angeles Los Angeles, CA
2019-2020	Whitcome Predoctoral Fellowship in Molecular Biology University of California, Los Angeles Los Angeles, CA
2019-2020	Technology Fellow UCLA Technology Development Group Los Angeles, CA
2020	Michael E. Jung Excellence in Teaching Award University of California, Los Angeles Los Angeles, CA
2020	Robert A. Smith Dissertation Award University of California, Los Angeles Los Angeles, CA

PUBLICATIONS

Fernández-del-Río L., Kelly M., Contreras J., **Bradley M.C.**, James A.M., Murphy M.P., Payne G.S., Clarke C.F. (2020) Genes and lipid molecules that impact the uptake and assimilation of exogenous coenzyme Q in *Saccharomyces cerevisiae*. *Free Radical Biology and Medicine,* 154: 105-118. doi: 10.1016/j.freeradbiomed.2020.04.029

Awad A.M., Nag A., Pham N.V.B., **Bradley M.C.**, Clarke C.F. (2020) Intragenic suppressor mutations of the *COQ8* protein kinase homolog restore coenzyme Q biosynthesis and function in *Saccharomyces cerevisiae*. *PLOS ONE*, **Submitted**.

Bradley M.C., Yang K., Fernández-del-Río L., Ngo J., Tsui S.T., Ayer A., Stocker R., Shirihai O.S., Barros M., Clarke C.F. (2020) *COQ11* deletion mitigates respiratory deficiency caused by mutations in the gene encoding the coenzyme Q chaperone protein Coq10. *The Journal of Biological Chemistry*, 295 (18): 6023-6042. doi: 10.1074/jbc.RA119.012420

Tsui S.T., Pham N.V.B., Amer B.R., **Bradley M.C.**, Gosschalk J.E., Gallagher-Jones M., Ibarra H., Rodriguez J., Clubb R.T., Blaby-Haas C., Clarke C.F. (2019) Human COQ10A and COQ10B are distinct lipid-binding START domain proteins required for coenzyme Q function. *The Journal of Lipid Research*, 60 (7):1293-1310. doi: 10.1194/jlr.M093534

Eisenberg-Bord M., Tsui H.S., Antunes D., Fernández-del-Río L., **Bradley M.C.**, Dunn C.D., Nguyen T.P.T., Rapaport D., Clarke C.F. (2019) Schuldiner M. The ER-Mitochondria contact site coordinates coenzyme Q biosynthesis. *Contact*, 2: 1- 14. doi: 10.1177/2515256418825409

Bernert A.C., Jacobs E.J., Buceta Roberts P.M., Reinl S.R., Culver J.C., Goodspeed C.R., Cronk J.D., **Bradley M.C.**, Clarke C.F., Basset G.J., Shepherd J.N. (2019) Recombinant RquA catalyzes the *in vivo* conversion of ubiquinone to rhodoquinone in *Escherichia coli* and *Saccharomyces cerevisiae*. *BBA - Molecular and Cell Biology of Lipids*, 1864 (9): 1226-1234. doi: 10.1016/j.bbalip.2019.05.007

Awad A.M., **Bradley M.C.**, Fernández-del-Río L., Nag A., Tsui H.S., Clarke C.F. (2018) Coenzyme Q_{10} deficiencies: pathways in yeast and humans. *Essays in Biochemistry*, 62 (3): 361-376. doi: 10.1042/EBC20170106

Awad A.M, Venkataramanan S., Nag A., Galivanche A.R., **Bradley M.C.**, Neves L.T., Douglass S., Clarke C.F., Johnson T.L. (2017) Chromatin-remodeling SWI/SNF complex regulates coenzyme Q_6 synthesis and a metabolic shift to respiration in yeast. *The Journal of Biological Chemistry*, 292 (36): 14851-14866. doi: 10.1074/jbc.M117.798397.

Bradley M.C., Ramirez I., Cheung K., Gholkar A.A., Torres J.Z. (2016) Inducible LAP-tagged Stable Cell Lines for Investigating Protein Function, Spatiotemporal Localization and Protein Interaction Networks. *Journal of Visualized Experiments:JoVE*, 118: 54870. doi:10.3791/54870.

CHAPTER 1

Coenzyme Q: Function, Biosynthesis, and Regulation

COENZYME Q INTRODUCTION

Coenzyme Q (ubiquinone or Q_n) is a small lipid biomolecule comprised of a fully-substituted benzoquinone ring attached to a polyisoprenyl side-chain. This crucial molecule is found in all eukaryotes and α-, β-, and γ-proteobacteria (1). Importantly, the Q_n benzoquinone ring is redox-active and is capable of carrying two electrons and protons in a reversible set of reactions; the fully oxidized Q_n accepts one election and one proton to produce the stable ubisemiquinone radical species ($Q_nH^{\cdot}$), which subsequently accepts a second proton and electron to form the fully reduced ubiquinol (Q_nH_2) (2). The hydrophobic side-chain anchors Q_n at the mid-plane of phospholipid bilayers within cellular membranes, where it is able to diffuse freely (2). While the benzoquinone ring is conserved, there is some variation in the length of the polyisprenoid group '*n*' between species: six isoprenyl-units in *Saccharomyces cerevisiae* (Q_6), Q_8 in *Escherichia coli*, a combination of Q_9 and Q_{10} in mice, and Q_{10} in humans (3). Previous studies have demonstrated that Q_6-Q_{10} may complement the function of Q_8 in *E. coli* (4,5), however, organisms do appear to have a preference towards their endogenous Q_n species (5,6).

The major function of Q_n is to serve as a mobile electron carrier inside the plasma membrane during respiratory electron transport (2,3,7). This electron transport process occurs at the inner mitochondrial membrane in eukaryotes and in prokaryotic plasma membranes (8).

In eukaryotes, Q_n accepts electrons from NADH or succinate via complex I or complex II, respectively, and donates them to cytochrome *c* at complex III (cytochrome bc_1 complex) through the protonmotive Q cycle (8,9). Each Q cycle results in the oxidation of Q_nH_2, reduction of two molecules of cytochrome *c*, and consumption of two protons on the negative side of the membrane, to result in the efficient transport of four protons to the positive side of the membrane (8). *S. cerevisiae* lacks complex I and alternatively uses internal and external NADH:ubiquinone

oxidoreduactases which, unlike complex I, do not generate a proton gradient (10). These complexes include Nde1 and Nde2 mitochondrial NADH dehydrogenases that act on the cytosolic side of the inner mitochondrial membrane, as well as Ndi1 that oxidizes NADH at the matrix side of the inner membrane (11).

The QH_2 reduced hydroquinone also serves as an important chain-breaking antioxidant shown to alleviate lipid peroxidative damage and regenerate alpha-tocopherol (vitamin E) (12). In fact, Q_nH_2 is the only lipid soluble antioxidant species synthesized endogenously (13). Yeast lacking Q_nH_2 are extremely sensitive to oxidative damage driven by exogenously added polyunsaturated fatty acids (PUFAs) (14-16), due to the loss of Q_nH_2 antioxidant protection (13). This effect is alleviated by site-specific reinforcement at bis-allylic hydrogen atoms with deuterium atoms (14,17).

A high Q_nH_2/Q_n ratio initiates reverse electron transport (RET) from complex II to complex I under physiological conditions in both *Drosophila* and mammalian cells in culture (18,19). Superoxide and secondary reactive species produced via complex I RET induced by high Q_nH_2, extended *Drosophila* lifespan and improved mitochondrial function in Parkinson's disease models (19).

The role of Q_n in electron transport is similarly fundamental for other pathways, including pyrimidine biosynthesis, and the oxidation of sulfide, proline, fatty acids, and branched-chain amino acids (9,20,21). Previous work has demonstrated that Q_{10} inhibits apoptosis independently from its role in radical scavenging, by preventing the opening of the mitochondrial permeability transition pore, thus inhibiting mitochondrial depolarization (22). Several studies have also suggested that Q_{10} may act as a cofactor for fatty acid-dependent proton transport by uncoupling proteins (23,24), and has an inducible effect on several genes that play

significant roles in the immune system inflammatory response (25). Additionally, Q_{10} is associated with an ever-increasing number of functions in other important metabolic processes including regulating the amount of integrins on the surface of monocytes and modulating physiochemical properties of cellular membranes (26).

OVERVIEW OF COENZYME Q BIOSYNTHESIS

While Q_n is found in all cellular membranes, the biosynthesis of Q_n occurs selectively within the mitochondria (2). The polyisoprenoid side-chain of Q_n is synthesized from the precursors isopentenyl pyrophosphate (IPP) and dimethylallyl pyrophosphate (DMAPP), which are generated from mevalonate in eukaryotes and 1-deoxy-D-xylulose-5-phosphate in prokaryotes (2,3,27). Elongation of the ployisopreoid tail occurs when IPP and DMAPP enzymatically condense via a head-to-tail reaction to form hexaprenyl diphosphate in yeast and decaprenyl diphosphate in humans (2). The major aromatic precursor compound for the Q_n benzoquinone head group is 4-hydroxybenzoic acid (4HB), produced from tyrosine in mammals, chorismate in *E. coli*, and both tyrosine and chorismate in yeast (28-30). Several other compounds including *para*-coumarate, resveratrol, vanillic acid, 3,4-diHB, and kaempferol have also been identified as efficient Q_n precursors (31-33). An additional ring precursor, *para*-aminobenzoic acid (pABA), is used in *S. cerevisiae* Q_6 biosynthesis but is not employed in humans or mice or *E. coli* (28).

S. cerevisiae is a useful model for studies of Q_n biosynthesis because yeast retain the ability to survive through fermentation metabolism in the absence of Q_6 (34). Previous studies have demonstrated that most yeast *coq* mutants are rescued by expression of their corresponding human homolog (2), indicating a high degree of functional conservation between yeast and

humans. In *S. cerevisiae*, fourteen mitochondrial proteins are required for efficient Q_6 biosynthesis: Coq1-Coq11, Yah1, Arh1, and Hfd1 (17). *YAH1* and *ARH1* are essential genes in yeast that are required for iron–sulphur cluster and heme A biosynthesis (35-37). The Yah1 and Arh1 polypeptides are additionally required for Q_6 production, serving as ferredoxin and ferredoxin reductase, respectively (38). Hfd1 is a mitochondrial outer membrane protein that catalyzes the oxidation of 4-hydroxybenzaldehyde to 4HB during the early steps of Q_6 biosynthesis (39,40). Deficiencies in Q_6 emanating from *HFD1* inactivation may be rescued by exogenous 4HB supplementation (40). Yeast *coq1-coq9* deletion mutants are Q_6-less, resulting in a subsequent failure to respire and grow on a non-fermentable carbon source (2,3). In contrast, *coq10* and *coq11* mutants still synthesize small amounts of Q_6 and retain the ability to grow on respiratory medium (15,41,42).

COQ1 encodes a species specific hexaprenyl diphosphate synthase that assembles the polyisoprenoid side-chain of Q_6 through the condensation of precursors DMAPP and IPP (43) (Fig. 1). Submitochondrial fractionation studies demonstrated that Coq1 is peripherally associated with the mitochondrial inner membrane on the matrix side (44). The *coq1*Δ mutant is rescued by polyprenyl diphosphate synthases from other organisms, and produces Q_n isoforms with varying tail lengths defined by the specific polyprenyl diphosphate synthase (4). In humans, the Coq1 homologs PDSS1 and PDSS2 form a heterotetramer essential for enzymatic activity and synthesis of the decaprenyl diphosphate side-chain for Q_{10} biosynthesis (45). Clinical phenotypes associated with partial defects in either PDSS1 and PDSS2 include mitochondrial oxidative phosphorylation disorders such as Leigh Syndrome (46).

Transfer of the polyisoprenoid side-chain to the benzoquinone ring precursors is catalyzed by the 4HB-polyprenyltrasferase, Coq2 (47), and produces 3-hexaprenyl-4-hydroxy

benzoic acid (HHB; Fig. 1). Coq2 is an integral membrane protein localized to the mitochondrial inner membrane (48). Yeast *coq3-coq9* null mutants, accumulate the early-stage hydrophobic Q_6-intermeadiate HHB (2,49). Expression of human *COQ2* cDNA in *coq2*Δ cells successfully restored Q_6 biosynthesis, demonstrating that Coq2 does not dictate the length of the polyprenyl tail (50). Patients with heterozygous *COQ2* deficiency allowing residual amount of Q_6 biosynthesis, present with steroid resistant nephrotic syndrome or adult onset encephalopathy, however, homozygous *COQ2* defects that fully prevent Q production manifest in more severe disease pathology (51).

The functional roles of the Coq3, Coq5, Coq6, and Coq7 ring-modifying enzymes have been studied widely and are largely defined. Yeast Coq3 is an S-adenosylmethionine (AdoMet, SAM)-dependent *O*-methyltransferase enzyme that catalyzes the two *O*-methylation steps of Q_6 biosynthesis (52,53). Coq3 binds SAM via four highly conserved structures typical of Class I SAM-dependent methyltransferases, that form a seven-strand twisted β sheet (54). Fractionation studies have determined that Coq3 is peripherally bound to the matrix-face of the inner mitochondrial membrane (53). Because Coq3 is phosphorylated in a Coq8-dependent manner (55), its molecular stability is dependent on Coq8 (48,56). Further, the low Coq4, Coq6, Coq7, and Coq9 polypeptide levels of the *coq3*Δ mutant are increased upon Coq8 overexpression (48). Expression of human COQ3 in *coq3*Δ yeast partially rescued Q_6 biosynthesis and restored growth on a non-fermentable carbon source (57); no mutations within the *COQ3* open reading frame are known to cause primary human Q_{10} deficiency. Analogous to Coq3, yeast Coq5 is peripherally associated with the matrix-side of the mitochondrial inner membrane (58), and is another SAM-dependent methyltransferase required for the Q_6 biosynthesis *C*-methylation step (34,59). The structure of yeast Coq5 has a characteristic seven β-strand Class I SAM

methyltransferase motif (60). Overexpression of Coq8 in the *coq5*Δ mutant restores Coq4, Coq7, Coq9 polypeptide amounts to those of wild type (48,61), and there is evidence that phosphorylation of Coq5 may be dependent on Coq8 (55). Interestingly, expression of human COQ5 was only successful in rescuing Q_6 biosynthesis of the *coq5* point mutants and *coq5*Δ overexpressing Coq8, but failed to have an effect on the *coq5*Δ mutant (62). Partial loss of COQ5 function was recently determined to be the causal mutation for Q_{10} deficiencies in several patients presenting with cerebellar ataxia of varying severity (63).

Yeast Coq6 is a flavin-dependent monooxygenase with consensus sequences for ADP, FAD, NAD(P)H, and ribityl binding (64). Consistent with enzymatic studies demonstrating that Coq6 is responsible for the hydroxylation of HHB and HAB at the C5 position on the ring, Coq6 co-purifies with a tightly bound FAD (65). Additionally, Coq6 is necessary for the C4-deamination reaction when pABA is used as a ring precursor for Q_6 biosynthesis (66). The hydroxylation reactions catalyzed by Coq6 are dependent on Yah1 and Arh1, ferredoxin and ferredoxin reductase, which serve as an electron source for the monooxygenase reaction (38). The Coq6 protein is peripherally bound to the inner mitochondrial membrane facing the matrix (64). Human *COQ6* expression complements the *S. cerevisiae coq6*Δ mutant (32,67), and patients with *COQ6* deficiencies have progressive nephrotic syndrome and deafness clinical phenotypes (67). Vanillic acid restored ATP production and Q_{10} biosynthesis in human cellular models of COQ6 deficiency (68), while 2,4-dihydroxybenzoic acid (2,4-diHB) treatment prevented Coq6 related disease progression in mice (69). This is surprising because 2,4-diHB was previously known to bypass COQ7 deficiencies (70).

The enzymatic hydroxylase activity of Coq7 was first illustrated in the observation that the *coq7* point mutant accumulated DMQ_6 (71). Structure modeling predicted Coq7 to be a di-

iron carboxylate protein, with a highly conserved four-helix bundle and a fifth helix facilitating Coq7 interfacial inner mitochondrial membrane association (48,72). The activity of Coq7 is mediated by Coq8-dependent phosphorylation (41,61); moreover, Coq7 phosphorylation status may be a regulator of respiratory-induced Q_6 biosynthesis (73). Expression of human COQ7 recovered Q_6 biosynthesis in *coq7*Δ yeast (74), validating it as a Coq7 functional ortholog. Primary Q_{10} deficiency resulting from COQ7 mutations manifests in a range of metabolic diseases that can benefit from treatment with 2,4-diHB, a 4HB analog that bypasses the COQ7-dependent hydroxylase step (75,76).

In contrast to the aforementioned Coq proteins, the responsibility of Coq4, Coq8, Coq9, and Coq10 within the Q_6 biosynthetic pathway is somewhat less clear. No enzymatic function has thus far been ascribed to Coq4, yet the *coq4*Δ mutant lacks detectable Q_6 and accumulates early-stage Q_6-intermeadiates (77). The Coq4 polypeptide is peripherally associated with the matrix side of the mitochondrial inner membrane and is required for Q_6 biosynthesis (77). Coq4 possess a bound geranylgeranyl monophosphate (78), suggesting that the function of Coq4 may be to bind the polyisoprenoid side-chain of Q_6-intermeadiates. Additionally, the structure contains a conserved $HDxxHx_{10–13}E$ putative zinc-binding motif, with a bound magnesium ion in close proximity to the phosphate head group (78,79). It is believed that Coq4 binds Q_6-intermediates and serves as a scaffold protein, effective in organizing several other Coq proteins (48,79). Human COQ4 was demonstrated to have conserved function with yeast Coq4 (80). Homozygous recessive *COQ4* mutant alleles were shown to drive early-onset mitochondrial diseases with debilitating phenotypes in patients (81), and intriguingly COQ4 haploinsufficiency also resulted in Q_{10} deficiency (82).

Yeast *COQ8* is a putative kinase that belongs to the ancient atypical kinase family (83), and harbors six of the twelve motifs present in canonical protein kinases (84). These proteins are capable of autophosphorylation and have a strong preference for ADP as phosphate group source (85). The phosphorylation state of Coq3, Coq5, and Coq7 is dependent on Coq8, which is similarly localized to the matrix side of the inner mitochondrial membrane (55). Expression of the human homolog of Coq8, COQ8A (ADCK3) or COQ8B (ADCK4) efficiently restored Q_6 biosynthesis, and COQ8A expression additional rescued phosphorylation of the aforementioned Coq polypeptides (55,86). Interestingly, COQ8A exhibits ATPase activity, rather than protein kinase activity, that is enhanced by small-molecule Q_6-intermediate mimetics and cardiolipin (87,88). It is thus tempting to speculate that yeast Coq8 and its homologs may work as chaperones to allow for the extraction of Q_6-intermediates from the membrane and into the aqueous matrix, to facilitate *de novo* Q_n biosynthesis (88). Diseases correlated with mutated *COQ8A* include childhood-onset cerebellar ataxia (84,89), and *COQ8B* associated steroid-resistant nephrotic disease (86,90).

The Coq9 protein in *S. cerevisiae* is peripherally associated with the matrix-face of the inner mitochondrial membrane, where it was identified as necessary for Q_6 biosynthesis (48). Yeast *coq9*Δ accumulates the early-stage Q_6-intermediate HHB (49). Further, the presence of Coq9 is necessary for the removal of the amino substituent at carbon 4 on Q_6 biosynthetic intermediate when pABA is provided as the ring precursor (91). The deamination also depends on the function of Coq6 hydroxylase activity; both c*oq9* mutants, and *coq6*Δ overexpressing *COQ8*, accumulate 3-hexaprenyl-4-aminophenol (4-AP) (61). Coq9 is also required for Coq7 hydroxylase activity (92). Taken together, these results demonstrate that Coq9 plays a supportive role for the hydroxylation steps catalyzed by Coq6 and Coq7. Human COQ9 has been effective

in the rescue of *coq9* temperature sensitive point mutants (93), yet thus far has not been shown to restore Q_6 biosynthesis in *coq9*Δ yeast (94,95).

Similar to Coq4, Coq8, and Coq9, the specific function of the Coq10 polypeptide remains undefined. Yeast *coq10*Δ is unique among the Q_6-less *coq1-coq9* mutants, because it synthesizes near wild-type amounts of Q_6 in stationary phase, yet produces Q_6 less efficiently during log phase growth (42,96). However, the *coq10*Δ mutant is respiratory deficient and has decreased NADH and succinate oxidase activities, and displays sickly, translating to anemic growth on respiratory medium (15,42,97). Cells lacking *COQ10* are particularly to lipid peroxidation initiated by exogenously supplemented polyunsaturated fatty acids (PUFAs), indicating that Coq10 is also required for antioxidant protection by Q_6 (96,97). The Coq10 polypeptide contains a steroidogenic acute regulatory (StAR)-related lipid transfer (StART) domain, shown to bind Q_6 and late-stage Q_6-intermediates both *in vitro* and *in vivo* via its hydrophobic tunnel (42,96,98,99). Therefore, it is likely that Coq10 acts as a lipid chaperone delivering Q_6 from its site of synthesis to where Q_6 functions as an antioxidant and to the respiratory complexes (96). Human COQ10A and COQ10B were unable to rescue Q_6 biosynthesis in *coq10*Δ yeast, however, expression of either mammalian homolog did restore mutant respiration on a nonfermentable carbon source and sensitivity to PUFA induced oxidative stress (97). There are currently no known disease phenotypes attributed to either COQ10A or COQ10B dysfunction.

FORMATION OF A 'COQ SYNTHOME' IS REQUIRED FOR Q BIOSYNTHESIS

Several genetic and biochemical analyses have determined that Coq3-Coq9, and Coq11, organize into a multi-subunit high molecular weight complex termed the 'CoQ synthome', that is required for Q_6 biosynthesis (41,79,100,101). Specifically, gel filtration chromatography and

two-dimensional Blue Native/SDS-PAGE investigations have presented evidence of high molecular weight migration of several Coq proteins (2). Co-immunoprecipitation experiments revealed direct interaction between numerous Coq polypeptides; biotinylated Coq3 co-purified with Coq4, and HA-tagged Coq9 co-precipitated Coq4, Coq5, Coq6, and Coq7 (100,101). Coq1 and Coq2 have not yet been identified to associate with the CoQ synthome component polypeptides. Nevertheless, polyisoprenylated Q_6-intermediates produced by Coq1 and Coq2 appear to be important for CoQ synthome formation and/or stabilization (48).

Experimental evidence suggests that polyisoprenylated Q_6-intermediates, in addition to Q_6 itself, directly interact with the CoQ synthome (9). Size exclusion chromatography of digitionin treated mitochondrial extracts showed that the late-stage Q_6-intermediate DMQ_6 co-eluted with Coq3 *O*-methyltransferase activity and high molecular mass Coq polypeptide sub-complexes (100).

In yeast *coq7*Δ mutants, addition of exogenous Q_6 to growth medium increased the steady-state levels of the Coq3 and Coq4 polypeptides and restored DMQ_6 synthesis (102). Overexpression of Coq8, shown to restore Coq proteins and CoQ synthome formation in some of the other *coq* null mutants (48,55,61), had no effect on *coq1*Δ and *coq2*Δ yeast, which fail to produce polyisoprenylated ring intermediates (61). This data implies that the presence of Q_6 and other Q_6-intermediates are crucial for Coq protein and CoQ synthome stability.

Deletion of *S. cerevisiae COQ1-COQ10* genes that are essential for Q_6 biosynthesis leads to destabilization of various other Coq polypeptides may result in CoQ synthome destabilization (101,103). Alternatively, *coq11*Δ yeast display increased protein amounts of Coq4, Coq6, Coq7, and Coq9, ultimately driving stabilization of the CoQ synthome (15). Two recent studies using *in vivo* visualization of tagged yeast Coq proteins indicated that the several Coq polypeptides

colocalize into discrete 'CoQ domains' at the inner mitochondrial membrane (103,104). The presence of these CoQ domains is contingent upon proper formation of the CoQ synthome (103). Mitochondria isolated from yeast lacking components of the CoQ synthome*, coq3-coq9*, and additionally the *coq10*Δ mutant, have a reduced number of CoQ domain puncta (103,104). This is driven by lower levels of specific Coq polypeptides and partial CoQ synthome destabilization in these mutants (2,48,96,97). The CoQ synthome is additionally required for the generation of ER-mitochondrial contact sites mediated by the ER-mitochondrial encounter structure (ERMES) complex (103,104). The ERMES complex mediates lipid trafficking between the ER and mitochondria (105). In fact, cells lacking *ERMES* proteins have dysfunctional Q_6 cellular distribution and a destabilized CoQ synthome (104). Experimental evidence has ultimately suggested that Q_6 circulation from the mitochondria to other organelles relies on CoQ synthome positioning next to the ERMES complex (104).

IDENTIFICATION OF A PUTATIVE COENZYME Q MODULATOR

Recently, a protein of unknown function encoded by the open reading frame *YLR290C* was identified to co-purify with Coq5, Coq7, and Coq9, as well as Q_6 and late-stage Q_6-intermediates (41). Yeast lacking *ylr290c* maintained respiratory growth on non-fermentable medium, despite producing significantly less *de novo* Q_6 compared to wild type (41). Taken together, this data indicated that YLR290C was a novel Coq protein, and it was therefore renamed 'Coq11'. Yeast Coq11 is a member of the short-chain dehydrogenase/reductase (SDR) superfamily of NAD(P)(H) dependent oxidoreductases (41,106). SDR superfamily proteins possess a conserved Rossmann fold, employed in the binding of nucleotide cofactors such as FAD, FMN, and NAD(P) (107). This enzyme class catalyzes various reactions including

isomerization, decarboxylation, epimerization, imine reduction, and carbonyl-alcohol oxidoreduction (106). Crystal structures revealed that enzymes containing Rossmann fold domains in both *Escherichia coli* and *Pseudomonas aeruginosa* catalyze FMN-dependent decarboxylation reactions in the species respective Q_n biosynthetic pathways (108). The decarboxylation step in *S. cerevisiae* Q_6 biosynthesis remains uncharacterized at present. These data have prompted speculation that Coq11 may use its Rossmann fold in conjunction with a nucleotide cofactor to perform similar redox chemistry in *S. cerevisiae* Q_6 biosynthesis.

In various fungi, Coq11 and Coq10 were found as protein fusions (41), indicating that Coq11 and Coq10 may be involved in the same biochemical pathway or physically interact (109). We have demonstrated that *coq10*Δ mutant phenotypes of respiratory deficiency, decreased Q_6 biosynthesis, and sensitivity to exogenous PUFA treatment, are rescued by deletion of *COQ11* (15). Additionally, *coq11*Δ yeast accumulated increased amounts of certain Coq polypeptides, and the destabilized Coq proteins in the *coq10*Δ mutant were restored in a *coq10*Δ*coq11*Δ double mutant (15). The *coq11*Δ mutant conferred a stabilized CoQ synthome (15), and displayed increased CoQ domain intensity, although the total number of domains was comparable to wild type (103). These observations have led to the hypothesis that Coq11 is involved with modulation of Q_6 biosynthesis; perhaps Coq11 is serving as a control point Q_6 production, catalyzing the transition between Q_6 redox states, or simply acting in tandem with Coq10 to facilitate the transportation of Q_6 and Q_6-intermediates.

The closest human homolog of *S. cerevisiae* Coq11 is NUDUFA9 (41)—an SDR subfamily protein, and an auxiliary subunit of complex I in humans (110,111). Genetic knockouts using Transcription Activator-like Effector Nucleases (TALENs) revealed that NDUFA9 is important for stabilization of the junction between the matrix and membrane arms of

complex I (112). Disruption of proteins involved in complex I formation disrupts respiratory electron transport (113,114), and perhaps Q_{10} biosynthesis as well. Patients with decreased levels of NDUFA9 are unable to assemble complex I properly and may develop a degenerative infancy respiratory disorder, known as Leigh syndrome (115,116). Although yeast do not possess complex I, it would be interesting to determine whether Coq11 localizes to yeast respiratory complexes in a similar manner to NDUFA9. The present work investigates various aspects of Coq11, towards understanding its role in the Q_6 biosynthetic pathway.

FIGURES

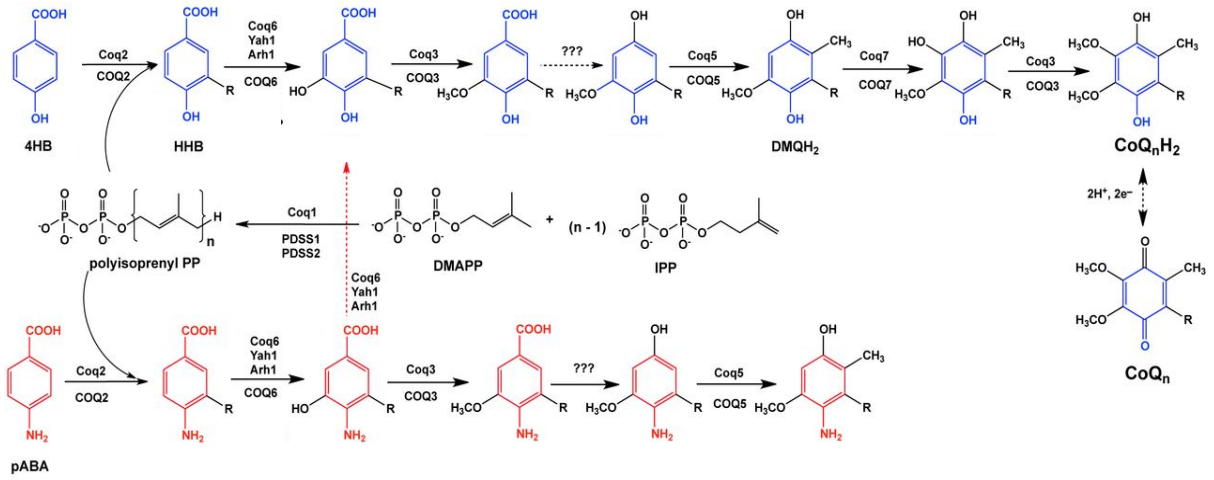

Figure 1. The coenzyme Q biosynthetic pathway within *S. cerevisiae* and humans. Figure is adapted from Ref. (2). At least fourteen known proteins are required to drive Q_6 biosynthesis in *S. cerevisiae* (Coq1-Coq11, Yah1, Arh1, and Hfd1), and the corresponding human genes are denoted below each arrow (2). A polyprenyl diphosphate is generated by a polyprenyl diphosphate synthase (Coq1, or PDSS1/PDSS2) using the precursors isopentenyl pyrophosphate (IPP) and dimethylallyl pyrophosphate (DMAPP). The isoprenoid side-chain is attached to an aromatic ring precursor by Coq2 or COQ2. Both yeast and human use 4-hydroxybenzoic acid (4HB) as a ring precursor (intermediates emanating from blue text) (3), while yeast additionally may utilize *para*-aminobenzoic acid (pABA) as an alternative ring precursor (red text) (117). Several Coq proteins (Coq6/COQ6, Coq3/COQ3, Coq5/COQ5, and Coq7/COQ7) decorate the $Q_{6/10}$ benzene ring to form the final product. Additional Coq proteins (Coq4/COQ4, Coq8/ADCK3+ADCK4, Coq9/COQ9, Coq10/COQ10A+COQ10B, and Coq11/?) may not directly catalyze an enzymatic step but are still required for efficient $Q_{6/10}$ biosynthesis. The steps donated "???" are not yet attributed to a particular protein.

REFERENCES

1. Nowicka, B., and Kruk, J. (2010) Occurrence, biosynthesis and function of isoprenoid quinones. *Biochim Biophys Acta* **1797**, 1587-1605
2. Awad, A. M., Bradley, M. C., Fernandez-Del-Rio, L., Nag, A., Tsui, H. S., and Clarke, C. F. (2018) Coenzyme Q_{10} deficiencies: pathways in yeast and humans. *Essays Biochem* **62**, 361-376
3. Wang, Y., and Hekimi, S. (2019) The Complexity of Making Ubiquinone. *Trends Endocrinol Metab*
4. Okada, K., Suzuki, K., Kamiya, Y., Zhu, X., Fujisaki, S., Nishimura, Y., Nishino, T., Nakagawa, T., Kawamukai, M., and Matsuda, H. (1996) Polyprenyl diphosphate synthase essentially defines the length of the side chain of ubiquinone. *Biochim Biophys Acta* **1302**, 217-223
5. Okada, K., Kainou, T., Matsuda, H., and Kawamukai, M. (1998) Biological significance of the side chain length of ubiquinone in *Saccharomyces cerevisiae*. *FEBS Lett* **431**, 241-244
6. Jonassen, T., Davis, D. E., Larsen, P. L., and Clarke, C. F. (2003) Reproductive fitness and quinone content of *Caenorhabditis elegans clk-1* mutants fed coenzyme Q isoforms of varying length. *J Biol Chem* **278**, 51735-51742
7. Crane, F. L. (2007) Discovery of ubiquinone (coenzyme Q) and an overview of function. *Mitochondrion* **7 Suppl**, S2-7
8. Brandt, U., and Trumpower, B. (1994) The protonmotive Q cycle in mitochondria and bacteria. *Crit Rev Biochem Mol Biol* **29**, 165-197

9. Turunen, M., Olsson, J., and Dallner, G. (2004) Metabolism and function of coenzyme Q. *Biochim Biophys Acta* **1660**, 171-199

10. Grandier-Vazeille, X., Bathany, K., Chaignepain, S., Camougrand, N., Manon, S., and Schmitter, J. M. (2001) Yeast mitochondrial dehydrogenases are associated in a supramolecular complex. *Biochemistry* **40**, 9758-9769

11. Luttik, M. A., Overkamp, K. M., Kotter, P., de Vries, S., van Dijken, J. P., and Pronk, J. T. (1998) The *Saccharomyces cerevisiae NDE1* and *NDE2* genes encode separate mitochondrial NADH dehydrogenases catalyzing the oxidation of cytosolic NADH. *J Biol Chem* **273**, 24529-24534

12. Frei, B., Kim, M. C., and Ames, B. N. (1990) Ubiquinol-10 is an effective lipid-soluble antioxidant at physiological concentrations. *Proc Natl Acad Sci U S A* **87**, 4879-4883

13. Bentinger, M., Brismar, K., and Dallner, G. (2007) The antioxidant role of coenzyme Q. *Mitochondrion* **7 Suppl**, S41-50

14. Hill, S., Hirano, K., Shmanai, V. V., Marbois, B. N., Vidovic, D., Bekish, A. V., Kay, B., Tse, V., Fine, J., Clarke, C. F., and Shchepinov, M. S. (2011) Isotope-reinforced polyunsaturated fatty acids protect yeast cells from oxidative stress. *Free Radic Biol Med* **50**, 130-138

15. Bradley, M. C., Yang, K., Fernandez-Del-Rio, L., Ngo, J., Ayer, A., Tsui, H. S., Novales, N. A., Stocker, R., Shirihai, O. S., Barros, M. H., and Clarke, C. F. (2020) *COQ11* deletion mitigates respiratory deficiency caused by mutations in the gene encoding the coenzyme Q chaperone protein Coq10. *J Biol Chem* **295**, 6023-6042

16. Poon, W. W., Do, T. Q., Marbois, B. N., and Clarke, C. F. (1997) Sensitivity to treatment with polyunsaturated fatty acids is a general characteristic of the ubiquinone-deficient yeast *coq* mutants. *Mol Aspects Med* **18 Suppl**, S121-127

17. Hill, S., Lamberson, C. R., Xu, L., To, R., Tsui, H. S., Shmanai, V. V., Bekish, A. V., Awad, A. M., Marbois, B. N., Cantor, C. R., Porter, N. A., Clarke, C. F., and Shchepinov, M. S. (2012) Small amounts of isotope-reinforced polyunsaturated fatty acids suppress lipid autoxidation. *Free Radic Biol Med* **53**, 893-906

18. Guaras, A., Perales-Clemente, E., Calvo, E., Acin-Perez, R., Loureiro-Lopez, M., Pujol, C., Martinez-Carrascoso, I., Nunez, E., Garcia-Marques, F., Rodriguez-Hernandez, M. A., Cortes, A., Diaz, F., Perez-Martos, A., Moraes, C. T., Fernandez-Silva, P., Trifunovic, A., Navas, P., Vazquez, J., and Enriquez, J. A. (2016) The $CoQH_2$/CoQ Ratio Serves as a Sensor of Respiratory Chain Efficiency. *Cell Rep* **15**, 197-209

19. Scialo, F., Sriram, A., Fernandez-Ayala, D., Gubina, N., Lohmus, M., Nelson, G., Logan, A., Cooper, H. M., Navas, P., Enriquez, J. A., Murphy, M. P., and Sanz, A. (2016) Mitochondrial ROS Produced via Reverse Electron Transport Extend Animal Lifespan. *Cell Metab* **23**, 725-734

20. Desbats, M. A., Lunardi, G., Doimo, M., Trevisson, E., and Salviati, L. (2015) Genetic bases and clinical manifestations of coenzyme Q_{10} (CoQ_{10}) deficiency. *J Inherit Metab Dis* **38**, 145-156

21. Alcazar-Fabra, M., Trevisson, E., and Brea-Calvo, G. (2018) Clinical syndromes associated with Coenzyme Q_{10} deficiency. *Essays Biochem* **62**, 377-398

22. Papucci, L., Schiavone, N., Witort, E., Donnini, M., Lapucci, A., Tempestini, A., Formigli, L., Zecchi-Orlandini, S., Orlandini, G., Carella, G., Brancato, R., and

Capaccioli, S. (2003) Coenzyme q_{10} prevents apoptosis by inhibiting mitochondrial depolarization independently of its free radical scavenging property. *J Biol Chem* **278**, 28220-28228

23. Divakaruni, A. S., and Brand, M. D. (2011) The regulation and physiology of mitochondrial proton leak. *Physiology (Bethesda)* **26**, 192-205

24. Echtay, K. S., Winkler, E., Frischmuth, K., and Klingenberg, M. (2001) Uncoupling proteins 2 and 3 are highly active $H(^{+})$ transporters and highly nucleotide sensitive when activated by coenzyme Q (ubiquinone). *Proc Natl Acad Sci U S A* **98**, 1416-1421

25. Schmelzer, C., Lindner, I., Vock, C., Fujii, K., and Doring, F. (2007) Functional connections and pathways of coenzyme Q_{10}-inducible genes: an *in-silico* study. *IUBMB Life* **59**, 628-633

26. Bentinger, M., Tekle, M., and Dallner, G. (2010) Coenzyme Q--biosynthesis and functions. *Biochem Biophys Res Commun* **396**, 74-79

27. Olson, R. E. (1966) Biosynthesis of ubiquinones in animals. *Vitam Horm* **24**, 551-574

28. Marbois, B., Xie, L. X., Choi, S., Hirano, K., Hyman, K., and Clarke, C. F. (2010) *para*-Aminobenzoic acid is a precursor in coenzyme Q_6 biosynthesis in *Saccharomyces cerevisiae*. *J Biol Chem* **285**, 27827-27838

29. Kawamukai, M. (2016) Biosynthesis of coenzyme Q in eukaryotes. *Biosci Biotechnol Biochem* **80**, 23-33

30. Pierrel, F. (2017) Impact of Chemical Analogs of 4-Hydroxybenzoic Acid on Coenzyme Q Biosynthesis: From Inhibition to Bypass of Coenzyme Q Deficiency. *Front Physiol* **8**, 436

31. Xie, L. X., Williams, K. J., He, C. H., Weng, E., Khong, S., Rose, T. E., Kwon, O., Bensinger, S. J., Marbois, B. N., and Clarke, C. F. (2015) Resveratrol and *para*-coumarate serve as ring precursors for coenzyme Q biosynthesis. *J Lipid Res* **56**, 909-919

32. Doimo, M., Trevisson, E., Airik, R., Bergdoll, M., Santos-Ocana, C., Hildebrandt, F., Navas, P., Pierrel, F., and Salviati, L. (2014) Effect of vanillic acid on *COQ6* mutants identified in patients with coenzyme Q_{10} deficiency. *Biochim Biophys Acta* **1842**, 1-6

33. Fernandez-Del-Rio, L., Nag, A., Gutierrez Casado, E., Ariza, J., Awad, A. M., Joseph, A. I., Kwon, O., Verdin, E., de Cabo, R., Schneider, C., Torres, J. Z., Buron, M. I., Clarke, C. F., and Villalba, J. M. (2017) Kaempferol increases levels of coenzyme Q in kidney cells and serves as a biosynthetic ring precursor. *Free Radic Biol Med* **110**, 176-187

34. Barkovich, R. J., Shtanko, A., Shepherd, J. A., Lee, P. T., Myles, D. C., Tzagoloff, A., and Clarke, C. F. (1997) Characterization of the *COQ5* gene from *Saccharomyces cerevisiae*. Evidence for a C-methyltransferase in ubiquinone biosynthesis. *J Biol Chem* **272**, 9182-9188

35. Sheftel, A., Stehling, O., and Lill, R. (2010) Iron-sulfur proteins in health and disease. *Trends Endocrinol Metab* **21**, 302-314

36. Manzella, L., Barros, M. H., and Nobrega, F. G. (1998) *ARH1* of *Saccharomyces cerevisiae*: a new essential gene that codes for a protein homologous to the human adrenodoxin reductase. *Yeast* **14**, 839-846

37. Barros, M. H., and Nobrega, F. G. (1999) *YAH1* of *Saccharomyces cerevisiae*: a new essential gene that codes for a protein homologous to human adrenodoxin. *Gene* **233**, 197-203

38. Ozeir, M., Muhlenhoff, U., Webert, H., Lill, R., Fontecave, M., and Pierrel, F. (2011) Coenzyme Q biosynthesis: Coq6 is required for the C5-hydroxylation reaction and substrate analogs rescue Coq6 deficiency. *Chem Biol* **18**, 1134-1142

39. Zahedi, R. P., Sickmann, A., Boehm, A. M., Winkler, C., Zufall, N., Schonfisch, B., Guiard, B., Pfanner, N., and Meisinger, C. (2006) Proteomic analysis of the yeast mitochondrial outer membrane reveals accumulation of a subclass of preproteins. *Mol Biol Cell* **17**, 1436-1450

40. Payet, L. A., Leroux, M., Willison, J. C., Kihara, A., Pelosi, L., and Pierrel, F. (2016) Mechanistic Details of Early Steps in Coenzyme Q Biosynthesis Pathway in Yeast. *Cell Chem Biol* **23**, 1241-1250

41. Allan, C. M., Awad, A. M., Johnson, J. S., Shirasaki, D. I., Wang, C., Blaby-Haas, C. E., Merchant, S. S., Loo, J. A., and Clarke, C. F. (2015) Identification of Coq11, a new coenzyme Q biosynthetic protein in the CoQ-synthome in *Saccharomyces cerevisiae*. *J Biol Chem* **290**, 7517-7534

42. Barros, M. H., Johnson, A., Gin, P., Marbois, B. N., Clarke, C. F., and Tzagoloff, A. (2005) The *Saccharomyces cerevisiae COQ10* gene encodes a START domain protein required for function of coenzyme Q in respiration. *J Biol Chem* **280**, 42627-42635

43. Ashby, M. N., and Edwards, P. A. (1990) Elucidation of the deficiency in two yeast coenzyme Q mutants. Characterization of the structural gene encoding hexaprenyl pyrophosphate synthetase. *J Biol Chem* **265**, 13157-13164

44. Gin, P., and Clarke, C. F. (2005) Genetic evidence for a multi-subunit complex in coenzyme Q biosynthesis in yeast and the role of the Coq1 hexaprenyl diphosphate synthase. *J Biol Chem* **280**, 2676-2681

45. Saiki, R., Nagata, A., Kainou, T., Matsuda, H., and Kawamukai, M. (2005) Characterization of solanesyl and decaprenyl diphosphate synthases in mice and humans. *FEBS J* **272**, 5606-5622

46. Lopez, L. C., Schuelke, M., Quinzii, C. M., Kanki, T., Rodenburg, R. J., Naini, A., Dimauro, S., and Hirano, M. (2006) Leigh syndrome with nephropathy and CoQ_{10} deficiency due to decaprenyl diphosphate synthase subunit 2 (PDSS2) mutations. *Am J Hum Genet* **79**, 1125-1129

47. Ashby, M. N., Kutsunai, S. Y., Ackerman, S., Tzagoloff, A., and Edwards, P. A. (1992) *COQ2* is a candidate for the structural gene encoding *para*-hydroxybenzoate:polyprenyltransferase. *J Biol Chem* **267**, 4128-4136

48. He, C. H., Xie, L. X., Allan, C. M., Tran, U. C., and Clarke, C. F. (2014) Coenzyme Q supplementation or over-expression of the yeast Coq8 putative kinase stabilizes multi-subunit Coq polypeptide complexes in yeast *coq* null mutants. *Biochim Biophys Acta* **1841**, 630-644

49. Johnson, A., Gin, P., Marbois, B. N., Hsieh, E. J., Wu, M., Barros, M. H., Clarke, C. F., and Tzagoloff, A. (2005) *COQ9*, a new gene required for the biosynthesis of coenzyme Q in *Saccharomyces cerevisiae*. *J Biol Chem* **280**, 31397-31404

50. Forsgren, M., Attersand, A., Lake, S., Grunler, J., Swiezewska, E., Dallner, G., and Climent, I. (2004) Isolation and functional expression of human *COQ2*, a gene encoding a polyprenyl transferase involved in the synthesis of CoQ. *Biochem J* **382**, 519-526

51. Desbats, M. A., Morbidoni, V., Silic-Benussi, M., Doimo, M., Ciminale, V., Cassina, M., Sacconi, S., Hirano, M., Basso, G., Pierrel, F., Navas, P., Salviati, L., and Trevisson, E.

(2016) The *COQ2* genotype predicts the severity of coenzyme Q_{10} deficiency. *Hum Mol Genet* **25**, 4256-4265

52. Clarke, C. F., Williams, W., and Teruya, J. H. (1991) Ubiquinone biosynthesis in *Saccharomyces cerevisiae*. Isolation and sequence of *COQ3*, the 3,4-dihydroxy-5-hexaprenylbenzoate methyltransferase gene. *J Biol Chem* **266**, 16636-16644

53. Poon, W. W., Barkovich, R. J., Hsu, A. Y., Frankel, A., Lee, P. T., Shepherd, J. N., Myles, D. C., and Clarke, C. F. (1999) Yeast and rat Coq3 and *Escherichia coli* UbiG polypeptides catalyze both O-methyltransferase steps in coenzyme Q biosynthesis. *J Biol Chem* **274**, 21665-21672

54. Niewmierzycka, A., and Clarke, S. (1999) S-Adenosylmethionine-dependent methylation in *Saccharomyces cerevisiae*. Identification of a novel protein arginine methyltransferase. *J Biol Chem* **274**, 814-824

55. Xie, L. X., Hsieh, E. J., Watanabe, S., Allan, C. M., Chen, J. Y., Tran, U. C., and Clarke, C. F. (2011) Expression of the human atypical kinase ADCK3 rescues coenzyme Q biosynthesis and phosphorylation of Coq polypeptides in yeast *coq8* mutants. *Biochim Biophys Acta* **1811**, 348-360

56. Tauche, A., Krause-Buchholz, U., and Rodel, G. (2008) Ubiquinone biosynthesis in *Saccharomyces cerevisiae*: the molecular organization of O-methylase Coq3p depends on Abc1p/Coq8p. *FEMS Yeast Res* **8**, 1263-1275

57. Jonassen, T., and Clarke, C. F. (2000) Isolation and functional expression of human *COQ3*, a gene encoding a methyltransferase required for ubiquinone biosynthesis. *J Biol Chem* **275**, 12381-12387

58. Baba, S. W., Belogrudov, G. I., Lee, J. C., Lee, P. T., Strahan, J., Shepherd, J. N., and Clarke, C. F. (2004) Yeast Coq5 C-methyltransferase is required for stability of other polypeptides involved in coenzyme Q biosynthesis. *J Biol Chem* **279**, 10052-10059

59. Dibrov, E., Robinson, K. M., and Lemire, B. D. (1997) The *COQ5* gene encodes a yeast mitochondrial protein necessary for ubiquinone biosynthesis and the assembly of the respiratory chain. *J Biol Chem* **272**, 9175-9181

60. Dai, Y. N., Zhou, K., Cao, D. D., Jiang, Y. L., Meng, F., Chi, C. B., Ren, Y. M., Chen, Y., and Zhou, C. Z. (2014) Crystal structures and catalytic mechanism of the C-methyltransferase Coq5 provide insights into a key step of the yeast coenzyme Q synthesis pathway. *Acta Crystallogr D Biol Crystallogr* **70**, 2085-2092

61. Xie, L. X., Ozeir, M., Tang, J. Y., Chen, J. Y., Jaquinod, S. K., Fontecave, M., Clarke, C. F., and Pierrel, F. (2012) Overexpression of the Coq8 kinase in *Saccharomyces cerevisiae coq* null mutants allows for accumulation of diagnostic intermediates of the coenzyme Q_6 biosynthetic pathway. *J Biol Chem* **287**, 23571-23581

62. Nguyen, T. P., Casarin, A., Desbats, M. A., Doimo, M., Trevisson, E., Santos-Ocana, C., Navas, P., Clarke, C. F., and Salviati, L. (2014) Molecular characterization of the human COQ5 C-methyltransferase in coenzyme Q_{10} biosynthesis. *Biochim Biophys Acta* **1841**, 1628-1638

63. Malicdan, M. C. V., Vilboux, T., Ben-Zeev, B., Guo, J., Eliyahu, A., Pode-Shakked, B., Dori, A., Kakani, S., Chandrasekharappa, S. C., Ferreira, C. R., Shelestovich, N., Marek-Yagel, D., Pri-Chen, H., Blatt, I., Niederhuber, J. E., He, L., Toro, C., Taylor, R. W., Deeken, J., Yardeni, T., Wallace, D. C., Gahl, W. A., and Anikster, Y. (2018) A novel

inborn error of the coenzyme Q_{10} biosynthesis pathway: cerebellar ataxia and static encephalomyopathy due to COQ5 C-methyltransferase deficiency. *Hum Mutat* **39**, 69-79

64. Gin, P., Hsu, A. Y., Rothman, S. C., Jonassen, T., Lee, P. T., Tzagoloff, A., and Clarke, C. F. (2003) The *Saccharomyces cerevisiae COQ6* gene encodes a mitochondrial flavin-dependent monooxygenase required for coenzyme Q biosynthesis. *J Biol Chem* **278**, 25308-25316

65. Ismail, A., Leroux, V., Smadja, M., Gonzalez, L., Lombard, M., Pierrel, F., Mellot-Draznieks, C., and Fontecave, M. (2016) Coenzyme Q Biosynthesis: Evidence for a Substrate Access Channel in the FAD-Dependent Monooxygenase Coq6. *PLoS Comput Biol* **12**, e1004690

66. Ozeir, M., Pelosi, L., Ismail, A., Mellot-Draznieks, C., Fontecave, M., and Pierrel, F. (2015) Coq6 is responsible for the C4-deamination reaction in coenzyme Q biosynthesis in *Saccharomyces cerevisiae*. *J Biol Chem* **290**, 24140-24151

67. Heeringa, S. F., Chernin, G., Chaki, M., Zhou, W., Sloan, A. J., Ji, Z., Xie, L. X., Salviati, L., Hurd, T. W., Vega-Warner, V., Killen, P. D., Raphael, Y., Ashraf, S., Ovunc, B., Schoeb, D. S., McLaughlin, H. M., Airik, R., Vlangos, C. N., Gbadegesin, R., Hinkes, B., Saisawat, P., Trevisson, E., Doimo, M., Casarin, A., Pertegato, V., Giorgi, G., Prokisch, H., Rotig, A., Nurnberg, G., Becker, C., Wang, S., Ozaltin, F., Topaloglu, R., Bakkaloglu, A., Bakkaloglu, S. A., Muller, D., Beissert, A., Mir, S., Berdeli, A., Varpizen, S., Zenker, M., Matejas, V., Santos-Ocana, C., Navas, P., Kusakabe, T., Kispert, A., Akman, S., Soliman, N. A., Krick, S., Mundel, P., Reiser, J., Nurnberg, P., Clarke, C. F., Wiggins, R. C., Faul, C., and Hildebrandt, F. (2011) COQ6 mutations in

human patients produce nephrotic syndrome with sensorineural deafness. *J Clin Invest* **121**, 2013-2024

68. Acosta Lopez, M. J., Trevisson, E., Canton, M., Vazquez-Fonseca, L., Morbidoni, V., Baschiera, E., Frasson, C., Pelosi, L., Rascalou, B., Desbats, M. A., Alcazar-Fabra, M., Rios, J. J., Sanchez-Garcia, A., Basso, G., Navas, P., Pierrel, F., Brea-Calvo, G., and Salviati, L. (2019) Vanillic Acid Restores Coenzyme Q Biosynthesis and ATP Production in Human Cells Lacking *COQ6*. *Oxid Med Cell Longev* **2019**, 3904905

69. Widmeier, E., Airik, M., Hugo, H., Schapiro, D., Wedel, J., Ghosh, C. C., Nakayama, M., Schneider, R., Awad, A. M., Nag, A., Cho, J., Schueler, M., Clarke, C. F., Airik, R., and Hildebrandt, F. (2019) Treatment with 2,4-Dihydroxybenzoic Acid Prevents FSGS Progression and Renal Fibrosis in Podocyte-Specific Coq6 Knockout Mice. *J Am Soc Nephrol*

70. Wang, Y., Oxer, D., and Hekimi, S. (2015) Mitochondrial function and lifespan of mice with controlled ubiquinone biosynthesis. *Nat Commun* **6**, 6393

71. Marbois, B. N., and Clarke, C. F. (1996) The *COQ7* gene encodes a protein in *Saccharomyces cerevisiae* necessary for ubiquinone biosynthesis. *J Biol Chem* **271**, 2995-3004

72. Stenmark, P., Grunler, J., Mattsson, J., Sindelar, P. J., Nordlund, P., and Berthold, D. A. (2001) A new member of the family of di-iron carboxylate proteins. Coq7 (clk-1), a membrane-bound hydroxylase involved in ubiquinone biosynthesis. *J Biol Chem* **276**, 33297-33300

73. Martin-Montalvo, A., Gonzalez-Mariscal, I., Padilla, S., Ballesteros, M., Brautigan, D. L., Navas, P., and Santos-Ocana, C. (2011) Respiratory-induced coenzyme Q

biosynthesis is regulated by a phosphorylation cycle of Cat5p/Coq7p. *Biochem J* **440**, 107-114

74. Vajo, Z., King, L. M., Jonassen, T., Wilkin, D. J., Ho, N., Munnich, A., Clarke, C. F., and Francomano, C. A. (1999) Conservation of the *Caenorhabditis elegans* timing gene clk-1 from yeast to human: a gene required for ubiquinone biosynthesis with potential implications for aging. *Mamm Genome* **10**, 1000-1004

75. Freyer, C., Stranneheim, H., Naess, K., Mourier, A., Felser, A., Maffezzini, C., Lesko, N., Bruhn, H., Engvall, M., Wibom, R., Barbaro, M., Hinze, Y., Magnusson, M., Andeer, R., Zetterstrom, R. H., von Dobeln, U., Wredenberg, A., and Wedell, A. (2015) Rescue of primary ubiquinone deficiency due to a novel COQ7 defect using 2,4-dihydroxybensoic acid. *J Med Genet* **52**, 779-783

76. Kwong, A. K., Chiu, A. T., Tsang, M. H., Lun, K. S., Rodenburg, R. J. T., Smeitink, J., Chung, B. H., and Fung, C. W. (2019) A fatal case of COQ7-associated primary coenzyme Q_{10} deficiency. *JIMD Rep* **47**, 23-29

77. Belogrudov, G. I., Lee, P. T., Jonassen, T., Hsu, A. Y., Gin, P., and Clarke, C. F. (2001) Yeast *COQ4* encodes a mitochondrial protein required for coenzyme Q synthesis. *Arch Biochem Biophys* **392**, 48-58

78. Rea, S. L., Graham, B. H., Nakamaru-Ogiso, E., Kar, A., and Falk, M. J. (2010) Bacteria, yeast, worms, and flies: exploiting simple model organisms to investigate human mitochondrial diseases. *Dev Disabil Res Rev* **16**, 200-218

79. Marbois, B., Gin, P., Gulmezian, M., and Clarke, C. F. (2009) The yeast Coq4 polypeptide organizes a mitochondrial protein complex essential for coenzyme Q biosynthesis. *Biochim Biophys Acta* **1791**, 69-75

80. Casarin, A., Jimenez-Ortega, J. C., Trevisson, E., Pertegato, V., Doimo, M., Ferrero-Gomez, M. L., Abbadi, S., Artuch, R., Quinzii, C., Hirano, M., Basso, G., Ocana, C. S., Navas, P., and Salviati, L. (2008) Functional characterization of human *COQ4*, a gene required for Coenzyme Q_{10} biosynthesis. *Biochem Biophys Res Commun* **372**, 35-39

81. Brea-Calvo, G., Haack, T. B., Karall, D., Ohtake, A., Invernizzi, F., Carrozzo, R., Kremer, L., Dusi, S., Fauth, C., Scholl-Burgi, S., Graf, E., Ahting, U., Resta, N., Laforgia, N., Verrigni, D., Okazaki, Y., Kohda, M., Martinelli, D., Freisinger, P., Strom, T. M., Meitinger, T., Lamperti, C., Lacson, A., Navas, P., Mayr, J. A., Bertini, E., Murayama, K., Zeviani, M., Prokisch, H., and Ghezzi, D. (2015) *COQ4* mutations cause a broad spectrum of mitochondrial disorders associated with CoQ_{10} deficiency. *Am J Hum Genet* **96**, 309-317

82. Salviati, L., Trevisson, E., Rodriguez Hernandez, M. A., Casarin, A., Pertegato, V., Doimo, M., Cassina, M., Agosto, C., Desbats, M. A., Sartori, G., Sacconi, S., Memo, L., Zuffardi, O., Artuch, R., Quinzii, C., Dimauro, S., Hirano, M., Santos-Ocana, C., and Navas, P. (2012) Haploinsufficiency of *COQ4* causes coenzyme Q_{10} deficiency. *J Med Genet* **49**, 187-191

83. Leonard, C. J., Aravind, L., and Koonin, E. V. (1998) Novel families of putative protein kinases in bacteria and archaea: evolution of the "eukaryotic" protein kinase superfamily. *Genome Res* **8**, 1038-1047

84. Lagier-Tourenne, C., Tazir, M., Lopez, L. C., Quinzii, C. M., Assoum, M., Drouot, N., Busso, C., Makri, S., Ali-Pacha, L., Benhassine, T., Anheim, M., Lynch, D. R., Thibault, C., Plewniak, F., Bianchetti, L., Tranchant, C., Poch, O., DiMauro, S., Mandel, J. L., Barros, M. H., Hirano, M., and Koenig, M. (2008) ADCK3, an ancestral kinase, is

mutated in a form of recessive ataxia associated with coenzyme Q_{10} deficiency. *Am J Hum Genet* **82**, 661-672

85. Stefely, J. A., Reidenbach, A. G., Ulbrich, A., Oruganty, K., Floyd, B. J., Jochem, A., Saunders, J. M., Johnson, I. E., Minogue, C. E., Wrobel, R. L., Barber, G. E., Lee, D., Li, S., Kannan, N., Coon, J. J., Bingman, C. A., and Pagliarini, D. J. (2015) Mitochondrial ADCK3 employs an atypical protein kinase-like fold to enable coenzyme Q biosynthesis. *Mol Cell* **57**, 83-94

86. Vazquez Fonseca, L., Doimo, M., Calderan, C., Desbats, M. A., Acosta, M. J., Cerqua, C., Cassina, M., Ashraf, S., Hildebrandt, F., Sartori, G., Navas, P., Trevisson, E., and Salviati, L. (2018) Mutations in COQ8B (ADCK4) found in patients with steroid-resistant nephrotic syndrome alter COQ8B function. *Hum Mutat* **39**, 406-414

87. Stefely, J. A., Licitra, F., Laredj, L., Reidenbach, A. G., Kemmerer, Z. A., Grangeray, A., Jaeg-Ehret, T., Minogue, C. E., Ulbrich, A., Hutchins, P. D., Wilkerson, E. M., Ruan, Z., Aydin, D., Hebert, A. S., Guo, X., Freiberger, E. C., Reutenauer, L., Jochem, A., Chergova, M., Johnson, I. E., Lohman, D. C., Rush, M. J. P., Kwiecien, N. W., Singh, P. K., Schlagowski, A. I., Floyd, B. J., Forsman, U., Sindelar, P. J., Westphall, M. S., Pierrel, F., Zoll, J., Dal Peraro, M., Kannan, N., Bingman, C. A., Coon, J. J., Isope, P., Puccio, H., and Pagliarini, D. J. (2016) Cerebellar Ataxia and Coenzyme Q Deficiency through Loss of Unorthodox Kinase Activity. *Mol Cell* **63**, 608-620

88. Reidenbach, A. G., Kemmerer, Z. A., Aydin, D., Jochem, A., McDevitt, M. T., Hutchins, P. D., Stark, J. L., Stefely, J. A., Reddy, T., Hebert, A. S., Wilkerson, E. M., Johnson, I. E., Bingman, C. A., Markley, J. L., Coon, J. J., Dal Peraro, M., and Pagliarini, D. J.

(2018) Conserved Lipid and Small-Molecule Modulation of COQ8 Reveals Regulation of the Ancient Kinase-like UbiB Family. *Cell Chem Biol* **25**, 154-165 e111

89. Mollet, J., Delahodde, A., Serre, V., Chretien, D., Schlemmer, D., Lombes, A., Boddaert, N., Desguerre, I., de Lonlay, P., de Baulny, H. O., Munnich, A., and Rotig, A. (2008) *CABC1* gene mutations cause ubiquinone deficiency with cerebellar ataxia and seizures. *Am J Hum Genet* **82**, 623-630

90. Ashraf, S., Gee, H. Y., Woerner, S., Xie, L. X., Vega-Warner, V., Lovric, S., Fang, H., Song, X., Cattran, D. C., Avila-Casado, C., Paterson, A. D., Nitschke, P., Bole-Feysot, C., Cochat, P., Esteve-Rudd, J., Haberberger, B., Allen, S. J., Zhou, W., Airik, R., Otto, E. A., Barua, M., Al-Hamed, M. H., Kari, J. A., Evans, J., Bierzynska, A., Saleem, M. A., Bockenhauer, D., Kleta, R., El Desoky, S., Hacihamdioglu, D. O., Gok, F., Washburn, J., Wiggins, R. C., Choi, M., Lifton, R. P., Levy, S., Han, Z., Salviati, L., Prokisch, H., Williams, D. S., Pollak, M., Clarke, C. F., Pei, Y., Antignac, C., and Hildebrandt, F. (2013) *ADCK4* mutations promote steroid-resistant nephrotic syndrome through CoQ_{10} biosynthesis disruption. *J Clin Invest* **123**, 5179-5189

91. He, C. H., Black, D. S., Nguyen, T. P., Wang, C., Srinivasan, C., and Clarke, C. F. (2015) Yeast Coq9 controls deamination of coenzyme Q intermediates that derive from *para*-aminobenzoic acid. *Biochim Biophys Acta* **1851**, 1227-1239

92. Padilla, S., Tran, U. C., Jimenez-Hidalgo, M., Lopez-Martin, J. M., Martin-Montalvo, A., Clarke, C. F., Navas, P., and Santos-Ocana, C. (2009) Hydroxylation of demethoxy-Q_6 constitutes a control point in yeast coenzyme Q_6 biosynthesis. *Cell Mol Life Sci* **66**, 173-186

93. He, C. H., Black, D. S., Allan, C. M., Meunier, B., Rahman, S., and Clarke, C. F. (2017) Human *COQ9* Rescues a *coq9* Yeast Mutant by Enhancing Coenzyme Q Biosynthesis from 4-Hydroxybenzoic Acid and Stabilizing the CoQ-Synthome. *Front Physiol* **8**, 463

94. Hayashi, K., Ogiyama, Y., Yokomi, K., Nakagawa, T., Kaino, T., and Kawamukai, M. (2014) Functional conservation of coenzyme Q biosynthetic genes among yeasts, plants, and humans. *PLoS One* **9**, e99038

95. Duncan, A. J., Bitner-Glindzicz, M., Meunier, B., Costello, H., Hargreaves, I. P., Lopez, L. C., Hirano, M., Quinzii, C. M., Sadowski, M. I., Hardy, J., Singleton, A., Clayton, P. T., and Rahman, S. (2009) A nonsense mutation in *COQ9* causes autosomal-recessive neonatal-onset primary coenzyme Q_{10} deficiency: a potentially treatable form of mitochondrial disease. *Am J Hum Genet* **84**, 558-566

96. Allan, C. M., Hill, S., Morvaridi, S., Saiki, R., Johnson, J. S., Liau, W. S., Hirano, K., Kawashima, T., Ji, Z., Loo, J. A., Shepherd, J. N., and Clarke, C. F. (2013) A conserved START domain coenzyme Q-binding polypeptide is required for efficient Q biosynthesis, respiratory electron transport, and antioxidant function in *Saccharomyces cerevisiae*. *Biochim Biophys Acta* **1831**, 776-791

97. Tsui, H. S., Pham, N. V. B., Amer, B. R., Bradley, M. C., Gosschalk, J. E., Gallagher-Jones, M., Ibarra, H., Clubb, R. T., Blaby-Haas, C. E., and Clarke, C. F. (2019) Human COQ10A and COQ10B are distinct lipid-binding START domain proteins required for coenzyme Q function. *J Lipid Res* **60**, 1293-1310

98. Cui, T. Z., and Kawamukai, M. (2009) Coq10, a mitochondrial coenzyme Q binding protein, is required for proper respiration in *Schizosaccharomyces pombe*. *FEBS J* **276**, 748-759

99. Busso, C., Bleicher, L., Ferreira-Junior, J. R., and Barros, M. H. (2010) Site-directed mutagenesis and structural modeling of Coq10p indicate the presence of a tunnel for coenzyme Q_6 binding. *FEBS Lett* **584**, 1609-1614

100. Marbois, B., Gin, P., Faull, K. F., Poon, W. W., Lee, P. T., Strahan, J., Shepherd, J. N., and Clarke, C. F. (2005) Coq3 and Coq4 define a polypeptide complex in yeast mitochondria for the biosynthesis of coenzyme Q. *J Biol Chem* **280**, 20231-20238

101. Hsieh, E. J., Gin, P., Gulmezian, M., Tran, U. C., Saiki, R., Marbois, B. N., and Clarke, C. F. (2007) *Saccharomyces cerevisiae* Coq9 polypeptide is a subunit of the mitochondrial coenzyme Q biosynthetic complex. *Arch Biochem Biophys* **463**, 19-26

102. Tran, U. C., Marbois, B., Gin, P., Gulmezian, M., Jonassen, T., and Clarke, C. F. (2006) Complementation of *Saccharomyces cerevisiae coq7* mutants by mitochondrial targeting of the *Escherichia coli* UbiF polypeptide: two functions of yeast Coq7 polypeptide in coenzyme Q biosynthesis. *J Biol Chem* **281**, 16401-16409

103. Subramanian, K., Jochem, A., Le Vasseur, M., Lewis, S., Paulson, B. R., Reddy, T. R., Russell, J. D., Coon, J. J., Pagliarini, D. J., and Nunnari, J. (2019) Coenzyme Q biosynthetic proteins assemble in a substrate-dependent manner into domains at ER-mitochondria contacts. *J Cell Biol* **218**, 1353-1369

104. Eisenberg-Bord, M., Tsui, H. S., Antunes, D., Fernandez-Del-Rio, L., Bradley, M. C., Dunn, C. D., Nguyen, T. P. T., Rapaport, D., Clarke, C. F., and Schuldiner, M. (2019) The Endoplasmic Reticulum-Mitochondria Encounter Structure Complex Coordinates Coenzyme Q Biosynthesis. *Contact (Thousand Oaks)* **2**, 2515256418825409

105. Murley, A., and Nunnari, J. (2016) The Emerging Network of Mitochondria-Organelle Contacts. *Mol Cell* **61**, 648-653

106. Marchler-Bauer, A., Zheng, C., Chitsaz, F., Derbyshire, M. K., Geer, L. Y., Geer, R. C., Gonzales, N. R., Gwadz, M., Hurwitz, D. I., Lanczycki, C. J., Lu, F., Lu, S., Marchler, G. H., Song, J. S., Thanki, N., Yamashita, R. A., Zhang, D., and Bryant, S. H. (2013) CDD: conserved domains and protein three-dimensional structure. *Nucleic Acids Res* **41**, D348-352

107. Rossmann, M. G., Moras, D., and Olsen, K. W. (1974) Chemical and biological evolution of nucleotide-binding protein. *Nature* **250**, 194-199

108. Kopec, J., Schnell, R., and Schneider, G. (2011) Structure of PA4019, a putative aromatic acid decarboxylase from *Pseudomonas aeruginosa*. *Acta Crystallogr Sect F Struct Biol Cryst Commun* **67**, 1184-1188

109. Marcotte, E. M., Pellegrini, M., Ng, H. L., Rice, D. W., Yeates, T. O., and Eisenberg, D. (1999) Detecting protein function and protein-protein interactions from genome sequences. *Science* **285**, 751-753

110. Pagliarini, D. J., Calvo, S. E., Chang, B., Sheth, S. A., Vafai, S. B., Ong, S. E., Walford, G. A., Sugiana, C., Boneh, A., Chen, W. K., Hill, D. E., Vidal, M., Evans, J. G., Thorburn, D. R., Carr, S. A., and Mootha, V. K. (2008) A mitochondrial protein compendium elucidates complex I disease biology. *Cell* **134**, 112-123

111. Hirst, J. (2011) Why does mitochondrial complex I have so many subunits? *Biochem J* **437**, e1-3

112. Stroud, D. A., Formosa, L. E., Wijeyeratne, X. W., Nguyen, T. N., and Ryan, M. T. (2013) Gene knockout using transcription activator-like effector nucleases (TALENs) reveals that human NDUFA9 protein is essential for stabilizing the junction between membrane and matrix arms of complex I. *J Biol Chem* **288**, 1685-1690

113. Ugalde, C., Vogel, R., Huijbens, R., Van Den Heuvel, B., Smeitink, J., and Nijtmans, L. (2004) Human mitochondrial complex I assembles through the combination of evolutionary conserved modules: a framework to interpret complex I deficiencies. *Hum Mol Genet* **13**, 2461-2472

114. Baertling, F., Sanchez-Caballero, L., van den Brand, M. A. M., Fung, C. W., Chan, S. H., Wong, V. C., Hellebrekers, D. M. E., de Coo, I. F. M., Smeitink, J. A. M., Rodenburg, R. J. T., and Nijtmans, L. G. J. (2018) *NDUFA9* point mutations cause a variable mitochondrial complex I assembly defect. *Clin Genet* **93**, 111-118

115. Leshinsky-Silver, E., Lev, D., Tzofi-Berman, Z., Cohen, S., Saada, A., Yanoov-Sharav, M., Gilad, E., and Lerman-Sagie, T. (2005) Fulminant neurological deterioration in a neonate with Leigh syndrome due to a maternally transmitted missense mutation in the mitochondrial *ND3* gene. *Biochem Biophys Res Commun* **334**, 582-587

116. van den Bosch, B. J., Gerards, M., Sluiter, W., Stegmann, A. P., Jongen, E. L., Hellebrekers, D. M., Oegema, R., Lambrichs, E. H., Prokisch, H., Danhauser, K., Schoonderwoerd, K., de Coo, I. F., and Smeets, H. J. (2012) Defective NDUFA9 as a novel cause of neonatally fatal complex I disease. *J Med Genet* **49**, 10-15

117. Pierrel, F., Hamelin, O., Douki, T., Kieffer-Jaquinod, S., Muhlenhoff, U., Ozeir, M., Lill, R., and Fontecave, M. (2010) Involvement of mitochondrial ferredoxin and *para*-aminobenzoic acid in yeast coenzyme Q biosynthesis. *Chem Biol* **17**, 449-459

CHAPTER 2

COQ11 deletion mitigates respiratory deficiency caused by mutations in the gene encoding the coenzyme Q chaperone protein Coq10

JBC ARTICLE

COQ11 deletion mitigates respiratory deficiency caused by mutations in the gene encoding the coenzyme Q chaperone protein Coq10

Received for publication, December 20, 2019, and in revised form, March 17, 2020 Published, Papers in Press, March 23, 2020, DOI 10.1074/jbc.RA119.012420

Michelle C. Bradley[‡], Krista Yang[‡], Lucía Fernández-del-Río[‡], Jennifer Ngo[‡§], Anita Ayer[¶‖], Hui S. Tsui[‡], Noelle Alexa Novales[‡], Roland Stocker[¶‖], Orian S. Shirihai[§], Mario H. Barros[**], and Catherine F. Clarke[‡1]

From the [‡]Department of Chemistry and Biochemistry, Molecular Biology Institute, UCLA, Los Angeles, California 90095-1569, the [§]Department of Molecular and Medical Pharmacology and Medicine, David Geffen School of Medicine, UCLA, Los Angeles, California 90095, the [¶]Vascular Biology Division, Victor Chang Cardiac Research Institute, Sydney, New South Wales 2010, Australia, the [‖]St. Vincent's Clinical School, University of New South Wales Medicine, Sydney, New South Wales 2050, Australia, and the [**]Departamento Microbiologia, Universidade de São Paulo, São Paulo 05508-900, Brazil

Edited by Dennis R. Voelker

Coenzyme Q (Q_n) is a vital lipid component of the electron transport chain that functions in cellular energy metabolism and as a membrane antioxidant. In the yeast *Saccharomyces cerevisiae*, *coq1–coq9* deletion mutants are respiratory-incompetent, sensitive to lipid peroxidation stress, and unable to synthesize Q_6. The yeast *coq10* deletion mutant is also respiratory-deficient and sensitive to lipid peroxidation, yet it continues to produce Q_6 at an impaired rate. Thus, Coq10 is required for the function of Q_6 in respiration and as an antioxidant and is believed to chaperone Q_6 from its site of synthesis to the respiratory complexes. In several fungi, Coq10 is encoded as a fusion polypeptide with Coq11, a recently identified protein of unknown function required for efficient Q_6 biosynthesis. Because "fused" proteins are often involved in similar biochemical pathways, here we examined the putative functional relationship between Coq10 and Coq11 in yeast. We used plate growth and Seahorse assays and LC-MS/MS analysis to show that *COQ11* deletion rescues respiratory deficiency, sensitivity to lipid peroxidation, and decreased Q_6 biosynthesis of the *coq10*Δ mutant. Additionally, immunoblotting indicated that yeast *coq11*Δ mutants accumulate increased amounts of certain Coq polypeptides and display a stabilized CoQ synthome. These effects suggest that Coq11 modulates Q_6 biosynthesis and that its absence increases mitochondrial Q_6 content in the *coq10*Δ*coq11*Δ double mutant. This augmented mitochondrial Q_6 content counteracts the respiratory deficiency and lipid peroxidation sensitivity phenotypes of the *coq10*Δ mutant. This study further clarifies the intricate connection between Q_6 biosynthesis, trafficking, and function in mitochondrial metabolism.

Coenzyme Q (ubiquinone or Q)[2] is a benzoquinone lipid that functions as an essential electron carrier within the electron transport chain (1). Because of its redox activities, Q is a versatile electron acceptor in biological pathways such as cellular respiration, oxidation of proline and sulfide, fatty acid β-oxidation, and pyrimidine biosynthesis (1–3). The reduced hydroquinone form of Q (ubiquinol or QH_2) also serves as an important chain-breaking antioxidant shown to alleviate lipid peroxidative damage in cellular membranes (4).

For proper functional localization, Q relies on its polyisoprenoid tail to remain anchored at the mid-plane of phospholipid bilayers. The number of isoprene units (*n*) that comprise the polyisoprenoid tail of Q_n depends on a species-specific polyprenyl diphosphate synthase (5), with Q_{10} representing the major isoform in humans (6). Patients unable to produce adequate levels of Q_{10} display a wide variety of health issues that stem from mitochondrial dysfunction across tissues (7). Attempts to ameliorate the consequences of primary Q_{10} deficiency by early Q_{10} supplementation have been partially successful in some cases (8); however, many patients fail to demonstrate full recovery, which is related to inefficient uptake of orally-supplied Q_{10}. Because of the striking homology between human *COQ* genes and those of *Saccharomyces cerevisiae* (7, 9), studies of Q_6 biosynthesis in *S. cerevisiae* may provide insight

This work was supported by National Science Foundation Grant MCB-1330803 (to C. F. C.), National Institutes of Health Grant T32 GM 007185 (to H. S. T. and M. C. B.) Ruth L. Kirschstein National Service (to M. C. B. and H. S. T.), the Whitcome Individual Predoctoral Fellowship (to M. C. B.), UCLA Summer Undergraduate Research Fellowship, Department of Chemistry and Biochemistry (to K. Y.), Fundação de Amparo a Pesquisa de São Paulo–FAPESP 2013/09482-8 and 2013/07937-8 (to M. H. B.), Gates Millennium Scholars Fellowship (to J. N.), and the Eugene V. Cota Robles Fellowship (to J. N.). The authors declare that they have no conflicts of interest with the contents of this article. The content is solely the responsibility of the authors and does not necessarily represent the official views of the National Institutes of Health.
This article contains Figs. S1–S3, Tables S1 and S2, and supporting Refs. 1–8.
[1] To whom correspondence should be addressed. Tel.: 310-825-0771; Fax: 310-206-5213; E-mail: cathy@chem.ucla.edu.

[2] The abbreviations used are: Q, ubiquinone; DMQ, demethoxy-Q; HHB, 3-hexaprenyl-4-hydroxybenzoic acid; Q_n, coenzyme Q_n (where *n* designates the number of isoprene units in the polyisoprenyl tail); QH_2, reduced coenzyme Q or ubiquinol; ORF, open reading frame; ER, endoplasmic reticulum; MIOREX complex, mitochondrial organization of gene expression complex; IMS, intermembrane space; OCR, oxygen consumption rate; FCCP, carbonyl cyanide *p*-trifluoromethoxyphenylhydrazone; PUFA, polyunsaturated fatty acid; qPCR, quantitative real-time PCR; ERMES, ER-mitochondrial encounter structure; START, steroidogenic acute regulatory protein–related lipid transfer; BisTris, 2-[bis(2-hydroxyethyl)amino]-2-(hydroxymethyl)propane-1,3-diol; SDR, short-chain dehydrogenase/reductase; 2D-BN/SDS-PAGE, two-dimensional blue native/SDS-PAGE; DOD, drop-out dextrose; SD, synthetic dextrose; lc*COQ11*, low-copy *COQ11*; RET, reverse electron transport; P, pellet; S, supernatant.

into human Q_{10} biosynthesis, leading to the discovery of potential therapeutic targets.

In *S. cerevisiae*, at least 14 nuclear-encoded mitochondrial proteins (Coq1–Coq11, Yah1, Arh1, and Hfd1) drive Q_6 biosynthesis (7, 9). Many Coq polypeptides (Coq3–Coq9, and Coq11) are localized to the matrix side of the mitochondrial inner membrane, where they organize into a high-molecular-weight multisubunit complex known as the "CoQ synthome" (7, 9). Several lines of evidence suggest that correct assembly of the CoQ synthome is necessary for efficient Q_6 biosynthesis (9–12). In fact, deletion of certain *COQ* genes results in decreased levels of other Coq polypeptides and contributes to a destabilized CoQ synthome in these mutants (12, 13). Recently, a protein of unknown function encoded by the ORF *YLR290C* was identified to associate with the CoQ synthome, via proteomic analysis of tandem affinity-purified tagged Coq proteins (14). YLR290C copurified with Coq5, Coq7, and Coq9, in addition to Q_6 and late-stage Q_6-intermediates (14). Furthermore, the *ylr290c*Δ mutant exhibited impaired *de novo* Q_6 biosynthesis, despite preserving growth on a nonfermentable carbon source (14). Given its effects on Q_6 biosynthesis and involvement with the CoQ synthome, YLR290C was renamed Coq11 (14).

In several fungi, Coq11 and Coq10 have evolved as fusion proteins (14), suggesting that Coq11 may have a functional relationship with Coq10 (15). High-throughput genetic analyses found *COQ11* to correlate with both *COQ2* and *COQ10* (16). Whereas the *coq* mutants generally lack Q_6, the *coq10*Δ mutant is different because it produces near WT amounts of Q_6 in stationary phase and only has decreased *de novo* Q_6 biosynthesis in log phase (17, 18). Although Q_6 biosynthesis is only minimally decreased in the absence of *COQ10*, the *coq10*Δ mutant has decreased NADH and succinate oxidase activity and displayed sickly growth on respiratory medium (18). The *coq10*Δ mutant is sensitive to lipid peroxidation initiated by exogenously supplemented polyunsaturated fatty acids (PUFAs), indicating that the Coq10 polypeptide is also required for antioxidant protection by Q_6 (17, 19).

The NMR structure of a Coq10 ortholog in *Caulobacter crescentus* was shown to possess a steroidogenic acute regulatory protein–related lipid transfer (START) domain (20) that can directly bind Q and late-stage Q-intermediates (17). Purified Coq10 from either *S. cerevisiae* or *Schizosaccharomyces pombe* eluted with the respective species' Q isoform (18, 21). This observation has prompted speculation that Coq10 acts as a Q_6 chaperone protein required for delivery of Q_6 from its synthesis site to sites where Q_6 functions as an antioxidant and to the respiratory complexes, thereby bridging efficient *de novo* Q_6 biosynthesis with respiration (17). Recent studies have shown a spatial compartmentalization of the mitochondrial inner membrane with the identification of different sites, such as the inner boundary membrane, the cristae membrane, and the ER-mitochondrial contact sites (22–25). Thus, for optimal respiratory competence, newly-synthesized Q_6 must move from its site of synthesis (*i.e.* the ER-mitochondrial contact sites (23, 24)) to the cristae membrane where the respiratory complexes are concentrated (22). The presence of Coq10–Coq11 fusions in fungal species indicates that Coq11 may have a functional association with the Coq10 chaperone to facilitate or regulate Q_6 transport for respiration in yeast.

In this work, the functional relationship between Coq10 and Coq11 was investigated using a series of single- and double-knockout mutants. Deletion of *COQ11* alleviated the *coq10*Δ respiratory defect, increased Coq polypeptides and CoQ synthome stability, and partially rescued Q_6 production. Based on this evidence, we propose a novel function for Coq11 as a negative modulator of Q_6 biosynthesis in the mitochondria.

Results

Coq10 and Coq11 reside in similar compartments within the mitochondria

Previous phylogenetic analyses of numerous fungi revealed that Coq11-like proteins are fused to Coq10 (14). Protein fusions often indicate a functional relationship between corresponding homologs in other organisms, such as direct protein–protein interaction or operation within the same biological pathway (15). Although Coq10 and Coq11 are not physically fused in yeast (Fig. 1*A*), we sought to investigate whether there is a functional link between the two proteins. Because protein localization is often associated with function, we first performed mitochondrial fractionation to localize both Coq10 and Coq11. Coq10 has been localized previously (18), but fractionation was re-performed here in the context of Coq11.

S. cerevisiae mitochondria were fractionated as described under "Experimental procedures." Purified mitochondria were incubated in hypotonic buffer to disrupt the outer membrane and release soluble components of the intermembrane space (IMS). The inner membrane was kept intact following hypotonic buffer treatment, protecting inner membrane and matrix proteins. Analysis of the fractions via immunoblot suggested that both Coq10 and Coq11 remained associated with the mitoplast fraction as opposed to colocalizing with the IMS marker cytochrome b_2. Mitoplasts were further fractionated after sonication to separate soluble matrix components (supernatant, S) from membrane components (pellet, P). The soluble matrix marker Hsp60 was partially released into the supernatant by sonication as demonstrated in earlier work (26). Although Coq11 remained associated with the membrane fraction, Coq10 was partially dissociated in a similar manner to Hsp60 (Fig. 1*B*). Previous Coq10 colocalization following sonication demonstrated that Coq10 was solely associated with the membrane fraction (18). The detection of Coq10 in the supernatant shown in Fig. 1*B* may be due to increased sensitivity of the polyclonal antisera used in this study.

Alternatively, mitoplasts were subjected to alkaline carbonate extraction to separate peripheral membrane components (supernatant, S) from integral membrane and matrix components (pellet, P) (27). Coq10 and Coq11 were released into the supernatant following alkaline treatment (Fig. 1*B*), matching the peripheral inner membrane marker Atp2 (28). There was no colocalization with the pellet fraction, marked by the integral membrane protein Cyt_1 (29). These results indicate that Coq10 and Coq11 are both peripheral inner membrane proteins, and Coq10 has additional localization to the matrix. The localization of Coq10 to the inner membrane is consistent with

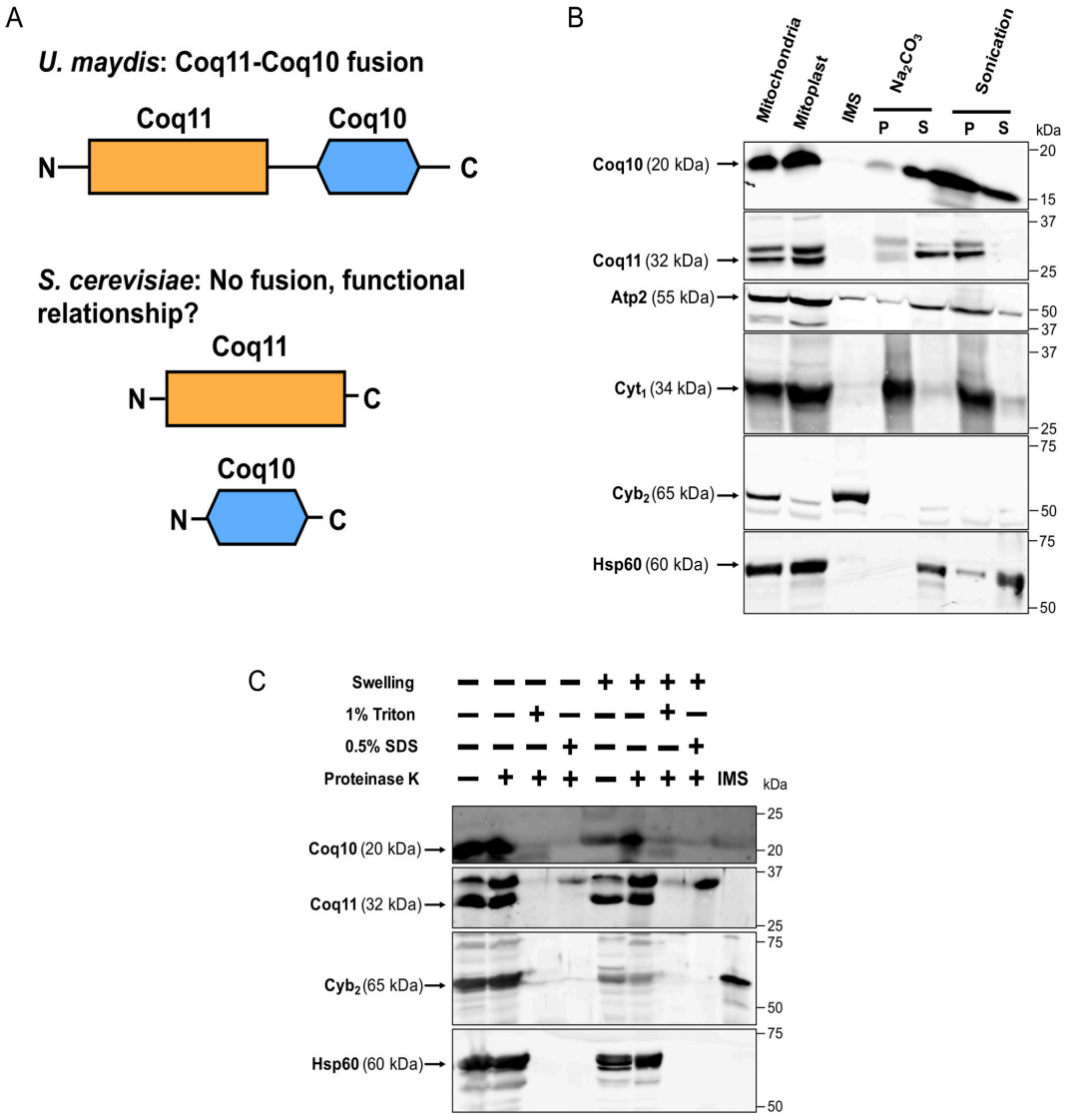

Figure 1. Coq11 and Coq10 are peripherally associated with the mitochondrial inner membrane facing the matrix, and Coq10 is additionally found in the mitochondrial matrix. *A*, Coq10 and Coq11 are fused in multiple fungi, suggesting an evolutionarily functional relationship between these proteins, although they are not found fused in *S. cerevisiae*. *B*, *S. cerevisiae* mitochondria purified from yeast strains cultured on YPGal medium were subjected to hypotonic swelling and centrifugation to separate the IMS proteins from mitoplasts. The mitoplasts were alkaline-treated (Na_2CO_3; pH 11.5) or sonicated and then separated by centrifugation (100,000 × *g* for 1 h) into supernatant (S) or pellet (P) fractions. *C*, intact mitochondria or mitoplasts were treated with 100 μg/ml proteinase K for 30 min on ice, with or without detergent. Mitochondrial polypeptide markers are as follows: *Atp2*, peripheral inner membrane protein; *Cyb_2*, intermembrane space protein; *Cyt_1*, integral inner membrane protein; and *Hsp60*, soluble matrix protein. Results are representative of two experiments.

its putative role as a START domain protein possessing a hydrophobic cavity to bind and chaperone Q_6 from its site of synthesis to complex III for respiration (17, 18). We hypothesize that dual mitochondrial matrix localization occurs when Coq10 is tightly bound to protein partners to decrease its hydrophobicity.

For better insight into the membrane association of Coq10 and Coq11, intact mitochondria or mitoplasts were treated with proteinase K in the absence or presence of two individual detergents (1% Triton X-100 or 0.5% SDS). Coq10 and Coq11 were both protected from protease treatment in purified mitochondria and mitoplasts, as was the matrix marker Hsp60 (Fig. 1*C*). When protease was used in the presence of either detergent in mitochondria or mitoplasts, all proteins became sensitive to the protease and were degraded. Expanding on the subfractionation results, these data indicate that Coq10 and Coq11 polypeptides are peripherally associated with the inner membrane facing the matrix side in yeast mitochondria, and Coq10 is also found in the mitochondrial matrix itself. The mitochondrial peripheral membrane association of these two proteins is also in agreement with their submitochondrial localization previously identified in a study of the yeast mitochondrial proteome (30).

Table 1
Genotype and source of yeast strains

Strain	Genotype	Source
W303-1B	MAT α *ade2-1 his3-1,15 leu2-,112trp1-1 ura3-1*	R. Rothstein[a]
BY4742	MAT α *his3Δ0 leu2Δ0 met15Δ0 ura3Δ0*	53
JM6	*MAT a his-4* ρ^0	68
JM8	*MAT* α *ade-1* ρ^0	68
BY4742 *coq1*Δ	MAT α *his3Δ0 leu2Δ0 met15Δ0 ura3Δ0 coq1::KanMX4*	69
BY4741 *coq2*Δ	MAT a *his3Δ0 leu2Δ0 met15Δ0 ura3Δ0 coq2::KanMX4*	69
BY4742 *coq3*Δ	MAT α *his3Δ0 leu2Δ0 met15Δ0 ura3Δ0 coq3::KanMX4*	69
BY4742 *coq4*Δ	MAT α *his3Δ0 leu2Δ0 met15Δ0 ura3Δ0 coq4::KanMX4*	69
BY4742 *coq5*Δ	MAT α *his3Δ0 leu2Δ0 met15Δ0 ura3Δ0 coq5:: KanMX4*	69
BY4741 *coq6*Δ	MAT a *his3Δ0 leu2Δ0 met15Δ0 ura3Δ0 coq6::KanMX4*	Dharmacon, Inc.
BY4742 *coq7*Δ	MAT α *his3Δ0 leu2Δ0 met15Δ0 ura3Δ0 coq7::KanMX4*	69
BY4742 *coq8*Δ	MAT α *his3Δ0 leu2Δ0 met15Δ0 ura3Δ0 coq8::KanMX4*	69
BY4742 *coq9*Δ	MAT α*his3Δ0 leu2Δ0 met15Δ0 ura3Δ0 coq9::KanMX4*	69
BY4742 *coq10*Δ	MAT α *his3Δ0 leu2Δ0 met15Δ0 ura3Δ0 coq10::KanMX4*	69
BY4742 *coq11*Δ	MAT α *his3Δ0 leu2Δ0 met15Δ0 ura3Δ0 coq11::LEU2*	This work
BY4742 *coq10*Δ*coq11*Δ	MAT α *his3Δ0 leu2Δ0 met15Δ0 ura3Δ0 coq10::HIS3 coq11::LEU2*	This work
W303 *coq10*Δ	MAT α *ade2-1 his3-1,15 leu2-3,112trp1-1 ura3-1 coq10::HIS3*	18
W303 *coq10*Δ	MAT a *ade2-1 his3-1,15 leu2-3,112trp1-1 ura3-1 coq10::HIS3*	18
W303 *coq10*rev	MAT α *ade2-1 his3-1,15 leu2-3,112trp1-1 ura3-1 coq10::HIS3 sup*	This work
MB-10	Diploid produced from W303 a *coq10*Δ x W303 α *coq10*Δrev	This work
W303 *coq11*Δ	MAT α *ade2-1 his3-1,15 leu2-3,112trp1-1 ura3-1 coq11::LEU2*	This work
W303 *coq10*Δ*coq11*Δ	MAT α *ade2-1 his3-1,15 leu2-3,112trp1-1 ura3-1 coq10::HIS3 coq11::LEU2*	This work
BY4741 *cor1*Δ	MAT a *his3Δ0 leu2Δ0 met15Δ0 ura3Δ0 cor1::KanMX4*	69

[a] Gift from Dr. Rodney Rothstein Department of Human Genetics, Columbia University.

*coq10*Δ respiratory defect is alleviated by deletion of *COQ11*

Based on similar mitochondria localization and genetic evolutionary evidence, a putative functional relationship between Coq10 and Coq11 was further probed using a series of *coq10* and *coq11* single- and double-knockout mutants. Strain descriptions are listed in Table 1. The Coq10 polypeptide is required for respiration in yeast, and mutants lacking *coq10* have poor growth on nonfermentable carbon sources, including YPGlycerol, hereafter referred to as "YPG" (18). Unlike deletion of *COQ10*, *coq11*Δ mutants are respiratory-capable and have comparable growth to WT on nonfermentable carbon sources (14). When *COQ11* was deleted in a *coq10*Δ mutant in two different yeast genetic backgrounds, the sickly growth of *coq10*Δ on nonfermentable YPG was rescued (Fig. 2*A*).

Quantitative respiratory capacity of each mutant was evaluated with an XF96 Extracellular Flux Analyzer (Fig. 2, *B* and *C*). Representative and normalized traces of oxygen consumption rates (OCR) of four independent experiments performed in nonrepressive medium (YPGal) are shown in Fig. 2*B*. Basal rates of OCR were measured prior to the addition of any small molecule inhibitors. Consistent with its slow growth on nonfermentable medium, the *coq10*Δ mutant had a low rate of basal oxygen consumption compared with WT ($p = 0.052$) (Fig. 2*C*). Basal OCR was rescued in the *coq10*Δ*coq11*Δ double mutant (Fig. 2*C*). Following the addition of two sequential injections of FCCP, a mitochondrial oxidative phosphorylation uncoupler, maximal respiration was also quantified. The maximal respiration of *coq10*Δ*coq11*Δ was rescued to that of WT (Fig. 2*C*). These results show that the deletion of *COQ11* in a *coq10*Δ mutant confers a beneficial effect, such that both growth on respiratory medium and OCR are rescued to WT.

Deletion of *COQ11* rescues PUFA sensitivity of the *coq10*Δ mutant

PUFA autoxidation is initiated by the radical-mediated abstraction of vulnerable hydrogen atoms at bis-allylic positions (31). The ensuing carbon-centered radical adds to molecular oxygen to form a lipid peroxyl radical that propagates lipid peroxidation, with the resulting lipid hydroperoxides ultimately driving cellular toxicity (32). The *coq10*Δ mutant is sensitive to treatment with exogenous PUFAs (Fig. 2*D*) (17, 19), likely because the Q_6 chaperone function of Coq10 is required for the antioxidant function of Q_6. Attenuated respiration in *coq10*Δ is rescued in the *coq10*Δ*coq11*Δ double knockout (Fig. 2, *A–C*), presumably through regained function of Q_6 in the electron transport chain. To test whether the antioxidant capability of Q_6 is also restored in the *coq10*Δ*coq11*Δ mutant, yeast strains were evaluated for sensitivity to added PUFAs (Fig. 2*D*). As anticipated, all strains were resistant to treatment with the monounsaturated oleic acid (Fig. 2*D*). Q_6-less *coq9*Δ was sensitive to α-linolenic acid due to the lack of Q_6 antioxidant protection (Fig. 2*D*). Conversely, the Q_6-replete yet respiratory-deficient *cor1*Δ remained resistant to α-linolenic acid (Fig. 2*D*). Deletion of *COQ11* rescued the α-linolenic acid sensitivity of the *coq10*Δ mutant, suggesting that the double knockout has restored Q_6 antioxidant protection (Fig. 2*D*) despite the absence of Coq10 as a Q_6 chaperone.

Independent *coq10* revertant with rescued growth on respiratory medium harbors a mutation within *COQ11*

Although the *coq10*Δ mutant is unable to grow robustly on nonfermentable medium, an earlier study identified a spontaneous *coq10* revertant (*coq10*rev) that arose when *coq10*Δ yeast was cultured for several weeks on nonfermentable medium containing ethanol and glycerol as carbon sources (18). Characterization of this revertant revealed a suppressor mutation within the *COQ11* ORF, resulting in a truncated Coq11 protein that is predicted to be nonfunctional (Fig. 3*A*). This mutation was further assessed for dominance to determine whether it was sufficient to explain the respiratory competence of *coq10*rev. A haploid *coq10*Δ mutant crossed with haploid *coq10*rev produced diploid MB-10 (Table 1), which was capable of growth on respiratory medium (Fig. 3*B*). Illustrated growth

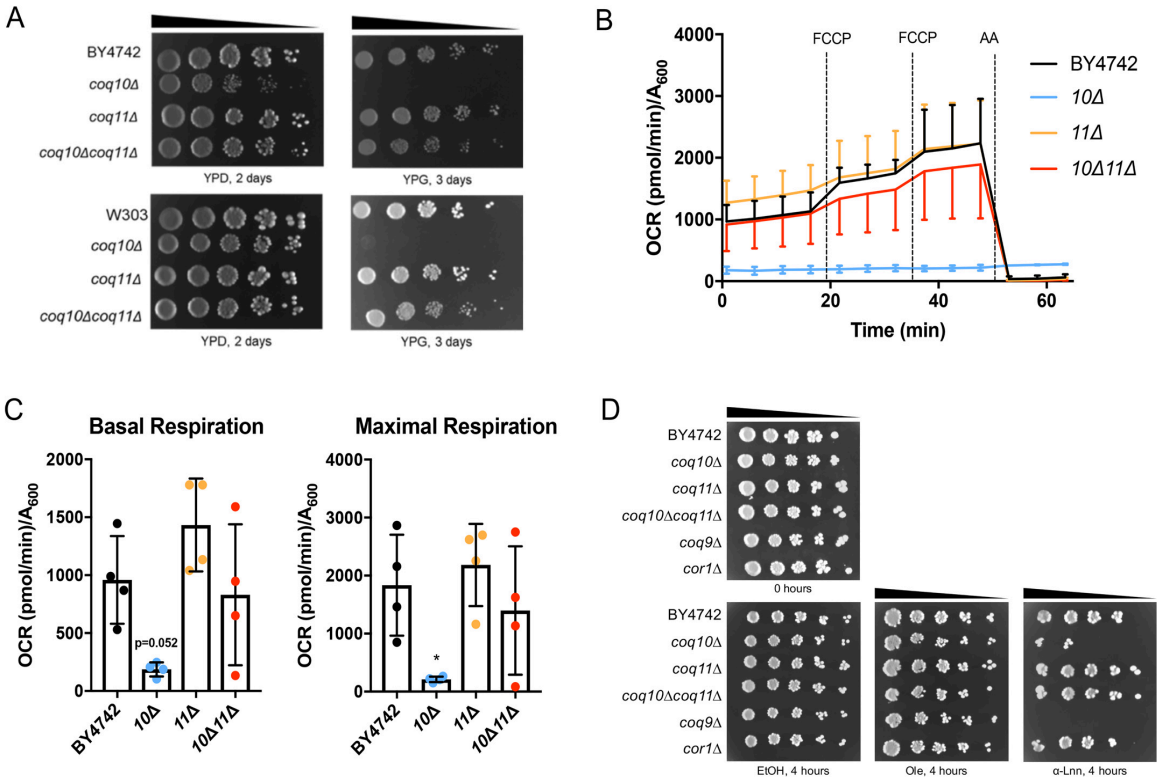

Figure 2. *COQ11* deletion rescues the lack of growth on YPG, low-oxygen consumption rates, and lost Q_6 antioxidant protection in the *coq10Δ* mutant. *A*, strains were grown overnight in 5 ml of YPD, diluted to an A_{600} = 0.2 with sterile PBS, and 2 μl of 5-fold serial dilutions were spotted onto fermentable (YPDextrose, *YPD*) or respiratory (YPGlycerol, *YPG*) medium, corresponding to a final A_{600} = 0.2, 0.04, 0.008, 0.0016, and 0.00032. Plates were incubated at 30 °C, and growth was captured after 2 or 3 days. *B* and *C*, quadruplicates of 25-ml cultures of WT, *coq10Δ*, *coq11Δ*, and *coq10Δcoq11Δ* yeast were grown in YPGal until they reached A_{600} ~4. Yeast were diluted to an A_{600} = 0.1 in fresh YPGal and collected by centrifugation on poly-D-lysine-coated Seahorse XF96 microplates to assess oxygen consumption. *B*, representative traces of OCR of yeast strains with the XF96 extracellular flux analyzer. FCCP and antimycin A (*AA*) were sequentially added to evaluate mitochondrial respiratory states. Measurements were taken approximately every 4 min, as represented by *points* and their respective *error bars*. Four independent experiments were performed (Fig. S1), and each group of average traces represents 8–10 technical replicates. *C*, quantification of basal and maximal (maximal electron transport activity induced by the uncoupler FCCP) OCR as obtained from four independent experiments (Fig. S1). The data show the mean ± S.D., and the statistical significance as compared with WT is represented by *, $p < 0.05$. *D*, deletion of *COQ11* in the *coq10Δ* rescues PUFA sensitivity. Results are representative of three experiments.

patterns suggest that the *coq11* truncated allele present in *coq10*rev is a dominant-negative mutation. Because the dominant mutation in *coq10*rev restores growth on respiratory medium via a functionally suppressive Coq11 truncation mutation, this mutant effectively validates the *coq10Δcoq11Δ* phenotype in an independent system.

Deletion of COQ11 fails to fully restore coq10Δ Q_6 biosynthesis in whole cells

When a *coq* mutant displays anemic growth on respiratory medium, it is often indicative of inefficient Q_6 biosynthesis (7, 9); yeast lacking *COQ10* exhibit both poor growth on respiratory medium and decreased Q_6 biosynthesis in log phase whole cells (17, 19). Although the *coq11Δ* mutant retains the ability to grow on nonfermentable medium, it is also characterized by impaired Q_6 biosynthesis (14). Only a small amount of Q_6 is required for growth on respiratory medium, ~0.2–3% of the total Q_6 found in WT (9, 33, 34). Because the *coq10Δcoq11Δ* double mutant has rescued respiration, we wanted to assess whether recovered growth was accompanied by increased Q_6 biosynthesis. Whole-cell *de novo*–synthesized $[^{13}C_6]Q_6$ and $[^{12}C]Q_6$ were measured in yeast by feeding the quinone ring-labeled precursor, $[^{13}C_6]$4HB, or EtOH vehicle control (Fig. 4). These analyses were performed in the fermentable, nonrepressive YPGal medium (35) to match the conditions of experiments involving purified mitochondria.

Consistent with previous results (14, 17), *coq10Δ* and *coq11Δ* had significantly decreased *de novo*-synthesized $[^{13}C_6]Q_6$ and $[^{12}C]Q_6$ compared with WT (Fig. 4*A*). The *coq10Δ* mutant had a lower total Q_6 content ($[^{13}C_6]Q_6$ + $[^{12}C]Q_6$) than WT and also a lower total Q_6 than *coq11Δ* (Fig. 4*B*). Deletion of *COQ11* in *coq10Δ* yeast led to a slight increase in *de novo*-synthesized $[^{13}C_6]Q_6$ and unchanged $[^{12}C]Q_6$ compared with *coq10Δ* (Fig. 4*A*). Therefore, the *coq10Δcoq11Δ* double mutant presented total Q_6 contents that were significantly lower than either WT or *coq11Δ* (Fig. 4*B*). Given the robust growth of the *coq10Δcoq11Δ* double mutant on YPG, restored respiration, and resistance to PUFA treatment, the low Q_6 concentrations observed are surprising.

Next, we quantified the concentrations of key Q_6-intermediates in the same whole-cell yeast pellets. As shown previously

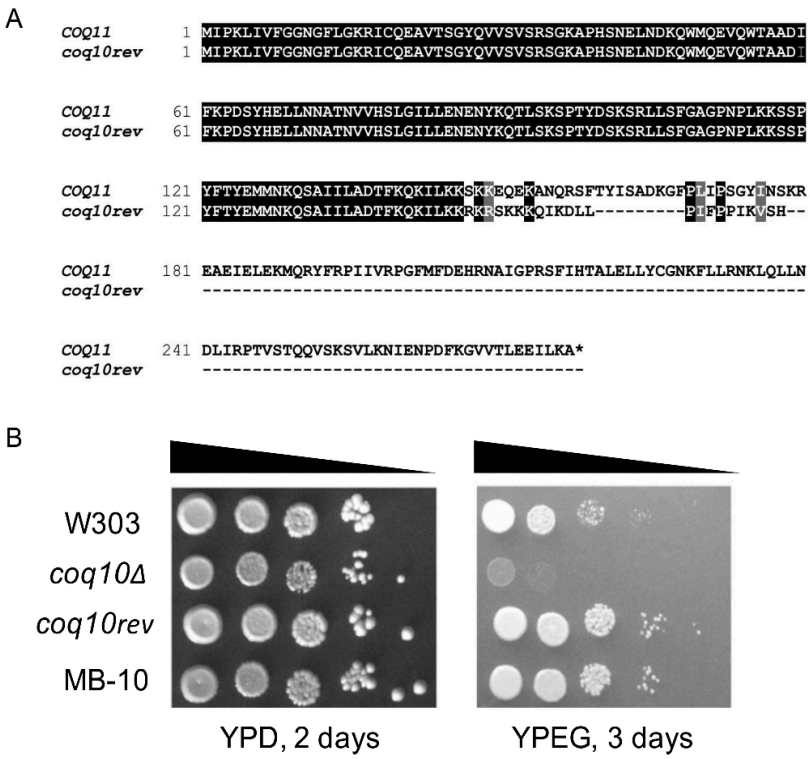

Figure 3. Spontaneous *coq10* revertant with rescued respiratory capacity was identified to possess a base-pair deletion in *COQ11*, encoding a truncated Coq11 protein. *A*, alignment of the amino acid sequence of WT *COQ11* ORF with the *coq11* allele (*coq10rev*) present in the *coq10* revertant. *B*, growth properties of WT were compared with *coq10* mutants and diploid MB-10 (defined in Table 1). Strains were grown overnight in 8 ml of YPDextrose (*YPD*), diluted to an A_{600} = 0.2 with sterile PBS, and 2 μl of 5-fold serial dilutions were spotted onto fermentable YPD or respiratory (YPEGlycerol (*YPEG*)) medium, corresponding to a final A_{600} = 0.2, 0.04, 0.008, 0.0016, and 0.00032. Plates were incubated at 30 °C, and growth was captured after 2 or 3 days. Results are representative of three experiments.

(17, 19), the *coq10*Δ mutant contained lower amounts of the late-stage intermediate [$^{13}C_6$]DMQ$_6$ and [^{12}C]DMQ$_6$ (Fig. 4*C*) than WT, and it accumulated the early-stage intermediate [$^{13}C_6$]HHB and [^{12}C]HHB (Fig. 4*D*). In contrast to *coq10*Δ, the *coq11*Δ mutant mirrored WT production of both *de novo*-synthesized and unlabeled early- and late-stage intermediates (Fig. 4, *C* and *D*), as shown previously (14). Q$_6$-intermediate trends in *coq10*Δ*coq11*Δ matched those of the *coq10*Δ mutant rather than *coq11*Δ (Fig. 4, *C* and *D*). The low Q$_6$ content and accumulation of early-stage Q$_6$-intermediates in the *coq10*Δ*coq11*Δ double knockout suggest the absence of *COQ10* still produces a notable effect on Q$_6$ biosynthesis, although respiratory capacity is rescued.

*coq10*Δ*coq11*Δ *double mutant has increased mitochondrial Q$_6$ compared with the coq10*Δ *single mutant*

Although Q$_6$ biosynthesis solely occurs within mitochondria, it is found in all cellular membranes (9). Therefore, Q$_6$ was quantified in both whole cells and purified mitochondria from mutant and WT cells cultured under the same conditions (36). Whole-cell Q$_6$ determined under mitochondrial purification conditions matched those determined in Figs. 4 and 5*A*. The *coq10*Δ*coq11*Δ double mutant made slightly more Q$_6$ than the *coq10*Δ single mutant, but overall less Q$_6$ compared with the *coq11*Δ single mutant. All mutants had lower whole-cell Q$_6$ amounts than WT (Fig. 5*A*).

Similarly, mitochondrial Q$_6$ content per microgram of mitochondrial protein was lower in *coq11*Δ than WT (Fig. 5*B*). However, deletion of *COQ11* in the *coq10*Δ mutant increased the mitochondrial Q$_6$ 5-fold (Fig. 5*B*). Despite these profound differences in mitochondrial Q$_6$ content, mitochondrial mass was consistent between strains as determined by three distinct assays (Fig. 5, *C–E*). Increased mitochondrial Q$_6$ in the *coq10*Δ*coq11*Δ double mutant compared with *coq10*Δ indicates that the absence of *COQ11* in part rescues defective Q$_6$ synthesis in the *coq10*Δ mutant.

*Low Coq protein content and destabilized CoQ synthome of the coq10*Δ *mutant are restored in the coq10*Δ*coq11*Δ *double mutant*

Proper formation of the CoQ synthome from component Coq polypeptides is required for efficient Q$_6$ biosynthesis in yeast (9, 12, 13). Deletion of *COQ10* causes a decrease in several other Coq polypeptides, including Coq3–Coq7, Coq9, as well as overall CoQ synthome destabilization (12, 13, 19). These results were confirmed when purified mitochondria from *coq10*Δ yeast were analyzed for each Coq polypeptide (Fig. 6*A*). The *coq10*Δ mutant had significantly decreased amounts of Coq3,

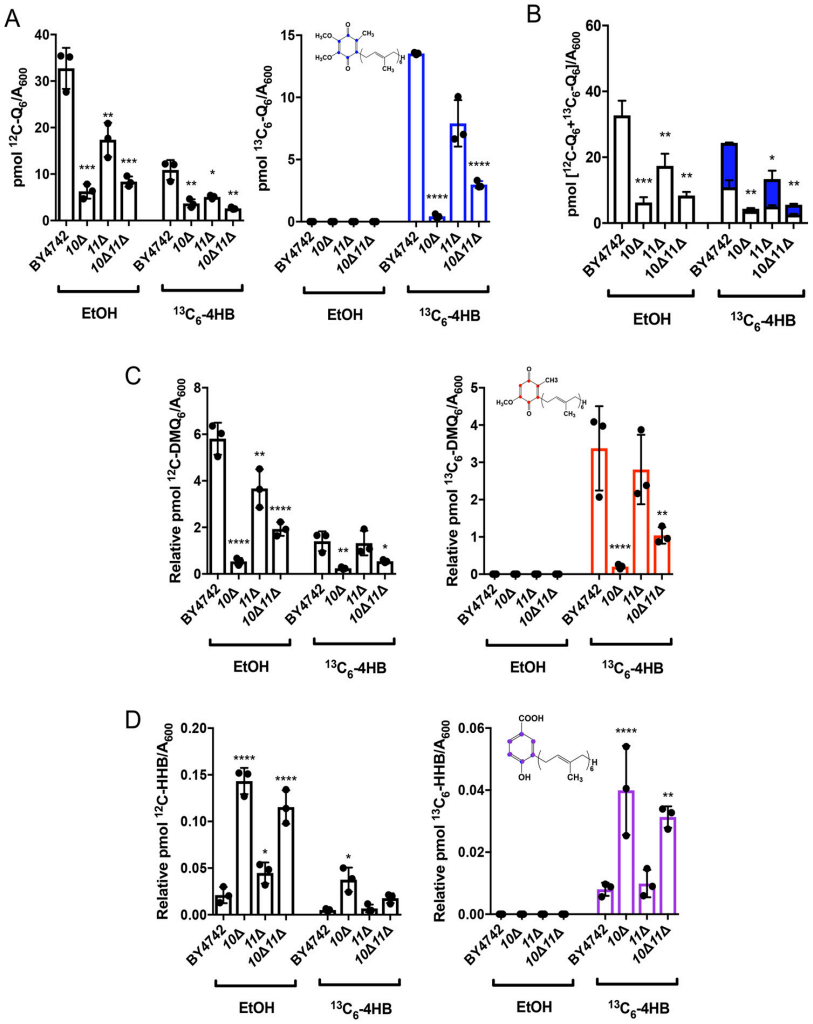

Figure 4. Low amounts of *de novo* [^{13}C$_6$]Q$_6$ in whole-cell lipid extracts of the *coq10*Δ mutant are only partially restored by deletion of *COQ11*. Triplicates of 6-ml cultures in YPGal were labeled at A_{600} ~1 with 5 μg/ml [^{13}C$_6$]4HB or EtOH vehicle control, and 5 ml of each culture were collected after 4 h, lipid-extracted, and analyzed by LC-MS/MS. *A*, unlabeled [^{12}C]Q$_6$ and *de novo*–synthesized [^{13}C$_6$]Q$_6$ (*blue*); *B*, total amount of Q$_6$ determined from the sum of [^{13}C$_6$]Q$_6$ and [^{12}C]Q$_6$; *C*, [^{12}C]DMQ$_6$ and [^{13}C$_6$]DMQ$_6$ (*red*); and *D*, [^{12}C]HHB and [^{13}C$_6$]HHB (*purple*) were measured from the whole-cell lipid extracts of WT and the *coq10*Δ, *coq11*Δ, and *coq10*Δ*coq11*Δ mutants. Values are the mean of three replicates. The data show mean ± S.D., and the statistical significance as compared with WT is represented by *, $p < 0.05$; ***, $p < 0.001$; and ****, $p < 0.0001$.

Coq4, Coq7, and Coq9 compared to and plotted as a percentage of WT (Fig. 6*B*).

In contrast to *coq10*Δ, the *coq11*Δ single mutant had elevated Coq4, Coq6, Coq7, and Coq9 (Fig. 6*A*), with protein quantification shown in Fig. 6*B*. Furthermore, the *coq10*Δ*coq11*Δ double mutant also had raised amounts of Coq4, Coq7, and Coq9 polypeptides compared with WT (Fig. 6, *A* and *B*). This increase in Coq proteins could not be explained by enhanced *COQ* transcription as there was no corresponding change in the concentration of the respective mRNAs, (Fig. 6*C*), although *COQ4* mRNA was not detected.

CoQ synthome formation was probed using two-dimensional blue native/SDS-PAGE (2D-BN/SDS-PAGE) with Coq4 and Coq9 serving as sensitive indicators of a high-molecular-weight complex (13). As expected, the CoQ synthome in WT yeast presented as a heterogeneous high-molecular-weight complex, spanning a range of ~140 kDa to >1 MDa for Coq4 (Fig. 7*A*) and from ~100 kDa to >1 MDa for Coq9 (Fig. 7*B*). Consistent with prior results (13, 19), the *coq10*Δ mutant displayed a highly-destabilized CoQ synthome, with a disappearance of large complexes that were replaced by lower-molecular-weight subcomplexes less than ~440 kDa for Coq4 (Fig. 7*A*) and less than ~232 kDa for Coq9 (Fig. 7*B*). The *coq11*Δ mutant had a stabilized CoQ synthome compared with WT, with high-molecular-weight complexes shifting to the left and collapsing into a more homogeneous complex spanning ~900 kDa to >1 MDa for both Coq4 (Fig. 7*A*) and Coq9 (Fig. 7*B*). When *COQ11* was deleted in combination with *COQ10*, there was a substantial rescue of high-molecular-weight complex formation compared with the *coq10*Δ single mutant (Fig. 7, *A* and *B*). The CoQ

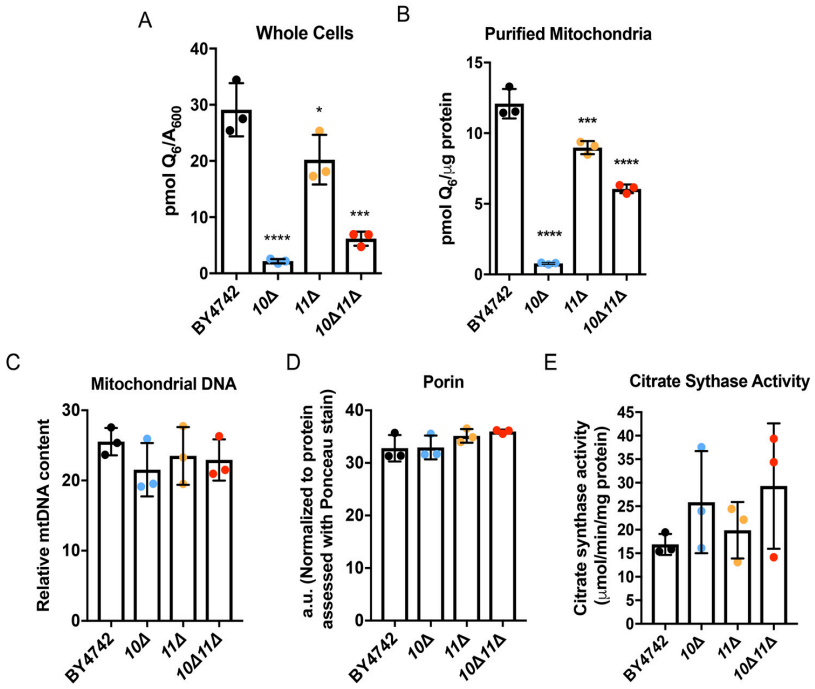

Figure 5. Deletion of *COQ11* in the *coq10*Δ mutant enhances mitochondrial Q_6 content. Triplicates of 30-ml cultures of WT, *coq10*Δ, *coq11*Δ, and *coq10*Δ*coq11*Δ yeast were grown in YPGal until they reached A_{600} ~4. *A*, 5 ml of whole cells from each culture were harvested, lipid-extracted, and analyzed by LC-MS/MS for Q_6 content. Alternatively, WT, *coq10*Δ, *coq11*Δ, and *coq10*Δ*coq11*Δ yeasts were grown in YPGal until they reached A_{600} ~4 and were subjected to mitochondrial preparation. *B*, lipids from triplicates of purified mitochondria (100 μg) were analyzed by LC-MS/MS for Q_6 content. *C–E*, mitochondrial mass was estimated using three distinct methods. *C*, relative mitochondrial DNA to actin was quantified by qPCR. *D*, porin protein amounts were quantified by hand using ImageStudioLite following immunoblot and normalized to total protein levels evaluated by Ponceau stain. *E*, citrate synthase activity was determined using a colorimetric assay as outlined under "Experimental procedures." Values are the mean of three replicates. The data show the mean ± S.D., and the statistical significance as compared with WT is represented by *, $p < 0.05$; ***, $p < 0.001$; and ****, $p < 0.0001$.

synthome of the *coq10*Δ*coq11*Δ double mutant appeared similar to that of *coq11*Δ complexes spanning ~66 kDa to > 1 MDa for Coq4 (Fig. 7*A*) and from ~66 kDa to > 1 MDa for Coq9 (Fig. 7*B*). However, the deletion of *COQ11* in *coq10*Δ does not negate the effect from the *COQ10* deletion, as it does not restore small subcomplexes <140 kDa to higher molecular weights (Fig. 7, *A* and *B*). These CoQ synthome signals for *coq11* mutants were complementary to the observed increased Coq polypeptides, indicating that the absence of *COQ11* enhanced the Q_6 biosynthetic machinery.

High-copy COQ8 does not restore Q_6 content in the coq10Δcoq11Δ single mutant

The Coq8 polypeptide is a member of an ancient atypical kinase family (37), with several conserved kinase motifs that are essential for Q biosynthesis (13, 38). Prior studies have demonstrated that overexpression of Coq8 in a *coq10*Δ mutant increased the otherwise low amounts of several key Coq polypeptides and stabilized CoQ synthome formation (13). This is similar to the phenotype observed when *COQ11* was deleted in the *coq10*Δ mutant. Furthermore, Coq8 overexpression has also been shown to influence Q_6 biosynthesis, including the restoration of late-stage Q_6-intermediates in *coq5–coq9* null mutants (39). Although the CoQ synthome of the *coq10*Δ mutant was stabilized by deletion of *COQ11*, Q_6 and late-stage Q_6-intermediates remained lower compared with WT and the *coq11*Δ single mutant (Fig. 4*C*). We hypothesized that the overexpression of Coq8 in the *coq10*Δ and *coq10*Δ*coq11*Δ mutant may restore Q_6 content in both mutants.

WT, *coq10*Δ, *coq11*Δ, and *coq10*Δ*coq11*Δ were analyzed for growth on nonfermentable medium and Q_6 biosynthesis upon transformation with high-copy *COQ8* (hc*COQ8*, Table 2) or empty vector control (Fig. 8). Similar to previous observations in a different yeast genetic background (18), *coq10*Δ-expressing hc*COQ8* regained the ability to grow on respiratory medium (Fig. 8*A*). This growth phenotype may be explained by a stabilized CoQ synthome in the *coq10*Δ mutant harboring hc*COQ8* (13). However, hc*COQ8* had no material effect on the growth properties of WT, *coq11*Δ, or *coq10*Δ*coq11*Δ strains on YPG (Fig. 8*A*).

Each strain was grown in minimal selection medium to maintain plasmid expression and was analyzed for Q_6 biosynthesis following metabolic labeling with the ring-labeled Q_6 precursor, [$^{13}C_6$]HB (Fig. 8, *B* and *C*). Changing the growth medium from rich (*i.e.* YPGal) to minimal synthetic (*i.e.* SD and dropout dextrose media (DOD)) changed the relative amounts of Q_6 content among the mutants (Figs. 4*B versus* 8*C*). Although WT [$^{13}C_6$]Q_6 and total Q_6 content is similar in Figs. 4*B* and 8*C*, the values for *coq11*Δ and the double mutant are quite different. When grown in YPGal, *coq10*Δ had the lowest Q_6 content, followed by the double mutant *coq10*Δ*coq11*Δ, with *coq11*Δ hav-

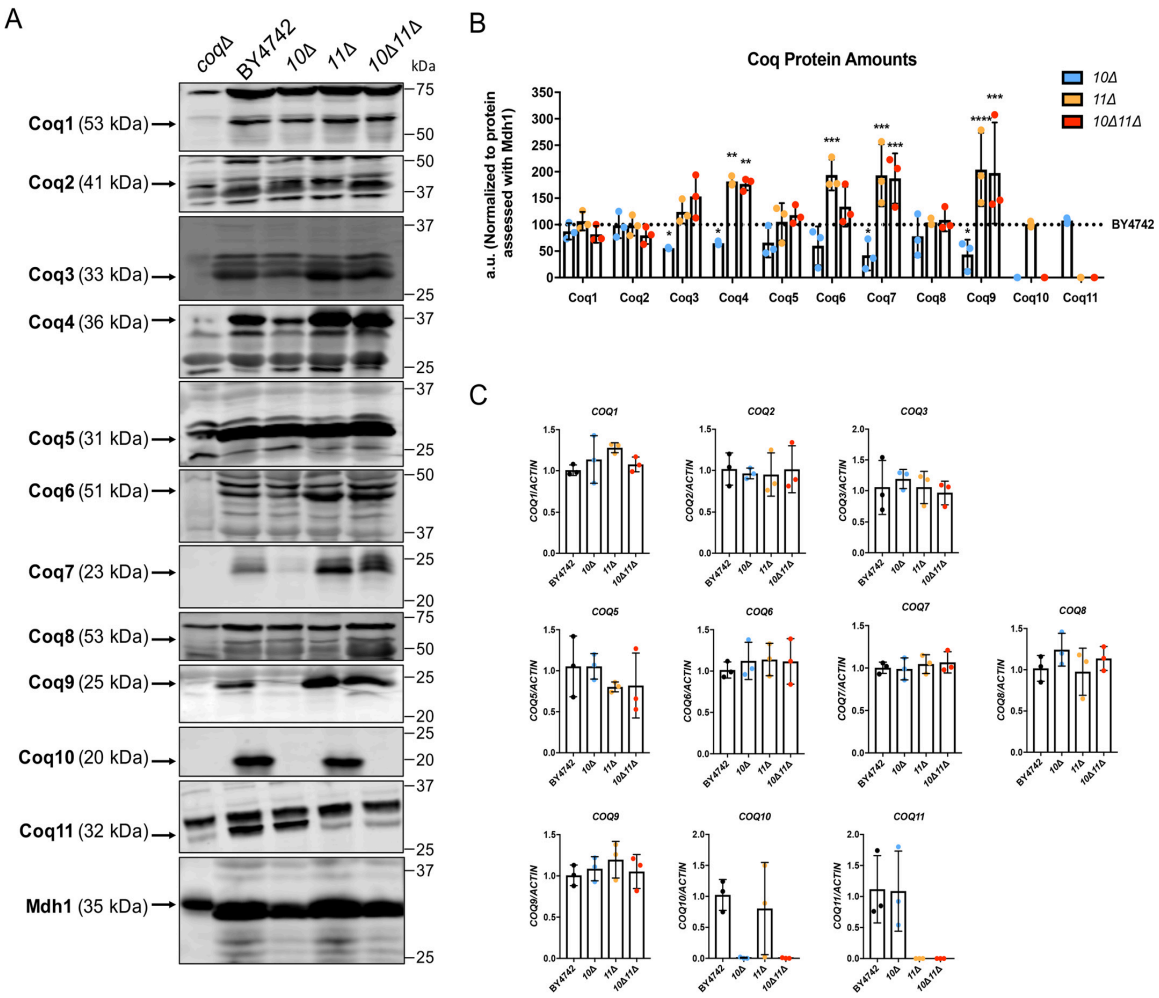

Figure 6. Several Coq polypeptides have increased abundance in *coq11*Δ and *coq10*Δ*coq11*Δ mutants compared with WT. *A*, aliquots of purified mitochondria (25 μg) from WT, *coq10*Δ, *coq11*Δ, and *coq10*Δ*coq11*Δ yeasts were subjected to 10 or 12% Tris-glycine SDS-PAGE. Mitochondrial malate dehydrogenase (Mdh1) was included as a loading control, with a representative blot shown. The Coq5 protein also serves as a qualitative loading control, because the Coq5 polypeptide amounts remain unchanged across the panel of *coq1*–*coq4* and *coq6*–*coq10* deletion mutants (12). Aliquots of purified *coq*Δ mitochondria (*coq1*Δ–*coq11*Δ) were included as negative controls for immunoblotting with antisera to each of the Coq polypeptides. *Black arrows* highlight the location of each protein on the membrane. *B*, ImageStudioLite was used to quantify triplicates of each Coq protein band's intensity by hand, which were normalized to Mdh1 and plotted as a percentage of WT. The data show mean ± S.D., and the statistical significance is as compared with WT is represented by *, $p < 0.05$; **, $p < 0.01$; ***, $p < 0.001$; and ****, $p < 0.0001$. *C*, qPCR was used to determine *COQ* gene expression from whole-cell cultures of WT, *coq10*Δ, *coq11*Δ, or *coq10*Δ*coq11*Δ, and data were normalized to actin. *COQ* RNA levels remain unchanged in the *coq10*Δ, *coq11*Δ, or *coq10*Δ*coq11*Δ mutants as compared with WT.

ing the closest Q_6 content to WT (Figs. 4, *A* and *B*, and 5*A* and Fig. S2, *A* and *B*). In contrast, when these strains are cultured in SD−Ura (Fig. 8, *B* and *C*), the double mutant *coq10*Δ*coq11*Δ had the lowest Q_6 content, as compared with either the *coq10*Δ or *coq11*Δ single mutant strains. Growth on minimal dextrose medium in the absence of plasmid selection produced similar trends (Fig. S2, *C* and *D*, and Fig. S3, *A* and *B*).

Upon Coq8 overexpression, *coq10*Δ had increased *de novo*-synthesized $[^{13}C_6]Q_6$ and $[^{12}C]Q_6$ (Fig. 8*B*), and total Q_6 concentrations ($[^{13}C_6]Q_6 + [^{12}C]Q_6$) were restored to those of WT (Fig. 8*C*). This finding is consistent with previous results, which also indicated that hc*COQ8* restored Q biosynthesis and amounts of Coq polypeptides and the CoQ synthome in the *coq10*Δ mutant (13, 17, 18). Intriguingly, expression of hc*COQ8* had no effect on *de novo* or unlabeled Q_6 content in either the *coq11*Δ single mutant or the *coq10*Δ*coq11*Δ double mutant (Fig. 8*B*). Total Q_6 contents of both *coq11*Δ and *coq10*Δ*coq11*Δ remained significantly decreased compared with WT (Fig. 8*C*). Together, these results show that the rescue of the *coq10*Δ mutant mediated by Coq8 overexpression requires Coq11.

*Expression of low-copy COQ11 rescues only some of the phenotypes of the coq10*Δ*coq11*Δ *mutant*

The functional complementation of *coq11*Δ single and *coq10*Δ*coq11*Δ double mutants with low-copy *COQ11* was assessed (lc*COQ11*, Table 2). As expected, the *coq10*Δ mutant, *coq10*Δ with empty vector, and *coq10*Δ complemented with lc*COQ11* showed slow growth on the nonfermentable carbon

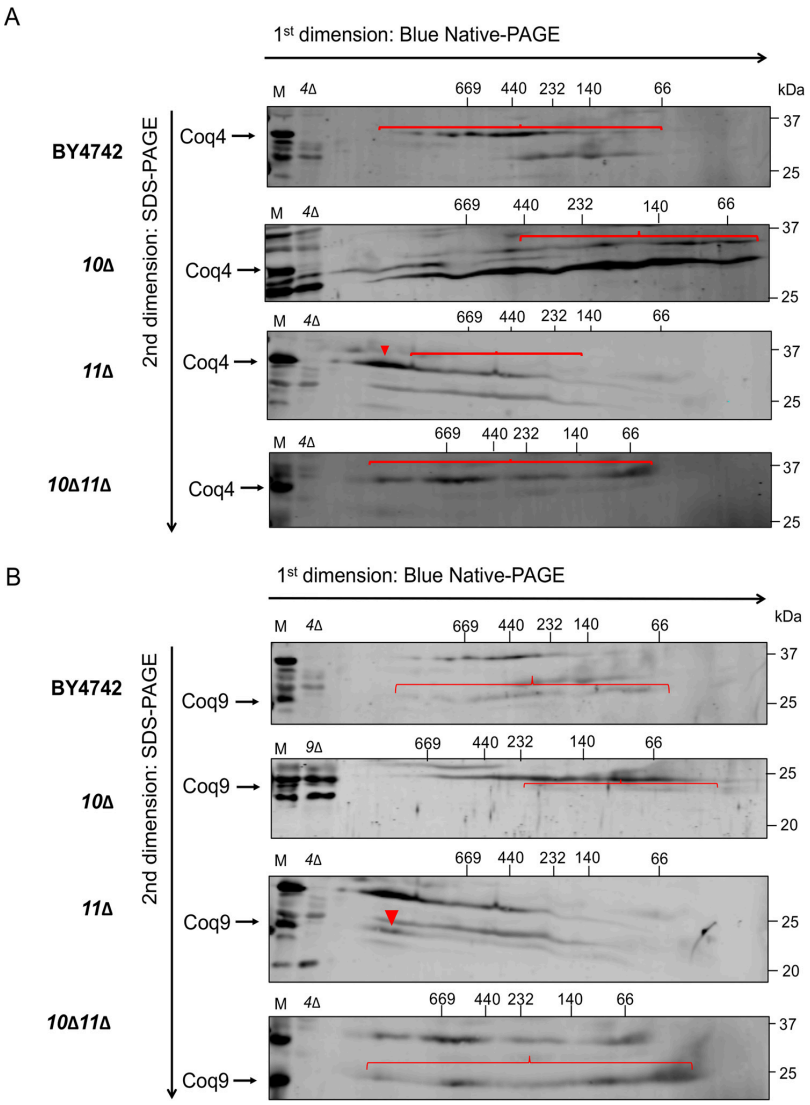

Figure 7. Deletion of *COQ11* in the *coq10*Δ mutant restores the CoQ synthome. Aliquots (100 μg) of purified mitochondria from WT, *coq10*Δ, *coq11*Δ, and *coq10*Δ*coq11*Δ yeasts cultured in YPGal were solubilized with digitonin and separated with two-dimensional BN/SDS-PAGE. Following transfer of proteins to membranes, the CoQ synthome was visualized as a heterogeneous signal from ~66 to ~669 kDa in WT control with antibodies to *A*, Coq4, or *B*, Coq9. Intact mitochondria (25 μg) from each designated strain was included as a loading control (*M*). Aliquots of *coq4*Δ- or *coq9*Δ-purified mitochondria (25 μg) were included as a negative control for the antisera to Coq4 and Coq9, as the Coq9 polypeptide is absent from the *coq4*Δ mutant. *Red arrowheads* and *brackets* indicate distinct complexes.

Table 2
Yeast expression vectors

Plasmid	Relevant genes/markers	Source
pRS305	Yeast vector with *LEU2* marker	70
pRS313	Yeast vector with *HIS3* marker	70
pRS316	Yeast shuttle vector; low-copy	70
lc*COQ11*	pRS316 with yeast *COQ11*; low-copy	This work
pRS426	Yeast shuttle vector; multi-copy	71
p4HN4	pRS426 with yeast *COQ8*; multi-copy	12

source YPGlycerol (Fig. 9*A*). Because yeast lacking *COQ11* retain respiratory capacity (Fig. 2) (14), *coq11*Δ complemented with lc*COQ11* had no detectable change in growth phenotype compared with either the *coq11*Δ mutant or *coq11*Δ with empty vector (Fig. 9*A*). Intriguingly, when lc*COQ11* was expressed in the *coq10*Δ*coq11*Δ double mutant, there was no repression of growth on YPG compared with that of the *coq10*Δ mutant (Fig. 9*A*).

This observation suggests that Q_6 biosynthesis in *coq10*Δ *coq11*Δ may not be affected by lc*COQ11*. To determine the effect of lc*COQ11* expression on mutant Q_6 biosynthesis, yeast was grown in selection medium to maintain plasmid expression. We tested whether lc*COQ11* expression rescued Q_6 content in the *coq11*Δ mutant. Expression of lc*COQ11* in *coq11*Δ efficiently rescued total Q_6 ($[^{13}C_6]Q_6$ + $[^{12}C]Q_6$) to WT amounts (Fig. 9*B*).

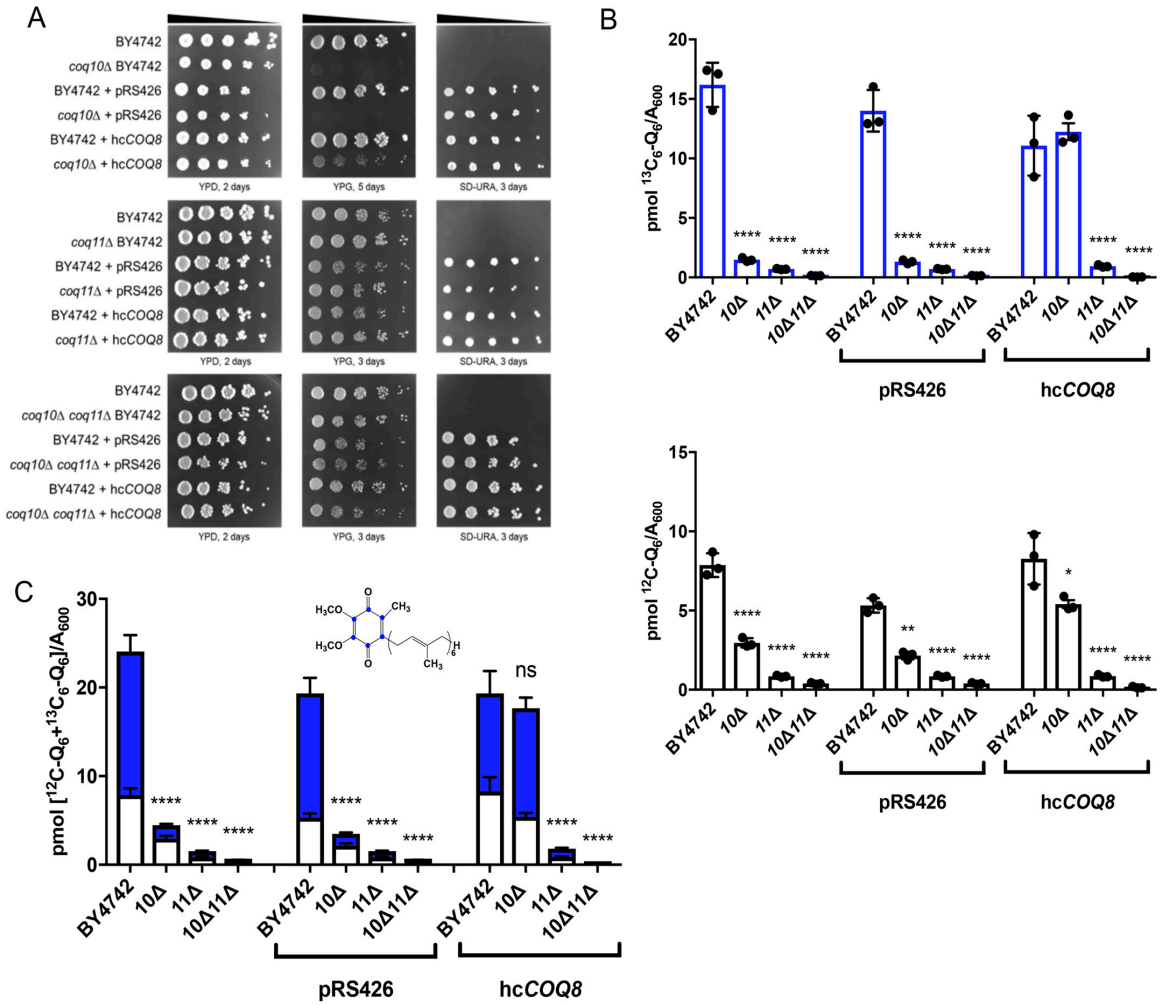

Figure 8. Overexpression of the CoQ synthome stabilizer, *COQ8*, has no effect on Q_6 synthesis in the *coq10Δcoq11Δ* mutant. WT, *coq10Δ*, *coq11Δ*, and *coq10Δcoq11Δ* mutants were transformed with high-copy *COQ8* (hc*COQ8*) or empty vector (pRS426) plasmids. *A*, strains were grown overnight in 5 ml of selection medium, diluted to an A_{600} = 0.2 with sterile PBS, and 2 μl of 5-fold serial dilutions were spotted onto YPD, YPG, or selection medium (SD−Ura), corresponding to a final A_{600} = 0.2, 0.04, 0.008, 0.0016, and 0.00032. Plates were incubated at 30 °C, and growth was captured after 2 or 3 days. Triplicates of 5 ml of culture in selection medium were labeled with 5 μg/ml [$^{13}C_6$]4HB, collected after 4 h, lipid-extracted, and analyzed by LC-MS/MS. *B*, [^{12}C]Q_6 (*white*) and *de novo* [$^{13}C_6$]Q_6 (*blue*). *C*, total amount of Q_6 was also plotted from the sum of [$^{13}C_6$]Q_6 and [^{12}C]Q_6. The values are the means of three replicates. The data show mean ± S.D., and the statistical significance as compared with WT is represented by *, $p < 0.05$; **, $p < 0.01$; ***, $p < 0.001$; and ****, $p < 0.0001$. The *ns* signifies that values are not significantly different from WT.

Finally, whole-cell steady-state Q_6 concentrations were evaluated in all mutants. Even though lc*COQ11* complementation did not suppress *coq10Δcoq11Δ* growth on YPGlycerol (Fig. 9*A*), Q_6 concentrations were increased in *coq10Δcoq11Δ* to a level comparable with that of *coq10Δ* (Fig. 9*C*). This implies that Coq11's role in Q_6 biosynthesis is not effective when the *COQ11* ORF is expressed on a single-copy plasmid in the absence of *COQ10*. Perhaps Coq11 expression from a plasmid does not account for multiple levels of regulation that occur through endogenous expression. Alternatively, the *coq10Δcoq11Δ* double mutant may have slightly lower amounts of the Coq11 polypeptide compared with *coq11Δ* when both are complemented by lc*COQ11* (Fig. 9*D*), and these lower levels may not be sufficient to suppress respiration (Fig. 9*A*).

Discussion

This work investigated a putative functional relationship between Coq10 and Coq11 within the *S. cerevisiae* Q_6 biosynthetic pathway. The presence of Coq10–Coq11 fusions in several Ustilaginaceae species suggests that these proteins may directly interact or participate in the same biological pathway in yeast (Fig. 1*A*) (14). Yeast Coq10 and its orthologs were previously shown to be required for efficient *de novo* Q biosynthesis and respiration (17, 18). We were surprised to discover that the yeast *coq10Δ* growth defect on nonfermentable medium and oxygen consumption rates were rescued upon deletion of *COQ11* (Fig. 2). Moreover, spontaneous revertants isolated from *coq10Δ* yeast were previously found to exhibit growth on

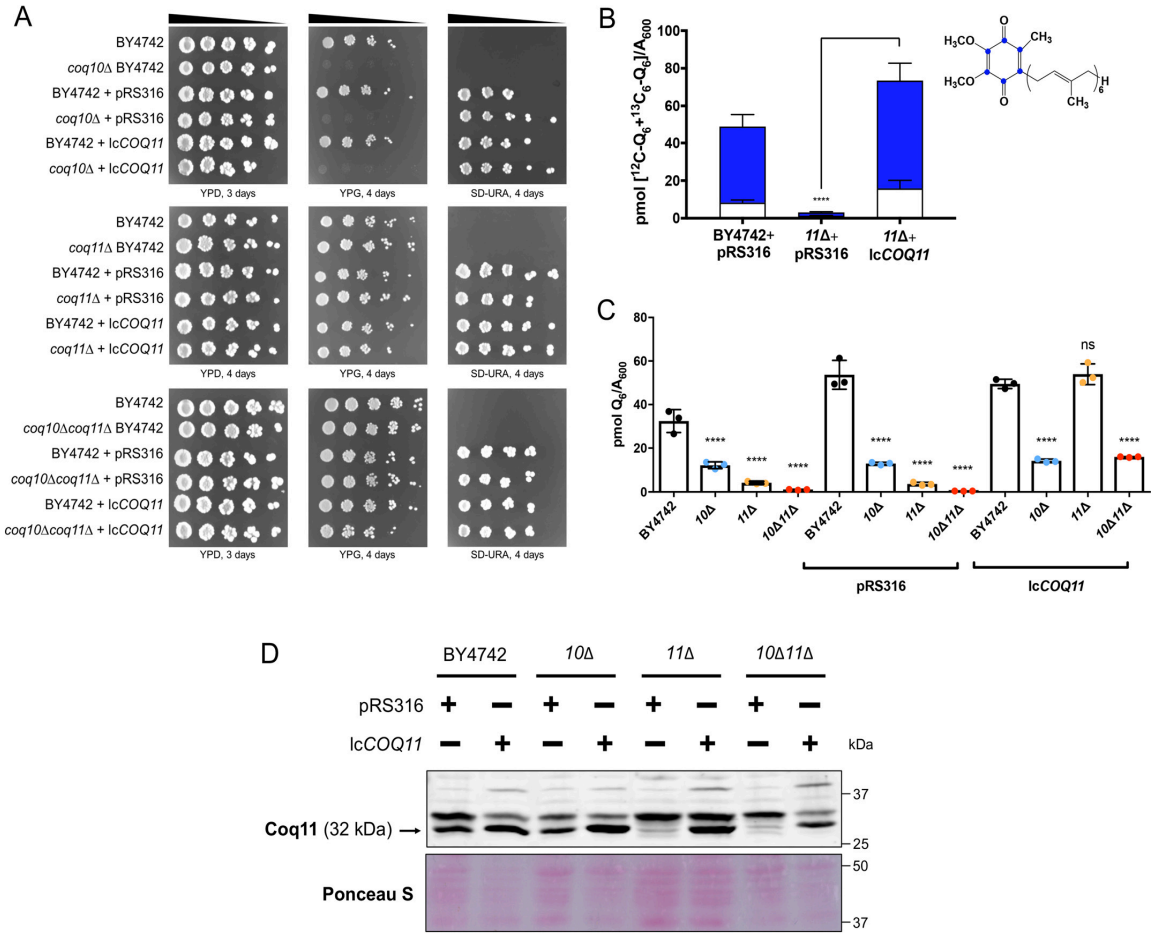

Figure 9. Low-copy *COQ11* rescues only some of the phenotypes of the *coq10Δcoq11Δ* double mutant. A low-copy plasmid expressing *COQ11* (*lcCOQ11*) and an empty vector control (pRS316) were transformed into WT, *coq10Δ*, *coq11Δ*, and *coq10Δcoq11Δ*. *A*, strains were grown overnight in 5 ml of YPDextrose (*YPD*) and diluted to an A_{600} = 0.2 with sterile PBS, and 2 μl of 5-fold serial dilutions were spotted onto YPDextrose, YPGlycerol (*YPG*), or selection medium (SD−Ura), corresponding to a final A_{600} = 0.2, 0.04, 0.008, 0.0016, and 0.00032. Plates were incubated at 30 °C, and growth was captured after 3 or 4 days. *B*, rescue of mutant *de novo* and unlabeled Q_6 production was initially demonstrated in *coq11Δ*. Triplicates of 6-ml cultures in selection medium were labeled with 5 μg/ml [$^{13}C_6$]4HB, and 5 ml of each culture was collected after 4 h, lipid-extracted, and analyzed by LC-MS/MS. Total amount of Q_6 was plotted from the sum of *de novo* [$^{13}C_6$]Q_6 (*blue*) and unlabeled [^{12}C]Q_6. Values are the mean of three replicates. *C*, rescue of mutant Q_6 content was evaluated in each mutant strain. Triplicates of 6-ml cultures in selection medium were grown until A_{600} ~4. Lipid extracts from 5 ml of each culture were analyzed by LC-MS/MS. The data show the means ± S.D., and the statistical significance as compared with WT is represented by *, $p < 0.05$; **, $p < 0.01$; ***, $p < 0.001$; and ****, $p < 0.0001$. *ns* signifies that values are not significantly different from WT. *D*, aliquots of purified mitochondria (25 μg) from WT and mutant yeast containing empty vector or lc*COQ11* were isolated in YPGal medium and were separated on 10% Tris-glycine SDS-polyacrylamide gels to determine Coq11 protein expression. Proteins stained with Ponceau stain were used as loading control.

nonfermentable medium (18). We have shown that this reversion is due to a dominant base pair deletion within the *COQ11* gene, likely resulting in a nonfunctional, truncated Coq11 protein (Fig. 3). Mutants lacking both *COQ10* and *COQ11* when cultured on YPGal have increased *de novo* Q_6 production (Fig. 4*A*) in addition to a 5-fold increase in mitochondrial Q_6 content compared with the *coq10Δ* single knockout (Fig. 5*B*). Therefore, we have demonstrated that deletion of the Coq11 polypeptide in a *coq10Δ* mutant confers a beneficial effect on both respiration and Q_6 biosynthesis (Fig. 10).

Enhanced Q_6 content in the *coq10Δcoq11Δ* double mutant compared with the *coq10Δ* single mutant may be partially due to increased amounts of several key Coq polypeptides (Fig. 6) and CoQ synthome stabilization (Fig. 7). The ring-modifying enzymes within the Q_6 biosynthetic pathway colocalize to numerous distinct "CoQ domains" *in vivo*, and proper assembly of the CoQ synthome components is required for the presence of these CoQ domains (23). Two recent studies demonstrated that mitochondria isolated from yeast lacking *COQ10* have a reduced number of CoQ domain puncta (23, 24). This is likely due to lower levels of certain Coq polypeptides and partial CoQ synthome destabilization in the *coq10Δ* mutant (17, 19), which was confirmed in this work (Figs. 6 and 7). In contrast, *coq11Δ* yeast displayed significantly higher amounts of Coq4, Coq6, Coq7, and Coq9 polypeptides (Fig. 6). The CoQ synthome was likewise shifted to a higher molecular weight in *coq11Δ* mitochondria compared with WT (Fig. 7). When Coq9–yEGFP was used as a marker for CoQ domains, *coq11Δ* had increased CoQ

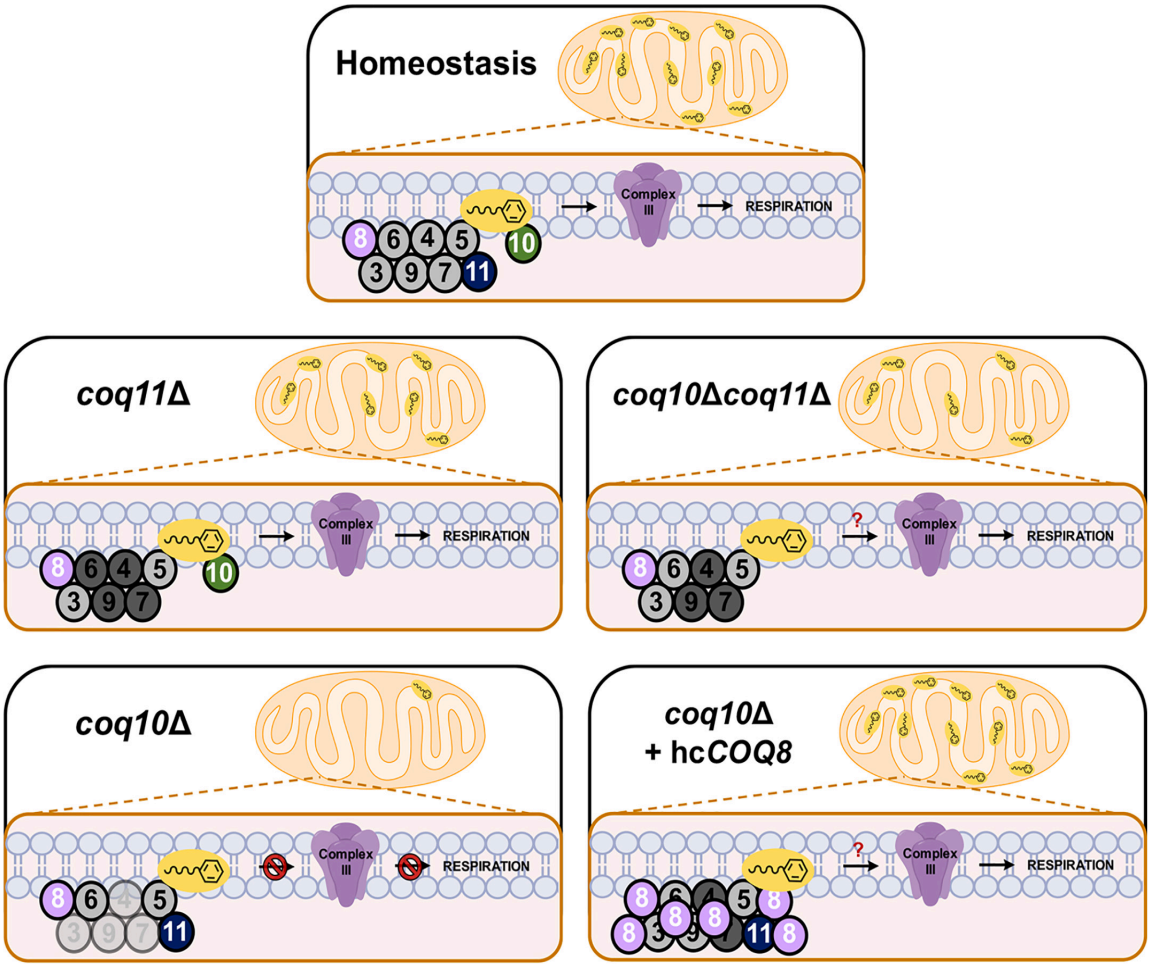

Figure 10. Scheme postulating Coq11 as a modulator of Q_6 synthesis in mitochondria. Under homeostasis, Coq11 associates with the CoQ synthome and acts as a modest negative regulator of Q_6 synthesis via Coq10. In the absence of *COQ11*, several Coq polypeptides are increased (*dark shading*), and the CoQ synthome is stabilized compared with WT cells, despite a slight decrease in Q_6 content. In contrast, the *coq10*Δ mutant is missing the Q_6 chaperone protein, resulting in a decreased amount (*light shading*) of Coq3, Coq4, Coq7, and Coq9, a destabilized CoQ synthome, substantially decreased Q_6 concentrations, and a lack of respiration. The deletion of *COQ11* in the *coq10*Δ mutant counterbalances the destabilized CoQ synthome and decreased Q_6 content phenotype of the *coq10*Δ mutant, allowing the *coq10*Δ*coq11*Δ double mutant to grow on YPG and respire. Expression of hc*COQ8* in the *coq10*Δ mutant produces many similar phenotypes to *COQ11* deletion in *coq10*Δ cells, including increased Coq polypeptides and a stabilized CoQ synthome (13), resulting in restored growth on YPG. Unlike the *coq10*Δ*coq11*Δ double mutant, *coq10*Δ + hc*COQ8* has rescued Q_6 content pointing to an additional role of Coq11 in Q_6 biosynthesis, redox regulation, or transportation.

domain intensity that stemmed from amplified expression of Coq9 –yEGFP, although the number of domains was similar to WT. Mutants lacking essential Coq polypeptides *coq1– coq9*, or *coq10*, displayed significantly less Coq9-labeled domains (24). The CoQ synthome stabilization seen in *coq11*Δ via 2D-BN/SDS-PAGE analyses performed in this work (Fig. 7) agrees with the observation of increased CoQ domains and argues that the CoQ synthome is truly stabilized upon deletion of *COQ11*, as opposed to inducing a greater number of domains.

These observations are consistent with the biochemical data that led to the notion of a CoQ synthome whose formation relies on the presence of prenylated Q-intermediates (13, 40, 41). The *coq10*Δ mutant produced more early-stage intermediates (HHB) and had less late-stage intermediates (DMQ_6) compared with WT (Fig. 4, *C* and *D*), resulting in less CoQ synthome formation (Fig. 7). Because *coq11*Δ yeast displayed comparable amounts of early- and late-stage Q_6-intermediates to WT (Fig. 4, *C* and *D*), this mutant retained the ability to fully form the CoQ synthome (Fig. 7). The double knockout synthesized varying amounts of early- and late-stage Q_6-intermediates that were largely in-between those of the single knockouts (Fig. 4, *C* and *D*). The CoQ synthome is thus able to form in *coq10*Δ*coq11*Δ yeast, albeit not to the efficiency of the *coq11*Δ single mutant (Fig. 7). We suspect that the accumulation of Coq polypeptides and restoration of the CoQ synthome in the *coq10*Δ*coq11*Δ double mutant are sufficient to allow for Q_6 to escape its site of synthesis and reach the respiratory complexes, despite an absence of the Coq10 Q_6 chaperone protein and lower Q_6 in this strain (Fig. 10). How this occurs is presently not known. One possible explanation could be that Coq11 inhibits

a currently unidentified Q_6 chaperone with lower efficiency than Coq10 that is able to rescue respiration only in the absence of both Coq10 and Coq11.

Overexpression of the Q_6-biosynthetic protein Coq8 also rescued *coq10*Δ mutant growth on nonfermentable medium (Fig. 8*A*) and *de novo* Q_6 biosynthesis (Fig. 8, *B* and *C*) (17). Coq8 has been implicated in the partial extraction of Q_6-intermediates out of the mitochondrial inner membrane for enzymatic modification by other Coq proteins, allowing for appropriate Q_6 biosynthesis (25). Prior investigations also revealed that Coq8 overexpression in *coq10*Δ yeast increased Coq4 and Coq9 polypeptides and stabilized the CoQ synthome (13, 24). Despite the substantial benefit of Coq8 overexpression in a *coq10*Δ single mutant, Coq8 overexpression failed to enhance Q_6 biosynthesis in the *coq10*Δ*coq11*Δ double knockout (Figs. 8, *B* and *C*, and 10). The absence of *COQ11* in the double mutant is sufficient to restore Coq polypeptides and CoQ synthome formation (Figs. 6, *A* and *B*, 7, and 10). Coq11 and Coq8 may therefore work by different mechanisms to serve opposing functions for CoQ synthome and Coq polypeptide stabilization. Furthermore, it is clear that Coq11 is required to perform an additional function to Coq8, as hc*COQ8* requires the presence of Coq11 to restore Q_6 biosynthesis (Figs. 8, *B* and *C*, and 10).

Proper CoQ synthome formation is not only required for efficient Q_6 biosynthesis, but it is also vital for the establishment of ER-mitochondrial contact sites mediated by the ER-mitochondrial encounter structure (ERMES) complex (23, 24). The ERMES complex is essential for lipid exchange between the ER and mitochondria (42). Specifically, *ERMES* null mutants have irregular Q_6 cellular distribution and a destabilized CoQ synthome (23). When *COQ10* was deleted in yeast expressing Coq6–GFP, there was a significant decrease in Coq6–GFP puncta colocalization with Mdm34–mCherry, a component of the ERMES complex (23). These results indicate that CoQ synthome positioning next to the ERMES complex, and subsequent Q_6 distribution from the mitochondria, depends on Coq10. Because *COQ11* deletion stabilizes the CoQ synthome (Figs. 6, *A* and *B*, and 7), it is possible that *coq11*Δ mutants have more ER-mitochondrial contacts through the ERMES complex and improved transfer of lipids between these organelles. Therefore, one possible role of Coq11 may be an auxiliary protein mediating lipid transport between the ER and mitochondria.

In a recent study, Coq11 was named Mrx2, as part of the mitochondrial organization of gene expression (MIOREX) complex involved in the mitochondrial genetic expression system (43). Considering the proposed regulatory function of Coq11 in CoQ synthome assembly, it is tempting to speculate that Coq11 offers a mechanism to couple Q_6 synthesis with the assembly of the respiratory complexes. When the synthesis of the respiratory complexes is more active, Coq11 is associated to the MIOREX complex, and Q_6 synthesis at ER junctions is stimulated. Coq11 dual localization in the mitochondrial inner membrane, to the MIOREX complex and the CoQ synthome, would also explain the sensitivity of yeast cells to the number of *COQ11* copies, as well as present another example of a loop system control for balanced expression of mitochondrial products (44).

Another potential explanation for the phenotypes induced by the knockout of Coq11 relates to its structural connection with the short-chain dehydrogenase/reductase (SDR) superfamily of NAD(P)(H)-dependent oxidoreductases (14, 45). These enzymes catalyze an assortment of reactions, including isomerization, decarboxylation, epimerization, imine reduction, and carbonyl–alcohol oxidoreduction (45). SDR superfamily proteins contain a conserved protein structural motif known as a Rossmann fold, a feature used in the binding of nucleotide cofactors such as FAD, FMN, and NAD(P) (46). The crystal structure of the *Pseudomonas aeruginosa* gene UbiX, which catalyzes the decarboxylation step in Q_9 biosynthesis, revealed a Rossmann fold with a bound FMN (47). Thus, Coq11 may use its Rossmann fold in conjunction with a nucleotide cofactor to perform similar redox chemistry in *S. cerevisiae* Q_6 biosynthesis. The ratio of QH_2/Q serves as a metabolic sensor for electron transport chain efficiency (48). High QH_2/Q ratios induce respiratory complex I-mediated reverse electron transport (RET) under physiological conditions in both *Drosophila* and mammalian cell lines (48, 49). Superoxide and secondary reactive species produced specifically through complex I RET extended *Drosophila* lifespan and improved mitochondrial function in a model of Parkinson's disease (49). RET induced by over-reduction of the Q pool presumably generates a superoxide-dependent signal essential for homeostasis, such that manipulation of the Q redox state is beneficial for mitochondrial function (48, 49). Mitochondrial phenotypes in the absence of *COQ11*, including restored respiration in *coq10*Δ *coq11*Δ and up-regulated Q_6 machinery (Figs. 2, *A–C*, 6, and 7), seem to correlate well with the aforementioned effects of Q_6H_2 accumulation. Yeast *coq11*Δ and *coq10*Δ*coq11*Δ mutants retain antioxidant protection by Q_6H_2, demonstrated by their resistance to treatment with exogenously-added PUFAs (Fig. 2*D*). Because cells lacking the Coq11 polypeptide maintain Q_6H_2 as an antioxidant, it follows that Coq11 could be involved in the oxidation of Q_6H_2 to Q_6.

The phenotypes of Coq10 and Coq11 seen in this work are similar to those in both fungi and mammalian hosts. Several fungi use Coq11 or Coq11-like proteins as NAD-dependent epimerases/dehydratases, NADH-ubiquinone oxidoreductases, and NADH dehydrogenase subunits (14). Coq11 orthologs are commonly found in plant and algae genomes, including the chloroplast-localized flavin reductase protein At1g32220 from the land plant *Arabidopsis thaliana*, which is thought to be involved in plastoquinone biosynthesis and storage (14, 50). The closest but distinct higher eukaryotic Coq11-like protein is the SDR subfamily protein NDUFA9 (14), an auxiliary subunit of complex I in humans (51). Patients with decreased NDUFA9 expression are unable to properly assemble complex I and may develop a degenerative infancy respiratory disorder known as Leigh syndrome (52). Although yeast cells do not possess complex I, this evidence indicates that Coq11 may play a crucial role in respiratory regulation or function, supporting the observations of this study.

The function of Coq10 is widely conserved across different organisms. Expression of the Coq10 homolog from *C. crescentus* (CC1736) rescues the impaired respiration and antioxidant function of Q_6 in *coq10* yeast mutants (17). The NMR structure

of CC1736 reveals a START domain, which is known to bind lipids via a hydrophobic tunnel (20). Studies of *S. pombe* Coq10 demonstrate that it is able to bind Q_{10} (21). One proposed function of Q binding by CC1736 and Coq10 from *S. pombe* may be to regulate Q delivery to its proper sites in the respiratory complexes. Humans have two distinct homologs of yeast Coq10: COQ10A and COQ10B. Expression of either human protein rescues the *coq10*Δ respiratory deficiency and sensitivity to oxidative stress, and it restores the amounts of Coq polypeptides to WT (19). The conserved function of yeast Coq10 with human COQ10A and COQ10B suggests that the findings of this work will shed light on the role of Coq10 as a chaperone in humans, leading to a better understanding of the pathobiology of Q_{10} diseases.

In summary, this work reveals that Coq11 plays a regulatory role to maintain Q_6 homeostasis in concert with Coq10 in *S. cerevisiae* (Fig. 10). The absence of *COQ11* caused an augmentation of Q_6 production and respiration in the *coq10*Δ mutant, indicating that Coq11 confers a negative effect on the CoQ synthome. Coq11 may be crucial for Q_6 function in addition to Q_6 biosynthesis, as total whole-cell and mitochondrial Q_6 content remained lower than WT in *coq11*Δ and *coq10*Δ*coq11*Δ mutants.

Experimental procedures

All reagents were obtained commercially from Thermo Fisher Scientific unless otherwise specified

Yeast strains and growth medium

S. cerevisiae strains used in this study are described in Table 1. Yeast strains were derived from S288C (BY4742 (53)) or W303 (54). Growth media were prepared as described previously (55), and plate medium contained 2% bacto-agar. Growth media included the following: YPD (2% glucose, 1% yeast extract, and 2% peptone), YPGal (2% galactose, 1% yeast extract, 2% peptone, and 0.1% dextrose), YPG (3% glycerol, 1% yeast extract, and 2% peptone), and YPEG (3% glycerol, 2% ethanol, 1% yeast extract, and 2% peptone). Synthetic dextrose/selection media (SD–Complete, SD−Ura, SD-Leu, SD-His, SD-His–Leu, SD−Ura–Leu) were prepared as described previously (55) and consisted of all components minus uracil, leucine, histidine, or both uracil and leucine. Drop-out dextrose (DOD) medium was prepared as described previously (14).

COQ11 was disrupted by the one-step gene replacement method (56). The *LEU2* gene from pRS305 was amplified by polymerase chain reaction (PCR), with *COQ11* upstream and downstream flanking sequences 5′-GGGAAATATGTATCGTATACAAAAATACAGCTAAAGCTTGAACTG and 3′-GTACTTAACTATATACAGCTTGGTATAATTTTAAAATGGTAATAAC. Transformations of PCR products into yeast cells were performed using the Li-acetate method (57). The double *coq10*Δ*coq11*Δ mutant was constructed via disruption of *COQ10* within the *coq11*Δ strain. The *HIS3* gene from pRS313 was amplified by PCR with *COQ10* upstream and downstream flanking sequences 5′-GGATAAGGAGCCAAACAATAAACGGCTAAAGATACCGTGG and 3′-CAGATAACAAAGATCATGCCATCCAGGATAAGCGTATGCA, and transformation was performed as for the *COQ11* disruption. Primers were designed using SnapGene (GSL Biotech, LLC, Chicago, IL).

Mitochondria isolation from BY4742 WT and mutant yeast

Yeast cultures of BY4742, *coq10*Δ, *coq11*Δ, and *coq10*Δ *coq11*Δ were grown overnight in 5 ml of YPD. Yeast-containing plasmids were grown overnight in 5 ml of selection medium (SD−Ura). All pre-cultures were back-diluted with YPGal and grown overnight with shaking (30 °C, 250 rpm) until cell density reached an A_{600} ~4. Spheroplasts were prepared with Zymolyase-20T (MP Biomedicals) and fractionated as described previously (36), in the presence of cOmplete™ EDTA-free protease inhibitor mixture tablets (Roche Applied Science), phosphatase inhibitor mixture set I (Sigma-Aldrich), phosphatase inhibitor mixture set II (Sigma-Aldrich), and phenylmethylsulfonyl fluoride (Thermo Fisher Scientific). Nycodenz (Sigma-Aldrich) density gradient purified mitochondria were frozen in liquid nitrogen, aliquoted, and stored at −80 °C until further use. Protein concentration of mitochondria was measured by the bicinchoninic acid (BCA) assay (Thermo Fisher Scientific).

Submitochondrial localization of Coq10 and Coq11 polypeptides

Purified mitochondria from BY4742 yeast (3 mg of protein, 150 μl) were subfractionated, as described previously (13). Proteinase K treatment of purified BY4742 mitochondria was also performed as described previously (13). Proteinase K-treated mitoplasts and control samples were resuspended in SDS sample buffer (50 mM Tris, pH 6.8, 10% glycerol, 2% SDS, 0.1% bromphenol blue, and 1.33% β-mercaptoethanol); equal aliquots were separated by SDS-gel electrophoresis on 10 or 12% Tris-glycine polyacrylamide gels as detailed below. Several mitochondrial compartment markers and proteins of interest, Coq10 and Coq11, were detected with rabbit polyclonal antibodies prepared in blocking buffer at dilutions listed in Table S1.

Oxygen consumption evaluation by Seahorse

Mitochondrial function was assessed using the XF96 extracellular flux analyzer (Seahorse Bioscience, Agilent Technologies). Seahorse plates were coated with 50 μg/ml poly-D-lysine (Sigma-Aldrich), diluted 1:1 in UltraPure distilled water (Thermo Fisher Scientific). Volumes of 25 μl were added to each well for 30 min at room temperature and then aspirated before plates were dried overnight at room temperature. The Seahorse XF96 sensor cartridge was hydrated with Seahorse XF calibrant solution (Agilent) and was incubated overnight at room temperature.

Yeast cultures of BY4742, *coq10*Δ, *coq11*Δ, and *coq10*Δ*coq11*Δ were grown overnight in 25 ml of YPGal medium. On the day of measurement, all cultures were diluted to seed an A_{600} = 0.1 cells/well of BY4742, *coq10*Δ, *coq11*Δ, and *coq10*Δ*coq11*Δ into a Seahorse XF96 microplate in a total volume of 175 μl YPGal. Four wells containing only medium were included for background measurement. The loaded plate was centrifuged at 500 × *g* for 3 min at room temperature (with no brakes). Following centrifugation, the loaded plate was incubated for 30

min at 37 °C with no CO_2 to aid in the transitioning of the plate into the Seahorse machine's temperature. Cells were stimulated sequentially with two injections of 4 μM FCCP in ports A and B (optimized for maximum oxygen consumption rate) (Enzo Life Sciences) and 2.5 μM antimycin A in port C (Enzo Life Sciences), delivered in YPGal. Mix, wait, and measure times were 2 min, 30 s, and 2 min, respectively. Basal respiration included four measurements, and then following each injection three measurements were made. All OCR were subtracted for nonmitochondrial respiration and normalized to A_{600} = 0.1. Basal respiration was calculated as an average of OCR prior to the first FCCP addition. Maximal respiration was calculated as an average of OCR following the second FCCP addition. Nonmitochondrial respiration was measured as average OCR following antimycin A addition.

Fatty acid sensitivity assay

Sensitivity of yeast cells to PUFA-induced oxidative stress was performed as described previously (19, 58, 59), with some modifications. Briefly, BY4742 WT, *cor1*Δ, *coq9*Δ, *coq10*Δ, *coq11*Δ, and *coq10*Δ*coq11*Δ were inoculated in 5 ml of YPD medium and incubated overnight at 30 °C, 250 rpm. Cultures were subinoculated to an A_{600} = 0.25 in 15 ml of fresh YPD medium and incubated at 30 °C, 250 rpm until they reached an A_{600} ~1. Cells were harvested, washed twice with 10 ml of sterile H_2O, and diluted in 0.1 M phosphate buffer with 0.2% dextrose, pH 6.2, to an A_{600} = 0.2. This cell suspension was divided into 5-ml aliquots and treated with an ethanol vehicle control (final concentration 0.1% v/v), ethanol-diluted oleic acid (Nu-Check Prep), or α-linolenic acid (Nu-Check Prep) to a final concentration of 200 μM. Fatty acid-treated cultures were incubated for 4 h at 30 °C, 250 rpm, after which cell viability was assessed via plate dilutions. Cell viability prior to the addition of fatty acids was determined via plate dilutions, represented in the 0-h plate.

Analysis of Q_6 and Q_6-intermediates

Standards of Q_6 were obtained from Avanti Polar Lipids, and Q_4 was from Sigma-Aldrich. Yeast cultures were grown overnight in 30 ml of YPGal, or selection medium (SD-complete or SD−Ura) for strains harboring plasmids. Cultures were diluted into triplicates of 6 ml of fresh medium to A_{600} = 0.5, and 5 ml of medium was harvested by centrifugation once they reached A_{600} ~4. Cell pellets were stored at −20 °C. Following collection, frozen cell pellets were lipid-extracted in the presence of internal standard Q_4 and analyzed for Q_6 and Q_6-intermediates by LC-MS/MS as described previously (19).

Stable isotope labeling for determination of de novo Q_6 and Q_6-intermediates

Yeast cultures were grown overnight in 30 ml of YPGal and diluted in triplicates of 6 ml of fresh medium to an A_{600} = 0.1. Cultures were incubated until they reached an A_{600} ~1, at which point ethanol vehicle control (0.1% v/v) or 5 μg/ml of the stable isotope [$^{13}C_6$]4HB (Cambridge Isotope Laboratories, Inc.) was added. Cultures were allowed to grow for an additional 4 h when 5 ml of each culture was harvested by centrifugation and stored at −20 °C. Cell pellets were lipid extracted and analyzed by LC-MS/MS as described previously (19).

Mitochondrial DNA determination by qPCR analysis

DNA was extracted from yeast cells as follows. Yeast pellets (10 ml) grown in YPGal were collected at an A_{600} ~4 by centrifugation at 3000 × *g* for 5 min, washed with 5 ml of H_2O, and transferred to 2-ml screw-cap tubes. Pellets were frozen at −80 °C until DNA extraction was carried out. Cell pellets were resuspended in 200 μl of lysis buffer (10 mM Tris-Cl, pH 8.0, 2% (v/v) Triton X-100, 1 mM EDTA, 100 mM NaCl, 1% SDS), and 200 μl of acid-washed glass beads with 200 μl of phenol/chloroform/isoamyl alcohol (25:24:1) were added to the cell suspension. Cells were lysed using a bead-beater (Precellys 24; Bertin Technologies) three times for 10 s at 6500 rpm with a 45-s break between rounds at 4 °C. Tris-EDTA (TE, 200 μl) was added, and the cell suspension was centrifuged at 13,000 × *g* for 5 min at room temperature. The aqueous layer was removed to a new tube containing 200 μl of chloroform, mixed by inversion, and centrifuged at 13,000 × *g* for 5 min at room temperature. This was repeated once more. The aqueous layer was then transferred to a 2-ml screw-cap tube containing 1 ml of 95% EtOH, mixed by inversion, and centrifuged at 13,000 × *g* for 2 min at room temperature. The resulting pellet was resuspended in 400 μl of TE containing 30 μg of RNase A and incubated at 37 °C for 30 min. Then, 10 μl of 3 M sodium acetate and 1 ml of 95% EtOH was added, mixed by inversion, and incubated at −20 °C for 1 h. After 1 h at −20 °C, the suspension was centrifuged at 13,000 × *g* for 5 min, and the pellet was washed twice with 70% EtOH and air-dried. The dried pellet was resuspended in 25 μl of TE; concentration was measured by Nanodrop (Thermo Fisher Scientific), and the pellet was stored at −20 °C until use.

qPCR was performed on a CFX384 instrument (Bio-Rad) using the SensiFAST™SYBR® NO ROX kit (Bioline) as per the manufacturer's instructions. Each sample was run in duplicate with 150 ng of total DNA used per reaction using the following thermocycling protocol (95 °C for 2 min, 95 °C for 5 s, 60 °C for 10 s, and 72 °C for 20 s, plate read and cycle repeated ×40, melt curve 40–92 °C with plate read and 40 °C for 10 s). Melting-curve analysis confirmed that all PCRs produced a single product. mtDNA-specific primers (forward (13,999), 5′-GTG CGT ATA TTT CGT TGA TGC GT-3′; reverse (14,297), 5′-TTC ACA CTG CCT GTG CTA TCT AA-3′ (60) and actin-specific primers (forward, 5′-GAA TTG AGA GTT GCC CCA GA-3′; reverse, 5′-ATC ACC GGA ATC CAA AAC AA-3) were used. The relative level of gene expression of mitochondrial DNA was normalized to the expression level of actin as described previously (61).

Citrate synthase activity

The measurement of citrate synthase activity in cells was carried out as described previously (62). Briefly, yeast pellets (10 ml) grown in YPGal were collected at an A_{600} ~4 by centrifugation at 3000 × *g* for 5 min, washed with 5 ml of H_2O, and transferred to 2-ml screw-cap tubes. Cell pellets were resuspended in 200 μl of lysis buffer (100 mM Tris-Cl, pH 7.4, 1% (v/v) Triton X-100, 1 mM EDTA, 1 mM phenylmethylsulfonyl fluoride, 1× cOmplete™ Protease Inhibitor Mixture (Roche

Applied Science)), and then 200 μl of acid-washed glass beads were added. Cells were lysed using a bead-beater (Precellys 24; Bertin Technologies) three times for 10 s at 6500 rpm with a 45-s break between rounds at 4 °C. The clarified cell lysate was collected after centrifugation at 16,000 $\times$ *g* for 10 min at 4 °C. The concentration of protein was determined with the BCA assay (Thermo Fisher Scientific). Cell lysates were normalized to 0.05 μg/μl protein. The colorimetric citrate synthase assay was carried out using a VersaMax plate reader (Molecular Devices) and a flat-bottom 96-well plate. First, 40 μl of 500 mM Tris-Cl, pH 7.4, 2 μl of 30 mM acetyl-CoA, 8 μl of 2.5 mM 5,5′-dithiobis(2-nitrobenzoic acid), 90 μl of H_2O, and 50 μl cell lysate (2.5 μg total protein) were added into each well. Then, 10 μl of 10 mM oxaloacetic acid were added per well and mixed by pipetting up and down. A_{412} was measured every 30 s at 25 °C. The initial slope was calculated by using data from the first 10 min and used to determine the enzyme reaction rate using the extinction coefficient for 2-nitro-5-thiobenzoate of 14.15 $mM^{-1}\,cm^{-1}$ (63).

Porin quantification

Porin content was quantified via immunoblot of yeast WT and mutant whole cells. Protein extraction from whole cells was performed (64), and 25 μg of each sample was separated by SDS-gel electrophoresis as described below. Three replicates of the immunoblots were performed and quantified by hand using ImageStudioLite software normalized to Ponceau total protein staining.

Quantitative real-time PCR (qRT-PCR)

Total RNA was isolated from yeast cells using TRIzol reagent (Invitrogen). DNA contamination from the resulting RNA was removed using the DNase TURBO kit as per the manufacturer's instructions (Invitrogen). RNA concentration was measured by Nanodrop (Thermo Fisher Scientific), and RNA was stored at −20 °C. Reverse transcription was carried out using the Superscript III first strand synthesis system using random hexamer primers (Invitrogen). cDNA was stored at −20 °C until qPCR analyses were carried out. Quantitative real-time PCR was performed on a CFX384 instrument (Bio-Rad) using the SensiFAST™SYBR® NO-ROX kit (Bioline) in duplicate. The relative levels of gene expression were normalized to the expression level of actin. Melting curve analysis confirmed that all PCRs produced a single product. The primers (forward/reverse) used in real-time PCR were designed using Primer3 on line (RRID: SCR_003139). Primers used are given in Table S2.

SDS-PAGE and immunoblot analysis

Purified mitochondria (25 μg) were resuspended in SDS sample buffer and separated by SDS-gel electrophoresis on 10 or 12% Tris-glycine polyacrylamide gels. Proteins were transferred to a 0.45-μm polyvinylidene difluoride membrane (Millipore) and blocked with blocking buffer (0.5% BSA, 0.1% Tween 20, 0.02% SDS in PBS). Representative Coq polypeptides and loading control mitochondrial malate dehydrogenase (Mdh1) were probed with rabbit polyclonal antibodies prepared in blocking buffer at dilutions listed in Table S1. IRDye 680LT goat anti-rabbit IgG secondary antibody (LiCOR) was used at a dilution of 1:10,000. Proteins were visualized using a LiCOR Odyssey IR Scanner (LiCOR). Immunoblots are representative of three replicates and were quantified by hand using ImageStudioLite software normalized to Mdh1.

Two-dimensional Blue Native/SDS-PAGE immunoblot analysis of high-molecular-weight complexes

2D-BN/SDS-PAGE was performed as described previously (13, 65, 66). Briefly, 200 μg of purified mitochondria were solubilized at 4 mg/ml for 1 h on ice with 16 mg/ml digitonin (Biosynth) in the presence of the protease and phosphatase inhibitors used during mitochondrial isolation. Protein concentration of solubilized mitochondria was determined by BCA assay. NativePAGE 5% G-250 sample additive (Thermo Fisher Scientific) was added to a final concentration of 0.25%. Solubilized mitochondria (100 μg) were separated on NativePAGE 4–16% BisTris gels (Thermo Fisher Scientific) in the first dimension, and native gel slices were further separated on 12% Tris-glycine polyacrylamide gel in the second dimension. Following the second-dimension separation, immunoblot analyses were performed as described above, using antibodies against Coq4 and Coq9 at the dilutions indicated in Table S1. Molecular weight standards for BN gel electrophoresis and SDS gel electrophoresis were obtained from GE Healthcare (Sigma-Aldrich) and Bio-Rad, respectively.

Construction of low-copy COQ11 yeast expression vectors

Plasmids used in this study are described in Table 2. A low-copy *COQ11*-containing plasmid was constructed using the pRS316 low-copy empty vector. The *COQ11* ORF and regions corresponding to 842 bp upstream and 256 bp downstream were cloned into pRS316 using Gibson Assembly (New England Biolabs). Clones were sequenced by Laragen, and successful clones were transformed into WT and mutant yeast, along with the corresponding empty vector (pRS316) control as described above.

Revertant isolation

As reported previously, *coq10* mutant growth deficiency on nonfermentable carbon sources (YPEG) spontaneously revert due to nuclear suppression mutations (18). Here, W303 *coq10*Δ yeast was grown on glucose to stationary phase, and ~10 million cells were plated on YPEG. After several weeks, a colony began to appear on this medium. The colony was purified, and its genome was sequenced.

Genome sequencing

The Wizard® genomic purification kit (Promega) was used to extract total DNA from the parental respiratory-deficient mutant W303 *coq10*Δ and from the spontaneous revertant W303 *coq10*rev. The DNA was quantified using the QUBIT DNA™ high-sensitivity assay, and 1 ng of the normalized DNA was tagged by the Nextera XTTM (Illumina) protocol. The libraries were amplified and pooled as described (67). The pooled libraries were subjected to sequencing with the NextSeq™ (Illumina) equipment in the Genome Investigation and Analysis Laboratory of the Institute of Biomedical Sciences at the University of Sao Paulo. The BWA Aligner tool,

version 1.1.4 (Base Space Labs-Illumina), was used to align ~23,000,000 reads obtained from each strain with the reference genomes of *S. cerevisiae*. The alignments were compared using the Integrative Genomics Viewer (Base Space Labs Illumina).

Statistical analyses

All data sets were tested for normality using GraphPad Prism 7 with the Shapiro-Wilk normality test. Because a majority of sets passed the normality test ($\alpha = 0.5$), statistical analyses were performed using GraphPad Prism 7 with parametric one-way analysis of variance correcting for multiple comparisons using Tukey's test, comparing the mean of each sample to the mean of its corresponding WT or empty vector control. The data show the means ± S.D., and the statistical significance as compared with WT or empty vector control is represented by the following: *, $p < 0.05$; **, $p < 0.01$; ***, $p < 0.001$; and ****, $p < 0.0001$. The denotation *ns* indicates values with "not significant" differences from the corresponding control.

Data availability

The MS source data for determination of Q_6 and Q_6 intermediates will be shared upon request. Please contact Catherine Clarke at cathy@chem.ucla.edu. All remaining data are contained within the article.

Author contributions—M. C. B., M. H. B., and C. F. C. conceptualization; M. C. B., J. N., A. A., H. S. T., O. S. S., M. H. B., and C. F. C. resources; M. C. B., K. Y., L. F.-dR., J. N., A. A., H. S. T., N. A. N., M. H. B., and C. F. C. data curation; M. C. B., J. N., A. A., and M. H. B. software; M. C. B., K. Y., L. F.-dR., J. N., A. A., H. S. T., N. A. N., R. S., M. H. B., and C. F. C. formal analysis; M. C. B., R. S., O. S. S., M. H. B., and C. F. C. supervision; M. C. B., J. N., H. S. T., M. H. B., and C. F. C. funding acquisition; M. C. B., K. Y., L. F.-dR., J. N., A. A., H. S. T., R. S., and M. H. B. validation; M. C. B., K. Y., L. F.-dR., J. N., A. A., H. S. T., N. A. N., R. S., M. H. B., and C. F. C. investigation; M. C. B., K. Y., L. F.-dR., J. N., A. A., H. S. T., N. A. N., M. H. B., and C. F. C. visualization; M. C. B., K. Y., L. F.-dR., J. N., A. A., H. S. T., N. A. N., R. S., M. H. B., and C. F. C. methodology; M. C. B. and C. F. C. writing-original draft; M. C. B., R. S., M. H. B., and C. F. C. project administration; M. C. B., K. Y., L. F.-dR., J. N., A. A., H. S. T., N. A. N., R. S., O. S. S., M. H. B., and C. F. C. writing-review and editing.

Acknowledgments—We thank the UCLA Molecular Instrumentation Core proteomics facility and Dr. Yu Chen for the use of the QTRAP4000 for lipid analysis. We thank undergraduate UCLA researcher Hope Ibarra for her contributions in assisting with experiments.

References

1. Turunen, M., Olsson, J., and Dallner, G. (2004) Metabolism and function of coenzyme Q. *Biochim. Biophys. Acta* **1660,** 171–199 CrossRef Medline
2. Alcázar-Fabra, M., Trevisson, E., and Brea-Calvo, G. (2018) Clinical syndromes associated with coenzyme Q_{10} deficiency. *Essays Biochem.* **62,** 377–398 CrossRef Medline
3. Desbats, M. A., Lunardi, G., Doimo, M., Trevisson, E., and Salviati, L. (2015) Genetic bases and clinical manifestations of coenzyme Q_{10} (CoQ 10) deficiency. *J. Inherit. Metab. Dis.* **38,** 145–156 CrossRef Medline
4. Frei, B., Kim, M. C., and Ames, B. N. (1990) Ubiquinol-10 is an effective lipid-soluble antioxidant at physiological concentrations. *Proc. Natl. Acad. Sci. U.S.A.* **87,** 4879–4883 CrossRef Medline
5. Okada, K., Suzuki, K., Kamiya, Y., Zhu, X., Fujisaki, S., Nishimura, Y., Nishino, T., Nakagawa, T., Kawamukai, M., and Matsuda, H. (1996) Polyprenyl diphosphate synthase essentially defines the length of the side chain of ubiquinone. *Biochim. Biophys. Acta* **1302,** 217–223 CrossRef Medline
6. Kawamukai, M. (2016) Biosynthesis of coenzyme Q in eukaryotes. *Biosci. Biotechnol. Biochem.* **80,** 23–33 CrossRef Medline
7. Stefely, J. A., and Pagliarini, D. J. (2017) Biochemistry of mitochondrial coenzyme Q biosynthesis. *Trends Biochem. Sci.* **42,** 824–843 CrossRef Medline
8. Montini, G., Malaventura, C., and Salviati, L. (2008) Early coenzyme Q_{10} supplementation in primary coenzyme Q_{10} deficiency. *N. Engl. J. Med.* **358,** 2849–2850 CrossRef Medline
9. Awad, A. M., Bradley, M. C., Fernández-Del-Río, L., Nag, A., Tsui, H. S., and Clarke, C. F. (2018) Coenzyme Q_{10} deficiencies: pathways in yeast and humans. *Essays Biochem* **62,** 361–376 CrossRef Medline
10. Tran, U. C., Marbois, B., Gin, P., Gulmezian, M., Jonassen, T., and Clarke, C. F. (2006) Complementation of *Saccharomyces cerevisiae coq7* mutants by mitochondrial targeting of the *Escherichia coli* UbiF polypeptide: two functions of yeast Coq7 polypeptide in coenzyme Q biosynthesis. *J. Biol. Chem.* **281,** 16401–16409 CrossRef Medline
11. Marbois, B., Gin, P., Faull, K. F., Poon, W. W., Lee, P. T., Strahan, J., Shepherd, J. N., and Clarke, C. F. (2005) Coq3 and Coq4 define a polypeptide complex in yeast mitochondria for the biosynthesis of coenzyme Q. *J. Biol. Chem.* **280,** 20231–20238 CrossRef Medline
12. Hsieh, E. J., Gin, P., Gulmezian, M., Tran, U. C., Saiki, R., Marbois, B. N., and Clarke, C. F. (2007) *Saccharomyces cerevisiae* Coq9 polypeptide is a subunit of the mitochondrial coenzyme Q biosynthetic complex. *Arch. Biochem. Biophys.* **463,** 19–26 CrossRef Medline
13. He, C. H., Xie, L. X., Allan, C. M., Tran, U. C., and Clarke, C. F. (2014) Coenzyme Q supplementation or overexpression of the yeast Coq8 putative kinase stabilizes multi-subunit Coq polypeptide complexes in yeast *coq* null mutants. *Biochim. Biophys. Acta* **1841,** 630–644 CrossRef Medline
14. Allan, C. M., Awad, A. M., Johnson, J. S., Shirasaki, D. I., Wang, C., Blaby-Haas, C. E., Merchant, S. S., Loo, J. A., and Clarke, C. F. (2015) Identification of Coq11, a new coenzyme Q biosynthetic protein in the CoQ-synthome in *Saccharomyces cerevisiae*. *J. Biol. Chem.* **290,** 7517–7534 CrossRef Medline
15. Marcotte, E. M., Pellegrini, M., Ng, H. L., Rice, D. W., Yeates, T. O., and Eisenberg, D. (1999) Detecting protein function and protein–protein interactions from genome sequences. *Science* **285,** 751–753 CrossRef Medline
16. Perocchi, F., Jensen, L. J., Gagneur, J., Ahting, U., von Mering, C., Bork, P., Prokisch, H., and Steinmetz, L. M. (2006) Assessing systems properties of yeast mitochondria through an interaction map of the organelle. *PLoS Genet.* **2,** e170 CrossRef Medline
17. Allan, C. M., Hill, S., Morvaridi, S., Saiki, R., Johnson, J. S., Liau, W. S., Hirano, K., Kawashima, T., Ji, Z., Loo, J. A., Shepherd, J. N., and Clarke, C. F. (2013) A conserved START domain coenzyme Q-binding polypeptide is required for efficient Q biosynthesis, respiratory electron transport, and antioxidant function in *Saccharomyces cerevisiae*. *Biochim. Biophys. Acta* **1831,** 776–791 CrossRef Medline
18. Barros, M. H., Johnson, A., Gin, P., Marbois, B. N., Clarke, C. F., and Tzagoloff, A. (2005) The *Saccharomyces cerevisiae COQ10* gene encodes a START domain protein required for function of coenzyme Q in respiration. *J. Biol. Chem.* **280,** 42627–42635 CrossRef Medline
19. Tsui, H. S., Pham, N. V. B., Amer, B. R., Bradley, M. C., Gosschalk, J. E., Gallagher-Jones, M., Ibarra, H., Clubb, R. T., Blaby-Haas, C. E., and Clarke, C. F. (2019) Human COQ10A and COQ10B are distinct lipid-binding START domain proteins required for coenzyme Q function. *J. Lipid Res.* **60,** 1293–1310 CrossRef Medline
20. Shen, Y., Goldsmith-Fischman, S., Atreya, H. S., Acton, T., Ma, L., Xiao, R., Honig, B., Montelione, G. T., and Szyperski, T. (2005) NMR structure of the 18 kDa protein CC1736 from *Caulobacter crescentus* identifies a member of the START domain superfamily and suggests residues mediating substrate specificity. *Proteins* **58,** 747–750 CrossRef Medline

21. Cui, T. Z., and Kawamukai, M. (2009) Coq10, a mitochondrial coenzyme Q binding protein, is required for proper respiration in *Schizosaccharomyces pombe*. *FEBS J.* **276,** 748–759 CrossRef Medline
22. Stoldt, S., Wenzel, D., Kehrein, K., Riedel, D., Ott, M., and Jakobs, S. (2018) Spatial orchestration of mitochondrial translation and OXPHOS complex assembly. *Nat. Cell Biol.* **20,** 528–534 CrossRef Medline
23. Eisenberg-Bord, M., Tsui, H. S., Antunes, D., Fernández-Del-Río, L., Bradley, M. C., Dunn, C. D., Nguyen, T. P. T., Rapaport, D., Clarke, C. F., and Schuldiner, M. (2019) The endoplasmic reticulum–mitochondria encounter structure complex coordinates coenzyme Q biosynthesis. *Contact* **2,** 2515256418825409 CrossRef Medline
24. Subramanian, K., Jochem, A., Le Vasseur, M., Lewis, S., Paulson, B. R., Reddy, T. R., Russell, J. D., Coon, J. J., Pagliarini, D. J., and Nunnari, J. (2019) Coenzyme Q biosynthetic proteins assemble in a substrate-dependent manner into domains at ER-mitochondria contacts. *J. Cell Biol.* **218,** 1353–1369 CrossRef Medline
25. Reidenbach, A. G., Kemmerer, Z. A., Aydin, D., Jochem, A., McDevitt, M. T., Hutchins, P. D., Stark, J. L., Stefely, J. A., Reddy, T., Hebert, A. S., Wilkerson, E. M., Johnson, I. E., Bingman, C. A., Markley, J. L., Coon, J. J., *et al.* (2018) Conserved lipid and small-molecule modulation of *COQ8* reveals regulation of the ancient kinase-like UbiB family. *Cell Chem. Biol.* **25,** 154–165.e11 CrossRef Medline
26. Reading, D. S., Hallberg, R. L., and Myers, A. M. (1989) Characterization of the yeast *HSP60* gene coding for a mitochondrial assembly factor. *Nature* **337,** 655–659 CrossRef Medline
27. Fujiki, Y., Hubbard, A. L., Fowler, S., and Lazarow, P. B. (1982) Isolation of intracellular membranes by means of sodium carbonate treatment: application to endoplasmic reticulum. *J. Cell Biol.* **93,** 97–102 CrossRef Medline
28. Chen, W. J., and Douglas, M. G. (1987) Phosphodiester bond cleavage outside mitochondria is required for the completion of protein import into the mitochondrial matrix. *Cell* **49,** 651–658 CrossRef Medline
29. Ohashi, A., Gibson, J., Gregor, I., and Schatz, G. (1982) Import of proteins into mitochondria. The precursor of cytochrome c_1 is processed in two steps, one of them heme-dependent. *J. Biol. Chem.* **257,** 13042–13047 Medline
30. Vögtle, F. N., Burkhart, J. M., Gonczarowska-Jorge, H., Kücükköse, C., Taskin, A. A., Kopczynski, D., Ahrends, R., Mossmann, D., Sickmann, A., Zahedi, R. P., and Meisinger, C. (2017) Landscape of submitochondrial protein distribution. *Nat. Commun.* **8,** 290 CrossRef Medline
31. Yin, H., Xu, L., and Porter, N. A. (2011) Free radical lipid peroxidation: mechanisms and analysis. *Chem. Rev.* **111,** 5944–5972 CrossRef Medline
32. Pryor, W. A., and Porter, N. A. (1990) Suggested mechanisms for the production of 4-hydroxy-2-nonenal from the autoxidation of polyunsaturated fatty acids. *Free Radic. Biol. Med.* **8,** 541–543 CrossRef Medline
33. Heeringa, S. F., Chernin, G., Chaki, M., Zhou, W., Sloan, A. J., Ji, Z., Xie, L. X., Salviati, L., Hurd, T. W., Vega-Warner, V., Killen, P. D., Raphael, Y., Ashraf, S., Ovunc, B., Schoeb, D. S., *et al.* (2011) COQ6 mutations in human patients produce nephrotic syndrome with sensorineural deafness. *J. Clin. Invest.* **121,** 2013–2024 CrossRef Medline
34. Nguyen, T. P., Casarin, A., Desbats, M. A., Doimo, M., Trevisson, E., Santos-Ocaña, C., Navas, P., Clarke, C. F., and Salviati, L. (2014) Molecular characterization of the human COQ5 *C*-methyltransferase in coenzyme Q_{10} biosynthesis. *Biochim. Biophys. Acta* **1841,** 1628–1638 CrossRef Medline
35. Conrad, M., Schothorst, J., Kankipati, H. N., Van Zeebroeck, G., Rubio-Texeira, M., and Thevelein, J. M. (2014) Nutrient sensing and signaling in the yeast *Saccharomyces cerevisiae*. *FEMS Microbiol. Rev.* **38,** 254–299 CrossRef Medline
36. Glick, B. S., and Pon, L. A. (1995) Isolation of highly purified mitochondria from *Saccharomyces cerevisiae*. *Methods Enzymol.* **260,** 213–223 CrossRef Medline
37. Stefely, J. A., Reidenbach, A. G., Ulbrich, A., Oruganty, K., Floyd, B. J., Jochem, A., Saunders, J. M., Johnson, I. E., Minogue, C. E., Wrobel, R. L., Barber, G. E., Lee, D., Li, S., Kannan, N., Coon, J. J., *et al.* (2015) Mitochondrial ADCK3 employs an atypical protein kinase-like fold to enable coenzyme Q biosynthesis. *Mol. Cell* **57,** 83–94 CrossRef Medline
38. Xie, L. X., Hsieh, E. J., Watanabe, S., Allan, C. M., Chen, J. Y., Tran, U. C., and Clarke, C. F. (2011) Expression of the human atypical kinase ADCK3 rescues coenzyme Q biosynthesis and phosphorylation of Coq polypeptides in yeast *coq8* mutants. *Biochim. Biophys. Acta* **1811,** 348–360 CrossRef Medline
39. Xie, L. X., Ozeir, M., Tang, J. Y., Chen, J. Y., Jaquinod, S. K., Fontecave, M., Clarke, C. F., and Pierrel, F. (2012) Overexpression of the Coq8 kinase in *Saccharomyces cerevisiae coq* null mutants allows for accumulation of diagnostic intermediates of the coenzyme Q_6 biosynthetic pathway. *J. Biol. Chem.* **287,** 23571–23581 CrossRef Medline
40. Tran, U. C., and Clarke, C. F. (2007) Endogenous synthesis of coenzyme Q in eukaryotes. *Mitochondrion* **7,** Suppl., S62–S71 CrossRef Medline
41. Wang, Y., and Hekimi, S. (2019) The complexity of making ubiquinone. *Trends Endocrinol. Metab.* **30,** 929–943 CrossRef Medline
42. Murley, A., and Nunnari, J. (2016) The emerging network of mitochondria-organelle contacts. *Mol. Cell* **61,** 648–653 CrossRef Medline
43. Kehrein, K., Möller-Hergt, B. V., and Ott, M. (2015) The MIOREX complex–lean management of mitochondrial gene expression. *Oncotarget* **6,** 16806–16807 CrossRef Medline
44. Fontanesi, F. (2013) Mechanisms of mitochondrial translational regulation. *IUBMB Life* **65,** 397–408 CrossRef Medline
45. Marchler-Bauer, A., Zheng, C., Chitsaz, F., Derbyshire, M. K., Geer, L. Y., Geer, R. C., Gonzales, N. R., Gwadz, M., Hurwitz, D. I., Lanczycki, C. J., Lu, F., Lu, S., Marchler, G. H., Song, J. S., Thanki, N., *et al.* (2013) CDD: conserved domains and protein three-dimensional structure. *Nucleic Acids Res.* **41,** D348–D352 CrossRef Medline
46. Rossmann, M. G., Moras, D., and Olsen, K. W. (1974) Chemical and biological evolution of nucleotide-binding protein. *Nature* **250,** 194–199 CrossRef Medline
47. Kopec, J., Schnell, R., and Schneider, G. (2011) Structure of PA4019, a putative aromatic acid decarboxylase from *Pseudomonas aeruginosa*. *Acta Crystallogr. Sect. F Struct. Biol. Cryst. Commun.* **67,** 1184–1188 CrossRef Medline
48. Guarás, A., Perales-Clemente, E., Calvo, E., Acín-Pérez, R., Loureiro-Lopez, M., Pujol, C., Martínez-Carrascoso, I., Nuñez, E., García-Marqués, F., Rodríguez-Hernández, M. A., Cortés, A., Diaz, F., Pérez-Martos, A., Moraes, C. T., Fernández-Silva, P., *et al.* (2016) The $CoQH_2$/CoQ ratio serves as a sensor of respiratory chain efficiency. *Cell Rep.* **15,** 197–209 CrossRef Medline
49. Scialò, F., Sriram, A., Fernández-Ayala, D., Gubina, N., Lõhmus, M., Nelson, G., Logan, A., Cooper, H. M., Navas, P., Enríquez, J. A., Murphy, M. P., and Sanz, A. (2016) Mitochondrial ROS produced via reverse electron transport extend animal lifespan. *Cell Metab.* **23,** 725–734 CrossRef Medline
50. UniProt Consortium (2018) UniProt: the universal protein knowledgebase. *Nucleic Acids Res.* **46,** 2699 CrossRef Medline
51. Pagliarini, D. J., Calvo, S. E., Chang, B., Sheth, S. A., Vafai, S. B., Ong, S. E., Walford, G. A., Sugiana, C., Boneh, A., Chen, W. K., Hill, D. E., Vidal, M., Evans, J. G., Thorburn, D. R., Carr, S. A., and Mootha, V. K. (2008) A mitochondrial protein compendium elucidates complex I disease biology. *Cell* **134,** 112–123 CrossRef Medline
52. van den Bosch, B. J., Gerards, M., Sluiter, W., Stegmann, A. P., Jongen, E. L., Hellebrekers, D. M., Oegema, R., Lambrichs, E. H., Prokisch, H., Danhauser, K., Schoonderwoerd, K., de Coo, I. F., and Smeets, H. J. (2012) Defective NDUFA9 as a novel cause of neonatally fatal complex I disease. *J. Med. Genet.* **49,** 10–15 CrossRef Medline
53. Brachmann, C. B., Davies, A., Cost, G. J., Caputo, E., Li, J., Hieter, P., and Boeke, J. D. (1998) Designer deletion strains derived from *Saccharomyces cerevisiae* S288C: a useful set of strains and plasmids for PCR-mediated gene disruption and other applications. *Yeast* **14,** 115–132 CrossRef Medline
54. Thomas, B. J., and Rothstein, R. (1989) Elevated recombination rates in transcriptionally active DNA. *Cell* **56,** 619–630 CrossRef Medline
55. Barkovich, R. J., Shtanko, A., Shepherd, J. A., Lee, P. T., Myles, D. C., Tzagoloff, A., and Clarke, C. F. (1997) Characterization of the *COQ5* gene from *Saccharomyces cerevisiae*. Evidence for a *C*-methyltransferase in ubiquinone biosynthesis. *J. Biol. Chem.* **272,** 9182–9188 CrossRef Medline

56. Rothstein, R. J. (1983) One-step gene disruption in yeast. *Methods Enzymol.* **101,** 202–211 CrossRef Medline
57. Gietz, R. D., and Woods, R. A. (2002) Transformation of yeast by lithium acetate/single-stranded carrier DNA/polyethylene glycol method. *Methods Enzymol.* **350,** 87–96 CrossRef Medline
58. Hill, S., Hirano, K., Shmanai, V. V., Marbois, B. N., Vidovic, D., Bekish, A. V., Kay, B., Tse, V., Fine, J., Clarke, C. F., and Shchepinov, M. S. (2011) Isotope-reinforced polyunsaturated fatty acids protect yeast cells from oxidative stress. *Free Radic. Biol. Med.* **50,** 130–138 CrossRef Medline
59. Hill, S., Lamberson, C. R., Xu, L., To, R., Tsui, H. S., Shmanai, V. V., Bekish, A. V., Awad, A. M., Marbois, B. N., Cantor, C. R., Porter, N. A., Clarke, C. F., and Shchepinov, M. S. (2012) Small amounts of isotope-reinforced polyunsaturated fatty acids suppress lipid autoxidation. *Free Radic. Biol. Med.* **53,** 893–906 CrossRef Medline
60. Santos, J. H., Mandavilli, B. S., and Van Houten, B. (2002) Measuring oxidative mtDNA damage and repair using quantitative PCR. *Methods Mol. Biol.* **197,** 159–176 CrossRef Medline
61. Gonzalez-Hunt, C. P., Rooney, J. P., Ryde, I. T., Anbalagan, C., Joglekar, R., and Meyer, J. N. (2016) PCR-based analysis of mitochondrial DNA copy number, mitochondrial DNA damage, and nuclear DNA damage. *Curr. Protoc. Toxicol.* **67,** 20.11.1–20.11.25 CrossRef Medline
62. Guo, X., Niemi, N. M., Hutchins, P. D., Condon, S. G. F., Jochem, A., Ulbrich, A., Higbee, A. J., Russell, J. D., Senes, A., Coon, J. J., and Pagliarini, D. J. (2017) Ptc7p dephosphorylates select mitochondrial proteins to enhance metabolic function. *Cell Rep.* **18,** 307–313 CrossRef Medline
63. Eyer, P., Worek, F., Kiderlen, D., Sinko, G., Stuglin, A., Simeon-Rudolf, V., and Reiner, E. (2003) Molar absorption coefficients for the reduced Ellman reagent: reassessment. *Anal. Biochem.* **312,** 224–227 CrossRef Medline
64. Zhang, T., Lei, J., Yang, H., Xu, K., Wang, R., and Zhang, Z. (2011) An improved method for whole protein extraction from yeast *Saccharomyces cerevisiae*. *Yeast* **28,** 795–798 CrossRef Medline
65. Schägger, H., Cramer, W. A., and von Jagow, G. (1994) Analysis of molecular masses and oligomeric states of protein complexes by blue native electrophoresis and isolation of membrane protein complexes by two-dimensional native electrophoresis. *Anal. Biochem.* **217,** 220–230 CrossRef Medline
66. Wittig, I., Braun, H. P., and Schägger, H. (2006) Blue NativePAGE. *Nat. Protoc.* **1,** 418–428 CrossRef Medline
67. Barros, M. H., and Tzagoloff, A. (2017) Aep3p-dependent translation of yeast mitochondrial *ATP8*. *Mol. Biol. Cell* **28,** 1426–1434 CrossRef Medline
68. Santos-Ocaña, C., Do, T. Q., Padilla, S., Navas, P., and Clarke, C. F. (2002) Uptake of exogenous coenzyme Q and transport to mitochondria is required for bc_1 complex stability in yeast *coq* mutants. *J. Biol. Chem.* **277,** 10973–10981 CrossRef Medline
69. Winzeler, E. A., Shoemaker, D. D., Astromoff, A., Liang, H., Anderson, K., Andre, B., Bangham, R., Benito, R., Boeke, J. D., Bussey, H., Chu, A. M., Connelly, C., Davis, K., Dietrich, F., Dow, S. W., *et al.* (1999) Functional characterization of the *S. cerevisiae* genome by gene deletion and parallel analysis. *Science* **285,** 901–906 CrossRef Medline
70. Sikorski, R. S., and Hieter, P. (1989) A system of shuttle vectors and yeast host strains designed for efficient manipulation of DNA in *Saccharomyces cerevisiae*. *Genetics* **122,** 19–27 Medline
71. Christianson, T. W., Sikorski, R. S., Dante, M., Shero, J. H., and Hieter, P. (1992) Multifunctional yeast high-copy-number shuttle vectors. *Gene* **110,** 119–122 CrossRef Medline

CHAPTER 3

Understanding the role of the uncharacterized polypeptide Coq11 in coenzyme Q biosynthesis

ABSTRACT

Coenzyme Q (ubiquinone or Q_n) is a polyisoprenylated benzoquinone lipid of varying tail length *n*, that is required for several vital cellular functions including bioenergetics, antioxidant defense, and as a co-factor to enzymes participating in pyrimidine biosynthesis and fatty acid β-oxidation. In *Saccharomyces cerevisiae*, a group of proteins work together towards the biosynthesis of Q_6. Several of these Coq proteins interact to form a high-molecular mass complex on the mitochondrial inner member termed the 'CoQ synthome'. Recently, a protein of unknown function, renamed Coq11, was discovered to be essential for efficient *de novo* Q_6 biosynthesis and co-purified with several members of the CoQ synthome. Attempts to elucidate the function of Coq11 have focused on its phylogenetic correlation with Coq10. Here, we present Coq11 protein purification strategies and constructs for Coq11 overexpression in yeast, to characterize its role in Q_6 biosynthesis. These data provide a valuable foundation for future studies clarifying the association of Coq11 with Q_6 biosynthetic pathway.

INTRODUCTION

Coenzyme Q (Q_n) is an essential lipid molecule component of the electron transport chain and serves an important role in cellular antioxidant defense (1). Patients with partial defects in Q biosynthesis suffer from a variety of health issues, including cerebellar ataxia, renal disease, cardiovascular complications, respiratory dysfunction, and neurodegenerative diseases (2-4). The major clinical strategy for treatment of Q_{10} deficiencies involves large scale Q_{10} supplementation, and such treatments have only been partially successful in most cases; however, many patients fail to demonstrate full recovery due to insufficient uptake of Q_{10} (4,5). Further, once severe Q_{10} deficits in the kidney or defects in neurological function occur, they are not reversible, even if Q_{10} supplementation efficacy were to be increased (6). Current efforts to improve Q_{10} therapeutics have been focused improving delivery strategies for Q_{10} (7,8), and developing compounds that enhance endogenous Q_{10} biosynthesis in patients (1,4,9,10). Due to the striking homology between human genes and those of *Saccharomyces cerevisiae*, studies of Q_6 biosynthesis in *S. cerevisiae* may provide insight into human Q_{10} biosynthesis towards the elucidation of potential therapeutic targets.

In *S. cerevisiae*, a cohort of at least fourteen mitochondrial proteins (Coq1-Coq11, Yah1, Arh1, and Hfd1) drive Q_6 biosynthesis (1,4,11). Several of these Coq polypeptides assemble into a multi-subunit CoQ synthome localized to the mitochondrial inner membrane (1). A novel polypeptide encoded by the open reading frame *YLR290C* was recently identified to co-purify with several members of the CoQ synthome (12). Based on this evidence and a requirement of YLR290C for efficient *de novo* Q_6 biosynthesis (12), the protein was renamed ‘Coq11’.

Although it is clear that Coq11 associates with the CoQ synthome, the functional roles, organization, and stoichiometry of Coq11 within the CoQ synthome are not yet understood.

Numerous features of Coq11 and its homologs solidify its link to Q_6 biosynthesis. In several fungal genomes, Coq11 and Coq10 have evolved as fusion proteins (12). When two proteins are encoded as fusions they often exist within the same biological pathway or may directly interact with one another (13). The *coq10*Δ mutant is unique among *coq* mutants because it has decreased *de novo* Q_6 biosynthesis in log phase, yet produces near wild-type concentrations of Q_6 in stationary phase (14,15). The deletion of *COQ10* causes sickly growth on respiratory medium and decreased antioxidant protection by Q_6 indicated by *coq10*Δ sensitivity to lipid peroxidation initiated by exogenously supplemented polyunsaturated fatty acids (PUFAs) (14-16). We have recently demonstrated that respiratory deficiency, sensitivity to lipid peroxidation, and decreased Q_6 biosynthesis of the *coq10*Δ mutant are rescued by deletion of *COQ11 (17)*. Immunoblotting demonstrated that *coq11*Δ yeast accumulate increased amounts of certain Coq polypeptides and possess a stabilized CoQ synthome, that rescues the Coq polypeptides and CoQ synthome decencies of the *coq10*Δ mutant (17). This relationship between Coq10 and Coq11 has implications about the role of Coq11 as a negative modulator of Q_6 biosynthesis within the mitochondria.

Sequence analyses additionally reveal that Coq11 is a member of the atypical short-chain dehydrogenase/reductase (SDR) superfamily of oxidoreductases that catalyze an assortment of reactions including isomerization, decarboxylation, epimerization, imine reduction, and carbonyl-alcohol oxidoreduction (18). SDR superfamily proteins contain a conserved Rossmann fold structural motif used in the binding of nucleotide co-factors such as FAD, FMN, and

NAD(P) (19). The crystal structure of *Pseudomonas aeruginosa* UbiX (PA4019), an enzyme catalyzing the decarboxylation in Q biosynthesis in combination with UbiD, contains a Rossmann fold with a bound FMN (20). The structure of Pad1, a paralog of *E. coli* UbiX with 51% identity, similarly includes a Rossmann fold in complex with FMN (21). Although the crystal structure of Coq11 remains unsolved, perhaps the Rossmann fold in Coq11 analogously catalyzes an FMN-dependent decarboxylation in Q_6 biosynthesis. Intriguingly, the *S. cerevisiae* homologs to UbiX and UbiD, Pad1 and Fdc1, participate in the same chemistry as phenylacrylic acid decarboxylases (22,23). Pad1 and Fdc1 have never been implicated to function specifically as Q_6 biosynthetic decarboxylases thus far, yet it is tempting to suggest that Coq11 may work together with these enzymes inside of the Q_6 biosynthetic pathway.

This study seeks to further understand the enzymatic function of Coq11 using a variety of techniques. We have determined that *coq11* deletion has background specific effects on *de novo* Q_6 production, and that Coq11, Pad1, and Fdc1 are not redundant decarboxylases in Q_6 biosynthesis. We also detail the attempts to over-express and purify Coq11 from *E. coli*; here we describe methods and four distinct constructs, to provide useful information for future purification attempts. Finally, Coq11 overexpression from several different plasmids was found to be intolerable to yeast cells. These results represent crucial steps towards the identification of the function of Coq11.

EXPERIMENTAL PROCEDURES

Yeast strains and growth medium

S. cerevisiae strains used in this study are described in Table 1. Yeast strains were derived from S288C (BY4742; (24)) or W303 (25). Growth media for yeast included YPD (2% glucose, 1% yeast extract, 2% peptone), YPG (3% glycerol, 1% yeast extract, 2% peptone) and YPGal (2% galactose, 1% yeast extract, 2% peptone, 0.1% dextrose) (26). Synthetic Dextrose/Minimal-Complete (SD–Complete) and Synthetic Dextrose/Minimal minus uracil (SD–Ura) (0.18% Difco yeast nitrogen base without amino acids and ammonium sulfate, 0.5% $(NH_4)_2SO_4$, 0.14% NaH_2PO_4, 2% dextrose, complete amino acid supplement, or amino acid supplement lacking uracil) were prepared as described (26). Drop out dextrose (DOD) medium was prepared as described (12). Solid media contained additional 2% Bacto agar.

COQ11 was disrupted in previously created *pad1*Δ*fdc1*Δ double mutants in W303 and BY4742 yeast genetic backgrounds, by the one-step gene replacement method (23,27). The *LEU2* gene from pRS305 was amplified by polymerase chain reaction (PCR), with *COQ11* upstream and downstream flanking sequences using the primers 5'-GGGAAATATGTATCGTATACAAAAATACAGCTAAAGCTTGAACTG-3' and 3'-GTACTTAACTATATACAGCTTGGTATAATTTTAAAATGGTAATAAC-5'. Transformations of PCR products into *pad1*Δ*fdc1*Δ double mutants in W303 and BY4742 yeast cells were performed using the Li-acetate method (28).

Generation of a Coq11 polyclonal antibody

A synthetic peptide-based antigen specific to the *COQ11* ORF, consisting of the amino acid sequence C- KKSKK EQEKA NQRSF –N, was designed by Cocalico Biologicals, Inc. This peptide was injected into two different rabbits a total of four times to elicit an immune response. Following bleed-out, antisera from both rabbits was diluted 1:500 in blocking buffer (0.5% BSA, 0.1% Tween 20, 0.02% SDS in phosphate-buffered saline) and used as a primary antibody against the Coq11 polypeptide (16).

Yeast mitochondria isolation

Yeast cultures were grown overnight in 5 mL of YPD or selection medium to maintain plasmid expression (SD−Ura). All pre-cultures were back-diluted with YPGal and grown overnight at 30 °C with shaking (250 rpm) until cell density reached an $A_{600} \sim 4$. Spheroplasts were prepared with Zymolyase-20T (MP Biomedicals) and fractionated as previously described (29), in the presence of cOmplete™ EDTA-free protease inhibitor cocktail tablets (Roche), phosphatase inhibitor cocktail set I (Sigma-Aldrich), phosphatase inhibitor cocktail set II (Sigma-Aldrich), and PMSF (Fisher Scientific). Nycodenz (Sigma-Aldrich) density gradient purified mitochondria were frozen in liquid nitrogen, aliquoted, and stored at −80 °C until further use. Mitochondria protein concentration was measured by the Bicinchoninic acid (BCA) assay (ThermoFisher Scientific).

SDS-PAGE and immunoblot analyses for Coq11 protein expression

Purified mitochondria (25 μg) were resuspended in SDS sample buffer and separated by SDS gel electrophoresis on 10% or 12% Tris-glycine polyacrylamide gels. Proteins were transferred to a 0.45 μm PVDF membrane (Millipore) and blocked with blocking buffer (0.5% BSA, 0.1% Tween 20, 0.02% SDS in phosphate-buffered saline). Coq11 was probed with its rabbit polyclonal antibody prepared in blocking buffer at a dilution of 1:500 (17). IRDye 680LT goat anti-rabbit IgG secondary antibody (LiCOR) was used at a dilution of 1:10,000. Coq11 was visualized using a LiCOR Odyssey Infrared Scanner (LiCOR).

Cloning of Coq11 and Coq11-tagged constructs for overexpression in bacteria using Gateway

Plasmids used in this study are listed in Table 2. The generation of a Coq11 bacterial overexpression vector for subsequent protein purification and structural characterization was first attempted using the Gateway™ system (Invitrogen). Briefly, the *COQ11* ORF was PCR amplified from yeast genomic DNA using primers 5'-GGGGACAAGTTTGTACAAAAAAGCAGGCTTCgagaatctttattttcagggc**GGCGGGGGCGGG**ATGATACCAAAGCTTATAGTTTTTGGAGGCAATGG-3' and 5'-GGGGACCACTTTGTACAAGAAAGCTGGGTGTCATTATGCTTTAAGTATTTCCTCAAGTGTAACTACCCC-3' into the pDONR221 vector (Invitrogen) with attB1/2 sequences (underlined). The forward primer contains a TEV site (lower case) for cleavage of protein tags, and a glycine linker (bold). Following generation of the entry clone, the gene of interest was recombined into the pDEST17 vector allowing inducible overexpression of 6xHis-tagged Coq11,

HC11 (Invitrogen). HC11 was transformed into DH5α competent *E. coli* cells (ThermoFisher) and single colonies were selected on LB plates with 100 μg/mL ampicillin incubated at 37 °C overnight. Correct clones were confirmed by DNA sequencing (Laragen).

Three additional Coq11 bacterial overexpression constructs were then constructed using Gibson Assembly (NEB). The *COQ11* ORF was PCR amplified from pRS426*COQ11* and cloned into either linearized pETSUMO (ThermoFisher) using the primers

5'-gaggctcacagagaacagattggtggtATGATACCAAAGCTTATAGTTTTTGGAGGC-3' and

3'-cactttgcgccgaataaatacctaagcttgtctttaTTATGCTTTAAGTATTTCCTCAAGTGTAACTA-5' to produce HSC11,

or linearized DCLIC (ThermoFisher) using the primers

5'-gctaaagcttgaactgaagtagaaaATGGGCAGCAGCCATCACCATCATCACCACAG-3' and

3'-ctataagctttggtatcatACCCTGGAAATACAAATTTTCGC-5' to produce HMC11. The pETSUMO vector produces a 6xHis- and SUMO-tagged proteins for overexpression in bacteria. Generation of the DCLIC bacterial coexpression vector was performed by Dr. Lukas Susac in the lab of Professor Juli Feigon UCLA. DCLIC was created by cloning into the pETDuet vector (Sigma Aldrich) from the NcoI and XhoI site, and contains a 6xHis and GFP sequence for dual protein expression with GFP. However, HMC11 contains the *COQ11* ORF including its stop codon to prevent GFP expression. HSC11 was transformed into DH5α competent *E. coli* cells (ThermoFisher) and single colonies were selected on LB plates with 50 μg/mL kanamycin. HMC11 was transformed into DH5α competent *E. coli* cells (ThermoFisher) and single colonies

were selected on LB plates with 100 μg/mL ampicillin incubated at 37 °C overnight. Correct clones were confirmed by DNA sequencing (Laragen).

His-MBP-Coq11-GFP (HMC11GFP) was constructed from HMC11 to allow for the co-expression of Coq11 and GFP. Q5 Site Directed Mutagenesis (NEB) was performed using the HMC11 plasmid with the primers 5'-tttccagggtaaatctcttatcgacgtc-3' and

3'-tacaaattttcTGCTTTAAGTATTTCCTCAAG-5', to mutate the Coq11 STOP codon from TAA to a cleavable TEV site. HMC11GFP was transformed into DH5α competent *E. coli* cells (ThermoFisher) and single colonies were selected on LB plates with 100 μg/mL ampicillin incubated at 37 °C overnight. Successful cloning was confirmed by DNA sequencing (Laragen).

Induction of Coq11 tagged constructs for overexpression in bacteria

Each of the following plasmids, HC11, HSC11, HMC11, and HMC11GFP, was transformed into *E. coli* BL21(DE3) (Invitrogen). The HC11 culture was grown in LB with 100 μg/mL ampicillin at 37 °C to an A_{600} = 0.6-0.8 before expression was induced with β-D thiogalactopyranoside (IPTG). The HSC11, HMC11, and HMC11GFP constructs were grown in M9 minimal media with appropriate selection at 37 °C to an A_{600} = 0.6-0.8, and transferred to 18 °C for 1 h prior to induction with IPTG. Specific expression conditions for each plasmid are listed in Table 3.

Purification of HC11

Induction of protein expression was assessed by taking a sample pre- and post-induction and visualizing eith commission stain prior to initiating each attempt at purification. Induced cells expressing HC11 were harvested by centrifugation at 5,000 × *g* for 10 min at 4 °C and lysed with sonication in lysis buffer (50 mM NaH_2PO_4, pH 8.0, 500 mM NaCl, 10 mM imidazole, 10% glycerol, 1 mM DTT, 0.1% Triton X-100, 1 mM phenylmethylsulfonyl fluoride, Complete EDTA-free protease inhibitor). Cell lysate was centrifuged at 10,000 × *g* for 45 min at 4 °C, at which point the soluble and insoluble fractions were collected separately. The soluble fraction was incubated for 2 h at 4 °C with Ni-NTA resin (Qiagen), pre-equilibrated overnight at 4 °C in 0.1 M NaH_2PO_4, 0.01 M Tris-Cl, 6M Guanidine HCl, pH 8.0. The Ni-NTA bound with protein were loaded into a gravity column, as washed three times with 2 column volumes (CV) of wash buffer (20 mM imidazole in 50 mM NaH_2PO_4, pH 8.0, 300 mM NaCl, 10% glycerol, 1 mM DTT, and 0.1% Triton X-100). Protein was eluted from the Ni-NTA resin twice with 1.5 CV of elution buffer (wash buffer with 500 mM imidazole).

Purification of HSC11 and HMC11

Induced cells expressing either HSC11 or HMC11 were harvested by centrifugation at 5,000 × *g* for 15 min at 4 °C. Pellets were resuspended in lysis buffer (50 mM Tris, 30 mM NaCl, 3 mM NaN_3, 30 mM imidazole, 10% glycerol, 0.1% Triton X-100), supplemented with lysozyme, and lysed by sonication. Lysates were clarified by ultracentrifugation 25,000 × *g* for 1 h at 4 °C, filtered, and the supernatant was applied to the Ni sepharose affinity column (HisTrap HP; GE Healthcare) by the AKTA purification system (GE Healthcare). Prior to application of

the supernatant, the column was flushed with 5 CV dH_2O followed by 5 CV wash buffer (50 mM Tris pH 7.5, 5% glycerol, 1 M NaCl, 1 mM TCEP, 30 mM imidazole, 3 mM NaN_3) with a flow rate of 5 mL/min. The soluble sample was purified using 5 CV of wash buffer and eluted from the column with 5 CV of elution buffer (wash buffer supplemented with 300 mM imidazole). About 1 mL of the eluate was collected based on the UV absorbance of the sample to ensure the protein of interest was not diluted with excess buffer.

Purification of HMC11GFP

Induced cells expressing HSC11GFP were purified using a Ni sepharose affinity column (HisTrap HP; GE Healthcare) by the AKTA purification system (GE Healthcare), as described above. The eluates of HSC11GFP that showed visible signs of full-length protein expression, fluorescing a green color, were pooled and concentrated with Amicon (Sigma). Concentrated samples were further purified by size exclusion chromatography (SEC; HiLoad 26/600 Superdex 75; GE Healthcare). The protein peak concentrations were measured.

Analysis of Q_6 and Q_6-intermediates

Yeast cultures were grown overnight in 25 mL of YPD. Cultures were diluted into triplicates of 6 mL fresh medium to $A_{600} = 0.5$, and 5 mL were harvested by centrifugation once they reached $A_{600} \sim 4$. The cell density was recorded at the time of harvest, and cell pellets were stored at −20 °C. Following collection, frozen cell pellets were lipid extracted in the presence of the internal standard Q_4 and analyzed for Q_6 and Q_6-intermediates by LC-MS/MS as described

(16). Standards of Q_6 and Q_4 were obtained from Avanti Polar Lipids and Sigma-Aldrich, respectively.

Stable isotope labeling for determination of *de novo* Q_6 and Q_6-intermediates

Yeast cultures were grown overnight in 25 mL of YPD, DOD, or selection (SD−Complete or SD−Ura) for strains harboring plasmids. Cultures were diluted in triplicates of 6 mL fresh medium to an $A_{600} = 0.1$. Cultures were incubated until they reached an $A_{600} \sim 0.5$, at which point ethanol vehicle control (0.1% vol/vol) or 5 μg/mL of the stable isotope $^{13}C_6$-4HB (Cambridge Isotope Laboratories, Inc.) was added. Cultures were allowed to grow over a period of 5 h, and at each hour time point (including 0 h) 5 mL of each culture was harvested by centrifugation, cell culture density was recorded, and pellets were stored at −20 °C. Cell pellets were lipid extracted in the presence of the Q_4 internal standard and analyzed by LC-MS/MS as described (16).

Construction of high-copy *COQ11* yeast expression vectors

Two high-copy *COQ11* containing plasmids were constructed using the pRS426 high-copy empty vector. The *COQ11* open reading frame and regions corresponding to 842 bp upstream and 256 bp downstream, or the reverse of this sequence, were PCR amplified from BY4742 yeast and cloned into pRS426 using Gibson Assembly (NEB). Primers were designed using SnapGene (GSL Biotech, LLC). Clones were sequenced by Laragen, and successful clones, along with the corresponding empty vector (pRS426) control, were transformed into wild type and mutant yeast as described (30).

RESULTS

The Coq11 polypeptide is detectable by a new Coq11 polyclonal antibody

Coq polypeptides serve important enzymatic roles in Q_6 biosynthesis and are crucial for appropriate CoQ synthome formation (1,4). Deletion of certain *COQ* genes results in destabilization of other Coq polypeptides, highlighting the functional relationship between Coq proteins (31). Detection of Coq polypeptide levels is typically accomplished via immunoblotting and use of primary antibodies against the protein of interest. Upon its identification as a member of the CoQ synthome, Coq11 protein levels could only be probed indirectly using antibodies to a tagged Coq11 isoform (12). Here, we have generated a novel Coq11 polyclonal antibody using a synthetic peptide-antigen to a unique sequence in the *COQ11* ORF (Fig. 1A). Antisera were diluted 1:500 in SDS-PAGE blocking buffer, and evaluated for its ability to detect Coq11.

In wild-type yeast mitochondria Coq11 migrated at about 32 kDa (Fig. 1B). The antisera consistently detected a doublet of bands at this molecular weight, and therefore *coq11*Δ mitochondria were included as a control to ensure the correct band corresponding to Coq11 was detected. Mitochondria prepared from *coq11*Δ showed a disappearance of the lower doublet band, while Coq11-CNAP showed a slight upward shift of the Coq11 band, indicated by the red arrow, corresponding to ~ 3 kDa increase in molecular weight due to the integrated protein tag (Fig. 1B). The absent Coq11 polypeptide in the *coq11*Δ mutant was restored in yeast *coq11*Δ cell expressing the lc*COQ11* plasmid (Fig. 1B). These data demonstrate that the new Coq11 antibody is capable of detecting Coq11 protein expression in yeast mitochondria.

Coq11 purification from *E. coli* for subsequent enzymatic and structural characterization remains challenging

Although it is clear that Coq11 associates with the CoQ synthome and is required for efficient Q_6 biosynthesis, the functional role of Coq11 within the Q_6 biosynthetic pathway has yet to be realized (12). Sequence analyses revealed Coq11 as a member of the SDR superfamily of oxidoreductases, which catalyze a variety of enzymatic reactions including isomerization, decarboxylation, epimerization, imine reduction, and carbonyl-alcohol oxidoreduction (12,18). SDR superfamily proteins possess a conserved Rossmann fold used in the binding of nucleotide co-factors that assist in enzymatic reactions (19). In order to perform Coq11 enzymatic activity assays, structurally characterize the protein, and identify any bound co-factors, we have attempted to overexpress and purify Coq11 from *E. coli*.

Coq11 was initially tagged with a 6xHis motif (HC11) on its N-terminus (Fig. 2A). This vector was tested for expression induction at different temperatures with varying concentrations of IPTG (Fig. 2B). A strong band corresponding to HC11 expression appeared at 34 kDa with induction using 4 mM IPTG at 37 °C for 2 h. However, only a small portion of the total HC11 resided in the soluble fraction following cell lysis by sonication (Fig. 2C). The soluble fraction was loaded onto Ni-NTA resin and purification of HC11 was performed with a gravity column (Fig. 2D). Several impurities remained following the purification, which were visualized in the eluate (E) lane (Fig. 2D).

Often, creating a protein fusion with small ubiquitin-related modifier (SUMO) or maltose-binding protein (MBP) in combination with 6xHis may increase protein solubility and overall yield of purified protein product (32). Due to loss of HC11 in the insoluble fraction and

difficulties isolating the protein with a simple purification workflow, both His-SUMO-Coq11 (HSC11) and His-MBP-Coq11 (HMC11) were generated to improve protein solubility and production (Fig. 3A,C). Optimal induction conditions for both constructs were evaluated and each was purified using the AKTA purification system (Fig. 3B, D). Because HSC11 was almost entirely insoluble purification was not successful (Fig. 3B). A portion of HMC11 was present in the soluble fraction of the lysate, and had a low recovery in the eluate following purification (Fig. 3D). There was also a considerable amount of suspected protein truncation products and contamination in the eluate of HMC11, encompassing the multiple bands below the band of interest (Fig. 3D). We hypothesize that protein truncation occurred because of the high levels of HMC11 expression triggering the *E. coli* to degrade the protein. Alternatively, degradation could be happening during the purification itself.

To distinguish full-length HMC11 from degradation products, a new construct was created to produce a read-through Coq11 protein fusion with green fluorescent protein (HMC11GFP) (Fig. 4A). This novel co-expression plasmid fluoresced a green color only when a full protein is produced. Expression induction gave a cell pellet with a distinctly green color (Fig. 4B). The cell pellet was lysed by sonication and the soluble fraction was purified using the AKTA purification system (Fig. 4C). Despite the presence of several assumed degradation products in the eluate, there was a prevalent band at the expected molecular weight for HMC11GFP (~ 103 kDa) (Fig. 4C). Eluates were pooled, run on a size-exclusion column (SEC), and several fractions were evaluated for the presence of HMC11GFP (Fig. 4D).

Because fractions 10-32 had varying levels of green fluorescence, an aliquot of every-other fraction in this range was visualized using SDS-PAGE (Fig. 4D). Fractions 10-18 were

slightly green, 20-22 were not very green, while 28-32 were extremely green. Based on UV-analysis of each of these fractions, it seems that 28-32 contain solely GFP with a strong 395 nm absorbance (data not shown). The most predominant band in these fractions has a molecular weight of ~ 27 kDa, corresponding to GFP (Fig. 4D). While fractions 10 and 12 also have a large 395 nm absorbance, the levels become incrementally lower in fractions 14-22 (data not shown).

This information nicely reflects the results depicted in Fig. 4D. The full-length HMC11GFP is present in the upper band in fractions 10-22 (Fig. 4D). The band is steadily decreasing with increasing fraction number, mirroring the decrease in GFP absorbance in these fractions. We suspect that the most prominent band in fractions 14-20 corresponds to a truncated version of the full-length HMC11GFP that is being degraded from the C-terminus (Fig. 4D), therefore missing GFP and not producing a strong green color nor exhibiting typical GFP UV-absorbance. This band also may contain N-terminal truncation products missing MBP. Although this construct appears to provide the most promising Coq11 purification products, there is still significant work needed in order to have a product pure enough for enzymatic assay and/or structural studies. It should be noted that the expression from each construct has not yet been tested on protein extracts using the Coq11 antibody.

Deletion of *COQ11* has a greater effect on *de novo* Q_6 biosynthesis in the BY4742 genetic background compared to the W303 genetic background

Previous work determined that *coq11*Δ mutants produce significantly less *de novo* Q_6 compared to wild type in the *S. cerevisiae* BY4741 genetic background (12). In the same study, Coq11-CNAP in W303 yeast was found to associate with several Coq polypeptides components

of the CoQ synthome (12). It is important to investigate the role of genes in multiple genetic backgrounds of yeast because the strains differ greatly—Coq11 may be required for proper Q biosynthesis in one background but not in the other (1). In order to confirm the requirement of Coq11 in Q_6 biosynthesis in both BY4742 and W303, whole cell *de novo* synthesized $^{13}C_6$-Q_6 and ^{12}C-Q_6 were measured in *coq11*Δ mutants in each genetic background by feeding the quinone ring-labeled precursor, $^{13}C_6$-4HB (Fig. 5). These analyses were performed in the minimal drop-out dextrose (DOD) media to match the conditions of the published results (12).

Consistent with prior results (12,17), the *coq11*Δ BY4742 mutant produced significantly decreased *de novo* synthesized $^{13}C_6$-Q_6 and ^{12}C-Q_6 compared to wild type (Fig. 5D,E). The *coq11*Δ mutant in the BY4742 genetic background also had lower total Q_6 content ($^{13}C_6$-Q_6 + ^{12}C-Q_6) than wild type (Fig. 5F). In contrast, the *coq11*Δ W303 mutant produced only slightly *de novo* synthesized $^{13}C_6$-Q_6 and ^{12}C-Q_6 compared to wild type, often not to a level of significance (Fig. 5A,B). Total Q_6 content ($^{13}C_6$-Q_6 + ^{12}C-Q_6) was not significantly lower in *coq11*Δ compared to wild type (Fig. 5C). These results demonstrate that there are significant genetic background differences in the role of Coq11 in Q_6 biosynthesis. Perhaps there is a Coq11 redundancy in W303 that is not present in BY4742, or W303 may simply be a more robust background than BY4742.

Coq11 is not a redundant decarboxylase to Pad1 and Fdc1

The challenges with Coq11 purification coupled with its background specific effects on Q_6 biosynthesis has made Coq11 characterization difficult. As mentioned previously, one potential function of Coq11 lies in its sequence similarities with the SDR superfamily of proteins

that contain a Rossmann fold used to catalyze a variety of enzymatic reactions (12). It is possible that Coq11 may use its Rossmann fold to catalyze an FMN-dependent decarboxylation reaction in Q_6 biosynthesis. The production of small amounts of Q_6 in *coq11*Δ mutants suggests that there may be redundant decarboxylases in the Q_6 biosynthetic pathway capable of bypassing Coq11 (Fig. 5). We hypothesized that these enzymes might be Pad1 and Fdc1, two phenylacrylic acid decarboxylases with homology to the *E. coli* Q_8 biosynthetic decarboxylases UbiD and UbiX (Fig. 6A) (22,33).

It has been previously shown that *pad1*Δ, *fdc1*Δ, and *pad1*Δ*fdc1*Δ mutants all contain normal Q_6 levels in *S. cerevisiae* W303 and YPH499 (23,34). A *pad1*Δ*fdc1*Δ*coq11*Δ triple mutant was generated in both W303 and BY4742 yeast and *de novo* Q_6 production was determined to assess whether Pad1, Fdc1, and Coq11 are redundant decarboxylases in Q_6 biosynthesis (Fig. 6 and Fig. 7). The *pad1*Δ*fdc1*Δ BY4742 mutant produced slightly decreased *de novo* synthesized $^{13}C_6$-Q_6 and ^{12}C-Q_6 compared to wild type over five hours (Fig. 6B,C). The inconsistency with prior results may be explained by the use of minimal media here compared with rich media, and the background differences in BY4742 yeast (23). Although *coq11*Δ BY4742 had significantly decreased *de novo* synthesized $^{13}C_6$-Q_6 and ^{12}C-Q_6 compared to wild type over five hours, the *pad1*Δ*fdc1*Δ*coq11*Δ BY4742 triple mutant had intermediate *de novo* synthesized $^{13}C_6$-Q_6 and ^{12}C-Q_6 to *coq11*Δ and *pad1*Δ*fdc1*Δ (Fig. 6B,C). There was similar trend of *pad1*Δ*fdc1*Δ*coq11*Δ BY4742 intermediate total Q_6 content ($^{13}C_6$-Q_6 + ^{12}C-Q_6) (Fig. 6D).

Due to the minimal effect of *COQ11* deletion on W303 Q_6 biosynthesis (Fig. 5), additional experiments were conducted with a *pad1*Δ*fdc1*Δ*coq11*Δ W303 triple mutant to complement the results in the BY4742 genetic background (Fig. 7). Consistent with previous

results (23), *pad1*Δ*fdc1*Δ W303 produced a similar amount *de novo* synthesized $^{13}C_6$-Q_6 and ^{12}C-Q_6 compared to wild type over five hours (Fig. 7A,B). Because the *coq11*Δ W303 mutant had no difference in *de novo* synthesized $^{13}C_6$-Q_6 and ^{12}C-Q_6 compared to wild type over five hours (Fig. 7A,B), the *pad1*Δ*fdc1*Δ*coq11*Δ BY4742 triple mutant also produced similar *de novo* synthesized $^{13}C_6$-Q_6 and ^{12}C-Q_6 to *coq11*Δ, *pad1*Δ*fdc1*Δ, and wild type (Fig. 7A,B). There was also no difference between the W303 mutants and wild type total Q_6 content ($^{13}C_6$-Q_6 + ^{12}C-Q_6) (Fig. 7C). Ultimately, these results demonstrate that Coq11, Pad1, and Fdc1 are not redundant decarboxylases within the Q_6 biosynthetic pathway, or there is yet another redundant decarboxylase involved in this step of Q_6 synthesis.

Coq11 overexpression in the *coq11*Δ mutant has been unsuccessful

Coq11 has been effectively expressed on a low copy plasmid (lc*COQ11*, Fig. 1B), and was shown to rescue *de novo* Q_6 biosynthesis in *coq11*Δ mutant yeast (17). Because the deletion of *COQ11* is beneficial to the mitochondria causing increased amounts of several key Coq polypeptides, a stabilized CoQ synthome, and increased respiration and mitochondrial Q_6 content in the context of a *coq11*Δ mutant (17), we hypothesized that Coq11 overexpression might be detrimental to the cell. Coq11 was overexpressed using the pRS426 vector and transformed into *coq11*Δ yeast (pRS426*COQ11*) along with the empty vector control (pRS426) (Table 2). Whole cell *de novo* synthesized $^{13}C_6$-Q_6 and ^{12}C-Q_6 were measured in the *coq11*Δ mutant or wild type cells expressing either empty vector or pRS426*COQ11* (Fig. 8A,B). Total Q_6 content ($^{13}C_6$-Q_6 + ^{12}C-Q_6) was not rescued in *coq11*Δ expressing pRS426*COQ11* versus *coq11*Δ harboring the

empty vector (Fig. 8A). Yet, mitochondria purified from *coq11*Δ + pRS426*COQ11* yeast had no detectable amounts of Coq11 protein (Fig. 8B).

In an attempt to truly overexpress Coq11, the same DNA sequence of *COQ11* from pRS426*COQ11* was cloned into pRS426 again, but in the reverse direction to produce pRS426*COQ11rev* (Table 2). Again, total Q_6 content ($^{13}C_6$-Q_6 + ^{12}C-Q_6) was not rescued in *coq11*Δ expressing pRS426*COQ11rev* (Fig. 8C) while mitochondria purified from *coq11*Δ + pRS426*COQ11rev* yeast also had no detectable amounts of Coq11 protein (Fig. 8D). Based on this data, Coq11 appears to be toxic to cells at high levels, causing it to be quickly degraded. Another explanation for these results is that Coq11 expression from this plasmid requires key regulatory elements that are outside of the cloned region.

Coq11 overexpression no effect on Q_6 content in wild-type yeast

Several Coq11 yeast expression constructs were generated and used to transform W303 yeast (Table 2, Fig. 9A): Integrated low copy Coq11 under control of its own promoter (p*COQ11*/ST1), high copy Coq11 under control of its own promoter (p*COQ11*/ST3), and integrated under control of the Gal promoter (pGal/*COQ11*). Whole cells expressing each plasmid showed no difference in Q_6 amount compared to wild type (Fig. 9B). While the pGal/*COQ11* strain did show high Coq11 protein levels, the majority of the strains showed no marked increase in Coq11 expression (Fig. 9C), as seen in overexpression attempts using the pRS426 vector (Fig. 8B, D). It will be interesting to determine how Coq11 overexpression from integrated pGal/*COQ11* effects Coq11 protein levels and Q_6 content in the *coq11*Δ mutant.

DISCUSSION & FUTURE DIRECTIONS

Genetic and biochemical experiments have recently determined that Coq11 associates with the CoQ synthome and is required for efficient *de novo* Q_6 biosynthesis (12). Here, we present several strategies to characterize the specific role of Coq11 within the Q_6 biosynthetic pathway. A polyclonal antibody has been developed that precisely recognizes epitopes on the Coq11 polypeptide (Fig. 1). This antibody has thus far been used to localize Coq11 within a discrete mitochondrial sub-compartment, determine protein levels in various mutants, and map the position of Coq11 within high molecular weight complexes (16,17). Future studies will have the capacity to show how Coq11 protein is effected in different strains and conditions.

Allan *et. al* discovered that Coq11 co-purifies with several Coq polypeptides in W303 yeast, yet experiments regarding the necessity of Coq11 for efficient *de novo* Q_6 biosynthesis were performed in BY4741 yeast (12). In fact, deletion of *COQ11* causes a greater defect in Q_6 biosynthesis in BY472 yeast compared with W303 yeast (Fig. 5). *S. cerevisiae* lab strains of different genetic backgrounds often vary in crucial properties including cell size, cell volume, robustness of growth on non-fermentable medium, salt tolerance, plasma membrane potential, and mitochondrial respiratory activity (17,35,36). Although Coq11 associates with the Q_6 biosynthetic machinery in W303, it appears to have a less direct role in the production of Q_6 in this genetic background. One explanation for this observation is that the robustness of the W303 strain outcompetes the effects of *coq11* deletion on W303 Q_6 biosynthesis. The *coq11*Δ BY4742 mutant may be unable to efficiently synthesize Q_6 due to an unknown catalytic, structural, or

transportation role Coq11 plays. However, this role is not a vital in W303, perhaps because this background is able to compensate for the loss of the Coq11 polypeptide via other proteins or another form of regulation, despite both BY4742 and W303 having identical *COQ11* genetic sequences. This is consistent with previous findings indicating that absence of *COQ11* is beneficial for cellular respiration, and increases the stability of several Coq polypeptides and overall CoQ synthome formation, in the context of a *coq10*Δ BY4742 mutant (17). If Coq11 is a negative regulator of Q_6, it follows that its deletion would not provide further benefits in a more vigorous cell line such as W303. We thus recommend continuing studies of Coq11 use the BY4742 yeast genetic background. Additionally, it may be interesting to study Coq11 in other yeast genetic backgrounds where its requirement in Q_6 biosynthesis has yet to be studied, including JM46 and CEN.PK.

Coq11 resides in a protein cluster defined largely by taxonomy with the SDR superfamily of proteins (12). This diverse family of oxidoreductases typically contain a conserved Rossmann fold that is used to bind nucleotide cofactors and carry out enzymatic reactions, including decarboxylations (19). Intriguingly, no enzyme is currently associated with the catalysis of the decarboxylation step in Q_6 biosynthesis. Coq11 overexpression and purification was carried out to reveal whether it possessed a conserved Rossmann fold capable of carrying out the decarboxylation of Q_6-intermediates and driving Q_6 biosynthesis (Figs. 2, 3 & 4). These purifications schemes have utilized various protein fusion tags including 6xHis, SUMO, MBP, and GFP. In each case, solubility of the fusion proteins overexpressed in *E. coli* has presented challenges. Coq11 has been previously localized as a mitochondrial inner membrane protein,

facing the matrix side (17). Coq11 mitochondrial membrane localization, in addition to the low abundance of Coq polypeptides, are potential explanations for Coq11 purification difficulties.

The most promising candidate for Coq11 purification from *E. coli* seems to be the 6xHis-MBP-Coq11-GFP (HMC11GFP) construct (Fig. 4). Full-length Coq11 was distinguished from truncation products, resulting from degradation during the purification process, using a GFP fusion protein that only fluoresced in the presence of read-through Coq11. However, there were still significant degradation contamination products present following SEC of the purified protein mixture (Fig. 4D). These degradation products need to be confirmed via immunoblotting with the Coq11 antibody. Future HMC11GFP purification strategies will include TEV cleavage from the two TEV sites within the fusion protein—following the 6xHis-MBP tag on the Coq11 N-terminus and preceding the GFP on the Coq11 C-terminus, with TEV protease applied only to SEC fractions most likely to contain HMC11GFP. Reverse immobilized-metal affinity chromatography (IMAC) may then be used on the cleavage product to isolate purified Coq11 from the severed fusion tags. Alternative purification attempts may be conducted using Coq11 overexpression constructs directly in yeast or other organisms, where the protein could be more stable than when it is expressed from *E. coli*.

Phylogenetic analyses suggest that Coq11 may use its Rossmann fold to catalyze decarboxylation in yeast Q_6 biosynthesis (12). The difficulties encountered during Coq11 purification shifted our focus from direct decarboxylation studies to evaluating Q_6 production of various mutants in the absence of *COQ11*. We hypothesized that Coq11 may work in conjunction with the phenylacrylic acid decarboxylases Pad1 and Fdc1 to perform FMN-dependent decarboxylation (Figs. 6 & 7), similar to the reaction mechanism of UbiX and UbiD

in *E. coli* Q_6 biosynthesis (22,34,37). Despite a clear decrease compared to wild type, there was still some level of *de novo* Q_6 biosynthesis in the *pad1*Δ*fdc1*Δ*coq11*Δ BY4742 triple mutant (Fig. 6). Pad1 and Fdc1 work cooperatively outside of the Q_6 synthetic pathway to increase cinnamic acid, ferulic acid, para-coumaric acid and caffeinic acid decarboxylase activity in *S. cerevisiae* (38). Perhaps these proteins and Coq11 play an ancillary role to modify alternative Q_6 ring-precursors that feed into the pathway, including para-coumarate (1,39). This theory parallels the observation that the *pad1*Δ*fdc1*Δ*coq11*Δ BY4742 triple mutant has increased total Q_6 compared the *coq11*Δ BY4742 single mutant (Fig. 6). In the absence of Pad1 and Fdc1, the cell is required to push through the more efficient route to Q_6 biosynthesis using a distinct 4-HB precursor (1), resulting in increased *de novo* Q_6 biosynthesis. Alternatively, Pad1 and Fdc1 may not partake in any facet of Q_6 production, and Coq11 could have a relationship with an additional redundant decarboxylase that supplements its function. This is not completely consistent, however, with data showing that Pad1 expression from a plasmid complements the *E. coli ubix* mutant (34). Fdc1 has not yet been tested for its ability to rescue the *E. coli ubiD* mutant and these experiments will be the subject of future work.

Another possible functional role of Coq11 relates to the recent finding that Coq11 is a negative modulator of Q_6 production (17). Expression of single-copy Coq11 on a plasmid rescued Coq11 protein expression and *de novo* Q_6 production in a *coq11*Δ mutant (17). In contrast, several attempts at Coq11 overexpression from a plasmid have proved unsuccessful rescuing Q_6 production or Coq11 protein expression, other than pGAL/*COQ11* showing prominent overexpression in wild-type cells (Figs. 8 & 9). The pGAL/*COQ11* construct has not yet been tested for its ability to restore Q_6 biosynthesis or Coq11 protein expression in a *coq11*Δ

mutant. Absence of Coq11 protein signal in Coq11 most overexpression conditions suggests one of three options, 1) the plasmids were missing regulatory features that are required for proper Coq11 expression, 2) Coq11 overexpression is toxic and therefore the cell is quickly degrading it, or 3) high-copy Coq11 is exerting a dominant negative effect. The first explanation seems unlikely since the exact same nucleotide sequence was used for Coq11 single-copy expression on pRS316, and produced a strong Coq11 signal (17). Upcoming experiments will employ alternative overexpression plasmids and use DNA sequences with larger flanking regions surrounding the *COQ11* ORF, to further rule out this possibly. Alternatively, it would be interesting to clone only the *COQ11* ORF into the pRCM vector where it would be under control of the CYC1 promoter, and properly imported into the mitochondria via the Coq3 mitochondrial leader sequence (40).

Formation of the CoQ synthome is a delicate process that may be disrupted by deletion of certain Coq polypeptides and other proteins (15,16,31,41), or stabilized by overexpression of other Coq polypeptides (42,43). If high levels of Coq11 are toxic to the cell and degraded immediately, or if Coq11 overexpression is dominant negative, the CoQ synthome will be dysregulated. The observation that *coq11*Δ + various *COQ11* overexpression plasmids still produce low levels of Q_6 is not consistent with this theory (Figs. 8 & 9); however, there may be compensatory mechanisms at work that allow minor amounts of CoQ synthome formation and Q_6 production, prior to degradation. The findings presented here demonstrate that while progress has been made towards characterization of Coq11 function, stoichiometry, and protein partners within the Q_6 biosynthetic pathway, there are still important studies to be performed.

Table 1. Genotype and source of yeast and *E. coli* strains.

Strain	*Genotype/Specifications*	*Source*
S. cerevisiae		
W303-1B	MAT α *ade2-1 his3-1,15 leu2-3,112trp1-1 ura3-1*	R. Rothstein[a]
BY4742	MAT α *his3Δ0 leu2Δ0 met15Δ0 ura3Δ0*	(24)
JM6	*MAT a his-4* ρ^0	(44)
JM8	*MAT α ade-1* ρ^0	(44)
BY4742 *coq11*Δ	MAT α *his3Δ0 leu2Δ0 met15Δ0 ura3Δ0 coq11::LEU2*	This work
BY4742 *pad1*Δ*fdc1*Δ	MAT α *his3Δ0 leu2Δ0 met15Δ0 ura3Δ0 pad1::HIS5 fdc1::HIS5*	(23)
BY4742 *coq11*Δ*pad1*Δ*fdc1*Δ	MAT α *his3Δ0 leu2Δ0 met15Δ0 ura3Δ0 coq11::LEU2 pad1::HIS5 fdc1::HIS5*	This work
W303 *coq11*Δ	MAT α *ade2-1 his3-1,15 leu2-3,112trp1-1 ura3-1 coq11::LEU2*	This work
W303 Coq11-CNAP	MAT **a** *ade2-1 his3-1,15 leu2-3,112 trp1-1 ura3-1 coq11*::*COQ11-CNAP-HIS3*	(12)
W303 *pad1*Δ*fdc1*Δ	MAT α *ade2-1 his3-1,15 leu2-3,112trp1-1 ura3-1 pad1::HIS5 fdc1::HIS5*	(23)

Table 1. Genotype and source of yeast and *E. coli* strains. (Cont.)

Strain	*Genotype/Specifications*	*Source*
W303 *coq11Δpad1Δfdc1Δ*	MAT α *ade2-1 his3-1,15 leu2-3,112trp1-1 ura3-1 coq11::LEU2 pad1::HIS5 fdc1::HIS5*	This work
E. coli		
BL21(DE3)	One Shot™ BL21(DE3) Chemically Competent	Invitrogen
DH5α	Subcloning Efficiency™ DH5α Competent Cells	ThermoFisher

[a]Dr. Rodney Rothstein. Department of Human Genetics, Columbia University.

Table 2. Yeast and bacterial expression vectors.

Plasmid	*Genotype/Specifications*	*Source*
lc*COQ11*	Yeast shuttle vector pRS316 with yeast *COQ11*; low-copy	(17)
pRS426	Yeast shuttle vector; multi-copy	(45)
pRS246*COQ11*	Yeast shuttle vector pRS426 with yeast *COQ11*; high-copy	This work
pRS426*COQ11rev*	Yeast shuttle vector pRS426 with reverse yeast *COQ11*; high-copy	This work
pDEST17	Bacteria Gateway™ destination vector; Inducible overexpression of 6xHis-tagged proteins	J. Torres[b]
HC11	Bacterial vector pDEST17 with yeast *COQ11*	This work
DCLIC	Bacterial coexpression vector with GFP; Created by cloning into pETDuet vector (EMD Biosciences) from NcoI and XhoI sites	J. Feigon[c]
HSC11	Bacterial expression vector pETSUMO with His_6-SUMO-*COQ11*	This work
HMC11	Bacterial coexpresison vector DCLIC with His_6-MBP-*COQ11*	This work

Table 2. Yeast and bacterial expression vectors. (Cont.)

Plasmid	*Genotype/Specifications*	*Source*
HMC11GFP	Bacterial coexpresison vector DCLIC with His_6-MBP-*COQ11*-GFP	This work
p*COQ11*/ST1	Yeast shuttle vector Ylp352 with yeast *COQ11*; low-copy	M. Barros[d]
p*COQ11*/ST3	Yeast shuttle vector YEp352 with yeast *COQ11*; high-copy	M. Barros[d]
pGal/*COQ11*	Yeast shuttle vector Ylp351-GAL with yeast *COQ11*; high-copy	M. Barros[d]
pDONR221	Gateway™ entry vector	J. Torres[b]
pETSUMO	Bacterial vector for inducible expression of N-terminally 6xHis- and SUMO-tagged proteins	J. Feigon[c]

[b]Dr. Jorge Torres. Department of Chemistry & Biochemistry, UCLA.

[c]Dr. Juli Feigon. Department of Chemistry & Biochemistry, UCLA.

[d]Dr. Mario Barros. Departamento Microbiologia, Universidade de São Paulo.

Table 3. Final expression induction conditions for indicated bacterial Coq11 plasmids.

Plasmid	*[IPTG]*	*Temperature*	*Length (time)*
HC11	4 mM	37 °C	2 h
HSC11	0.5 mM	18 °C	18 h
HMC11	0.5 mM	18 °C	18 h
HMC11GFP	0.5 mM	18 °C	18 h

FIGURES

Figure 1. A polyclonal Coq11 antibody is able to detect the Coq11 polypeptide in isolated mitochondria (17). *A*, A synthetic peptide-antigen corresponding to a segment of the Coq11 polypeptide was injected into rabbits for the production of a polyclonal antibody. Following several injections, antisera was received and tested for its ability to detect the Coq11 protein in yeast. *B*, Aliquots of purified mitochondria (25 μg) isolated from wild type, Coq11-CNAP, *coq11*Δ, and *coq11*Δ + lc*COQ11* were separated on a 10% Tris-Glycine SDS-PAGE gel to determine whether the new Coq11 antisera was able to detect the presence of Coq11. The position of Coq11 (32 kDa) and Coq11-CNAP (35 kDa) are indicated by black and red arrows, respectively.

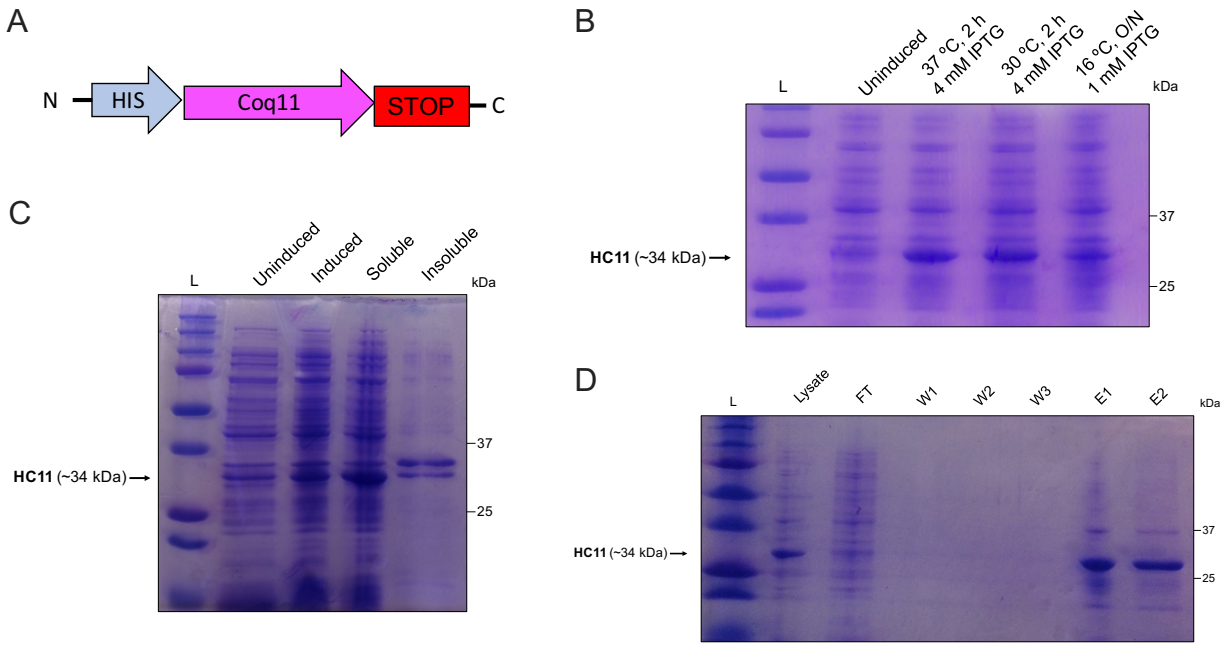

Figure 2. A representative purification scheme of His-Coq11 suggests that this construct is not sufficient for large-scale Coq11 purification without impurities. *A*, The *COQ11* ORF including a 6xHis tag (HC11) on its N-terminus was cloned into the pDEST17 vector as described in Experimental Procedures. *B*, Coq11 expression was induced with IPTG under various conditions to evaluate Coq11 overexpression. *C*, Coq11 expression was induced (4 mM IPTG, 37 °C, 2 h) and the presence of HC11 in either the soluble or insoluble fractions of the clear lysate was evaluated. *D*, HC11 was purified over a Ni-NTA gravity column; FT, column flow through; W, wash 1-3; E, eluate. An aliquot of 5 µL sample was loaded into each lane, and separated on 12% SDS-PAGE. The gel was subsequently stained with Coomassie and destained for visualization.

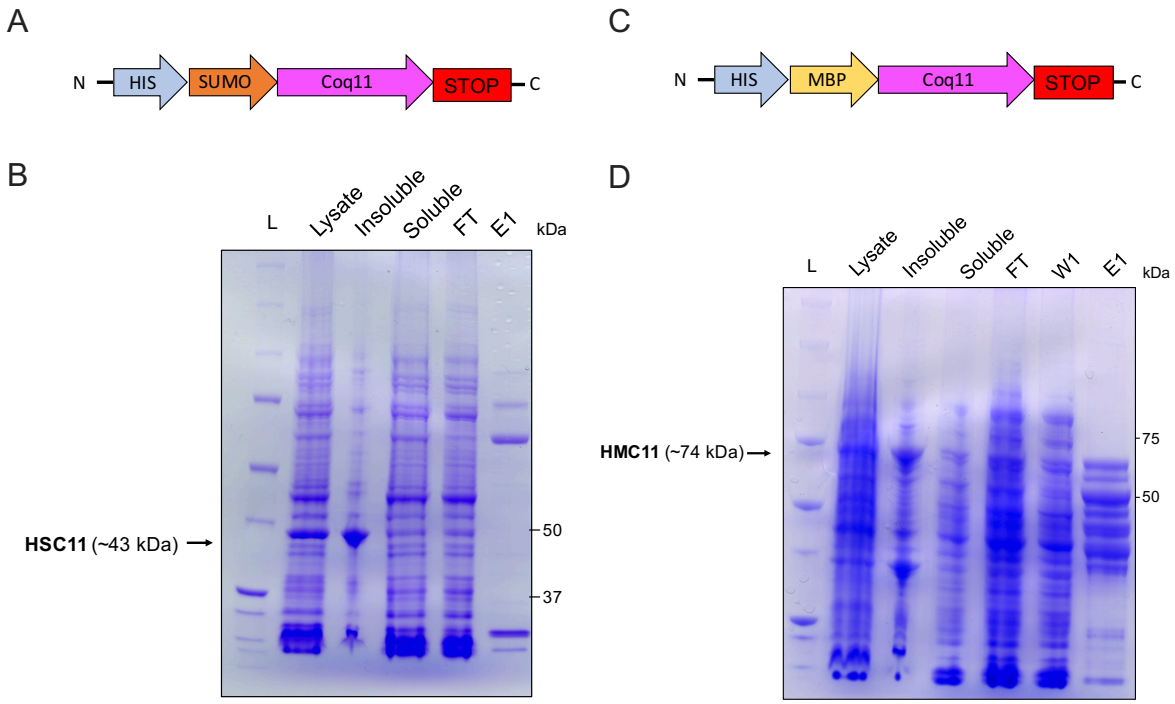

Figure 3. His-Coq11 tagged in combination with either SUMO or MBP does not improve Coq11 purification yield and results in truncated protein products. The *COQ11* ORF was cloned into the pETSUMO or DCLIC vectors (Experimental Procedures, Table 2) as a protein fusion with *A*, SUMO or *C*, MBP, to increase overall protein expression and solubility. *B & D*, Each plasmid was expressed (0.5 mM IPTG, 18 ºC, O/N) and purified from 2 L of *E. coli* by application to an Ni-NTA column via an AKTA chromatography system; FT, column flow through; E, eluate. An aliquot of 5 µL sample was loaded into each lane, and separated on 12% SDS-PAGE. The gel was subsequently stained with Coomassie and destained for visualization.

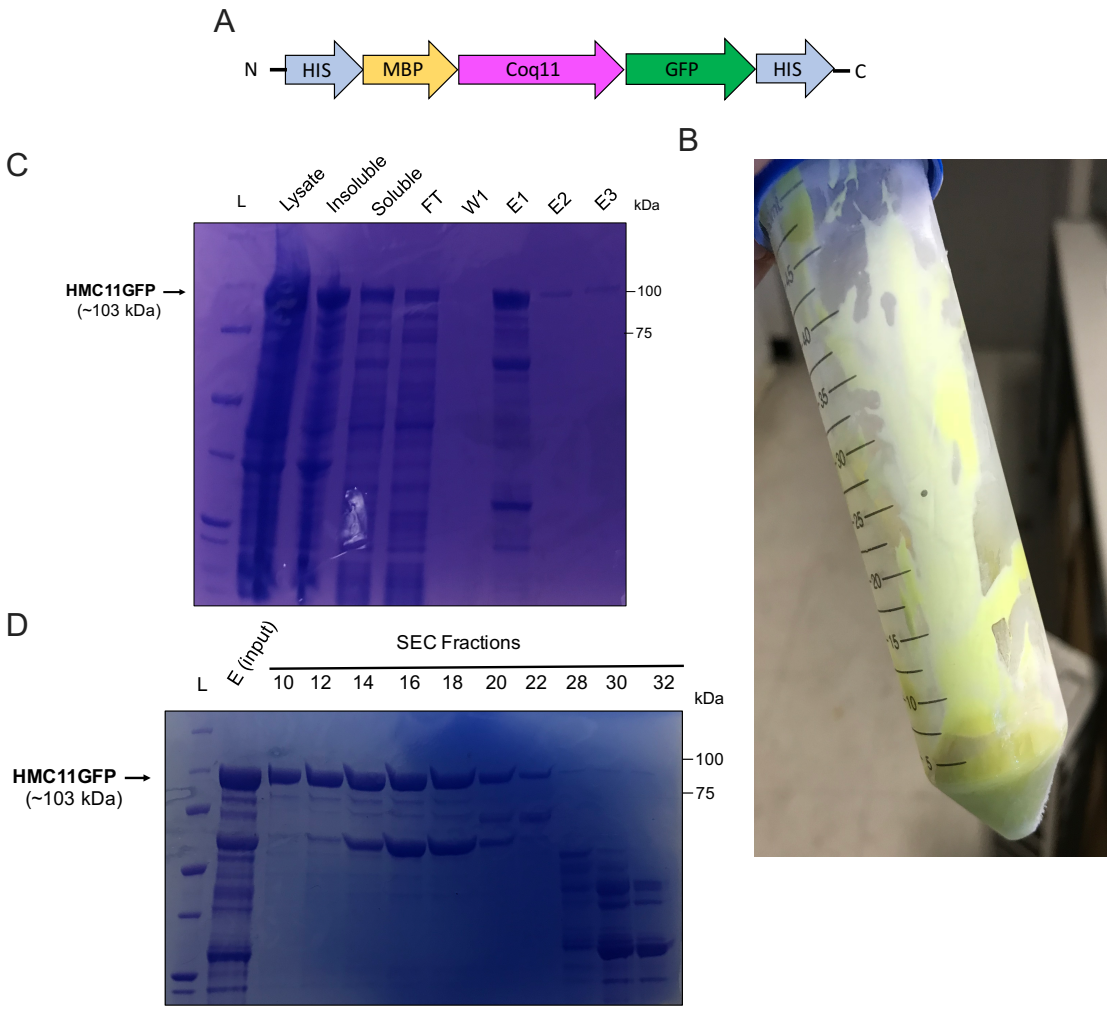

Figure 4. Protein purification of MBP-Coq11-GFP results in similar protein truncation products that are challenging to circumvent. *A*, Final Coq11 purification construct attempted, His-MBP-Coq11-GPF (HMC11GFP). B, The protein is expressing GFP and harvested cells have a distinctly green color. *C*, The plasmid was expressed (0.5 mM IPTG, 18 ºC, O/N) and purified from 2 L of *E. coli* by application to an Ni-NTA column via an AKTA chromatography system; FT, column flow through; W, wash; E, eluate. *D*, The pooled elutes from '*B*' were run on SEC, individual fractions were collected, and 5 µL from each fraction was loaded and separated on 12% SDS-PAGE. The gels were subsequently stained with Coomassie and destained for visualization.

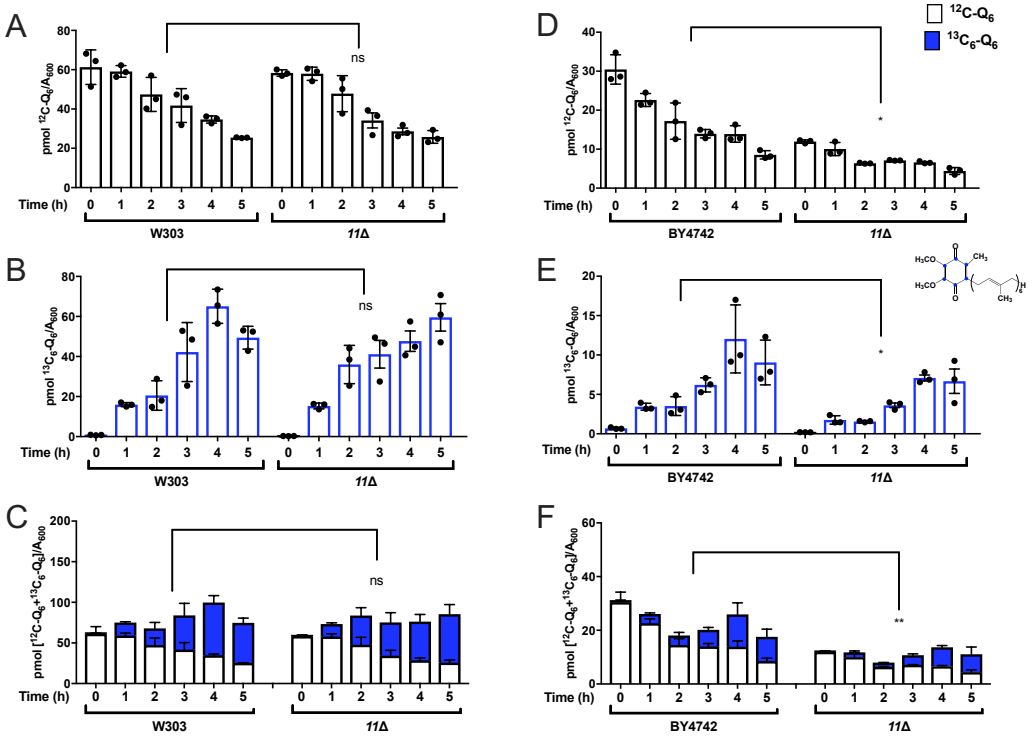

Figure 5. Deletion of *COQ11* has a greater effect on *de novo* Q_6 production in the BY4742 genetic background compared to the W303 genetic background. Triplicates of 6 mL cultures in DOD minimal medium were grown to A_{600} ~ 0.5 and labeled with 5 µg/mL $^{13}C_6$-4HB. At hour intervals from 0 – 5 h, 5 mL of each culture was collected, lipid extracted, and analyzed by LC-MS/MS. *A & D*, Unlabeled ^{12}C-Q_6; *B & E*, *De novo* synthesized $^{13}C_6$-Q_6 (*blue*); and *C & F,* Total amount of Q_6 determined from the sum of $^{13}C_6$-Q_6 and ^{12}C-Q_6, were measured from the whole-cell lipid extracts of wild type and *coq11*Δ mutants in both the W303 (*A-C*) and BY4742 (*D-F*) genetic background. The values are the mean of three replicates. The data show mean ± SD, and the statistical significance as compared to wild type is represented by *p < 0.05, **p < 0.01, ***p < 0.001 and ****p < 0.0001. The 'ns' denotation signifies that values are not significantly different than wild type.

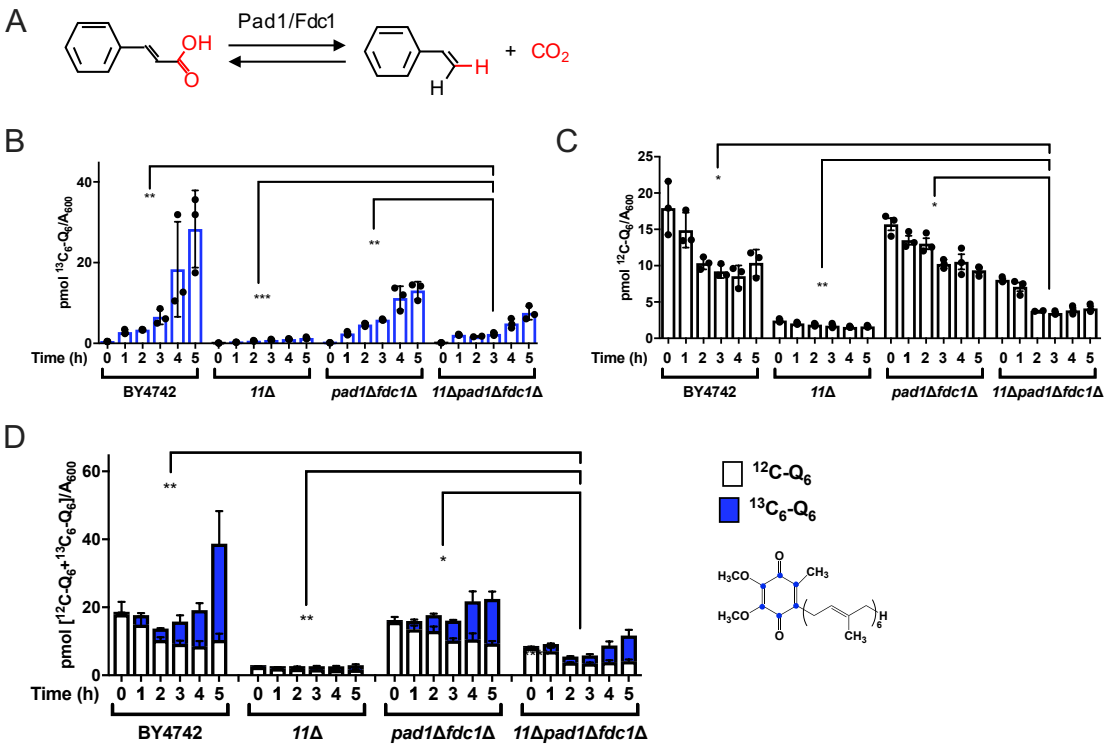

Figure 6. Coq11, Pad1, and Fdc1 are not redundant decarboxylases in Q_6 biosynthesis. *A*, Schematic of Pad1/Fdc1 involvement in decarboxylation. Triplicates of 6 mL cultures in DOD minimal medium were grown to $A_{600} \sim 0.5$ and labeled with 5 µg/mL $^{13}C_6$-4HB. At hour intervals from 0 – 5 h, 5 mL of each culture was collected, lipid extracted, and analyzed by LC-MS/MS. *B*, *De novo* synthesized $^{13}C_6$-Q_6 (*blue*); *C,* Unlabeled ^{12}C-Q_6; and *D*, Total amount of Q_6 determined from the sum of $^{13}C_6$-Q_6 and ^{12}C-Q_6, were measured from the whole-cell lipid extracts of BY4742 and the *coq11*Δ, *pad1*Δ*fdc1*Δ, and *coq11*Δ*pad1*Δ*fdc1*Δ mutants in the BY4742 genetic background. The values are the mean of three replicates. The data show mean ± SD, and the statistical significance as compared to wild type is represented by *p < 0.05, **p < 0.01, ***p < 0.001 and ****p < 0.0001. The 'ns' denotation signifies that values are not significantly different than wild type.

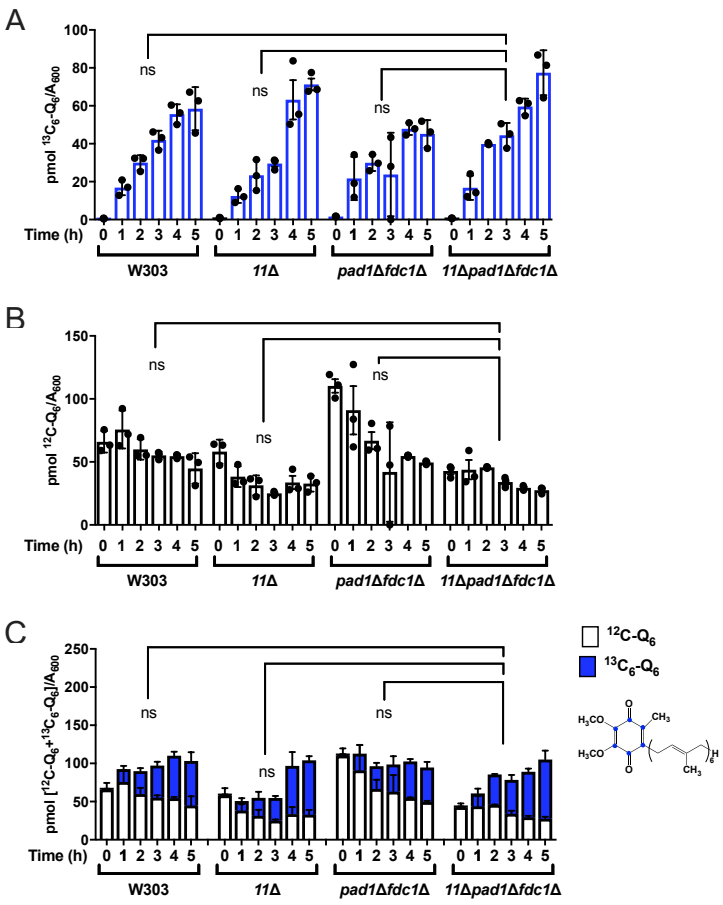

Figure 7. Coq11, Pad1, Fdc1 mutants have little or no effect on *de novo* Q_6 biosynthesis in the W303 background. Triplicates of 6 mL cultures in DOD minimal medium were grown to A_{600} ~ 0.5 and labeled with 5 µg/mL $^{13}C_6$-4HB. At hour intervals from 0 – 5 h, 5 mL of each culture was collected, lipid extracted, and analyzed by LC-MS/MS. *A*, *De novo* synthesized $^{13}C_6$-Q_6 (*blue*); *B,* Unlabeled ^{12}C-Q_6; and *C*, Total amount of Q_6 determined from the sum of $^{13}C_6$-Q_6 and ^{12}C-Q_6, were measured from the whole-cell lipid extracts of W303 and the *coq11*Δ, *pad1*Δ*fdc1*Δ, and *coq11*Δ*pad1*Δ*fdc1*Δ mutants in the W303 genetic background. The values are the mean of three replicates. The data show mean ± SD, and the statistical significance as compared to wild type is represented by *p < 0.05, **p < 0.01, ***p < 0.001 and ****p < 0.0001. The 'ns' denotation signifies that values are not significantly different than wild type.

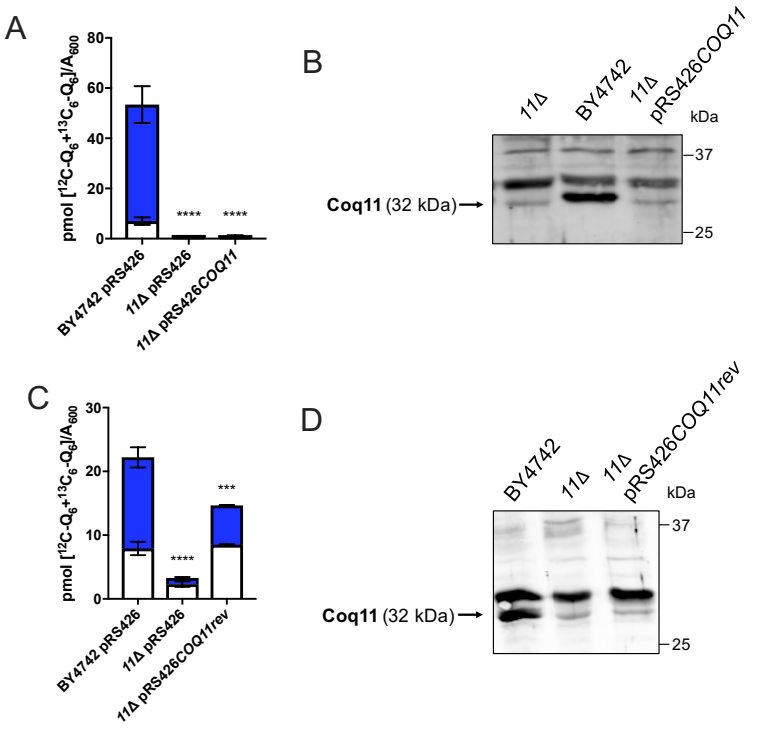

Figure 8. Rescue of *coq11*Δ mutant *de novo* Q_6 production is unsuccessful using two different overexpression constructs. Wild type and *coq11*Δ yeast was transformed with two Coq11 overexpression constructs, pRS426*COQ11* or pRS426*COQ11rev*, and the empty vector control (Table 2). *A & C*, Triplicates of 6 mL culture in selection medium were labeled at A_{600} ~ 0.5 with 5 μg/mL $^{13}C_6$-4HB. After 4 h, 5 mL of each culture was harvest, lipid extracted, and analyzed by LC-MS/MS. Total amount of Q_6 was plotted, from the sum of ^{12}C-Q_6 (*white*) and *de novo* $^{13}C_6$-Q_6 (*blue*). The values are the mean of three replicates. The data show mean ± SD, and the statistical significance as compared to wild type is represented by *p < 0.05, **p < 0.01, ***p < 0.001 and ****p < 0.0001. *B & D*, Aliquots of purified mitochondria (25 μg) from wild type and mutant yeast containing empty vector or each Coq11 overexpression construct were isolated in YPGal medium and separated on 10% Tris-Glycine SDS-PAGE gels. Coq11 is not effectively overexpressed from either high-copy plasmid.

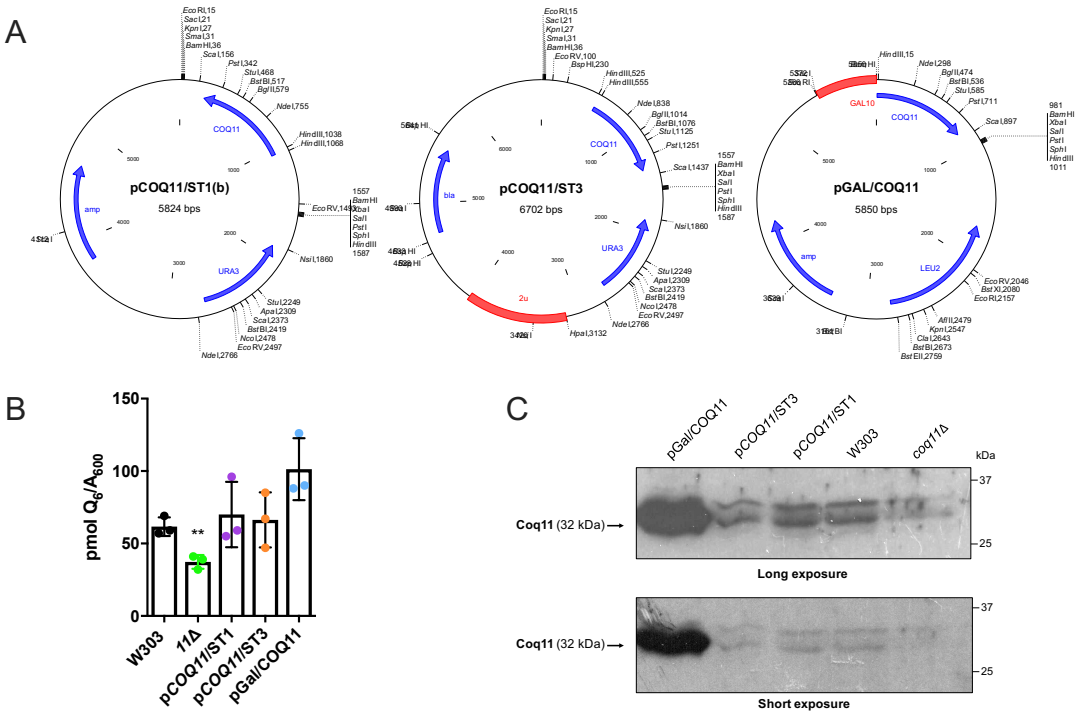

Figure 9. Coq11 low-copy and high-copy expression from three different constructs in W303 wild type yeast does significantly effect Q_6 production. *A*, Three plasmids were constructed to express Coq11; Low-copy, integrated (p*COQ11*/ST1); High-copy (p*COQ11*/ST3); and high-copy under control of the Gal promotor (pGal/*COQ11*), integrated. *B*, Triplicates of 6 mL cultures of W303 wild type, *coq11*Δ W303, and W303 expressing each of the aforementioned plasmids. in YPD media were seeded at A_{600} ~ 1, allowed to grow for 4 h, and then 5 mL were harvested by centrifugation. Each cell pellet was lipid extracted, and analyzed by LC-MS/MS for Q_6 content. The values are the mean of three replicates. The data show mean ± SD, and the statistical significance as compared to wild type is represented by **p < 0.01. *C*, Aliquots of purified mitochondria (25 μg) from the aforementioned strains were isolated in YPGal medium and were separated on 10% Tris-Glycine SDS-PAGE gels to determine Coq11 protein expression.

REFERENCES

1. Awad, A. M., Bradley, M. C., Fernandez-Del-Rio, L., Nag, A., Tsui, H. S., and Clarke, C. F. (2018) Coenzyme Q_{10} deficiencies: pathways in yeast and humans. *Essays Biochem* **62**, 361-376
2. Frei, B., Kim, M. C., and Ames, B. N. (1990) Ubiquinol-10 is an effective lipid-soluble antioxidant at physiological concentrations. *Proc Natl Acad Sci U S A* **87**, 4879-4883
3. Quinzii, C. M., Kattah, A. G., Naini, A., Akman, H. O., Mootha, V. K., DiMauro, S., and Hirano, M. (2005) Coenzyme Q deficiency and cerebellar ataxia associated with an aprataxin mutation. *Neurology* **64**, 539-541
4. Wang, Y., and Hekimi, S. (2019) The Complexity of Making Ubiquinone. *Trends Endocrinol Metab*
5. Muller, T., Buttner, T., Gholipour, A. F., and Kuhn, W. (2003) Coenzyme Q_{10} supplementation provides mild symptomatic benefit in patients with Parkinson's disease. *Neurosci Lett* **341**, 201-204
6. Hernandez-Camacho, J. D., Bernier, M., Lopez-Lluch, G., and Navas, P. (2018) Coenzyme Q_{10} Supplementation in Aging and Disease. *Front Physiol* **9**, 44
7. Zaki, N. M. (2016) Strategies for oral delivery and mitochondrial targeting of CoQ_{10}. *Drug Deliv* **23**, 1868-1881
8. Lee, J. S., Suh, J. W., Kim, E. S., and Lee, H. G. (2017) Preparation and Characterization of Mucoadhesive Nanoparticles for Enhancing Cellular Uptake of Coenzyme Q_{10}. *J Agric Food Chem* **65**, 8930-8937

9. Herebian, D., Lopez, L. C., and Distelmaier, F. (2018) Bypassing human CoQ_{10} deficiency. *Mol Genet Metab* **123**, 289-291

10. Berenguel Hernandez, A. M., de la Cruz, M., Alcazar-Fabra, M., Prieto-Rodriguez, A., Sanchez-Cuesta, A., Martin, J., Tormo, J. R., Rodriguez-Aguilera, J. C., Cortes-Rodriguez, A. B., Navas, P., Reyes, F., Vicente, F., Genilloud, O., and Santos-Ocana, C. (2020) Design of High-Throughput Screening of Natural Extracts to Identify Molecules Bypassing Primary Coenzyme Q Deficiency in *Saccharomyces cerevisiae*. *SLAS Discov* **25**, 299-309

11. Stefely, J. A., and Pagliarini, D. J. (2017) Biochemistry of Mitochondrial Coenzyme Q Biosynthesis. *Trends Biochem Sci* **42**, 824-843

12. Allan, C. M., Awad, A. M., Johnson, J. S., Shirasaki, D. I., Wang, C., Blaby-Haas, C. E., Merchant, S. S., Loo, J. A., and Clarke, C. F. (2015) Identification of Coq11, a new coenzyme Q biosynthetic protein in the CoQ-synthome in *Saccharomyces cerevisiae*. *J Biol Chem* **290**, 7517-7534

13. Marcotte, E. M., Pellegrini, M., Ng, H. L., Rice, D. W., Yeates, T. O., and Eisenberg, D. (1999) Detecting protein function and protein-protein interactions from genome sequences. *Science* **285**, 751-753

14. Allan, C. M., Hill, S., Morvaridi, S., Saiki, R., Johnson, J. S., Liau, W. S., Hirano, K., Kawashima, T., Ji, Z., Loo, J. A., Shepherd, J. N., and Clarke, C. F. (2013) A conserved START domain coenzyme Q-binding polypeptide is required for efficient Q biosynthesis, respiratory electron transport, and antioxidant function in *Saccharomyces cerevisiae*. *Biochim Biophys Acta* **1831**, 776-791

15. Barros, M. H., Johnson, A., Gin, P., Marbois, B. N., Clarke, C. F., and Tzagoloff, A. (2005) The *Saccharomyces cerevisiae COQ10* gene encodes a START domain protein required for function of coenzyme Q in respiration. *J Biol Chem* **280**, 42627-42635

16. Tsui, H. S., Pham, N. V. B., Amer, B. R., Bradley, M. C., Gosschalk, J. E., Gallagher-Jones, M., Ibarra, H., Clubb, R. T., Blaby-Haas, C. E., and Clarke, C. F. (2019) Human COQ10A and COQ10B are distinct lipid-binding START domain proteins required for coenzyme Q function. *J Lipid Res* **60**, 1293-1310

17. Bradley, M. C., Yang, K., Fernandez-Del-Rio, L., Ngo, J., Ayer, A., Tsui, H. S., Novales, N. A., Stocker, R., Shirihai, O. S., Barros, M. H., and Clarke, C. F. (2020) *COQ11* deletion mitigates respiratory deficiency caused by mutations in the gene encoding the coenzyme Q chaperone protein Coq10. *J Biol Chem* **295**, 6023-6042

18. Marchler-Bauer, A., Zheng, C., Chitsaz, F., Derbyshire, M. K., Geer, L. Y., Geer, R. C., Gonzales, N. R., Gwadz, M., Hurwitz, D. I., Lanczycki, C. J., Lu, F., Lu, S., Marchler, G. H., Song, J. S., Thanki, N., Yamashita, R. A., Zhang, D., and Bryant, S. H. (2013) CDD: conserved domains and protein three-dimensional structure. *Nucleic Acids Res* **41**, D348-352

19. Rossmann, M. G., Moras, D., and Olsen, K. W. (1974) Chemical and biological evolution of nucleotide-binding protein. *Nature* **250**, 194-199

20. Kopec, J., Schnell, R., and Schneider, G. (2011) Structure of PA4019, a putative aromatic acid decarboxylase from *Pseudomonas aeruginosa*. *Acta Crystallogr Sect F Struct Biol Cryst Commun* **67**, 1184-1188

21. Rangarajan, E. S., Li, Y., Iannuzzi, P., Tocilj, A., Hung, L. W., Matte, A., and Cygler, M. (2004) Crystal structure of a dodecameric FMN-dependent UbiX-like decarboxylase (Pad1) from *Escherichia coli* O157: H7. *Protein Sci* **13**, 3006-3016

22. White, M. D., Payne, K. A., Fisher, K., Marshall, S. A., Parker, D., Rattray, N. J., Trivedi, D. K., Goodacre, R., Rigby, S. E., Scrutton, N. S., Hay, S., and Leys, D. (2015) UbiX is a flavin prenyltransferase required for bacterial ubiquinone biosynthesis. *Nature* **522**, 502-506

23. Gulmezian, M. (2006) *Characterization of Escherichia coli ubiX, Saccharomyces cerevisiae PAD1 and YDR539W, and a Complex of Polypeptides Involved in Coenzyme Q Biosynthesi.* Ph.D., University of California Los Angeles

24. Brachmann, C. B., Davies, A., Cost, G. J., Caputo, E., Li, J., Hieter, P., and Boeke, J. D. (1998) Designer deletion strains derived from *Saccharomyces cerevisiae* S288C: a useful set of strains and plasmids for PCR-mediated gene disruption and other applications. *Yeast* **14**, 115-132

25. Thomas, B. J., and Rothstein, R. (1989) Elevated recombination rates in transcriptionally active DNA. *Cell* **56**, 619-630

26. Barkovich, R. J., Shtanko, A., Shepherd, J. A., Lee, P. T., Myles, D. C., Tzagoloff, A., and Clarke, C. F. (1997) Characterization of the *COQ5* gene from *Saccharomyces cerevisiae*. Evidence for a C-methyltransferase in ubiquinone biosynthesis. *J Biol Chem* **272**, 9182-9188

27. Rothstein, R. J. (1983) One-step gene disruption in yeast. *Methods Enzymol* **101**, 202-211

28. Gietz, R. D., and Woods, R. A. (2002) Transformation of yeast by lithium acetate/single-stranded carrier DNA/polyethylene glycol method. *Methods Enzymol* **350**, 87-96

29. Glick, B. S., and Pon, L. A. (1995) Isolation of highly purified mitochondria from *Saccharomyces cerevisiae*. *Methods Enzymol* **260**, 213-223

30. Elble, R. (1992) A simple and efficient procedure for transformation of yeasts. *Biotechniques* **13**, 18-20

31. Hsieh, E. J., Gin, P., Gulmezian, M., Tran, U. C., Saiki, R., Marbois, B. N., and Clarke, C. F. (2007) *Saccharomyces cerevisiae* Coq9 polypeptide is a subunit of the mitochondrial coenzyme Q biosynthetic complex. *Arch Biochem Biophys* **463**, 19-26

32. Bell, M. R., Engleka, M. J., Malik, A., and Strickler, J. E. (2013) To fuse or not to fuse: what is your purpose? *Protein Sci* **22**, 1466-1477

33. Mukai, N., Masaki, K., Fujii, T., Kawamukai, M., and Iefuji, H. (2010) *PAD1* and *FDC1* are essential for the decarboxylation of phenylacrylic acids in *Saccharomyces cerevisiae*. *J Biosci Bioeng* **109**, 564-569

34. Gulmezian, M., Hyman, K. R., Marbois, B. N., Clarke, C. F., and Javor, G. T. (2007) The role of UbiX in Escherichia coli coenzyme Q biosynthesis. *Arch Biochem Biophys* **467**, 144-153

35. Petrezselyova, S., Zahradka, J., and Sychrova, H. (2010) *Saccharomyces cerevisiae* BY4741 and W303-1A laboratory strains differ in salt tolerance. *Fungal Biol* **114**, 144-150

36. Bruder, S., Reifenrath, M., Thomik, T., Boles, E., and Herzog, K. (2016) Parallelised online biomass monitoring in shake flasks enables efficient strain and carbon source dependent growth characterisation of *Saccharomyces cerevisiae*. *Microb Cell Fact* **15**, 127

37. Marshall, S. A., Payne, K. A. P., Fisher, K., White, M. D., Ni Cheallaigh, A., Balaikaite, A., Rigby, S. E. J., and Leys, D. (2019) The UbiX flavin prenyltransferase reaction mechanism resembles class I terpene cyclase chemistry. *Nat Commun* **10**, 2357

38. Richard, P., Viljanen, K., and Penttila, M. (2015) Overexpression of PAD1 and FDC1 results in significant cinnamic acid decarboxylase activity in *Saccharomyces cerevisiae*. *AMB Express* **5**, 12

39. Xie, L. X., Williams, K. J., He, C. H., Weng, E., Khong, S., Rose, T. E., Kwon, O., Bensinger, S. J., Marbois, B. N., and Clarke, C. F. (2015) Resveratrol and *para*-coumarate serve as ring precursors for coenzyme Q biosynthesis. *J Lipid Res* **56**, 909-919

40. Hsu, A. Y., Poon, W. W., Shepherd, J. A., Myles, D. C., and Clarke, C. F. (1996) Complementation of coq3 mutant yeast by mitochondrial targeting of the *Escherichia coli* UbiG polypeptide: evidence that UbiG catalyzes both O-methylation steps in ubiquinone biosynthesis. *Biochemistry* **35**, 9797-9806

41. Lapointe, C. P., Stefely, J. A., Jochem, A., Hutchins, P. D., Wilson, G. M., Kwiecien, N. W., Coon, J. J., Wickens, M., and Pagliarini, D. J. (2018) Multi-omics Reveal Specific Targets of the RNA-Binding Protein Puf3p and Its Orchestration of Mitochondrial Biogenesis. *Cell Syst* **6**, 125-135 e126

42. Xie, L. X., Ozeir, M., Tang, J. Y., Chen, J. Y., Jaquinod, S. K., Fontecave, M., Clarke, C. F., and Pierrel, F. (2012) Overexpression of the Coq8 kinase in *Saccharomyces cerevisiae coq* null mutants allows for accumulation of diagnostic intermediates of the coenzyme Q_6 biosynthetic pathway. *J Biol Chem* **287**, 23571-23581

43. He, C. H., Xie, L. X., Allan, C. M., Tran, U. C., and Clarke, C. F. (2014) Coenzyme Q supplementation or over-expression of the yeast Coq8 putative kinase stabilizes multi-

subunit Coq polypeptide complexes in yeast *coq* null mutants. *Biochim Biophys Acta* **1841**, 630-644

44. Santos-Ocana, C., Do, T. Q., Padilla, S., Navas, P., and Clarke, C. F. (2002) Uptake of exogenous coenzyme Q and transport to mitochondria is required for bc_1 complex stability in yeast *coq* mutants. *J Biol Chem* **277**, 10973-10981

45. Christianson, T. W., Sikorski, R. S., Dante, M., Shero, J. H., and Hieter, P. (1992) Multifunctional yeast high-copy-number shuttle vectors. *Gene* **110**, 119-122

CHAPTER 4

Deficiency in phosphatidylethanolamine methyltransferase increases Q_6 content and has beneficial effects on the CoQ synthome

ABSTRACT

Coenzyme Q (Q_n) is a hydrophobic biomolecule consisting of a fully-substituted benzoquinone ring and a polyisoprenoid tail. Redox-active Q_n is the only endogenously synthesized lipid antioxidant, and is responsible for mitochondrial bioenergetics as a key player of the electron transport chain. In humans, patients unable to produce adequate levels of Q_{10} display a wide variety of health issues often stemming from mitochondrial dysfunction. The most productive treatment strategy available for Q_{10} deficiency is Q_{10} supplementation; while beneficial in some cases, the poor solubility of Q_{10} limits treatment efficacy. A more comprehensive understanding of Q_{10} uptake and assimilation, as well as endogenous biosynthesis, will greatly improve Q_{10} therapeutics. Previously, Dr. Anita Ayer conducted a large-scale screen of the *Saccharomyces cerevisiae* diploid homozygous knockout library for mutants displaying significantly different Q_6 content than wild type. Two phosphatidylethanolamine methyltransferase gene deletion mutants, *cho2* and *opi3*, were identified to have considerably elevated amounts of Q_6, with *cho2*Δ producing as much as a five-fold Q_6 increase compared to wild type. In collaboration with Dr. Lucía Fernández-del-Río, we revealed that both *cho2*Δ and *opi3*Δ yeast show normal amounts of Coq polypeptides, yet display a stabilized CoQ synthome. Further, the *cho2*Δ mutant has increased Q_6 antioxidant protection from exogenously added PUFAs. Our study demonstrates that Cho2 and Opi3 are novel regulators of Q_6 homeostasis.

INTRODUCTION

Coenzyme Q (Q_n) is an essential redox-active lipid that mediates electron transport during mitochondrial respiration (1). The oxidized quinone accepts electrons from NADH via Complex I, or succinate via Complex II, and the reduced hydroquinone then donates these electrons to Complex III to ultimately drive ATP synthesis (1,2). In this manner, Q_n is an electron acceptor for other enzymes involved in fatty acid β-oxidation, the oxidation of proline, sulfide, and pyrimidine biosynthesis (3-5). The reduced hydroquinone additionally serves as an important chain-terminating lipid soluble antioxidant, effective in quenching lipid peroxidative damage forming within cellular membranes (6,7). These vital functions of Q_n depend upon proper synthesis and formation of its fully substituted benzoquinone ring with a species-specific polyisoprenyl tail, where *n* designates the number of isoprenoid units (1).

Patients with partial defects in Q_{10} biosynthesis suffer from mitochondrial dysfunction resulting in such disease pathology as cerebellar ataxia, renal disease, cardiovascular complications, respiratory dysfunction, and neurodegenerative diseases (6-8). The current industry standard treatment to mitigate adverse symptoms of Q_{10} deficiency are high doses of Q_{10} supplementation (7). However, absorption of orally supplemented Q_{10} is inefficient due to its low solubility, resulting in limited disease recovery for most patients (7,9). Present research is focused on developing novel Q_{10} delivery strategies (10,11), or using alternative Q_{10} precursors or by-pass molecules to enhance endogenous Q_{10} biosynthesis (12,13).

In order to improve the therapeutic efficiency of Q_{10} supplementation, the mechanisms of its synthesis, uptake, distribution, and degradation within cells must be fully understood. *Saccharomyces cerevisiae* is an excellent model for studies of Q_{10} since many of the *COQ* genes involved in Q_{10} biosynthesis are functionally conserved between yeast and humans (1,14).

Additionally, yeast retains the ability to survive via fermentation in the absence of Q_6, has well characterized molecular genetics, is highly genetically malleable, and is easy to maintain in culture (15). A cohort of fourteen known enzymes participate in Q_6 biosynthesis in *Saccharomyces cerevisiae*, many of which organize into a high molecular weight complex at the mitochondrial inner membrane, known as the CoQ synthome (1,14). Deletion of essential *COQ* genes (*COQ1-COQ9*) results in a loss of Q_6 synthesis, and a subsequent failure to respire on a non-fermentable carbon source (1,2). While significant progress has been made in determining the role of each enzyme in Q_6 biosynthesis, the function of several Coq proteins remains uncharacterized (1,15).

Although Q_n is found in all cellular membranes in yeast and humans, Q_n biosynthesis occurs exclusively within the mitochondria (1,2). The presence of Q_n in membranes distant from its site of synthesis indicates the existence of a transportation mechanism from the mitochondria to other organelles (16,17). The assimilation of exogenously supplied Q_n in yeast, mice, and humans with Q_{10} deficiencies, is evidence for additional transportation of Q_n across the plasma membrane and into the mitochondrial inner membrane (18,19). Recently, six novel *S. cerevisiae* genes (*CDC10*, *RTS1*, *RVS161*, *RVS167*, *VPS1*, and *NAT3*) have been identified as necessary for efficient trafficking of Q_6 to mitochondria (Fernandez-del-Rio, et al., submitted). However, these mechanisms of Q_n transportation are largely unknown.

There are clearly large gaps in the scientific literature encompassing every aspect of Q_6 homeostasis. Perhaps most glaring is the lack of information surrounding regulation of the amount of cellular Q_6; the Q_6 content in different cellular membranes must be communicated to the Q_6 biosynthetic machinery in order to preserve optimal levels. To investigate Q_6 regulatory mechanisms, Dr. Anita Ayer from the Stocker laboratory at the Victor Chang Cardiac Research

Institute (Sydney, Australia), conducted a genome-wide screen of ~ 5,000 *S. cerevisiae* homozygous diploid deletion mutants. Genes required for maintaining Q_6 homeostasis were isolated by measuring Q_6 content in each mutant with HPLC-EC detection. This high-throughput screen identified eight mutants displaying significantly lower Q_6 content, and 30 mutants displaying significantly higher Q_6 content compared wild type. Among the mutants presenting with increased Q_6 compared to wild type was *cho2*—a gene that encodes a methyltransferase that catalyzes the first reaction in the conversion of phosphatidylethanolamine (PE) to phosphatidylcholine (PC) (20). Successive methyltransferase reactions in the phosphatidylethanolamine methyltransferase (PEMT) pathway of PC biosynthesis are catalyzed by Opi3 (21), which was also identified in Dr. Ayer's genetic screen to produce higher content of Q_6 (Fig. 1B). In this study, we evaluated the effect of the *cho2*Δ and *opi3*Δ mutants on Q_6 biosynthesis, biosynthetic machinery, and Q_6 antioxidant protection. Our results demonstrate that Cho2 and Opi3 are novel regulators of Q_6 biosynthesis in *S. cerevisiae*.

EXPERIMENTAL PROCEDURES

Yeast strains and growth medium

The *S. cerevisiae* strains used in this study are listed in Table 1. Yeast strains were derived from S288C (BY4743, BY4742, or BY4741 (22)), and were grown in synthetic defined medium lacking pABA (6.7 g YNB-pABA/L (Sunrise Scientific), 2% glucose, 1X amino acid/base solution) at 30 ºC. The amino acid solution was diluted from a 1 L, 10X solution prepared in H_2O and filter sterilized, containing the following amino acids: Leucine (2.6 g), lysine monohydride chloride (1.8 g), isoleucine (0.76 g), valine (1.2 g), tryptophan (0.9 g), histidine (0.46 g), adenine hemisulfate (0.55 g), and uracil (0.22 g). Additional growth media used included YPD (2% glucose, 1% yeast extract, 2% peptone) and YPGal (2% galactose, 1% yeast extract, 2% peptone, 0.1% dextrose) (23). Solid media was prepared with 2% Bacto agar.

Genetic screen of the diploid knockout *S. cerevisiae* library

The *S. cerevisiae* homozygous diploid knockout collection (~ 5,000 BY4743 mutants; Euroscaf) was used to conduct a genetic screen to identify genes contributing to Q_6 content regulation. Briefly, cells were inoculated from –80 °C stocks with 2.4 µL of defrosted culture, inoculated into 96-well plates containing 195 µL SD-pABA media. Cells were grown for two days at 30 °C with shaking. Following growth for two days, 2.4 µL of culture was sub-inoculated into 96-well plates containing 195 µL fresh media, and cells were grown for an additional 18 h at 30 °C with shaking. The A_{600} was measured (Pherastar 96-well plate spectrophotometer) after 18 h, and cells were pelleted by centrifugation. The supernatant was removed from each well and the cell pellet in each well resuspended in 50 µL of 155 mM ammonium acetate. The 96-well plate was frozen at –20 °C for future use. On the day of Q_6 analysis, plates were defrosted and 50

μL of cell suspension were used for Q_6 analysis as described below. Separately, wild-type cells were grown to A_{600} ~ 1, frozen in aliquots, and used as quality control (QC) for each plate. Wells A1, E6 and H12 of each plate were used for the QC samples with 50 μL of QC sample placed into each well on the day of analysis. For each plate to pass 'QC', the Q_6 content of the QC wells had to be within 20% of each other. Cells were lysed and Q_6 extracted and analyzed as outlined below.

Determination of Q_6 in *S. cerevisiae* during genetic screen

Each well was lipid extracted as described (24), with slight modifications. Ammonium acetate (0.155 mM, 50 μL) was added to cell pellets and the suspension was transferred to a glass-coated 96 deep well plate containing 50 μL glass beads per well. Cells were then lysed using a Thermomixer C (Eppendorf, 1,400 rpm, 2 h, 4 °C). Acidified methanol (0.02% acetic acid; 200 μL) and water-washed hexane (500 μL) was added to each sample with shaking (1,000 rpm, 1 min, 4 °C). An aliquot of the hexane layer (300 μL) was removed, 500 μL fresh hexane was added, and the plate was shaken again. This process was repeated five, to give a total of 2 mL hexane collected. The collected hexane was dried under nitrogen in a fume hood for 1 h at room temperature. The resulting lipids were resuspended in 150-180 μL ice-cold mobile phase (ethanol:methanol:isopropanol:ammonium acetate pH 4.4, 65:30:3:2, vol/vol/vol/vol) and transferred into HPLC vials. Samples were stored at 4 °C until analysis via HPLC coupled to UV and electrochemical detection (HPLC-UV/EC). For HPLC-UV/EC analyses, 100 μL of sample was injected onto a Supelcosil LC-C18 column (5 μm, 250 mm x 4.6 mm), eluted at 1 mL min^{-1}, and connected to UV and electrochemical (ESA CoulArray 5600A) detectors. Q_6 was detected at -700, +700, and +700 mV. Q_6 standards obtained from Avanti Polar Lipids.

Yeast mitochondria isolation

Yeast cultures of BY4743, *cho2*Δ BY4743, and *opi3*Δ BY4743 were grown overnight in 20 mL SD-pABA. Cultures were diluted with SD-pABA and grown overnight at 30 °C with shaking (250 rpm) until cell density reached an A_{600} ~ 1. Spheroplasts were generated using Zymolyase-20T (MP Biomedicals) and mitochondria were fractionated as previously described (25), in the presence of cOmplete™ EDTA-free protease inhibitor cocktail tablets (Roche), phosphatase inhibitor cocktail set I (Sigma-Aldrich), phosphatase inhibitor cocktail set II (Sigma-Aldrich), and PMSF (Fisher Scientific). Nycodenz (Sigma-Aldrich) density gradient purified mitochondria were aliquoted, frozen in liquid nitrogen, and stored at −80 °C until further use. Mitochondria protein concentration was measured by the Bicinchoninic acid (BCA) assay (ThermoFisher Scientific).

Analysis of Q_6 content of whole cells and purified mitochondria

Yeast cultures were grown overnight in 50 mL of SD-pABA. Cultures were diluted into triplicates of 20 mL fresh medium to A_{600} = 0.1, and 10 mL were harvested by centrifugation once they reached A_{600} ~ 1. Cell pellets were stored at −20 °C. Frozen cell pellets were lipid extracted in the presence of internal standard Q_4 and analyzed for Q_6 by LC-MS/MS as described (26). Standards of Q_6 were obtained from Avanti Polar Lipids, and Q_4 from Sigma-Aldrich. Alternatively, triplicates of 100 μg of purified mitochondria (purification described above) were lipid extracted in the presence of internal standard Q_4 and analyzed for Q_6 by LC-MS/MS as described (26).

SDS-PAGE and immunoblot analysis of Coq proteins

Aliquots of purified mitochondria (25 μg) were incubated with SDS sample buffer (50 mM Tris-HCl pH 6.8, 10% glycerol, 2% SDS, 0.1% bromophenol blue, 1.33% beta-mercaptoethanol) and separated on 10% or 12% Tris-glycine polyacrylamide gels by electrophoresis. Proteins were transferred to a 0.45 μm PVDF membrane (Millipore) at 100 V for 45 min, and the resulting membranes were stained with Ponceau for 5 min. Following the capture of each image, the blots were destained with dH_2O and blocked overnight in blocking buffer (0.5% BSA, 0.1% Tween 20, 0.02% SDS in phosphate-buffered saline). Molecular weight standards for SDS gel electrophoresis were obtained from Bio-Rad. Membranes were then probed for representative Coq polypeptides and Mdh1 loading control with rabbit polyclonal antibodies prepared in blocking buffer at the dilutions listed in Table 2. IRDye 680LT goat anti-rabbit IgG secondary antibody (LiCOR) was used at a dilution of 1:10,000. Proteins were visualized using a LiCOR Odyssey Infrared Scanner (LiCOR). Immunoblots are representative of three replicates and were quantified by hand using ImageStudioLite software normalized to Mdh1 and Ponceau.

Two-dimensional Blue Native/SDS-PAGE immunoblot analysis of high molecular weight complexes

Two-dimensional Blue Native (BN)/SDS-PAGE was performed as previously described (19,27,28). In brief, 200 μg of purified mitochondria were solubilized at 4 mg/mL for 1 h on ice with 16 mg/mL digitonin (Biosynth) in the presence of of cOmplete™ EDTA-free protease inhibitor cocktail tablets (Roche), phosphatase inhibitor cocktail set I (Sigma-Aldrich), phosphatase inhibitor cocktail set II (Sigma-Aldrich), and PMSF (Fisher Scientific). Protein

concentration of solubilized mitochondria was determined by the BCA assay (ThermoFisher Scientific). NativePAGE 5% G-250 sample additive (ThermoFisher Scientific) was added to the supernatant to a final concentration of 0.25%. Solubilized mitochondria (80 μg) were separated on NativePAGE 4-16% Bis-Tris gels (ThermoFisher Scientific) in the first-dimension, and native gel slices were soaked in SDS sample buffer, and further separated on 12% Tris-glycine polyacrylamide. Immunoblot analyses were performed as described above, using antibodies against Coq4 (Table 2). Molecular weight standards for BN gel electrophoresis and SDS gel electrophoresis were obtained from GE Healthcare (Sigma-Aldrich) and Bio-Rad, respectively.

Fatty acid sensitivity assay

Sensitivity of yeast cells to PUFA-induced oxidative stress was performed as described (26,29,30), with minor modifications. Strains were grown overnight in 30 mL SD-pABA medium at 30 ºC, 250 rpm, and then diluted to A_{600} = 0.25 in 15 mL of fresh SD-pABA medium. Cells were harvested at an A_{600}~1, washed twice with 10 mL sterile H_2O, and diluted to an A_{600} = 0.2 in 0.1 M phosphate buffer with 0.2% dextrose, pH 6.2 to an A_{600} = 0.2. Aliquots (5 mL) of each cell suspension was treated with an ethanol vehicle control (final concentration 0.1% vol/vol), ethanol-diluted oleic acid (Nu-Check Prep), or ethanol-diluted α-linolenic acid (Nu-Check Prep) to a 200 μM final concentration. The treated cultures were grown for 4 h at 34 ºC or 37 ºC. Cell viability was assessed via serial dilutions on YPD plate medium, which were incubated for 2 days at 30 ºC. Cell viability prior to the addition of fatty acids was determined via plate dilutions, represented in the 0 h plate.

RESULTS

cho2 and *opi3* BY4743 knockout mutants were identified in a high-throughput screen to have increased Q_6 content

The biosynthesis, trafficking, and degradation of Q_n are intricately connected and subject to multiple levels of regulation (1,2). The Stocker laboratory (Sydney, Australia) performed a high-throughput screen of the *S. cerevisiae* diploid homozygous knockout collection to identify novel genes involved in Q_6 content regulation. This library comprises knockouts of ~ 95% of non-essential genes in *S. cerevisiae*, or about ~ 5,000 total mutants, that were evaluated for altered levels of Q_6 using HPLC-EC detection. Following several rounds of analysis, 38 genes were selected as candidates with statistically significant differences in Q_6 compared to BY4743 wild-type yeast (Fig. 1A). Each of the eight mutants presenting with decreased amounts of Q_6 are genes directly involved in the Q_6 biosynthetic pathway. The 30 mutants with high Q_6 represent novel cellular processes that may regulate Q_6 production: Lipid metabolism, aminophospholipid flippase activity, mitochondrial function, vesicular trafficking, DNA repair, mRNA processing, and the RpdL3 Histone deacetylase complex (Fig. 1A). In particular, the *cho2*Δ mutant displayed about five-times the Q_6 content of wild type. This mutant was selected for continued study due to several crucial considerations—there was a mammalian homolog (PEMT), there was a mouse mutant available, the existing mount mutant was viable, and the existing mouse model had been characterized and correlated with Q_{10} related diseases (31,32) (Fig. 1A). Ultimately, we wanted to link the yeast genetics of cho2 and opi3 mutants with mammals

PC is the most abundant phospholipid in every mammalian and yeast cell type, including subcellular organelles (33). Phospholipids such as PC play a crucial role in controlling the formation and stability of lipoproteins (33). Using *S*-adenosyl-L-methionine (AdoMet, SAM),

Cho2 catalyzes the first of three methylation steps in biosynthesis of PC from PE (34,35) (Fig. 1B). The Cho2 homolog PEMT is the enzyme responsible for all three methylation steps in both mice and humans (32). Because Opi3 is associated with two methylation reactions in the *S. cerevisiae* PEMT pathway (Fig. 1B), Opi3 was included, in addition to Cho2, for subsequent studies of PC biosynthesis. Confirming the results of the initial screen, both *cho2*Δ and *opi3*Δ yeast had significantly increased Q_6 content in whole cells compared to BY4743 wild type (Fig. 2A). However, the effects of *cho2* deletion on Q_6 levels were more prominent than the effects of *opi3* deletion in purified mitochondria (Fig. 2B). This suggests a novel role for these proteins and phospholipid methylation in Q_6 homeostasis.

The CoQ synthome is stabilized in the absence of *CHO2* and *OPI3*

Previous studies have investigated the effects of *COQ* deletions on the amounts of Coq polypeptides forming the CoQ synthome (1). These Coq proteins serve as structural components required for CoQ synthome formation and stability, in addition to catalyzing essential enzymatic reactions towards the production of Q_6 (1,19,36). Here, Coq protein levels were investigated in *cho2*Δ and *opi3*Δ mutants compared to BY4743 wild type, to determine if the increased mitochondrial Q_6 could be explained by an increase in the Q_6 biosynthetic proteins (Fig. 3). To match the conditions used previously in this study for assays of Q_6 content, BY4743, *cho2*Δ, and *opi3*Δ mitochondrial lysates were prepared from yeast harvested at A_{600} = 1 cultured on SD-pABA. We anticipated that the increased Q_6 content in the *cho2*Δ and *opi3*Δ mutants (Figs. 1 & 2) might translate to up-regulated Q_6 biosynthetic machinery, including higher levels of *COQ* gene and protein expression. However, Coq protein expression remained consistent between wild type and both mutants (Fig. 3A). The *cho2*Δ and *opi3*Δ mutants did not have statistically

significant differences in Coq protein levels when quantified and normalized to either total protein Ponceau stain or a mitochondrial matrix marker (Mdh1), and plotted as a percentage of wild type (Fig. 3B,C). Although Coq7 appears elevated in both deletion mutants compared to wild type, these results did not show statistical significance because only two replicates were included in the analysis.

Decreased steady state levels of Coq polypeptides in yeast *coq* mutants often directly correlate with destabilization of the CoQ synthome (19,26,36), while increased amounts of Coq polypeptides are related to stabilization of the CoQ synthome (15). CoQ synthome stability was assessed in *cho2*Δ and *opi3*Δ mutants by two-dimensional Blue Native/SDS-PAGE (BN/SDS-PAGE) with the Coq4 signal denoting high molecular weight complex formations (19). In wild-type yeast, the CoQ synthome is represented by distinct signal at ~ 66 kDa (Fig. 4). This is a downward shift in molecular weight from prior studies, wherein the wild-type CoQ synthome is present in a diverse array of high molecular mass complexes and sub-complexes spanning a range of ~ 140 kDa to > 1 MDa for Coq4 (15,26). Reasons for these inconsistences may include the difference in carbon source and amino acid content in the medium used to culture the samples, the culture density at the time of harvest, or the diploid state. There is an additional signal in wild type just below the Coq4 signal that is non-specific, and is present in both *cho2*Δ and *opi3*Δ samples as well (Fig. 4).

Surprisingly, the CoQ synthome in the *cho2*Δ and *opi3*Δ mutants appear stabilized, indicated by the disappearance of complexes smaller than 440 kDa, and an appearance of complexes spanning ~ 440 kDa to > 1 MDa (Fig. 4). Deletion of *cho2* had the most prominent stabilization effect of the CoQ synthome compared to wild type (Fig. 4). Although the absence of *CHO2* or *OPI3* does not directly increase component Coq polypeptides, these knockout

mutations result in significant stabilization of the CoQ synthome that may partially explain the increase in Q_6 production (Figs. 1 & 2). Conversely, the increased Q_6 biosynthesis may lead to a stabilized CoQ synthome.

The yeast *cho2*Δ mutant confers increased resistance to PUFA induced peroxidative damage

PUFA peroxidation is initiated by radical-dependent hydrogen atom abstraction at bis-allylic positions, generating a carbon centered free radical (37). These radicals set in motion a chain reaction of lipid peroxidation in the presence of oxygen, driving cellular oxidative damage and the formation of protein-protein cross links, protein fragmentation, and DNA mutations (38). Yeast *coq* mutants unable to produce Q_6, such as *coq9*Δ, are sensitive to treatment with α-linolenic acid because they lack Q_6 antioxidant protection (29,30) (Fig. 5). In contrast, wild-type yeast is typically protected from α-linolenic acid treatment by Q_6 (15). Wild-type cells gradually become sensitive to PUFA treatment at non-permissible temperatures as the stress associated with heat shock imposes sensitivity, even though Q_6 is present (29,30). Thus, we evaluated whether the increased Q_6 production of the *cho2*Δ mutant is sufficient to rescue sensitivity to PUFA treatment observed in wild-type yeast in response to either 34 °C or 37 °C heat shock. Deletion of *cho2* rescued wild type sensitivity to treatment with α-linolenic acid (Fig. 5). As anticipated, all strains were resistant to monounsaturated oleic acid at both temperatures tested (Fig. 5). These results suggest that Cho2 may play a role in the conversion of redox states between reduced Q_6H_2 and oxidized Q_6. It is also possible that the higher Q_6 content in the *cho2*Δ mutant results in more Q_6 and Q_6H_2.

DISCUSSION AND FUTURE DIRECTIONS

The processes of Q_n biosynthesis, assimilation, and trafficking must be tightly regulated in order to maintain cellular bioenergetics and the antioxidant defense system (5,39). The Stocker laboratory has identified several novel regulators of *S. cerevisiae* Q_6 homeostasis from a high-throughput screen of the yeast diploid homozygous knockout collection (unpublished) (Fig. 1). Here, we confirm that deletion of *cho2* and *opi3* results in significantly increased amounts of Q_6 (Fig. 2).

CHO2 and *OPI3* encode two distinct phosphatidylethanolamine methyltransferase enzymes that catalyze the conversion of PE to PC via three consecutive methylation reactions (Fig. 1) (33). The major function of PC in humans and yeast is to maintain the integrity of membranes, in order to modulate the transport of molecules across the plasma membrane and other organelle membranes (21). PC is synthesized in mammalian cells from choline via the CDP-choline pathway, also known as the Kennedy pathway (Fig. 1) (40). In human liver, approximately 30% of PC synthesis occurs via the sequential methylation of PE (41), catalyzed by the *CHO2* mammalian homolog phosphatidylethanolamine *N*-methyltransferase (*PEMT*). Therefore, the results of this current study regarding Cho2 and Opi3 may give insights into the PEMT pathway of mammalian PC biosynthesis. Future experiments will assess whether expression of mammalian *PEMT* cDNA restores normal Q_6 content in the *cho2*Δ*opi3*Δ double mutant to confirm that these proteins are functional orthologs. Experiments have already been conducted to show that *PEMT* expression restores the PC deficiencies in the *cho2*Δ mutant (data not shown), however other *cho2*Δ phenotypes were evaluated.

Prior investigations revealed that *PEMT* regulates susceptibility to atherosclerotic cardiovascular disease and is required for normal lipoprotein metabolism (20,42). PEMT has also

been associated with cellular bioenergetics; PEMT protein expression was increased in adipocyte models of insulin resistance (43). While *Pemt* $^{+/+}$ mice fed high-fat diets displayed weight gain, plasma hyperlipidemia, and insulin resistance, *Pemt* $^{-/-}$ mice were protected against these phenotypes including diet-induced obesity (21). The accumulation of Q_6 in yeast *cho2*Δ and *opi3*Δ deletion mutants (Fig. 2) suggests that increased Q_n may be the protective mechanism against insulin resistance in *Pemt* $^{-/-}$ mice. Intriguingly, mitochondrial $Q_{9/10}$ deficiency has been implicated as a primary driver of insulin resistance *in vitro* and in mice fed a high-fat high sucrose diet (32). These data complement the results of our study nicely, implying that mechanisms that restore Q_{10}, including the deletion or inhibition of *PEMT*, might serve as novel therapeutic targets for insulin resistant patients. Ongoing studies in the Stocker lab are seeking to determine whether Cho2 (PEMT) is a conserved regulator of Q_n in mice and human adipocytes.

Both *cho2*Δ and *opi3*Δ yeast presented a stabilized CoQ synthome (Fig, 4), however, component Coq polypeptides were not elevated, with the possible exception of Coq7 (Fig. 3). The mechanism for increased Q_6 content in these mutants therefore cannot be fully explained by a comprehensive up-regulation of the Q_6 biosynthetic machinery. Mitochondrial oxidative stress is a hallmark of insulin resistance models in mice and humans (44-46). Mice harboring *Pemt*$^{-/-}$ homozygous deletion develop hypermetabolism that protects against insulin resistance, indicating that PEMT and choline are crucial regulators of energy metabolism (21). We hypothesized that Cho2, and by extension PEMT, may control mitochondrial energy production and perturb oxidative damage by regulating the flux between Q_6 redox states. Previous work has demonstrated that yeast mutants lacking Q_6 are sensitive to treatment with exogenously added polyunsaturated fatty acids (PUFAs) due to lack of antioxidant defense by Q_6H_2 (15,47). Under temperature stress conditions, *cho2*Δ showed increased protection from α-linolenic acid

compared to wild type (Fig. 5). Perhaps the higher amount of Q_6 in *cho2*Δ (Fig. 2) results in a corresponding increase in Q_6H_2 that confers additional antioxidant protection for this mutant (Fig. 5). The ratio of Q_6:Q_6H_2 could also be altered in *cho2*Δ yeast. Additional experiments need to be conducted in order to determine whether Q_6 redox state is dependent on the presence of *CHO2*. The *cho2*Δ mutant was found to have increased resistance to heat shock in a genetic screen (48). It would be interesting to determine if the Q_6 increase seen in the *cho2*Δ mutant is related to heat shock stress response.

Efficiency of the PEMT-phosphatidylcholine biosynthetic pathway not only requires Cho2 and Opi3, but also relies on SAM, the biological methyl donor (33,49). Once its methyl group is transferred to a substrate, SAM is converted to S-adenosylhomocysteine (AdoHcy, SAH), the product of Cho2 and Opi3. SAM-dependent methyltransferase reactions that also acts as a feedback inhibitor for SAM (50). Lack of Cho2/Opi3 activity leads to greater amounts of SAM co-substrate and consequently increase the SAM:SAH ratio (51). Due to the ubiquity of SAM substrates, the ratio of SAM:SAH is commonly used as sensitive indicator of cellular methylation capacity (52). Unrestricted SAM that is no longer needed for PE conversion to PC is now free to participate in alternate methylation reactions. There are three methyltransferase reactions in the Q_6 biosynthetic pathway that require SAM as a co-substrate (1); elevated concentrations of SAM might increase the rate of Q_6 biosynthesis, resulting in higher total Q_6.

Another possible explanation for the observed rise in *cho2*Δ and *opi3*Δ Q_6 content is metabolic flux through the Q_6 pathway. The polyisoprenyl tail of Q_n is synthesized from dimethylallyl diphosphate and isopentenyl diphosphate, derived from mevalonate in eukaryotes and 1-deoxy-D-xylulose-5-phosphate in prokaryotes (1). The Q_n benzoquinone ring is produced from 4-hydroxybenzoic acid (4HB), a phenolic derivative of benzoic acid that is synthesized

from tyrosine in mammals and both tyrosine and chorismate in *S. cerevisiae* (1,53). These inputs or 'fuel' are essential molecules that regulate flow into Q_n biosynthesis as opposed to other metabolic synthesis pathways. The Stocker lab has recently used an untargeted metabolomics approach coupled with mass spectrometry to compare metabolites in *cho2*Δ with wild type (data not shown). Importantly, they found decreased amounts of several Q_6 benzoquinone ring-precursor compounds in the absence of *cho2* (data not shown), indicating that Cho2 may indeed regulate the Q_6 head-group synthesis pathway. We suspect this regulation by Cho2 may involve previously unrecognized 4-HB precursors.

This study has provided crucial information towards determining the mechanism behind Cho2 and Opi3 regulation of Q_6 homeostasis. Future work by the Stocker lab will extend our findings into both *Pemt*$^{-/-}$ mouse and adipocyte cellular models. These results suggest that PEMT enzymes are novel regulators of Q_6 biosynthesis, and may be intricately connected with insulin resistance pathology.

Table 1. Genotype and source of yeast strains.

Strain	*Genotype/Specifications*	*Source*
BY4743	MAT **a**/α *his3Δ0 leu2Δ0 met15Δ0 ura3Δ0*	R. Stocker[a]
BY4743 *cho2*Δ	MAT **a**/α *his3Δ0 leu2Δ0 met15Δ0 ura3Δ0 cho2::KanMX4*	R. Stocker[a]
BY4743 *opi3*Δ	MAT **a**/α *his3Δ0 leu2Δ0 met15Δ0 ura3Δ0 opi3::KanMX4*	R. Stocker[a]
BY4742 *coq1*Δ	MAT α *his3Δ0 leu2Δ0 met15Δ0 ura3Δ0 coq1::KanMX4*	(54)
BY4742 *coq3*Δ	MAT α *his3Δ0 leu2Δ0 met15Δ0 ura3Δ0 coq3::KanMX4*	(54)
BY4742 *coq4*Δ	MAT α *his3Δ0 leu2Δ0 met15Δ0 ura3Δ0 coq4::KanMX4*	(54)
BY4742 *coq5*Δ	MAT α *his3Δ0 leu2Δ0 met15Δ0 ura3Δ0 coq5:: KanMX4*	(54)
BY4741 *coq6*Δ	MAT **a** *his3Δ0 leu2Δ0 met15Δ0 ura3Δ0 coq6::KanMX4*	Dharmacon, Inc.
BY4742 *coq7*Δ	MAT α *his3Δ0 leu2Δ0 met15Δ0 ura3Δ0 coq7::KanMX4*	(54)

Table 1. Genotype and source of yeast strains. (Cont.)

Strain	*Genotype/Specifications*	*Source*
BY4742 *coq8*Δ	MAT α *his3Δ0 leu2Δ0 met15Δ0 ura3Δ0 coq8::KanMX4*	(54)
BY4742 *coq10*Δ	MAT α *his3Δ0 leu2Δ0 met15Δ0 ura3Δ0 coq10::KanMX4*	(54)
BY4742 *coq11*Δ	MAT α *his3Δ0 leu2Δ0 met15Δ0 ura3Δ0 coq11::LEU2*	(15)
JM6	*MAT a his-4* ρ^0	(18)
JM8	*MAT α ade-1* ρ^0	(18)

[a]Prof. Roland Stocker. Victor Chang Cardiac Research Institute, Sydney, Australia.

Table 2. Description and source of antibodies.

Antibody	*Working dilution*	*Source*
Coq1	1:10,000	(55)
Coq3	1:200	(56)
Coq4	1:2,000	(57)
Coq5	1:5,000	(58)
Coq6	1:200	(59)
Coq7	1:1,000	(60)
Coq8	Affinity purified, 1:30	(36)
Coq10	Affinity purified, 1:400	(26)
Coq11	1:500	(26)
Mdh1	1:10,000	Lee McAlister-Henn[b]

[b] Dr. Lee McAlister-Henn, Department of Molecular Biophysics and Biochemistry, University of Texas Health Sciences Center, San Antonio, TX.

FIGURES

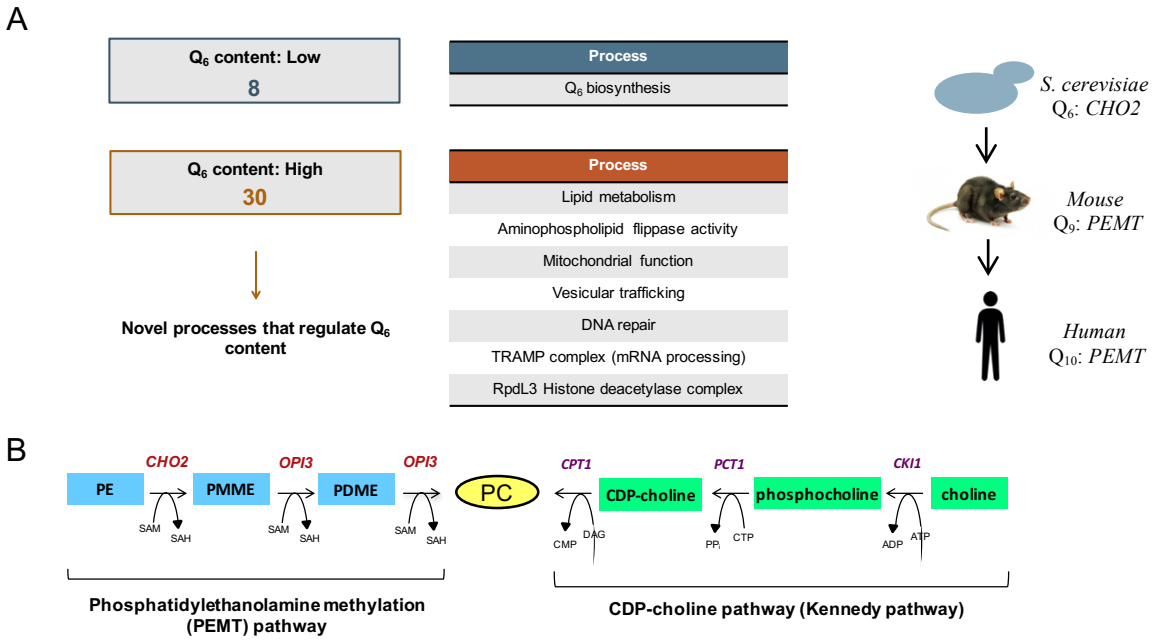

Figure 1. Cho2 and Opi3 may be involved in regulation of Q_6 content (adapted from Dr. Anita Ayer, 2018). *A*, A genetic screen of the *S. cerevisiae* homozygous diploid knockout collection performed by Dr. Anita Ayer and colleagues identified 34 mutants with significantly altered Q_6 content. Among those genes, 30 mutants displayed high Q_6 compared to BY4743 wild type, representing novel processes that regulate Q_6 content through a variety of cellular processes. In particular, the *cho2*Δ mutant had a five-fold increase in Q_6 levels versus wild type, had a viable mammalian homolog (*PEMT*), and a developed mouse mutant model (*PEMT*) with a known phenotype. *B*, Cho2 is an N-methyltransferase functioning in the biosynthesis of phosphatidylcholine (PC). Opi3, the N-methyltransferase that catalyzes the two subsequent methylation reactions towards the biosynthesis of PC, was also included in this study. Abbreviations: PE, phosphatidylethanolamine; PMME, phosphatidylmonomethyl ethanolamine; PDME, phosphatidyldimethyl ethanolamine; SAM, S-adenosylmethionine; SAH, S-adenosylhomocysteine.

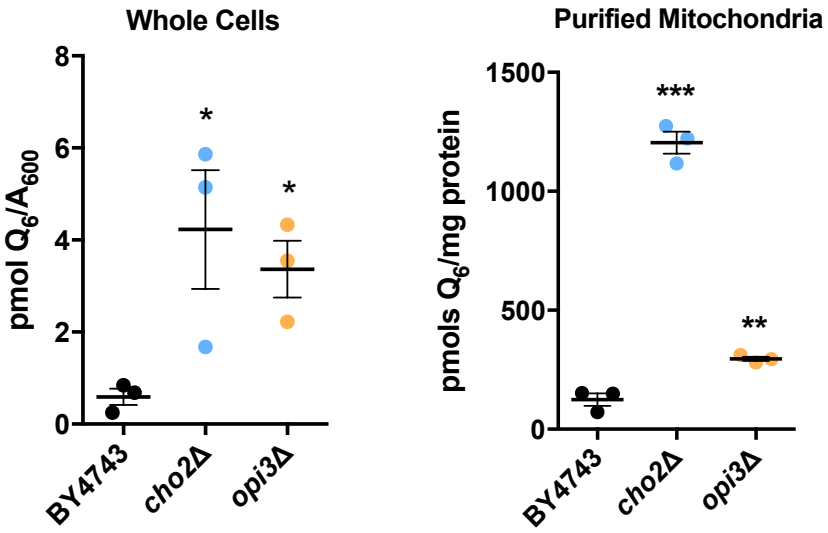

Figure 2. Total and mitochondrial Q_6 content is increased in *cho2*Δ and *opi3*Δ whole cells compared to wild type. Triplicates of 30 mL cultures of wild type BY4743, *cho2*Δ BY4743, and *opi3*Δ BY4743 yeast were grown in SD-pABA until they reached A_{600} ~ 1. *A*, 10 mL of whole cells from each culture were harvested, lipid extracted, and analyzed by LC-MS/MS for Q_6 content. Alternatively, wild type BY4743, *cho2*Δ BY4743, and *opi3*Δ BY4743 yeast were grown in SD-pABA until they reached A_{600}~1 and subject to mitochondrial preparation. *B*, Lipids from triplicates of purified mitochondria (100 μg) were analyzed by LC-MS/MS for Q_6 content. Values are the mean of three replicates. The data show mean ± SD, and the statistical significance as compared to wild type is represented by *p < 0.05, **p < 0.01, and ***p < 0.001.

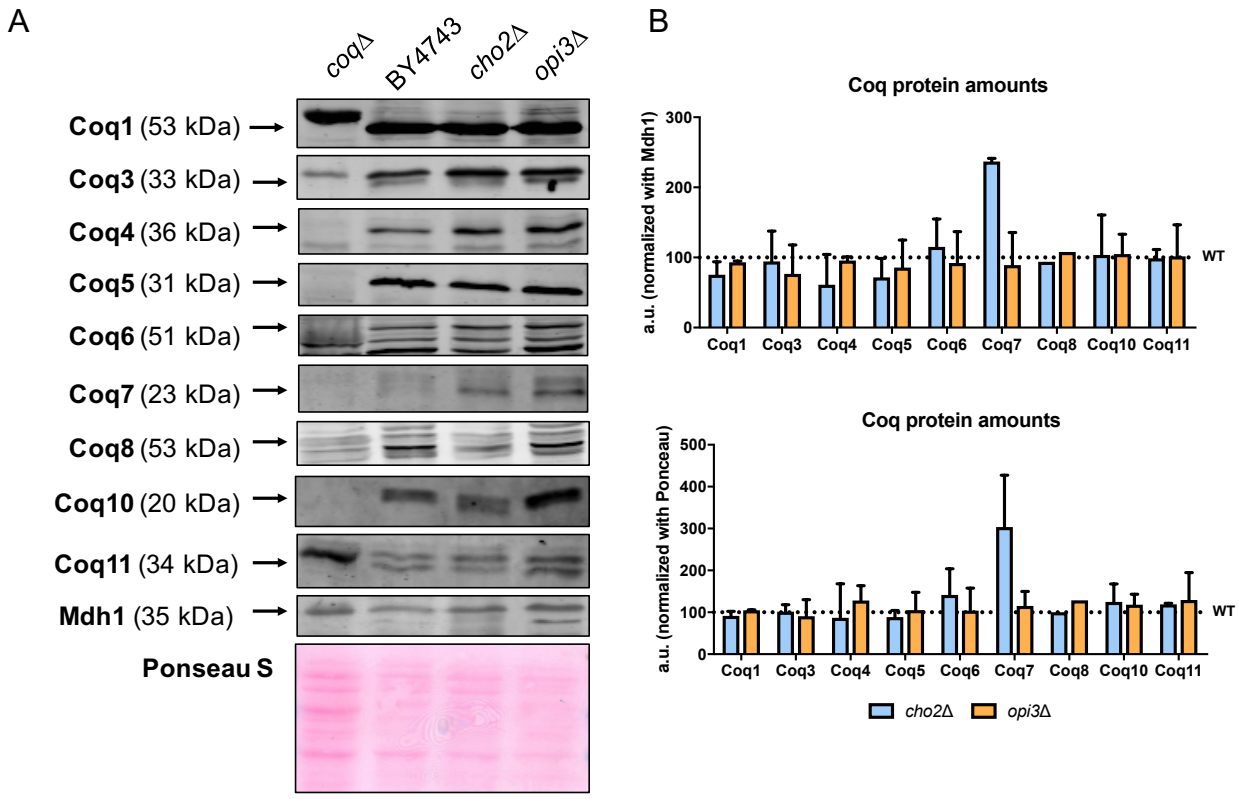

Figure 3. Coq polypeptides appear largely consistent in *cho2*Δ and *opi3*Δ mutants compared to wild type. *A*, Aliquots of intact mitochondria (25 μg) from wild type BY4743, *cho2*Δ BY4743, and *opi3*Δ BY4743 were separated on 10% or 12% Tris-Glycine SDS-PAGE and evaluated for the presence of several Coq polypeptides. Mitochondrial malate dehydrogenase (Mdh1) was included as a loading control, with a representative blot shown. Proteins were also stained with Ponceau stain as an additional loading control, with a representative image of two independent experiemtns shown. Aliquots of purified *coq*Δ (*coq1*Δ-*coq11*Δ) mitochondria were included as negative controls for immunoblotting with antisera to each of the Coq polypeptides. Black arrows indicate the position of each protein on the membrane. The Coq2 and Coq9 polypeptides were not detected. *B*, Duplicates of each Coq protein band intensity was quantified by hand using ImageStudioLite, normalized to Mdh1 or Ponceau stain, and plotted as a percentage of wild type. The data show mean ± SD.

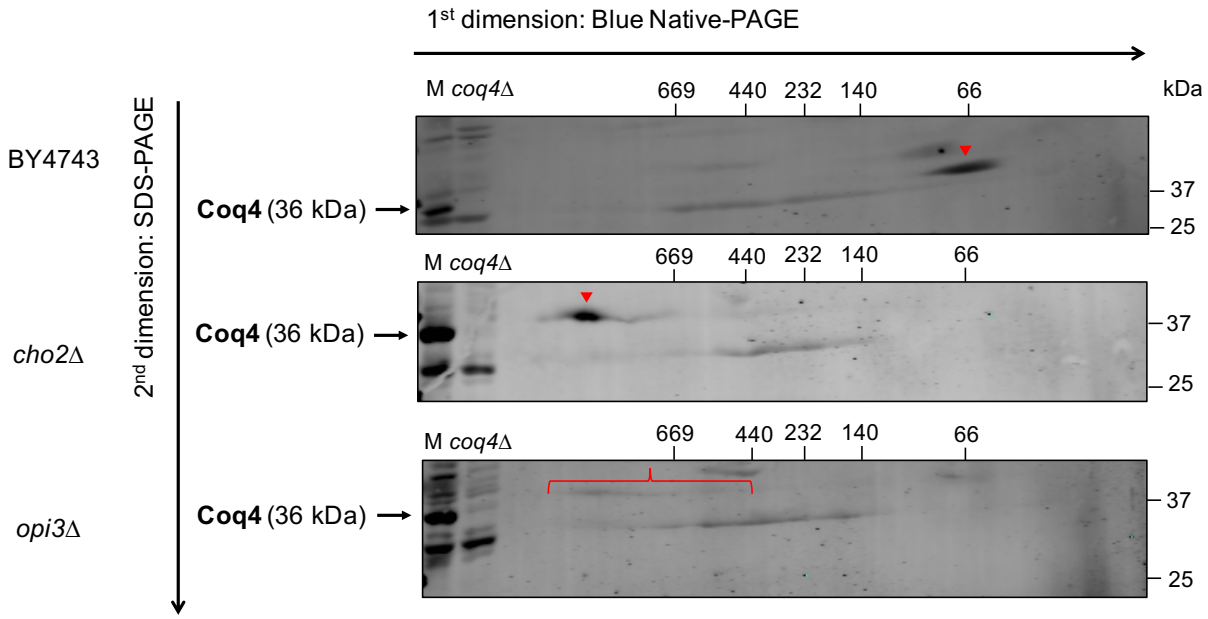

Figure 4. The CoQ synthome is stabilized in *cho2*Δ and *opi3*Δ mutants compared to wild type. Aliquots (100 µg) of purified mitochondria from wild type BY4743, *cho2*Δ BY4743, and *opi3*Δ BY4743 were solubilized with digitonin and separated with two-dimensional BN/SDS-PAGE. The CoQ synthome appeared as a singal from ~ 66 kDa to ~ 669 kDa in each sample with antibodies to Coq4. Aliquots of *coq4*Δ purified mitochondria (25 µg) were included as negative control for the antisera to Coq4. Intact mitochondria (25 µg) from each strain was included as a loading control ("M"). Red arrowheads and brackets indicate distinct complexes.

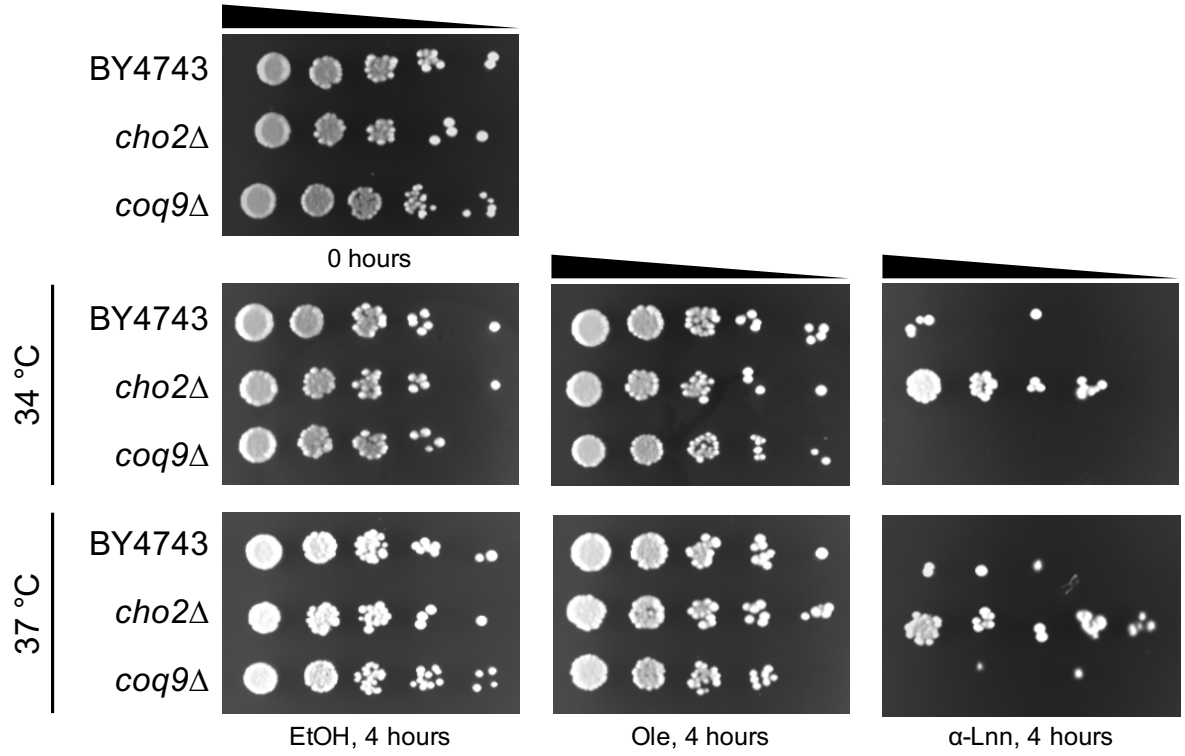

Figure 5. Mutants lacking *cho2* have increased tolerance to oxidative damage driven by exogenously added PUFAs. Wild type BY4743, *cho2Δ* BY4743, and Q_6-less *coq9Δ* BY4742 were grown at 30 °C in SD-pABA media until they reached log phase. Cells were washed twice with sterile H_2O and resuspended in phosphate buffer with 0.2% dextrose, pH 6.2 to 0.2 A_{600}/mL. The resuspended cells were incubated at 34 °C or 37 °C with oleic acid, or α-linolenic acid prepared in ethanol at a final concentration of 200 μM for 4 hours. Cells were also incubated with only ethanol as vehicle control. At time 0 or following 4 hours of fatty acid incubation, cell viability was assessed by plate dilution assay. An aliquot of 2 μL was plated in each spot in five-fold serial dilutions onto YPD, corresponding to a final A_{600} = 0.2, 0.04, 0.008, 0.0016, and 0.00032. Growth was captured after incubation at 30 °C for two days.

REFERENCES

1. Awad, A. M., Bradley, M. C., Fernandez-Del-Rio, L., Nag, A., Tsui, H. S., and Clarke, C. F. (2018) Coenzyme Q_{10} deficiencies: pathways in yeast and humans. *Essays Biochem* **62**, 361-376
2. Wang, Y., and Hekimi, S. (2019) The Complexity of Making Ubiquinone. *Trends Endocrinol Metab*
3. Alcazar-Fabra, M., Trevisson, E., and Brea-Calvo, G. (2018) Clinical syndromes associated with Coenzyme Q_{10} deficiency. *Essays Biochem* **62**, 377-398
4. Desbats, M. A., Lunardi, G., Doimo, M., Trevisson, E., and Salviati, L. (2015) Genetic bases and clinical manifestations of coenzyme Q_{10} (CoQ_{10}) deficiency. *J Inherit Metab Dis* **38**, 145-156
5. Turunen, M., Olsson, J., and Dallner, G. (2004) Metabolism and function of coenzyme Q. *Biochim Biophys Acta* **1660**, 171-199
6. Bentinger, M., Tekle, M., and Dallner, G. (2010) Coenzyme Q--biosynthesis and functions. *Biochem Biophys Res Commun* **396**, 74-79
7. Gutierrez-Mariscal, F. M., Yubero-Serrano, E. M., Villalba, J. M., and Lopez-Miranda, J. (2019) Coenzyme Q_{10}: From bench to clinic in aging diseases, a translational review. *Crit Rev Food Sci Nutr* **59**, 2240-2257
8. Quinzii, C. M., Kattah, A. G., Naini, A., Akman, H. O., Mootha, V. K., DiMauro, S., and Hirano, M. (2005) Coenzyme Q deficiency and cerebellar ataxia associated with an aprataxin mutation. *Neurology* **64**, 539-541
9. Hernandez-Camacho, J. D., Bernier, M., Lopez-Lluch, G., and Navas, P. (2018) Coenzyme Q_{10} Supplementation in Aging and Disease. *Front Physiol* **9**, 44

10. Sato, Y., Yokoyama, S., Yamaki, Y., Nishimura, Y., Miyashita, M., Maruyama, S., Takekuma, Y., and Sugawara, M. (2020) Enhancement of intestinal absorption of coenzyme Q_{10} using emulsions containing oleyl polyethylene acetic acids. *Eur J Pharm Sci* **142**, 105144

11. Lee, J. S., Suh, J. W., Kim, E. S., and Lee, H. G. (2017) Preparation and Characterization of Mucoadhesive Nanoparticles for Enhancing Cellular Uptake of Coenzyme Q_{10}. *J Agric Food Chem* **65**, 8930-8937

12. Herebian, D., Lopez, L. C., and Distelmaier, F. (2018) Bypassing human CoQ_{10} deficiency. *Mol Genet Metab* **123**, 289-291

13. Berenguel Hernandez, A. M., de la Cruz, M., Alcazar-Fabra, M., Prieto-Rodriguez, A., Sanchez-Cuesta, A., Martin, J., Tormo, J. R., Rodriguez-Aguilera, J. C., Cortes-Rodriguez, A. B., Navas, P., Reyes, F., Vicente, F., Genilloud, O., and Santos-Ocana, C. (2020) Design of High-Throughput Screening of Natural Extracts to Identify Molecules Bypassing Primary Coenzyme Q Deficiency in *Saccharomyces cerevisiae*. *SLAS Discov* **25**, 299-309

14. Stefely, J. A., and Pagliarini, D. J. (2017) Biochemistry of Mitochondrial Coenzyme Q Biosynthesis. *Trends Biochem Sci* **42**, 824-843

15. Bradley, M. C., Yang, K., Fernandez-Del-Rio, L., Ngo, J., Ayer, A., Tsui, H. S., Novales, N. A., Stocker, R., Shirihai, O. S., Barros, M. H., and Clarke, C. F. (2020) *COQ11* deletion mitigates respiratory deficiency caused by mutations in the gene encoding the coenzyme Q chaperone protein Coq10. *J Biol Chem* **295**, 6023-6042

16. Takahashi, T., Okamoto, T., Mori, K., Sayo, H., and Kishi, T. (1993) Distribution of ubiquinone and ubiquinol homologues in rat tissues and subcellular fractions. *Lipids* **28**, 803-809

17. Bentinger, M., Dallner, G., Chojnacki, T., and Swiezewska, E. (2003) Distribution and breakdown of labeled coenzyme Q_{10} in rat. *Free Radic Biol Med* **34**, 563-575

18. Santos-Ocana, C., Do, T. Q., Padilla, S., Navas, P., and Clarke, C. F. (2002) Uptake of exogenous coenzyme Q and transport to mitochondria is required for bc_1 complex stability in yeast *coq* mutants. *J Biol Chem* **277**, 10973-10981

19. He, C. H., Xie, L. X., Allan, C. M., Tran, U. C., and Clarke, C. F. (2014) Coenzyme Q supplementation or over-expression of the yeast Coq8 putative kinase stabilizes multi-subunit Coq polypeptide complexes in yeast *coq* null mutants. *Biochim Biophys Acta* **1841**, 630-644

20. Noga, A. A., Zhao, Y., and Vance, D. E. (2002) An unexpected requirement for phosphatidylethanolamine N-methyltransferase in the secretion of very low density lipoproteins. *J Biol Chem* **277**, 42358-42365

21. Jacobs, R. L., Zhao, Y., Koonen, D. P., Sletten, T., Su, B., Lingrell, S., Cao, G., Peake, D. A., Kuo, M. S., Proctor, S. D., Kennedy, B. P., Dyck, J. R., and Vance, D. E. (2010) Impaired *de novo* choline synthesis explains why phosphatidylethanolamine N-methyltransferase-deficient mice are protected from diet-induced obesity. *J Biol Chem* **285**, 22403-22413

22. Brachmann, C. B., Davies, A., Cost, G. J., Caputo, E., Li, J., Hieter, P., and Boeke, J. D. (1998) Designer deletion strains derived from *Saccharomyces cerevisiae* S288C: a useful

set of strains and plasmids for PCR-mediated gene disruption and other applications. *Yeast* **14**, 115-132

23. Barkovich, R. J., Shtanko, A., Shepherd, J. A., Lee, P. T., Myles, D. C., Tzagoloff, A., and Clarke, C. F. (1997) Characterization of the *COQ5* gene from *Saccharomyces cerevisiae*. Evidence for a C-methyltransferase in ubiquinone biosynthesis. *J Biol Chem* **272**, 9182-9188

24. Gay, C. A., and Stocker, R. (2004) Simultaneous determination of coenzyme Q_{10}, cholesterol, and major cholesterylesters in human blood plasma. *Methods Enzymol* **378**, 162-169

25. Glick, B. S., and Pon, L. A. (1995) Isolation of highly purified mitochondria from *Saccharomyces cerevisiae*. *Methods Enzymol* **260**, 213-223

26. Tsui, H. S., Pham, N. V. B., Amer, B. R., Bradley, M. C., Gosschalk, J. E., Gallagher-Jones, M., Ibarra, H., Clubb, R. T., Blaby-Haas, C. E., and Clarke, C. F. (2019) Human COQ10A and COQ10B are distinct lipid-binding START domain proteins required for coenzyme Q function. *J Lipid Res* **60**, 1293-1310

27. Schagger, H., Cramer, W. A., and von Jagow, G. (1994) Analysis of molecular masses and oligomeric states of protein complexes by blue native electrophoresis and isolation of membrane protein complexes by two-dimensional native electrophoresis. *Anal Biochem* **217**, 220-230

28. Wittig, I., Braun, H. P., and Schagger, H. (2006) Blue native PAGE. *Nat Protoc* **1**, 418-428

29. Hill, S., Hirano, K., Shmanai, V. V., Marbois, B. N., Vidovic, D., Bekish, A. V., Kay, B., Tse, V., Fine, J., Clarke, C. F., and Shchepinov, M. S. (2011) Isotope-reinforced

polyunsaturated fatty acids protect yeast cells from oxidative stress. *Free Radic Biol Med* **50**, 130-138

30. Hill, S., Lamberson, C. R., Xu, L., To, R., Tsui, H. S., Shmanai, V. V., Bekish, A. V., Awad, A. M., Marbois, B. N., Cantor, C. R., Porter, N. A., Clarke, C. F., and Shchepinov, M. S. (2012) Small amounts of isotope-reinforced polyunsaturated fatty acids suppress lipid autoxidation. *Free Radic Biol Med* **53**, 893-906

31. Fazakerley, D. J., Minard, A. Y., Krycer, J. R., Thomas, K. C., Stockli, J., Harney, D. J., Burchfield, J. G., Maghzal, G. J., Caldwell, S. T., Hartley, R. C., Stocker, R., Murphy, M. P., and James, D. E. (2018) Mitochondrial oxidative stress causes insulin resistance without disrupting oxidative phosphorylation. *J Biol Chem* **293**, 7315-7328

32. Fazakerley, D. J., Chaudhuri, R., Yang, P., Maghzal, G. J., Thomas, K. C., Krycer, J. R., Humphrey, S. J., Parker, B. L., Fisher-Wellman, K. H., Meoli, C. C., Hoffman, N. J., Diskin, C., Burchfield, J. G., Cowley, M. J., Kaplan, W., Modrusan, Z., Kolumam, G., Yang, J. Y., Chen, D. L., Samocha-Bonet, D., Greenfield, J. R., Hoehn, K. L., Stocker, R., and James, D. E. (2018) Mitochondrial CoQ deficiency is a common driver of mitochondrial oxidants and insulin resistance. *Elife* **7**

33. van der Veen, J. N., Kennelly, J. P., Wan, S., Vance, J. E., Vance, D. E., and Jacobs, R. L. (2017) The critical role of phosphatidylcholine and phosphatidylethanolamine metabolism in health and disease. *Biochim Biophys Acta Biomembr* **1859**, 1558-1572

34. Kodaki, T., and Yamashita, S. (1987) Yeast phosphatidylethanolamine methylation pathway. Cloning and characterization of two distinct methyltransferase genes. *J Biol Chem* **262**, 15428-15435

35. Han, G. S., O'Hara, L., Carman, G. M., and Siniossoglou, S. (2008) An unconventional diacylglycerol kinase that regulates phospholipid synthesis and nuclear membrane growth. *J Biol Chem* **283**, 20433-20442

36. Hsieh, E. J., Gin, P., Gulmezian, M., Tran, U. C., Saiki, R., Marbois, B. N., and Clarke, C. F. (2007) *Saccharomyces cerevisiae* Coq9 polypeptide is a subunit of the mitochondrial coenzyme Q biosynthetic complex. *Arch Biochem Biophys* **463**, 19-26

37. Yin, H., Xu, L., and Porter, N. A. (2011) Free radical lipid peroxidation: mechanisms and analysis. *Chem Rev* **111**, 5944-5972

38. Andreyev, A. Y., Tsui, H. S., Milne, G. L., Shmanai, V. V., Bekish, A. V., Fomich, M. A., Pham, M. N., Nong, Y., Murphy, A. N., Clarke, C. F., and Shchepinov, M. S. (2015) Isotope-reinforced polyunsaturated fatty acids protect mitochondria from oxidative stress. *Free Radic Biol Med* **82**, 63-72

39. Gonzalez-Mariscal, I., Garcia-Teston, E., Padilla, S., Martin-Montalvo, A., Pomares Viciana, T., Vazquez-Fonseca, L., Gandolfo Dominguez, P., and Santos-Ocana, C. (2014) The regulation of coenzyme q biosynthesis in eukaryotic cells: all that yeast can tell us. *Mol Syndromol* **5**, 107-118

40. Vance, D. E., Li, Z., and Jacobs, R. L. (2007) Hepatic phosphatidylethanolamine N-methyltransferase, unexpected roles in animal biochemistry and physiology. *J Biol Chem* **282**, 33237-33241

41. DeLong, C. J., Shen, Y. J., Thomas, M. J., and Cui, Z. (1999) Molecular distinction of phosphatidylcholine synthesis between the CDP-choline pathway and phosphatidylethanolamine methylation pathway. *J Biol Chem* **274**, 29683-29688

42. Noga, A. A., and Vance, D. E. (2003) Insights into the requirement of phosphatidylcholine synthesis for liver function in mice. *J Lipid Res* **44**, 1998-2005

43. Fu, S., Yang, L., Li, P., Hofmann, O., Dicker, L., Hide, W., Lin, X., Watkins, S. M., Ivanov, A. R., and Hotamisligil, G. S. (2011) Aberrant lipid metabolism disrupts calcium homeostasis causing liver endoplasmic reticulum stress in obesity. *Nature* **473**, 528-531

44. Anderson, E. J., Lustig, M. E., Boyle, K. E., Woodlief, T. L., Kane, D. A., Lin, C. T., Price, J. W., 3rd, Kang, L., Rabinovitch, P. S., Szeto, H. H., Houmard, J. A., Cortright, R. N., Wasserman, D. H., and Neufer, P. D. (2009) Mitochondrial H_2O_2 emission and cellular redox state link excess fat intake to insulin resistance in both rodents and humans. *J Clin Invest* **119**, 573-581

45. Houstis, N., Rosen, E. D., and Lander, E. S. (2006) Reactive oxygen species have a causal role in multiple forms of insulin resistance. *Nature* **440**, 944-948

46. Hoehn, K. L., Salmon, A. B., Hohnen-Behrens, C., Turner, N., Hoy, A. J., Maghzal, G. J., Stocker, R., Van Remmen, H., Kraegen, E. W., Cooney, G. J., Richardson, A. R., and James, D. E. (2009) Insulin resistance is a cellular antioxidant defense mechanism. *Proc Natl Acad Sci U S A* **106**, 17787-17792

47. Poon, W. W., Do, T. Q., Marbois, B. N., and Clarke, C. F. (1997) Sensitivity to treatment with polyunsaturated fatty acids is a general characteristic of the ubiquinone-deficient yeast *coq* mutants. *Mol Aspects Med* **18 Suppl**, S121-127

48. Jarolim, S., Ayer, A., Pillay, B., Gee, A. C., Phrakaysone, A., Perrone, G. G., Breitenbach, M., and Dawes, I. W. (2013) *Saccharomyces cerevisiae* genes involved in survival of heat shock. *G3 (Bethesda)* **3**, 2321-2333

49. Mato, J. M., Alvarez, L., Ortiz, P., and Pajares, M. A. (1997) S-adenosylmethionine synthesis: molecular mechanisms and clinical implications. *Pharmacol Ther* **73**, 265-280

50. Hoffman, D. R., Cornatzer, W. E., and Duerre, J. A. (1979) Relationship between tissue levels of S-adenosylmethionine, S-adenylhomocysteine, and transmethylation reactions. *Can J Biochem* **57**, 56-65

51. Ye, C., Sutter, B. M., Wang, Y., Kuang, Z., and Tu, B. P. (2017) A Metabolic Function for Phospholipid and Histone Methylation. *Mol Cell* **66**, 180-193 e188

52. Caudill, M. A., Wang, J. C., Melnyk, S., Pogribny, I. P., Jernigan, S., Collins, M. D., Santos-Guzman, J., Swendseid, M. E., Cogger, E. A., and James, S. J. (2001) Intracellular S-adenosylhomocysteine concentrations predict global DNA hypomethylation in tissues of methyl-deficient cystathionine beta-synthase heterozygous mice. *J Nutr* **131**, 2811-2818

53. Olson, R. E. (1966) Biosynthesis of ubiquinones in animals. *Vitam Horm* **24**, 551-574

54. Winzeler, E. A., Shoemaker, D. D., Astromoff, A., Liang, H., Anderson, K., Andre, B., Bangham, R., Benito, R., Boeke, J. D., Bussey, H., Chu, A. M., Connelly, C., Davis, K., Dietrich, F., Dow, S. W., El Bakkoury, M., Foury, F., Friend, S. H., Gentalen, E., Giaever, G., Hegemann, J. H., Jones, T., Laub, M., Liao, H., Liebundguth, N., Lockhart, D. J., Lucau-Danila, A., Lussier, M., M'Rabet, N., Menard, P., Mittmann, M., Pai, C., Rebischung, C., Revuelta, J. L., Riles, L., Roberts, C. J., Ross-MacDonald, P., Scherens, B., Snyder, M., Sookhai-Mahadeo, S., Storms, R. K., Veronneau, S., Voet, M., Volckaert, G., Ward, T. R., Wysocki, R., Yen, G. S., Yu, K., Zimmermann, K., Philippsen, P., Johnston, M., and Davis, R. W. (1999) Functional characterization of the *S. cerevisiae* genome by gene deletion and parallel analysis. *Science* **285**, 901-906

55. Gin, P., and Clarke, C. F. (2005) Genetic evidence for a multi-subunit complex in coenzyme Q biosynthesis in yeast and the role of the Coq1 hexaprenyl diphosphate synthase. *J Biol Chem* **280**, 2676-2681

56. Poon, W. W., Barkovich, R. J., Hsu, A. Y., Frankel, A., Lee, P. T., Shepherd, J. N., Myles, D. C., and Clarke, C. F. (1999) Yeast and rat Coq3 and *Escherichia coli* UbiG polypeptides catalyze both O-methyltransferase steps in coenzyme Q biosynthesis. *J Biol Chem* **274**, 21665-21672

57. Belogrudov, G. I., Lee, P. T., Jonassen, T., Hsu, A. Y., Gin, P., and Clarke, C. F. (2001) Yeast *COQ4* encodes a mitochondrial protein required for coenzyme Q synthesis. *Arch Biochem Biophys* **392**, 48-58

58. Baba, S. W., Belogrudov, G. I., Lee, J. C., Lee, P. T., Strahan, J., Shepherd, J. N., and Clarke, C. F. (2004) Yeast Coq5 C-methyltransferase is required for stability of other polypeptides involved in coenzyme Q biosynthesis. *J Biol Chem* **279**, 10052-10059

59. Gin, P., Hsu, A. Y., Rothman, S. C., Jonassen, T., Lee, P. T., Tzagoloff, A., and Clarke, C. F. (2003) The *Saccharomyces cerevisiae COQ6* gene encodes a mitochondrial flavin-dependent monooxygenase required for coenzyme Q biosynthesis. *J Biol Chem* **278**, 25308-25316

60. Tran, U. C., Marbois, B., Gin, P., Gulmezian, M., Jonassen, T., and Clarke, C. F. (2006) Complementation of *Saccharomyces cerevisiae coq7* mutants by mitochondrial targeting of the *Escherichia coli* UbiF polypeptide: two functions of yeast Coq7 polypeptide in coenzyme Q biosynthesis. *J Biol Chem* **281**, 16401-16409

APPENDIX I

Genes and lipids that impact uptake and assimilation of exogenous coenzyme Q in *Saccharomyces cerevisiae*

Contents lists available at ScienceDirect

Free Radical Biology and Medicine

journal homepage: www.elsevier.com/locate/freeradbiomed

Original article

Genes and lipids that impact uptake and assimilation of exogenous coenzyme Q in *Saccharomyces cerevisiae*

Lucía Fernández-del-Río[a], Miranda E. Kelly[a], Jaime Contreras[a], Michelle C. Bradley[a], Andrew M. James[b], Michael P. Murphy[b,c], Gregory S. Payne[d], Catherine F. Clarke[a,*]

[a] Department of Chemistry and Biochemistry and the Molecular Biology Institute, University of California, Los Angeles, USA
[b] MRC Mitochondrial Biology Unit, University of Cambridge, UK
[c] Department of Medicine, University of Cambridge, UK
[d] Department of Biological Chemistry, David Geffen School of Medicine, University of California, Los Angeles, USA

ARTICLE INFO

Keywords:
Coenzyme Q
Ubiquinone
Transport
Uptake
Endocytosis
CoQ_6 rescue
Saccharomyces cerevisiae

ABSTRACT

Coenzyme Q (CoQ) is an essential player in the respiratory electron transport chain and is the only lipid-soluble antioxidant synthesized endogenously in mammalian and yeast cells. In humans, genetic mutations, pathologies, certain medical treatments, and aging, result in CoQ deficiencies, which are linked to mitochondrial, cardiovascular, and neurodegenerative diseases. The only strategy available for these patients is CoQ supplementation. CoQ supplements benefit a small subset of patients, but the poor solubility of CoQ greatly limits treatment efficacy. Consequently, the efficient delivery of CoQ to the mitochondria and restoration of respiratory function remains a major challenge. A better understanding of CoQ uptake and mitochondrial delivery is crucial to make this molecule a more efficient and effective therapeutic tool. In this study, we investigated the mechanism of CoQ uptake and distribution using the yeast *Saccharomyces cerevisiae* as a model organism. The addition of exogenous CoQ was tested for the ability to restore growth on non-fermentable medium in several strains that lack CoQ synthesis (*coq* mutants). Surprisingly, we discovered that the presence of CoQ biosynthetic intermediates impairs assimilation of CoQ into a functional respiratory chain in yeast cells. Moreover, a screen of 40 gene deletions considered to be candidates to prevent exogenous CoQ from rescuing growth of the CoQ-less *coq2Δ* mutant, identified six novel genes (*CDC10, RTS1, RVS161, RVS167, VPS1,* and *NAT3*) as necessary for efficient trafficking of CoQ to mitochondria. The proteins encoded by these genes represent essential steps in the pathways responsible for transport of exogenously supplied CoQ to its functional sites in the cell, and definitively associate CoQ distribution with endocytosis and intracellular vesicular trafficking pathways conserved from yeast to human cells.

1. Introduction

Coenzyme Q (CoQ) is essential for energy production in mitochondria. It functions as an electron carrier in the respiratory chain, moving electrons from Complex I (NADH oxidase in *Saccharomyces cerevisiae*), II, and several other enzymes, to Complex III [1,2]. In this manner, CoQ participates in multiple cellular pathways including β-oxidation and *de novo* synthesis of pyrimidines. In addition, $CoQH_2$ (the reduced or hydroquinone form) has an important role as an antioxidant, protecting DNA, lipids, and proteins from oxidative stress [3,4]. CoQ is composed of a benzoquinone ring connected to a polyisoprenoid side chain, whose length is species-specific [1,2]. Six isoprene subunits are present in *Saccharomyces cerevisiae* (CoQ_6), eight in *Escherichia coli* (CoQ_8), and nine and ten (CoQ_9 and CoQ_{10}) in rodents and humans, although CoQ_9 predominates in rodents and CoQ_{10} is most prevalent in humans [1,2]. Almost all cells have the capacity to produce CoQ, and at least 13 genes are necessary for its endogenous production in yeast (see Fig. 1) [1,2,5].

In humans, insufficient CoQ_{10} can result in profound deficits in mitochondrial function [9,10]. Mutations in genes that participate directly in CoQ_{10} biosynthesis lead to primary CoQ_{10} deficiencies, rare conditions that severely affect multiple organ systems, such as the central and peripheral nervous systems, kidney, skeletal muscle, heart, or sensory systems, in highly variable manners [11]. CoQ_{10} content may also be decreased in other conditions attributed to secondary deficiencies, in which depletion of CoQ_{10} is caused by mutations in genes unrelated to CoQ_{10} biosynthesis including genes involved in mitochondrial myopathies or in the mitochondrial DNA depletion syndrome [12,13]. Secondary deficiencies can also result from non-genetic conditions such as

* Corresponding author. Department of Chemistry & Biochemistry, University of California, Los Angeles, CA, 90095-1569, USA.
E-mail address: cathy@chem.ucla.edu (C.F. Clarke).

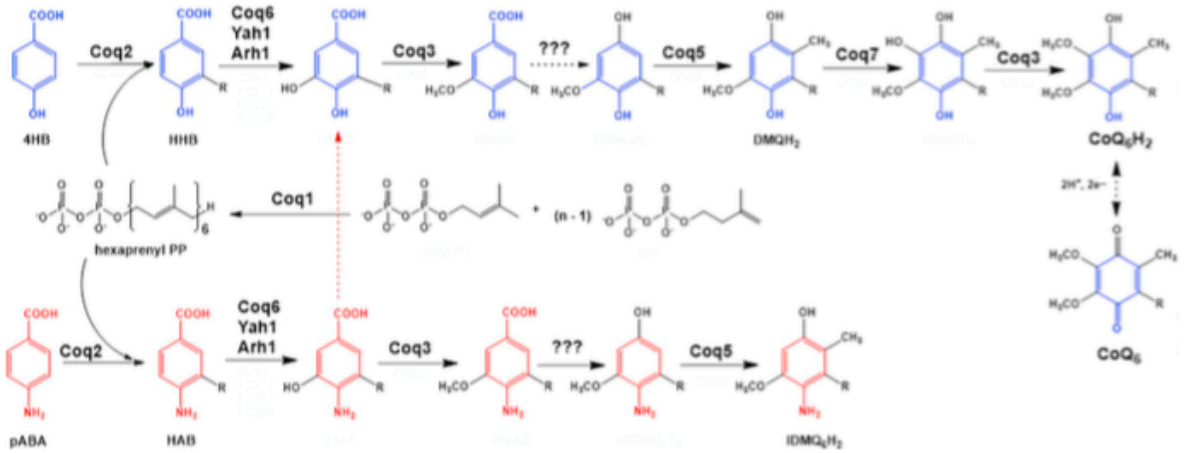

Fig. 1. Coenzyme Q biosynthetic pathway in *S. cerevisiae*. Adapted from Ref. [1]. At least 13 proteins are necessary for efficient CoQ biosynthesis in *S. cerevisiae* (Coq1-11, Yah1 and Arh1) [1]. The polyprenyl diphosphate is produced by a hexaprenyl diphosphate synthase (Coq1) [6]. Coq2 mediates the condensation of the isoprenoid tail with the aromatic ring precursor, generating a membrane-bound CoQ intermediate. In yeast, both 4HB and pABA can be used as ring precursors for CoQ_6 biosynthesis [7,8]. Intermediates originating from 4HB are depicted in *blue*, while intermediates originating from pABA are depicted in *red*. Several Coq proteins (Coq6, Coq3, Coq5 and Coq7) modify the hexaprenylated CoQ precursor to form the final product. Other Coq proteins (Coq4, Coq8, Coq9, Coq10 and Coq11) are essential for efficient CoQ production. For simplicity, only the relevant intermediates to understand further analysis have been named. 4HB = 4-hydroxybenzoic acid; pABA = para-aminobenzoic acid; HHB = 3-hexaprenyl-4-hydroxybenzoic acid; HAB = 3-hexaprenyl-4-aminobenzoic acid; $DMQH_2$ = demethoxy-QH_2; $IDMQH_2$ = 4-imino-demethoxy-QH_2; CoQ_6H_2 = reduced coenzyme Q_6H_2; CoQ_6 = oxidized coenzyme Q_6. (For interpretation of the references to colour in this figure legend, the reader is referred to the Web version of this article.)

fibromyalgia, clinical treatments (e.g. hypercholesterolemia treatment with statins) [14,15], environmental toxins, metabolic disorders, aging [16], and age-related diseases [2,4]. Secondary deficiencies are more common than primary deficiencies and reflect the diversity of biological functions and metabolic pathways that involve CoQ_{10} [11,12].

To date, the only treatment to ameliorate the symptoms of human CoQ_{10} deficiencies is CoQ_{10} supplementation. At high doses, CoQ_{10} supplements increase CoQ_{10} levels in all tissues, especially with certain formulations, and are beneficial for various pathophysiological conditions [11,17]. For example, the Q-SYMBIO study demonstrated that CoQ_{10} supplementation improves heart failure symptoms with a significant reduction in major adverse cardiovascular events and mortality [4,18]. Other studies reported that CoQ_{10} supplementation could stop the progression of encephalopathy [19] and ameliorate the symptoms of renal disease in patients with defects in *COQ2*, *COQ6*, or *ADCK4* (the human homolog of yeast Coq8) [20,21]. However, bioavailability studies show that the response of individuals to CoQ_{10} supplementation is inconsistent, and treatment failure is common [1,17]. The absorption of CoQ_{10} is slow and limited due to its high molecular weight and negligible aqueous solubility, making delivery by oral supplementation inefficient [11,17,22]. Thus, developing therapies for CoQ_{10} deficiencies remains a challenge. Current efforts are focused on new delivery strategies for CoQ [23–25], as well as on alternative approaches using compounds that enhance endogenous CoQ_{10} synthesis in CoQ_{10}-deficient patients [1,5,11,26–29].

In order to improve the therapeutic efficacy of CoQ_{10} supplementation, it is crucial to define the mechanisms responsible for the uptake and distribution of CoQ within cells. However, complete understanding of these mechanisms remains elusive. In mammalian cells and yeast, CoQ is synthesized in the inner membrane and matrix of mitochondria, yet is found in all cellular membranes, indicating the existence of a transport mechanism from the mitochondria to the rest of the cell [30–32]. Conversely, transport to the mitochondria can also occur from the extracellular environment through the plasma membrane as shown by uptake and assimilation of exogenously supplied CoQ in studies with yeast [33,34] and mice [35], as well as through successful CoQ_{10} supplementation in patients with CoQ_{10} deficiencies [36]. Bidirectionality of CoQ transport, from the extracellular media to the mitochondria and from the mitochondria to other cellular membranes, has been attributed to endomembrane trafficking, yet the pathways and mechanisms remain obscure [32,33].

In the yeast *S. cerevisiae*, CoQ_6 is not essential for viability as strains that lack CoQ_6 (*coq* mutants) can grow by fermentation on glucose without the involvement of the respiratory chain. However, *coq* mutants are unable to grow on non-fermentable carbon sources unless they are supplemented with exogenous CoQ, thereby restoring mitochondrial oxidative phosphorylation [34,37,38]. In this study, we investigated the mechanism of CoQ uptake and intracellular distribution in yeast. To do this, we interrogated a series of *ORFΔcoq2Δ* double mutants for their ability to grow in a non-fermentable glycerol-based medium (designated YPG) in the presence of exogenous CoQ_6. These mutants harbor the deletion of one gene necessary for CoQ biosynthesis (*coq2Δ*) in conjunction with the deletion of another gene hypothesized to be involved with CoQ transport. The inability of some of these *ORFΔcoq2Δ* double mutants to recover growth in YPG even in the presence of CoQ_6 allowed us to identify six genes that are important for CoQ_6 trafficking, highlighting key components of the intracellular CoQ transport pathway. Intriguingly, our results showed that single *coqΔ* mutants differ in their ability to be rescued with exogenous CoQ_6 and demonstrated that the presence of CoQ_6-hexaprenylated biosynthetic intermediates impairs the assimilation of exogenous CoQ_6 in yeast cells.

2. Materials and methods

2.1. Coenzyme Q isoforms

CoQ_2 was obtained from Cayman Chemical, CoQ_6 from Avanti, and CoQ_4 and CoQ_{10} from Millipore-Sigma. Each was dissolved in ethanol and the concentration was calculated using the absorbance at 275 nm and the corresponding molar extinction coefficients (13,700 $M^{-1}cm^{-1}$ for CoQ_2; 14,200 $M^{-1}cm^{-1}$ for CoQ_4; 14,700 $M^{-1}cm^{-1}$ for CoQ_6 and 15,200 $M^{-1}cm^{-1}$ for CoQ_{10}).

2.2. Determination of CoQ_6 movement in mixed vesicle populations

The methodology used was a combination of previously described methods [39–41]. Briefly, LUVETs (large unilamellar vesicles produced by extrusion) were created from 25 mg/mL L-α-phosphatidylcholine (PC) from soybean (Type III-S, Millipore-Sigma) in chloroform, supplemented with 1-pyrene dodecanoic acid (Pyr_{12}, Santa Cruz Biotechnology) to achieve a final concentration of 4 μM. The mixture was evaporated until dry under a stream of nitrogen gas, re-hydrated with MBSE buffer (0.15 M NaCl/0.01 M MOPS pH7/0.1 M EDTA) to a final PC concentration of 1 mg/mL, and subjected to ten freeze-thaw cycles in a solid CO_2/ethanol bath. The multilamellar vesicles were extruded through two polycarbonate filters in tandem using the Avestin Lipofast system (Avestin, Inc). A second population was created as described above, with the addition of CoQ_2, CoQ_4, CoQ_6, or CoQ_{10} to the chloroform to achieve a final concentration of 200 μM after re-hydration. To monitor the ability of the different CoQ isoforms to move between vesicles, Pyr_{12} quenching was monitored. Two mL of the initial LUVETs population was placed in a stirred cuvette in a Photon Technology International QuantaMaster Spectrofluorimeter (Horiba) (λ_{ex} 346 nm and λ_{em} 377 nm) at 30 °C. After 90 s, 0.5 mL of a CoQ-containing vesicle population was added and the fluorescence was monitored for a total of 10 min. CoQ collisionally quenches Pyr_{12} fluorescence if both are present in the same vesicle and are capable of physical interaction [39,42]. On mixing the two populations of vesicles, a further decrease in the fluorescence signal can only occur if the CoQ_n isoform is able to move from vesicle to vesicle. This is because the gain in fluorescence in the CoQ_n vesicle population from CoQ loss is less than the loss in fluorescence in the previously CoQ_n-less population from the gain of CoQ (for a discussion see Ref. [39]). Data are expressed as the ratio of fluorescence at a given point in time (I) to initial fluorescence just before the addition of the second population of vesicles (I_0).

2.3. Yeast strains, growth media, and verification of the mutants

S. cerevisiae strains used in this study are described in Table S1. Standard growth media for yeast included YPD (1% Bacto yeast extract, 2% Bacto peptone, 2% dextrose) and YPG (1% Bacto yeast extract, 2% Bacto peptone, 3% glycerol). Solid plate medium contains additional 2% Bacto agar. To select for mutants that contain a *kanMX* cassette, YPD + 200 mg/L G418 (Santa Cruz Biotechnology) plates were used. To select for *ORFΔcoq2Δ* mutants obtained from a previously created library [39], synthetic dextrose media without arginine and histidine (SD –His –Arg) (20 g/L glucose, 1.7 g/L yeast nitrogen base without amino acids and ammonium sulfate, 1 g/L monosodium glutamic acid, and 2 g/L of amino acid supplement lacking histidine and arginine) plates were used. These SD –His –Arg plates were supplemented with 200 mg/L G418, 70 mg/L canavanine (Millipore-Sigma) and 100 mg/L nourseothricin sulfate (ClonNat) (Gold Biotechnology). For mutants of new creation (see method below), SD –Leu (0.18% Difco yeast nitrogen base without amino acids and ammonium sulfate, 0.5% $(NH_4)_2SO_4$, 0.14% NaH_2PO_4, 2% dextrose and amino acid supplement lacking leucine) plate medium was used. For plasmid selection (see below), SD –Ura (0.18% Difco yeast nitrogen base without amino acids and ammonium sulfate, 0.5% $(NH_4)_2SO_4$, 0.14% NaH_2PO_4, 2% dextrose and amino acid supplement lacking uracil) liquid and plate media were used.

Deletions in each and every strain (both *ORF* and *COQ2* deletions) were confirmed by PCR, using primer pairs A - KanB or D - KanC. Primer A and D are specific for each *ORF* while KanB and KanC are located within the *kanMX* cassette. Primers were obtained from the *Saccharomyces* Genome Deletion Project database (http://www-sequence.stanford.edu/group/yeast_deletion_project/deletions3.html). T_m ranged between 57 and 62 °C. The *rho* status of the cells was also confirmed using JM6 and JM8 as *rho*0 test strains [34]. Additionally, prior to the initiation of CoQ_6 rescue experiments, we confirmed the ability of each of the corresponding single selected *ORFΔ* mutants to grow on YPG. The deletion of a single gene could compromise the ability of a mutant to grow on YPG if the gene is involved in respiratory activity. Demonstrated growth of the single *ORFΔ* on YPG ensures that recovery of respiration of the corresponding *ORFΔcoq2Δ* mutants with exogenous CoQ_6 is theoretically possible. Any single mutant unable to grow on YPG automatically eliminated the corresponding *ORFΔcoq2Δ* from the study.

2.4. Generation of double deletion mutants

Some non-available mutants of interest for the study were created *de novo* using a PCR-based gene deletion strategy [43]. In all cases, the *ORF* of interest was replaced with a *LEU2* auxotrophic marker amplified from the pRS305 vector using primers *Leu forward: 5′-TGCCCTCCTCCTTGTC AATA-3′* and *Leu reverse: 5′- GGCGCCTGATTCAAGAAATA-3′*, to which homologous sequences to the upstream of *ORF* start codon and downstream of the *ORF* stop codon were attached. Details about these homologous sequences are described in Table S2. Following PCR clean-up (Thermo Fisher Scientific), the PCR products were used to transform corresponding *ORFΔ* mutant strain using the lithium acetate/single-stranded carrier DNA/Polyethylene Glycol method [44], and transformed cells were selected twice on SD –Leu plates. Genomic DNA isolation following by PCR and DNA sequencing (Laragen, Inc.) were used to verify the correct integration of the auxotrophic marker at the correct gene locus. In these verification steps, specific primers A and D from the *Saccharomyces* Genome Deletion Project database were used, together with two internal primers inside the LEU vector (*5′-CCATCACCATCGTCTTC CTT-3′* and *5′-CTGTGGGTGGTCCTAAATGG-3′*) for DNA sequencing.

2.5. Generation of rho negative yeast

To generate *rho*0 BY4741 yeast, cells were incubated on YPD media plus 25 μg/mL ethidium bromide for two subsequent overnight periods. After that, cells were diluted (1:20,000 from a 1 A_{600nm}/mL solution) and plated on YPD. After 1–2 days, cells were replica plated to YPG plate medium to test their ability to respire. Colonies unable to grow on YPG were considered *rho*0. To further confirm the absence of mtDNA, two distant mitochondrial DNA loci, *COX3* and *OLI1*, were checked by PCR (**COX3-F**: *5′-GGTAATAT GAATATGGTATATTTAGC-3′*; **COX3-R**: *5′-GTTACAGTAGCACCAGAAGATA ATAAG-3′*; **OLI1-F**: *5′-ATGCAATTAGTATTAGCAGCTAAAT-3′*; **OLI1-R**: *5′-CCGAATAATAATAAGAATGAAACCATTA-3′*) [45]. The *ERG2* locus was included as a positive control for a nuclear gene, using erg2A and erg2D primers from the *Saccharomyces* Deletion Project Database.

2.6. Exogenous CoQ rescue assays

Yeast mutants were grown overnight in YPD at 30 °C 250 rpm. The next day, the A_{600nm}/mL was measured and yeast strains were sub-inoculated into tubes containing 5 mL of YPG supplemented with CoQ (2 μM of CoQ_6 [33] or 100 μM of CoQ_2 [39]) or with the corresponding amount of ethanol at a cell density of 0.1 A_{600nm}/mL. In all experiments the amount of ethanol added to the culture (containing CoQ or as vehicle) was less than 1% of the culture volume. Yeast were allowed to grow at 30 °C 250 rpm for 7 days. To construct the growth curves (see examples in Fig. S4), A_{600nm} measurements were taken at approximately 0, 7, 24, 30, 48, 54, 72, 78, and 144 h. An aliquot of each culture (200 μL) was transferred to a 96-well plate and A_{600nm} was measured in a TECAN M1000 plate reader. 1/10 dilutions were made if necessary. With the exception of Fig. S4, CoQ rescue is always represented as a percentage of a designated control, considered as 100% and represented as a dashed line in the graphics. A_{600nm} from the last time point, 144 h, was used to calculate the degree of rescue.

2.7. Determination of CoQ_6 and CoQ_6 intermediates

To determine the content of CoQ_6 and CoQ_6 intermediate in *coqΔ* mutants, 15 mL of yeast grown on YPD were harvested at

approximately 1 A_{600nm}/mL. Lipid extractions and the following analysis of CoQ content in a 4000 QTRAP linear MS/MS spectrometer (Applied Biosystems) were performed as described [46]. Aliquots of the culture were saved prior to lipid extraction to determine protein concentration using Bradford assay [47].

2.8. Immunoblot analysis

Three mL of yeast grown on YPD were harvested at approximately 1 A_{600nm}/mL. Pellets were resuspended in 100 µL 2 M lithium acetate and incubated on ice for 5 min. Samples were centrifuged and pellets were resuspended in 100 µL 0.4 M NaOH, then incubated on ice for 5 min. After this step, a 10 µL aliquot of each sample was saved for further protein quantification. Samples were resuspended in 100 µL 1X SDS sample buffer (50 mM Tris pH 6.8, 10% glycerol, 2% SDS, 0.1% bromophenol blue, and 1.33% β-mercaptoethanol) and boiled for 5 min. After centrifugation, supernatants were moved to clean tubes and stored at −20 °C until further use. 30–50 µg of protein was loaded in individual lanes and separated by SDS gel electrophoresis on 12% Tris-glycine polyacrylamide gels. Proteins were subsequently transferred to 0.45 µm Immobilon-P membrane (Bio-Rad). Blots were stained with Ponceau S dye for visualization of protein lanes and assessment of equal protein loading. After blocking (blocking buffer: 0.5% BSA, 0.1% Tween 20, 0.02% SDS in phosphate-buffered saline), blots were incubated with 1:1,000 primary anti-Porin 1 (obtained from Dr. Carla Koehler, University of California, Los Angeles) and 1:20,000 secondary IRDye 680LT goat anti-rabbit IgG antibody (LiCOR). Immunoblot images were visualized with a LiCOR Odyssey infrared scanner (LiCOR), and relative protein levels were quantified by band densitometry using both Image Studio Lite 5.2 and ImageJ.

2.9. Complementation of ORFΔcoq2Δ mutants with yeast COQ2

To re-introduce *COQ2* in the *ORFΔcoq2Δ* double mutants, the vector pRSQ2 was constructed. The sequence of yeast *COQ2* plus 350 bp of the upstream sequence was cloned into the vector pRS316 [48] using the BamHI restriction site. Then, the empty vector, as well as pRSQ2, were each used to transform *coq2Δ*, *cdc10Δcoq2Δ*, *rts1Δcoq2Δ*, *rvs161Δcoq2Δ*, *rvs167Δcoq2Δ* and *nat3Δcoq2Δ*. Transformation of WT and the corresponding single *ORFΔ* with pRS316 served as controls. Cells containing the plasmid were double selected on SD −Ura plates. The ability of the *ORFΔcoq2Δ* to recover their respiratory capacity after *COQ2* was analyzed using spot plate assays. Briefly, plasmid-containing cells were grown overnight in SD −Ura at 30 °C 250 rpm. The next morning, A_{600nm}/mL was measured, cells were diluted to 0.2 A_{600nm}/mL in PBS, and a series of 5-fold dilutions were prepared. 2 µL of each dilution were plated onto YPD, YPG and SD −Ura plates. Plates were incubated at 30 °C and after 3–4 days, pictures were taken.

2.10. Statistical analysis

Data shown in this work represent mean ± standard deviation (SD) from at least three biological replicates. Statistical analyses and graphics were performed with Graphpad Prism 7 (Graphpad Software Inc., San Diego, CA, USA). When a specific mutant is compared to WT or to a designated normalization variable (specific *coqΔ* + CoQ_6 or *ORFΔ*) a *paired t-test* analysis was performed. When comparing two specific mutants between each other, an *unpaired t-test* analysis was used. Significant differences were referred as *p < 0.05, **p < 0.01, ***p < 0.001, and ****p < 0.0001.

3. Results

3.1. CoQ_6 does not move passively between non-contiguous membranes

Growth of *coqΔ* strains on YPG with exogenous CoQ_6 [33,34] indicated that a sufficient quantity of the supplied CoQ_6 reached the mitochondrial inner membrane. However, the uptake of a particular CoQ isoform depends on the length of the isoprenoid chain. A previous study assessed the ability of different CoQ isoforms to diffuse between non-contiguous membranes [39]. Short CoQ isoforms such as CoQ_2 and CoQ_4 that are more water soluble, freely exchanged between phospholipid bilayers, while a long CoQ isoform (CoQ_9) did not due to its extreme hydrophobicity, and thus required a mechanism of transport [39]. The behavior of the *S. cerevisiae* isoform CoQ_6 has not been evaluated. Therefore, to assess the ability of CoQ_6 to move between non-contiguous membranes, fluorescence quenching experiments were performed with two populations of phosphatidylcholine vesicles. Both populations contained equal concentrations of the fluorophore Pyr_{12}, but only the second population contained the specified isoform of CoQ_n. In this second population, the presence of CoQ_n fully quenches Pyr_{12} fluorescence by collisional quenching. On mixing the two populations of vesicles, a further decrease in the fluorescence signal can only occur if the CoQ_n isoform is able to move from vesicle to vesicle [39,49]. Results showing the behavior of CoQ_6 in comparison with CoQ_2, CoQ_4 and CoQ_{10} are depicted in Fig. 2. When the population of CoQ-loaded vesicles was added, the fluorescence decreased dramatically when CoQ_2 or CoQ_4 were present, while fluorescence was maintained when the vesicles were loaded with either CoQ_6 or CoQ_{10}. These results indicated that CoQ_2 and CoQ_4 were able to move rapidly between the different vesicles, in agreement with previous results [39], while CoQ_{10} and CoQ_6 were non-diffusible. The inability of CoQ_6 to move between synthetic phospholipid membranes supports the idea that a transport/distribution mechanism is needed due to its negligible water solubility.

3.2. Yeast mutants harboring deletions in distinct COQ genes show different degrees of rescue in response to exogenous CoQ_6

Previous work indicated that at least four genes of the endocytic pathway are required for rescue of *S. cerevisiae* by exogenous CoQ_6

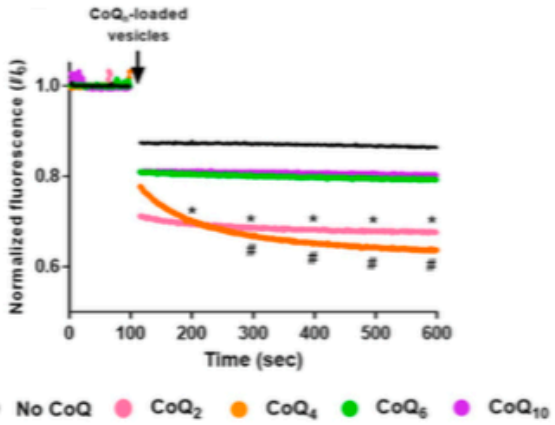

Fig. 2. CoQ_6 and CoQ_{10} isoforms fail to move freely between phosphatidylcholine vesicles. The membrane behavior of different CoQ_n isoforms was analyzed using a fluorescence-quenching assay. An initial population of vesicles containing 4 µM Pyr_{12} was mixed with 500 µL of a second population of vesicles that contained 4 µM Pyr_{12} and either a control, with no addition (*black*), or a CoQ isoform: CoQ_2 (*pink*), CoQ_4 (*orange*), CoQ_6 (*green*) or CoQ_{10} (*purple*). Fluorescence was monitored for 600 s and data points were collected every second. The data are expressed as the relative amount of fluorescence at a given point in time (I) to the initial fluorescence just before the addition of the CoQ_n-loaded vesicles (I_0). Dots represent the average, at each point, of at least three independent experiments. Standard deviations have been omitted for clarity in this figure but they are provided in Fig. S1. At intervals of 100 s, the (*) symbol represents significant differences ($p < 0.05$) between CoQ_2 and the no-CoQ condition, while (#) represents differences between CoQ_4 and the no-CoQ condition. (For interpretation of the references to colour in this figure legend, the reader is referred to the Web version of this article.)

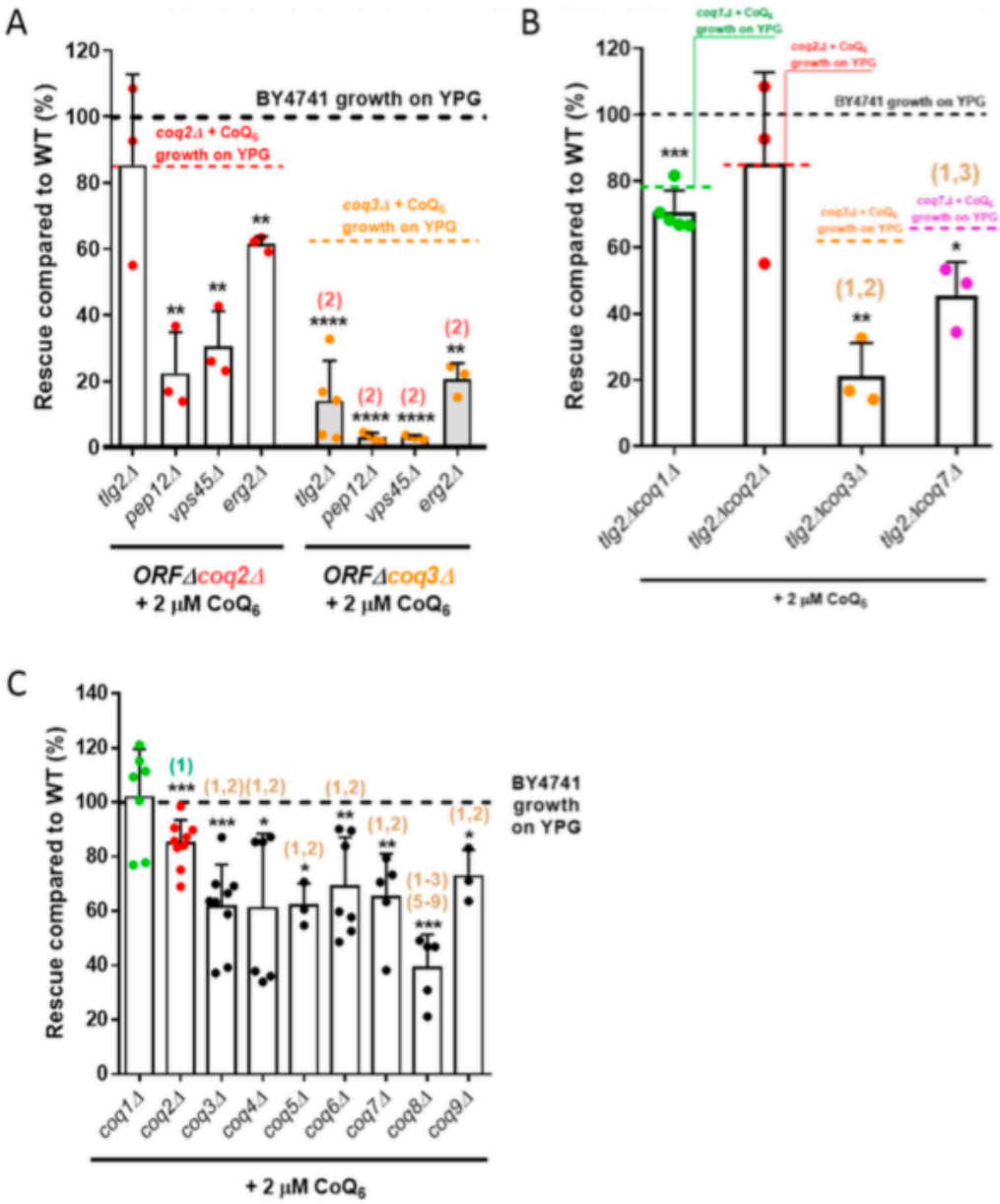

Fig. 3. Yeast mutants harboring deletions in distinct *COQ* genes show different degrees of rescue in response to exogenously added CoQ_6. **(A)** Yeast *coq2Δ* mutants harboring additional deletions in *tlg2Δ*, *pep12Δ*, *vps45Δ* or *erg2Δ* showed a more pronounced YPG growth rescue by CoQ_6 than do the comparable *coq3Δ* double mutants. **(B)** The *tlg2Δcoq1Δ*, *tlg2Δcoq3Δ* and *tlg2Δcoq7Δ* double mutants presented an impaired degree of rescue as compared to WT. The decrease of rescue was more pronounced in *tlg2Δcoq3Δ* and *tlg2Δcoq7Δ*, but especially in the *tlg2Δcoq3Δ* mutant. **(C)** Yeast mutants harboring deletions in either the *COQ1* or *COQ2* gene showed more robust rescue in response to exogenous CoQ_6 treatment than do the other single *coq* null mutants (*coq3Δ - coq9Δ*). In all cases, columns represent the degree of rescue (in %) ± SD of a strain compared to WT, which is defined as 100% and represented as a dashed line. In A and B, the average of rescue of the specific positive controls (*coq1Δ* + CoQ_6, *coq2Δ* + CoQ_6, *coq3Δ* + CoQ_6, or *coq7Δ* + CoQ_6), which were analyzed in parallel with the samples, is represented as a dashed line. Three or more independent rescue experiments were performed for every strain. Asterisks on top of the columns represent significant differences when compared to WT (*$p < 0.05$, **$p < 0.01$, ***$p < 0.001$, and ****$p < 0.0001$). Statistically significant differences between a specific *coqΔ* mutant (or *ORFΔcoqΔ* mutant) and one of its counterparts (another *coqΔ* or *ORFΔcoqΔ* mutant) are denoted with numbers in parentheses on top of the columns: (1) represents differences comparing to *coq1Δ*, (2) represents differences comparing to *ORFΔcoq2Δ* (panel A) or *coq2Δ* (panel B–C), (3) represents differences comparing to *coq3Δ*, etc. Statistical comparisons not detailed in the figure are provided in Table S3.

[33]. In that study, *ERG2*, *TLG2*, *PEP12*, or *VPS45* deleted in combination with a *COQ3* deletion inhibited growth of the resulting double mutants on YPG supplemented with CoQ_6. CoQ_6 is produced in the mitochondrial inner membrane by a large multiprotein complex (the CoQ synthome) formed by several Coq proteins (Coq3-Coq9, Coq11) [1]. The absence of one Coq polypeptide can result in the loss of other

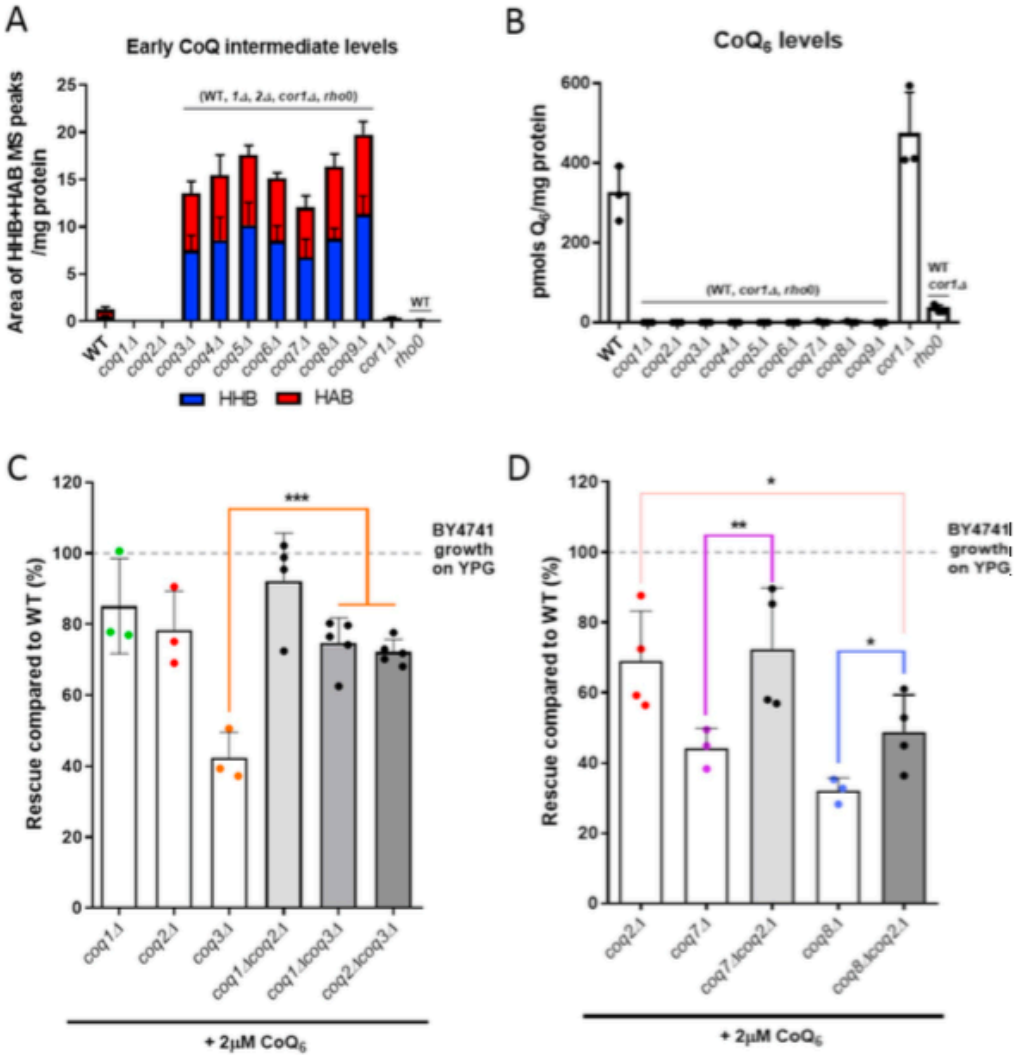

Fig. 4. The elimination of HHB and HAB intermediates augments the degree of rescue with exogenous CoQ_6. **(A)** Each of the *coq* mutants, from *coq3Δ* to *coq9Δ*, accumulated early CoQ_6 intermediates (HHB and HAB). The amount of HHB and HAB was calculated as the area of the MS peak/mg protein. **(B)** CoQ_6 was not detected in any of the *coqΔ* mutants. CoQ_6 (pmol/mg protein) was determined based on a CoQ_6 standard curve as described in Ref. [46]. **(C)** Additional deletions of either *COQ1* or *COQ2* restored the deficient CoQ_6-rescue of a *coq3Δ* mutant, but do not affect the phenotype observed in *coq1Δ* or *coqΔ2* strains. **(D)** Similar results were observed when *COQ2* is deleted in a *coq7Δ* strain, but only a partial improvement was observed in a *coq8Δ* mutant. In A and B, columns represent mean ± SD and strains named in parentheses on top of the columns denote statistically significant differences ($p < 0.01$). In C and D, columns represent the degree of rescue (in %) ± SD of a strain in comparison to WT (considered 100% and represented as a dashed line). Asterisks denote significant differences as compared to the single *coqΔ* strain (*$p < 0.05$, **$p < 0.01$, and ***$p < 0.001$). In all cases, three or more independent biological replicates were performed.

Coq proteins [1,50]. Given the effects of distinct *COQ* gene deletions on the CoQ synthome composition, we tested whether there is a difference in the ability of CoQ_6 to rescue strains carrying different *COQ* deletions in combination with the endocytic pathway mutations. Deletions of either *COQ2* or *COQ3* were combined with *erg2Δ*, *tlg2Δ*, *pep12Δ*, or *vps45Δ*, and the resulting strains were assessed for the degree of rescue by CoQ_6 (Fig. 3A, Table S3). When normalized to the wild-type parental strain (WT), rescue of the four *ORFΔcoq2Δ* double mutants by exogenous CoQ_6 was more robust than rescue of the *ORFΔcoq3Δ* counterparts. Similar results were observed if the degree of rescue was compared to the corresponding positive control (either *coq2Δ* + CoQ_6 or *coq3Δ* + CoQ_6), instead of to WT growth (Fig. 3A, Table S3). These results suggested that *coq3Δ* cells are sensitized to the effects of endocytic pathway mutations on CoQ_6 rescue compared to *coq2Δ* cells. This was most apparent in the case of *tlg2Δ*, which severely inhibited rescue in *coq3Δ* cells but had no effect on rescue in *coq2Δ* cells. It thus seemed possible that the presence of different CoQ_6 synthesis intermediates might influence the rescue with exogenous CoQ_6. In a *coq3Δ* mutant, the Coq2 polypeptide is present and active, resulting in the production of two hexaprenylated CoQ_6 intermediates: 3-hexaprenyl-4-hydroxybenzoic acid (HHB), and 3-hexaprenyl-4-aminobenzoic acid (HAB) (Fig. 1) [1]. On the other hand, in a *coq2Δ* mutant, CoQ biosynthesis is blocked at the hexaprenyl transfer step, and neither HHB nor HAB can be formed.

To further examine whether the accumulation of early CoQ_6 synthesis intermediates influences the degree of rescue by exogenous CoQ_6, we

focused on a particular endocytosis-defective mutant, *tlg2Δ*, and constructed *COQ1* and *COQ7* deletion strains. Coq1 synthesizes the CoQ polyisoprenoid tail, so its deletion prevents the formation of any hexaprenylated CoQ precursors (Fig. 1) [1]. Coq7 is a hydroxylase responsible for catalyzing the penultimate step of the CoQ biosynthetic pathway. However, because it is also a required structural component of the CoQ synthome, its deletion leads to the accumulation of HHB and HAB [1]. As shown in Fig. 3B, the degree of rescue of either *tlg2Δcoq3Δ* or *tlg2Δcoq7Δ* was significantly different from the mutants carrying *tlg2Δcoq1Δ* or *tlg2Δcoq2Δ*. It is notable that the *tlg2Δcoq3Δ* exhibits the most severely impaired degree of rescue (Fig. 3B, Table S3). The same general trend was observed when the degree of rescue is compared to each of the corresponding positive controls (e.g. *coq1Δ* + CoQ_6; *coq2Δ* + CoQ_6; *etc.*), instead of to WT growth (Fig. 3B, Table S3). These results suggest that the accumulation of CoQ hexaprenylated intermediates can affect the restoration of respiratory chain function by exogenous CoQ_6.

We then assessed the degree of rescue of each of the *coq1Δ* to *coq9Δ* single mutants in presence of exogenous CoQ_6 (Fig. 3C). The *coq1Δ* mutant grew to WT levels under these conditions (Fig. 3C, Table S3). Although exogenous CoQ_6 does not completely restore the *coq2Δ* growth to WT levels, the response of the *coq2Δ* mutant is significantly better as compared to each of the other mutants, from *coq3Δ* to *coq9Δ* (Fig. 3C, Table S3). Interestingly, the *coq8Δ* mutant is more impaired than most of the other mutants (Fig. 3C, Table S3). This finding might suggests an active role of Coq8 in CoQ_6 transport. As *coq3Δ* - *coq9Δ* mutants are reported to accumulate hexaprenylated CoQ_6 intermediates, these results further support the hypothesis that the presence of such intermediates inhibits rescue of respiratory defective cells by CoQ_6.

3.3. The accumulation of early CoQ_6 hexaprenylated intermediates impairs CoQ_6 rescue

The presence of HHB and HAB in *coq3Δ-coq9Δ* mutants has been described previously [1,2,5], but a direct comparison of intermediates between the different strains is not available. We now show this comparison in Fig. 4A. These experiments revealed the loss of CoQ_6 in each of the *coqΔ* mutant strains (Fig. 4B) and a similar accumulation of HHB and HAB in *coq3Δ* - *coq9Δ* mutants (Fig. 4A, Fig. S2). None of the *coqΔ* mutants accumulated late-stage CoQ_6 intermediates (Fig. S2). In all cases, several controls were included: WT, which defines normal content of CoQ_6 and CoQ_6 biosynthetic intermediates in yeast cells; *cor1Δ*, as an example of a mutant with normal CoQ_6 content but an inability to respire due to the deletion of *COR1*, an essential component of complex III; and a *rho0* mutant on the same genetic background, to evaluate the absence of mitochondrial DNA (mtDNA) on CoQ_6 content. The absence of mtDNA can be considered a secondary CoQ deficiency [2,51], and accordingly a dramatic decrease of CoQ_6 is observed (Fig. 4B). Additionally, to investigate whether altered mitochondrial mass might affect the degree of rescue of *coq3Δ-coq9Δ* mutants, we measured levels of the porin 1 polypeptide as a mitochondrial mass marker. Mitochondrial mass was not altered in any of the nuclear mutants (Fig. S3).

If accumulation of hexaprenylated CoQ_6 intermediates HAB and HHB caused by *coq3Δ* - *coq9Δ* mutations is responsible for impaired rescue by exogenous CoQ_6, then deletion of either *COQ1* or *COQ2*, which prevent the prenylation, should improve growth of *coq3Δ* - *coq9Δ* in the presence of CoQ_6. As predicted, deletion of *COQ1* or *COQ2* in a *coq3Δ* mutant provided a degree of CoQ_6 rescue comparable to either the *coq1Δ* and *coq2Δ* single mutant, and approximately double that of a *coq3Δ* mutant (Fig. 4C). Similarly, deletion of *COQ2* in either a *coq7Δ* or a *coq8Δ* mutant enhanced rescue by exogenous CoQ_6 as compared with the rescue of either the *coq7Δ* or *coq8Δ* single mutants (Fig. 4D). Interestingly, the rescue of the *coq8Δcoq2Δ* mutant was still lower than the rescue of a single *coq2Δ* strain (Fig. 4D). Together, our data indicate that the accumulation of HHB and HAB intermediates in *coq3Δ-coq9Δ* mutants impairs rescue by exogenous CoQ_6.

3.4. Genes that diminish growth response to exogenous CoQ_6

To identify genes involved in CoQ_6 uptake and trafficking to mitochondria, we used a library of double *ORFΔcoq2Δ* mutants, and tracked their ability to recover growth on YPG when supplemented with exogenous CoQ_6. This library was previously developed to identify proteins or pathways that might be involved in CoQ_2 or CoQ_4-dependent growth on non-fermentable substrates [39]. Based on the results described above, the use of *coq2Δ* in the library avoids potential complications from accumulation of HHB and HAB. Rescue with exogenous CoQ_6 requires vigorous aeration of liquid cultures, which does not occur in high throughput multi-well assays [52]. Therefore, we selected 48 candidate genes that previous literature suggests may be involved in CoQ_6 uptake/distribution [32,33,39]. The genes can be grouped into seven categories (Table 1): 16 genes described to have diminished response to exogenous CoQ_2 and CoQ_4 [39] plus two extra genes involved in phospholipid and sterol transport (*CSR1* and *HES1*) with limited growth on exogenous CoQ_2 and CoQ_4; 15 genes implicated in yeast clathrin-mediated endocytosis [53]; four genes that assemble the endoplasmic reticulum (ER)-mitochondria encounter structure (ERMES) [54]; two genes that encode the nucleus-vacuole junction (NVJ); three genes that represent the vacuole-mitochondria patch (vCLAMP) [55,56]; four endocytosis genes already described to play a role in CoQ_6 transport [33]; and two genes that form the N-terminal acetyltransferase B (Nat B) complex. Some *ORFΔcoq2Δ* double mutants were not recoverable from the library (see Table 1), so a total of 40 mutants were ultimately analyzed.

The ability of each *ORFΔcoq2Δ* double mutant to recover respiratory growth on YPG in the presence of 2 μM CoQ_6 was monitored for seven days. In all experiments, WT, *coq2Δ* and *cor1Δ* strains were included as controls in the presence and absence of CoQ_6. This screen identified 23 mutants that showed significantly diminished rescue compared to the positive control (*coq2Δ* + 2 μM CoQ_6) (Fig. 5A), indicating that the presence of these particular *ORF*s may be necessary for optimal CoQ_6 rescue. A representative *ORFΔcoq2Δ* mutant growth curve from each group is displayed in Fig. S4. Almost all double mutants from the heterogeneous Group 1 had diminished ability to be rescued by CoQ_6, in agreement with the deficient response to addition of CoQ_2 or CoQ_4 [39]. Four affected candidates were yeast endocytic factors (Group 2), while six other members of this group retained the ability to be rescued with exogenous CoQ_6. This result suggests that the entire endocytic pathway may not be necessary for CoQ_6 transport, or that alternative or redundant mechanisms of CoQ_6 transport may compensate for the deletion of a particular gene. A strong deficiency in rescue was also observed in three of the four gene deletions previously studied [33] (Group 6) and in the members of the Nat B complex. Interestingly, the groups representing the connections between organelles were in general not affected. These results may either exclude gene products involved in organelle connections as participants in the mechanism of CoQ_6 transport, or suggest that CoQ_6 transport has more than one path and so the elimination of one organelle connection is not sufficient to produce a defective phenotype.

Deletions of certain genes may not completely abolish the ability of mutants to grow on YPG, but can still compromise growth. To examine this, a second round of screening was performed and the ability of the *ORFΔcoq2Δ* mutants to grow in the presence of exogenous CoQ_6 was compared with the corresponding single *ORFΔ*. We analyzed the 23 candidates identified in Fig. 5A for their degree of rescue when compared to the single *ORFΔ*. It should be noted that two double mutants were excluded: *qcr9Δcoq2Δ* and *emi1Δcoq2Δ*. The growth of the single *qcr9Δ* in YPG was highly inconsistent, for reasons that are unclear. In the case of the *emi1Δcoq2Δ* mutant, the phenotype observed was unlikely to be related to CoQ_6 transport, and is being investigated separately. Of the remaining 21 *ORFΔcoq2Δ* mutants, 17 candidates were

Table 1
Yeast gene candidates selected for screening.

Group 1	Genes with diminished response to exogenous CoQ_2 and CoQ_4 [39]	*ZDS1, RTS1, IKI3, ELP4, QCR9, ACO1, MDL2, SAC1, SWF1, ARV1, CDC10, KCS1, EMI1, MET18, RPL31A, HTA1, CSR1, HES1*
Group 2	Yeast major clathrin-mediated endocytic factors [53]	*SYP1, EDE1, CHC1, CLC1, SLA2, END3, SLA1, VRP1, BZZ1, MYO3, MYO5, BBC1, RVS161, RVS167, ABP1*
Group 3	ER-mitochondria encounter structure (ERMES)	*MMM1, MDM10, MDM12, MDM34*
Group 4	Nucleous-vacuole junction (NVJ)	*VAC8, NVJ1*
Group 5	Vacuole-mitochondria patch (vCLAMP)	*YPT7, VAM6, VAM7*
Group 6	Genes previously described to be required for CoQ_6 rescue [33]	*TLG2, PEP12, ERG2, VPS45*
Group 7	Nat B complex	*MDM20, NAT3*

Genes depicted in light grey represent the *ORFΔcoq2Δ* double mutants that were not recoverable for the *ORFΔcoq2Δ* library.

significantly different from the corresponding *ORFΔ* (Fig. 5B), suggesting they are involved in CoQ_6 transport. The four *ORFΔ* that were eliminated were each rescued to their maximum potential level, indicating that the slow YPG growth is unrelated to CoQ_6 transport. A good example of this phenomenon can be observed in Fig. S4B, where the growth of *ede1Δcoq2Δ* + CoQ_6 is similar to the growth of *ede1Δ*, and both display decreased growth as compared to the positive control.

3.5. Comparison of the CoQ_2 and CoQ_6 rescue phenotypes identifies six candidates necessary for CoQ_6 transport

In order to identify the most relevant genes in the transport of CoQ_6, we analyzed the rescue phenotype of the 17 previously identified candidates in response to exogenous CoQ_2. We hypothesized that if the growth defect of the *ORFΔcoq2Δ* mutants is in fact due to the uptake and/or distribution of CoQ_6, a shorter, diffusible isoform of CoQ such as CoQ_2 should allow for a better degree of rescue than CoQ_6. In this scenario, CoQ_2 will be able to reach the mitochondria of the mutants even when the mechanisms of transport are impaired. It is important to note that the degree of rescue of the *coq2Δ* mutant in the presence of CoQ_2 was significantly lower than that observed in the presence of CoQ_6 (Fig. S5A). It is possible that the more rapid diffusion of CoQ_2 between membranes due to its far lower hydrophobicity limits its accumulation in the mitochondria where it must partition to recover respiratory function.

Comparison between CoQ_2 and CoQ_6 rescue phenotypes of each of the 17 *ORFΔcoq2Δ* mutants is depicted in Fig. 6A. The CoQ_2 rescue phenotype of the mutants on their own can be observed in Fig. S5B. Of the 17 *ORFΔcoq2Δ* mutants analyzed, eight showed statistically significant differences between CoQ_2 and CoQ_6 rescue. However, only five *ORFΔcoq2Δ* candidates fit the criterion of having a degree of CoQ_2 rescue significantly greater than that by CoQ_6. Thus, these five genes (*CDC10, RTS1, RVS161, RVS167,* and *NAT3*) seem good candidates to encode proteins that are required for CoQ_6 uptake and/or distribution to mitochondria within yeast cells. The known functions of these proteins are summarized in Table 2. In Fig. S6, we showed that the transformation of the final five *ORFΔcoq2Δ* candidates with the plasmid pRSQ2 (containing the *COQ2* gene) restores the growth of the *ORFΔ* on YPG plates.

Two of the five identified proteins, Rvs161 and Rvs167, function together in the vesicle scission step of the clathrin-mediated endocytosis pathway. Multiple studies have identified Vps1 as a third player in this mechanism [61,62]. Moreover, Vps1 and Rvs167 have been reported to function together during endocytosis [63]. *VPS1* was not part of our initial selection of candidates, but due to its functional relationship with Rvs161 and Rvs167, we hypothesized that it might also function in CoQ_6 transport. The degree of rescue with exogenous CoQ_6 of the *vps1Δcoq2Δ* mutant, in comparison to the positive control and also with *vps1Δ*, is represented in Fig. 6B and C. In both cases, the degree of CoQ_6 rescue is dramatically impaired. In addition, the degree of rescue with exogenous CoQ_2 was analyzed, and the comparison with the CoQ_6 rescue phenotype showed that the "CoQ_2 rescue > CoQ_6 rescue" criteria is fulfilled (Fig. 6D). These results confirmed *VPS1* as an additional gene required for CoQ_6 transport.

4. Discussion

CoQ_{10} is among the most widely used dietary and nutritional supplements on the market, ranging from an over-the-counter supplement to more specific administration for particular disorders [64]. Numerous disease processes associated with CoQ_{10} deficiency may benefit from CoQ_{10} supplementation, including primary and secondary CoQ_{10} deficiencies, mitochondrial diseases, fibromyalgia, cardiovascular disease, neurodegenerative diseases, cancer, diabetes mellitus, infertility, and periodontal disease [17,65,66]. However, CoQ_{10} is not an efficient oral supplement. Its high lipophilicity and poor solubility lead to low bioavailability due to limited absorption into systemic circulation, making the effective delivery of CoQ_{10} to the mitochondria a major challenge [23,67]. Understanding the mechanism(s) used to uptake and distribute CoQ_{10} within cells is of great relevance to help CoQ_{10} become an efficient therapy. Towards this end, the studies in yeast reported here uncovered an unexpected inhibitory effect of prenylated CoQ intermediates on exogenous CoQ assimilation and identified six genes required for functional rescue of CoQ-deficiency by exogenous supplementation with the normal cellular form of CoQ. While we have utilized respiration as a means to identify genes that transport CoQ, CoQ supplementation via these transport pathways could offer antioxidant protection against mitochondrial-derived oxidants.

Multiple lines of evidence support the existence of one or more import pathways for exogenous CoQ_6 and CoQ_{10}, as well as an intracellular distribution mechanism for *de novo* synthesized CoQ from the mitochondria to other cellular membranes [30–34]. Results presented in Fig. 2 establish the necessity of transport systems for movement of CoQ_{10} and CoQ_6 between membranes, supporting the view that CoQ transport requires the endomembrane system [32,33]. To address the mechanism of transport, we adopted a genetic strategy in which gene deletions were screened for effects on the ability of exogenous CoQ_6 to rescue the growth of a *coqΔ* strain deficient in CoQ synthesis. During the course of these experiments, we observed differential responses of *coqΔ* mutants to exogenous CoQ_6 due to reduced rescue in

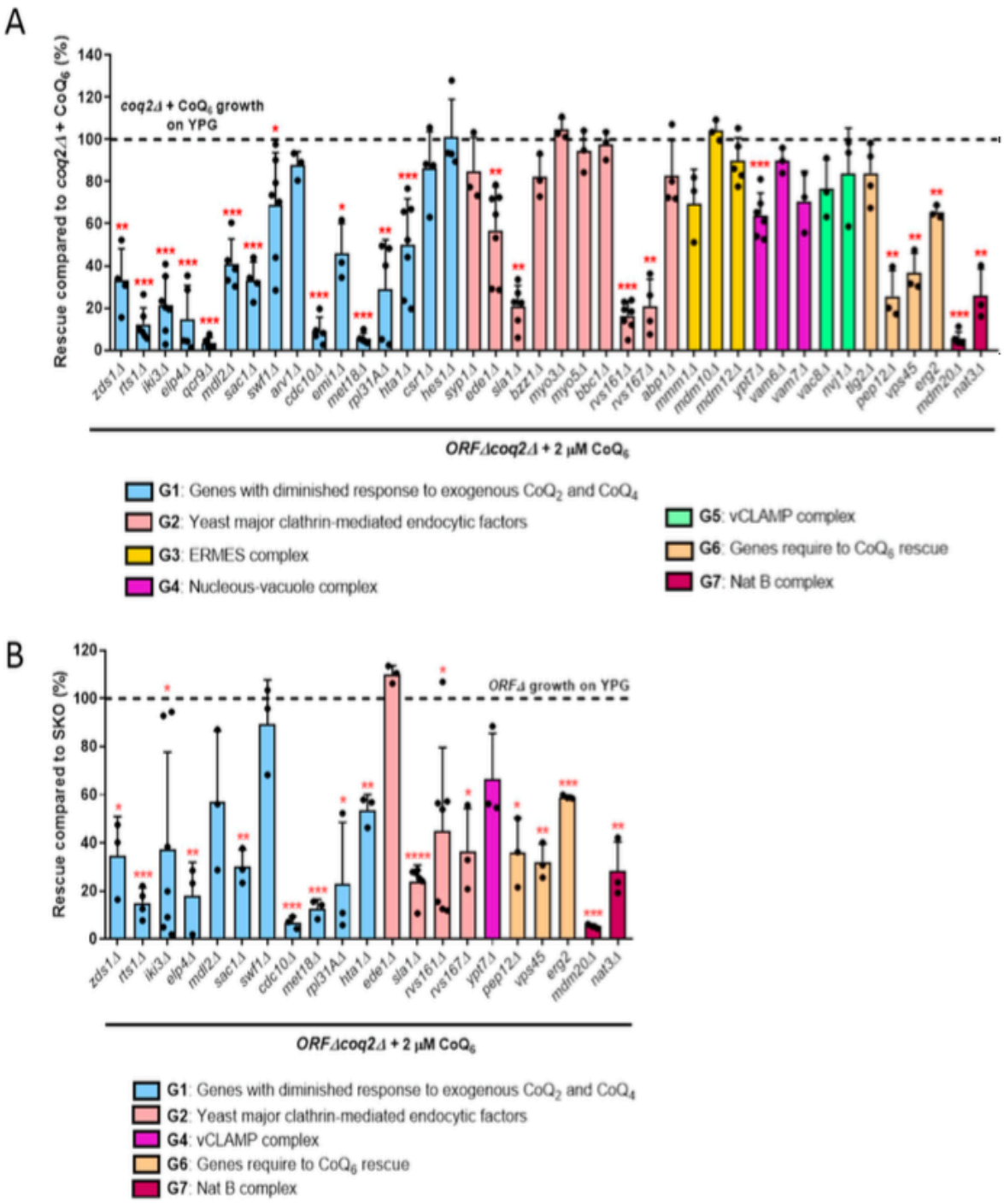

Fig. 5. Two rounds of screening identified 17 *ORFΔcoq2Δ* double mutants to have a diminished response to exogenous CoQ_6. (A) First, the degree of rescue of the *ORFΔcoq2Δ* candidates was calculated in comparison with the positive control: *coq2Δ* + CoQ_6. Of a total of 40 candidates, 23 showed a significantly decreased ability to rescue in presence of exogenous CoQ_6. **(B)** Since a single deletion can compromise the ability of a mutant to grow on YPG, the degree of rescue of the previous significant candidates was calculated in comparison to the corresponding *ORFΔ* in the second phase of the screening. The *emi1Δcoq2Δ* and *qcr9Δcoq2Δ* mutants were eliminated for further analysis due to special phenotypes (see main text). 17 candidates display impaired rescue in response to treatment with exogenous CoQ_6. In both cases, columns represent the average degree of rescue (in %) ± SD of mutants growing on YPG in presence of 2 µM CoQ_6 for 7 days. Three or more replicas were included for all candidates. The normalization variable is considered 100% and represented as a dashed line. Asterisks denote the different degrees of significance: *$p < 0.05$, **$p < 0.01$, ***$p < 0.001$, and ****$p < 0.0001$.

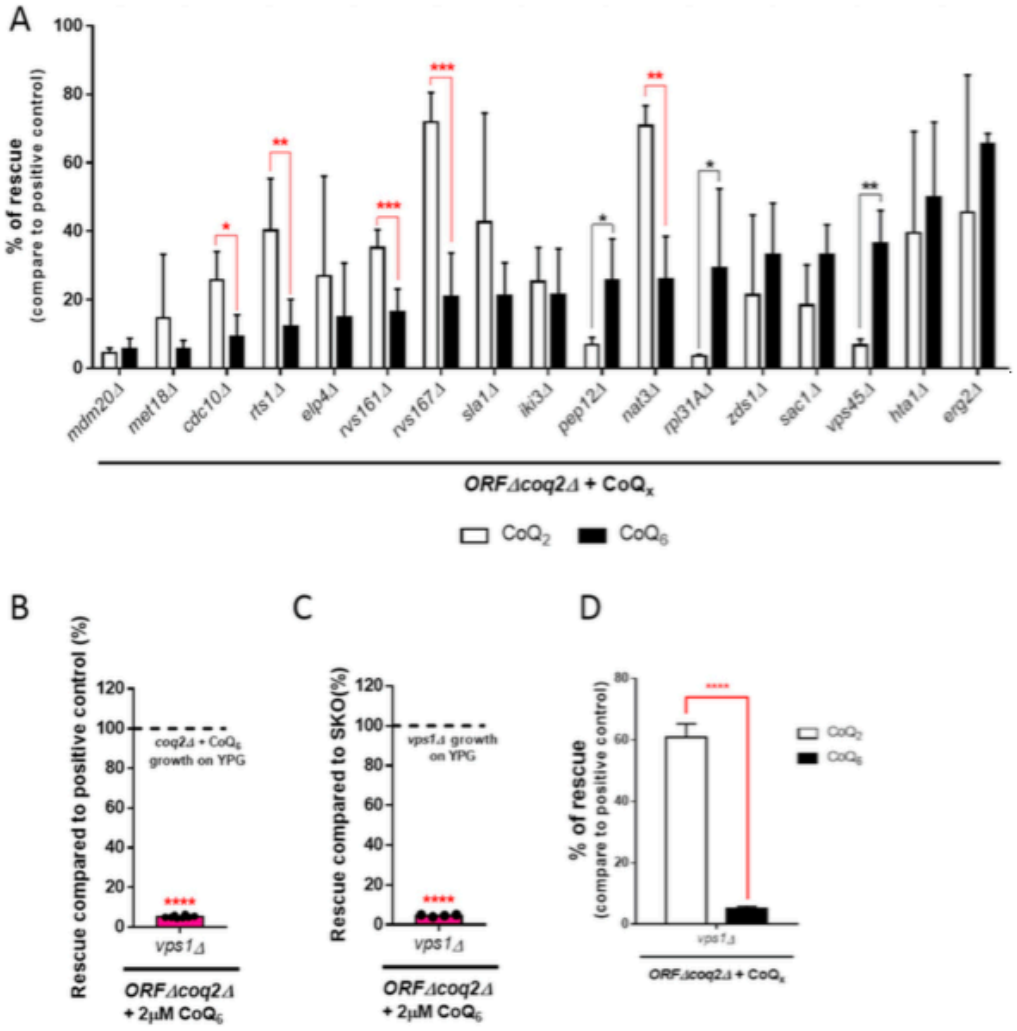

Fig. 6. Comparison of the CoQ_2 and CoQ_6 rescue phenotypes identifies six genes necessary for CoQ_6 transport. (A) The degree of CoQ_2 and CoQ_6 rescue, compared to the corresponding positive control (*coq2Δ* + CoQ_2 or *coq2Δ* + CoQ_6), are represented side by side (from low to high degree of CoQ_6 rescue). Five candidates (denoted with red lines) fulfilled the "CoQ_6 rescue < CoQ_2 rescue" criteria and have been identified as involved in CoQ_6 transport. This panel merges data from Fig. 5A and Fig. S5B to allow for a straightforward comparison. **(B)** The degree of rescue of *vps1Δcoq2Δ* was observed to be dramatically low when compared to the positive control. **(C)** Similar results were observed when the rescue of the *vps1Δcoq2Δ* mutant was compared to *vps1Δ*. **(D)** The degree of rescue with the addition of exogenous CoQ_2 was superior to the one observed with the addition of CoQ_6. Degree of rescue is referred to the corresponding positive control (*coq2Δ* + CoQ_2 or *coq2Δ* + CoQ_6). In all cases, columns represent the average degree of rescue (in %) ± SD of mutants growing on YPG in presence of CoQ for 7 days. At least three replicas were included in all determinations. The normalization variable is considered 100% and represented as a dashed line. Asterisks denote: $^*p < 0.05$, $^{**}p < 0.01$, $^{***}p < 0.001$, and $^{****}p < 0.0001$. (For interpretation of the references to colour in this figure legend, the reader is referred to the Web version of this article.)

strains (*coq3Δ-coq9Δ*) that accumulate early-stage prenylated CoQ_6 intermediates, HHB and HAB (Figs. 3 and 4). This likely also explains the previous observation that exogenous decylubiquinone blunts rescue by exogenous CoQ_2 in *coq2Δ* mutants [39].

The exact reason why the presence of early CoQ_6 hexaprenylated intermediates prevents the rescue with exogenous CoQ_6 is not clear, but different hypotheses can be proposed: CoQ_6 intermediates could (i) produce a certain level of toxicity that affects the normal operation of the cells; (ii) mimic the behavior of detergents by trapping CoQ_6 in micelles and prevent its correct delivery to the mitochondrial inner membrane; (iii) impede incorporation of CoQ_6 into the mitochondrial inner membrane by saturating the bilayer or transport proteins with polyisoprenoids; or (iv) interact with CoQ-utilizing proteins and prevent the proper function of imported exogenous CoQ_6. It is also possible that the slight rescue deficiency observed in *coq2Δ* (Fig. 3C) is due to the presence of hexaprenyl-diphosphate in the membranes. The accumulation of CoQ prenylated intermediates is not as well explored in human cells as it is in yeast cells. However the accumulation of DMQ_{10} has been reported in fibroblasts derived from patients with inherited COQ4, COQ7, and COQ9 deficiencies [64,68,69], as well as in fibroblasts where *COQ3*, *COQ5*, or *COQ6* were knocked down with siRNAs [64]. DMQ is considered a late-stage CoQ intermediate and it is not clear whether this precursor negatively affects CoQ rescue. However, if this is the case, patients with CoQ_{10} deficiencies that accumulate

Table 2
Genes identified to be related to CoQ_6 transport.

ORFΔ (protein name)	ORF description (www.yeastgenome.org)	Human homolog
YCR002C (Cdc10)	Subunit of the septin complex with GTPase activity. Localizes to the bud neck septin ring, and can function as scaffolds for recruiting cell division factors and as barriers to prevent diffusion of specific proteins.	**SEPT9**
YOR014W (Rts1)	Protein phosphatase regulator involved in protein dephosphorylation, mitotic spindle orientation checkpoint, and septin ring organization and disassembly.	**PPP2R5C**
YCR009C (Rvs161)	N-BAR domain protein that interacts with Rvs167 and regulates polarization of the actin cytoskeleton, endocytosis, cell polarity, cell fusion and viability following starvation or osmotic stress.	**BIN3**
YDR388W (Rvs167)	N-BAR domain protein with roles in endocytic membrane tabulation, constriction and exocytosis. Interacts with Rvs161 to regulate actin cytoskeleton, endocytosis and viability following starvation or osmotic stress.	**BIN1, AMPH** [57–59]
YPR131C (Nat3)	Catalytic subunit of the NatB N-terminal acetyltransferase complex, which is in charge of the N-acetylation of the amino-terminal methionine residues of all proteins beginning with Met-Asp or Met-Glu and of some proteins beginning with Met-Asn or Met-Met (approximately 20% of proteins in yeast).	**NAA20**
YKR001C (Vps1)	Dynamin-like GTPase required for vacuolar sorting, protein retention in Golgi apparatus, peroxisome organization and fission, endocytosis, and actin cytoskeleton organization.	**Dynamin** [57,60]

Unless otherwise is indicated, the closest human homolog genes were located in the HomoloGene tool from the NCBI database.

DMQ_{10} might not respond well to CoQ_{10} supplementation and alternative treatments, such as the induction of internal CoQ_{10} synthesis, should be considered instead. Based on our results, in addition to CoQ_{10} intermediates serving as a potentially important biomarker for the diagnosis of CoQ_{10} deficiency disorders [64], they may also impact selection of an appropriate treatment.

Our use of *coq2Δ* cells to screen for genes involved in CoQ_6 transport avoids complications that could arise from accumulation of prenylated CoQ_6 intermediates. This was evident in our analyses of *TLG2*, previously identified as required for CoQ_6 uptake using *coq3Δ* cells. In our experiments, whereas deletion of *TLG2* in a *coq3Δ* strain impaired rescue by exogenous CoQ_6, the same deletion in a *coq2Δ* mutant had no significant impact on rescue, indicating that *TLG2* does not play a significant role in CoQ_6 transport in cells that do not accumulate HHB and HAB (Fig. 3).

Comparison of rescue by CoQ_6 and CoQ_2 provided a way to distinguish mutations that specifically impeded CoQ_6 transport (preferentially rescued by CoQ_2) from those that generally prevented utilization of CoQ. For example, in addition to *TLG2*, three other genes were identified using *ORFΔcoq3Δ* mutants: *ERG2*, *PEP12* and *VPS45* (30). Unlike deletion of TLG2, deletion of these genes in *coq2Δ* strains still reduced CoQ_6 rescue, though not to the extent observed with *coq3Δ* cells. However, the *coq2Δ* strains harbouring deletions of *ERG2, PEP12 or VPS45* were not preferentially rescued by CoQ_2 (Fig. 6A), suggesting that defective transport of CoQ_6 is not the underlying issue. Like the *erg2Δcoq2Δ* mutant, many other *ORFΔcoq2Δ* strains in Fig. 6A responded similarly to exogenous CoQ_2 and CoQ_6, indicating that the defect in these strains is also more likely to be related to CoQ utilization. Notably, *pep12Δcoq2Δ* and *vps45Δcoq2Δ*, as well as *rpl31AΔcoq2Δ*, responded better to CoQ_6 than to CoQ_2. The basis for this phenotype remains to be determined, but may be due to lower levels of delivery to the vacuole and degradation.

The Coq8 polypeptide is a member of an ancient atypical kinase family [70], with several conserved kinase motifs that are essential for CoQ biosynthesis [71,72]. Unique characteristics have been attributed to Coq8, including the observation that its overexpression in *coqΔ* mutants augments the levels of several Coq polypeptides, stabilizes CoQ synthome formation, and restores the formation of CoQ domains [73–77]. We find it intriguing that *coq8Δ* mutant yeast also displayed an unique phenotype with regard to rescue by exogenous CoQ_6. Its degree of rescue is lower as compared to most of the other *coqΔ* mutants (Fig. 3C), and the additional deletion of *COQ2* only partially augmented rescue (Fig. 4D). Together, these observations might suggest an active role of Coq8 in CoQ_6 transportation. Such a role is in agreement with previous studies, where Coq8 has been proposed to function as a chaperone that facilitates the partial extraction of lipophilic CoQ intermediates out of the inner mitochondrial membrane and into the aqueous matrix environment promoting the enzymatic reactions catalyzed by other Coq proteins [78].

Due to their endosymbiotic origin, mitochondria are not embedded within the vesicular trafficking system [79]. Instead, they are connected to other cellular organelles by multiple membrane contact sites [79,80]. Recently, it has been described that the CoQ synthome is localized to distinct puncta within the inner mitochondrial membrane, termed CoQ domains [76]. The CoQ domains are non-randomly localized to adjacent ER-mitochondria contact sites [76,81]. Moreover, it was observed that the disruption of ERMES alters the distribution of CoQ_6 and its precursors [81]. These observations suggest a role for ER-mitochondria contacts in CoQ domain formation and CoQ_6 production and distribution from mitochondria to the rest of the cell. Our screen to identify genes involved in CoQ_6 transport revealed that *ORFΔcoq2Δ* strains missing an ERMES gene were not affected in their ability to be rescued by exogenous CoQ_6. Deletion of genes belonging to the vCLAMP or the NVJ families also had no significant impact on rescue by exogenous CoQ_6. These results may suggest that exogenous CoQ_6 is reaching the mitochondria by a mechanism unrelated to these organelle connections, perhaps by means of the novel clathrin-mediated vesicle transport from the plasma membrane to the mitochondria [82], or via a still-unknown transport process. It is also possible that transport of CoQ_6 through organelle connections occurs via redundant steps. It has been shown previously that for phospholipid exchange, mitochondria are dependent on at least one functional contact site with the endomembrane system: ERMES or vCLAMP, whose functions are tightly co-regulated [83]. In this case, the loss of one system elicits a compensatory response in the other, and loss of both is lethal. Thus, the cell is able to adapt and, in the absence of one structure, an increase in the other serves as a "backup" path for small-molecule transport [83].

We identified six *ORFΔcoq2Δ* double mutants that are compromised in their CoQ_6 rescue, and perform better when diffusible CoQ_2 is supplied instead (Figs. 5 and 6). These six *ORFs* (*CDC10*, *RTS1*, *RVS161*, *RVS167*, *NAT3*, and *VPS1*) encode proteins that are necessary for CoQ_6 transport and identify essential steps that cannot be compensated by other proteins or pathways. Three of these proteins (Rvs161, Rvs167, and Vps1) are directly involved in the endocytosis process at the plasma membrane. Rvs161 and Rvs167 are Bin/amphiphysin/Rvs (BAR) domain proteins that form a heterodimeric protein complex capable of deforming the membrane, and are necessary for invagination and scission of vesicles in the final step of clathrin-mediated endocytosis [84]. In mammalian cells, in addition to Rvs161/167 homologues, the GTPase dynamin (Vps1 human homolog) is essential for scission of clathrin-coated vesicles. In yeast, the role of Vps1 in endocytosis has been controversial [84], but recent reports demonstrated that Vps1 functions with the Rvs161/167 heterodimer to facilitate scission and release of the vesicles [61–63,85]. Indeed, Vps1 and Rvs167 were found to physically interact with each other [63]. The *rvs161Δ* and *rvs167Δ* mutants have a specific defect: a significant fraction of the endocytic patches begins to be internalized and move inward from the cell surface but are then retracted toward the cortex [86]. This defective phenotype

might impair the uptake of exogenous CoQ_6, resulting in the poor rescue phenotype observed in *rvs161Δcoq2Δ* and *rvs167Δcoq2Δ* double mutants (Figs. 5 and 6A). Invaginations do not form correctly in the absence of Vps1 either [61]. Vps1 plays a significant role in endosomal trafficking, and the *vps1Δ* mutant accumulates endosomes in the cytoplasm [60]. Perhaps these attributes of the *vps1Δ* mutant account for the extremely deficient rescue phenotype of the *vps1Δcoq2Δ* double mutant (< 5% of the positive control) (Fig. 6B).

Cdc10 was also identified in our screens as a protein involved in CoQ_6 transport (Figs. 5 and 6A). Cdc10 is one of the four core septin proteins in *S. cerevisiae*, a group of GTPases that assemble into filaments and higher-order structures [87–89]. In yeast cells, septin filaments assemble at the bud neck in a 'septin ring', which is essential in cytokinesis during which it acts as a scaffold to recruit cytokinetic factors to the site of cell division [88,90]. In addition to scaffolding, the other main function of septins is to serve as cortical barriers to prevent the free diffusion of membrane proteins between different compartments [88,90]. Septins may play a role in endocytosis since they interact with a subset of endocytic proteins, including Vps1, and the accessory proteins Syp1 and Sla2 [91]. SEPT9, the human homolog of Cdc10, has been implicated in endosomal sorting [92]. Interaction partners previously identified suggested a role for SEPT9 in vesicle transport to and from the plasma membrane [93]. The other three core septins (Cdc3, Cdc11 and Cdc12) are encoded by essential genes and therefore the null mutants cannot be interrogated [94]. Whether the involvement of Cdc10 (or potentially other septins) in CoQ_6 uptake/transport is related to the role of septins in endocytosis or to a different septin function, will require further experimentation.

The remaining two proteins identified as necessary for CoQ_6 transport, Rts1 and Nat3, may function as regulators. Rts1 is one of the two regulatory subunits of protein phosphatase 2A (PP2A), a major class of serine/threonine protein phosphatases that play an important role in many biological processes [95,96]. The regulatory subunit is thought to determine substrate specificity, targeting $PP2A^{Rts1}$ for regulation of the mitotic spindle orientation checkpoint, cell size control, and septin ring organization and disassembly during cytokinesis [96]. Phosphoproteomic analyses in *rts1Δ* cells reveals 156 hyperphosphorylated proteins, highlighting the multitude of $PP2A^{Rts1}$ complex targets [97]. The cytokinesis defect observed in *rts1Δ* cells is in agreement with the role of $PP2A^{Rts1}$ in the regulation of septin dynamics, possibly by dephosphorylating some factor(s) at the bud neck [98]. $PP2A^{Rts1}$ reverses phosphorylation of (at least) septin Shs1 and contributes to timely septin disassembly after cytokinesis [90]. Yet-to-be-identified relationships between septins and $PP2A^{Rts1}$ are possible as suggested by data from other fungal species. AspB (the *CDC3* ortholog in *Aspergillus fumigatus*) is dephosphorylated in a PP2A-dependent manner [99]. To the best of our knowledge, there is no direct association between $PP2A^{Rts1}$ and Cdc10, although Rts1 has a strong potential to serve as a regulator during CoQ_6 transport even if it is not related with septins. Almost all endocytic proteins participating in clathrin-mediated endocytosis are phosphorylated [100], including Rvs161, Rvs167, and Vps1 [100–102], and are excellent targets for phospho/dephosphorylation regulation.

The final gene influencing CoQ_6 uptake or transport is Nat3, the catalytic subunit of the NatB complex. Together with its auxiliary subunit (Mdm20), Nat3 mediates the N-terminal acetyl transfer of about 20% of proteins in yeast and humans [103–105]. In yeast, there are four functional NATs, and each has distinct substrate specificity [105,106]. Could N-acetylation modifications play a role in some of the proteins involved in CoQ_6 transport? This seems less likely given that *mdm20Δcoq2Δ* had profound rescue defects in response to both exogenous CoQ_2 and CoQ_6 (Fig. 6A), excluding *MDM20* from consideration as an *ORF* related with CoQ_6 transport. Thus, we believe that Nat3 and CoQ_6 may be connected through an unknown, but NatB-independent, function of this protein. Although *nat3Δ* and *mdm20Δ* share several phenotypes, *nat3Δ* mutants possess additional unique phenotypes [104]. Moreover, Mdm20 has recently been related with several cellular functions independent of Nat3 [107,108], supporting the idea that Nat3 participates in additional pathways, either by itself or in conjunction with another auxiliary protein. It is also possible that the deficient rescue displayed by *mdm20Δcoq2Δ* (Fig. 6A) is a consequence of multiple defects in this strain, and that N-acetylation modifications somehow regulate CoQ_6 transport.

5. Conclusion

Our studies have revealed deleterious effects of CoQ_6 hexaprenylated intermediates on rescue with exogenous CoQ_6. Additionally, our research defines six novel proteins as necessary for appropriate CoQ_6 uptake and transport, and strongly connects CoQ_6 distribution with endocytosis and membrane trafficking pathways.

Funding sources

Work in CFC laboratory was supported by the National Science Foundation Grant (MCB-1330803), a National Institutes of Health Grant T32 Ruth L. Kirschstein National Service (GM 007185, to M.C. Bradley), a Whitcome Individual Predoctoral Fellowship (to M.C. Bradley), and a Whitcome Summer Undergraduate Research Fellowship of the Department of Chemistry & Biochemistry at UCLA (to M.E. Kelly). Work in MPM laboratory was supported by the Medical Research Council UK (MC_U105663142) and a Wellcome Trust Investigator award (110159/Z/15/Z).

Declaration of competing interest

The authors declare no conflict of interest for any of the work presented in this article.

Acknowledgements

We thank the UCLA Molecular Instrumentation Core proteomics facility, and Dr. Yu Chen, for the use of the QTRAP4000 for lipid analysis. We thank undergraduate UCLA researcher Peter Lee for the creation of the pRSQ2 plasmid. We thank Kelly Quinn and Christopher P. Kampmeyer for their participation in the early stages of the project.

Appendix A. Supplementary data

Supplementary data to this article can be found online at https://doi.org/10.1016/j.freeradbiomed.2020.04.029.

References

[1] A.M. Awad, M.C. Bradley, L. Fernandez-del-Rio, A. Nag, H. Tsui, C.F. Clarke, Coenzyme Q_{10} deficiencies: pathways in yeast and humans, Essays Biochem. 62 (3) (2018) 361–376.

[2] Y. Wang, S. Hekimi, The complexity of making ubiquinone, Trends Endocrinol. Metabol. 30 (12) (2019) 923–943.

[3] M. Bentinger, M. Tekle, G. Dallner, Coenzyme Q-biosynthesis and functions, Biochem. Biophys. Res. Commun. 396 (1) (2010) 74–79.

[4] F.M. Gutierrez-Mariscal, E.M. Yubero-Serrano, J.M. Villalba, J. Lopez-Miranda, Coenzyme Q_{10}: from bench to clinic in aging diseases, a translational review, Crit. Rev. Food Sci. Nutr. 59 (14) (2018) 2240–2257.

[5] J.A. Stefely, D.J. Pagliarini, Biochemistry of mitochondrial coenzyme Q biosynthesis, Trends Biochem. Sci. 42 (10) (2017) 824–843.

[6] R. Saiki, A. Nagata, T. Kainou, H. Matsuda, M. Kawamukai, Characterization of solanesyl and decaprenyl diphosphate synthases in mice and humans, FEBS J. 272 (21) (2005) 5606–5622.

[7] B. Marbois, L.X. Xie, S. Choi, K. Hirano, K. Hyman, C.F. Clarke, para-Aminobenzoic acid is a precursor in coenzyme Q_6 biosynthesis in *Saccharomyces cerevisiae*, J. Biol. Chem. 285 (36) (2010) 27827–27838.

[8] F. Pierrel, O. Hamelin, T. Douki, S. Kieffer-Jaquinod, U. Muhlenhoff, M. Ozeir, R. Lill, M. Fontecave, Involvement of mitochondrial ferredoxin and para-aminobenzoic acid in yeast coenzyme Q biosynthesis, Chem. Biol. 17 (5) (2010) 449–459.

[9] D. Yubero, R. Montero, C. Santos-Ocana, L. Salviati, P. Navas, R. Artuch, Molecular diagnosis of coenzyme Q_{10} deficiency: an update, Expert Rev. Mol. Diagn 18 (6) (2018) 491–498.

[10] D. Yubero, G. Allen, R. Artuch, R. Montero, The value of coenzyme Q_{10} determination in mitochondrial patients, J. Clin. Med. 6 (4) (2017) 1–10.
[11] M. Alcazar-Fabra, E. Trevisson, G. Brea-Calvo, Clinical syndromes associated with Coenzyme Q_{10} deficiency, Essays Biochem. 62 (3) (2018) 377–398.
[12] M.A. Desbats, G. Lunardi, M. Doimo, E. Trevisson, L. Salviati, Genetic bases and clinical manifestations of coenzyme Q_{10} (CoQ_{10}) deficiency, J. Inherit. Metab. Dis. 38 (1) (2015) 145–156.
[13] M. Doimo, M.A. Desbats, C. Cerqua, M. Cassina, E. Trevisson, L. Salviati, Genetics of coenzyme Q_{10} deficiency, Mol Syndromol 5 (3–4) (2014) 156–162.
[14] G.P. Littarru, P. Langsjoen, Coenzyme Q_{10} and statins: biochemical and clinical implications, Mitochondrion 7 (Suppl) (2007) S168–S174.
[15] S. Passi, A. Stancato, E. Aleo, A. Dmitrieva, G.P. Littarru, Statins lower plasma and lymphocyte ubiquinol without affecting other antioxidants and PUFA, Biofactors 18 (1–4) (2003) 113–124.
[16] I.P. Barcelos, R.H. Haas, CoQ_{10} and aging, Biology 8 (2) (2019) 1–22.
[17] J.D. Hernández-Camacho, M. Bernier, G. López-Lluch, P. Navas, Coenzyme Q_{10} supplementation in aging and disease, Front. Physiol. 9 (44) (2018) 1–11.
[18] S. Oleck, H.O. Ventura, Coenzyme Q_{10} and utility in heart failure: just another supplement? Curr. Heart Fail. Rep. 13 (4) (2016) 190–195.
[19] L. Salviati, S. Sacconi, L. Murer, G. Zacchello, L. Franceschini, A.M. Laverda, G. Basso, C. Quinzii, C. Angelini, M. Hirano, A.B. Naini, P. Navas, S. DiMauro, G. Montini, Infantile encephalomyopathy and nephropathy with CoQ_{10} deficiency: a CoQ_{10}-responsive condition, Neurology 65 (4) (2005) 606–608.
[20] G. Montini, C. Malaventura, L. Salviati, Early coenzyme Q_{10} supplementation in primary coenzyme Q_{10} deficiency, N. Engl. J. Med. 358 (26) (2008) 2849–2850.
[21] M.J. Acosta, L. Vazquez Fonseca, M.A. Desbats, C. Cerqua, R. Zordan, E. Trevisson, L. Salviati, Coenzyme Q biosynthesis in health and disease, Biochim. Biophys. Acta 1857 (8) (2016) 1079–1085.
[22] G. Lopez-Lluch, J. Del Pozo-Cruz, A. Sanchez-Cuesta, A.B. Cortes-Rodriguez, P. Navas, Bioavailability of coenzyme Q_{10} supplements depends on carrier lipids and solubilization, Nutrition 57 (2018) 133–140.
[23] N.M. Zaki, Strategies for oral delivery and mitochondrial targeting of CoQ_{10}, Drug Deliv. 23 (6) (2016) 1868–1881.
[24] J.S. Lee, J.W. Suh, E.S. Kim, H.G. Lee, Preparation and characterization of mucoadhesive nanoparticles for enhancing cellular uptake of coenzyme Q_{10}, J. Agric. Food Chem. 65 (40) (2017) 8930–8937.
[25] Y. Sato, S. Yokoyama, Y. Yamaki, Y. Nishimura, M. Miyashita, S. Maruyama, Y. Takekuma, M. Sugawara, Enhancement of intestinal absorption of coenzyme Q_{10} using emulsions containing oleyl polyethylene acetic acids, Eur. J. Pharmaceut. Sci. 142 (2019) 105–144.
[26] D. Herebian, L.C. Lopez, F. Distelmaier, Bypassing human CoQ_{10} deficiency, Mol. Genet. Metabol. 123 (3) (2018) 289–291.
[27] A.M. Berenguel Hernandez, M. de la Cruz, M. Alcazar-Fabra, A. Prieto-Rodriguez, A. Sanchez-Cuesta, J. Martin, J.R. Tormo, J.C. Rodriguez-Aguilera, A.B. Cortes-Rodriguez, P. Navas, F. Reyes, F. Vicente, O. Genilloud, C. Santos-Ocana, Design of high-throughput screening of natural extracts to identify molecules bypassing primary coenzyme Q deficiency in *Saccharomyces cerevisiae*, SLAS Discov 21 (2019) 1–11.
[28] L.X. Xie, K.J. Williams, C.H. He, E. Weng, S. Khong, T.E. Rose, O. Kwon, S.J. Bensinger, B.N. Marbois, C.F. Clarke, Resveratrol and para-coumarate serve as ring precursors for coenzyme Q biosynthesis, J. Lipid Res. 56 (4) (2015) 909–919.
[29] L. Fernandez-Del-Rio, A. Nag, E. Gutierrez Casado, J. Ariza, A.M. Awad, A.I. Joseph, O. Kwon, E. Verdin, R. de Cabo, C. Schneider, J.Z. Torres, M.I. Buron, C.F. Clarke, J.M. Villalba, Kaempferol increases levels of coenzyme Q in kidney cells and serves as a biosynthetic ring precursor, Free Radic. Biol. Med. 110 (2017) 176–187.
[30] T. Takahashi, T. Okamoto, K. Mori, H. Sayo, T. Kishi, Distribution of ubiquinone and ubiquinol homologues in rat tissues and subcellular fractions, Lipids 28 (9) (1993) 803–809.
[31] M. Bentinger, G. Dallner, T. Chojnacki, E. Swiezewska, Distribution and breakdown of labeled coenzyme Q_{10} in rat, Free Radic. Biol. Med. 34 (5) (2003) 563–575.
[32] D.J. Fernandez-Ayala, G. Brea-Calvo, G. Lopez-Lluch, P. Navas, Coenzyme Q distribution in HL-60 human cells depends on the endomembrane system, Biochim. Biophys. Acta 1713 (2) (2005) 129–137.
[33] S. Padilla-Lopez, M. Jimenez-Hidalgo, A. Martin-Montalvo, C.F. Clarke, P. Navas, C. Santos-Ocana, Genetic evidence for the requirement of the endocytic pathway in the uptake of coenzyme Q_6 in *Saccharomyces cerevisiae*, Biochim. Biophys. Acta 1788 (6) (2009) 1238–1248.
[34] C. Santos-Ocana, T.Q. Do, S. Padilla, P. Navas, C.F. Clarke, Uptake of exogenous coenzyme Q and transport to mitochondria is required for bc1 complex stability in yeast *coq* mutants, J. Biol. Chem. 277 (13) (2002) 10973–10981.
[35] Y. Wang, S. Hekimi, Mitochondrial respiration without ubiquinone biosynthesis, Hum. Mol. Genet. 22 (23) (2013) 4768–4783.
[36] C. Weber, A. Bysted, G. Holmer, Coenzyme Q_{10} in the diet-daily intake and relative bioavailability, Mol. Aspect. Med. 18 (Suppl) (1997) S251–S254.
[37] C. Santos-Ocana, J.M. Villalba, F. Cordoba, S. Padilla, F.L. Crane, C.F. Clarke, P. Navas, Genetic evidence for coenzyme Q requirement in plasma membrane electron transport, J. Bioenerg. Biomembr. 30 (5) (1998) 465–475.
[38] T. Jonassen, M. Proft, F. Randez-Gil, J.R. Schultz, B.N. Marbois, K.D. Entian, C.F. Clarke, Yeast Clk-1 homologue (Coq7/Cat5) is a mitochondrial protein in coenzyme Q synthesis, J. Biol. Chem. 273 (6) (1998) 3351–3357.
[39] A.M. James, H.M. Cocheme, M. Murai, H. Miyoshi, M.P. Murphy, Complementation of coenzyme Q-deficient yeast by coenzyme Q analogues requires the isoprenoid side chain, FEBS J. 277 (9) (2010) 2067–2082.
[40] R.C. MacDonald, R.I. MacDonald, B.P. Menco, K. Takeshita, N.K. Subbarao, L.R. Hu, Small-volume extrusion apparatus for preparation of large, unilamellar vesicles, Biochim. Biophys. Acta 1061 (2) (1991) 297–303.
[41] A.M. James, M.S. Sharpley, A.R. Manas, F.E. Frerman, J. Hirst, R.A. Smith, M.P. Murphy, Interaction of the mitochondria-targeted antioxidant MitoQ with phospholipid bilayers and ubiquinone oxidoreductases, J. Biol. Chem. 282 (20) (2007) 14708–14718.
[42] A.M. James, H.M. Cocheme, R.A. Smith, M.P. Murphy, Interactions of mitochondria-targeted and untargeted ubiquinones with the mitochondrial respiratory chain and reactive oxygen species. Implications for the use of exogenous ubiquinones as therapies and experimental tools, J. Biol. Chem. 280 (22) (2005) 21295–21312.
[43] A. Baudin, O. Ozier-Kalogeropoulos, A. Denouel, F. Lacroute, C. Cullin, A simple and efficient method for direct gene deletion in *Saccharomyces cerevisiae*, Nucleic Acids Res. 21 (14) (1993) 3329–3330.
[44] R.D. Gietz, R.A. Woods, Yeast transformation by the LiAc/SS Carrier DNA/PEG method, Methods Mol. Biol. 313 (2006) 107–120.
[45] L. Dirick, W. Bendris, V. Loubiere, T. Gostan, E. Gueydon, E. Schwob, Metabolic and environmental conditions determine nuclear genomic instability in budding yeast lacking mitochondrial DNA, G3 (Bethesda) 4 (3) (2014) 411–423.
[46] H.S. Tsui, N.V.B. Pham, B.R. Amer, M.C. Bradley, J.E. Gosschalk, M. Gallagher-Jones, H. Ibarra, R.T. Clubb, C.E. Blaby-Haas, C.F. Clarke, Human COQ10A and COQ10B are distinct lipid-binding START domain proteins required for coenzyme Q function, J. Lipid Res. 60 (7) (2019) 1293–1310.
[47] C.M. Stoscheck, Quantitation of protein, Methods Enzymol. 182 (1990) 50–68.
[48] R.S. Sikorski, P. Hieter, A system of shuttle vectors and yeast host strains designed for efficient manipulation of DNA in *Saccharomyces cerevisiae*, Genetics 122 (1) (1989) 19–27.
[49] J.M. Harnly, S. Bhagwat, L.Z. Lin, Profiling methods for the determination of phenolic compounds in foods and dietary supplements, Anal. Bioanal. Chem. 389 (1) (2007) 47–61.
[50] E.J. Hsieh, P. Gin, M. Gulmezian, U.C. Tran, R. Saiki, B.N. Marbois, C.F. Clarke, *Saccharomyces cerevisiae* Coq9 polypeptide is a subunit of the mitochondrial coenzyme Q biosynthetic complex, Arch. Biochem. Biophys. 463 (1) (2007) 19–26.
[51] D. Cotan, M.D. Cordero, J. Garrido-Maraver, M. Oropesa-Avila, A. Rodriguez-Hernandez, L. Gomez Izquierdo, M. De la Mata, M. De Miguel, J.B. Lorite, E.R. Infante, S. Jackson, P. Navas, J.A. Sanchez-Alcazar, Secondary coenzyme Q_{10} deficiency triggers mitochondria degradation by mitophagy in MELAS fibroblasts, Faseb. J. 25 (8) (2011) 2669–2687.
[52] U.C. Tran, C.F. Clarke, Endogenous synthesis of coenzyme Q in eukaryotes, Mitochondrion 7 (Suppl) (2007) S62–S71.
[53] D.R. Boettner, R.J. Chi, S.K. Lemmon, Lessons from yeast for clathrin-mediated endocytosis, Nat. Cell Biol. 14 (1) (2011) 2–10.
[54] A.H. Michel, B. Kornmann, The ERMES complex and ER-mitochondria connections, Biochem. Soc. Trans. 40 (2) (2012) 445–450.
[55] Y. Tamura, T. Endo, Role of intra- and inter-mitochondrial membrane contact sites in yeast phospholipid biogenesis, Adv. Exp. Med. Biol. 997 (2017) 121–133.
[56] Y. Tamura, S. Kawano, T. Endo, Organelle contact zones as sites for lipid transfer, J. Biochem. 165 (2) (2019) 115–123.
[57] A.S. Robertson, E. Smythe, K.R. Ayscough, Functions of actin in endocytosis, Cell. Mol. Life Sci. 66 (13) (2009) 2049–2065.
[58] R. Lombardi, H. Riezman, Rvs161p and Rvs167p, the two yeast amphiphysin homologs, function together *in vivo*, J. Biol. Chem. 276 (8) (2001) 6016–6022.
[59] G. Ren, P. Vajjhala, J.S. Lee, B. Winsor, A.L. Munn, The BAR domain proteins: molding membranes in fission, fusion, and phagy, Microbiol. Mol. Biol. Rev. 70 (1) (2006) 37–120.
[60] M. Williams, K. Kim, From membranes to organelles: emerging roles for dynamin-like proteins in diverse cellular processes, Eur. J. Cell Biol. 93 (7) (2014) 267–277.
[61] R. Smaczynska-de II, E.G. Allwood, S. Aghamohammadzadeh, E.H. Hettema, M.W. Goldberg, K.R. Ayscough, A role for the dynamin-like protein Vps1 during endocytosis in yeast, J. Cell Sci. 123 (Pt 20) (2010) 3496–3506.
[62] D. Wang, J. Sletto, B. Tenay, K. Kim, Yeast dynamin implicated in endocytic scission and the disassembly of endocytic components, Commun. Integr. Biol. 4 (2) (2011) 178–181.
[63] R. Smaczynska-de II, E.G. Allwood, R. Mishra, W.I. Booth, S. Aghamohammadzadeh, M.W. Goldberg, K.R. Ayscough, Yeast dynamin Vps1 and amphiphysin Rvs167 function together during endocytosis, Traffic 13 (2) (2012) 317–328.
[64] D. Herebian, A. Seibt, S.H.J. Smits, G. Bunning, C. Freyer, H. Prokisch, D. Karall, A. Wredenberg, A. Wedell, L.C. Lopez, E. Mayatepek, F. Distelmaier, Detection of 6-demethoxyubiquinone in CoQ_{10} deficiency disorders: insights into enzyme interactions and identification of potential therapeutics, Mol. Genet. Metabol. 121 (3) (2017) 216–223.
[65] S. Shukla, K.K. Dubey, CoQ_{10} a super-vitamin: review on application and biosynthesis, 3 Biotech 8 (5) (2018) 249.
[66] J. Garrido-Maraver, M.D. Cordero, M. Oropesa-Avila, A.F. Vega, M. de la Mata, A.D. Pavon, E. Alcocer-Gomez, C.P. Calero, M.V. Paz, M. Alanis, I. de Lavera, D. Cotan, J.A. Sanchez-Alcazar, Clinical applications of coenzyme Q_{10}, Front. Biosci. 19 (2014) 619–633.
[67] S. Beg, S. Javed, K. Kohli, Bioavailability enhancement of coenzyme Q_{10}: an extensive review of patents, Recent Pat. Drug Deliv. Formulation 4 (3) (2010) 245–255.
[68] A.C. Smith, Y. Ito, A. Ahmed, J.A. Schwartzentruber, C.L. Beaulieu, E. Aberg, J. Majewski, D.E. Bulman, K. Horsting-Wethly, D.V. Koning, C. Care4Rare Canada, R.J. Rodenburg, K.M. Boycott, L.S. Penney, A family segregating lethal neonatal coenzyme Q_{10} deficiency caused by mutations in COQ9, J. Inherit. Metab. Dis. 41 (4) (2018) 719–729.

[69] K. Danhauser, D. Herebian, T.B. Haack, R.J. Rodenburg, T.M. Strom, T. Meitinger, D. Klee, E. Mayatepek, H. Prokisch, F. Distelmaier, Fatal neonatal encephalopathy and lactic acidosis caused by a homozygous loss-of-function variant in COQ9, Eur. J. Hum. Genet. 24 (3) (2016) 450–454.
[70] J.A. Stefely, A.G. Reidenbach, A. Ulbrich, K. Oruganty, B.J. Floyd, A. Jochem, J.M. Saunders, I.E. Johnson, C.E. Minogue, R.L. Wrobel, G.E. Barber, D. Lee, S. Li, N. Kannan, J.J. Coon, C.A. Bingman, D.J. Pagliarini, Mitochondrial ADCK3 employs an atypical protein kinase-like fold to enable coenzyme Q biosynthesis, Mol Cell 57 (1) (2015) 83–94.
[71] W. Cheng, W. Li, Structural insights into ubiquinone biosynthesis in membranes, Science 343 (6173) (2014) 878–881.
[72] L.X. Xie, E.J. Hsieh, S. Watanabe, C.M. Allan, J.Y. Chen, U.C. Tran, C.F. Clarke, Expression of the human atypical kinase ADCK3 rescues coenzyme Q biosynthesis and phosphorylation of Coq polypeptides in yeast coq8 mutants, Biochim. Biophys. Acta 1811 (5) (2011) 348–360.
[73] C.H. He, L.X. Xie, C.M. Allan, U.C. Tran, C.F. Clarke, Coenzyme Q supplementation or over-expression of the yeast Coq8 putative kinase stabilizes multi-subunit Coq polypeptide complexes in yeast *coq* null mutants, Biochim. Biophys. Acta Mol. Cell Biol. Lipids 1841 (4) (2014) 630–644.
[74] L.X. Xie, M. Ozeir, J.Y. Tang, J.Y. Chen, S.K. Jaquinod, M. Fontecave, C.F. Clarke, F. Pierrel, Overexpression of the Coq8 kinase in *Saccharomyces cerevisiae* coq null mutants allows for accumulation of diagnostic intermediates of the coenzyme Q_6 biosynthetic pathway, J. Biol. Chem. 287 (28) (2012) 23571–23581.
[75] A. Tauche, U. Krause-Buchholz, G. Rodel, Ubiquinone biosynthesis in *Saccharomyces cerevisiae*: the molecular organization of O-methylase Coq3p depends on Abc1p/Coq8p, FEMS Yeast Res. 8 (8) (2008) 1263–1275.
[76] K. Subramanian, A. Jochem, M. Le Vasseur, S. Lewis, B.R. Paulson, T.R. Reddy, J.D. Russell, J.J. Coon, D.J. Pagliarini, J. Nunnari, Coenzyme Q biosynthetic proteins assemble in a substrate-dependent manner into domains at ER-mitochondria contacts, J. Cell Biol. 218 (4) (2019) 1353–1369.
[77] M.C. Bradley, K. Yang, L. Fernandez-Del-Rio, J. Ngo, A. Ayer, H.S. Tsui, N.A. Novales, R. Stocker, O.S. Shirihai, M.H. Barros, C.F. Clarke, COQ11 deletion mitigates respiratory deficiency caused by mutations in the gene encoding the coenzyme Q chaperone protein Coq10, J. Biol. Chem. 295 (18) (2020) 6023–6042.
[78] A.G. Reidenbach, Z.A. Kemmerer, D. Aydin, A. Jochem, M.T. McDevitt, P.D. Hutchins, J.L. Stark, J.A. Stefely, T. Reddy, A.S. Hebert, E.M. Wilkerson, I.E. Johnson, C.A. Bingman, J.L. Markley, J.J. Coon, M. Dal Peraro, D.J. Pagliarini, Conserved lipid and small-molecule modulation of COQ8 reveals regulation of the ancient kinase-like UbiB family, Cell Chem Biol 25 (2) (2018) 154–165.
[79] L. Ellenrieder, H. Rampelt, T. Becker, Connection of protein transport and organelle contact sites in mitochondria, J. Mol. Biol. 429 (14) (2017) 2148–2160.
[80] K.S. Dimmer, D. Rapaport, Mitochondrial contact sites as platforms for phospholipid exchange, Biochim. Biophys. Acta 1862 (1) (2017) 69–80.
[81] M. Eisenberg-Bord, H.S. Tsui, D. Antunes, L. Fernandez-Del-Rio, M.C. Bradley, C.D. Dunn, T.P.T. Nguyen, D. Rapaport, C.F. Clarke, M. Schuldiner, The endoplasmic reticulum-mitochondria encounter structure complex coordinates coenzyme Q biosynthesis, Contact (Thousand Oaks) 2 (2019) 1–14.
[82] Z. Wei, W. Su, H. Lou, S. Duan, G. Chen, Trafficking pathway between plasma membrane and mitochondria via clathrin-mediated endocytosis, J. Mol. Cell Biol. 10 (6) (2018) 539–548.
[83] Y. Elbaz-Alon, E. Rosenfeld-Gur, V. Shinder, A.H. Futerman, T. Geiger, M. Schuldiner, A dynamic interface between vacuoles and mitochondria in yeast, Dev. Cell 30 (1) (2014) 95–102.
[84] J. Weinberg, D.G. Drubin, Clathrin-mediated endocytosis in budding yeast, Trends Cell Biol. 22 (1) (2012) 1–13.
[85] S. Nannapaneni, D. Wang, S. Jain, B. Schroeder, C. Highfill, L. Reustle, D. Pittsley, A. Maysent, S. Moulder, R. McDowell, K. Kim, The yeast dynamin-like protein Vps1:vps1 mutations perturb the internalization and the motility of endocytic vesicles and endosomes via disorganization of the actin cytoskeleton, Eur. J. Cell Biol. 89 (7) (2010) 499–508.
[86] M. Kaksonen, C.P. Toret, D.G. Drubin, A modular design for the clathrin- and actin-mediated endocytosis machinery, Cell 123 (2) (2005) 305–320.
[87] S. Mostowy, P. Cossart, Septins: the fourth component of the cytoskeleton, Nat. Rev. Mol. Cell Biol. 13 (3) (2012) 183–194.
[88] O. Glomb, T. Gronemeyer, Septin organization and functions in budding yeast, Front Cell Dev Biol 4 (2016) 123.
[89] M.A. McMurray, A. Bertin, G. Garcia 3rd, L. Lam, E. Nogales, J. Thorner, Septin filament formation is essential in budding yeast, Dev. Cell 20 (4) (2011) 540–549.
[90] M.A. Juanes, S. Piatti, The final cut: cell polarity meets cytokinesis at the bud neck in *S. cerevisiae*, Cell. Mol. Life Sci. 73 (16) (2016) 3115–3136.
[91] C. Renz, S. Oeljeklaus, S. Grinhagens, B. Warscheid, N. Johnsson, T. Gronemeyer, Identification of cell cycle dependent interaction partners of the septins by quantitative mass spectrometry, PloS One 11 (2) (2016) e0148340.
[92] K. Song, G. Russo, M. Krauss, Septins as modulators of endo-lysosomal membrane traffic, Front Cell Dev Biol 4 (2016) 124.
[93] M. Hecht, R. Rosler, S. Wiese, N. Johnsson, T. Gronemeyer, An interaction network of the human SEPT9 established by quantitative mass spectrometry, G3 (Bethesda) 9 (6) (2019) 1869–1880.
[94] A. Mela, M. Momany, Septin mutations and phenotypes in *S. cerevisiae*, Cytoskeleton (Hoboken) 76 (1) (2019) 33–44.
[95] Q. Han, C. Pan, Y. Wang, N. Wang, Y. Wang, J. Sang, The PP2A regulatory subunits, Cdc55 and Rts1, play distinct roles in *Candida albicans*' growth, morphogenesis, and virulence, Fungal Genet. Biol. 131 (2019) 103240.
[96] J. Arino, D. Velazquez, A. Casamayor, Ser/Thr protein phosphatases in fungi: structure, regulation and function, Microb Cell 6 (5) (2019) 217–256.
[97] J. Zapata, N. Dephoure, T. Macdonough, Y. Yu, E.J. Parnell, M. Mooring, S.P. Gygi, D.J. Stillman, D.R. Kellogg, PP2ARts1 is a master regulator of pathways that control cell size, J. Cell Biol. 204 (3) (2014) 359–376.
[98] J. Dobbelaere, M.S. Gentry, R.L. Hallberg, Y. Barral, Phosphorylation-dependent regulation of septin dynamics during the cell cycle, Dev. Cell 4 (3) (2003) 345–357.
[99] J.M. Vargas-Muniz, H. Renshaw, A.D. Richards, G. Waitt, E.J. Soderblom, M.A. Moseley, Y. Asfaw, P.R. Juvvadi, W.J. Steinbach, Dephosphorylation of the core septin, AspB, in a protein phosphatase 2A-dependent manner impacts its localization and function in the fungal pathogen *Aspergillus fumigatus*, Front. Microbiol. 7 (2016) 997.
[100] R. Lu, D.G. Drubin, Y. Sun, Clathrin-mediated endocytosis in budding yeast at a glance, J. Cell Sci. 129 (8) (2016) 1531–1536.
[101] H. Friesen, K. Murphy, A. Breitkreutz, M. Tyers, B. Andrews, Regulation of the yeast amphiphysin homologue Rvs167p by phosphorylation, Mol. Biol. Cell 14 (7) (2003) 3027–3040.
[102] R. Smaczynska-de II, C.J. Marklew, E.G. Allwood, S.E. Palmer, W.I. Booth, R. Mishra, M.W. Goldberg, K.R. Ayscough, Phosphorylation regulates the endocytic function of the yeast dynamin-related protein Vps1, Mol. Cell Biol. 36 (5) (2015) 742–755.
[103] B. Polevoda, T.S. Cardillo, T.C. Doyle, G.S. Bedi, F. Sherman, Nat3p and Mdm20p are required for function of yeast NatB Nalpha-terminal acetyltransferase and of actin and tropomyosin, J. Biol. Chem. 278 (33) (2003) 30686–30697.
[104] J.M. Singer, J.M. Shaw, Mdm20 protein functions with Nat3 protein to acetylate Tpm1 protein and regulate tropomyosin-actin interactions in budding yeast, Proc. Natl. Acad. Sci. U. S. A. 100 (13) (2003) 7644–7649.
[105] H. Aksnes, K. Hole, T. Arnesen, Molecular, cellular, and physiological significance of N-terminal acetylation, Int Rev Cell Mol Biol 316 (2015) 267–305.
[106] T. Arnesen, P. Van Damme, B. Polevoda, K. Helsens, R. Evjenth, N. Colaert, J.E. Varhaug, J. Vandekerckhove, J.R. Lillehaug, F. Sherman, K. Gevaert, Proteomics analyses reveal the evolutionary conservation and divergence of N-terminal acetyltransferases from yeast and humans, Proc. Natl. Acad. Sci. U. S. A. 106 (20) (2009) 8157–8162.
[107] K. Yasuda, M. Takahashi, N. Mori, Mdm20 modulates actin remodeling through the mTORC2 pathway via its effect on rictor expression, PloS One 10 (11) (2015) e0142943.
[108] K. Yasuda, K. Ohyama, K. Onga, A. Kakizuka, N. Mori, Mdm20 stimulates polyQ aggregation via inhibiting autophagy through Akt-Ser473 phosphorylation, PloS One 8 (12) (2013) e82523.

Abbreviations

CoQn: coenzyme Q containing a polyisoprenyl tail of *n* isoprene units
CoQ_6: oxidized coenzyme Q_6
CoQ_6H_2: reduced coenzyme Q_6H_2
Coq1: polypeptide encoded by the *COQ1* gene in *Saccharomyces cerevisiae*
coq1Δ: yeast mutant harboring a deletion in the *COQ1* gene
$DMQH_2$: demethoxy-QH_2
ERMES: endoplasmic reticulum-mitochondria encounter structure
HAB: 3-hexaprenyl-4-aminobenzoic acid
4HB: 4-hydroxybenzoic acid
HHB: 3-hexaprenyl-4-hydroxybenzoic acid
$IDMQH_2$: 4-imino-demethoxy-QH_2
LUVET: large unilamellar vesicles produced by extrusion
mtDNA: mitochondrial DNA
NatB: N-acetyltransferase B complex
NVJ: nucleus vacuole junction
ORFΔcoq2Δ: yeast double mutant harboring a gene deletion in a designated open reading frame plus a deletion in *COQ2*
pABA: para-aminobenzoic acid
PC: phosphatidylcholine
Pyr_{12}: 1-pyrene dodecanoic acid
SD: synthetic dextrose medium
vCLAMP: vacuole-mitochondria patch
WT: wild-type parental yeast strain
YPD: rich growth medium containing dextrose as a fermentable carbon source
YPG: rich growth medium contain glycerol as the sole non-fermentable carbon source

APPENDIX II

Intragenic suppressor mutations of the COQ8 protein kinase homolog restore coenzyme Q biosynthesis and function in *Saccharomyces cerevisiae*

ABSTRACT

Saccharomyces cerevisiae Coq8 is a member of the ancient UbiB atypical protein kinase family. Coq8, and its orthologs UbiB, ABC1, ADCK3, and ADCK4, are required for the biosynthesis of coenzyme Q in yeast, *E. coli*, *A. thaliana*, and humans. Each Coq8 ortholog retains nine highly conserved protein kinase-like motifs, yet its functional role in coenzyme Q biosynthesis remains mysterious. Coq8 may function as an ATPase whose activity is stimulated by coenzyme Q intermediates and phospholipids. A key yeast point mutant expressing Coq8-A197V was previously shown to result in a coenzyme Q-less, respiratory deficient phenotype. The A197V substitution occurs in the crucial Ala-rich protein kinase-like motif I of yeast Coq8. Here we show that long-term culture of mutants expressing Coq8-A197V produces spontaneous revertants with the ability to grow on medium containing a non-fermentable carbon source. Each revertant is shown to harbor a secondary intragenic suppressor mutation within the *COQ8* gene. The intragenic suppressors restore the synthesis of coenzyme Q. One class of the suppressors fully restores the levels of coenzyme Q and key Coq polypeptides necessary for the maintenance and integrity of the high-molecular mass CoQ synthome (also termed complex Q), while the other class provides only a partial rescue. Mutants harboring the first class of suppressors grow robustly under respiratory conditions, while mutants containing the second class grow more slowly under these conditions. Our work provides insight into the function of this important yet still enigmatic Coq8 family.

INTRODUCTION

Coenzyme Q (also termed ubiquinone, CoQ or Q) serves as a vital redox active lipid and antioxidant molecule necessary for energy production (1,2). Q is composed of a fully substituted benzoquinone ring and a polyisoprenoid tail whose length is species dependent (3). *Homo sapiens* produce Q_{10} with a decaprenyl tail, *Escherichia coli* produce Q_8, and *Saccharomyces cerevisiae* produce Q_6. A primary role of Q in the inner mitochondrial membrane is to serve as a reversible electron and proton carrier (4). Q accepts electrons and protons from Complexes I and II in the respiratory electron transport chain, and QH_2 (ubiquinol or reduced $CoQH_2$) donates electrons and protons to Complex III (5). Q also functions as an electron acceptor in other biochemical pathways, such as pyrimidine synthesis, sulfide oxidation, and fatty acid β-oxidation (4,6,7). Human Q_{10} deficiencies often affect multiple organ systems, including the central and peripheral nervous systems, kidney, skeletal muscle, heart, and sensory systems (6). Mouse knockout studies show that a complete lack of Q is embryonic lethal (8). In contrast, yeast mutants lacking Q_6 are unable to grow on nonfermentable carbon sources, but are able to grow on fermentable carbon sources, because ATP is generated via substrate-level phosphorylation.

Fourteen nuclear encoded mitochondrial proteins are necessary for the efficient production of Q_6 in *S. cerevisiae* (Fig 1A) (9,10). Coq1 is responsible for the synthesis of hexaprenyl diphosphate, and Coq2 attaches the hexaprenyl group to 4-hydroxybenzoic acid (4-HB). Other Coq polypeptides work to catalytically modify the head group via decarboxylation, hydroxylation, and methylation steps, in order to produce QH_2. Several of the Coq proteins involved in the synthesis of Q_6 in *S. cerevisiae* associate in a high molecular mass complex termed the CoQ synthome, and localize to the inner mitochondrial membrane on the matrix side (Fig 1B) (9,11). Coq4 serves as a scaffolding protein and is the central organizer of the CoQ synthome (12). Many

of the other Coq polypeptides, including Coq3, Coq5, Coq6, Coq7, Coq8, Coq9, and Coq11 are partner proteins required for CoQ synthome stability, assembly, or enzyme activity (9,11).

Coq8 is a member of the ancient protein kinase-like (PKL) UbiB family of proteins, as well as a member of the superfamily of putative atypical protein kinases termed "ADCKs" (aarF-domain containing kinases) (13). The UbiB PKL family comprises nearly a quarter of all known microbial PKL proteins, is involved in isoprenoid lipid synthesis, and is necessary for the aerobic production of Q (14). In humans, there are five UbiB-like homologs, termed ADCK1 - ADCK5; deficiencies in ADCK1, ADCK2, ADCK3 or ADCK4 have been implicated in various diseases. ADCK3 (COQ8A) and ADCK4 (COQ8B) are co-orthologs of yeast Coq8, since each can rescue the yeast *coq8* null mutant (15,16). Patients harboring mutations in *ADCK3* develop cerebellar ataxia (17,18), while patients with mutations in *ADCK4* develop steroid resistant nephrotic syndrome (16,19). Both types of patients have significantly decreased levels of Q_{10}. Recently, *ADCK2* haploinsufficiency was observed to cause liver dysfunction, impaired fatty acid oxidation, and mitochondrial myopathy in skeletal muscle in one patient and in a mouse model (20).

Structural and biochemical studies of human COQ8A revealed an atypical kinase-like fold, and ATP and ADP were bound in a divalent cation-dependent manner (13). Sequence alignments identified nine conserved PKL subdomains (13). Analyses of yeast *coq8* mutants with mutations present within the PKL motifs suggest that these conserved motifs are essential for Q biosynthesis (13,15). Creation of an ATP analog-sensitive version of yeast Coq8 showed that chemical inhibition with targeted ATP-based inhibitors could be used to rapidly induce a respiratory deficient phenotype and depletion of Q_6 (21). These studies indicate that ATP binding and hydrolysis is essential to the function of Coq8 and COQ8A in the biosynthesis of Q. An atypical Ala-rich loop defines the PKL-motif 1 of COQ8A and replaces the Gly-rich loop present in the

active site of canonical protein kinases (13). The mutation of a single alanine residue (A339) to a glycine within the Ala-rich loop of kinase-like motif 1 elicited enhanced autophosphorylation of COQ8A, but decreased Q production. The A339 of human COQ8A corresponds to A197 of yeast Coq8; the Coq8-A197V mutation was shown to abolish Q_6 production in yeast (15).

Several Coq polypeptides are shown to be phosphorylated in a Coq8-dependent manner—particularly Coq3, Coq5, and Coq7—although there is no direct evidence that Coq8 is the kinase that is responsible for this phosphorylation (15). Instead, mammalian COQ8A and COQ8B, and yeast Coq8, have been proposed to function as ATPases or small molecule kinases, rather than as canonical protein kinases (22). In this capacity Coq8 may somehow act to assist the formation or stability of the CoQ synthome. Coq8 and its ATPase activity are also required for the organization of the CoQ synthome into puncta or discrete domains that occur at contact sites between the mitochondria and ER (23,24). Coq4, Coq7, and Coq9 polypeptides are often used as sensitive indicator polypeptides of the CoQ synthome (12,25). Overexpression of Coq8 augments the steady state levels of these indicator Coq polypeptides and stabilizes the CoQ synthome (12,25,26).

In this study, we employed a yeast *coq8*-3 mutant harboring an A197V mutation that was previously characterized as "Q-less" and unable to grow on rich medium containing glycerol (YPG) (15). We recovered spontaneous revertants that acquired the ability to grow on YPG. Surprisingly, characterization of the revertants reveals that each contains a secondary mutation within the *COQ8* gene, and thus are intragenic suppressors. Overall, we identify and characterize three novel point mutations that appear to be highly influential in the mode of action of Coq8 and its contribution to Q production and CoQ synthome stability.

EXPERIMENTAL PROCEDURES

All reagents were obtained commercially from Fisher Scientific unless otherwise specified.

Yeast strains and culture conditions

The *S. cerevisiae* strains used in this study are listed in Table 1. All strains were derived from the W303 genetic background. Liquid yeast culture medium was prepared as described (11) and included YPD (2% glucose, 1% yeast extract, 2% peptone), YPGal (2% galactose, 0.1% glucose, 1% yeast extract, 2% peptone), and YPG (3% glycerol, 1% yeast extract, 2% peptone). Yeast plate medium was prepared by adding 2% Agar (Bacto) to the above mentioned liquid media. Yeast strains were stored in 30% (v/v) sterile glycerol at −80 ^{o}C. Prior to each experiment, the corresponding strains were plated on to YPD plates, incubated at 30 ^{o}C for two to three days, and the plates with yeast colonies were stored at 4 ^{o}C for up to two weeks.

Use of CRISPR/Cas9 to generate NP-183A and NP-183AL

pCAS plasmid was obtained from Addgene (plasmid #60847) (27) (Table 2). NP-183A and NP-183AL strains harboring the *coq8-3* point mutation were prepared via standard yeast transformation protocol (28) with inclusion of 1 μg of the pCas9 plasmid along with the standard repair DNA for homologous recombination. The *COQ8* sequence in proximity of the *coq8-3* point mutation (C590T encoding A197V) was designed following a Protospace Adjacent Motif (PAM) sequence. A 60-basepair repair double stranded DNA that emulated the *coq8-3* point mutation was prepared through restriction free cloning with the QuikChange II Site-directed mutagenesis kit (Agilent, Santa Clara, CA). The newly desired plasmid and the repair DNA were used to transform W303-1A. Transformants were plated on YPD with G418 and incubated at 37 ^{o}C for one to two

days to activate the Cas9 enzyme. Colonies observed on YPD with G418 were isolated and grown on YPD at 30 ^{o}C. The *COQ8* gene sequence was verified through sequencing and over the region of the *COQ8* gene, NP-183A and NP-183AL (Table 1) each contained just the *coq8-3* mutation.

Yeast mating type switch

Mating type switch for NP-183A was performed with the pGal-HO plasmid as described (29). Single colonies were selected and tested for intact mitochondrial genome by mating with JM6 and JM8 *rho*^{0} tester strains (Table 1). The rho test also provided verification of the mating type switch.

Yeast sporulation and tetrad dissection

Diploid cells were induced to sporulate and tetrads dissected as described (30). Respiratory defective yeast diploid strains were transformed with p3HN4 expressing the wild-type *COQ8* gene prior to sporulation. Treatment with 5-fluoro-orotic acid (5-FOA) was used to remove p3HN4 from resulting haploid progeny (30).

Site-directed mutagenesis

Site-directed mutagenesis was performed with the QuikChange Lightning mutagenesis kit and the XL10 transformation according to the manufacturer's directions (Agilent, Santa Clara, CA).

Purification of mitochondria

Yeast cells were grown in 5 ml of YPGal plus 0.1% dextrose precultures and inoculated into 600-ml YPGal plus 0.1% dextrose cultures for overnight growth in a shaking incubator (30 °C, 250 rpm). Cells were harvested at an A_{600nm} of 3.5–4.0, and mitochondria were purified as described (31) and (11). Protein concentration was measured with a BCA assay using bovine serum albumin as the standard.

SDS-PAGE and Immunoblot analyses

Protein samples incubated with SDS sample buffer (50 mM Tris-HCl, pH 6.8, 10% glycerol, 2% SDS, 0.1% bromphenol blue, 1.33% β-mercaptoethanol) were separated on 12% Tris-glycine SDS-polyacrylamide gels by electrophoresis (32) for 2 hrs at 135 V followed by transfer to Immobilon-P PVDF membranes (Millipore) at 150 V for 1 hr. Membranes were then blocked overnight in 3% nonfat milk, phosphate-buffered saline (140.7 mM NaCl, 9.3 mM Na_2HPO_4, pH 7.4), 0.1% Tween 20 or BSA based blocking buffer for compatibility with LiCor imaging. Membranes were then probed with primary antibodies (Table 3) in 2% nonfat milk, phosphate buffered saline, 0.1% Tween 20 or with antibodies diluted in BSA-based buffer compatible with LiCor imaging. Goat anti-rabbit secondary antibody conjugated to horseradish peroxidase (Calbiochem) was used at 1:10,000 dilutions. Blots were visualized using Supersignal West Pico chemiluminescent substrate or directly via the LiCor system when secondary antibody used was conjugated to a fluorescent signal probe.

Metabolic labeling of Q_6 with $^{13}C_6$-labeled precursors

In order to assess the content of de novo synthesized Q_6, yeast strains were grown as described (33). Briefly yeast strains were incubated overnight in 5 ml of YPD in a shaking incubator (30 °C, 250 rpm) and diluted to an A_{600nm} of 0.1 in 6 ml of fresh YPD the next morning. The cultures were incubated as before to an A_{600nm} of 0.5 (mid-log phase) and subsequently treated with $^{13}C_6$-4HB at 10 μg/ml final concentration (ethanol 0.015%, v/v). At designated time periods, cells were harvested by centrifugation at 3000 × *g* for 5 min, from 5 ml aliquots. Cell pellets were stored at −20 °C.

Analysis of Q_6 and Q_6 intermediates

Q_6 was obtained from Avanti Polar Lipids, Inc. Lipid extraction of cell pellets was conducted as described (33) with methanol and petroleum ether. Prior to extraction Q_4 was added as the internal standard. To determine the Q_6 content in yeast strains cultured on YPG plates, the strains were applied to YPG plates and incubated at 30°C 4-5 days before harvesting. Cells recovered from the solid plate medium were suspended in YPG liquid medium and the A_{600} determined. Cells were then collected by centrifugation and subjected to lipid extraction. Yeast strains that failed to grow on YPG were subjected to the same analysis, except that a section of the solid plate medium harboring the inoculated yeast cells was excised and subjected to the lipid extraction protocol. This was performed in order to recover cells that were applied to the plate medium but failed to grow. Lipid measurements were performed by HPLC-MS/MS and normalized to total OD. Prior to mass spectrometry analyses, all samples were treated with 1.0 mg/ml benzoquinone to oxidize hydroquinones to quinones. Mass spectrometry analyses utilized a 4000 QTRAP linear MS/MS spectrometer (Applied Biosystems), and data were acquired and

analyzed using Analyst version 1.4.2 and 1.5.2 software (Applied Biosystems). Separation of lipid quinones was performed with a binary HPLC delivery system and a Luna 5µ phenyl-hexyl column (100 × 4.6 mm, 5 µm; Phenomenex). The mobile phase consisted of a 95:5 methanol/isopropyl alcohol solution with 2.5 mM ammonium formate as solution A and a 100% isopropyl alcohol solution with 2.5 mM ammonium formate as solution B. The percentage of solution B was increased linearly from 0 to 5% over 6 min, whereby the flow rate was increased from 600 to 800 µl. Initial flow rate and mobile phase conditions were changed back to initial phase conditions linearly over 3.5 min. Each sample was analyzed using multiple reaction monitoring mode. The following precursor-to-product ion transitions were detected as well as the +17 m/z ammoniated adducts for each of the metabolic products: $^{13}C_6$-HHB m/z 553.4/157.0 (ammoniated: 570.4/157.0), ^{12}C-HHB m/z 547.4/151.0 (ammoniated: 564.4/151.0), $^{13}C_6$-DMQ_6 m/z 567.6/173.0 (ammoniated: 584.6/173.0), ^{12}C-DMQ_6 m/z 561.6/167.0 (ammoniated: 578.6/167.0), $^{13}C_6$-Q_6 m/z 597.4/203.1 (ammoniated: 614.4/203.1), ^{12}C-Q_6 m/z 591.4/197.1 (ammoniated: 608.4/197.1), and ^{12}C-Q_4 m/z 455.4/197.0 (ammoniated: 472.4/197.0).

Plate dilution assays

Strains were grown overnight in 5 ml of YPD as described (33) and diluted to an A_{600} of 0.2 in sterile PBS. A 5-fold serial dilution in PBS was performed, after which 2 µl of each dilution (1 X, 5 X, 25 X, 125 X, and 625 X) were spotted onto the designated plate growth medium. The final A_{600} of the aforementioned dilution series are 0.2, 0.04, 0.008, 0.0016, and 0.00032, respectively. The plates were incubated at 30 ^{o}C for the designated time periods in days and subsequently imaged.

PHYRE homology modeling

S. cerevisiae Coq8 was modeled with the PHYRE2 intensive modeling mode (34). A 44% identity was obtained compared to PDB ID 4PED, a crystal structure determined for an amino-terminal truncated human COQ8A. The modeled structure lacks the first 32 amino acids of yeast Coq8, predicted to function as the mitochondrial targeting sequence. This sequence is excised upon transport of Coq8 to the mitochondria, resulting in the mature Coq8 polypeptide.

RESULTS

Single nucleotide mutations within *COQ8* restore respiratory growth of the Coq8-A197V mutant

A yeast mutant harboring the *coq8-3* allele (see Table 1 for the complete genotype), is respiratory defective, fails to grow on medium with glycerol as the sole carbon source, and lacks Q_6 (15,35). The *coq8-3* mutation was identified as A197V, resulting from C590T in the DNA sequence of the *COQ8* gene (Table 4) (15). In order to isolate and characterize spontaneous *coq8-3* revertants, we recreated the Coq8-A197V mutation in the W303-1A wild-type genetic background. To accomplish this, the C590T mutation was introduced into the W303-1A genome via CRISPR/Cas9 as described in *Materials and Methods*, and gave rise to yeast strains NP-183A and NP-183AL, that each expressed Coq8-A197V (Table 1). Three independent screens were performed to search for spontaneous revertants, with the acquired ability to grow on YPG plate medium after incubation at 30 °C for three to four weeks. Colonies observed on the YPG screening plates were not always capable of sustained growth when reapplied to fresh YPG plate medium. Thus, colonies were assessed by plate dilution assays prior to being identified as potential revertants.

This procedure produced five independent revertant yeast strains termed Rev-AL, Rev-BL, Rev-CL, Rev-DL, and Rev-EL that carry suppressor mutations (Table 1). Qualitatively, the robust growth of Rev-CL, Rev-DL and Rev-EL was comparable to wild type, while less robust growth was observed for Rev-AL and Rev-BL on YPG (Fig 2). Sequence analyses of the *coq8* locus in each of the five revertant yeast strains showed retention of the parental Coq8-A197V mutation (Table 4). Surprisingly, each of the revertants also harbored a second mutation within the *coq8* locus, indicating that the revertant phenotypes were perhaps due to intragenic suppression. Thus, in addition to the introduced A197V mutation, Rev-AL acquired the L237P mutation, Rev-BL acquired the P220S mutation, and Rev-CL, Rev-DL, and Rev-EL each acquired the same S232N mutation resulting from G695A (Table 4).

Dominance tests reveal Rev-AL and Rev-BL are recessive and Rev-CL, Rev-DL, and Rev-EL are dominant

To test dominance, each haploid revertant was mated with NP-183BH to create diploids (Table 1). The NPD-A and NPD-B diploids derived from Rev-AL and Rev-BL, respectively, were unable to grow on YPG, indicating that the L237P and P220S mutations were recessive suppressors (Figure 3A). Conversely, the NPD-C, NPD-D and NPD-E diploids each grew on YPG plate medium, and showed the S232N mutation was a dominant suppressor (Fig 3A). To examine whether each of the revertant phenotypes could be attributed to a single nuclear mutation, the diploids were sporulated, and four to ten tetrads were dissected for each of the NPD-A, NPD-C, NPD-D and NPD-E diploids (S1-S3 Figs). In order to permit sporulation, the respiratory defective NPD-A and NPD-B diploids were first rescued by transformation with a low copy plasmid expressing wild-type *COQ8* (p3HN4, Table 2). Although this procedure enabled tetrad dissection

of spores derived from NPD-A, we were not able to obtain tetrads from NPD-B. Four dissected spores from each tetrad were grown on YPD plate medium and replica-plated onto YPG plate medium. The haploid spores derived from NPD-A were first cured of p3HN4 prior to testing on YPG medium as described in *Materials and methods*. Each of the diploid strains yielded tetrads that segregated 2:2 for respiration (S1-S3 Figs). These results indicated that the ability of Rev-AL, Rev-CL, Rev-DL and Rev-EL to respire was due to a single nuclear mutation.

The S232N amino acid substitution is solely responsible for restoration of the growth of Rev-CL yeast on a non-fermentable carbon source

We wanted to determine whether the S232N change was responsible for the gain of function in the Rev-CL, Rev-DL and Rev-EL revertants expressing Coq8-A197V/S232N. To test this, p3HN4, a low copy plasmid carrying *COQ8*, was modified to create different variants. One variant possessed just the A197V mutation, a second had only the S232N mutation, and the final variant contained both point mutations (Table 4). The parental mutant, NP-183AL was transformed with each plasmid and tested for growth on a non-fermentable carbon source. As expected, NP-183AL with the plasmid expressing Coq8-A197V failed to grow on YPG plate medium (Fig 3B). However, significant growth was observed for NP-183AL containing the plasmid plc-Coq8-A197V/S232N and for the plasmid plc-Coq8-S232N (Fig 3B). This result confirmed that the S232N amino acid substitution was solely responsible for the gain of function of respiratory growth observed in the Rev-CL, Rev-DL and Rev-EL revertants. In subsequent studies, Rev-CL was used as the representative mutant for S232N.

Structural prediction of yeast Coq8 reveals putative spatial organization of revertant mutations

A crystal structure for the yeast Coq8 polypeptide has not yet been reported. However, a partial human COQ8A (ADCK3) structure was characterized and deposited as 4PED in the protein databank (13). PHYRE2 homology modeling software was used to predict the putative structure of yeast Coq8, which was modeled at 44% identity to the partial human COQ8A structure 4PED (Fig 4A) (34). Modeling yeast Coq8 in this manner relates the predicted locations of the suppressor mutations with respect to the previously published COQ8A domains. Yeast Coq8-A197 is the site of the A197V parental mutation, and is located in the Ala-rich loop of Protein Kinase-Like Motif I (PKLI), within the beta sheets that are part of the N-lobe (Figure 4; (13)). The suppressor mutations are all located next to, or within, the GQα5 motif, in what is termed the "N-lobe insert" (Fig 4; (13)). The relative predicted locations of L237 (L237P in Rev-AL), P220 (P220S in Rev-BL), and S232 (S232N in Rev-CL, Rev-DL and Rev-EL) are in close proximity to A197V in the primary sequence (Fig 4C). However, the mutations in Rev-AL and Rev-CL are estimated to reside 19 Å from the A197V mutation, and the P220S in Rev-BL is estimated to reside 13.4 Å from the A197V mutation (Figure 4A, inset). Moreover, it is apparent that L237, P220, and S232 residues are located on the surface of Coq8, remote from the predicted active site residues in the Ala-rich region of the PKL1 motif.

Amino acid alignment indicates that S232N in Rev-CL is sustained as a conserved Asn in other eukaryotic Coq8 homologs

A multiple sequence alignment of yeast Coq8, *E. coli* UbiB, *A. thaliana* ABC1, *C. elegans* COQ-8, mouse COQ8A and COQ8B, and human COQ8A and COQ8B homologs shows the

relative positions of the A197V and the three amino acid substitutions recovered in the revertants (Fig 4C). The mutations in Rev-AL (L237P) and in Rev-BL (P220S) both correspond to highly conserved residues in all eight Coq8 homologs. Intriguingly, with the exception of *S. cerevisiae*, all eukaryotic sequences examined in Fig 4C have a conserved Asn present at the relative position of yeast Coq8-S232. Since the Coq8-S232N substitution confers a dominant phenotype that over-rides the inactive Coq8-A197V mutation, it is possible that the Asn naturally present at this corresponding position in the other eukaryotic Coq8 homologs may confer an inherently more active state.

Analyses of Q_6 synthesis and content in the three revertant yeast strains as compared to wild-type yeast

Growth of WT, *coq8*Δ, NP-183A (containing Coq8-A197V), Rev-AL, Rev-BL, and Rev-CL was assessed in various types of growth medium. When rich medium containing dextrose was provided as the sole fermentable carbon source (YPD), the six strains followed a nearly identical logarithmic growth trend over the first five hours (S4A Fig). When glycerol was provided as the sole carbon source (YPG), initial growth during the first five hours represented two to three doublings, and was presumably due to utilization of a small amount of dextrose introduced by the inoculum of yeast cultured in YPD. Over the course of 24 hours, WT and Rev-CL showed similar vigorous growth, while Rev-AL displayed slower growth on YPG (S4B Fig). When galactose was provided as a main carbon source (YPGal supplemented with 0.1% dextrose) WT showed the highest growth, followed closely by Rev-CL, then NP-183A, the *coq8*Δ mutant, and Rev-AL, and with Rev BL showing the slowest growth in this condition (S4C Fig). YPGal medium provides a fermentable but non-repressive carbon source, and is used for experiments that involve

mitochondrial extraction and purification (36). It is useful here to establish these growth behaviors for each strain of interest in order to determine the optimal time course of incubation.

Q_6 *de novo* synthesis was measured following incubation with $^{13}C_6$-4HB, a ring precursor of Q_6 (Fig 1). In addition, total Q_6 content, and Q_6-intermediates were quantified in each of the six strains grown in YPD. Over the course of five hours, cells were harvested and lipid extracts were analyzed for unlabeled ^{12}C-Q_6 and *de novo* $^{13}C_6$-Q_6 levels using HPLC-tandem mass spectrometry. Rev-CL produced nearly comparable levels of unlabeled Q_6 as WT, while producing slightly lower levels of *de novo* $^{13}C_6$-Q_6 (Figs 5A and 5B). The expanded scale presented in Figs 5C and 5D, shows that Rev-AL has significantly lower levels of unlabeled and *de novo* $^{13}C_6$-Q_6. Conversely, in these YPD cultures Rev-BL lacks detectable levels of unlabeled Q_6 or labeled $^{13}C_6$-Q_6. In this regard it behaves identically to the Q-less *coq8*Δ and NP-183A mutants.

WT and Rev-CL yeast strains that produced high levels of unlabeled Q_6 and *de novo* $^{13}C_6$-Q_6, also contained comparable levels of unlabeled DMQ_6 and *de novo* $^{13}C_6$-DMQ_6 (Figs 6A and 6B), the penultimate intermediate in Q_6 biosynthesis (Fig 1). Rev-AL and Rev-BL, as well as the *coq8*Δ and NP-183A mutants produced substantially lower or undetectable levels of DMQ_6 (Figs 6A and 6B). In contrast, these four mutant yeast strains contained relatively high levels of unlabeled HHB and $^{13}C_6$-HHB as compared to WT (Figs 6C and 6D). HHB is an early intermediate in Q_6 biosynthesis that frequently accumulates in yeast *coq*3 – *coq11* mutants with deficiencies in Q_6 biosynthesis (9). The relatively high accumulation of $^{13}C_6$-HHB in Rev-CL suggests that *de novo* synthesis of $^{13}C_6$-Q_6 is impaired as compared to WT.

Overall, the lipid analyses in YPD medium over a five-hour time course show that the secondary mutation S232N in Rev-CL restored the capacity to produce Q_6 to levels comparable to

WT, while Rev-AL makes substantially lower levels of Q_6. Surprisingly, Rev-BL failed to produce detectable amounts of unlabeled Q_6 or labeled $^{13}C_6$-Q_6.

Both Rev-CL and Rev-AL are able to synthesize Q_6 in non-fermentable YPG medium

The lack of detectable Q_6 in the YPD cultures of Rev-BL raised the question, how is this mutant able to grow successfully on YPG plates? In order to interrogate this further, each of the six strains was cultured in a YPG glycerol-based medium (non-fermentable) and in the YPD dextrose-based (fermentable) medium, and analyzed for unlabeled and *de novo* $^{13}C_6$-Q_6 production after five hours of incubation. Rev-CL exhibited comparable levels of unlabeled and *de novo* $^{13}C_6$-Q_6 to WT, in both types of medium (Figs 7A and 7B), and total (^{12}C-Q_6 +$^{13}C_6$-Q_6) levels in Rev-CL were nearly identical to WT in YPG (Fig 7C). Rev-AL contained low amounts of unlabeled Q_6, a trait that was more pronounced in YPG medium (Fig 7A). Curiously, neither unlabeled Q_6 nor labeled $^{13}C_6$-Q_6 was detected in the Rev-BL yeast under these conditions (Fig 7).

Rev-BL grown on solid YPG plate medium contains Q_6

Since culture for five hours in liquid YPG medium failed to allow Rev-BL to produce any detectable amounts of Q_6, we recovered yeast from colonies that were cultured on YPG plate medium. Under these growth conditions, WT, Rev-AL, Rev-BL and Rev-CL showed growth (Fig 2) and successful production of Q_6 (Fig 8A). In fact, WT, Rev-CL, and Rev-AL showed comparable levels of Q_6, while Rev-BL produced lower amounts of Q_6 (Fig 8A). These results show that under conditions of growth on YPG plate medium, Rev-BL is able to produce Q_6. It has been shown that growth on YPG plate medium requires only 0.2 to 3% of the "baseline" levels of Q_6 (9,11,37,38). This may explain the low but comparable growth of Rev-BL and Rev-AL

observed on YPG plate medium (Fig 2B). As controls, the *coq8Δ* and NP-183A yeast strains were also applied to the YPG plate medium. Although these yeast fail to grow on YPG medium, the region of the plate containing the applied yeast cells was recovered, and analyzed for Q_6 and Q_6-intermediates as described in *Materials and Methods*. Neither Q_6 nor DMQ_6 were detected in these lipid extracts, although an early Q_6-intermediate HHB, was detected (Fig 8).

Growth in nutrient conditions that facilitate the study of mitochondrial function reveals the capacity of all three revertants to produce Q_6

In order to study mitochondrial function in yeast strains, rich growth medium containing 2% galactose (YPGal) is often used as a non-repressing carbon source (36). The use of this growth medium circumvents the repression of mitochondrial function mediated by dextrose. For this analysis, a predominantly galactose carbon source was used (YPGal with 0.1% dextrose). Under this condition, Rev-CL showed a decreased capacity to produce both unlabeled and *de novo* $^{13}C_6$-Q_6, as compared to WT (Fig 9A), while Rev-AL and Rev-BL produced substantially lower amounts of unlabeled and $^{13}C_6$-Q_6 than Rev-CL (Fig 9A, inset). Indeed, only WT and Rev CL showed detectable levels of DMQ_6, while all the strains except WT showed accumulation of the early precursor, HHB (Figs 9B and 9C).

The suppressor mutations in Rev-AL, Rev-BL, and Rev-CL result in different levels of the CoQ synthome polypeptides

We sought to investigate the effects of the Coq8 suppressors on the levels of sensitive indicator Coq polypeptides. These indicator polypeptides include Coq4, Coq7, and Coq9, because they serve key roles in maintaining the high molecular mass CoQ synthome (12). In order to track

these indicator Coq polypeptides, mitochondria were subjected to immunoblotting with the primary antibodies described in Table 3. Interestingly, Rev-CL contained nearly wild-type content of the Coq4 and Coq9 polypeptides, while Rev-AL and particularly Rev-BL had decreased amounts of Coq4 and Coq9 (Fig 10). This is quite intriguing, since Coq4 has previously been shown to serve as a central organizer of the CoQ synthome (12). The content of Coq7 is retained at near WT levels in Rev-CL and Rev-AL, but was slightly decreased in Rev-BL. This is consistent with the higher content of Q_6 in Rev-CL, since Q_6 production relies on Coq4, Coq7, and Coq9 (9). It appears as though the Rev-AL and Rev-CL exhibit a near normal amount of Coq8 polypeptide as compared to WT, while the level of Coq8 polypeptide is lower in Rev-BL mitochondria (Fig 10).

DISCUSSION

Coq8 is a member of an ancient family of atypical protein kinases with essential roles in Q_6 biosynthesis. Coq8 facilitates the assembly of the CoQ synthome, a multisubunit complex that is essential for the biosynthesis of Q_6 in yeast (12). Coq8 also mediates the organization of the CoQ synthome into discrete domains within mitochondria, observed as puncta located adjacent to ER-mitochondria contact sites (23). These functions are conserved in COQ8A, the human ortholog of yeast Coq8 (23). *E. coli* UbiB, yeast Coq8 and human COQ8A possess ATPase activity that is stimulated by analogs of Q-intermediates (21), although the mechanism(s) by which Coq8 or COQ8A mediate the assembly or spatial organization of the CoQ synthome (or Complex Q) is still mysterious (23,39).

In this study we used a yeast Coq8-A197V mutant previously characterized as Q-less and respiratory deficient (15). The A197V mutation occurs within the crucial Ala-rich PKL-motif I of

yeast Coq8, that replaces the Gly-rich nucleotide-binding loop normally present in canonical protein kinases (13) (Fig 4C). Thus, the A197V mutation occurs within the presumed active site of the Coq8 polypeptide, and is likely to impact the binding of ATP and its hydrolysis. Here, we characterized spontaneous revertants of the Coq8-A197V mutant that were isolated following long-term culture in growth medium containing glycerol, a non-fermentable carbon source. Each revertant (Rev-AL, Rev-BL, Rev-CL, Rev-DL and Rev-EL) acquired the ability to grow on medium containing glycerol and to synthesize Q_6. Surprisingly, each revertant was found to contain a secondary mutation within the *COQ8* gene, suggesting that the recovery of glycerol growth and Q_6 synthesis resulted from an intragenic suppressor mutation.

Each of the intragenic suppressor mutations was determined to reside next to or within the GQα5 helix of Coq8. The GQα5 helix is one of two helices that form an insert located between the beta sheet (β3) and the αC helix (Fig 4). This insert is part of a distinct and conserved feature present in each of the PKL members of the UbiB family (13). Each intragenic suppressor mutation was predicted to lie near the surface of Coq8, and to range a distance of 14 - 19 Å from the A197V mutation (Fig 4). It is tempting to speculate that the surface location of the Coq8 suppressor mutations allows them to mediate interactions of Coq8 with other Coq subunit proteins of the CoQ synthome. Because expression of Coq8-A197V/S232N is able to dominantly suppress the parental mutant phenotype, it may serve to displace the Coq8-A197V polypeptide. In contrast the recessive intragenic suppressors are unlikely to be able to displace the Coq8-A197V polypeptide (Fig 11).

Differences between the two classes of revertants (dominant and recessive) are also evident from their capacity to synthesize Q_6. Rev-CL displayed the capacity to synthesize levels of Q_6 comparable to wild-type yeast. Rev-AL and Rev-BL, however, produced much lower amounts of Q_6, yet still showed the ability to make significant quantities, when cultured on YPGal + 0.1%

dextrose liquid medium or when cultured on YPGlycerol plate medium. Thus, we hypothesized that the Coq8-A197/S232N polypeptide present in Rev-CL may act to restore levels of the Coq polypeptides that are components of the CoQ synthome.

Determining the levels of sensitive indicator Coq polypeptides tested this idea. Rev-CL displayed robust levels of Coq4, Coq7, and Coq9 polypeptides. The Coq8-A197V/S232N polypeptide was also present at levels comparable to Coq8 in wild-type yeast. This is consistent with the high levels of Q_6 synthesis in the Rev-CL yeast. In contrast, the recessive revertants, Rev-Al and Rev-BL produced much less Q_6, and retained low amounts of the Coq4 and Coq9 indicator polypeptides.

It is notable that the Coq8-A197V/S232N polypeptide in Rev-CL allows for efficient respiration and a near perfect restoration of Q_6 production. In eukaryotic Coq8 homologs, an Asn residue normally occupies this same location as S232 (Fig 4C). It is possible that the yeast Coq8-S232N point mutation restores Q_6 biosynthesis by mimicking the sequence of higher order eukaryotic Coq8 orthologs.

A distinct mutation of A197G in Coq8 has been shown to decrease Q_6 content and inhibit growth on glycerol containing medium (13), and also results in enhanced ATPase activity and cis-autophosphorylation (21,22). Similar trends of ATPase and cis-autophosphorylation are noted for the A339G mutation in human COQ8A, which corresponds to Coq8-A197G (21,22). It would be interesting to perform similar activity assays on the Coq8-A197V and each of the three revertants.

Protein kinase activity in trans has not been demonstrated for any of the UbiB, Coq8, or COQ8A PKL orthologs (22). It is possible that the full-length activity of Coq8 may show different properties than the truncated versions used in activity assays to date (40). A recent report identifies a PKL family member with distinct ATP-dependent ligation activity (41). There is precedent in *A.*

thaliana for trans phosphorylation mediated by an ABC1K homolog of the UbiB family. ABC1K1 has been shown to phosphorylate VTE1, a plastoglobule protein involved in vitamin E synthesis (42). ABC1K1 is one of five ABC1K homologs located within the plastoglobule, a lipid droplet within the plastid that contains prenylated lipids including plastoquinone and vitamin E (43). Finally, it is possible that phosphorylation sites may control transport into the mitochondria, since several sites present in Coq7 and Coq9 polypeptides are located near the amino terminus, and are not present in the full length polypeptide (15,44,45). The phosphatase Ptc7 in yeast and PPTC7 in human cells have recently been shown to aid in import of mitochondrial proteins (46). It will be important to determine the effect of the revertant mutations on the role of full-length Coq8 in order to understand its mechanisms of action in Q biosynthesis.

ACKNOWLEDGMENTS

We thank and acknowledge the UCLA Molecular Instrumentation Core proteomics facility and Dr. Yu Chen for his advice and the use of the QTRAP4000 for lipid analysis. We thank and acknowledge Dr. Guillaume Chanfreau and Mr. Charles Wang, for their assistance and guidance on *CRISPR/Cas9* methodology and procedures. We thank Dr. Carol Dieckmann for advice and consultation on this project. We thank Dr. Theresa Nguyen and Ms. Hei Tong Nikki Lam for their contributions related to this project, and the members of the Clarke lab for discussions and input on the manuscript. We acknowledge the authors of the PHYRE2 web portal for the protein modeling, prediction, and analysis presented in this work.

Table 1. Genotypes and sources of yeast strains

Strain	Genotype or description	Source
W303-1A	MAT **a** *leu2-3,112 trp1-1 can1-100 ura3-1 ade2-1 his3-11,15*	R. Rothstein[a]
C183	MAT α *met6 coq8-3*	(35)
W183-2A	MAT **a** *his3-1,15 trp1-1 ura3-1 coq8-3*	(15)
JM6	MAT **a** *his4 rho^0*	J.E. McEwen[b]
JM8	MAT α *ade1 rho^0*	J.E. McEwen[b]
W303Δ*coq8*	MAT **a** *ade2-1 his3-1,15 leu2-3,112 trp1-1, ura3-1 coq8::HIS3*	(47)
NP-183A	MAT **a** *leu2-3,112 trp1-1 can1-100 ura3-1 ade2-1 his3-11,15 coq8-3*	This work
NP-183AL	MAT **a** *trp1-1 can1-100 ura3-1 ade2-1 his3-11,15 coq8-3*	This work
NP-183B	MAT α *leu2-3,112 trp1-1 can1-100 ura3-1 ade2-1 his3-11,15 coq8-3*	This work
NP-183BH	MAT α *leu2-3,112 trp1-1 can1-100 ura3-1 ade2-1 coq8-3*	This work
Rev-AL	MAT **a** *trp1-1 can1-100 ura3-1 ade2-1 his3-11,15 coq8-3 SupRA*	This work
Rev-BL	MAT **a** *trp1-1 can1-100 ura3-1 ade2-1 his3-11,15 coq8-3 SupRB*	This work
Rev-CL	MAT **a** *trp1-1 can1-100 ura3-1 ade2-1 his3-11,15 coq8-3 SupRC*	This work
Rev-DL	MAT **a** *trp1-1 can1-100 ura3-1 ade2-1 his3-11,15 coq8-3 SupRD*	This work
Rev-EL	MAT **a** *trp1-1 can1-100 ura3-1 ade2-1 his3-11,15 coq8-3 SupRE*	This work
NPD-NP	diploid produced from NP-183BH × NP-183AL	This work
NPD-A	diploid produced from NP-183BH × Rev-AL	This work
NPD-B	diploid produced from NP-183BH × Rev-BL	This work
NPD-C	diploid produced from NP-183BH × Rev-CL	This work
NPD-D	diploid produced from NP-183BH × Rev-DL	This work
NPD-E	diploid produced from NP-183BH × Rev EL	This work

[a] Dr. Rodney Rothstein, Columbia University, [b] Dr. Joan E. McEwen

Table 2. Plasmid constructs used in this study

Plasmid	Construct Description	Copy Number	Source
pCAS	Expresses *S. pyogenes* Cas9 plus a HDV ribozyme-sgRNA for genome editing in yeast	Multi copy	(27)
p3HN4	Yeast ABC1/COQ8	Low copy	(48)
p4HN4	Yeast ABC1/COQ8	Multi copy	(49)
plc-Coq8-A197V	Yeast ABC1/COQ8 with Coq8-A197V	Low copy	This work
plc-Coq8-S232N	Yeast ABC1/COQ8 with Coq8-S232N	Low copy	This work
plc-Coq8-A197V/S232N	Yeast ABC1/COQ8 with Coq8-A197V and S232N	Low copy	This work

Table 3. Antibodies used in this study

Antibody	Working solution	Source
Coq4	1:1000	(50)
Coq7	1:500	(51)
Coq8	1:30 (affinity purified)	(52)
Coq9	1:1000	(52)
Mdh1	1:10,000	Lee McAlister-Henn[a]

Table 4. Amino acid and nucleotide substitution of *coq8* alleles

NP-183AL	A197V (C590T)
Rev-AL	A197V (C590T) and L237P (T710C)
Rev-BL	A197V (C590T) and P220S (C658T)
Rev-CL	A197V (C590T) and S232N (G695A)
Rev-DL	A197V (C590T) and S232N (G695A)
Rev-EL	A197V (C590T) and S232N (G695A)

FIGURES

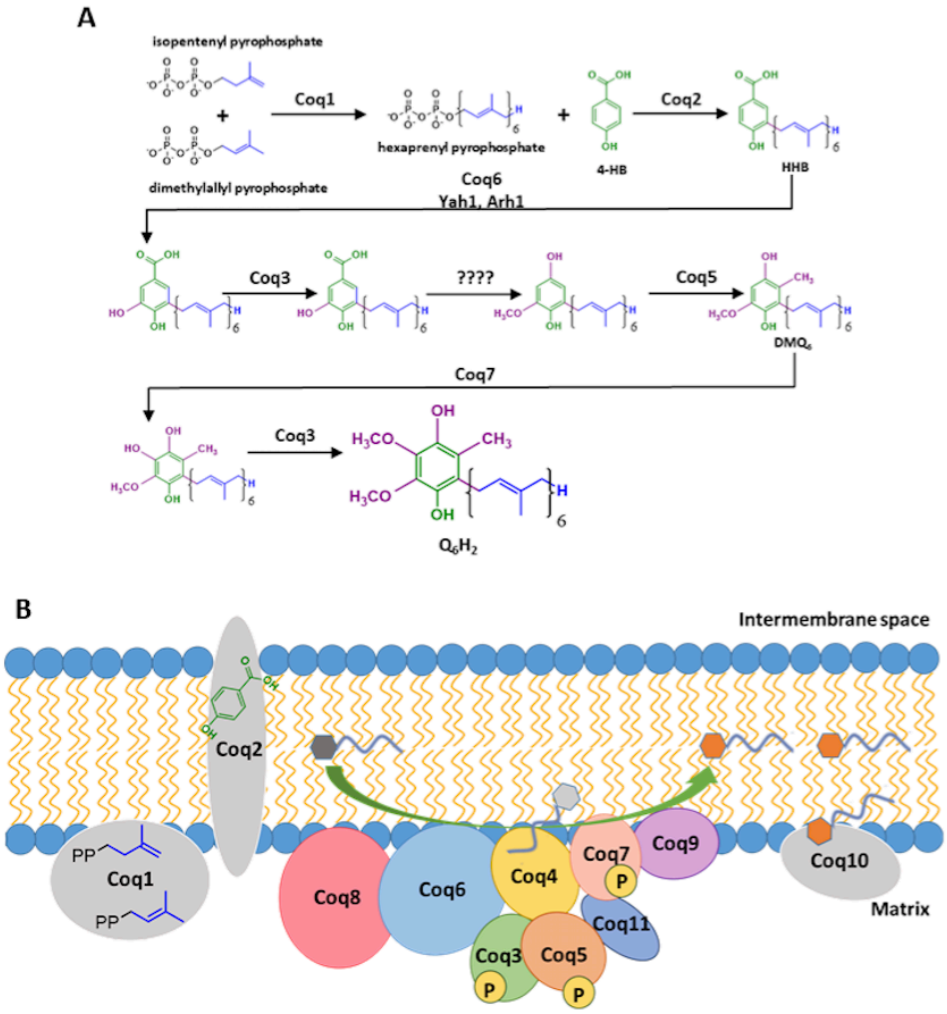

Fig 1. Coenzyme Q biosynthetic pathway in *S. cerevisiae* and the formation of the high-molecular mass CoQ synthome. *A*, The pathway for the enzymatic formation of Q_6 in yeast, starting with 4-hydroxybenzoic acid as the ring precursor. Questions marks indicate unknown steps involved in the decarboxylation and hydroxylation of the intermediate(s) leading to reduced coenzyme Q_6H_2. *B*, The schematic of a high-molecular mass complex in yeast, termed the CoQ synthome. Coq1, Coq2, and Coq10 polypeptides are not observed as members of the high-

molecular mass complex. Coq1 and Coq2 produce HHB (designated by the dark gray hexagon). This early CoQ-intermediate is converted by subsequent action of Coq6 and other Coq polypeptides to an essential lipid component of the CoQ synthome (shown as a light gray hexagon in association with Coq4). Coq8 physically associates with Coq6 and is an ancient atypical kinase, thought to be responsible for the regulatory phosphorylation of Coq3, Coq5 and Coq7 and/or ATPase activity. Q_6, the product of the CoQ synthome, is designated by the orange hexagon.

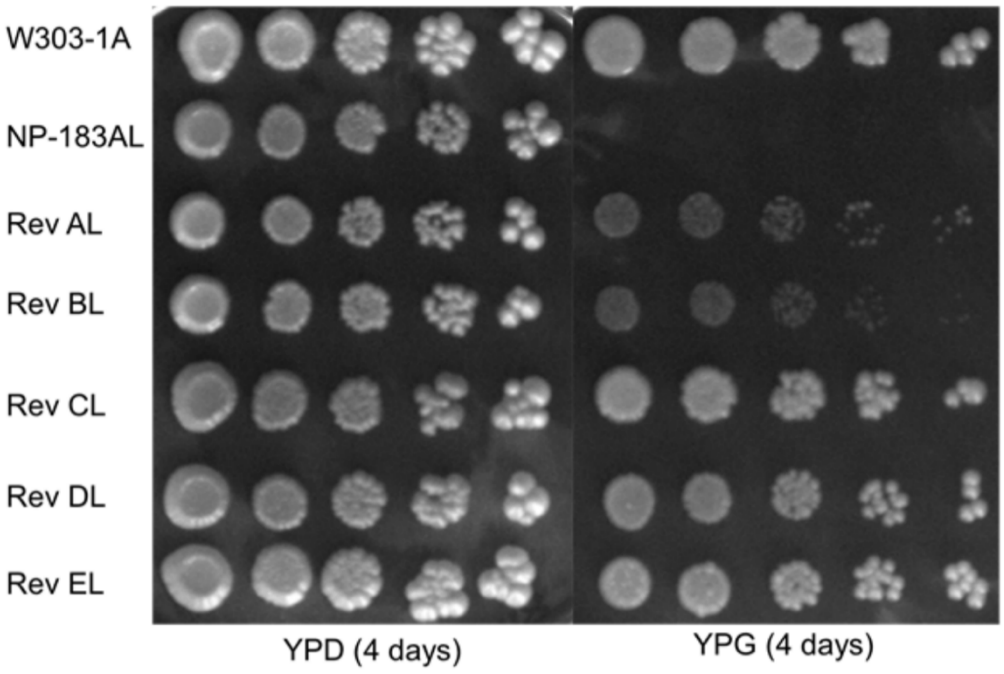

Fig 2. Spontaneous revertants of NP-183AL expressing Coq8-A197V show respiratory growth on YPG plate medium. The designated yeast strains (Table 1) were each grown overnight in 5 mL of YPD, diluted to an A_{600nm} of 0.2 with sterile PBS, and 2 μL of 5-fold serial dilutions were spotted onto the designated plate medium, corresponding to a final OD_{600nm} of 0.2, 0.04, 0.008, 0.0016, and 0.00032. Plates were incubated at 30 °C, and growth is depicted after four days. Results shown are representative of four independent biological replicate experiments.

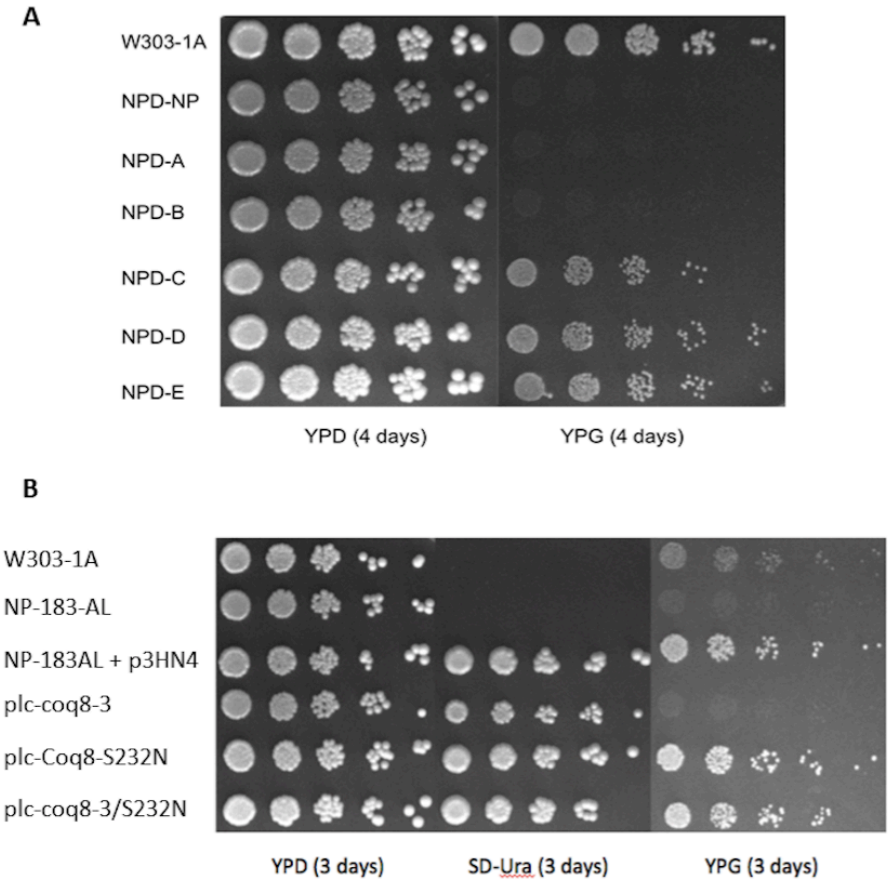

Fig 3. The Coq8-S232N substitution present in Rev-CL, Rev-DL, and Rev-EL is dominant, and its presence is sufficient to restore growth of the Coq8-A197V mutant on YPG. *A*, Each isolated revertant (Rev-AL, Rev-BL, Rev-CL, Rev-DL, and Rev-EL) was mated with parental mutant, NP-183BH and the respective diploid strains (NPD-A, NPD-B, NPD-C, NPD-D, and NPD-E) were isolated as described in *Experimental Procedures*. As a control, NP-183AL was mated with NP-183BH to form a diploid strain NPD-NP containing two copies of the *coq8-3* mutation. The derived diploid strains were then plated on YPD, a fermentable carbon source, and YPG, a non-fermentable carbon source. The haploid wild-type strain, W303-1A, was also included. Plates were incubated at 30 °C for 4 days Panel *A* is representative of two independent biological replicate experiments. *B*, Expression of Coq8 harboring the dominant *SupRC* mutation

present in Rev-CL rescues the growth of the NP183AL *coq8-3* mutant on non-fermentable carbon source medium. Yeast plate dilution assay was conducted on parental mutant, NP-183AL, transformed with the designated plasmids: plc-Coq8 (p3HN4), yeast low-copy *COQ8*; plc-A197V, yeast low-copy Coq8-A197V; plc-S232N, yeast low copy Coq8-S232N; or plc-A197V/S232N, yeast low copy Coq8-A197V/S232N. Each strain was cultured overnight in SD−Ura selective plate media, and the optical density (A_{600nm}) adjusted to 0.2 with sterile PBS, and 2 μL of 5-fold serial dilutions were spotted onto each type of plate medium, as described in Fig 2. Cells were incubated at 30° C for 3 days. Panel *B* is representative of two independent biological replicate experiments.

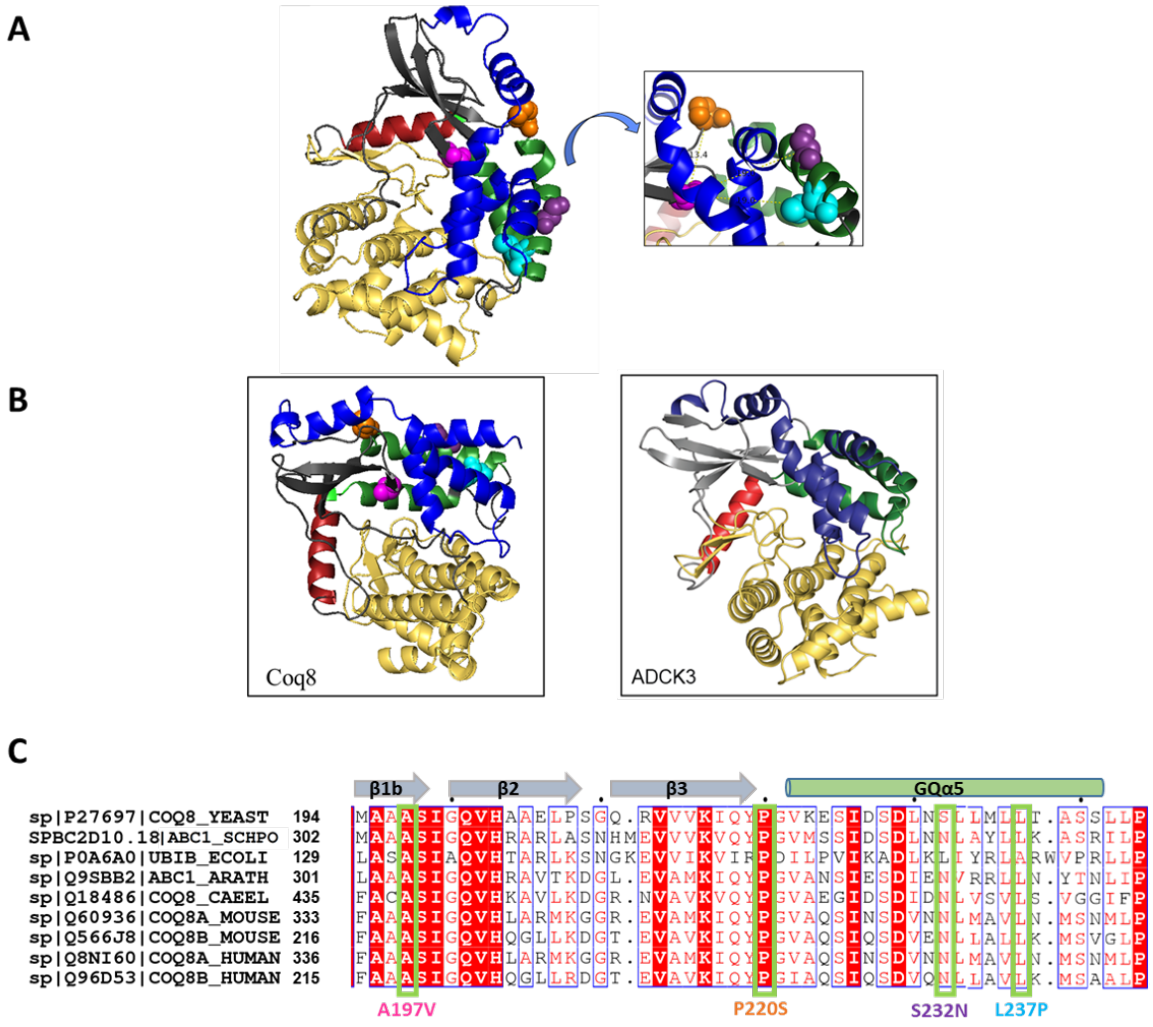

Fig 4. Structural prediction of *S. cerevisiae* Coq8 and sequence alignment with Coq8 homologs depict the sites of the A197V and suppressor mutations. *A,* PHYRE2 homology prediction of yeast Coq8, modeled to a 44% identity to PDB 4PED, corresponds to the partial structure of crystallized human COQ8A (13,34). The structural features of Coq8 and COQ8A are color-coded as described previously (13): The N-lobe folds into β-sheets, *gray* and a single helix αC, *red*; inserted between these features are the GQα5 and GQα6 helices, *green*; the C-lobe is shown in *yellow*; an N-terminal extension is shown in *blue*. The color-coding of the amino acids

are: A197, *pink*; L237, *cyan*; P220, *orange;* and S232, *purple*. These locations are the sites of the parental mutant, Coq8-A197V and the three revertants, Rev-AL (L237P), Rev-BL (P220S), and Rev-CL (S232N). Rev-DL and Rev-EL also contained S232N.The predicted 32 amino acid mitochondrial targeting sequence of Coq8 (53) has been removed from the model to allow for the accurate depiction of the mature polypeptide. *A inset,* The predicted distances between the A197 and each of the amino acid substitutions present in Rev-AL, Rev-BL, and Rev-CL are shown on the structure following its rotation of 90° counterclockwise. *B*, Yeast Coq8 is depicted in the same orientation and color-coding as for the previously published ADCK3 (13). *C,* Multiple sequence alignment and depiction of the locations of the mutations present in each of the yeast revertants. Secondary structure as predicted in the model of Coq8 is depicted above the yeast Coq8 sequence. A197V is present within the *coq8-3* parental mutant, and is present in each of the revertants. In addition, L237P occurs in Rev-AL, the P220S in Rev-BL, and the S232N is present in Rev-CL, Rev-DL and Rev-EL. The alignment included the designated Coq8 homologs from *S. cerevisiae*, *S. pombe*, *E. coli*, *A. thaliana*, *C. elegans*, *M. musculus*, and *H. sapiens*. The amino acid alignment was built using MUSCLE and visualized using EsPript (54).

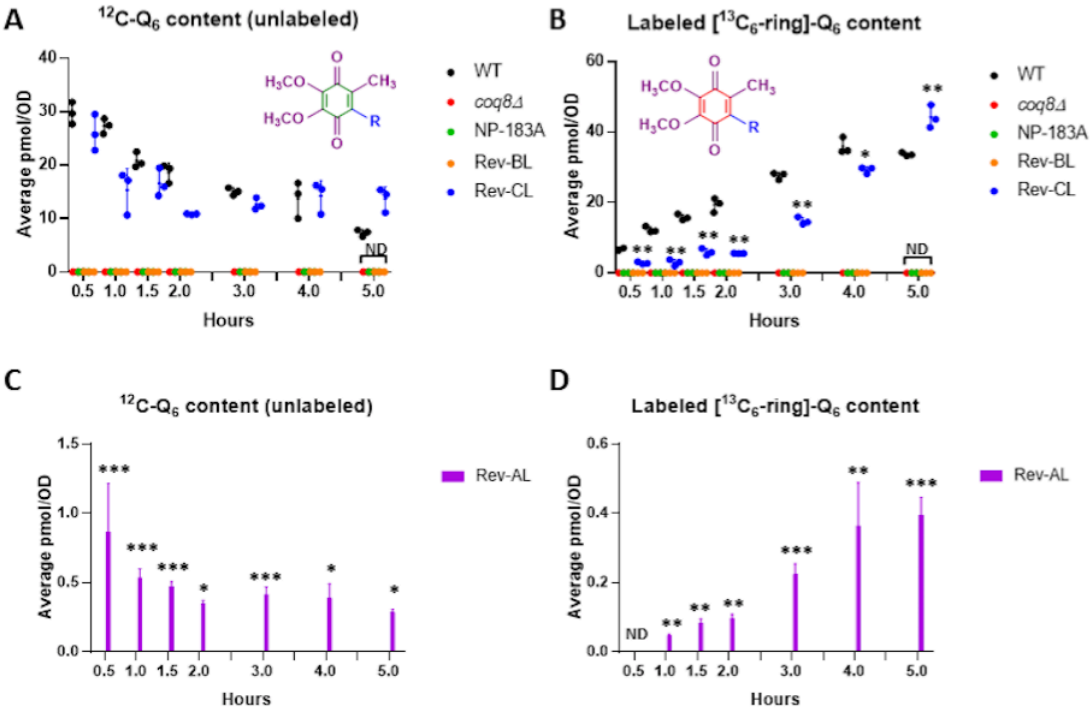

Fig 5. In YPD liquid medium, biosynthesis of Q_6 in Rev-CL is nearly comparable to WT, while Rev-AL produces substantially lower levels of Q_6 compared to WT, and in Rev-BL Q_6 is not detected. *A*, Levels of unlabeled Q_6 (^{12}C-Q_6) and *B, de novo* synthesized $^{13}C_6$-Q_6 ($^{13}C_6$-Q_6) in each strain were determined at the designated time points after labeling with $^{13}C_6$-4HB in YPD medium. Unlabeled Q_6 and de novo labeled $^{13}C_6$-Q_6 were not detected in *coq8Δ*, NP-183A or in Rev-BL at any of the time points; this is denoted as "ND" at the 5 h time point for simplicity. *C* and *D,* The expanded scales show the levels of unlabeled and *de novo* $^{13}C_6$-Q_6 present in the Rev-AL strain. Error bars, S.D. of n=3 biological replicates (unpaired Student's t test between all strains compared to WT, with statistical significance represented by: *p<0.05, **p<0.005, ***p<0.0005). Results are shown for three independent biological replicate experiments.

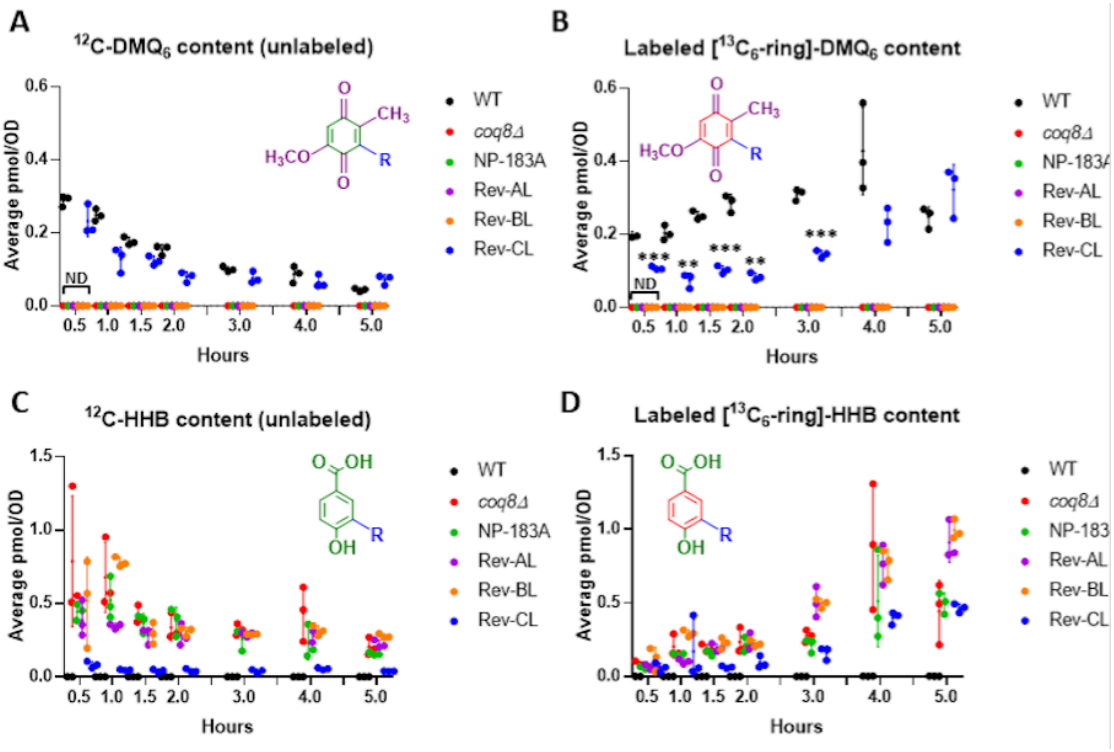

Fig 6. Rev-CL synthesizes late-stage intermediate DMQ_6, while Rev-AL and Rev-BL accumulate the early-stage intermediate, HHB. *A*, Levels of unlabeled ^{12}C-DMQ_6; *B, de novo* synthesized $^{13}C_6$-DMQ_6; *C,* unlabeled ^{12}C-HHB; and *D, de novo* synthesized $^{13}C_6$-HHB were determined in WT, *coq8*Δ, NP-183A, Rev-AL, Rev-BL, and Rev-CL at the designated time points after labeling with $^{13}C_6$-4HB in YPD medium. Error bars, S.D. of n=3 biological replicates (unpaired Student's t test between all strains compared to WT, with statistical significance represented by: *p<0.05, **p<0.005, ***p<0.0005). Panel A and B show non-detectable values for the lipids analyzed for *coq8*Δ, NP-183A, Rev AL, and Rev BL for all time points, indicated as "ND" for the first time point for simplicity. Panels *C* and *D* show non-detectable levels of HHB in WT. Results are shown for three independent biological replicate experiments.

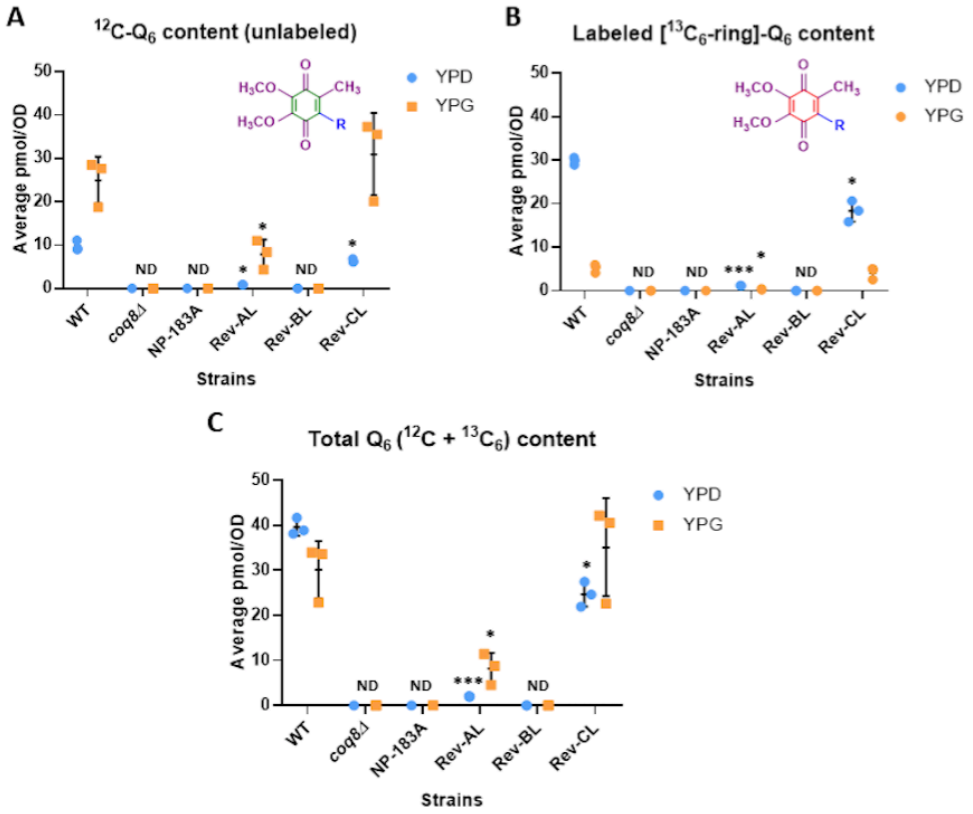

Fig 7. Rev-CL and Rev-AL are able to synthesize Q_6 in YPG liquid medium, and Rev-CL produces comparable levels of total Q_6 (^{12}C-Q_6 + ^{13}C$_6$-Q_6) as WT. *A*, Levels of unlabeled Q_6 (^{12}C-Q_6) and *B, de novo* synthesized ^{13}C$_6$-Q_6 (^{13}C$_6$-Q_6) in WT, *coq8*Δ, NP-183A, Rev AL, Rev BL, and Rev CL were determined after labeling with ^{13}C$_6$-4HB for 5 hours in YPD or YPG liquid medium. *C*, Total Q_6 (^{12}C-Q_6 + ^{13}C$_6$-Q_6) content is shown for all labeled strains in both YPD and YPG medium. Error bars, S.D. of n=3 biological replicates (unpaired Student's t test between all strains compared to WT in the same type of medium, with statistical significance represented by: *p<0.05, **p<0.005, ***p<0.0005). "ND" indicates lipids levels that were non-detectable in the indicated strains. Results are shown for three independent biological replicate experiments.

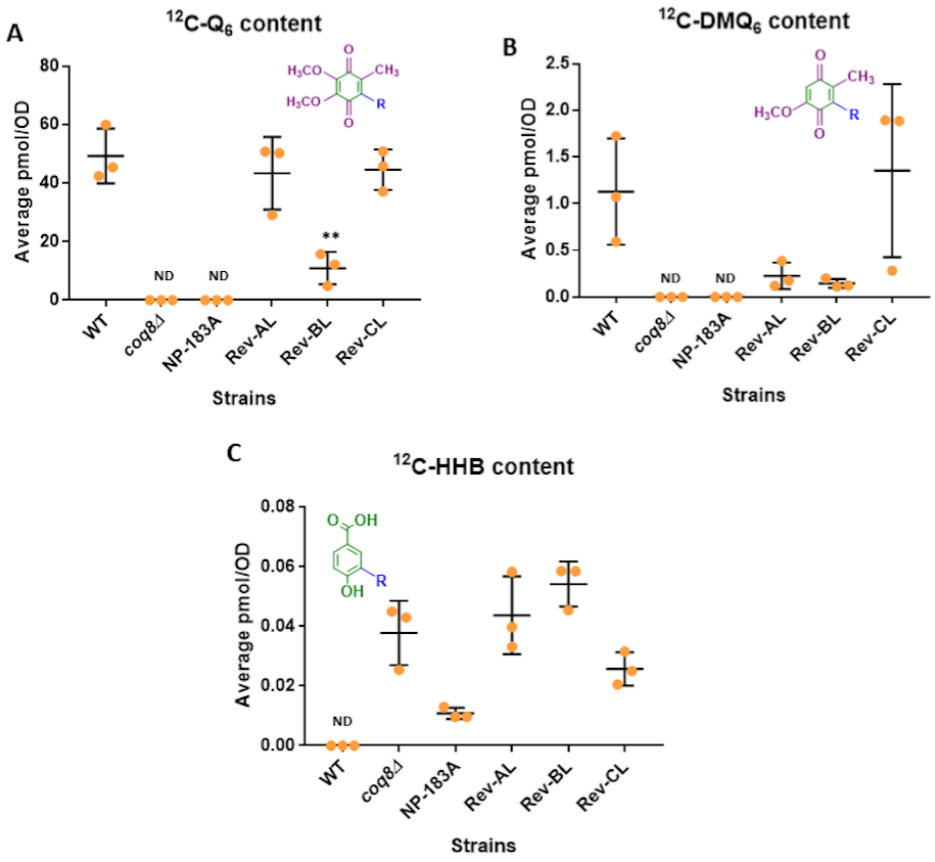

Fig 8. Assessment of Q_6 and Q_6-intermediates in strains following incubation on YPG plate medium reveals the presence of Q_6 in Rev-BL. *A*, Levels of unlabeled ^{12}C-CoQ_6; *B,* ^{12}C-DMQ_6; and *C,* ^{12}C-HHB in WT, *coq8*Δ*,* NP-183A, Rev AL, Rev BL, and Rev CL were determined on colonies that were cultured on YPG solid medium for two days. Error bars, S.D. of n=3 biological replicates (unpaired Student's t test between all strains compared to WT, with statistical significance set at $p<0.05$). "ND" indicates lipids levels that were undetectable in the indicated strains. Results are shown for three independent biological replicate experiments.

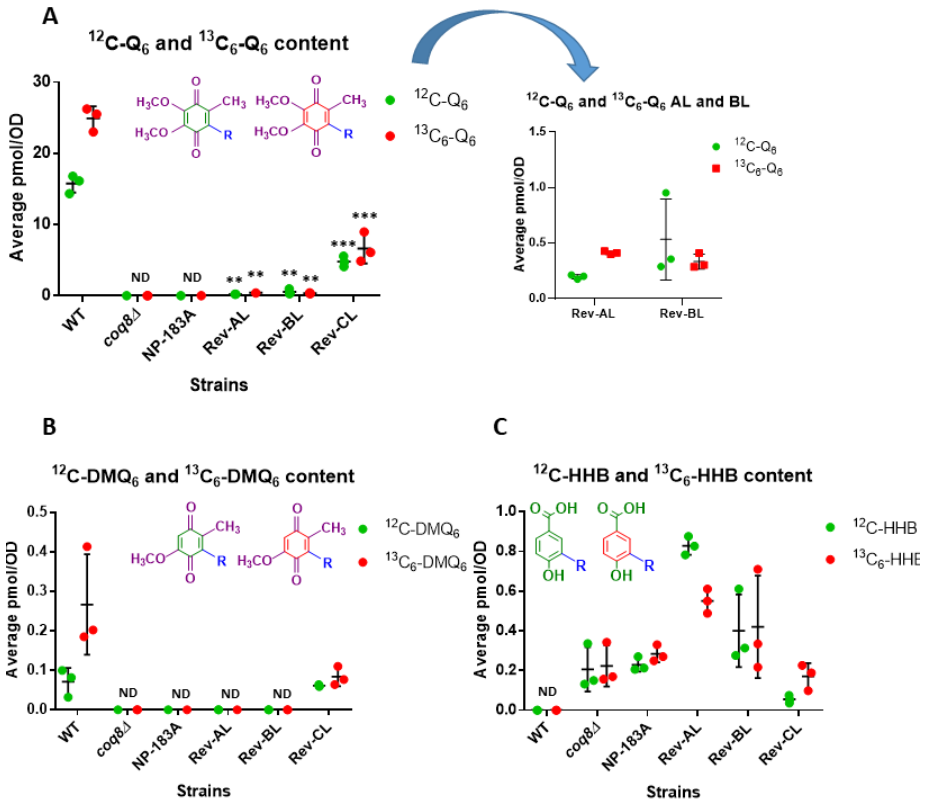

Fig 9. Growth in YPGal (a nonrepressive carbon source) reveals all three revertants are capable of *de novo* $^{13}C_6$-Q_6 production. *A*, Levels of unlabeled ^{12}C-Q_6 and *de novo* $^{13}C_6$-Q_6; *B,* unlabeled ^{12}C-DMQ_6 and *de novo* $^{13}C_6$-DMQ_6; *C*, unlabeled ^{12}C-HHB and *de novo* $^{13}C_6$-HHB in WT, *coq8*Δ*,* NP-183A, Rev-AL, Rev-BL, and Rev-CL were determined in cultures of yeast labeled for 5 hours with $^{13}C_6$-4HB in YPGal + 0.1% Dextrose liquid media. The expanded y axis in the panel *A* inset demonstrates the levels of Q_6 production in Rev-AL and Rev-BL. Error bars, S.D. of n=3 biological replicates (unpaired Student's t test between all strains compared to WT, with statistical significance represented by: *p<0.05, **p<0.005, ***p<0.0005). "ND" indicates lipids levels that were non-detectable and lower than background in the indicated strains. Results are shown for three independent biological replicate experiments.

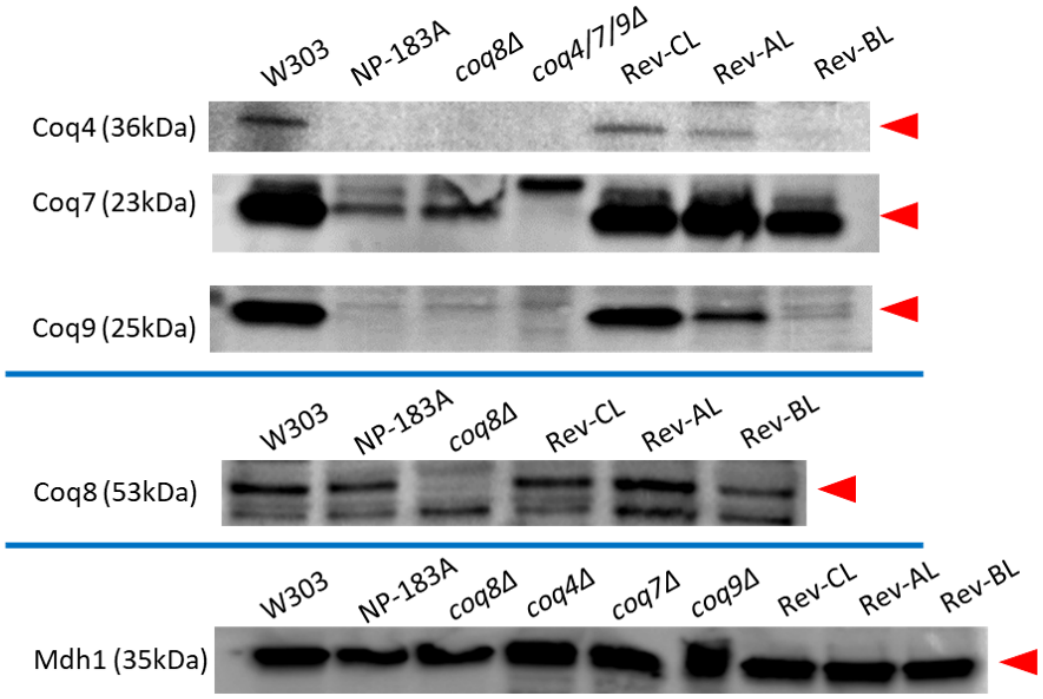

Fig 10. Amounts of indicator Coq polypeptides in mitochondria isolated from Rev-CL are restored to near WT levels. Levels of Coq4, Coq7, Coq8, and Coq9 polypeptides were determined by SDS-PAGE and immunoblotting. Samples were separated on 12% SDS-PAGE gels and then transferred to PVDF membranes for immunoblotting with antisera to the designated yeast Coq polypeptides. 25 μg of purified mitochondria was analyzed for each strain. Arrows indicate each antibody-detected protein in their respective blots; a *coq* null strain in each respective Coq polypeptide blot was used as a reference for the absence of the desired band of interest. Blots were performed two times each. The Mdh1 blot serves to validate the samples used in all the blots; the samples that were loaded in the Mdh1 blot are those of the same preparation as used for the Coq4, Coq7, Coq8, and Coq9 blots.

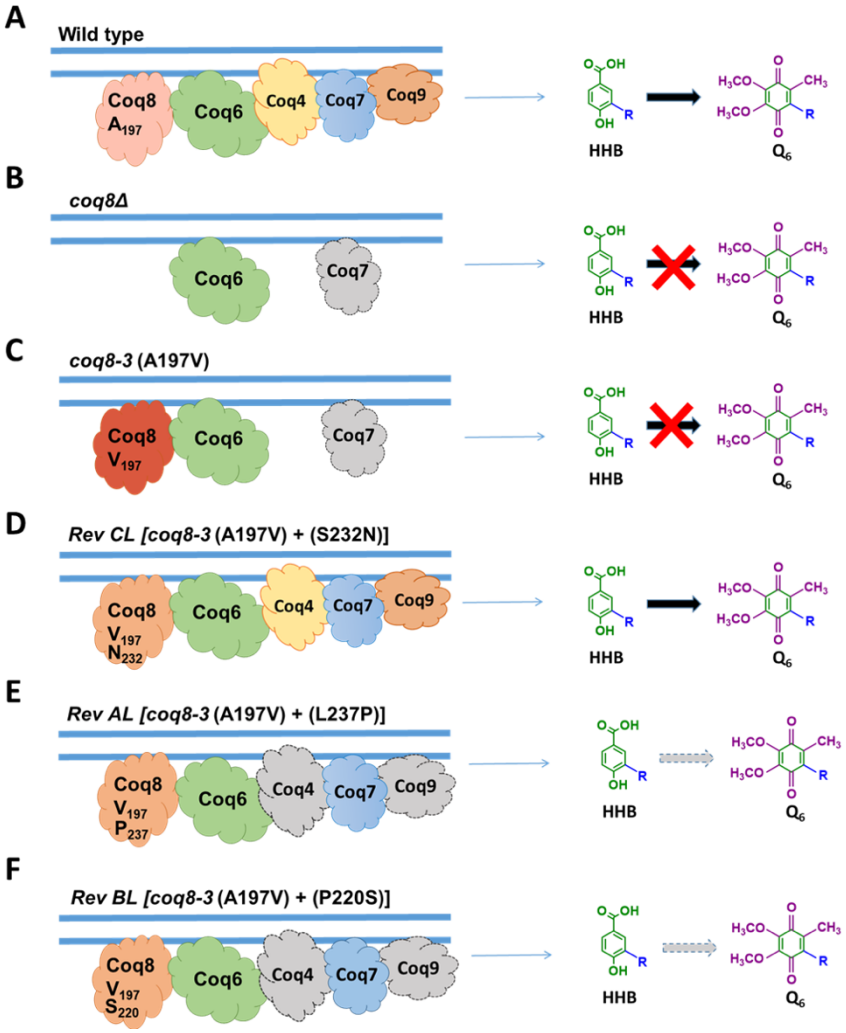

Fig 11. Model for the restoration of Q_6 biosynthesis in three revertants. *A*, Under conditions of Coq8 expression in wild-type yeast, benchmark values of Q_6 production are noted and the wild-type amounts of key Coq polypeptides (Coq4, Coq7, Coq8, and Coq9) are defined. *B*, the yeast *coq8*Δ mutant lacks Q_6, has a lower content of the Coq7 polypeptide, the Coq4, Coq8, and Coq9 polypeptides are not detectable, and the early intermediate HHB accumulates. *C*, the yeast mutant expressing the Coq8-A197V polypeptide lacks Q_6, has a lower content of the Coq7 polypeptide, the Coq4 and Coq9 polypeptides are not detectable, and the early intermediate HHB accumulates.

D, The dominant Rev-CL revertant restores Q_6 production and the stability of the Coq4, Coq7 and Coq9 polypeptides. *E*, The recessive Rev-AL revertant has partially restored Q_6 biosynthesis. However, amounts of the Coq4 and Coq9 polypeptides are low and this results in greatly impaired synthesis of Q_6. *F*, The recessive Rev-BL revertant exhibits very low levels of Q_6 biosynthesis, and has dramatically decreased content of the Coq4 and Coq9 polypeptides, even though Coq8 and Coq7 polypeptides remain readily detectable.

REFERENCES

1. Bentinger, M., Brismar, K., and Dallner, G. (2007) The antioxidant role of coenzyme Q. *Mitochondrion* **7S**, S41-S50
2. Turunen, M., Olsson, J., and Dallner, G. (2004) Metabolism and function of coenzyme Q. *Biochim. Biophys. Acta* **1660**, 171-199
3. Crane, F. L., and Barr, R. (1985) Chemical structure and properties of coenzyme Q and related compounds. in *Coenzyme Q: Biochemistry, Bioenergetics, and Clinical Applications* (Lenaz, G. ed.), John Wiley & Sons, New York, NY. pp 1-37
4. Bentinger, M., Tekle, M., and Dallner, G. (2010) Coenzyme Q--biosynthesis and functions. *Biochemical and biophysical research communications* **396**, 74-79
5. Brandt, U., and Trumpower, B. (1994) The protonmotive Q cycle in mitochondria and bacteria. *Crit Rev Biochem Mol Biol* **29**, 165-197
6. Alcazar-Fabra, M., Trevisson, E., and Brea-Calvo, G. (2018) Clinical syndromes associated with Coenzyme Q10 deficiency. *Essays Biochem* **62**, 377-398
7. Luna-Sanchez, M., Hidalgo-Gutierrez, A., Hildebrandt, T. M., Chaves-Serrano, J., Barriocanal-Casado, E., Santos-Fandila, A., Romero, M., Sayed, R. K., Duarte, J., Prokisch, H., Schuelke, M., Distelmaier, F., Escames, G., Acuna-Castroviejo, D., and Lopez, L. C. (2017) CoQ deficiency causes disruption of mitochondrial sulfide oxidation, a new pathomechanism associated with this syndrome. *EMBO molecular medicine* **9**, 78-95
8. Wang, Y., and Hekimi, S. (2013) Molecular genetics of ubiquinone biosynthesis in animals. *Critical Reviews in Biochemistry and Molecular Biology* **48**, 69-88

9. Awad, A. M., Bradley, M. C., Fernandez-Del-Rio, L., Nag, A., Tsui, H. S., and Clarke, C. F. (2018) Coenzyme Q10 deficiencies: pathways in yeast and humans. *Essays Biochem* **62**, 361-376

10. Stefely, J. A., and Pagliarini, D. J. (2017) Biochemistry of Mitochondrial Coenzyme Q Biosynthesis. *Trends Biochem Sci* **42**, 824-843

11. Allan, C. M., Awad, A. M., Johnson, J. S., Shirasaki, D. I., Wang, C., Blaby-Haas, C. E., Merchant, S. S., Loo, J. A., and Clarke, C. F. (2015) Identification of Coq11, a new coenzyme Q biosynthetic protein in the CoQ-Synthome in *Saccharomyces cerevisiae*. *The Journal of biological chemistry* **290**, 7517-7534

12. He, C. H., Xie, L. X., Allan, C. M., Tran, U. C., and Clarke, C. F. (2014) Coenzyme Q supplementation or over-expression of the yeast Coq8 putative kinase stabilizes multi-subunit Coq polypeptide complexes in yeast *coq* null mutants. *Biochimica et Biophysica Acta (BBA) - Molecular and Cell Biology of Lipids* **1841**, 630-644

13. Stefely, J. A., Reidenbach, A. G., Ulbrich, A., Oruganty, K., Floyd, B. J., Jochem, A., Saunders, J. M., Johnson, I. E., Minogue, C. E., Wrobel, R. L., Barber, G. E., Lee, D., Li, S., Kannan, N., Coon, J. J., Bingman, C. A., and Pagliarini, D. J. (2015) Mitochondrial ADCK3 employs an atypical protein kinase-like fold to enable coenzyme Q biosynthesis. *Mol Cell* **57**, 83-94

14. Kannan, N., Taylor, S. S., Zhai, Y., Venter, J. C., and Manning, G. (2007) Structural and functional diversity of the microbial kinome. *PLoS biology* **5**, e17

15. Xie, L. X., Hsieh, E. J., Watanabe, S., Allan, C. M., Chen, J. Y., Tran, U. C., and Clarke, C. F. (2011) Expression of the human atypical kinase ADCK3 rescues coenzyme Q

biosynthesis and phosphorylation of Coq polypeptides in yeast coq8 mutants. *Biochim Biophys Acta* **1811**, 348-360

16. Vazquez Fonseca, L., Doimo, M., Calderan, C., Desbats, M. A., Acosta, M. J., Cerqua, C., Cassina, M., Ashraf, S., Hildebrandt, F., Sartori, G., Navas, P., Trevisson, E., and Salviati, L. (2018) Mutations in COQ8B (ADCK4) found in patients with steroid-resistant nephrotic syndrome alter COQ8B function. *Hum Mutat* **39**, 406-414

17. Lagier-Tourenne, C., Tazir, M., Lopez, L. C., Quinzii, C. M., Assoum, M., Drouot, N., Busso, C., Makri, S., Ali-Pacha, L., Benhassine, T., Anheim, M., Lynch, D. R., Thibault, C., Plewniak, F., Bianchetti, L., Tranchant, C., Poch, O., DiMauro, S., Mandel, J. L., Barros, M. H., Hirano, M., and Koenig, M. (2008) ADCK3, an ancestral kinase, is mutated in a form of recessive ataxia associated with coenzyme Q_{10} deficiency. *Am. J. Hum. Genet.* **82**, 661-672

18. Mollet, J., Delahodde, A., Serre, V., Chretien, D., Schlemmer, D., Lombes, A., Boddaert, N., Desguerre, I., de Lonlay, P., de Baulny, H. O., Munnich, A., and Rotig, A. (2008) *CABC1* gene mutations cause ubiquinone deficiency with cerebellar ataxia and seizures. *Am. J. Hum. Genet.* **82**, 623-630

19. Ashraf, S., Gee, H. Y., Woerner, S., Xie, L. X., Vega-Warner, V., Lovric, S., Fang, H., Song, X., Cattran, D. C., Avila-Casado, C., Paterson, A. D., Nitschke, P., Bole-Feysot, C., Cochat, P., Esteve-Rudd, J., Haberberger, B., Allen, S. J., Zhou, W., Airik, R., Otto, E. A., Barua, M., Al-Hamed, M. H., Kari, J. A., Evans, J., Bierzynska, A., Saleem, M. A., Bockenhauer, D., Kleta, R., El Desoky, S., Hacihamdioglu, D. O., Gok, F., Washburn, J., Wiggins, R. C., Choi, M., Lifton, R. P., Levy, S., Han, Z., Salviati, L., Prokisch, H., Williams, D. S., Pollak, M., Clarke, C. F., Pei, Y., Antignac, C., and Hildebrandt, F. (2013)

ADCK4 mutations promote steroid-resistant nephrotic syndrome through CoQ10 biosynthesis disruption. *J Clin Invest* **123**, 5179-5189

20. Vazquez-Fonseca, L., Schaefer, J., Navas-Enamorado, I., Santos-Ocana, C., Hernandez-Camacho, J. D., Guerra, I., Cascajo, M. V., Sanchez-Cuesta, A., Horvath, Z., Siendones, E., Jou, C., Casado, M., Gutierrez, P., Brea-Calvo, G., Lopez-Lluch, G., Fernandez-Ayala, D. J. M., Cortes-Rodriguez, A. B., Rodriguez-Aguilera, J. C., Matte, C., Ribes, A., Prieto-Soler, S. Y., Dominguez-Del-Toro, E., Francesco, A. D., Aon, M. A., Bernier, M., Salviati, L., Artuch, R., Cabo, R., Jackson, S., and Navas, P. (2019) ADCK2 Haploinsufficiency Reduces Mitochondrial Lipid Oxidation and Causes Myopathy Associated with CoQ Deficiency. *Journal of clinical medicine* **8**, E1374

21. Reidenbach, A. G., Kemmerer, Z. A., Aydin, D., Jochem, A., McDevitt, M. T., Hutchins, P. D., Stark, J. L., Stefely, J. A., Reddy, T., Hebert, A. S., Wilkerson, E. M., Johnson, I. E., Bingman, C. A., Markley, J. L., Coon, J. J., Dal Peraro, M., and Pagliarini, D. J. (2018) Conserved Lipid and Small-Molecule Modulation of COQ8 Reveals Regulation of the Ancient Kinase-like UbiB Family. *Cell Chem Biol* **25**, 154-165 e111

22. Stefely, J. A., Licitra, F., Laredj, L., Reidenbach, A. G., Kemmerer, Z. A., Grangeray, A., Jaeg-Ehret, T., Minogue, C. E., Ulbrich, A., Hutchins, P. D., Wilkerson, E. M., Ruan, Z., Aydin, D., Hebert, A. S., Guo, X., Freiberger, E. C., Reutenauer, L., Jochem, A., Chergova, M., Johnson, I. E., Lohman, D. C., Rush, M. J., Kwiecien, N. W., Singh, P. K., Schlagowski, A. I., Floyd, B. J., Forsman, U., Sindelar, P. J., Westphall, M. S., Pierrel, F., Zoll, J., Dal Peraro, M., Kannan, N., Bingman, C. A., Coon, J. J., Isope, P., Puccio, H., and Pagliarini, D. J. (2016) Cerebellar ataxia and coenzyme Q deficiency through loss of unorthodox kinase activity. *Molecular cell* **63**, 608-620

23. Subramanian, K., Jochem, A., Le Vasseur, M., Lewis, S., Paulson, B. R., Reddy, T. R., Russell, J. D., Coon, J. J., Pagliarini, D. J., and Nunnari, J. (2019) Coenzyme Q biosynthetic proteins assemble in a substrate-dependent manner into domains at ER-mitochondria contacts. *J Cell Biol* **218**, 1353-1369

24. Eisenberg-Bord, M., Tsui, H. S., Antunes, D., Fernandez-Del-Rio, L., Bradley, M. C., Dunn, C. D., Nguyen, T. P. T., Rapaport, D., Clarke, C. F., and Schuldiner, M. (2019) The Endoplasmic Reticulum-Mitochondria Encounter Structure Complex Coordinates Coenzyme Q Biosynthesis. *Contact (Thousand Oaks)* **2**, 2515256418825409

25. Xie, L. X., Ozeir, M., Tang, J. Y., Chen, J. Y., Jaquinod, S. K., Fontecave, M., Clarke, C. F., and Pierrel, F. (2012) Overexpression of the Coq8 kinase in Saccharomyces cerevisiae coq null mutants allows for accumulation of diagnostic intermediates of the coenzyme Q6 biosynthetic pathway. *J Biol Chem* **287**, 23571-23581

26. Tauche, A., Krause-Buchholz, U., and Rodel, G. (2008) Ubiquinone biosynthesis in *Saccharomyces cerevisiae*: The molecular organization of *O*-methylase Coq3p depends on Abc1p/Coq8p. *FEMS Yeast Res* **8**, 1263-1275

27. Ryan, O. W., Skerker, J. M., Maurer, M. J., Li, X., Tsai, J. C., Poddar, S., Lee, M. E., DeLoache, W., Dueber, J. E., Arkin, A. P., and Cate, J. H. (2014) Selection of chromosomal DNA libraries using a multiplex CRISPR system. *eLife* **3**

28. Gietz, R. D., and Schiestl, R. H. (2007) High-efficiency yeast transformation using the LiAc/SS carrier DNA/PEG method. *Nature protocols* **2**, 31-34

29. Herskowitz, I., and Jensen, R. E. (1991) Putting the HO gene to work: practical uses for mating-type switching. *Methods in enzymology* **194**, 132-146

30. Burke, D., Dawson, D., and Stearns, T. . (2000) Methods in Yeast Genetics. *Cold spring Harbor Laboratory Press*

31. Glick, B. S., and Pon, L. A. (1995) Isolation of highly purified mitochondria from Saccharomyces cerevisiae. *Methods Enzymol* **260**, 213-223

32. Laemmli, U. K. (1970) Cleavage of structural proteins during the assembly of the head of bacteriophage T4. *Nature* **227**, 680-685

33. Awad, A. M., Venkataramanan, S., Nag, A., Galivanche, A. R., Bradley, M. C., Neves, L. T., Douglass, S., Clarke, C. F., and Johnson, T. L. (2017) Chromatin-remodeling SWI/SNF complex regulates coenzyme Q_6 synthesis and a metabolic shift to respiration in yeast. *The Journal of biological chemistry* **292**, 14851-14866

34. Kelley, L. A., Mezulis, S., Yates, C. M., Wass, M. N., and Sternberg, M. J. (2015) The Phyre2 web portal for protein modeling, prediction and analysis. *Nature protocols* **10**, 845-858

35. Tzagoloff, A., and Dieckmann, C. L. (1990) *PET* genes of *Saccharomyces cerevisiae*. *Microbiol. Rev.* **54**, 211-225

36. Conrad, M., Schothorst, J., Kankipati, H. N., Van Zeebroeck, G., Rubio-Texeira, M., and Thevelein, J. M. (2014) Nutrient sensing and signaling in the yeast Saccharomyces cerevisiae. *FEMS Microbiol Rev* **38**, 254-299

37. Nguyen, T. P., Casarin, A., Desbats, M. A., Doimo, M., Trevisson, E., Santos-Ocana, C., Navas, P., Clarke, C. F., and Salviati, L. (2014) Molecular characterization of the human COQ5 C-methyltransferase in Coenzyme Q biosynthesis. *Biochimica et biophysica acta*

38. Heeringa, S. F., Chernin, G., Chaki, M., Zhou, W., Sloan, A. J., Ji, Z., Xie, L. X., Salviati, L., Hurd, T. W., Vega-Warner, V., Killen, P. D., Raphael, Y., Ashraf, S., Ovunc, B.,

Schoeb, D. S., McLaughlin, H. M., Airik, R., Vlangos, C. N., Gbadegesin, R., Hinkes, B., Saisawat, P., Trevisson, E., Doimo, M., Casarin, A., Pertegato, V., Giorgi, G., Prokisch, H., Rotig, A., Nurnberg, G., Becker, C., Wang, S., Ozaltin, F., Topaloglu, R., Bakkaloglu, A., Bakkaloglu, S. A., Muller, D., Beissert, A., Mir, S., Berdeli, A., Varpizen, S., Zenker, M., Matejas, V., Santos-Ocana, C., Navas, P., Kusakabe, T., Kispert, A., Akman, S., Soliman, N. A., Krick, S., Mundel, P., Reiser, J., Nurnberg, P., Clarke, C. F., Wiggins, R. C., Faul, C., and Hildebrandt, F. (2011) *COQ6* mutations in human patients produce nephrotic syndrome with sensorineural deafness. *The Journal of clinical investigation* **121**, 2013-2024

39. Wang, Y., and Hekimi, S. (2019) The Complexity of Making Ubiquinone. *Trends Endocrinol Metab*

40. Gogl, G., Kornev, A. P., Remenyi, A., and Taylor, S. S. (2019) Disordered Protein Kinase Regions in Regulation of Kinase Domain Cores. *Trends in biochemical sciences* **44**, 300-311

41. Black, M. H., Osinski, A., Gradowski, M., Servage, K. A., Pawlowski, K., Tomchick, D. R., and Tagliabracci, V. S. (2019) Bacterial pseudokinase catalyzes protein polyglutamylation to inhibit the SidE-family ubiquitin ligases. *Science* **364**, 787-792

42. Martinis, J., Glauser, G., Valimareanu, S., Stettler, M., Zeeman, S. C., Yamamoto, H., Shikanai, T., and Kessler, F. (2014) ABC1K1/PGR6 kinase: a regulatory link between photosynthetic activity and chloroplast metabolism. *The Plant journal : for cell and molecular biology* **77**, 269-283

43. van Wijk, K. J., and Kessler, F. (2017) Plastoglobuli: Plastid Microcompartments with Integrated Functions in Metabolism, Plastid Developmental Transitions, and Environmental Adaptation. *Annual review of plant biology* **68**, 253-289

44. Martin-Montalvo, A., Gonzalez-Mariscal, I., Padilla, S., Ballesteros, M., Brautigan, D. L., Navas, P., and Santos-Ocana, C. (2011) Respiratory-induced coenzyme Q biosynthesis is regulated by a phosphorylation cycle of Cat5p/Coq7p. *Biochem. J.* **440**, 107-114

45. Chi, A., Huttenhower, C., Geer, L. Y., Coon, J. J., Syka, J. E., Bai, D. L., Shabanowitz, J., Burke, D. J., Troyanskaya, O. G., and Hunt, D. F. (2007) Analysis of phosphorylation sites on proteins from Saccharomyces cerevisiae by electron transfer dissociation (ETD) mass spectrometry. *Proceedings of the National Academy of Sciences of the United States of America* **104**, 2193-2198

46. Niemi, N. M., Wilson, G. M., Overmyer, K. A., Vogtle, F. N., Myketin, L., Lohman, D. C., Schueler, K. L., Attie, A. D., Meisinger, C., Coon, J. J., and Pagliarini, D. J. (2019) Pptc7 is an essential phosphatase for promoting mammalian mitochondrial metabolism and biogenesis. *Nature communications* **10**, 3197

47. Hsu, A. Y., Do, T. Q., Lee, P. T., and Clarke, C. F. (2000) Genetic evidence for a multi-subunit complex in the O-methyltransferase steps of coenzyme Q biosynthesis. *Biochimica et Biophysica Acta (BBA) - Molecular and Cell Biology of Lipids* **1484**, 287-297

48. Do, T. Q., Hsu, A. Y., Jonassen, T., Lee, P. T., and Clarke, C. F. (2001) A defect in coenzyme Q biosynthesis is responsible for the respiratory deficiency in Saccharomyces cerevisiae abc1 mutants. *The Journal of biological chemistry* **276**, 18161-18168

49. Hsieh, E. J., Dinoso, J. B., and Clarke, C. F. (2004) A tRNA(TRP) gene mediates the suppression of cbs2-223 previously attributed to ABC1/COQ8. *Biochem Biophys Res Commun* **317**, 648-653

50. Belogrudov, G. I., Lee, P. T., Jonassen, T., Hsu, A. Y., Gin, P., and Clarke, C. F. (2001) Yeast *COQ4* encodes a mitochondrial protein required for coenzyme Q synthesis. *Archives of Biochemistry and Biophysics* **392**, 48-58

51. Tran, U. C., Marbois, B., Gin, P., Gulmezian, M., Jonassen, T., and Clarke, C. F. (2006) Complementation of *Saccharomyces cerevisiae coq7* mutants by mitochondrial targeting of the *Escherichia coli* UbiF polypeptide. Two functions of yeast Coq7 polypeptide in coenzyme Q biosynthesis. *Journal of Biological Chemistry* **281**, 16401-16409

52. Hsieh, E. J., Gin, P., Gulmezian, M., Tran, U. C., Saiki, R., Marbois, B. N., and Clarke, C. F. (2007) *Saccharomyces cerevisiae* Coq9 polypeptide is a subunit of the mitochondrial coenzyme Q biosynthetic complex. *Archives of biochemistry and biophysics* **463**, 19-26

53. Vogtle, F. N., Wortelkamp, S., Zahedi, R. P., Becker, D., Leidhold, C., Gevaert, K., Kellermann, J., Voos, W., Sickmann, A., Pfanner, N., and Meisinger, C. (2009) Global analysis of the mitochondrial N-proteome identifies a processing peptidase critical for protein stability. *Cell* **139**, 428-439

54. Edgar, R. C. (2004) MUSCLE: multiple sequence alignment with high accuracy and high throughput. *Nucleic acids research* **32**, 1792-1797

APPENDIX III

Coenzyme Q_{10} deficiencies: pathways in yeast and humans

Essays in Biochemistry (2018) **62** 361–376
https://doi.org/10.1042/EBC20170106

PORTLAND PRESS

Review Article

Coenzyme Q_{10} deficiencies: pathways in yeast and humans

Agape M. Awad, Michelle C. Bradley, Lucía Fernández-del-Río, Anish Nag, Hui S. Tsui and Catherine F. Clarke

Department of Chemistry and Biochemistry, Molecular Biology Institute, UCLA, Los Angeles, CA 90095, U.S.A.

Correspondence: Catherine F. Clarke (cathy@chem.ucla.edu)

Coenzyme Q (ubiquinone or CoQ) is an essential lipid that plays a role in mitochondrial respiratory electron transport and serves as an important antioxidant. In human and yeast cells, CoQ synthesis derives from aromatic ring precursors and the isoprene biosynthetic pathway. *Saccharomyces cerevisiae coq* mutants provide a powerful model for our understanding of CoQ biosynthesis. This review focusses on the biosynthesis of CoQ in yeast and the relevance of this model to CoQ biosynthesis in human cells. The *COQ1–COQ11* yeast genes are required for efficient biosynthesis of yeast CoQ. Expression of human homologs of yeast *COQ1–COQ10* genes restore CoQ biosynthesis in the corresponding yeast *coq* mutants, indicating profound functional conservation. Thus, yeast provides a simple yet effective model to investigate and define the function and possible pathology of human *COQ* (yeast or human gene involved in CoQ biosynthesis) gene polymorphisms and mutations. Biosynthesis of CoQ in yeast and human cells depends on high molecular mass multisubunit complexes consisting of several of the *COQ* gene products, as well as CoQ itself and CoQ intermediates. The CoQ synthome in yeast or Complex Q in human cells, is essential for *de novo* biosynthesis of CoQ. Although some human CoQ deficiencies respond to dietary supplementation with CoQ, in general the uptake and assimilation of this very hydrophobic lipid is inefficient. Simple natural products may serve as alternate ring precursors in CoQ biosynthesis in both yeast and human cells, and these compounds may act to enhance biosynthesis of CoQ or may bypass certain deficient steps in the CoQ biosynthetic pathway.

Introduction

Coenzyme Q (ubiquinone or CoQ) is a vital lipid component in mitochondrial energy metabolism. It is a two-part molecule containing a long polyisoprenyl tail of *n* isoprene units positioning the molecule in the mid-plane of membrane bilayer, and a fully substituted benzoquinone ring that undergoes reversible reduction and oxidation. The redox chemistry of CoQ and $CoQH_2$ (ubiquinol, a hydroquinone) allows it to play its best-known role in mitochondrial respiration, accepting electrons and protons from Complex I or Complex II and donating them to Complex III, thereby establishing a proton gradient across the mitochondrial inner membrane. CoQ also serves as an essential electron and proton acceptor in other aspects of metabolism including fatty acid β-oxidation, uridine biosynthesis, and oxidation of sulphide, proline, glycerol-3-phosphate, choline, dimethylglycine, and sarcosine [1,2]. $CoQH_2$ also serves a crucial antioxidant function, protecting membranes as a chain terminator of lipid peroxidation reactions, and in the maintenance of reduced forms of vitamin E [1,3]. $CoQ/CoQH_2$ is a component of lipoproteins and is present in all cellular membranes including the plasma membrane where it functions in cellular redox regulation as part of the plasma membrane oxidoreductase system [1].

The focus of this review is on the biosynthesis of CoQ_6 in the yeast *Saccharomyces cerevisiae* and the relevance of this model to the biosynthesis of CoQ_{10} in human cells. Readers are directed to other

Received: 26 February 2018
Revised: 08 April 2018
Accepted: 14 May 2018

Version of Record published: 06 July 2018

Essays in Biochemistry (2018) **62** 361–376
https://doi.org/10.1042/EBC20170106

recent reviews that discuss the biosynthesis of CoQ in prokaryotes such as *Escherichia coli* [4], and in eukaryotes including *Schizosaccharomyces pombe*, plants, *Caenorhabditis elegans*, *Mus musculus*, and humans [5-7]. For an in-depth discussion of the effects of CoQ_{10} deficiencies and the clinical syndromes associated with these deficiencies, readers are directed to the article by Brea-Calvo and colleagues [8] in this issue of *Essays in Biochemistry*.

Overview of CoQ biosynthesis

S. cerevisiae is an extraordinarily useful model for understanding the biosynthesis of CoQ. Early yeast classic and molecular genetics combined with subcellular fractionation, biochemical assays, and lipid chemistry have helped to identify many of the steps required for CoQ biosynthesis. In particular, the collection of respiratory deficient *coq* mutants identified by Tzagoloff [9,10] set the stage for isolation and characterization of the yeast *COQ* genes. A particular advantage is that the CoQ-less *coq* mutants are viable when cultured on growth medium containing a fermentable carbon source, but are incapable of growth on medium containing a non-fermentable carbon source. In most cases, expression of the human COQ (human polypeptide involved in CoQ_{10} biosynthesis) homolog restores function in the corresponding yeast *coq* mutant. This rescue of yeast *coq* mutants by human *COQ* genes is a powerful and simple functional assay still being used to ascertain the effects of human mutations or polymorphisms on human *COQ* gene function. Thus, what we have learned about the biosynthesis of CoQ_6 in the yeast model is highly relevant to the biosynthesis of CoQ_{10} in humans (Figure 1).

The yeast model also provided early evidence that the eukaryotic CoQ biosynthetic pathway was localized to mitochondria. The Coq (denotes *S. cerevisiae* polypeptide involved in CoQ_6 biosynthesis) polypeptides are nuclear encoded, and amino-terminal mitochondrial targetting sequences are needed to direct their transport to the mitochondrial matrix (Coq1, Coq3–Coq11) or to the inner mitochondrial membrane (Coq2). Assembly of Coq3–Coq9 plus Coq11 polypeptides into a high molecular mass complex termed the CoQ synthome in yeast (Figure 2) and Complex Q in human cells is another conserved feature of CoQ biosynthesis [7,11]. These complexes are essential for the biosynthesis of CoQ in yeast and human cells, and may serve to enhance catalytic efficiency and to minimize the escape of intermediates that may be toxic due to their redox or electrophilic properties. The CoQ-intermediates are quite hydrophobic and at least some of them appear to be essential partners in the assembly of the membrane-bound CoQ synthome [12] and Complex Q [7,13].

Ring precursors utilized in biosynthesis of CoQ

Origin of 4-hydroxybenzoic acid

In yeast and human cells, the primary precursor molecule that leads to the biosynthesis of CoQ is 4-hydroxybenzoic acid (4HB). Yeast cells generate 4HB via the shikimate pathway, but also utilize tyrosine as a ring precursor [14]. Unlike yeast, human cells contain phenylalanine hydroxylase, and so either phenylalanine or tyrosine may be utilized as precursors for the biosynthesis of 4HB. Many steps involved in the generation of 4HB from tyrosine are yet to be characterized [15,16]. However, two recent studies have shed light on the first and the last steps involved in yeast 4HB biosynthesis [17,18]. The first step involves the deamination of tyrosine to 4-hydroxyphenylpyruvate (4-HPP), catalyzed by either of the aminotransferases Aro8 or Aro9 [17]. Payet et al. [17] also identified 4-hydroxybenzaldehyde (4HBz) as the final intermediate leading to the biosynthesis of 4HB. The oxidation of 4HBz to 4HB is catalyzed by the aldehyde dehydrogenase Hfd1. Hfd1 is a mitochondrial outer membrane protein [19] indicating that 4HB is synthesized in the cytosol, and must be imported into the mitochondrial matrix, where it is incorporated into CoQ. Hence, there should be a mitochondrial transporter for 4HB that remains to be identified [7], and is responsible for use of exogenously added 4HB. Inactivation of *HFD1* results in CoQ_6 deficiency that may be complemented by the addition of exogenous 4HB. Expression of the human homolog ALDH3A1 restored CoQ_6 biosynthesis in the *hfd1* yeast mutant, and was shown to oxidize 4HBz to 4HB [17]. In an independent study Stefely et al. [18] confirmed these findings; MS was used to characterize the proteomes, lipidomes, and metabolomes of a large selection of yeast strains, each lacking a distinct gene related to mitochondrial biology. This multi-omic approach revealed that yeast Hfd1 and human ALDH3A1 serve as the aldehyde dehydrogenases responsible for the oxidation of 4HBz to 4HB. It will be important to determine whether human *ALDH3A1* is required for CoQ_{10} biosynthesis in human cells; if so, it may be a potential target gene that should be considered when screening for CoQ_{10} deficiencies in patients.

Other aromatic ring precursors of CoQ

In addition to 4HB, yeast utilize *para*-aminobenzoic acid (pABA) as a ring precursor of CoQ_6 [20,21]. Yeast Coq6 and Coq9 polypeptides are required for this metabolism. Yeast Coq6 is required for the oxidative deamination of

Essays in Biochemistry (2018) **62** 361–376
https://doi.org/10.1042/EBC20170106

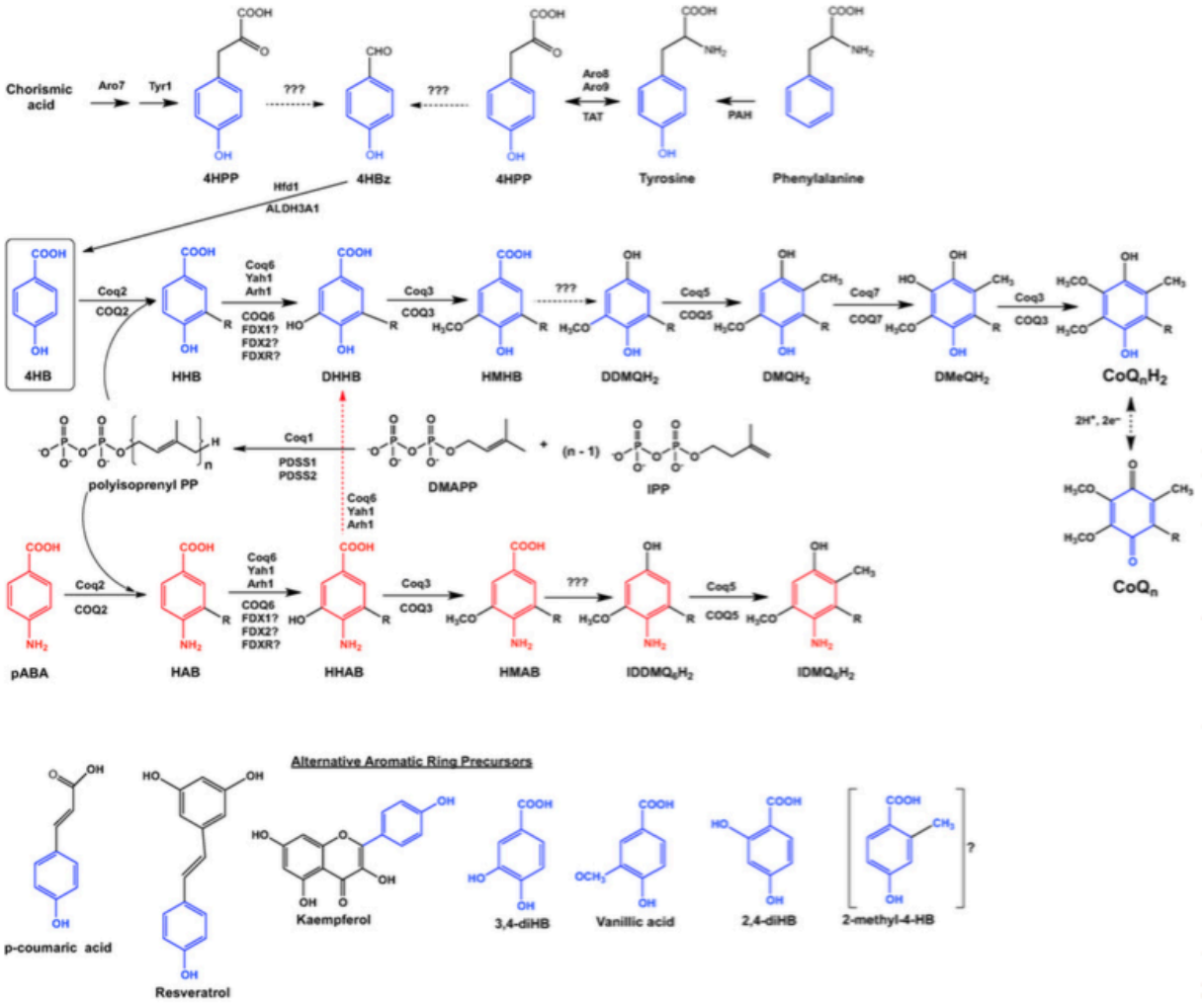

Figure 1. CoQ biosynthetic pathways in the yeast *S. cerevisiae* and in humans

The CoQ biosynthetic pathway has been shown to involve at least 14 nuclear-encoded proteins that are necessary for mitochondrial CoQ biosynthesis in *S. cerevisiae*. Black dotted arrows denote more than one step. Solid arrows denote a single step attributed to the corresponding yeast polypeptide named above each arrow. The corresponding human homologs are named below each arrow. The main ring precursor used by both yeast and humans is 4-hydroxybenzoic acid (4HB). Yeasts synthesize 4HB *de novo* from chorismate or may obtain it from the metabolism of tyrosine. Humans rely on tyrosine to produce 4HB (or on phenylalanine and phenylalanine hydroxylase to produce tyrosine). Yeast and human cells produce isopentenyl pyrophosphate (IPP) and dimethylally pyrophosphate (DMAPP) as precursors to form hexaprenyl diphosphate (n=6) via Coq1 in yeast or decaprenyl diphosphate (n=10) via PDSS1/PDSS2 in humans. Yeast Coq2 and human COQ2 attach the polyisoprenyl tail to 4HB. Subsequent to this step, the next three intermediates are identified as yeast hexaprenyl-intermediates: HHB, 3-hexaprenyl-4HB; DHHB, 3-hexaprenyl-4,5-dihydroxybenzoic acid; HMHB, 3-hexaprenyl-4-hydroxy-5-methoxybenzoic acid. The next three intermediates are hydroquinones: $DDMQH_2$, 2-hexaprenyl-6-methoxy-1,4-benzenediol; $DMQH_2$, 2-hexaprenyl-3-methyl-6-methoxy-1,4-benzenediol; $DMeQH_2$, 2-hexaprenyl- 3-methyl-6-methoxy-1,4,5-benzenetriol; to ultimately produce the final reduced product (CoQ_nH_2). Red text identifies *para*-aminobenzoic acid (pABA) as an alternate ring precursor utilized by yeast (but not by humans). The next three intermediates are identified as yeast hexaprenyl-intermediates: HAB, 4-amino-3-hexaprenylbenzoic acid; HHAB, 4-amino-3-hexaprenyl-5-hydroxybenzoic acid; HMAB, 4-amino-3-hexaprenyl-5-methoxybenzoic acid. The next two intermediates are: $IDDMQH_2$, 4-amino-3-hexaprenyl-5-methoxyphenol; $IDMQH_2$, 4-amino-3-hexaprenyl-2-methyl-5-methoxyphenol. The step denoted by the red dotted arrow depends on yeast Coq6 and converts HHAB into DHHB. Interconversion of (CoQ_nH_2) and (CoQ_n) is shown via a reversible two-electron reduction and oxidation. Steps indicated by '???' are catalyzed by as yet unknown enzymes. Alternative compounds that may serve as ring precursors in CoQ biosynthesis are shown at the bottom of the

Essays in Biochemistry (2018) **62** 361–376
https://doi.org/10.1042/EBC20170106

panel: *p*-coumaric acid, resveratrol, and kaempferol. Analogs of 4HB that can function to bypass certain deficiencies in the CoQ biosynthetic pathway include: 3,4-dihydroxybenzoic acid (3,4-diHB), vanillic acid and 2,4-dihydroxybenzoic acid (2,4-diHB). It is not yet known whether 2-methyl-4HB (2-methyl-4HB) may also serve a bypass function.

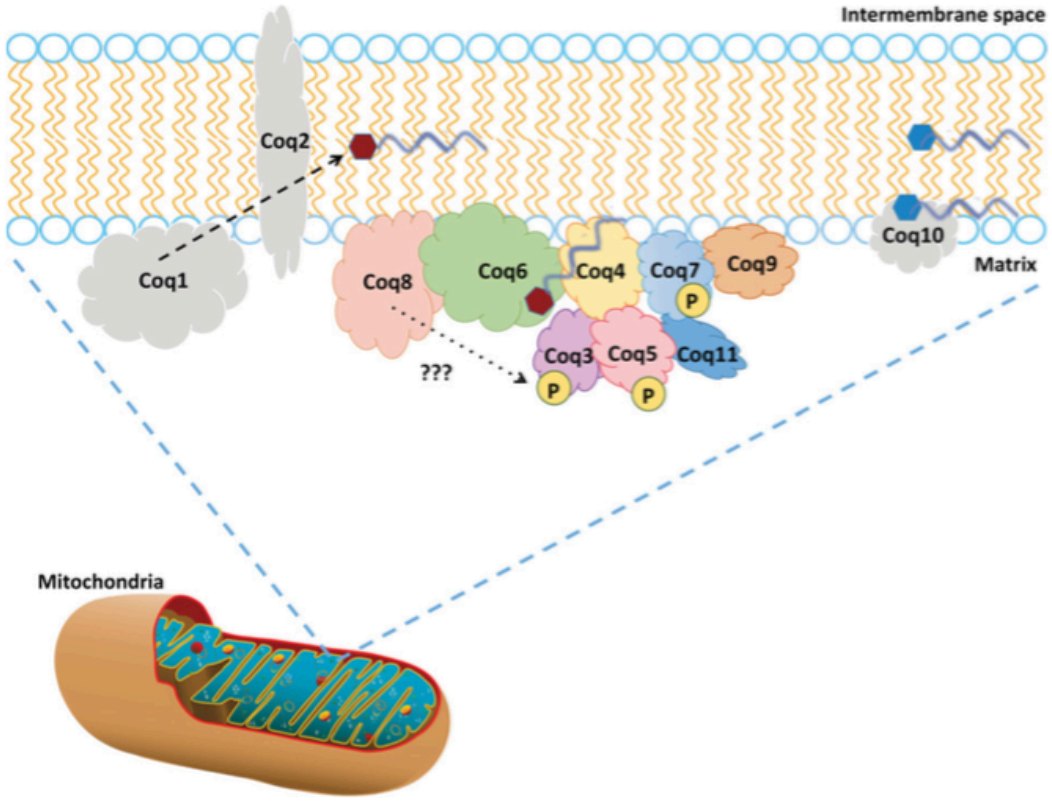

Figure 2. A model of the CoQ Synthome in the yeast *S. cerevisiae*

Studies in *S. cerevisiae* have provided evidence for a high-molecular mass multisubunit protein and lipid complex, the CoQ synthome (see text for references). The Coq3–Coq9 and Coq11 polypeptides, designated in color, co-purify, and are members of this complex that is peripherally associated with the matrix-side of the inner mitochondrial membrane. Coq1, Coq2, and Coq10 are individual polypeptides that do not associate with the complex (indicated in gray). Coq1 and Coq2 synthesize the early intermediates HHB and HAB (denoted by red hexagon with a gray hexaprenyl tail). Coq10 binds CoQ (and also late-stage CoQ-intermediates denoted as blue hexagons with a gray tail), and functions as a chaperone for this hydrophobic lipid that normally resides at the mid-plane of the membrane bilayer. The Coq3, Coq5, and Coq7 polypeptides are phosphorylated in a Coq8-dependent manner (shown by '???'). The function of Coq8 is still under investigation; although part of a family of atypical kinases, Coq8 has been shown to autophosphorylate, but not yet shown to phosphorylate any other proteins, *in vitro* or *in vivo*. It is speculated to have ATPase function and potentially has the ability to phosphorylate lipids or other small molecules. Hence the phosphorylation of Coq3, Coq5, and Coq7 may be from Coq8 or be produced via another kinase that is recruited to the CoQ synthome to act upon those particular polypeptides. In yeast, it has been shown that the phosphatase that dephosphorylates Coq7 is $Ptc7_s$, the product of the spliced form of *PTC7* (not shown).

the ring nitrogen substituent [22]. Coq9 is also required for Coq6 activity, including the Coq6-mediated deamination function [23,24]. Analogs of 4HB, including 2,4-dihydroxybenzoic acid (2,4-diHB), 3,4-dihydroxybenzoic acid (3,4-diHB) and vanillic acid may be incorporated into CoQ_6 [16] (Figure 1). These analogs may allow for the bypass of CoQ_6 biosynthetic defects in certain yeast *coq6* and *coq7* mutants [16,24,25], as discussed in 'Yeast and human

genes essential for CoQ biosynthesis'. Additional aromatic ring precursors incorporated into CoQ_6 in yeast include *p*-coumarate and the polyphenols resveratrol and kaempferol [26,27] (Figure 1), although the use of kaempferol by yeast is very marginal.

In contrast, pABA is not utilized for CoQ synthesis by human or mouse cells [26], and instead it acts to inhibit the incorporation of 4HB into CoQ [16,28,29]. In mammalian cells, *p*-coumarate, vanillic acid, 3,4-diHB, resveratrol, and kaempferol also serve as CoQ ring precursors, with the difference that in this case kaempferol is a very efficient precursor that is even able to up-regulate CoQ_9 and CoQ_{10} levels in human and mouse kidney cells [27]. While the mechanism underlying the use of polyphenols is still unknown, it is clear that a highly specific process occurs because other polyphenols with similar structures, such as piceatannol or apigenin, are not used for CoQ synthesis in mammalian cells [27].

A hypothesis for the use of *p*-coumarate, resveratrol, and kaempferol as ring precursors of CoQ is that they are metabolized to produce 4HB. The set of reactions that allow this conversion is not yet identified but, independent of the metabolic route involved, an increase in alternative CoQ ring precursors in cells will only turn into higher CoQ levels if cells have a low availability of endogenous 4HB, which is the primary precursor of CoQ. The fact that the availability of 4HB is a rate-limiting step in the CoQ biosynthetic pathway has been previously described in yeast and in mammalian kidney cells [21,27]. Supplementing mammalian kidney cells with exogenous 4HB resulted in an increase in CoQ levels four- to six-fold higher as compared with the non-supplemented control [27]. This observation led the authors to propose the possibility that increasing the availability of CoQ precursors in cells could move the metabolic flux in favor of the biosynthesis of CoQ, helping to ameliorate the phenotype associated with certain Q deficiencies.

Yeast and human genes essential for CoQ biosynthesis

Yeast *COQ1*; human *PDSS1* and *PDSS2*

In yeast and human cells, the synthesis of the polyisoprenyl diphosphate tail derives from a non-sterol branch of the mevalonate pathway [7]. Yeast Coq1 is responsible for the synthesis of the hexaprenyl diphosphate tail moiety from the precursors dimethylallyl diphosphate and isopentenyl diphosphate [30]. The Coq1 polypeptide is peripherally associated with the matrix side of the inner mitochondrial membrane [31]. The analogous polyprenyl diphosphate synthases in other species determine the tail length (*n*) of the CoQ_n (ubiquinone-n or coenzyme Q_n (refers to a specific isoform, where n is number of isoprenyl units in the tail of CoQ_n, e.g. CoQ_{10} in humans, CoQ_6 in *S. cerevisiae*)) produced [32], and when expressed in yeast direct the synthesis of corresponding isoforms of CoQ_n [33]. The yeast Coq1 polypeptide is not associated with the CoQ synthome, but its lipid product is essential for the formation and/or stabilization of this complex [31,34].

PDSS1 and PDSS2 form a heterotetramer responsible for the synthesis of the decaprenyl-diphosphate tail precursor used to synthesize CoQ_{10} in human cells [35]. Patients with partial deficiencies in PDSS1 [36] and PDSS2 [37] show severe disruptions in multiple organ systems. As reviewed in this volume [8], the complexity of phenotypes is a hallmark of mitochondrial deficiency diseases.

Yeast *COQ2*; human *COQ2*

The yeast Coq2 polypeptide is required for the attachment of the polyisoprenyl 'tail' to 4HB [38]. In yeast, Coq2 generates 3-hexaprenyl-4-hydroxy benzoic acid (HHB; Figure 1), the first polyisoprenylated ring CoQ-intermediate in the biosynthetic pathway. This early hydrophobic CoQ-intermediate was found to accumulate in many of the yeast *coq* null mutants, including the *coq3-coq9* null mutants [39,40]. Coq2 is imported into mitochondria via the Tim23 pathway [41], and is an integral membrane protein of the inner mitochondrial membrane [34]. It was originally hypothesized that Coq2 might serve to anchor the CoQ-synthome to the inner mitochondrial membrane [11], however there is no evidence that Coq2 is associated with the other Coq polypeptides that assemble into the CoQ-synthome [12]. Instead it appears that polyisoprenylated CoQ-intermediates produced by Coq1 and Coq2 are important for the stabilization of the CoQ synthome [34] (Figure 2).

Forsgren et al. [42] isolated human *COQ2* cDNA and showed its expression in a yeast *coq2* null mutant restored CoQ_6 biosynthesis. Recently, Desbats et al. [43] have defined the 5′ transcription start sites of the human *COQ2* transcript, indicating that of four potential upstream ATG translation initiation codons, the first two are rarely (if ever) used and that it is the fourth ATG that is in fact predominant. All isoforms of COQ2 were shown to co-localize to mitochondria. This finding argues against the previous hypothesis that the shorter COQ2 isoforms may represent non-mitochondrial polypeptides that may mediate cytoplasmic prenylation of 4HB [42]. The predominant use of the fourth ATG results in a shorter COQ2 polypeptide and the authors suggest new numbering that should be used to

Essays in Biochemistry (2018) **62** 361–376
https://doi.org/10.1042/EBC20170106

designate mutations of human COQ2 [43]. Desbats et al. [43] found a good correlation between disease severity in patients and the effect of *COQ2* mutations on the decreased production of CoQ_6 in a yeast complementation assay. Patients who harbored two alleles that markedly impair CoQ biosynthesis manifested multisystem severe clinical symptoms at birth or infancy, while patients who had a least one allele with residual CoQ biosynthesis manifested isolated steroid resistant nephrotic syndrome (SRNS) or adult onset encephalopathy [43].

Based on two structures determined for prokaryotic homologs of COQ2 (UbiA family aromatic prenyltransferases), human COQ2 is proposed to contain nine transmembrane helices [43]. The C-terminus of human COQ2 resides in the intermembrane space in mitochondria of HEK293 cells [43]. A recent structural model is compatible with this suggestion and predicts that the active site of human COQ2 faces the matrix [44]. Two of the disease-related mutations (given in the old nomenclature) are posited to interfere with the binding of the polyisoprenyl diphosphate (R197H) or to clash with the Mg^{2+} ions that participate in catalysis (A302V) [44].

A recent study by Herebian et al. [45] demonstrated that supplementation with 4HB fully restores endogenous CoQ_{10} biosynthesis in partially deficient COQ2 human fibroblasts harboring homozygous mutant alleles, including the A302V severe allele. Based on an *in silico* model of human COQ2, the authors identified several binding sites for 4HB and posited a channel for 4HB transport across the inner mitochondrial membrane. The authors proposed that the rescue of CoQ_{10} synthesis in fibroblasts from COQ2-deficient patients by treatment with 4HB may represent amelioration of a 4HB transport deficit and/or an enhancement of activity by increased supply of the ring substrate [45]. It will be important to experimentally determine whether the COQ2 polypeptide also functions as a 4HB transporter. In addition to restoring CoQ_{10} levels, the 4HB treatment also increased the steady state levels of COQ4 and COQ7 proteins involved in CoQ biosynthesis, and enhanced cell viability in response to stress conditions. This finding makes sense in light of the important role that CoQ and CoQ-intermediates play in stabilizing the CoQ-synthome in yeast and Complex Q in human cells [7,12,34]. This rescue of COQ2-deficient cells by 4HB treatment is quite striking and deserves further testing as a potential therapy. Even a small enhancement in the biosynthesis of CoQ is able to restore a wide array of phenotypes associated with CoQ deficiency [46].

Yeast *COQ3*; human *COQ3*

Yeast Coq3 is an *S*-adenosylmethionine (AdoMet)-dependent methyltransferase required for the two *O*-methylation steps of CoQ biosynthesis [47-49]. Coq3 is peripherally associated with the matrix-side of the mitochondrial inner membrane [49]. Recent studies reveal that *E. coli* UbiG, a functional homolog of Coq3, binds to liposomes containing cardiolipin [50]. Structural determination of UbiG identifies it as a seven β-strand AdoMet-dependent methyltransferase that contains an unusual insertion sequence that mediates UbiG binding to membranes, and is required for CoQ biosynthesis [50].

Assays with farnesylated analogs of CoQ-intermediates provided early evidence that a complex of yeast Coq polypeptides is required to observe the Coq3 *O*-methyltransferase activity and hence CoQ biosynthesis [39,51]. Recovery of the yeast Coq3-consecutive non-denaturing affinity purification (CNAP) tagged polypeptide from digitonin-solubilized mitochondrial extracts showed that it co-purified with Coq4, Coq5, Coq6, Coq7, Coq9, and Coq11 polypeptides, in a high molecular mass complex that contained CoQ_6 and several CoQ_6-intermediates [12]. Thus Coq3 is an integral member of the CoQ synthome in yeast. The phosphorylation state of Coq3 may modulate the stability of the Coq3 polypeptide and that of the CoQ synthome [52,53]. Overexpression of Coq8, an atypical putative protein kinase, has been shown to stabilize several Coq polypeptides and the CoQ synthome in certain yeast *coq* null mutants [24,34]. Indeed, overexpression of Coq8 in the yeast *coq3* null mutant increased steady state levels of the Coq4, Coq6, Coq7, and Coq9 polypeptides, and stabilized the CoQ synthome. Treatment of *coq3* null mutants overexpressing Coq8 with vanillic acid (a 4HB analog that should bypass the first hydroxylation and first methylation steps) resulted in the production of the late stage CoQ-intermediate DMQ_6 [24] (Figure 1). This finding indicates the potential difficulties in using analogs of 4HB to bypass deficiencies in Coq3, due to its involvement in two *O*-methylation steps, and to the apparent absence of Coq7 hydroxylase activity. It is tempting to speculate that treatment with 2,3-dimethoxy-4HB might serve to bypass both *O*-methyltransferase deficient steps in the *coq3* null mutant. Such bypass would require that this analog could still be prenylated by Coq2, and subjected to decarboxylation, hydroxylation and *C*-methylation steps.

Expression of human COQ3 in yeast *coq3* null mutants rescued growth on a non-fermentable source and partially restored the biosynthesis of CoQ_6 [54]. Assays with farnesylated analogs of CoQ-intermediates showed that mitochondria prepared from *coq3* null mutant yeast expressing human COQ3 performed both *O*-methylation steps [54]. Many lines of evidence indicate a similar Complex Q containing the COQ3–COQ9 polypeptides is involved in

Essays in Biochemistry (2018) **62** 361–376
https://doi.org/10.1042/EBC20170106

human CoQ_{10} biosynthesis [7]. So far, no mutations causing primary CoQ_{10} deficiency have been reported for the human *COQ3* gene.

Yeast *COQ4*; human *COQ4*

Yeast Coq4 is required for CoQ_6 biosynthesis in yeast, and is peripherally associated with the inner mitochondrial membrane on the matrix side [55]. It is thought to serve as a scaffold or organizer for the CoQ synthome [34,56], as it is associated with Coq3, Coq6, and Coq9 [12,51,57]. No enzyme activity or exact function has been associated with the Coq4 polypeptide. A known crystal structure of the Coq4 domain, determined as part of the structural genomics effort (PDB: 3KB4, Northeastern structural genomics program) identified long hydrophobic α helices bound to a geranylgeranyl monophosphate lipid. A conserved $HDxxHx_{10-13}E$ motif [56] chelated a magnesium ion (Mg^{2+}) near to the phosphate head group [57]. From this structure, the function of Coq4 is speculated to bind the long polyisoprenyl tail of CoQ-intermediates and/or CoQ and to organize the enzymes that perform the ring modifications [34,57] (Figure 2).

Human COQ4 was shown to be a functional ortholog of yeast Coq4, and is capable of restoring CoQ_6 biosynthesis in the yeast *coq4* null mutant [58]. Distinct *COQ4* RNA transcripts indicated the potential for two different isoforms of the human COQ4 polypeptide; the longest isoform was shown to possess a mitochondrial targetting sequence, was localized to mitochondria in HeLa cells, and restored CoQ_6 biosynthesis in the yeast *coq4* null mutant. The functional significance of the shorter isoform is not known; it lacks the mitochondrial targetting sequence and failed to rescue *coq4* mutant yeast.

Patients who harbor two recessive *COQ4* mutant alleles exhibit a broad spectrum of mitochondrial disorders associated with CoQ_{10} deficiencies [59]. Intriguingly, haploinsufficiency of *COQ4* also causes CoQ_{10} deficiency in both human and yeast diploid cells [60]. Recently a heterozygous missense E161D mutation in *COQ4* was reported in a patient with lethal rhabdomyolysis; introduction of the missense mutation was introduced to iPSCs, and recapitulated the muscle-specific CoQ_{10} deficiency [61].

Yeast *COQ5*; human *COQ5*

The yeast Coq5 polypeptide is an AdoMet-dependent methyltransferase required for the *C*-methylation step of CoQ biosynthesis [62,63]. It is peripherally associated with the matrix-side of the mitochondrial inner membrane [64]. Dai et al. [65] determined the structure of yeast Coq5; it has a typical seven β-strand AdoMet methyltransferase structure, and the protein was crystallized both in the presence and absence of AdoMet. The catalytic mechanism is yet to be determined; based on modeling the authors proposed an active site highly conserved Arg^{201} or Tyr^{78} act to deprotonate a water molecule that then acts as the base to deprotonate the C5-ring H from $DDMQ_6H_2$ [65]. Yeast *coq5* point mutants that harbor mutations in the Class I methyltransferase motifs result in a loss of *C*-methyltransferase function, but retain steady state levels of the Coq5 polypeptide, and of the Coq polypeptide partner proteins of the CoQ synthome. In contrast, these CoQ synthome partner proteins are destabilized in the *coq5* null mutant [64]. Overexpression of Coq8 in the *coq5* null yeast mutant results in the increased steady-state levels of the Coq4, Coq7, Coq9 polypeptides, the stabilization of the CoQ synthome, and the accumulation of $DDMQ_6H_2$, the substrate of Coq5 [24,34] (Figure 1). It is possible that the 4HB analog 2-methyl-4-BH might function to bypass the defect in *coq5* point mutants with stable Coq5 polypeptide, however, this has not yet been tested.

Regulated expression of yeast Coq5 is necessary for the correct assembly of the CoQ synthome. Recently, two mechanisms of COQ5 post-transcriptional regulation have been elucidated. The RNA binding protein Puf3 regulates the translation of appropriate amounts of Coq5 so the CoQ synthome can be assembled [66]. Oct1 is a mitochondrial matrix-localized protease that removes eight residues from the amino-terminal mitochondrial targetting sequence of Coq5 and is essential for formation of the mature amino-terminus of Coq5 and its stability [67]. There is also evidence that yeast Coq5 is phosphorylated in a Coq8-dependent manner [53].

Expression of the human COQ5 polypeptide was found to rescue the CoQ_6 biosynthetic defect of the *coq5* point mutants or in a *coq5* null mutant overexpressing Coq8, but not a *coq5* null mutant [68]. Thus, human COQ5 is an ortholog of yeast Coq5, but can rescue yeast only when the other yeast Coq partner proteins are present and the CoQ synthome is assembled. Primary CoQ_{10} deficiency has been recently diagnosed due to a partial loss of function of COQ5 [69]. The deficiency is shown to be due to a duplication of the *COQ5* gene, and that due to alternative splicing appears to generate an unstable *COQ5* mRNA with a long 3′-UTR. Steady state levels of the COQ5 polypeptide were dramatically decreased in fibroblasts from the affected homozygous patients as compared with controls. The affected patients had variable degrees of cerebellar ataxia, and showed a modest decrease in the levels of CoQ_{10} in peripheral blood leukocytes, and a more dramatic decrease in CoQ_{10} levels in a skeletal muscle biopsy [69]. The reduction in

Essays in Biochemistry (2018) 62 361–376
https://doi.org/10.1042/EBC20170106

CoQ_{10} levels is consistent with the observation that decreases in COQ5-containing mitochondrial protein complex impairs the production of CoQ_{10} [70].

Yeast *COQ6*; human *COQ6*

The yeast Coq6 polypeptide is characterized as a flavin-dependent monooxygenase [71]. Conserved catalytic regions in Coq6 include the ADP binding fingerprint, the NAD(P)H/FAD binding motif, and the ribityl binding region [71]. Yeast Coq6 co-purifies with a tightly bound FAD, and modeling studies are consistent with its proposed activity as a ring hydroxylase [72]. Yeast Coq6 is responsible for the first hydroxylation step (ring C5) in CoQ biosynthesis [73]. It is also necessary for the deamination of ring C4 in *S. cerevisiae* when pABA is used an aromatic ring precursor [22]. The yeast Coq6 polypeptide is peripherally associated with inner mitochondrial membrane on the matrix side [71], and associates with Coq4, Coq5, Coq7, Coq8, and Coq9 polypeptides of the CoQ synthome [12]. Recent investigations discovered a physical association of Coq6 with Coq8 [12]. Yeast *coq6* point mutants that affect the active site but preserve steady state levels of the Coq6 polypeptide and assembly of the CoQ synthome may be rescued by providing alternate ring precursors such as 3,4-diHB and vanillic acid (Figure 1). These alternate ring precursors, once prenylated by Coq2, allow the defective *coq6* step to be bypassed [73]. Such bypass is also effective in *coq6* null yeast mutants provided yeast *COQ8* is overexpressed [24].

The human homolog COQ6, is able to rescue a yeast *coq6* null mutant [25,74], and interacts with human COQ8B (ADCK4) and COQ7 [75]. Yeast *coq6* null mutants expressing certain hypomorphic mutations of human *COQ6* are rescued by treatment with either 3,4-diHB or vanillic acid [25]. The effectiveness of such bypass therapies as treatments for patients with mutations in *COQ6* remains to be explored. It seems possible that these alternate ring precursors might serve to restore endogenous CoQ_{10} biosynthesis in patients with *COQ6* deficiencies.

Mutations in human *COQ6* have been implicated in an autosomal recessive disease characterized by severe progressive nephrotic syndrome and deafness [74]. It has been suggested that kidney biopsy should be performed on young children present with SRNS and sensorineural hearing loss [76]. The rationale for this suggestion is that the abnormal mitochondria in podocytes may provide an early diagnostic clue of mutations in CoQ biosynthetic genes. Supplementation with high doses of CoQ_{10} can stop the progression of kidney disease, and this therapy should be started immediately at first suspicion of CoQ_{10} deficiency [76,77].

Yeast *YAH1* and *ARH1*; human *FDX1*, *FDX2*, and *FDXR*

Unlike most flavin-dependent monooxygenases that utilize NAD(P)H directly as a source of electrons, the electrons from NAD(P)H are funneled indirectly to yeast Coq6 via the coupled system of ferredoxin (Yah1) an iron–sulphur protein, and ferredoxin reductase (Arh1) [73]. Yeast engineered to be transiently depleted in Yah1 or Arh1 were shown to be defective in the same C5 ring-hydroxylation step, and to accumulate the same polyisoprenylated ring-intermediates as yeast mutants harboring inactive *coq6* alleles [21,73]. *YAH1* and *ARH1* are essential genes in yeast, and in addition to CoQ biosynthesis, are also required for iron–sulphur cluster biosynthesis [78].

There are two human homologs of yeast Yah1 – FDX1 and FDX2. Human FDX2 was shown to complement the iron–sulphur cluster biosynthetic defect of Yah1 depleted yeast [79]. However, neither human FDX1 nor FDX2 were able to complement the CoQ_6 biosynthetic defect of Yah1 depleted yeast [73]. The human homolog of Arh1 is termed as FDXR, which functions as an electron transfer protein in cholesterol biosynthesis and overall steroid metabolism, as well as iron–sulphur cluster biosynthesis [78]. Whether FDX1, FDX2, or FDXR function to assist human COQ6 catalytic activity in the biosynthesis of CoQ_{10} is not yet known.

Yeast *COQ7 (CAT5)* and *PTC7*; human *COQ7* (*CAT5*, *CLK-1*) and *PPTC7*

Yeast Coq7 is a hydroxylase responsible for catalyzing the penultimate step of the CoQ biosynthetic pathway [80-82]. The hydroxylase activity depends on a carboxylate-bridged diiron binding motif, first identified as a highly conserved sequence across a wide array of organisms, and predicted to mediate hydroxylation similar to other members of the carboxylate-bridged diiron protein family, such as methane monoxygenase, ribonucleotide reductase, and phenol-hydroxylase [82]. Modeling predicted Coq7 to be a four-helix bundle protein with an additional helix mediating an interfacial association with the membrane [82]. Experiments with isolated mitochondria and mitoplasts show yeast Coq7 polypeptide is peripherally associated with inner mitochondrial membrane on the matrix side [34].

Expression of human COQ7 rescues the CoQ_6 deficiency of yeast *coq7* null mutants [83], indicating profound conservation of function. Overexpression of a soluble fusion protein containing human COQ7 polypeptide fused to an immunoglobulin-binding domain of protein G was purified (termed as GB1-hCLK-1) and spectroscopic and kinetic methods provided evidence for the presence of the diiron center [84]. Binding of the substrate analogs DMQ_0 or

DMQ_2 to GB1-hCLK1 mediated the reduction in the diiron site by NADH and in the presence of O_2 the hydroxylation step was catalyzed [84].

Yeast *coq7* null mutants accumulate the early CoQ-intermediates HHB and HAB, while *coq7* point mutants [80] and *coq7* null mutants overexpressing Coq8 accumulate DMQ_6 the penultimate intermediate in the pathway [24,85]. Expression of the unrelated *E. coli* UbiF hydroxylase rescued a *coq7* point mutant, but failed to rescue the *coq7* null mutant [86]. These findings indicated Coq7 is an important polypeptide partner of the CoQ synthome; indeed, Coq7 co-purifies with tagged forms of Coq3, Coq6, and Coq9 polypeptides [12].

A mutation in the human *COQ7* gene is associated with a primary ubiquinone deficiency, and results in multiple organ involvement [87]. Interestingly, the deficiencies in CoQ_{10} content and mitochondrial respiratory activities in fibroblasts isolated from this patient were improved following treatment with 2,4-diHB, a 4HB analog that bypasses the COQ7-dependent hydroxylase step [87]. The effectiveness of treatment with 2,4-diHB depends on the type of *COQ7* mutation(s) present in patients [88]. It is likely that the success of these bypass therapies will depend on the stable presence of other COQ polypeptides and their ability to form the CoQ synthome (or complex Q) [16,24]. Regulated expression of COQ7 has been shown to impact the rates of CoQ_{10} biosynthesis, both at the level of NF-κB transcriptional up-regulation of *COQ7* gene expression [89], and at the level of RNA binding proteins that mediate stability of *COQ7* mRNA [90]. The regulated expression of COQ7 and the other component polypeptides of the CoQ synthome seem likely to influence its assembly and function, and so impact biosynthesis of CoQ_{10}.

Yeast Coq7 is modified by phosphorylation [12,53]. Predictive algorithms suggested that the phosphorylation status of Coq7 was regulatory for CoQ_6 biosynthesis, with at least three predicted phosphorylation sites on Ser^{20}, Ser^{28}, and Thr^{32} [91]. When these residues are replaced with alanine, phosphorylation was abolished and CoQ_6 levels were significantly increased in yeast expressing Coq7 with the triple-Alanine substitution. In contrast, yeast expressing the Coq7 with substitution of acidic residues at these residues (Asp^{20}, Glu^{28}, and Asp^{32}) had decreased levels of CoQ_6 and accumulated DMQ_6, indicating that the non-phosphorylatable form of Coq7 is the active form that catalyzes the penultimate pathway step [91]. Other sites of phosphorylation may also influence Coq7 activity; yeast expressing Coq7 harboring the phosphomimetic Ser^{114}Glu substitution also produced lower amounts of CoQ_6 and accumulated DMQ_6 [92].

The phosphatase responsible for Coq7 dephosphorylation is Ptc7, a *bona fide* mitochondrial serine/threonine protein phosphatase belonging to the PPM family of phosphatases [93]. It was recently discovered that two distinct forms of *PTC7* RNA exist, spliced and non-spliced forms, displaying a rare case of alternative splicing in yeast that results in two viable isoforms of a spliced protein [94,95]. The previously reported Ptc7 phosphatase was shown to be the spliced form ($Ptc7_s$) that resides in the mitochondria, while the non-spliced form ($Ptc7_{ns}$) is a nuclear membrane localized protein that contains a transmembrane helix that anchors it to the nuclear membrane [94]. Exclusive expression of $Ptc7_s$ showed significantly higher *de novo* CoQ biosynthesis, as compared with $Ptc7_{ns}$. These findings suggest that the mitochondrial targetting of the Ptc7s results in Coq7 dephosphorylation, and allows Coq7 to catalyze the penultimate step of the CoQ biosynthetic pathway [95]. Ptc7s acts to dephosphorylate other mitochondrial proteins, and deletion of *ptc7* perturbs mitochondrial function [96]. PPTC7 is the human serine/threonine phosphatase homolog of yeast Ptc7, however it is not known whether phosphorylation regulates human COQ7, and if so, whether PPTC7 recognizes it as a substrate.

Yeast *COQ8*; human *COQ8A* (*ADCK3*) and *COQ8B* (*ADCK4*)

The *S. cerevisiae* Coq8 polypeptide is identified as a putative kinase in the biosynthetic pathway of CoQ_6. Coq8 harbors six of twelve motifs present in protein kinases and is required to observe the presence of phosphorylated forms of Coq3, Coq5, and Coq7 polypeptides [53]. Coq8 co-purifies with the CoQ synthome [12]. Further, overexpression of Coq8 in certain of the *coq* null strains restores steady state levels of Coq4, Coq7, and Coq9, and stabilizes the formation of the CoQ synthome [24,34].

Expression of human COQ8A (ADCK3) in yeast *coq8* mutant strains restored CoQ_6 biosynthesis and the phosphorylation state of several of the yeast Coq polypeptides, indicating a profound conservation of function [53]. Rescue of yeast *coq8* mutants by human COQ8A depended on fusion to a yeast mitochondrial targetting sequence [53]. Yeast Coq8 and human COQ8A are homologs of atypical protein kinases. These proteins are able to autophosphorylate and show a surprising affinity and selectivity for ADP, as opposed to ATP [97]. Human COQ8A lacks *in vitro* protein kinase activity and instead shows ATPase activity that is essential for CoQ biosynthesis [98]. The ATPase activity is strongly activated by cardiolipin and small molecule mimics of CoQ intermediates [99]. Thus, the ATPase function of yeast Coq8 and human COQ8A is proposed to function in a chaperone-like activity to facilitate the assembly of the CoQ synthome and *de novo* [65] biosynthesis of CoQ [99].

Essays in Biochemistry (2018) **62** 361–376
https://doi.org/10.1042/EBC20170106

Expression of human COQ8B (ADCK4) also rescues CoQ_6 biosynthesis in yeast *coq8* mutants [100]. Although the amino terminus of COQ8B has a typical mitochondrial matrix targetting sequence, rescue of *coq8* mutant yeast by COQ8B depends on the addition of a yeast mitochondrial targetting sequence [100]. The effect of a *COQ8B* polymorphism present in 50% of the European population (COQ8B-H174R) was tested in the yeast expression model. Yeast *coq8* mutants expressing the human COQ8B-His^{174} polypeptide had decreased steady state levels of the COQ8B polypeptide, decreased growth on medium containing a non-fermentable carbon source, and decreased CII + CIII activity as compared with mutants expressing the COQ8B-Arg^{174} polypeptide [100]. Thus, it is possible that this common COQ8B polymorphism may represent a risk factor for secondary CoQ_{10} deficiencies. Various human diseases are directly associated with mutations in the *COQ8A* and *COQ8B* genes. Most prevalent are recessive ataxia and childhood-onset cerebellar ataxia associated with mutated *COQ8A* [101,102], and a steroid-resistant nephrotic disease related to mutated *COQ8B* [75,100].

Yeast *COQ9*; human *COQ9*

In *S. cerevisiae*, Coq9 is required for CoQ biosynthesis, is a member of the CoQ synthome, and is peripherally associated with the inner mitochondrial membrane, on the matrix side [34,103]. A temperature-sensitive *coq9* mutant (*coq9-ts19*) shifted to the non-permissive temperature results in the disassembling of the CoQ synthome, demonstrating that Coq9 is essential for the formation and stabilization of the high-molecular mass complex [23]. Coq9 is required for the deamination of Carbon 4 on CoQ-intermediates when pABA is utilized as the ring precursor in yeast [23]. The removal of the ring nitrogen substituent depends on the function of Coq6, and yeast with *coq9* mutations accumulate 3-hexaprenyl-4-aminophenol (4-AP), an intermediate that has also been shown to build up in a *coq6* null mutant overexpressing *COQ8* [24]. It is therefore likely that both Coq6 and Coq9 are needed for the 5-hydroxylation and 4-deamination steps of CoQ-intermediates. Additionally, an accumulation of late-stage intermediates suggests Coq7 is not active in the absence of Coq9 [6,24]. In summary, the yeast Coq9 polypeptide is required for both Coq6 and Coq7 hydroxylation steps, via an indirect or supportive role.

Attempts to rescue yeast *coq9* null mutants by expression of human COQ9 have so far failed [104-106]. However, expression of human COQ9 rescued the yeast *coq9-ts19* mutant [106]. Under these conditions, a small amount of the human COQ9 polypeptide enhanced the synthesis of CoQ_6 from 4HB (but not from pABA) and co-purified with the yeast Coq6-CNAP tagged polypeptide, indicating that human COQ9 is able to interact with the yeast CoQ synthome.

The presence of both human COQ9 and human COQ7 are needed for the hydroxylation step catalyzed by COQ7, and the two polypeptides interact [13]. Human cells with deficiencies in COQ9 accumulate DMQ_{10}, the same intermediate that accumulates in COQ7 deficient cells [107]. Both COQ7 and COQ9 deficient cell lines respond to treatment with 2,4-diHB, another example of bypass therapy [108,109]. In fact, human fibroblasts with mutations in COQ9 show decreased steady state levels of the COQ7 polypeptide [109]. Interestingly, treatment with vanillic acid also restored function in the COQ9 deficient cells, but not the COQ7 deficient cells [108]. Perhaps human COQ9 and COQ6 function may also be linked, similar to the situation in yeast. In humans, *COQ9* mutations result in various disease states, including predominant encephalomyopathy and an autosomal-recessive neonatal-onset CoQ deficiency [104,107].

Yeast and human genes required for efficient CoQ biosynthesis

Yeast *COQ10*; human *COQ10A, COQ10B*

Unlike the completely CoQ-less *coq1–coq9* null mutants, the yeast *coq10* null mutant produces near wild-type levels of CoQ at stationary phase, but synthesizes CoQ less efficiently during log phase growth [110,111]. While CoQ is eventually produced at near normal levels, the *coq10* null mutant still has severe defects in respiratory electron transport and is sensitive to treatment with polyunsaturated fatty acids, phenotypes that are hallmarks of the *coq1–coq9* null mutants [110]. Thus, even though CoQ_6 content is similar to that of wild-type yeast, Coq10 is required for efficient function and biosynthesis of CoQ_6. The Coq10 polypeptide contains a steroidogenic acute regulatory (StAR)-related lipid transfer (StART) domain, and binds CoQ and late-stage CoQ-intermediates both *in vitro* and *in vivo*, suggesting Coq10 may function as a lipid chaperone involving delivery of CoQ from site of synthesis to sites of function [110-114].

Humans have two homologs of yeast *COQ10*, namely *COQ10A* and *COQ10B*. Each isoform has several transcript variants as a result of alternative transcription initiation and/or alternative splicing [6]. The function of the COQ10 polypeptide is widely conserved across different organisms; expression of homologs from either *Caulobacter crescentus* or human COQ10A rescue the impaired growth of yeast *coq10Δ* mutant yeast [110]. Currently, there is no

known disease phenotype associated with mutations in human *COQ10A* or *COQ10B*. However, the postulated lipid chaperone function of COQ10A and COQ10B makes these polypeptides intriguing targets for study of the movement of CoQ between mitochondrial membranes and the respiratory complexes.

Yeast *COQ11*; human *NDUFA9*

COQ11 (*YLR290C*) was recently identified to be required for efficient *de novo* CoQ biosynthesis in *S. cerevisiae*. Affinity purification of CNAP-tagged Coq11 showed Coq11-CNAP co-purified with Coq4, Coq5, and Coq7 – members of the high molecular mass CoQ synthome [12]. A separate high throughput study also identified Coq11 as a mitochondrial protein, confirming its localization to the portion of the cell where CoQ is synthesized [115]. Due to its novelty, the functional roles, organization, and stoichiometry of Coq11 within the CoQ-synthome are not yet fully understood. However, numerous features of Coq11 and its homologs solidify its link to CoQ biosynthesis. In five fungal genomes, the existence of Coq11-Coq10 fusion proteins suggests these proteins may have a functional relationship [12]. High throughput studies found *COQ11* to have a genetic correlation with both *COQ2* and *COQ10*, which further supports this hypothesis [115]. Sequence analyses establish Coq11 as a member of the atypical short-chain dehydrogenase/reductase superfamily of oxidoreductases (SDR). SDR superfamily proteins contain a conserved Rossmann fold, a protein structural motif used to bind nucleotide co-factors such as FAD, FMN, and NAD(P) [116]. This bound co-factor is then used to assist the protein in its catalysis of different chemical reactions including isomerization, decarboxylation, epimerization, imine reduction, and carbonyl-alcohol oxidoreduction [116,117]. It is therefore tempting to speculate that Coq11 may use its Rossmann fold to perform enzymatic reactions within the CoQ biosynthetic pathway.

Interestingly, a protein similarity network analysis reveals that the taxonomy of YLR290C-like proteins includes the SDR subfamily protein NDUFA9, an auxiliary subunit of Complex I in humans important for complex stability [12,118-120]. Patients with decreased levels of NDUFA9 are unable to assemble Complex I properly and may develop a degenerative infancy respiratory disorder known as Leigh syndrome, which is often fatal in the first years of life [121,122]. Differences in *NDUFA9* deficiency produce phenotypic variations in patients [46]. It will be challenging to evaluate whether NDUFA9 deficiencies impact CoQ biosynthesis directly, because the deficiencies resulting from Complex I defects (and other mitochondrial defects) may secondarily influence CoQ biosynthesis [123,124]. Further exploration of Coq11 homology with NDUFA9 will help define their functional relationship.

Summary

- The *COQ1–COQ11* genes identified in the *S. cerevisiae* yeast model are required for efficient biosynthesis of CoQ_6.
- Expression of human homologs of yeast *COQ1–COQ10* genes restore CoQ biosynthesis in the corresponding yeast *coq* mutants, indicating profound functional conservation.
- Yeast provides a simple yet powerful model to investigate and define the function and possible pathology of human *COQ* gene polymorphisms and mutations.
- Simple natural products may serve as alternate ring precursors in CoQ biosynthesis, and these compounds may act to enhance biosynthesis of CoQ or may bypass select deficient steps.
- Biosynthesis of CoQ in yeast and human cells depends on high molecular mass multi-subunit complexes consisting of several of the *COQ* gene products, as well as CoQ itself and CoQ-intermediates.
- Thus the CoQ synthome in yeast, or Complex Q in human cells is essential for *de novo* biosynthesis of CoQ.

Acknowledgements

We thank Dr A. Tzagoloff (Columbia University) for the original yeast *coq* mutant strains. We also thank the UCLA Molecular Instrumentation Core for the use of the QTRAP 4000.

Essays in Biochemistry (2018) **62** 361–376
https://doi.org/10.1042/EBC20170106

Competing interests

The authors declare that there are no competing interests associated with this manuscript.

Funding

This work was supported in part by the National Science Foundation [grant number MCB-1330803 (to C.F.C.)]; and the National Institutes of Health [grant number T32 GM 008496 (to M.C.B. and H.T.)].

Author contribution

A.M.A., M.C.B., L.F.-d.-R., A.N., H.T., and C.F.C. contributed to drafting this review, revising it for intellectual content and approved the final version. A.M.A., A.N., L.F.-d.R., and C.F.C. contributed to preparation of the figures.

Abbreviations

AdoMet, *S*-adenosylmethionine; CNAP, consecutive non-denaturing affinity purification; CoQ, ubiquinone or coenzyme Q; $CoQH_2$, ubiquinol or CoQ hydroquinone; CoQ_n, ubiquinone-n or coenzyme Q_n (refers to a specific isoform, where n is number of isoprenyl units in the tail of CoQ_n, e.g. CoQ_{10} in humans, CoQ_6 in *Saccharomyces cerevisiae*); Coq, *Saccharomyces cerevisiae* polypeptide involved in CoQ_6 biosynthesis; COQ, human polypeptide involved in CoQ_{10} biosynthesis; *COQ*, yeast or human gene involved in CoQ biosynthesis; pABA, *para*-aminobenzoic acid; SDR, short-chain dehydrogenase/reductase superfamily of oxidoreductases; SRNS, steroid resistant nephrotic syndrome; 2,4-diHB, 2,4-dihydroxybenzoic acid; 3,4-diHB, 3,4-dihydroxybenzoic acid; 4HB, 4-hydroxybenzoic acid; 4HBz, 4-hydroxybenzaldehyde.

References

1 Turunen, M., Olsson, J. and Dallner, G. (2004) Metabolism and function of coenzyme Q. *Biochim. Biophys. Act.* **1660**, 171–199, https://doi.org/10.1016/j.bbamem.2003.11.012
2 Crane, F.L. (2001) Biochemical functions of coenzyme Q_{10}. *J. Am. Coll. Nutr.* **20**, 591–598, https://doi.org/10.1080/07315724.2001.10719063
3 Bentinger, M., Brismar, K. and Dallner, G. (2007) The antioxidant role of coenzyme Q. *Mitochondrion* **7S**, S41–S50, https://doi.org/10.1016/j.mito.2007.02.006
4 Aussel, L., Pierrel, F., Loiseau, L., Lombard, M., Fontecave, M. and Barras, F. (2014) Biosynthesis and physiology of coenzyme Q in bacteria. *Biochim. Biophys. Acta* **1837**, 1004–1011, https://doi.org/10.1016/j.bbabio.2014.01.015
5 Hayashi, K., Ogiyama, Y., Yokomi, K., Nakagawa, T., Kaino, T. and Kawamukai, M. (2014) Functional conservation of coenzyme Q biosynthetic genes among yeasts, plants, and humans. *PLoS ONE* **9**, 14, https://doi.org/10.1371/journal.pone.0099038
6 Wang, Y. and Hekimi, S. (2013) Molecular genetics of ubiquinone biosynthesis in animals. *Crit. Rev. Biochem. Mol. Biol.* **48**, 69–88, https://doi.org/10.3109/10409238.2012.741564
7 Stefely, J.A. and Pagliarini, D.J. (2017) Biochemistry of mitochondrial coenzyme Q biosynthesis. *Trends Biochem. Sci.* **42**, 824–843, https://doi.org/10.1016/j.tibs.2017.06.008
8 Alcázar-Fabra, M., Trevisson, E. and Brea-Calvo, G. (2018) Clinical syndromes associated with Coenzyme Q_{10} deficiency. *Essays Biochem.* **62**, 377–398, https://doi.org/10.1042/EBC20170107
9 Tzagoloff, A., Akai, A. and Needleman, R.B. (1975) Assembly of the mitochondrial membrane system. Characterization of nuclear mutants of *Saccharomyces cerevisiae* with defects in mitochondrial ATPase and respiratory enzymes. *J. Biol. Chem.* **250**, 8228–8235
10 Tzagoloff, A. and Dieckmann, C.L. (1990) *PET* genes of *Saccharomyces cerevisiae*. *Microbiol. Rev.* **54**, 211–225
11 Tran, U.C. and Clarke, C.F. (2007) Endogenous synthesis of coenzyme Q in eukaryotes. *Mitochondrion* **7S**, S62–S71, https://doi.org/10.1016/j.mito.2007.03.007
12 Allan, C.M., Awad, A.M., Johnson, J.S., Shirasaki, D.I., Wang, C., Blaby-Haas, C.E. et al. (2015) Identification of Coq11, a new coenzyme Q biosynthetic protein in the CoQ-Synthome in *Saccharomyces cerevisiae*. *J. Biol. Chem.* **290**, 7517–7534, https://doi.org/10.1074/jbc.M114.633131
13 Lohman, D.C., Forouhar, F., Beebe, E.T., Stefely, M.S., Minogue, C.E., Ulbrich, A. et al. (2014) Mitochondrial COQ9 is a lipid-binding protein that associates with COQ7 to enable coenzyme Q biosynthesis. *Proc. Natl. Acad. Sci. U.S.A.* **111**, E4697–E4705, https://doi.org/10.1073/pnas.1413128111
14 Clarke, C.F. (2000) New advances in coenzyme Q biosynthesis. *Protoplasma* **213**, 134–147, https://doi.org/10.1007/BF01282151
15 Kawamukai, M. (2016) Biosynthesis of coenzyme Q in eukaryotes. *Biosci. Biotechnol. Biochem.* **80**, 23–33, https://doi.org/10.1080/09168451.2015.1065172
16 Pierrel, F. (2017) Impact of chemical analogs of 4-hydroxybenzoic acid on coenzyme Q biosynthesis: from inhibition to bypass of coenzyme Q deficiency. *Front. Physiol.* **8**, 436, https://doi.org/10.3389/fphys.2017.00436
17 Payet, L.A., Leroux, M., Willison, J.C., Kihara, A., Pelosi, L. and Pierrel, F. (2016) Mechanistic details of early steps in coenzyme Q biosynthesis pathway in yeast. *Cell Chem. Biol.* **23**, 1241–1250, https://doi.org/10.1016/j.chembiol.2016.08.008
18 Stefely, J.A., Kwiecien, N.W., Freiberger, E.C., Richards, A.L., Jochem, A., Rush, M. J.P. et al. (2016) Mitochondrial protein functions elucidated by multi-omic mass spectrometry profiling. *Nat. Biotechnol.* **34**, 1191–1197, https://doi.org/10.1038/nbt.3683
19 Zahedi, R.P., Sickmann, A., Boehm, A.M., Winkler, C., Zufall, N., Schonfisch, B. et al. (2006) Proteomic analysis of the yeast mitochondrial outer membrane reveals accumulation of a subclass of preproteins. *Mol. Biol. Cell* **17**, 1436–1450, https://doi.org/10.1091/mbc.e05-08-0740

20 Marbois, B., Xie, L.X., Choi, S., Hirano, K., Hyman, K. and Clarke, C.F. (2010) para-Aminobenzoic acid is a precursor in coenzyme Q_6 biosynthesis in *Saccharomyces cerevisiae*. *J. Biol. Chem.* **285**, 27827–27838, https://doi.org/10.1074/jbc.M110.151894
21 Pierrel, F., Hamelin, O., Douki, T., Kieffer-Jaquinod, S., Muhlenhoff, U., Ozeir, M. et al. (2010) Involvement of mitochondrial ferredoxin and para-aminobenzoic acid in yeast coenzyme Q biosynthesis. *Chem. Biol.* **17**, 449–459, https://doi.org/10.1016/j.chembiol.2010.03.014
22 Ozeir, M., Pelosi, L., Ismail, A., Mellot-Draznieks, C., Fontecave, M. and Pierrel, F. (2015) Coq6 is responsible for the C4-deamination reaction in coenzyme Q biosynthesis in *Saccharomyces cerevisiae*. *J. Biol. Chem.* **290**, 24140–24151, https://doi.org/10.1074/jbc.M115.675744
23 He, C.H., Black, D.S., Nguyen, T.P., Wang, C., Srinivasan, C. and Clarke, C.F. (2015) Yeast Coq9 controls deamination of coenzyme Q intermediates that derive from para-aminobenzoic acid. *Biochim. Biophys. Acta* **1851**, 1227–1239, https://doi.org/10.1016/j.bbalip.2015.05.003
24 Xie, L.X., Ozeir, M., Tang, J.Y., Chen, J.Y., Jaquinod, S.K., Fontecave, M. et al. (2012) Overexpression of the Coq8 kinase in *Saccharomyces cerevisiae coq* null mutants allows for accumulation of diagnostic intermediates of the coenzyme Q_6 biosynthetic pathway. *J. Biol. Chem.* **287**, 23571–23581, https://doi.org/10.1074/jbc.M112.360354
25 Doimo, M., Trevisson, E., Airik, R., Bergdoll, M., Santos-Ocana, C., Hildebrandt, F. et al. (2014) Effect of vanillic acid on *COQ6* mutants identified in patients with coenzyme Q_{10} deficiency. *Biochim. Biophys. Acta* **1842**, 1–6, https://doi.org/10.1016/j.bbadis.2013.10.007
26 Xie, L.X., Williams, K.J., He, C.H., Weng, E., Khong, S., Rose, T.E. et al. (2015) Resveratrol and para-coumarate serve as ring precursors for coenzyme Q biosynthesis. *J. Lipid Res.* **56**, 909–919, https://doi.org/10.1194/jlr.M057919
27 Fernandez-Del-Rio, L., Nag, A., Gutierrez Casado, E., Ariza, J., Awad, A.M., Joseph, A.I. et al. (2017) Kaempferol increases levels of coenzyme Q in kidney cells and serves as a biosynthetic ring precursor. *Free Radic. Biol. Med.* **110**, 176–187, https://doi.org/10.1016/j.freeradbiomed.2017.06.006
28 Alam, S.S., Nambudiri, A.M. and Rudney, H. (1975) J-Hydroxybenzoate: polyprenyl transferase and the prenylation of 4-aminobenzoate in mammalian tissues. *Arch. Biochem. Biophys.* **171**, 183–190, https://doi.org/10.1016/0003-9861(75)90022-3
29 Gonzalez-Aragon, D., Buron, M.I., Lopez-Lluch, G., Herman, M.D., Gomez-Diaz, C., Navas, P. et al. (2005) Coenzyme Q and the regulation of intracellular steady-state levels of superoxide in HL-60 cells. *Biofactors* **25**, 31–41, https://doi.org/10.1002/biof.5520250105
30 Ashby, M.N. and Edwards, P.A. (1990) Elucidation of the deficiency in two yeast coenzyme Q mutants. Characterization of the structural gene encoding hexaprenyl pyrophosphate synthetase. *J. Biol. Chem.* **265**, 13157–13164
31 Gin, P. and Clarke, C.F. (2005) Genetic evidence for a multi-subunit complex in coenzyme Q biosynthesis in yeast and the role of the Coq1 hexaprenyl diphosphate synthase. *J. Biol. Chem.* **280**, 2676–2681, https://doi.org/10.1074/jbc.M411527200
32 Okada, K., Suzuki, K., Kamiya, Y., Zhu, X., Fujisaki, S., Nishimura, Y. et al. (1996) Polyprenyl diphosphate synthase essentially defines the length of the side chain of ubiquinone. *Biochim. Biophys. Acta* **1302**, 217–223, https://doi.org/10.1016/0005-2760(96)00064-1
33 Okada, K., Kainou, T., Matsuda, H. and Kawamukai, M. (1998) Biological significance of the side chain length of ubiquinone in *Saccharomyces cerevisiae*. *FEBS Lett.* **431**, 241–244, https://doi.org/10.1016/S0014-5793(98)00753-4
34 He, C.H., Xie, L.X., Allan, C.M., Tran, U.C. and Clarke, C.F. (2014) Coenzyme Q supplementation or over-expression of the yeast Coq8 putative kinase stabilizes multi-subunit Coq polypeptide complexes in yeast *coq* null mutants. *Biochim. Biophys. Acta* **1841**, 630–644, https://doi.org/10.1016/j.bbalip.2013.12.017
35 Saiki, R., Nagata, A., Kainou, T., Matsuda, H. and Kawamukai, M. (2005) Characterization of solanesyl and decaprenyl diphosphate synthases in mice and humans. *FEBS J.* **272**, 5606–5622, https://doi.org/10.1111/j.1742-4658.2005.04956.x
36 Mollet, J., Giurgea, I., Schlemmer, D., Dallner, G., Chretien, D., Delahodde, A. et al. (2007) Prenyldiphosphate synthase, subunit 1 (*PDSS1*) and OH-benzoate polyprenyltransferase (*COQ2*) mutations in ubiquinone deficiency and oxidative phosphorylation disorders. *J. Clin. Invest.* **117**, 765–772, https://doi.org/10.1172/JCI29089
37 Lopez, L.C., Schuelke, M., Quinzii, C.M., Kanki, T., Rodenburg, R.J., Naini, A. et al. (2006) Leigh syndrome with nephropathy and CoQ_{10} deficiency due to decaprenyl diphosphate synthase subunit 2 (*PDSS2*) mutations. *Am. J. Hum. Genet.* **79**, 1125–1129, https://doi.org/10.1086/510023
38 Ashby, M.N., Kutsunai, S.Y., Ackerman, S., Tzagoloff, A. and Edwards, P.A. (1992) *COQ2* is a candidate for the structural gene encoding para-hydroxybenzoate:polyprenyltransferase. *J. Biol. Chem.* **267**, 4128–4136
39 Hsu, A.Y., Do, T.Q., Lee, P.T. and Clarke, C.F. (2000) Genetic evidence for a multi-subunit complex in the O-methyltransferase steps of coenzyme Q biosynthesis. *Biochim. Biophys. Acta* **1484**, 287–297, https://doi.org/10.1016/S1388-1981(00)00019-6
40 Johnson, A., Gin, P., Marbois, B.N., Hsieh, E.J., Wu, M., Barros, M.H. et al. (2005) *COQ9*, a new gene required for the biosynthesis of coenzyme Q in *Saccharomyces cerevisiae*. *J. Biol. Chem.* **280**, 31397–31404, https://doi.org/10.1074/jbc.M503277200
41 Leuenberger, D., Bally, N.A., Schatz, G. and Koehler, C.M. (1999) Different import pathways through the mitochondrial intermembrane space for inner membrane proteins. *EMBO J.* **18**, 4816–4822, https://doi.org/10.1093/emboj/18.17.4816
42 Forsgren, M., Attersand, A., Lake, S., Grunler, J., Swiezewska, E., Dallner, G. et al. (2004) Isolation and functional expression of human *COQ2*, a gene encoding a polyprenyl transferase involved in the synthesis of CoQ. *Biochem. J.* **382**, 519–526, https://doi.org/10.1042/BJ20040261
43 Desbats, M.A., Morbidoni, V., Silic-Benussi, M., Doimo, M., Ciminale, V., Cassina, M. et al. (2016) The *COQ2* genotype predicts the severity of coenzyme Q_{10} deficiency. *Hum. Mol. Genet.* **25**, 4256–4265, https://doi.org/10.1093/hmg/ddw257
44 Li, W. (2016) Bringing bioactive compounds into membranes: the UbiA superfamily of intramembrane aromatic prenyltransferases. *Trends Biochem. Sci.* **41**, 356–370, https://doi.org/10.1016/j.tibs.2016.01.007
45 Herebian, D., Seibt, A., Smits, S. H.J., Rodenburg, R.J., Mayatepek, E. and Distelmaier, F. (2017) 4-Hydroxybenzoic acid restores CoQ_{10} biosynthesis in human COQ2 deficiency. *Ann. Clin. Transl. Neurol.* **4**, 902–908, https://doi.org/10.1002/acn3.486
46 Baertling, F., Sanchez-Caballero, L., van den Brand, M. A.M., Fung, C.W., Chan, S.H., Wong, V.C. et al. (2018) *NDUFA9* point mutations cause a variable mitochondrial complex I assembly defect. *Clin. Genet.* **93**, 111–118, https://doi.org/10.1111/cge.13089
47 Clarke, C.F., Williams, W. and Teruya, J.H. (1991) Ubiquinone biosynthesis in *Saccharomyces cerevisiae*. Isolation and sequence of *COQ3*, the 3,4-dihydroxy-5-hexaprenylbenzoate methyltransferase gene. *J. Biol. Chem.* **266**, 16636–16644

48 Hsu, A.Y., Poon, W.W., Shepherd, J.A., Myles, D.C. and Clarke, C.F. (1996) Complementation of *coq3* mutant yeast by mitochondrial targeting of the *Escherichia coli* UbiG polypeptide: evidence that UbiG catalyzes both O-methylation steps in ubiquinone biosynthesis. *Biochemistry* **35**, 9797–9806, https://doi.org/10.1021/bi9602932

49 Poon, W.W., Barkovich, R.J., Hsu, A.Y., Frankel, A., Lee, P.T., Shepherd, J.N. et al. (1999) Yeast and rat Coq3 and *Escherichia coli* UbiG polypeptides catalyze both *O*-methyltransferase steps in coenzyme Q biosynthesis. *J. Biol. Chem.* **274**, 21665–21672, https://doi.org/10.1074/jbc.274.31.21665

50 Zhu, Y., Wu, B., Zhang, X., Fan, X., Niu, L., Li, X. et al. (2015) Structural and biochemical studies reveal UbiG/Coq3 as a class of novel membrane-binding proteins. *Biochem. J.* **470**, 105–114, https://doi.org/10.1042/BJ20150329

51 Marbois, B., Gin, P., Faull, K.F., Poon, W.W., Lee, P.T., Strahan, J. et al. (2005) Coq3 and Coq4 define a polypeptide complex in yeast mitochondria for the biosynthesis of coenzyme Q. *J. Biol. Chem.* **280**, 20231–20238, https://doi.org/10.1074/jbc.M501315200

52 Tauche, A., Krause-Buchholz, U. and Rodel, G. (2008) Ubiquinone biosynthesis in *Saccharomyces cerevisiae*: the molecular organization of *O*-methylase Coq3p depends on Abc1p/Coq8p. *FEMS Yeast Res.* **8**, 1263–1275, https://doi.org/10.1111/j.1567-1364.2008.00436.x

53 Xie, L.X., Hsieh, E.J., Watanabe, S., Allan, C.M., Chen, J.Y., Tran, U.C. et al. (2011) Expression of the human atypical kinase ADCK3 rescues coenzyme Q biosynthesis and phosphorylation of Coq polypeptides in yeast *coq8* mutants. *Biochim. Biophys. Acta* **1811**, 348–360, https://doi.org/10.1016/j.bbalip.2011.01.009

54 Jonassen, T. and Clarke, C.F. (2000) Isolation and functional expression of human *COQ3*, a gene encoding a methyltransferase required for ubiquinone biosynthesis. *J. Biol. Chem.* **275**, 12381–12387, https://doi.org/10.1074/jbc.275.17.12381

55 Belogrudov, G.I., Lee, P.T., Jonassen, T., Hsu, A.Y., Gin, P. and Clarke, C.F. (2001) Yeast *COQ4* encodes a mitochondrial protein required for coenzyme Q synthesis. *Arch. Biochem. Biophys.* **392**, 48–58, https://doi.org/10.1006/abbi.2001.2448

56 Marbois, B., Gin, P., Gulmezian, M. and Clarke, C.F. (2009) The yeast Coq4 polypeptide organizes a mitochondrial protein complex essential for coenzyme Q biosynthesis. *Biochim. Biophys. Acta* **1791**, 69–75, https://doi.org/10.1016/j.bbalip.2008.10.006

57 Rea, S.L., Graham, B.H., Nakamaru-Ogiso, E., Kar, A. and Falk, M.J. (2010) Bacteria, yeast, worms, and flies: exploiting simple model organisms to investigate human mitochondrial diseases. *Dev. Disabil. Res. Rev.* **16**, 200–218, https://doi.org/10.1002/ddrr.114

58 Casarin, A., Jimenez-Ortega, J.C., Trevisson, E., Pertegato, V., Doimo, M., Ferrero-Gomez, M.L. et al. (2008) Functional characterization of human *COQ4*, a gene required for Coenzyme Q_{10} biosynthesis. *Biochem. Biophys. Res. Commun.* **372**, 35–39, https://doi.org/10.1016/j.bbrc.2008.04.172

59 Brea-Calvo, G., Haack, T.B., Karall, D., Ohtake, A., Invernizzi, F., Carrozzo, R. et al. (2015) *COQ4* mutations cause a broad spectrum of mitochondrial disorders associated with CoQ_{10} deficiency. *Am. J. Hum. Genet.* **96**, 309–317, https://doi.org/10.1016/j.ajhg.2014.12.023

60 Salviati, L., Trevisson, E., Rodriguez Hernandez, M.A., Casarin, A., Pertegato, V., Doimo, M. et al. (2012) Haploinsufficiency of *COQ4* causes coenzyme Q_{10} deficiency. *J. Med. Genet.* **49**, 187–191, https://doi.org/10.1136/jmedgenet-2011-100394

61 Romero-Moya, D., Santos-Ocana, C., Castano, J., Garrabou, G., Rodriguez-Gomez, J.A., Ruiz-Bonilla, V. et al. (2017) Genetic rescue of mitochondrial and skeletal muscle impairment in an induced pluripotent stem cells model of coenzyme Q_{10} deficiency. *Stem Cells* **35**, 1687–1703, https://doi.org/10.1002/stem.2634

62 Barkovich, R.J., Shtanko, A., Shepherd, J.A., Lee, P.T., Myles, D.C., Tzagoloff, A. et al. (1997) Characterization of the *COQ5* gene from *Saccharomyces cerevisiae*. Evidence for a C-methyltransferase in ubiquinone biosynthesis. *J. Biol. Chem.* **272**, 9182–9188, https://doi.org/10.1074/jbc.272.14.9182

63 Dibrov, E., Robinson, K.M. and Lemire, B.D. (1997) The *COQ5* gene encodes a yeast mitochondrial protein necessary for ubiquinone biosynthesis and the assembly of the respiratory chain. *J. Biol. Chem.* **272**, 9175–9181, https://doi.org/10.1074/jbc.272.14.9175

64 Baba, S.W., Belogrudov, G.I., Lee, J.C., Lee, P.T., Strahan, J., Shepherd, J.N. et al. (2004) Yeast Coq5 C-methyltransferase is required for stability of other polypeptides involved in coenzyme Q biosynthesis. *J. Biol. Chem.* **279**, 10052–10059, https://doi.org/10.1074/jbc.M313712200

65 Dai, Y.N., Zhou, K., Cao, D.D., Jiang, Y.L., Meng, F., Chi, C.B. et al. (2014) Crystal structures and catalytic mechanism of the C-methyltransferase Coq5 provide insights into a key step of the yeast coenzyme Q synthesis pathway. *Acta Crystallogr. Sec. D Biol. Crystallogr.* **70**, 2085–2092, https://doi.org/10.1107/S1399004714011559

66 Lapointe, C.P., Stefely, J.A., Jochem, A., Hutchins, P.D., Wilson, G.M., Kwiecien, N.W. et al. (2018) Multi-omics reveal specific targets of the RNA-binding protein Puf3p and its orchestration of mitochondrial biogenesis. *Cell Syst.* **6**, 125–135.e126

67 Veling, M.T., Reidenbach, A.G., Freiberger, E.C., Kwiecien, N.W., Hutchins, P.D., Drahnak, M.J. et al. (2017) Multi-omic mitoprotease profiling defines a role for Oct1p in coenzyme Q production. *Mol. Cell* **68**, 970–977.e911, https://doi.org/10.1016/j.molcel.2017.11.023

68 Nguyen, T.P., Casarin, A., Desbats, M.A., Doimo, M., Trevisson, E., Santos-Ocana, C. et al. (2014) Molecular characterization of the human COQ5 C-methyltransferase in Coenzyme Q biosynthesis. *Biochim. Biophys. Acta*, https://doi.org/10.1016/j.bbalip.2014.08.007

69 Malicdan, M. C.V., Vilboux, T., Ben-Zeev, B., Guo, J., Eliyahu, A., Pode-Shakked, B. et al. (2018) A novel inborn error of the coenzyme Q_{10} biosynthesis pathway: cerebellar ataxia and static encephalomyopathy due to COQ5 C-methyltransferase deficiency. *Hum. Mutat.* **39**, 69–79, https://doi.org/10.1002/humu.23345

70 Yen, H.C., Liu, Y.C., Kan, C.C., Wei, H.J., Lee, S.H., Wei, Y.H. et al. (2016) Disruption of the human COQ5-containing protein complex is associated with diminished coenzyme Q_{10} levels under two different conditions of mitochondrial energy deficiency. *Biochim. Biophys. Acta* **1860**, 1864–1876, https://doi.org/10.1016/j.bbagen.2016.05.005

71 Gin, P., Hsu, A.Y., Rothman, S.C., Jonassen, T., Lee, P.T., Tzagoloff, A. et al. (2003) The *Saccharomyces cerevisiae COQ6* gene encodes a mitochondrial flavin-dependent monooxygenase required for coenzyme Q biosynthesis. *J. Biol. Chem.* **278**, 25308–25316, https://doi.org/10.1074/jbc.M303234200

72 Ismail, A., Leroux, V., Smadja, M., Gonzalez, L., Lombard, M., Pierrel, F. et al. (2016) Coenzyme Q biosynthesis: evidence for a substrate access channel in the FAD-dependent monooxygenase Coq6. *PLoS Comput. Biol.* **12**, e1004690, https://doi.org/10.1371/journal.pcbi.1004690

73 Ozeir, M., Muhlenhoff, U., Webert, H., Lill, R., Fontecave, M. and Pierrel, F. (2011) Coenzyme Q biosynthesis: Coq6 is required for the C5-hydroxylation reaction and substrate analogs rescue Coq6 deficiency. *Chem. Biol.* **18**, 1134–1142, https://doi.org/10.1016/j.chembiol.2011.07.008

74 Heeringa, S.F., Chernin, G., Chaki, M., Zhou, W., Sloan, A.J., Ji, Z. et al. (2011) *COQ6* mutations in human patients produce nephrotic syndrome with sensorineural deafness. *J. Clin. Invest.* **121**, 2013–2024, https://doi.org/10.1172/JCI45693
75 Ashraf, S., Gee, H.Y., Woerner, S., Xie, L.X., Vega-Warner, V., Lovric, S. et al. (2013) *ADCK4* mutations promote steroid-resistant nephrotic syndrome through CoQ_{10} biosynthesis disruption. *J. Clin. Invest.* **123**, 5179–5189, https://doi.org/10.1172/JCI69000
76 Park, E., Ahn, Y.H., Kang, H.G., Yoo, K.H., Won, N.H., Lee, K.B. et al. (2017) *COQ6* mutations in children with steroid-resistant focal segmental glomerulosclerosis and sensorineural hearing loss. *Am. J. Kidney Dis.* **70**, 139–144, https://doi.org/10.1053/j.ajkd.2016.10.040
77 Gigante, M., Diella, S., Santangelo, L., Trevisson, E., Acosta, M.J., Amatruda, M. et al. (2017) Further phenotypic heterogeneity of CoQ_{10} deficiency associated with steroid resistant nephrotic syndrome and novel *COQ2* and *COQ6* variants. *Clin. Genet.* **92**, 224–226, https://doi.org/10.1111/cge.12960
78 Sheftel, A., Stehling, O. and Lill, R. (2010) Iron-sulfur proteins in health and disease. *Trends Endocrinol. Metab.* **21**, 302–314, https://doi.org/10.1016/j.tem.2009.12.006
79 Sheftel, A.D., Stehling, O., Pierik, A.J., Elsasser, H.P., Muhlenhoff, U., Webert, H. et al. (2010) Humans possess two mitochondrial ferredoxins, Fdx1 and Fdx2, with distinct roles in steroidogenesis, heme, and Fe/S cluster biosynthesis. *Proc. Natl. Acad. Sci. U.S.A.* **107**, 11775–11780, https://doi.org/10.1073/pnas.1004250107
80 Marbois, B.N. and Clarke, C.F. (1996) The *COQ7* gene encodes a protein in *Saccharomyces cerevisiae* necessary for ubiquinone biosynthesis. *J. Biol. Chem.* **271**, 2995–3004, https://doi.org/10.1074/jbc.271.6.2995
81 Jonassen, T., Proft, M., Randez-Gil, F., Schultz, J.R., Marbois, B.N., Entian, K.D. et al. (1998) Yeast Clk-1 homologue (Coq7/Cat5) is a mitochondrial protein in coenzyme Q synthesis. *J. Biol. Chem.* **273**, 3351–3357, https://doi.org/10.1074/jbc.273.6.3351
82 Stenmark, P., Grunler, J., Mattsson, J., Sindelar, P.J., Nordlund, P. and Berthold, D.A. (2001) A new member of the family of di-iron carboxylate proteins. Coq7 (clk-1), a membrane-bound hydroxylase involved in ubiquinone biosynthesis. *J. Biol. Chem.* **276**, 33297–33300, https://doi.org/10.1074/jbc.C100346200
83 Vajo, Z., King, L.M., Jonassen, T., Wilkin, D.J., Ho, N., Munnich, A. et al. (1999) Conservation of the *Caenorhabditis elegans* timing gene *clk-1* from yeast to human: a gene required for ubiquinone biosynthesis with potential implications for aging. *Mamm. Genome* **10**, 1000–1004, https://doi.org/10.1007/s003359901147
84 Lu, T.T., Lee, S.J., Apfel, U.P. and Lippard, S.J. (2013) Aging-associated enzyme human clock-1: substrate-mediated reduction of the diiron center for 5-demethoxyubiquinone hydroxylation. *Biochemistry* **52**, 2236–2244, https://doi.org/10.1021/bi301674p
85 Padilla, S., Tran, U.C., Jimenez-Hidalgo, M., Lopez-Martin, J.M., Martin-Montalvo, A., Clarke, C.F. et al. (2009) Hydroxylation of demethoxy-Q_6 constitutes a control point in yeast coenzyme Q_6 biosynthesis. *Cell. Mol. Life Sci.* **66**, 173–186, https://doi.org/10.1007/s00018-008-8547-7
86 Tran, U.C., Marbois, B., Gin, P., Gulmezian, M., Jonassen, T. and Clarke, C.F. (2006) Complementation of *Saccharomyces cerevisiae coq7* mutants by mitochondrial targeting of the *Escherichia coli* UbiF polypeptide. Two functions of yeast Coq7 polypeptide in coenzyme Q biosynthesis. *J. Biol. Chem.* **281**, 16401–16409, https://doi.org/10.1074/jbc.M513267200
87 Freyer, C., Stranneheim, H., Naess, K., Mourier, A., Felser, A., Maffezzini, C. et al. (2015) Rescue of primary ubiquinone deficiency due to a novel *COQ7* defect using 2,4-dihydroxybensoic acid. *J. Med. Genet.* **52**, 779–783, https://doi.org/10.1136/jmedgenet-2015-102986
88 Wang, Y., Smith, C., Parboosingh, J.S., Khan, A., Innes, M. and Hekimi, S. (2017) Pathogenicity of two *COQ7* mutations and responses to 2,4-dihydroxybenzoate bypass treatment. *J. Cell. Mol. Med.* **21**, 2329–2343, https://doi.org/10.1111/jcmm.13154
89 Brea-Calvo, G., Siendones, E., Sanchez-Alcazar, J.A., de Cabo, R. and Navas, P. (2009) Cell survival from chemotherapy depends on NF-kappaB transcriptional up-regulation of coenzyme Q biosynthesis. *PLoS ONE* **4**, e5301, https://doi.org/10.1371/journal.pone.0005301
90 Cascajo, M.V., Abdelmohsen, K., Noh, J.H., Fernandez-Ayala, D.J., Willers, I.M., Brea, G. et al. (2016) RNA-binding proteins regulate cell respiration and coenzyme Q biosynthesis by post-transcriptional regulation of COQ7. *RNA Biol.* **13**, 622–634, https://doi.org/10.1080/15476286.2015.1119366
91 Martin-Montalvo, A., Gonzalez-Mariscal, I., Padilla, S., Ballesteros, M., Brautigan, D.L., Navas, P. et al. (2011) Respiratory-induced coenzyme Q biosynthesis is regulated by a phosphorylation cycle of Cat5p/Coq7p. *Biochem. J.* **440**, 107–114, https://doi.org/10.1042/BJ20101422
92 Busso, C., Ferreira-Junior, J.R., Paulela, J.A., Bleicher, L., Demasi, M. and Barros, M.H. (2015) Coq7p relevant residues for protein activity and stability. *Biochimie* **119**, 92–102, https://doi.org/10.1016/j.biochi.2015.10.016
93 Martin-Montalvo, A., Gonzalez-Mariscal, I., Pomares-Viciana, T., Padilla-Lopez, S., Ballesteros, M., Vazquez-Fonseca, L. et al. (2013) The phosphatase Ptc7 induces coenzyme Q Biosynthesis by activating the hydroxylase Coq7 in yeast. *J. Biol. Chem.* **288**, 28126–28137, https://doi.org/10.1074/jbc.M113.474494
94 Juneau, K., Nislow, C. and Davis, R.W. (2009) Alternative splicing of *PTC7* in *Saccharomyces cerevisiae* determines protein localization. *Genetics* **183**, 185–194, https://doi.org/10.1534/genetics.109.105155
95 Awad, A.M., Venkataramanan, S., Nag, A., Galivanche, A.R., Bradley, M.C., Neves, L.T. et al. (2017) Chromatin-remodeling SWI/SNF complex regulates coenzyme Q_6 synthesis and a metabolic shift to respiration in yeast. *J. Biol. Chem.* **292**, 14851–14866, https://doi.org/10.1074/jbc.M117.798397
96 Guo, X., Niemi, N.M., Hutchins, P.D., Condon, S.G., Jochem, A., Ulbrich, A. et al. (2017) Ptc7p dephosphorylates select mitochondrial proteins to enhance metabolic function. *Cell Rep.* **18**, 307–313, https://doi.org/10.1016/j.celrep.2016.12.049
97 Stefely, J.A., Reidenbach, A.G., Ulbrich, A., Oruganty, K., Floyd, B.J., Jochem, A. et al. (2015) Mitochondrial ADCK3 employs an atypical protein kinase-like fold to enable coenzyme Q biosynthesis. *Mol. Cell* **57**, 83–94, https://doi.org/10.1016/j.molcel.2014.11.002
98 Stefely, J.A., Licitra, F., Laredj, L., Reidenbach, A.G., Kemmerer, Z.A., Grangeray, A. et al. (2016) Cerebellar ataxia and coenzyme Q deficiency through loss of unorthodox kinase activity. *Mol. Cell* **63**, 608–620, https://doi.org/10.1016/j.molcel.2016.06.030
99 Reidenbach, A.G., Kemmerer, Z.A., Aydin, D., Jochem, A., McDevitt, M.T., Hutchins, P.D. et al. (2018) Conserved lipid and small-molecule modulation of COQ8 reveals regulation of the ancient kinase-like UbiB family. *Cell Chem. Biol.* **25**, 154–165.e111, https://doi.org/10.1016/j.chembiol.2017.11.001

100 Vazquez Fonseca, L., Doimo, M., Calderan, C., Desbats, M.A., Acosta, M.J., Cerqua, C. et al. (2018) Mutations in *COQ8B* (*ADCK4*) found in patients with steroid-resistant nephrotic syndrome alter COQ8B function. *Hum. Mutat.* **39**, 406–414, https://doi.org/10.1002/humu.23376

101 Lagier-Tourenne, C., Tazir, M., Lopez, L.C., Quinzii, C.M., Assoum, M., Drouot, N. et al. (2008) ADCK3, an ancestral kinase, is mutated in a form of recessive ataxia associated with coenzyme Q_{10} deficiency. *Am. J. Hum. Genet.* **82**, 661–672, https://doi.org/10.1016/j.ajhg.2007.12.024

102 Mollet, J., Delahodde, A., Serre, V., Chretien, D., Schlemmer, D., Lombes, A. et al. (2008) *CABC1* gene mutations cause ubiquinone deficiency with cerebellar ataxia and seizures. *Am. J. Hum. Genet.* **82**, 623–630, https://doi.org/10.1016/j.ajhg.2007.12.022

103 Hsieh, E.J., Gin, P., Gulmezian, M., Tran, U.C., Saiki, R., Marbois, B.N. et al. (2007) *Saccharomyces cerevisiae* Coq9 polypeptide is a subunit of the mitochondrial coenzyme Q biosynthetic complex. *Arch. Biochem. Biophys.* **463**, 19–26, https://doi.org/10.1016/j.abb.2007.02.016

104 Duncan, A.J., Bitner-Glindzicz, M., Meunier, B., Costello, H., Hargreaves, I.P., Lopez, L.C. et al. (2009) A nonsense mutation in *COQ9* causes autosomal-recessive neonatal-onset primary coenzyme Q_{10} deficiency: a potentially treatable form of mitochondrial disease. *Am. J. Hum. Genet.* **84**, 558–566, https://doi.org/10.1016/j.ajhg.2009.03.018

105 Hayashi, K., Ogiyama, Y., Yokomi, K., Nakagawa, T., Kaino, T. and Kawamukai, M. (2014) Functional conservation of coenzyme Q biosynthetic genes among yeasts, plants, and humans. *PLoS ONE* **9**, e99038, https://doi.org/10.1371/journal.pone.0099038

106 He, C.H., Black, D.S., Allan, C.M., Meunier, B., Rahman, S. and Clarke, C.F. (2017) Human COQ9 rescues a *coq9* yeast mutant by enhancing coenzyme Q biosynthesis from 4-hydroxybenzoic acid and stabilizing the CoQ-synthome. *Front. Physiol.* **8**, 463, https://doi.org/10.3389/fphys.2017.00463

107 Danhauser, K., Herebian, D., Haack, T.B., Rodenburg, R.J., Strom, T.M., Meitinger, T. et al. (2016) Fatal neonatal encephalopathy and lactic acidosis caused by a homozygous loss-of-function variant in COQ9. *Eur. J. Hum. Genet.* **24**, 450–454, https://doi.org/10.1038/ejhg.2015.133

108 Herebian, D., Seibt, A., Smits, S. H.J., Bunning, G., Freyer, C., Prokisch, H. et al. (2017) Detection of 6-demethoxyubiquinone in CoQ_{10} deficiency disorders: Insights into enzyme interactions and identification of potential therapeutics. *Mol. Genet. Metab.* **121**, 216–223, https://doi.org/10.1016/j.ymgme.2017.05.012

109 Luna-Sanchez, M., Diaz-Casado, E., Barca, E., Tejada, M.A., Montilla-Garcia, A., Cobos, E.J. et al. (2015) The clinical heterogeneity of coenzyme Q_{10} deficiency results from genotypic differences in the *Coq9* gene. *EMBO Mol. Med.* **7**, 670–687, https://doi.org/10.15252/emmm.201404632

110 Allan, C.M., Hill, S., Morvaridi, S., Saiki, R., Johnson, J.S., Liau, W.S. et al. (2013) A conserved START domain coenzyme Q-binding polypeptide is required for efficient Q biosynthesis, respiratory electron transport, and antioxidant function in *Saccharomyces cerevisiae*. *Biochim. Biophys. Acta* **1831**, 776–791, https://doi.org/10.1016/j.bbalip.2012.12.007

111 Barros, M.H., Johnson, A., Gin, P., Marbois, B.N., Clarke, C.F. and Tzagoloff, A. (2005) The *Saccharomyces cerevisiae COQ10* gene encodes a START domain protein required for function of coenzyme Q in respiration. *J. Biol. Chem.* **280**, 42627–42635, https://doi.org/10.1074/jbc.M510768200

112 Busso, C., Bleicher, L., Ferreira, J.R. and Barros, M.H. (2010) Site-directed mutagenesis and structural modeling of Coq10p indicate the presence of a tunnel for coenzyme Q_6 binding. *FEBS Lett.* **584**, 1609–1614, https://doi.org/10.1016/j.febslet.2010.03.024

113 Cui, T.Z. and Kawamukai, M. (2009) Coq10, a mitochondrial coenzyme Q binding protein, is required for proper respiration in *Schizosaccharomyces pombe*. *FEBS J.* **276**, 748–759, https://doi.org/10.1111/j.1742-4658.2008.06821.x

114 Shen, Y., Goldsmith-Fischman, S., Atreya, H.S., Acton, T., Ma, L., Xiao, R. et al. (2005) NMR structure of the 18 kDa protein CC1736 from *Caulobacter crescentus* identifies a member of the START domain superfamily and suggests residues mediating substrate specificity. *Proteins* **58**, 747–750, https://doi.org/10.1002/prot.20365

115 Perocchi, F., Jensen, L.J., Gagneur, J., Ahting, U., von Mering, C., Bork, P. et al. (2006) Assessing systems properties of yeast mitochondria through an interaction map of the organelle. *PLoS Genet.* **2**, e170, https://doi.org/10.1371/journal.pgen.0020170

116 Marchler-Bauer, A., Zheng, C., Chitsaz, F., Derbyshire, M.K., Geer, L.Y., Geer, R.C. et al. (2013) CDD: conserved domains and protein three-dimensional structure. *Nucleic Acids Res.* **41**, D348–D352, https://doi.org/10.1093/nar/gks1243

117 Rossmann, M.G., Moras, D. and Olsen, K.W. (1974) Chemical and biological evolution of nucleotide-binding protein. *Nature* **250**, 194–199, https://doi.org/10.1038/250194a0

118 Pagliarini, D.J., Calvo, S.E., Chang, B., Sheth, S.A., Vafai, S.B., Ong, S.E. et al. (2008) A mitochondrial protein compendium elucidates complex I disease biology. *Cell* **134**, 112–123, https://doi.org/10.1016/j.cell.2008.06.016

119 Hirst, J. (2011) Why does mitochondrial complex I have so many subunits? *Biochem. J.* **437**, e1–e3, https://doi.org/10.1042/BJ20110918

120 Stroud, D.A., Formosa, L.E., Wijeyeratne, X.W., Nguyen, T.N. and Ryan, M.T. (2013) Gene knockout using transcription activator-like effector nucleases (TALENs) reveals that human NDUFA9 protein is essential for stabilizing the junction between membrane and matrix arms of complex I. *J. Biol. Chem.* **288**, 1685–1690, https://doi.org/10.1074/jbc.C112.436766

121 Leshinsky-Silver, E., Lev, D., Tzofi-Berman, Z., Cohen, S., Saada, A., Yanoov-Sharav, M. et al. (2005) Fulminant neurological deterioration in a neonate with Leigh syndrome due to a maternally transmitted missense mutation in the mitochondrial ND3 gene. *Biochem. Biophys. Res. Commun.* **334**, 582–587, https://doi.org/10.1016/j.bbrc.2005.06.134

122 van den Bosch, B.J., Gerards, M., Sluiter, W., Stegmann, A.P., Jongen, E.L., Hellebrekers, D.M. et al. (2012) Defective NDUFA9 as a novel cause of neonatally fatal complex I disease. *J. Med. Genet.* **49**, 10–15, https://doi.org/10.1136/jmedgenet-2011-100466

123 Kuhl, I., Miranda, M., Atanassov, I., Kuznetsova, I., Hinze, Y., Mourier, A. et al. (2017) Transcriptomic and proteomic landscape of mitochondrial dysfunction reveals secondary coenzyme Q deficiency in mammals. *Elife* **6**, https://doi.org/10.7554/eLife.30952

124 Yubero, D., Montero, R., Martin, M.A., Montoya, J., Ribes, A., Grazina, M. et al. (2016) Secondary coenzyme Q_{10} deficiencies in oxidative phosphorylation (OXPHOS) and non-OXPHOS disorders. *Mitochondrion* **30**, 51–58, https://doi.org/10.1016/j.mito.2016.06.007

APPENDIX IV

Human COQ10A and COQ10B are distinct lipid-binding START domain proteins required for coenzyme Q function

Human COQ10A and COQ10B are distinct lipid-binding START domain proteins required for coenzyme Q function[S]

Hui S. Tsui,* Nguyen V. B. Pham,* Brendan R. Amer,* Michelle C. Bradley,* Jason E. Gosschalk,*,† Marcus Gallagher-Jones,* Hope Ibarra,* Robert T. Clubb,* Crysten E. Blaby-Haas,§ and Catherine F. Clarke[1,*]

Department of Chemistry and Biochemistry and Molecular Biology Institute,* and UCLA-Department of Energy Institute of Genomics and Proteomics,† University of California, Los Angeles, Los Angeles, CA 90095; and Department of Biology,§ Brookhaven National Laboratory, Upton, NY 11973

Abstract **Coenzyme Q (CoQ or ubiquinone) serves as an essential redox-active lipid in respiratory electron and proton transport during cellular energy metabolism. CoQ also functions as a membrane-localized antioxidant protecting cells against lipid peroxidation. CoQ deficiency is associated with multiple human diseases; CoQ_{10} supplementation in particular has noted cardioprotective benefits. In *Saccharomyces cerevisiae*, Coq10, a putative START domain protein, is believed to chaperone CoQ to sites where it functions. Yeast *coq10* deletion mutants (*coq10Δ*) synthesize CoQ inefficiently during log phase growth and are respiratory defective and sensitive to oxidative stress. Humans have two orthologs of yeast *COQ10*, *COQ10A* and *COQ10B*. Here, we tested the human co-orthologs for their ability to rescue the yeast mutant. We showed that expression of either human ortholog, COQ10A or COQ10B, rescues yeast *coq10Δ* mutant phenotypes, restoring the function of respiratory-dependent growth on a nonfermentable carbon source and sensitivity to oxidative stress induced by treatment with PUFAs. These effects indicate a strong functional conservation of Coq10 across different organisms. However, neither COQ10A nor COQ10B restored CoQ biosynthesis when expressed in the yeast *coq10Δ* mutant. The involvement of yeast Coq10 in CoQ biosynthesis may rely on its interactions with another protein, possibly Coq11, which is not found in humans. Coexpression analyses of yeast *COQ10* and human *COQ10A* and *COQ10B* provide additional insights to functions of these START domain proteins and their potential roles in other biologic pathways.**—Tsui, H. S., N. V. B. Pham, B. R. Amer, M. C. Bradley, J. E. Gosschalk, M. Gallagher-Jones, H. Ibarra, R. T. Clubb, C. E. Blaby-Haas, and C. F. Clarke. **Human COQ10A and COQ10B are distinct lipid-binding START domain proteins required for coenzyme Q function. *J. Lipid Res.* 2019.** 60: **1293–1310.**

Supplementary key words antioxidants • lipids/chemistry • lipids/peroxidation • mass spectrometry • mitochondria • *Saccharomyces cerevisiae* • ubiquinone • steroidogenic acute regulatory protein-related lipid transfer

Coenzyme Q (CoQ) is a lipid composed of a fully substituted redox-active benzoquinone ring attached to a long polyisoprenoid chain. The polyisoprenoid chain of CoQ_n, with $n \geq 6$ isoprene units, anchors CoQ at the mid-plane of the membrane phospholipid bilayers. The reversible reduction and oxidation of CoQ and $CoQH_2$ enables the transport of electrons and protons necessary for cellular respiration. CoQ also serves as an important electron acceptor for enzymes involved in fatty acid β-oxidation, oxidation of proline and sulfide, and pyrimidine biosynthesis (1–3). The reduced or hydroquinone form of $CoQH_2$ serves as a chain-terminating antioxidant that slows lipid peroxidation (2).

Although CoQ exists in most biological membranes, its synthesis occurs exclusively inside the mitochondria in eukaryotes, or in the cytosol in *Escherichia coli*, catalyzed by a cohort of enzymes, many of which are organized in a complex known as the CoQ synthome (also known as complex Q) in eukaryotes, or the Ubi metabolon in *E. coli* (4–6). In *Saccharomyces cerevisiae*, currently known members of the

This work was supported by National Science Foundation Grant MCB-1330803 (to C.F.C.) and National Institutes of Health Grant T32 GM 008496 (to H.S.T. and M.C.B.). C.E.B-H. is supported by the U.S. Department of Energy, Office of Science, Office of Biological and Environmental Research. M.G-J. is supported by the Quantitative and Computational Biosciences Collaboratory Postdoctoral Fellowship. The content is solely the responsibility of the authors and does not necessarily represent the official views of the National Institutes of Health.

Manuscript received 25 February 2019 and in revised form 12 April 2019.

Published, JLR Papers in Press, May 2, 2019
DOI https://doi.org/10.1194/jlr.M093534

Abbreviations: BN/SDS-PAGE, Blue Native/SDS-PAGE; CoQ, coenzyme Q or ubiquinone; $CoQH_2$, reduced coenzyme QH_2 hydroquinone or ubiquinol; CoQ_n, coenzyme Q_n or ubiquinone-n (refers to a specific isoform of CoQ_n, where n designates the number of isoprene units in the tail of CoQ_n, e.g., CoQ_6 in *Saccharomyces cerevisiae* or CoQ_{10} in humans); DMQ_6H_2, demethoxy-Q_6H_2; DMQ_8, demethoxy-coenzyme Q_8; ERMES, ER-mitochondria encounter structure; HAB, 4-amino-3-hexaprenylbenzoic acid; 4HB, 4-hydroxybenzoic acid; HHB, 4-hydroxy-3-hexaprenylbenzoic acid; $IDMQ_6H_2$, 4-imino-demethoxy-Q_6H_2; MFN, mitofusin; MLN64, metastatic lymph node 64; MSA, multiple sequence alignment; pABA, *para*-aminobenzoic acid; ROS, reactive oxygen species; SD-Complete, synthetic dextrose/minimal-complete; SDR, short-chain dehydrogenase/reductase; SD-Ura, synthetic dextrose/minimal minus uracil; START, steroidogenic acute regulatory protein-related lipid transfer.

[1] To whom correspondence should be addressed.
e-mail: cathy@chem.ucla.edu

[S] The online version of this article (available at http://www.jlr.org) contains a supplement.

CoQ synthome consist of Coq3–Coq9 and Coq11 (4, 5). Together, they modify the quinone head group through a series of methylation (Coq3 and Coq5), deamination (Coq6, Coq9), and hydroxylation (Coq6, Coq7, Coq9) reactions (4, 5). The definitive functions of the remaining members of the CoQ synthome (Coq4, Coq8, and Coq11) are yet to be fully characterized. Attachment of the polyisoprenoid chain to the aromatic ring precursor precedes the ring modification steps. Coq1, a hexaprenyl pyrophosphate synthetase, condenses farnesyl pyrophosphate with three molecules of isopentenyl pyrophosphate to form hexaprenyldiphosphate, which is transferred to the 4-hydroxybenzoic acid (4HB) or *para*-aminobenzoic acid (pABA) ring at the C3 position by Coq2 (4, 5). The number of isoprene units (n) in the polyisoprenoid chain of CoQ_n varies between organisms, as determined by the specific polyprenyl diphosphate synthase (7), and consists of six isoprene units in *S. cerevisiae* (CoQ_6), eight isoprene units in *E. coli* (CoQ_8), and predominantly ten isoprene units in *Schizosaccharomyces pombe* and humans (CoQ_{10}) (8). Each of the yeast *coq1Δ–coq9Δ* mutants shows complete abolishment of CoQ_6 biosynthesis and fails to respire (5). Their defects in respiration can be readily restored by exogenous supplementation with CoQ_6 (5).

The *coq10Δ* mutant is unusual among the yeast *coq* mutants because it produces wild-type content of CoQ_6 at stationary phase, yet its de novo synthesis of CoQ_6 during log phase is inefficient (9, 10). Despite having normal or nearly normal steady state levels of CoQ_6, the *coq10Δ* mutant displays a respiratory-deficient phenotype shown by anemic growth on medium containing a nonfermentable carbon source and decreased NADH and succinate oxidase activities (10). In addition, the *coq10Δ* mutant is sensitive to lipid peroxidation induced by exogenously added PUFAs (9). Thus, the CoQ_6 present in the *coq10Δ* mutant is not utilized efficiently for either respiration or for its function as an antioxidant.

The NMR structure of CC1736, a Coq10 ortholog in *Caulobacter crescentus*, identified it as a member of the steroidogenic acute regulatory protein-related lipid transfer (START) domain superfamily (11). This family includes proteins that bind polycyclic compounds, such as cholesterol and polyketides, in a signature hydrophobic cavity (11). The START domain typically spans ~210 residues (12) and folds into a helix-grip structure consisting of antiparallel β-sheets flanked by one α-helix on each side (13). START domain-containing proteins are primarily involved in nonvesicular transport of lipids between membranes (14). For instance, STARD4 is a START domain protein that binds and transports cholesterol from the plasma membrane to mitochondria, the ER, and the endocytic recycling compartment, equilibrating cholesterol content among cellular membranes to fit their biophysical properties and physiological needs (15). Purified CC1736 binds to CoQ_n with variable polyisoprenoid chain lengths and to the farnesylated analog of a late-stage CoQ intermediate, demethoxy-CoQ_3 (DMQ_3) (9). Coq10 polypeptides isolated from *S. cerevisiae* and *S. pombe* copurify with CoQ_6 and CoQ_{10}, respectively (10, 16). Similarly, CoQ_8 copurifies with the *S. pombe* Coq10 polypeptide expressed in *E. coli* (16). These observations have led to the current hypothesis that the Coq10 polypeptide is a putative CoQ_n chaperone, necessary for delivering CoQ from its site of synthesis and/or the pool of free CoQ to sites of function.

Complex III inhibitors, antimycin A and myxothiazol, enhance reactive oxygen species (ROS) formation by blocking oxidation of cytochrome b_H at the N-site or inhibiting reduction of cytochrome b_L at the P-site, respectively (17–19). Thereby, antimycin A induces ROS through reverse electron flow from cytochrome b_L to CoQ to form the semiquinone radical (20), whereas myxothiazol-dependent ROS production results from incomplete $CoQH_2$ oxidation by slow reduction of the Rieske iron-sulfur protein (18, 19). Mitochondria isolated from yeast *coq10Δ* produce significantly elevated ROS in the presence of antimycin A, but not myxothiazol, suggesting that in the absence of the Coq10 polypeptide, electron transfer from $CoQH_2$ to the Rieske iron-sulfur protein is defective (20). This specific requirement for the presence of the Coq10 START domain polypeptide for functional electron transfer by complex III is further substantiated by the binding of both oxidized and reduced forms of a photo-reactive azido-quinone probe to the Coq10 polypeptide (21).

CoQ deficiencies are associated with human disease and the beneficial effects of CoQ_{10} supplementation in therapeutic regimens are increasingly appreciated (1, 4). Mutations in several genes encoding CoQ biosynthetic enzymes result in primary CoQ deficiency and cause encephalopathy, cerebellar ataxia, cardiomyopathy, nephrotic syndrome, and myopathy (1, 4). CoQ deficiency can also occur secondary to mutations in aprataxin, electron transfer flavoprotein dehydrogenase, or serine/threonine-protein kinase B-Raf (3). CoQ_{10} supplementation rescues the proteinuria in patients with nephrotic syndrome, provided that therapy is initiated early (22). Patients who develop myalgia under statin administration are often prompted to take CoQ_{10} supplements to mitigate adverse symptoms (23). Long term CoQ_{10} treatment has also been shown to improve symptoms and reduce major adverse cardiovascular events when it is used as adjunctive treatment in patients with chronic heart failure (24, 25).

Yeast is a superb model organism in which to study CoQ biosynthesis because many of the enzymes involved in CoQ biosynthesis are functionally conserved from yeast to humans (4, 5). In this work, we test the human co-orthologs of yeast Coq10, COQ10A and COQ10B, for their ability to complement the yeast *coq10Δ* mutant. We show that expression of human COQ10A or COQ10B rescues yeast *coq10Δ*-defective respiration and its sensitivity to oxidative stress, and restores steady-state levels of Coq polypeptides. However, neither COQ10A nor COQ10B expression is able to stabilize the yeast CoQ synthome or rescue the partial defect in de novo CoQ_6 biosynthesis characteristic of the yeast *coq10Δ* mutant.

MATERIALS AND METHODS

Yeast strains and growth media

S. cerevisiae strains used in this study are described in **Table 1**. Growth media for yeast included YPD (1% Bacto yeast extract, 2% Bacto peptone, 2% dextrose), YPG (1% Bacto yeast extract, 2%

TABLE 1. Genotype and source of yeast strains

Strain	Genotype[a]	Source
W303 1B	MAT α, *ade2-1 can1-100 his3-11,15 leu2-3,112 trp1-1 ura3-1*	R. Rothstein[b]
W303 *coq1Δ*	MAT α, *ade2-1 can1-100 his3-11,15 leu2-3,112 trp1-1 ura3-1 coq1::LEU2*	(99)
CC303	MAT α, *ade2-1 can1-100 his3-11,15 leu2-3,112 trp1-1 ura3-1 coq3::LEU2*	(100)
W303 *coq4Δ*	MAT **a**, *ade2-1 can1-100 his3-11,15 leu2-3,112 trp1-1 ura3-1 coq4::TRP1*	(101)
W303 *coq5Δ*	MAT α, *ade2-1 can1-100 his3-11,15 leu2-3,112 trp1-1 ura3-1 coq5::HIS3*	(27)
W303 *coq6Δ*	MAT **a**, *ade2-1 can1-100 his3-11,15 leu2-3,112 trp1-1 ura3-1 coq6::LEU2*	(102)
W303 *coq7Δ*	MAT α, *ade2-1 can1-100 his3-11,15 leu2-3,112 trp1-1 ura3-1 coq7::LEU2*	(103)
W303 *coq8Δ*	MAT **a**, *ade2-1 can1-100 his3-11,15 leu2-3,112 trp1-1 ura3-1 coq8::HIS3*	(101)
W303 *coq9Δ*	MAT α, *ade2-1 can1-100 his3-11,15 leu2-3,112 trp1-1 ura3-1 coq9::URA3*	(104)
W303 *coq10Δ*	MAT **a**, *ade2-1 can1-100 his3-11,15 leu2-3,112 trp1-1 ura3-1 coq10::HIS3*	(10)
W303 *coq11Δ*	MAT **a**, *ade2-1 can1-100 his3-11,15 leu2-3,112 trp1-1 ura3-1 coq11::HIS3*	This study

[a]Mating type **a** (MAT **a**) is in bold to distinguish it from mating type α (MAT α).
[b]Dr. Rodney Rothstein, Department of Human Genetics, Columbia University, New York, NY.

Bacto peptone, 3% glycerol), and YPGal (1% Bacto yeast extract, 2% Bacto peptone, 2% galactose, 0.1% dextrose) (26). Synthetic dextrose/minimal-complete (SD-Complete) and synthetic dextrose/minimal minus uracil (SD-Ura) [0.18% Difco yeast nitrogen base without amino acids and ammonium sulfate, 0.5% $(NH_4)_2SO_4$, 0.14% NaH_2PO_4, 2% dextrose, complete amino acid supplement, or amino acid supplement lacking uracil] were prepared as described (27). Solid media contained an additional 2% Bacto agar.

Construction of single- and multi-copy yeast expression vectors of human COQ10A and COQ10B

Plasmids used in this study are listed in **Table 2**. Generation of single-copy (pQM) and multi-copy (pRCM) yeast expression vectors was previously described (9, 28). Both pQM and pRCM contain the yeast *CYC1* promoter and the first 35 residues of the yeast *COQ3* ORF, corresponding to the proposed Coq3 mitochondrial leader sequence to direct import of human proteins into yeast mitochondria. To generate the single- and multi-copy yeast expression vectors of human COQ10A, the human *COQ10A* ORF (mRNA #1, Fig. 1A), encoding residues 44-247, was PCR amplified from pHCOQ10/ST1 (10) with primers 5′-ggccATCGATATGAGGTTTCTGACCTCCTGC-3′ and 5′-ggccGGTACCTCAAGTCTGGTGCACCTC-3′, and cloned into pQM and pRCM vectors using the restriction enzymes, *Cla*I and *Kpn*I (New England BioLabs), to generate pQM COQ10A and pRCM COQ10A, respectively. Similarly, full-length human *COQ10B* ORF (mRNA #1, Fig. 1A), encoding residues 1-238, was PCR amplified from COQ10B cDNA clone (GeneCopoeia) with primers 5′-ggccATCGATATGGCAGCTCGGACTGGTCAT-3′ and 5′-ggccGGTACCTTATGTGTGATGGACTTCATGAAGCATTAACTCC-3′ to generate pQM COQ10B and pRCM COQ10B.

Complementation of yeast *coq10Δ* by human COQ10A and COQ10B

Each of the following plasmids, pQM (empty vector), pQM COQ10A, pQM COQ10B, pRCM (empty vector), pRCM COQ10A, and pRCM COQ10B, was transformed into wild-type W303 or *coq10Δ*, and the transformed cells were selected on SD-Ura plates as described (29). A single colony from each SD-Ura plate was inoculated in SD-Ura liquid medium. Wild-type W303 and *coq10Δ* were each inoculated in SD-Complete liquid medium. Cultures were incubated overnight at 30°C 250 rpm. The overnight cultures were diluted to 0.2 OD_{600}/ml with sterile water, from which a series of 5-fold dilutions were prepared. An aliquot of 2 μl of sample from the dilution series was plated onto YPD and YPG plate medium and incubated at 30°C. Pictures were taken after 3–4 days.

TABLE 2. Yeast expression vectors

Plasmid	Relevant Genes/Markers	Source
pQM	pAH01 with *COQ3* mito leader, single-copy	(28)
pQM COQ10A	pQM with human *COQ10A*; single-copy	This work
pQM COQ10B	pQM with human *COQ10B*; single-copy	This work
pRCM	pCH1 with *COQ3* mito leader; multi-copy	(9)
pRCM COQ10A	pRCM with human *COQ10A*; multi-copy	This work
pRCM COQ10B	pRCM with human *COQ10B*; multi-copy	This work

Fatty acid sensitivity assay

A fatty acid sensitivity assay was performed as described (30, 31) with slight modifications. Briefly, yeast W303 wild-type, *cor1Δ*, *coq9Δ*, and *coq10Δ* were inoculated in SD-Complete liquid medium, and *coq10Δ*s harboring the designated plasmids were inoculated in SD-Ura liquid medium and incubated overnight at 30°C 250 rpm. Overnight cultures were back diluted to 0.2 OD_{600}/ml with fresh SD-Complete or SD-Ura liquid medium and incubated for 6 h at 30°C 250 rpm to logarithmic phase. The cells were harvested, washed twice with sterile water, and suspended in 0.1 M phosphate buffer with 0.2% dextrose (pH 6.2) to a cell density of 0.2 OD_{600}/ml. To test yeast sensitivity to PUFA-induced oxidative stress, ethanol-diluted oleic acid (Nu-Chek Prep) or α-linolenic acid (Nu-Check Prep) was added to aliquots of 5 ml cell suspension in phosphate buffer with 0.2% dextrose to a final concentration of 200 μM. Identical 5 ml cell suspensions were prepared with 0.1% (v/v) ethanol as a vehicle control. After a 4 h incubation at 30°C 250 rpm, cell viability was assessed with plate dilution assay by spotting 2 μl of sample from a series of 5-fold dilution onto YPD plates. Cell viability was also ascertained before addition of fatty acids, and labeled as 0 h.

Mitochondria isolation from yeast *coq10Δ* expressing human COQ10A or COQ10B

Precultures of yeast *coq10Δ* transformed with pQM COQ10A, pQM COQ10B, pRCM COQ10A, or pRCM COQ10B in YPD were back diluted with YPGal and grown overnight at 30°C 250 rpm until the cell density had reached ~3.0 OD_{600}/ml. Preparation of spheroplasts with Zymolyase-20T (MP Biomedicals) and extraction of mitochondria in the presence of Complete EDTA-free protease inhibitor mixture (Roche), phosphatase inhibitor cocktail set II (EMD Millipore), and phosphatase inhibitor cocktail set 3 (Sigma-Aldrich) over Nycodenz (Sigma-Aldrich) density gradient were previously described (32). Purified mitochondria were flash-frozen in liquid nitrogen and stored at −80°C until use.

Immunoblot analysis of steady state Coq polypeptide levels

Protein concentration in gradient-purified mitochondria was measured by the BCA assay (Thermo Fisher Scientific). Purified mitochondria were resuspended in SDS sample buffer [50 mM Tris

(pH 6.8), 10% glycerol, 2% SDS, 0.1% bromophenol blue, and 1.33% β-mercaptoethanol], and an aliquot of 25 μg of mitochondrial protein from each sample was loaded in individual lanes and separated by SDS gel electrophoresis on 12% Tris-glycine polyacrylamide gels. Proteins were subsequently transferred to 0.45 μm nitrocellulose membrane (Bio-Rad) and blocked with blocking buffer (0.5% BSA, 0.1% Tween 20, 0.02% SDS in phosphate-buffered saline). Representative Coq polypeptides and mitochondrial malate dehydrogenase Mdh1 (loading control) were detected with rabbit polyclonal antibodies prepared in blocking buffer at the dilutions listed in **Table 3**. Polyclonal antibodies against human COQ10A (Proteintech) and COQ10B (Abcam) were commercially obtained and used at dilutions recommended by the companies. The secondary IRDye 680LT goat anti-rabbit IgG antibody (LiCOR) was used at 1:10,000 dilution in the same blocking buffer. Immunoblot images were visualized with a LiCOR Odyssey infrared scanner (LiCOR), and relative protein levels were quantified by band densitometry using ImageJ software (https://imagej.nih.gov/ij/).

Analysis of high molecular weight complexes with two-dimensional Blue Native/SDS-PAGE

Two-dimensional Blue Native/SDS-PAGE (BN/SDS-PAGE) was performed as described (33–35). Purified mitochondria at 4 mg/ml were solubilized for 1 h in ice-cold solubilization buffer [11 mM HEPES (pH 7.4), 0.33 M sorbitol, 1× NativePAGE sample buffer (Thermo Fisher Scientific), 16 mg/ml digitonin (Biosynth)] in the presence of the previously described mixtures of protease and phosphatase inhibitors. After centrifugation (100,000 *g*, 10 min), the protein concentration in the soluble fraction was measured by BCA assay, and NativePAGE 5% G-250 sample additive (Thermo Fisher Scientific) was added to the soluble fraction to a final concentration of 0.25%. Soluble protein from each sample (80 μg) was separated on NativePAGE 4–16% Bis-Tris gel (Thermo Fisher Scientific) in the first dimension, followed by separation on 12% Tris-glycine polyacrylamide gel in the second dimension. The molecular weight standards for Blue Native gel electrophoresis and SDS gel electrophoresis were obtained from GE Healthcare (Sigma-Aldrich) and Bio-Rad, respectively. Immunoblot analysis of the CoQ synthome was performed as described above using antibodies against Coq4 and Coq9. A separate COQ10A- or COQ10B-containing complex was detected using commercial antibodies against COQ10A and COQ10B, respectively.

Analyses of de novo and steady state levels of CoQ_6 and CoQ_6-intermediates

Metabolic labeling with $^{13}C_6$-labeled ring precursors and subsequent analyses of labeled and unlabeled CoQ_6 and CoQ_6-intermediates in yeast whole-cell lipid extract by RP-HPLC MS/MS were previously described (9, 36). Briefly, overnight cultures of yeast wild-type, *coq10Δ* in SD-Complete medium, and *coq10Δ* expressing pQM, pQM COQ10A, pQM COQ10B, pRCM, pRCM COQ10A, or pRCM COQ10B in SD-Ura medium were back diluted with fresh SD-Complete or SD-Ura medium to 0.1 OD_{600}/ml and grown to 0.5 OD_{600}/ml (early-log phase) at 30°C 250 rpm. The $^{13}C_6$-labeled precursors, pABA or 4HB, were dissolved in ethanol and added to yeast cultures at a final concentration of 5 μg/ml (equivalent to 34.9 μM $^{13}C_6$-pABA and 34.7 μM $^{13}C_6$-4HB). Vehicle control samples contained a final concentration of 0.1% (v/v) ethanol. The cultures were incubated with the labeled precursors or ethanol for 5 h at 30°C 250 rpm before triplicates of 5 ml culture were harvested for lipid extraction. The cell density measured by OD_{600} at the time of harvest was recorded.

For lipid extraction, collected yeast cell pellets were dissolved in 2 ml of methanol, and lipids were extracted twice in the presence of internal standard CoQ_4, each time with 2 ml of petroleum ether followed by vigorous vortex. The organic phase from two extractions was combined and dried under a stream of N_2 gas. A series of CoQ_6 standards (Avanti) containing CoQ_4 were prepared and lipid extracted concurrently with yeast samples to construct a CoQ_6 standard curve. The dried lipids were reconstituted in 200 μl of 0.5 mg/ml benzoquinone prepared in ethanol to oxidize all lipid species for MS analysis with a 4000 QTRAP linear MS/MS spectrometer (Applied Biosystems). Aliquots (20 μl) of each reconstituted lipid extract were injected into a Luna phenyl-hexyl column (100 × 4.6 mm, 5 μm; Phenomenex). The HPLC mobile phase consisted of solvent A (95:5 methanol/isopropanol, 2.5 mM ammonium formate) and solvent B (isopropanol, 2.5 mM ammonium formate). As the percentage of solution B was increased linearly from 0% to 10%, representative CoQ_6 and CoQ_6-intermediates eluted off the column at distinct retention times and were monitored under multiple reaction monitoring mode scanning the precursor to product ion transitions listed in **Table 4**. For each analyte, the precursor to product ion transitions of both protonated ion species and its ammonium adduct ion species were tracked. The ammonium adducts provide much stronger ion signals for detection of isoprenoids by positive-ion electrospray ionization MS. Analyst 1.4.2 software (Applied Biosystems) was used for data acquisition and processing. In each sample, the amount of CoQ_6 and CoQ_6-intermediates was calculated from the sum of peak areas of each analyte and its corresponding ammonium adduct at a specific retention time, corrected for the recovery of internal standard CoQ_4. Statistical analyses were performed using GraphPad Prism with two-way ANOVA multiple comparisons comparing the mean of each sample to the mean of its corresponding empty vector control, and comparing the mean of wild-type to the mean of *coq10Δ*.

TABLE 3. Description and source of antibodies

Antibody	Working Dilution	Source
Coq1	1:10,000	(99)
Coq3	1:200	(105)
Coq4	1:2,000	(106)
Coq5	1:5,000	(107)
Coq6	1:200	(102)
Coq7	1:1,000	(108)
Coq8	Affinity purified, 1:30	(63)
Coq9	1:1,000	(109)
Coq10	Affinity purified, 1:400	This work
Coq11	1:500	This work
Mdh1	1:10,000	L. McAlister-Henn[a]
COQ10A	1:500	Proteintech
COQ10B	1 μg/ml	Abcam

[a]Dr. Lee McAlister-Henn, Department of Molecular Biophysics and Biochemistry, University of Texas Health Sciences Center, San Antonio, TX.

TABLE 4. Precursor-to-product ion transitions

	m/z $[M+H]^+$	m/z $[M+NH_4]^+$
HAB	546.4/150.0	563.0/150.0
$^{13}C_6$-HAB	552.4/156.0	569.0/156.0
HHB	547.4/151.0	564.0/151.0
$^{13}C_6$-HHB	553.4/157.0	570.4/157.0
DMQ_6	561.4/167.0	578.0/167.0
$^{13}C_6$-DMQ_6	567.4/173.0	584.0/173.0
$IDMQ_6$	560.6/166.0	577.0/166.0
$^{13}C_6$-$IDMQ_6$	566.6/172.0	583.0/172.0
CoQ_4	455.4/197.0	472.0/197.0
CoQ_6	591.4/197.0	608.0/197.0
$^{13}C_6$-CoQ_6	597.4/203.0	614.0/203.0

Homology modeling of human COQ10A and COQ10B

Secondary structural elements and disordered regions within the COQ10A and COQ10B ORFs were predicted using PsiPred (37) and DisoPred (38). Secondary structural alignments and initial model generation were performed using the SwissModel server (39). Using COQ10A as the query sequence, 50 homologous protein templates were identified with sequence identities ranging from 6.94% to 28.68%, and sequence similarity between 25% and 30%. Nine templates with the best alignment of the secondary structural elements were selected for model building in SwissModel. Of the nine models generated, four models with either low QMEAN scores or high identity to the template were selected for further improvement. As the sequence coverage of the models differs from each other, a combination of all four models was used to generate the final model that covers residues 87-228 of COQ10A. The final steps of model refinement, rebuilding strange loops, and improvement of side chain packing and backbone distortion were completed using custom script in PyRosetta (40). A total of 16,000 decoys were generated and the convergence of the refinement was assessed by checking RMSD of all decoys to the lowest energy decoy versus Rosetta energy. The top five decoys with the lowest Rosetta energy were selected and model quality was assessed via Qmean (41), Verify3D (42), Errat (43), and MolProbity (44). The decoy that scored equally well in all four metrics was chosen as the final model of COQ10A. A similar approach was used to create a homology model of COQ10B from a combination of six models that covered residues 79-219 of COQ10B.

Molecular docking of CC1736

Molecular docking was completed using Autodock vina (45), and substrate molecules were produced using phenix.ELBOW (46) and verified with phenix.REEL (46). Docking of each substrate was executed with a 20 × 20 × 20 Å grid box that encompassed the entirety of the hydrophobic pocket of CC1736. Docking was performed with an exhaustiveness of 18 and nine docking solutions were produced per run.

Yeast Coq10 ortholog similarity clustering and Coq10 coexpression analysis

The protein similarity network was constructed using the EFI-EST tool (http://efi.igb.illinois.edu/efi-est/) (47) with an alignment score of 30, with human COQ10A as the BLASTp seed sequence, retrieving 8,095 hits. Protein nodes were collapsed at >75% identity. The network was visualized with the yFiles organic layout provided with the Cytoscape software (48). The nodes in the network were colored by taxonomy as provided by the UniProt database (49). Information associated with proteins included in this analysis can be found in supplemental Table S2. Gene neighborhoods of bacterial homologs were retrieved with the EFI-GNT tool (https://efi.igb.illinois.edu/efi-gnt/). The phylogenetic analysis was performed using MAFFT (50) for sequence alignment and IQ Tree (51) as implemented on the CIPRES (52, 53) web portal with 1,000 bootstrap replicates (54). Before tree reconstruction, the multiple sequence alignment (MSA) was trimmed to remove poorly aligned sequence at the N terminus, and the edited MSA can be found in supplemental Table S2.

RESULTS

Expression of either COQ10A or COQ10B from humans restores respiratory growth of the yeast *coq10Δ* mutant

Human *COQ10A* and *COQ10B* are co-orthologs of yeast *COQ10* located on human chromosome 12 and chromosome 2, respectively (55). The polymorphisms in COQ10A (P79H, P231S) and COQ10B (L48F) are thought to be one of the genetic factors predisposing patients to statin-associated myopathy (56, 57). The underlying molecular mechanisms of statin-associated myopathy are proposed to be isoprenoid depletion, inhibition of CoQ biosynthesis, disruption of cholesterol homeostasis, or disturbance of calcium metabolism (58). *COQ10A* and *COQ10B* each contain six exons, which give rise to two isoforms of COQ10A and four isoforms of COQ10B as a result of alternative splicing and translation initiation (**Fig. 1A**). Each of the two *COQ10A* mRNA transcripts contains a unique 5′ UTR and translation initiation site (Fig. 1A, supplemental Table S1). According to the UniProt database (49), *COQ10A* mRNA #1 encodes the longer isoform of COQ10A, with the first 15 residues predicted to be the mitochondrial targeting sequence (supplemental Table S1). *COQ10A* mRNA #2 encodes COQ10A isoform 2 with a unique N terminus. Two of the *COQ10B* mRNA transcripts share an identical 5′ UTR and translation initiation site, whereas the other two *COQ10B* mRNA transcripts each have a unique 5′ UTR and translation initiation site (Fig. 1A, supplemental Table S1). Based on the UniProt database, *COQ10B* mRNA #1 encodes the longest isoform, and its mitochondrial targeting sequence consists of the first 37 residues (supplemental Table S1). COQ10B isoform 2 encoded by mRNA #2 lacks one of the exons present in mRNA #1 (Fig. 1A). COQ10B isoforms 3 and 4 contain distinct N-terminal sequences and their subcellular localization is unknown (Fig. 1A, supplemental Table S1). Although RNA processing predicts several isoforms of COQ10A and COQ10B, both isoforms of COQ10A and all four isoforms of COQ10B retain amino acid residues important for START domain formation.

Expression of human COQ10A from a multi-copy vector was previously shown to complement respiratory growth of the yeast *coq10Δ* mutant on a nonfermentable carbon source (10, 16). Here, we examined the functional complementation of the yeast *coq10Δ* by both single-copy (pQM) and multi-copy (pRCM) expression of human COQ10A or COQ10B. The cDNA expressed for COQ10A corresponded to residues 44-247 of isoform 1 (*COQ10A* mRNA #1), and the cDNA expressed for COQ10B corresponded to residues 1-238 of isoform 1 (*COQ10B* mRNA #1). Yeast *coq10Δ* and *coq10Δ* with empty vectors pQM or pRCM show slow growth on nonfermentable glycerol-containing medium (Fig. 1B). Expression of either COQ10A or COQ10B in single-copy or multi-copy rescued the glycerol growth of the *coq10Δ* mutant (Fig. 1B). Interestingly, single-copy COQ10A and both single- and multi-copy COQ10B seem to complement the defective growth of the *coq10Δ* mutant better as compared with multi-copy COQ10A (Fig. 1B). These results identify human COQ10A and COQ10B as functional co-orthologs of yeast Coq10.

Human COQ10A and COQ10B share low sequence identity but high structural similarity with other Coq10 orthologs

In vitro lipid binding assays have shown that the *C. crescentus* Coq10 ortholog, CC1736, binds to isoforms of CoQ_n

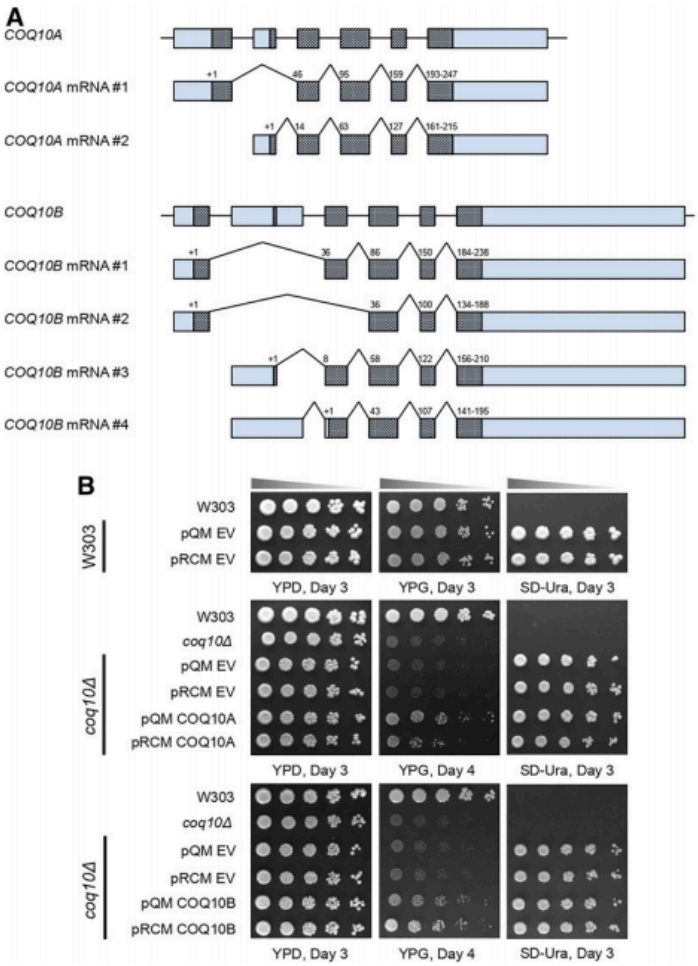

Fig. 1. Expression of either human COQ10A or COQ10B restores respiratory growth of the yeast *coq10Δ* mutant. A: A schematic representation of alternative splicing of human *COQ10A* and *COQ10B* mRNA. Alternative splicing and different translation initiation sites result in two isoforms of COQ10A and four isoforms of COQ10B. Boxes represent the exons, and the protein coding sequences are shaded within the exons. Both exons and the protein coding sequences were drawn relative to their corresponding number of base pairs. The introns are represented by horizontal lines and are not drawn to scale. The translation initiation sites were marked as "+1" on top of the protein coding sequence, and the numbers denote the amino acid residue numbers at the beginning of the coding sequence within each exon. The N-terminal sequences of all isoforms of COQ10A and COQ10B are listed in supplemental Table S1, with predicted mitochondria targeting sequence highlighted in bold. B: Wild-type W303, *coq10Δ* mutant, *coq10Δ* expressing single-copy (pQM), multi-copy (pRCM) human COQ10A, COQ10B, or their respective empty vectors were inoculated in SD-Complete or SD-Ura liquid medium overnight, from which a series of 5-fold dilutions of the overnight culture were prepared and plated on to YPD, YPG, and SD-Ura plate medium. Aliquots of 2 μl of samples from serial dilutions were plated in each spot, starting at 0.2 OD_{600}/ml in the first spot to the left. Pictures were taken 3–4 days after incubation at 30°C.

with varying polyisoprenoid chain length (n = 2, 3, 6, or 10) and to a farnesylated analog (n = 3) of a late-stage CoQ intermediate, DMQ_3 (9). CC1736 does not bind to a farnesylated analog of an early-stage CoQ intermediate, farnesylhydroxybenzoate (9). This observation strongly implies that the quinone moiety, but not the polyisoprenoid chain, is the structural determinant of Coq10 ligand interaction. Several amino acid residues have been identified through site-directed mutagenesis, and a substitution of these residues on Coq10 orthologs results in altered ligand-binding affinity and respiratory defects (9, 16, 21, 59). Among these residues, a combination of positive charge provided by residue K8, paired hydrophobic residues A55 and V70, and a salt bridge formed by E64 and K115 are thought to confer the ligand specificity of CC1736 (11). Mutations in the equivalent residues in *S. cerevisiae* Coq10 result in defects in respiration as measured by oxygen consumption, H_2O_2 release, or NADH-cytochrome *c* reductase activity (9, 59). Here, we constructed sequence alignment of four Coq10 orthologs and mapped these residues relative to positions in isoform 1 of the human COQ10A and COQ10B amino acid sequence (**Fig. 2A**). From the MSA, we noticed several additional conserved residues (shaded blue and lilac in Fig. 2A) besides those previously identified. Most noticeably, aromatic amino acids (tyrosine, phenylalanine, and tryptophan) and nonpolar amino acids (valine, leucine, and alanine) are highly enriched among these conserved residues (Fig. 2A). Residues F39 and P41 of *S. pombe* Coq10 are believed to be within the region for CoQ binding, and mutation of F39A and P41A reduces the photo-labeling yield with azido-quinone to about 50% of the wild-type control (21). Replacement of L63 or W104 with alanine on *S. pombe* Coq10 reduces CoQ binding affinity to about 50%, and a double point mutant further reduces the binding affinity to only 25% (16). Based on homology modeling, the N-terminal regions of human COQ10A and COQ10B do not seem to form defined secondary structure and were excluded from the predicted secondary structures shown in Fig. 2A. Thus, exon skipping in COQ10B isoform 2 (Fig. 1A) as well as variable N-terminal sequences on all COQ10A and COQ10B isoforms that result from alternative splicing and translation initiation (Fig. 1A) are not expected to change the secondary structural elements of the START domain of COQ10A and COQ10B.

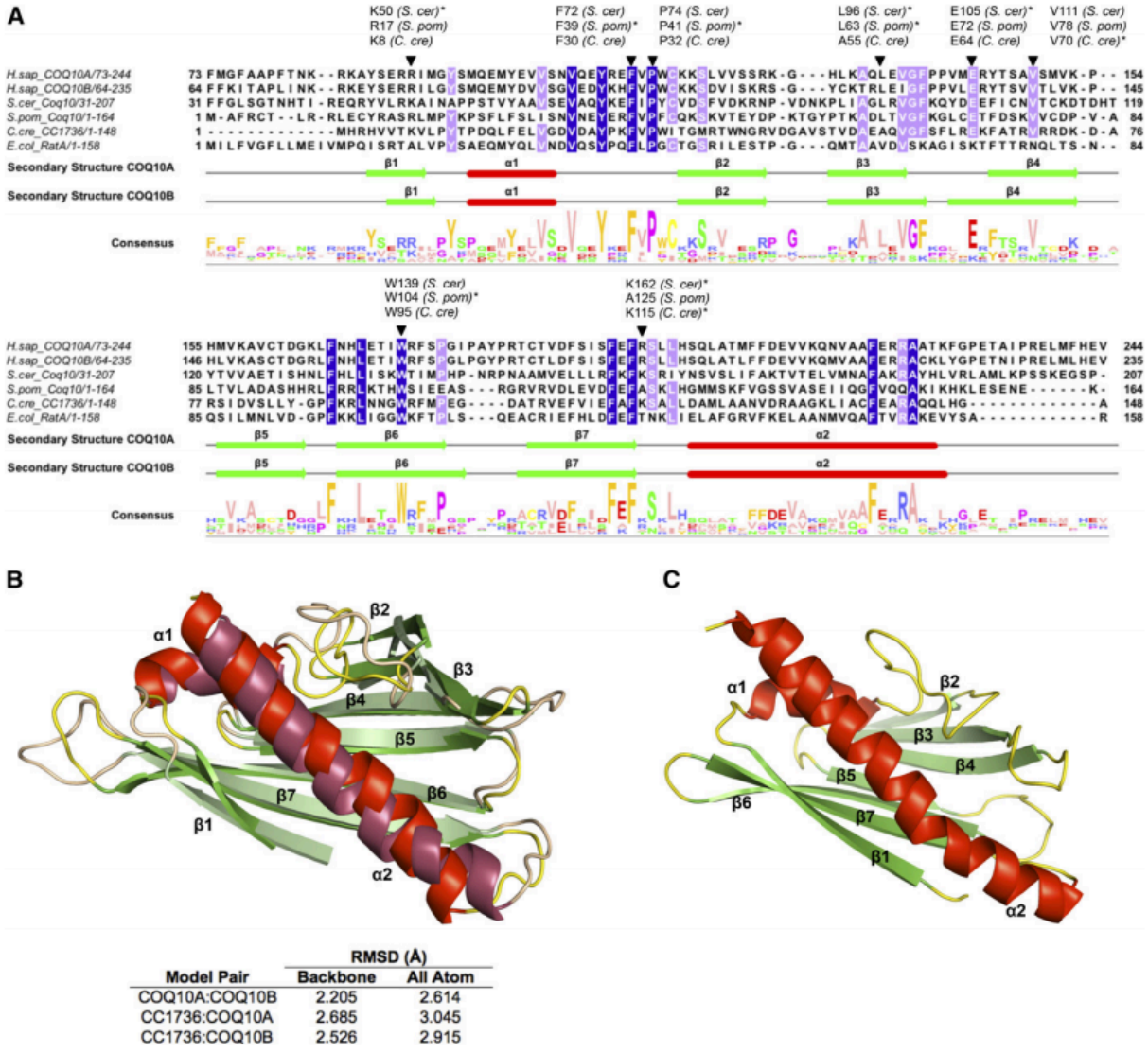

Model Pair	RMSD (Å) Backbone	All Atom
COQ10A:COQ10B	2.205	2.614
CC1736:COQ10A	2.685	3.045
CC1736:COQ10B	2.526	2.915

Fig. 2. Human COQ10A and COQ10B share low sequence identity with Coq10 orthologs, but are predicted to contain conserved START domain structures for lipid binding. A: Sequence alignment of human COQ10A (residues 73-244) and COQ10B (residues 64-235) with Coq10 orthologs in *S. cerevisiae, S. pombe, C. crescentus,* and *E. coli.* MSA was constructed using Tcoffee, with identical residues shaded in blue and highly conserved residues shaded in lilac. Residues that have been previously tested and deemed critical for ligand binding are indicated with an inverted triangle, and the asterisk indicates the organism in which the site-directed mutagenesis study was performed. The secondary structures of COQ10A and COQ10B were predicted using JPred and adjusted based on their refined models in B. Alpha-helices are shown in red and labeled α1-α2 and β-sheets are shown in green and labeled β1–β7. The figure was assembled in Jalview. B: Overlay of predicted homologous models of human COQ10A and COQ10B were generated using the structures of MSMEG_0129 from *Mycobacterium smegmatis* [Protein Data Bank identification (PDB ID): 5Z8O] as a template. The predicted structures of COQ10A (dark shade) and COQ10B (bright shade) were colored respectively, based on their predicted secondary structures. The COQ10A and COQ10B share a similar START domain, a hydrophobic cavity consists of α-helix (red) and anti-parallel β-sheets (green). C: NMR structure of CC1736 (PDB ID: 1T17), a Coq10 ortholog in *C. crescentus* (11). Structures in B and C were generated using PyMOL.

Based on the MSA, we also noticed that although human COQ10A and COQ10B exhibit relatively low sequence identity with other Coq10 orthologs (~26–31%), they are predicted to share similar helix-grip structures (Fig. 2B). The predicted structures of COQ10A and COQ10B are almost identical to each other (Fig. 2B) and similar to the solved structure of CC1736 (Fig. 2C). The core of both COQ10A and COQ10B consists of two α-helices and seven antiparallel β-sheets, and is predicted to form a hydrophobic cavity shielding its CoQ lipid ligand from the aqueous environment (Fig. 2B). The structural feature of a helix-grip fold identifies both COQ10A and COQ10B as distinctive members of the START domain protein family.

In order to reveal the most likely binding site for the CoQ lipid ligand and to identify additional residues that may confer CoQ lipid ligand binding specificity in COQ10A and COQ10B, we attempted to dock CoQ_6 to the known structure of CC1736. Consistent with previous in vitro binding assay results, we observed that docking of farnesylhydroxybenzoate to CC1736 occurred with free energy values significantly higher (more positive and less favorable) than CoQ_6 docked at the central cavity of CC1736 (**Fig. 3A**, B). The docking solutions of CoQ_6 to CC1736 consistently showed that the CoQ_6 folds into a boomerang-like structure, with its hexaprenyl tail making contact with residues A55, V70, and W95 lining the surface inside the cavity (Fig. 3A). However, the orientation of the benzoquinone head group was slightly more variable between docking solutions. Several START domain proteins have been reported to undergo ligand-induced conformational change such that the readily accessible entryway to the central cavity becomes partially constricted, shielding the ligand from the aqueous environment (60–62). Thus, it is highly likely that the flexible orientation of the quinone head group may be a result of a less compact conformation of the central cavity in the structure of a ligand-free CC1736. Further studies that would allow a more in-depth characterization of the conformational change of Coq10 or its orthologs are needed to decipher the CoQ ligand binding interaction.

Expression of human COQ10A or COQ10B restores steady state levels of Coq polypeptides

Coq polypeptide components of the CoQ synthome serve as enzymes required for CoQ biosynthesis and/or play structural roles necessary for formation or stability of the CoQ synthome (5, 34, 63). Yeast Coq10 has not been detected as part of the CoQ synthome, but its absence causes destabilization of Coq3, Coq4, Coq6, Coq7, and Coq9, as well as the overall CoQ synthome (34, 63). We tested the ability of human COQ10A or COQ10B to restore steady state levels of Coq polypeptides when expressed in the yeast *coq10Δ* mutant. We noticed that the steady state level of Coq5 is slightly reduced and the level of Coq8 is slightly increased in the *coq10Δ* mutant, in addition to other affected Coq polypeptide levels shown previously (63). The presence of single-copy pQM COQ10A fully restores steady state levels of Coq5 and Coq6 (**Fig. 4**, supplemental Fig. S1) and partially restores steady state levels of Coq3, Coq4, Coq7, and Coq9 (Fig. 4, supplemental Fig. S1). The single-copy pQM COQ10B fully restores the steady state level of Coq5 (Fig. 4, supplemental Fig. S1) and restores steady-state levels of Coq4, Coq7, and Coq9 to a minimal degree (Fig. 4, supplemental Fig. S1), but seems to have a negative effect on the levels of Coq3, Coq6, and Coq8 (Fig. 4, supplemental Fig. S1). Neither COQ10A nor COQ10B expressed on a multi-copy pRCM vector functions as well as the corresponding single-copy pQM vector, despite the fact that COQ10A and COQ10B are barely detected when expressed from a single-copy vector (Fig. 4). The multi-copy pRCM COQ10A restores the steady state level of Coq6 and partially restores the levels of Coq5 and Coq9 (Fig. 4, supplemental Fig. S1), while the steady state levels of Coq3, Coq4, and Coq7 remain similar to the *coq10Δ* mutant, if not lower (Fig. 4, supplemental Fig. S1). Yeast cells expressing COQ10A from a multi-copy vector show a nearly 50% reduction of Coq8 content compared with the wild-type control (Fig. 4, supplemental Fig. S1). Overexpression of Coq8 promotes assembly of subcomplexes of the CoQ synthome (34), and Coq8 deficit may explain the ineffective rescue of *coq10Δ* by the multi-copy COQ10A and its corresponding poor growth phenotype on YPG plate medium (Fig. 1B). The multi-copy pRCM COQ10B restores Coq5 and Coq9 (Fig. 4, supplemental Fig. S1), but has no effect on the Coq3, Coq4, Coq6, and Coq7 levels (Fig. 4, supplemental Fig. S1). Opposite from the effect of expressing multi-copy pRMC COQ10A, the presence of multi-copy pRCM COQ10B leads to a 50% increase of Coq8 compared with the wild-type cells (Fig. 4, supplemental Fig. S1). It is quite intriguing that pRCM COQ10B results in a slight reduction of the Coq1 level, while the level of Coq11 is nearly 2.5-fold more compared with the wild-type cells (Fig. 4, supplemental Fig. S1). The anti-COQ10A antibody specifically recognizes COQ10A and does not cross-react with human COQ10B (Fig. 4). Anti-COQ10B antibody is also antigen-specific, but it gives two intense bands, migrating at ~30 kDa and ~17 kDa (Fig. 4). In human cells, only the higher molecular mass band is detected, and the lower molecular mass band may correspond to a processed form of COQ10B unique to the yeast cells.

Expression of human COQ10A or COQ10B fails to restore the CoQ synthome in the yeast *coq10Δ* mutant

The decreased steady state levels of component Coq polypeptides in the yeast *coq10Δ* mutant are directly related to the destabilization of the CoQ synthome (34). Here, we assessed the stability of the CoQ synthome in *coq10Δ* expressing single- or multi-copy COQ10A or COQ10B by two-dimensional BN/SDS-PAGE. In the first dimension, multi-subunit protein complexes are resolved under

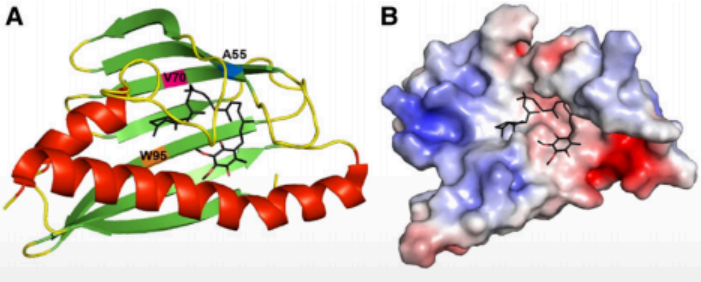

Fig. 3. CoQ_6 docks in the hydrophobic cavity of CC1736. A: CoQ_6 (colored in black) was docked to the NMR structure of CC1736 using AutoDock. The α-helices are shown in red and β-sheets are shown in green. Docking structures were produced using Autodock vina (45). B: Electrostatic surface of CC1736 showing the cavity docked with CoQ_6 with some residues hidden for clarity (red, negative; blue, positive). The polyisoprenoid chain is threaded through the hydrophobic cleft created by residues Ala55, Val70, and Trp95.

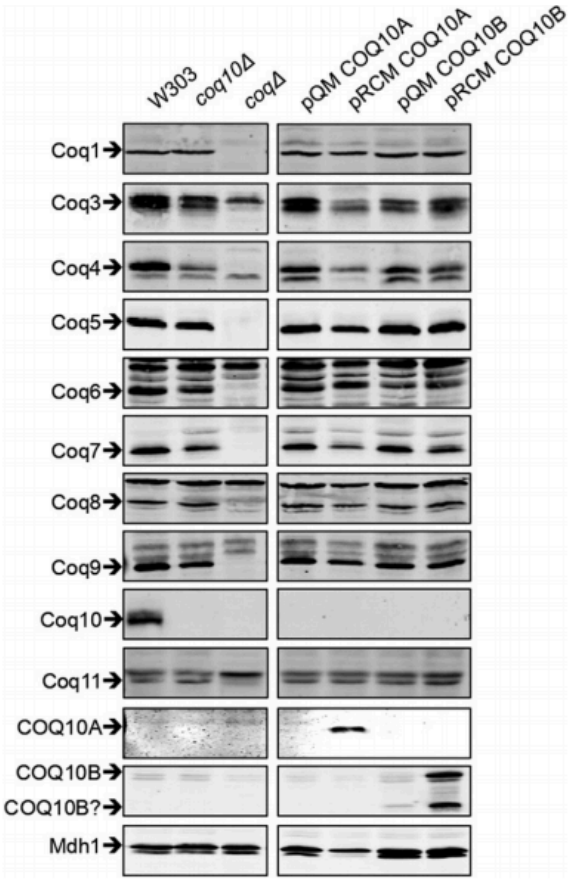

Fig. 4. Expression of human COQ10A or COQ10B restores steady state levels of Coq polypeptides. An aliquot of 25 μg of purified mitochondrial protein from wild-type, *coq10Δ*, or *coq10Δ* expressing single- or multi-copy COQ10A or COQ10B was applied to each lane and separated on 12% Tris-glycine SDS-PAGE gels. Purified mitochondria from *coq1Δ* and *coq3Δ–coq11Δ* mutants were included as negative controls for Western blotting against each of the Coq polypeptides. Purified mitochondria from *coq10Δ* were used as *coqΔ* control for blotting against human COQ10A and COQ10B. Yeast mitochondrial malate dehydrogenase (Mdh1) was included as loading control. Two panels (left and right) are immunoblots derived from the same nitrocellulose membrane. Relative protein levels were quantified by band densitometry in supplemental Fig. S1 using ImageJ software.

nondenaturing native conditions, followed by separation into individual polypeptide constituents in the second dimension by traditional SDS-PAGE under denaturing conditions. Proteins that represent subunits from the same multi-subunit complex are found in one vertical line, and a designated polypeptide component that is present in several distinct complexes or subcomplexes is indicated by a horizontal signal. Thus, the CoQ synthome that is represented by its component Coq4 or Coq9 polypeptide is shown by two horizontal lines that align with the Coq4 and Coq9 bands present in the sample of intact mitochondria from each sample in the lane labeled as "M" (**Fig. 5**). In wild-type yeast cells, the CoQ synthome is represented by a complex array of high molecular mass signals, spanning a range of about 400 kDa to >1 MDa for Coq4 and from ~140 kDa to >1 MDa for Coq9 (Fig. 5A). In contrast, the CoQ synthome in the *coq10Δ* mutant appears destabilized, indicated by the disappearance of complexes much larger than 669 kDa and an appearance of complexes limited to a distribution between 140 kDa and slightly greater than 669 kDa for both Coq4 and Coq9 signals (Fig. 5A). Although expression of single-copy pQM COQ10A restored the steady state polypeptide levels of both Coq4 and Coq9 (Fig. 4), the distribution of high molecular mass signals for Coq4 and Coq9 remains limited to a range similar to that of the *coq10Δ* mutant (Fig. 5A). Single-copy pQM COQ10B reinforced the CoQ synthome assemblies below 440 kDa, as shown by intense Coq9 signal (Fig. 5A), but it also failed to restore the CoQ synthome at a much greater molecular mass (Fig. 5A). Neither multi-copy COQ10A nor COQ10B expression appears to confer a stabilization effect on the CoQ synthome (Fig. 5A). Thus, the expression of either COQ10A or COQ10B, while having a rather dramatic effect on steady state Coq polypeptide levels, exerts a negligible effect on the high molecular mass signals that characterize efficient CoQ synthesis and the presence of the CoQ synthome.

Coq10 comigrates with Coq2 and Coq8 on two-dimensional BN/SDS-PAGE (64), but so far there is no direct evidence showing Coq10 interaction with other known Coq polypeptides or with the CoQ synthome. On a sucrose gradient, native Coq10 from yeast mitochondrial extract sediments at a fraction that corresponds to a molecular mass of approximately 140 kDa (10). Given that the monomeric molecular mass of mature Coq10 is 20 kDa, Coq10 must be present in a complex that consists of an oligomeric form of Coq10 and/or with other partner proteins (10). We tested to determine whether human COQ10A or COQ10B might also assemble into complexes. Because the signal intensities of both COQ10A and COQ10B expressed from single-copy vectors are quite weak, we decided to examine their complex formation when expressed from the multi-copy vector. On the two-dimensional BN/SDS-PAGE, wild-type yeast Coq10-containing complex is distributed across the entire range of high molecular mass standards, but predominantly concentrated between 66 and 232 kDa (Fig. 5B), and the Coq10-containing complex is absent in the *coq10Δ* mutant (Fig. 5B). Although the signal intensities of COQ10A and COQ10B are low, it appears that COQ10A forms a discrete complex at ~140 kDa (Fig. 5B), and COQ10B is dispersed across between 232 and 440 kDa (Fig. 5B). Knowing the total amount of protein subjected to analysis by BN/SDS-PAGE, it is possible that a significant amount of COQ10A and COQ10B may migrate at a much smaller size corresponding to its monomeric molecular mass, not observed by the first dimension gel matrix.

Expression of human COQ10A or COQ10B fails to restore CoQ biosynthesis in the yeast *coq10Δ* mutant

In yeast, CoQ is produced from two distinct quinone ring precursors, pABA or 4HB (5). Early-stage intermediates, 4-amino-3-hexaprenylbenzoic acid (HAB) and

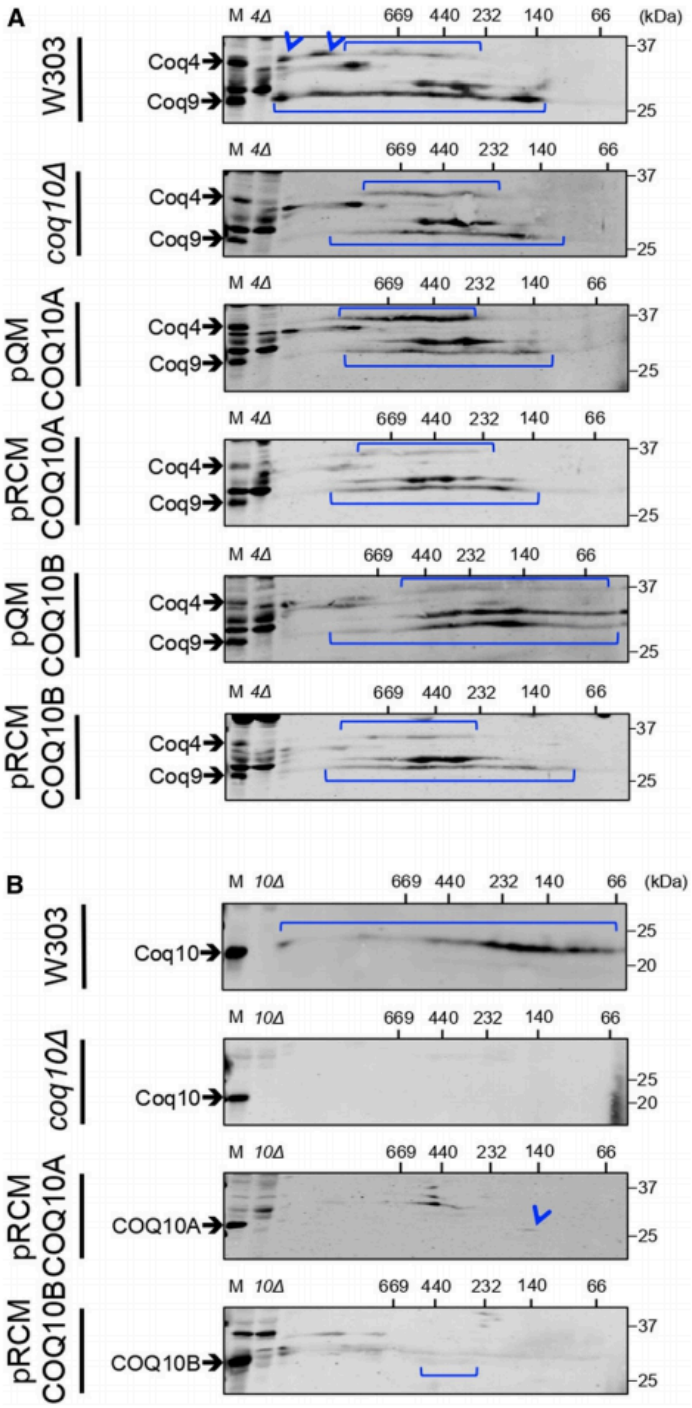

Fig. 5. Expression of either human COQ10A or COQ10B partially restores the yeast CoQ synthome. An aliquot of 80 μg of purified mitochondrial protein from wild-type, *coq10Δ*, or *coq10Δ* expressing single- or multi-copy COQ10A or COQ10B was resolved on a two-dimensional BN/SDS-PAGE and blotted against Coq4 and Coq9 (A) or against Coq10, COQ10A, or COQ10B (B). An aliquot of 25 μg of unsolubilized intact mitochondria from each designated sample was loaded in the lane labeled "M", and the same amount of intact *coq4Δ* or *coq10Δ* mitochondria were included as negative controls. The yeast *coq4Δ* mutant lacks both Coq4 and Coq9 polypeptides (63) and was used as a negative control for blotting against both proteins on the same membrane.

4-hydroxy-3-hexaprenylbenzoic acid (HHB), are the first polyisoprenylated intermediates emerging from pABA and 4HB, respectively (5). Subsequent modifications of the ring of HAB or HHB give rise to late-stage intermediates, 4-imino-demethoxy-Q_6H_2 ($IDMQ_6H_2$) or demethoxy-Q_6H_2 (DMQ_6H_2). It is believed that only DMQ_6H_2 gets directly converted to CoQ_6H_2, whereas $IDMQ_6H_2$ represents a dead-end late-stage product; the deamination of HAB is mediated by the Coq6/Coq9 step in the pABA pathway (5). To examine how well single- and multi-copy COQ10A or COQ10B rescue yeast *coq10Δ* de novo CoQ biosynthesis, we labeled the cells with $^{13}C_6$-pABA or $^{13}C_6$-4HB in order to

measure the efficiency of CoQ production from both pathways.

Consistent with previously published results (9), we observed that the yeast *coq10Δ* mutant produced less $^{13}C_6$-CoQ_6 (**Fig. 6A**) but significantly higher amounts of the early intermediates, $^{13}C_6$-HAB (supplemental Fig. S2A) and $^{13}C_6$-HHB (supplemental Fig. S2B) during log phase growth. The yeast *coq10Δ* mutant also makes less late-stage intermediates, $^{13}C_6$-DMQ_6 (supplemental Fig. S2C) and $^{13}C_6$-$IDMQ_6$ (supplemental Fig. S2D), de novo compared with the wild-type cells. One caveat to this result is that when the yeast *coq10Δ* mutant is transformed with empty vector pQM or pRCM, these empty vectors seem to make a significant difference on the levels of all representative CoQ_6-intermediates as well as in CoQ_6 when compared with the *coq10Δ* mutant (Fig. 6, supplemental Fig. S2). We suspected that this might be a result of different medium used to culture the *coq10Δ* mutant (SD-Complete) and *coq10Δ* mutant with empty vectors (SD-Ura). Therefore, we compared the yeast *coq10Δ* expressing single- or multi-copy COQ10A or COQ10B to their respective empty vector controls for the statistical analyses. If COQ10A or COQ10B were to restore efficient de novo CoQ biosynthesis, we would expect lower amounts of $^{13}C_6$-HAB and $^{13}C_6$-HHB and a higher amount of $^{13}C_6$-CoQ_6. However, expression of either COQ10A or COQ10B has only a minimal effect on the de novo biosynthesis of $^{13}C_6$-CoQ_6. Single-copy COQ10A seems to make slightly more $^{13}C_6$-CoQ_6 from labeled pABA and 4HB (Fig. 6A), and has slightly higher levels of total CoQ_6 (Fig. 6B) when compared with the empty vector control. In contrast, expression of COQ10B, particularly in multi-copy, decreases de novo $^{13}C_6$-CoQ_6 as well as the total CoQ_6 content (Fig. 6A, B). While single- and multi-copy COQ10A and multi-copy COQ10B synthesize $^{13}C_6$-DMQ_6 (supplemental Fig. S2C) and $^{13}C_6$-$IDMQ_6$ (supplemental Fig. S2D), the conversion from early-stage intermediates to late-stage intermediates is slow, as indicated by a buildup of the labeled $^{13}C_6$-HAB (supplemental Fig. S2A) and $^{13}C_6$-HHB (supplemental Fig. S2B).

In addition to $^{13}C_6$-labeled CoQ_6 and CoQ_6-intermediates, we also quantified the unlabeled CoQ_6 and CoQ_6-intermediates (Fig. 6B, supplemental Fig. S2E–H). Similar to what we observed with the $^{13}C_6$-labeled CoQ_6 and CoQ_6-intermediates, the yeast *coq10Δ* mutant expressing single- or multi-copy COQ10A or COQ10B has only a negligible effect on the steady state levels of CoQ_6 and CoQ_6-intermediates. To summarize, neither single- nor multi-copy expression of COQ10A or COQ10B functionally restores de novo CoQ biosynthesis to the wild-type level, and has negligible effects on the synthesis of early stage CoQ_6-intermediates relative to the empty vector control. Given that the high molecular weight CoQ synthome is known to be necessary for efficient CoQ_6 biosynthesis in yeast, it is not surprising that each of the human COQ10 orthologs fails to restore the yeast de novo CoQ_6 production.

Human COQ10A rescues PUFA sensitivity of the yeast *coq10Δ* mutant

PUFAs are particularly susceptible to oxidative damage caused by ROS-dependent abstraction of hydrogen atoms at bis-allylic positions, generating carbon-centered free radicals (65). In the presence of oxygen, the resulting peroxyl radicals trigger a chain reaction of lipid peroxidation and propagate oxidative damage to other macromolecules.

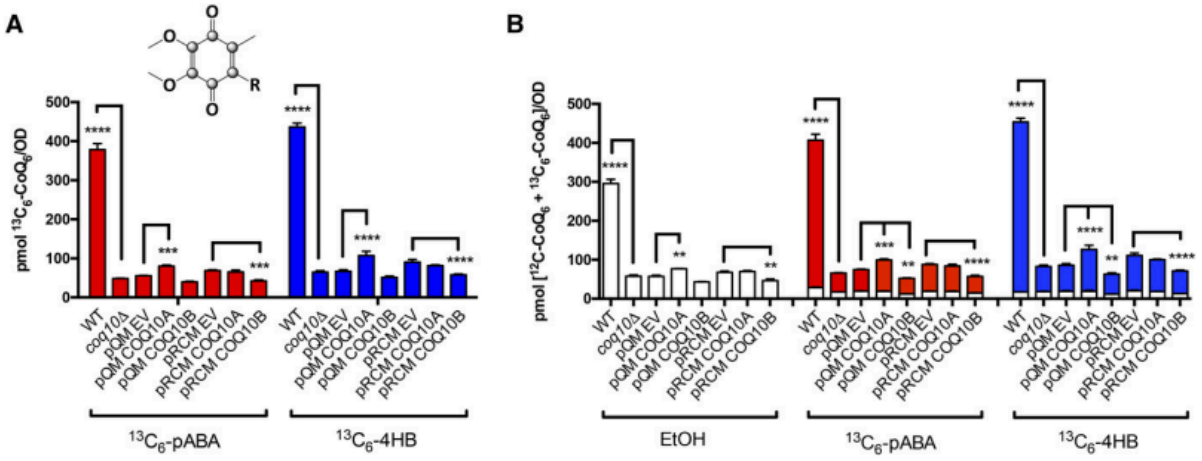

Fig. 6. Expression of human COQ10A or COQ10B has a minimal effect on de novo CoQ_6 biosynthesis and total CoQ_6 content. The de novo production of CoQ_6 was measured from yeast whole-cell lipid extracts from wild-type, *coq10Δ*, *coq10Δ* expressing single- or multi-copy COQ10A or COQ10B, or their respective empty vector labeled with $^{13}C_6$-pABA (red) or $^{13}C_6$-4HB (blue) for 5 h. Expression of single- or multi-copy COQ10A or COQ10B has almost negligible effect on both de novo $^{13}C_6$-CoQ_6 (A) and total CoQ_6 (B) when compared with their respective empty vector controls. The statistical analyses were performed using two-way ANOVA multiple comparisons from three biological replicates, comparing yeast *coq10Δ* expressing single- or multi-copy COQ10A or COQ10B to their respective empty vector controls, and comparing yeast *coq10Δ* mutant to the wild-type control. The error bar indicates mean ± SD, and the statistical significance is represented by $^*P < 0.05$, $^{**}P < 0.01$, $^{***}P < 0.001$, and $^{****}P < 0.0001$.

Collectively, this oxidative damage results in DNA mutations, protein fragmentation, and formation of protein-protein cross-links (66). As shown in **Fig. 7**, the yeast CoQ-less mutant (*coq9Δ*) is sensitive to α-linolenic acid due to the absence of antioxidant protection offered by CoQ (30, 31). The yeast *coq10Δ* mutant is also sensitive to treatment with α-linolenic acid, presumably because the chaperone function of the Coq10 polypeptide is necessary for the ability of CoQ to function as an antioxidant (9). This chaperone function of Coq10 is independent of its role in respiration per se, because a CoQ-replete respiratory-deficient mutant lacking a subunit of complex III (*cor1Δ*) is resistant to α-linolenic acid (Fig. 7). Thus, we assessed whether the sensitivity to PUFA treatment of yeast *coq10Δ* was rescued by the expression of single- or multi-copy human COQ10A or COQ10B. Expression of either single- or multi-copy COQ10A rescued yeast *coq10Δ* sensitivity to treatment with α-linolenic acid (Fig. 7). Multi-copy COQ10B partially rescued yeast *coq10Δ* sensitivity to α-linolenic acid, while single-copy COQ10B did not have a significant effect (Fig. 7). As expected, yeast strains tested were resistant to monounsaturated oleic acid (Fig. 7). Thus, our data suggest that COQ10A and COQ10B are only partially able to complement the yeast *coq10Δ* mutant; both human co-orthologs are capable of rescuing defective respiration and PUFA sensitivity in the yeast *coq10Δ* mutant, but fail to rescue the defect in CoQ_6 biosynthesis.

COQ10 family analysis

A protein sequence similarity network analysis reveals that the COQ10-like family can be divided into six main similarity clusters that are generally grouped by taxonomy (**Fig. 8A**). The COQ10-like proteins from land plants and green algae (with the exception of prasinophyte homologs) are closely related to animal homologs and, in the phylogenetic tree reconstruction, are nestled within the metazoan clade (Fig. 8B). Two groups of bacterial proteins are found in the COQ10-like family. Proteins encoded by genes (referred to as *yfjG/ratA* in *E. coli*) in the highly conserved *smpB-ratA-yfjF* gene neighborhood (67, 68) dominate bacterial cluster 1. RatA from *E. coli* (see sequence alignment in Fig. 2A) has a proposed role in cell cycle arrest as a response to stresses such as nutrient starvation (69). Upon induction, RatA blocks 70S ribosome association and inhibits the translation initiation step (69). The first gene in the neighborhood, *smpB*, also encodes a protein that interacts with the ribosome through a complex formed with tmRNA that is essential for rescuing stalled ribosomes (70, 71). The third gene in the conserved operon, *yfjF*, encodes a protein of unknown function, which was renamed RatB, an assumed antitoxin of RatA, but evidence suggests that RatB does not function as an antitoxin to RatA (69). YfjF is homologous to RnfH, a *Rhodobacter capsulatus* homolog encoded by a gene at the end of the *rnf* operon (72). Rnf is an enzyme complex homologous to but distinct from the bacterial respiratory complex, Na^+-dependent NADH:ubiquinone oxidoreductase (Na^+-NQR) (73). However, a role for RnfH in the Rnf complex is unsubstantiated and many *rnf* operons do not encode an RnfH orthologs (74).

Proteins encoded by genes that are often physically clustered with *lipA* orthologs, which encode lipoyl synthases, dominate bacterial cluster 2. Mining coexpression databases revealed that the characterized *COQ10* from *S. pombe* is coexpressed with *AIM22* (second-ranked coexpressed gene) (75), encoding a putative lipoate-protein ligase A. These two functional inferences (conserved gene clusters in bacteria and coexpression in *S. pombe*) may point to a yet uncharacterized role of COQ10 in lipoic acid biosynthesis or regulation; lipoic acid is a prosthetic group covalently attached to several dehydrogenases within the mitochondria. We also note that the top-ranked coexpressed gene in *S. cerevisiae*, *MDM12*, is positioned head-to-head with

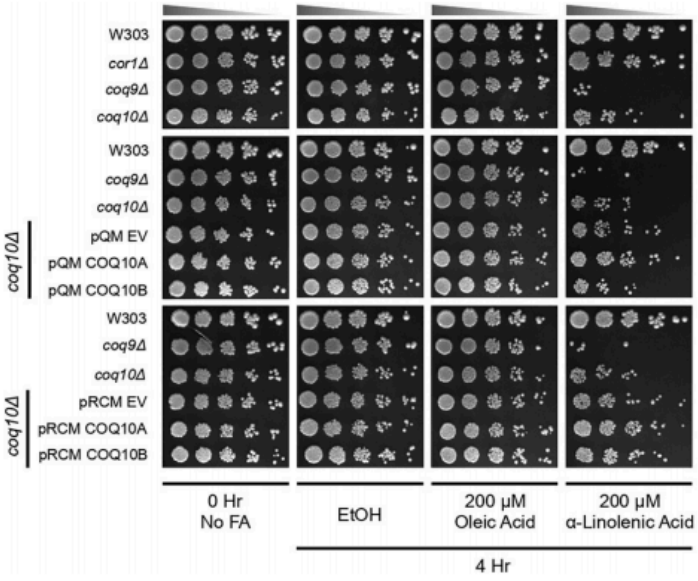

Fig. 7. Human COQ10A rescues PUFA sensitivity of the yeast *coq10Δ* mutant. Wild-type W303, respiratory-deficient mutant *cor1Δ*, CoQ-less mutant *coq9Δ*, *coq10Δ*, and *coq10Δ* expressing single- or multi-copy COQ10A or COQ10B, or their respective empty vector were grown in SD-Complete or SD-Ura liquid medium to log phase. Harvested cells were washed twice with sterile water and resuspended in phosphate buffer with 0.2% dextrose (pH 6.2) to 0.2 OD_{600}/ml. The resuspended cells were incubated with oleic acid or α-linolenic acid prepared in ethanol at a final concentration of 200 μM for 4 h. Cells were also incubated with only ethanol as vehicle control. Aliquots of cell suspension from each sample were removed before addition of fatty acids [0 h (0 Hr), no fatty acids], and 4 h (4 Hr) post fatty acid incubation to assess cell viability by plate dilution assay. An aliquot of 2 μl of a series of 5-fold diluted samples was plated in each spot starting at 0.2 OD_{600}/ml in the first spot on YPD plate medium. Pictures were taken 2 days after incubation at 30°C.

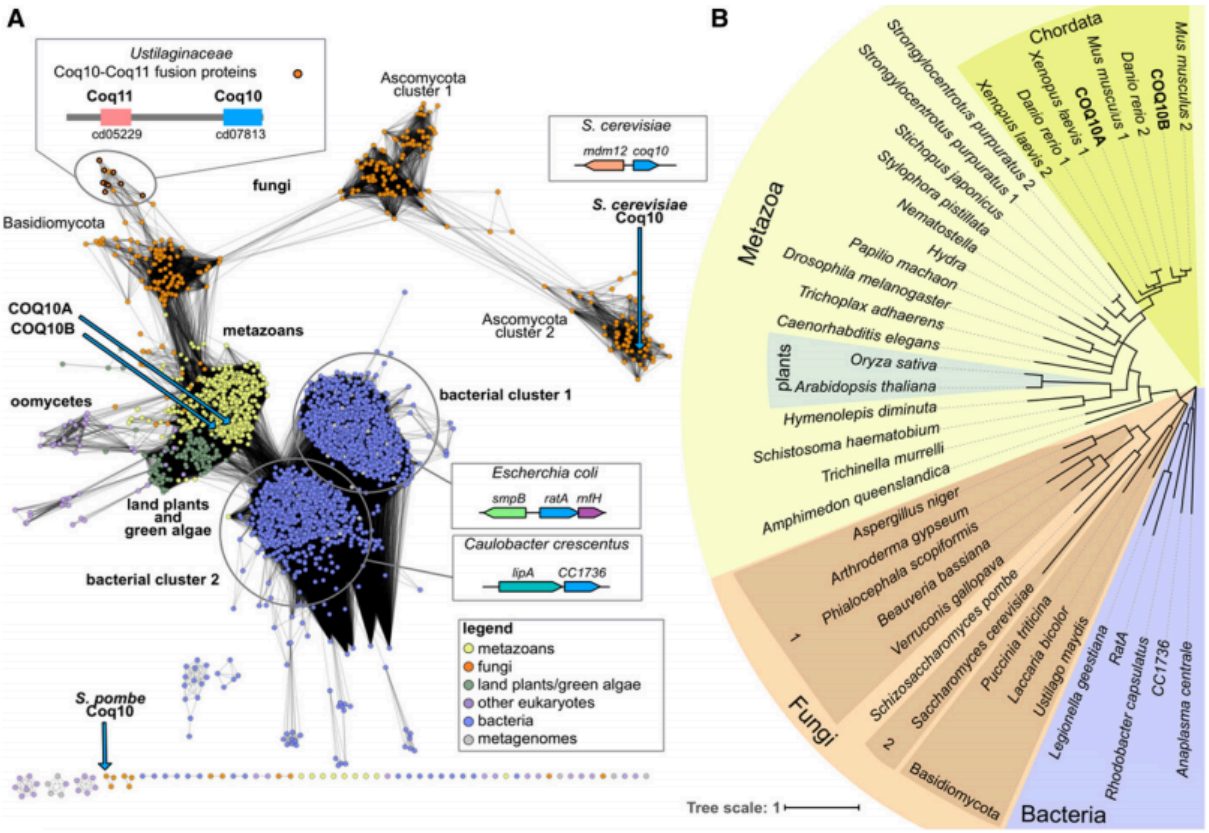

Fig. 8. The COQ10 family of proteins. A: A protein similarity network of proteins similar to COQ10 is shown. Each node (circle) represents one or more protein sequences, and each edge (solid line) represents similarity between two proteins (threshold set at an alignment score of 30). Nodes are colored by taxonomy as indicated in the legend. The locations of nodes representing human COQ10A and COQ10B, as well as previously characterized Coq10 orthologs from *S. cerevisiae* and *S. pombe*, are indicated with blue arrows. The disconnection of *S. pombe* Coq10 from the rest of the network is due to the low similarity (as measured by the BLASTp Evalue) between *S. pombe* Coq10 and other COQ10 homologs (with the exception of Coq10 from other *Schizosaccharomyces* species). The predominant operons observed for the two distinct bacterial clusters represented by *E. coli* and *C. crescentus* are shown as cartoons. A schematic of the Coq11-Coq10 protein fusion observed in genomes from *Ustilaginaceae* is also shown, and corresponding nodes are indicated with a thick border. Coq11 contains the cd05229 domain, an atypical SDR domain, and Coq10 contains the cd07813 domain, a SRPBCC (START/RHO_α_C/PITP/Bet_v1/CoxG/CalC) domain with a deep hydrophobic ligand-binding pocket. Protein and organism information for each node is available in supplemental Table S2. B: A phylogenetic tree of selected COQ10 homologs from each of the sequence similarity network protein clusters. Background shading corresponds to taxonomy as indicated. Branches with less than 50% bootstrap support were deleted.

COQ10 (75), suggesting that the two genes share a bidirectional promoter. The mitochondrial distribution and morphology protein (Mdm12) is the cytosolic subunit of the ER-mitochondria encounter structure (ERMES) for establishing the ER-mitochondria contact sites, the absence of which causes severe mitochondrial morphological defects, defects in respiration, and rapid loss of mitochondrial DNA (76, 77).

The Coq10-Coq11 fusion proteins found in genomes from *Ustilaginaceae* (78) are also shown in Fig. 8. Additional domains found in the present analysis fused to the COQ10 domain (PF03364) (encoded by at least two different species) include PF00098 (zinc-finger domain), PF00227/PF10584 (proteasome subunits), and PF00378 (enoyl-CoA hydratase/isomerase family). Additionally, both COQ10A and COQ10B were previously found to interact with the enoyl-CoA hydratase, ECH1, which in turn has been observed to interact with COQ2, COQ3, COQ4, COQ6, COQ7, and COQ8A (79, 80). Mining coexpression databases, both *COQ3* and *COQ8A* also coexpress with *COQ10A* (81). The human ECH1 localizes to the matrix of mitochondria and participates in β-oxidation of unsaturated fatty acids (82), and the interaction of ECH1 with both COQ10A and COQ10B aligns well with their roles as chaperones to deliver CoQ as a cofactor for the reaction.

DISCUSSION

This study provides another piece of evidence supporting the functional conservation of yeast and human proteins

involved in CoQ biosynthesis. Unlike yeast, humans have two isoforms of COQ10, which may have evolved by a duplication event during chordate evolution (Fig. 8B). RNA-seq analysis of different human tissues suggests that although both COQ10A and COQ10B are universally expressed, COQ10A seems predominantly expressed in heart and skeletal muscle cells (83, 84). Knowing that COQ10A and COQ10B share 66% sequence identity (84% similarity), the enrichment of COQ10A in human heart and skeletal muscle implies a functional specialization of the protein. From our experimental results, it is curious to note that single-copy COQ10A performs the best in terms of restoring steady state Coq polypeptide levels (Fig. 4), stabilizing the CoQ synthome (Fig. 5), and restoring resistance against PUFAs (Fig. 7), despite the finding that single-copy COQ10A seems to restore respiratory growth phenotype just as well as both single- and multi-copy COQ10B on YPG plate medium (Fig. 1B). In contrast, neither COQ10A nor COQ10B expression restores de novo CoQ synthesis in yeast when compared with the *coq10Δ* empty vector control (Fig. 6, supplemental Fig. S2). Efficient CoQ biosynthesis requires a properly assembled CoQ synthome, but neither COQ10A nor COQ10B expression fully restores the CoQ synthome assembly (Fig. 5). Importantly, neither COQ10A nor COQ10B expression restores the steady state levels of Coq4, which is known to be the central organizer protein of the CoQ synthome (34). Additionally, the assembly and stability of the CoQ synthome relies on the presence of CoQ_6 and CoQ_6-intermediates. Studies have shown that reestablishment of de novo CoQ_6 biosynthesis and the levels of certain CoQ_6-intermediates restores the CoQ synthome assembly and CoQ domain formation (34, 85). The CoQ synthome is responsible for efficient de novo CoQ biosynthesis, and the resulting CoQ and CoQ-intermediates are in turn necessary to stabilize the CoQ synthome. Because neither COQ10A nor COQ10B rescues the defect in de novo CoQ_6 production, the amounts of CoQ_6 or CoQ_6-intermediates may not be sufficient to restore and stabilize the CoQ synthome. However, expression of either of the human orthologs, COQ10A or COQ10B, complemented the *coq10Δ* glycerol growth (Fig. 1B). Thus, human COQ10A and COQ10B fulfill two independent functions in yeast: *1*) both facilitate the function of CoQ in respiration; and *2*) both enable CoQ to function as a chain-terminating antioxidant. However, neither COQ10A nor COQ10B function to restore the efficient CoQ biosynthesis in yeast.

One possibility is that a coordinated action of both yeast Coq10 and Coq11 is necessary to restore efficient CoQ biosynthesis in the yeast *coq10Δ* mutant. In mammalian cells, it is common that the START domain may be coupled with other motifs/domains on the same protein, offering additional functions, such as localization, enzymatic activity, or signaling (12, 13, 86). For instance, the metastatic lymph node 64 (MLN64) is a cholesterol-specific START protein, and it contains a conserved membrane-spanning (MLN64 N terminal) MENTAL domain in addition to the START domain (87). The NMENTAL domain anchors MLN64 to the late endosome membranes, from which the MENTAL domain can capture cholesterol and subsequently transfer it to the cytoplasmic START domain (14, 87, 88). Yeast Coq11 belongs to the short-chain dehydrogenase/reductase (SDR) superfamily, which contains a conserved Rossmann fold with an N-terminal binding site for NAD(H) or NADP(H) (89). The *S. cerevisiae coq11Δ* does not exhibit an apparent growth defect on a nonfermentable carbon source, but its de novo $^{13}C_6$-CoQ_6 production is significantly lower compared with the wild-type cells (78). *S. cerevisiae coq10Δ* shares a very similar phenotype except that its growth on nonfermentable carbon sources is impaired but not completely abolished. Thus, it may be possible that, in yeast, the Coq10 and Coq11 functions need to be coordinated in order to achieve wild-type level efficiency for de novo CoQ_6 biosynthesis. The presence of Coq10-Coq11 fusion protein in several *Ustilaginaceae* species (Fig. 8) further consolidates a potential functional link conferred by their physical interaction and/or function in the same biological pathway. In mammalian cells, the closest but distinct homolog to yeast Coq11 is NDUFA9, a NADH dehydrogenase and a complex I ubiquinone reduction-module (Q-module) subunit (78, 90). However, because humans do not have Coq11, a similar interaction between Coq10 and Coq11 either never evolved or was lost during evolution. Therefore, we postulate that neither human COQ10A nor COQ10B was able to interact with yeast Coq11, hence failing to restore de novo CoQ biosynthesis (Fig. 6, supplemental Fig. S2). In contrast, plants and algae do have orthologs of yeast Coq11 and have evolved to use Coq11 or Coq11-like proteins (78). The *Arabidopsis thaliana* genome encodes four Coq11 orthologs (At1g32220, At5g15910, At5g15480, and At5g10730), and the chloroplast-localized flavin reductase-related protein, At1g32220, is thought to be involved in plastoquinone biosynthesis (49, 78). In COXPRESdb, *COQ10A* is coexpressed with SDR39U1, which, like Coq11, belongs to the SDR superfamily (75), and SDR39U1 was found to coelute with human COQ9 from a hydroxyapatite column in mitochondria solubilized with Triton X-100 (91). These functional inferences may supply a link between human COQ10 and Coq11-like proteins in CoQ production.

So far, most of the publications on yeast Coq10 are focused on its putative function as a CoQ chaperone for its function in respiration and as a lipophilic antioxidant. The Coq10 similarity network analysis (Fig. 8A) suggests that Coq10 homologs may be functionally linked to lipoic acid synthesis and/or regulation. Lipoic acid is a sulfur-containing cofactor and is essential for enzymatic functions of pyruvate dehydrogenase and α-ketoglutarate dehydrogenase, as well as the glycine cleavage system (92). Lipoic acid is assembled on its cognate proteins from precursor octanoic acid from the fatty acid biosynthesis pathway to a specific lysine residue of the cognate protein by octanoyl transferase (LipB), followed by insertion of sulfur by lipoyl synthetase (LipA) (92). Eukaryotes contain a conserved mitochondrial fatty acid synthetic pathway, independent from cytosolic fatty acid biosynthesis machinery (93). The respiratory competence in yeast is dependent on the ability of mitochondria to synthesize fatty acids, and yeast deletion

mutants of enzymes involved in mitochondrial fatty acid synthesis exhibit a respiratory-deficient phenotype and small mitochondria, possibly mediated by inefficient tRNA processing by RNase P cleavage (93). A role for Coq10 or Coq10 homologs in fatty acid synthesis has not been substantiated, but because yeast *coq10Δ* is respiratory-defective, it would be interesting to examine the mitochondrial morphology in this particular mutant and assess the lipoic acid-dependent enzyme activities.

Another possible functional role of Coq10 relates to the coexpression of *COQ10* and *MDM12* from a shared promoter in *S. cerevisiae* (Fig. 8A) (94). The arrangement and coregulation of different genes via promoter sharing is indicative of functional connection and/or physical interactions between the two gene products. In yeast, Mdm12 is positioned on the mitochondrial outer membrane as part of the ERMES complex subunit; Mdm12 bridges Mmm1 localized at the ER membrane with Mdm10 and Mdm34 at the cytosolic site (76). The ERMES complex mediates ER-mitochondrial contacts, essential for lipid exchange between the two organelles (76). Recently, polypeptide members of the CoQ synthome (Coq3–Coq7, Coq9, and Coq11) have been shown to localize selectively to multiple domains (CoQ domains) (85, 95). These CoQ domains are marked by ER-mitochondria contact sites and are established by a START-like domain containing ER membrane sterol transporter protein, Ltc1, in complex with the mitochondrial outer membrane protein, Tom71, as well as by the ERMES complex (85, 95). Presence of the CoQ domain relies on the cooperative assembly of the CoQ synthome components (85). Absence of any one subunit of the ERMES complex also elicits a dramatic effect on the overall stability of the CoQ synthome and CoQ domain formation, but only a negligible effect on the steady state levels of the constituent Coq polypeptides of the CoQ synthome (85, 95). Deletion of *LTC1* in the *mmm1Δ* mutant further enhanced the defect of CoQ domain formation, suggesting a redundant functional role of these two ER-mitochondria tethers for domain positioning in the mitochondria (85). The *ERMESΔ* mutants accumulate steady state and $^{13}C_6$-labeled CoQ_6-intermediates as a result of inefficient CoQ_6 biosynthesis from destabilized CoQ synthome (95). Interestingly, these *ERMESΔ* mutants retain more $^{13}C_6$-labeled CoQ_6 even though their steady state CoQ_6 levels inside the mitochondria are lower compared with the wild-type cells (95). The disruption of CoQ_6 homeostasis presumably results from the reduced sequestration of CoQ_6 within the mitochondria and/or compromised degradation of CoQ_6 at the peroxisomes, which have been reported to colocalize with the ERMES complex at specific mitochondrial subdomains (95, 96). Inside the yeast mitochondria, two separate studies have observed a reduced number of CoQ synthome domain formations in the yeast *coq10Δ* mutant, which is likely contributed by the partial destabilization of the CoQ synthome as well as component Coq polypeptides in the absence of Coq10 (63, 85, 95). The establishment of CoQ domains within mitochondria relies on CoQ-intermediates and substrate flux (85), which seems to correlate well with the role of Coq10 in mediating efficient CoQ production. However, the exact mechanism underlying the role of Coq10 in coordination of the ER-mitochondria contact sites and CoQ biosynthesis remains to be elucidated.

Similar CoQ domains are also observed in human cells (85). However, mammalian cells do not have orthologs of ERMES polypeptides, and the physical contact between ER and mitochondria is established by homo- or heterodimerization of ER-localized mitofusin (MFN)2, with MFN1 or MFN2 on the mitochondrial outer membrane (97). Loss of MFN2 impairs respiration capacity, originating from a depletion of mitochondrial CoQ content and reduced CoQ-dependent NADH-cytochrome *c* reductase and succinate-cytochrome *c* reductase activities (98). Proteomic and metabolic analyses suggest that loss of MFN2 likely affects the isoprene biosynthesis pathway that is upstream of both CoQ and cholesterol biosynthesis, but the effect is only observed as decreased CoQ but not cholesterol levels (98). Similar to the yeast system, the enzymes involved in the isoprene biosynthetic pathway exist in different organelles, including mitochondria, ER, and peroxisomes (98); however, the functional implications of the involvement of human COQ10A and COQ10B in physical coordination of these organelles remain to be uncovered.

In summary, this study indicates that although expression of the human COQ10A or COQ10B orthologs failed to restore efficient de novo synthesis of CoQ_6, they nonetheless rescued the respiratory deficiency and the sensitivity to oxidative stress of the yeast *coq10Δ* mutant. These results indicate that the Coq10 START domain functions as a CoQ chaperone, necessary for respiration-dependent cellular bioenergetics and defense mechanisms against oxidative stress. The COQ10 family protein analyses provide additional insights into the possible roles of Coq10-dependent transport of CoQ, necessary for its function as a cofactor in biological pathways and trafficking between organelles.

The authors thank Dr. Carol Dieckmann from the University of Arizona for her comments and suggestions on this work.

REFERENCES

1. Alcázar-Fabra, M., E. Trevisson, and G. Brea-Calvo. 2018. Clinical syndromes associated with coenzyme Q_{10} deficiency. *Essays Biochem.* **62:** 377–398.
2. Turunen, M., J. Olsson, and G. Dallner. 2004. Metabolism and function of coenzyme Q. *Biochim. Biophys. Acta.* **1660:** 171–199.
3. Desbats, M. A., G. Lunardi, M. Doimo, E. Trevisson, and L. Salviati. 2015. Genetic bases and clinical manifestations of coenzyme Q_{10} (CoQ_{10}) deficiency. *J. Inherit. Metab. Dis.* **38:** 145–156.
4. Stefely, J. A., and D. J. Pagliarini. 2017. Biochemistry of mitochondrial coenzyme Q biosynthesis. *Trends Biochem. Sci.* **42:** 824–843.
5. Awad, A. M., M. C. Bradley, L. Fernández-del-Río, A. Nag, H. S. Tsui, and C. F. Clarke. 2018. Coenzyme Q_{10} deficiencies: pathways in yeast and humans. *Essays Biochem.* **62:** 361–376.
6. Hajj Chehade, M., L. Pelosi, C. D. Fyfe, L. Loiseau, B. Rascalou, S. Brugière, K. Kazemzadeh, C-D-T. Vo, L. Ciccone, L. Aussel, et al. 2019. A soluble metabolon synthesizes the isoprenoid lipid ubiquinone. *Cell Chem. Biol.* **26:** 482–492.e7.
7. Okada, K., K. Suzuki, Y. Kamiya, X. Zhu, S. Fujisaki, Y. Nishimura, T. Nishino, T. Nakagawa, M. Kawamukai, and H. Matsuda. 1996.

Polyprenyl diphosphate synthase essentially defines the length of the side chain of ubiquinone. *Biochim. Biophys. Acta.* **1302:** 217–223.
8. Kawamukai, M. 2016. Biosynthesis of coenzyme Q in eukaryotes. *Biosci. Biotechnol. Biochem.* **80:** 23–33.
9. Allan, C. M., S. Hill, S. Morvaridi, R. Saiki, J. S. Johnson, W. S. Liau, K. Hirano, T. Kawashima, Z. Ji, J. A. Loo, et al. 2013. A conserved START domain coenzyme Q-binding polypeptide is required for efficient Q biosynthesis, respiratory electron transport, and antioxidant function in *Saccharomyces cerevisiae*. *Biochim. Biophys. Acta.* **1831:** 776–791.
10. Barros, M. H., A. Johnson, P. Gin, B. N. Marbois, C. F. Clarke, and A. Tzagoloff. 2005. The *Saccharomyces cerevisiae COQ10* gene encodes a START domain protein required for function of coenzyme Q in respiration. *J. Biol. Chem.* **280:** 42627–42635.
11. Shen, Y., S. Goldsmith-Fischman, H. S. Atreya, T. Acton, L. Ma, R. Xiao, B. Honig, G. T. Montelione, and T. Szyperski. 2005. NMR structure of the 18 kDa protein CC1736 from *Caulobacter crescentus* identifies a member of the START domain superfamily and suggests residues mediating substrate specificity. *Proteins.* **58:** 747–750.
12. Ponting, C. P., and L. Aravind. 1999. START: a lipid-binding domain in StAR, HD-ZIP and signalling proteins. *Trends Biochem. Sci.* **24:** 130–132.
13. Iyer, L. M., E. V. Koonin, and L. Aravind. 2001. Adaptations of the helix-grip fold for ligand binding and catalysis in the START domain superfamily. *Proteins.* **43:** 134–144.
14. Alpy, F., and C. Tomasetto. 2014. START ships lipids across interorganelle space. *Biochimie.* **96:** 85–95.
15. Martin, L. A., B. E. Kennedy, and B. Karten. 2016. Mitochondrial cholesterol: mechanisms of import and effects on mitochondrial function. *J. Bioenerg. Biomembr.* **48:** 137–151.
16. Cui, T. Z., and M. Kawamukai. 2009. Coq10, a mitochondrial coenzyme Q binding protein, is required for proper respiration in *Schizosaccharomyces pombe*. *FEBS J.* **276:** 748–759.
17. Wikström, M. K., and J. A. Berden. 1972. Oxidoreduction of cytochrome *b* in the presence of antimycin. *Biochim. Biophys. Acta.* **283:** 403–420.
18. Starkov, A. A., and G. Fiskum. 2001. Myxothiazol induces H_2O_2 production from mitochondrial respiratory chain. *Biochem. Biophys. Res. Commun.* **281:** 645–650.
19. Drõse, S., and U. Brandt. 2008. The mechanism of mitochondrial superoxide production by the cytochrome *bc1* complex. *J. Biol. Chem.* **283:** 21649–21654.
20. Busso, C., E. B. Tahara, R. Ogusucu, O. Augusto, J. R. Ferreira-Junior, A. Tzagoloff, A. J. Kowaltowski, and M. H. Barros. 2010. *Saccharomyces cerevisiae coq10* null mutants are responsive to antimycin A. *FEBS J.* **277:** 4530–4538.
21. Murai, M., K. Matsunobu, S. Kudo, K. Ifuku, M. Kawamukai, and H. Miyoshi. 2014. Identification of the binding site of the quinone-head group in mitochondrial Coq10 by photoaffinity labeling. *Biochemistry.* **53:** 3995–4003.
22. Montini, G., C. Malaventura, and L. Salviati. 2008. Early coenzyme Q_{10} supplementation in primary coenzyme Q_{10} deficiency. *N. Engl. J. Med.* **358:** 2849–2850.
23. Marcoff, L., and P. D. Thompson. 2007. The role of coenzyme Q_{10} in statin-associated myopathy: a systematic review. *J. Am. Coll. Cardiol.* **49:** 2231–2237.
24. Ayer, A., P. Macdonald, and R. Stocker. 2015. CoQ_{10} function and role in heart failure and ischemic heart disease. *Annu. Rev. Nutr.* **35:** 175–213.
25. Mortensen, S. A., F. Rosenfeldt, A. Kumar, P. Dolliner, K. J. Filipiak, D. Pella, U. Alehagen, G. Steurer, G. P. Littarru, and Q. S. S. Investigators. 2014. The effect of coenzyme Q_{10} on morbidity and mortality in chronic heart failure: results from Q-SYMBIO: a randomized double-blind trial. *JACC Heart Fail.* **2:** 641–649.
26. Burke, D., D. Dawson, and T. Stearns. 2000. Methods in Yeast Genetics. Cold Spring Harbor Laboratory Press, Plainview, NY.
27. Barkovich, R. J., A. Shtanko, J. A. Shepherd, P. T. Lee, D. C. Myles, A. Tzagoloff, and C. F. Clarke. 1997. Characterization of the *COQ5* gene from *Saccharomyces cerevisiae*. Evidence for a C-methyltransferase in ubiquinone biosynthesis. *J. Biol. Chem.* **272:** 9182–9188.
28. Hsu, A. Y., W. W. Poon, J. A. Shepherd, D. C. Myles, and C. F. Clarke. 1996. Complementation of *coq3* mutant yeast by mitochondrial targeting of the *Escherichia coli* UbiG polypeptide: evidence that UbiG catalyzes both O-methylation steps in ubiquinone biosynthesis. *Biochemistry.* **35:** 9797–9806.
29. Elble, R. 1992. A simple and efficient procedure for transformation of yeasts. *Biotechniques.* **13:** 18–20.
30. Hill, S., K. Hirano, V. V. Shmanai, B. N. Marbois, D. Vidovic, A. V. Bekish, B. Kay, V. Tse, J. Fine, C. F. Clarke, et al. 2011. Isotope-reinforced polyunsaturated fatty acids protect yeast cells from oxidative stress. *Free Radic. Biol. Med.* **50:** 130–138.
31. Hill, S., C. R. Lamberson, L. Xu, R. To, H. S. Tsui, V. V. Shmanai, A. V. Bekish, A. M. Awad, B. N. Marbois, C. R. Cantor, et al. 2012. Small amounts of isotope-reinforced polyunsaturated fatty acids suppress lipid autoxidation. *Free Radic. Biol. Med.* **53:** 893–906.
32. Glick, B. S., and L. A. Pon. 1995. Isolation of highly purified mitochondria from *Saccharomyces cerevisiae*. *Methods Enzymol.* **260:** 213–223.
33. Schägger, H., W. A. Cramer, and G. von Jagow. 1994. Analysis of molecular masses and oligomeric states of protein complexes by blue native electrophoresis and isolation of membrane protein complexes by two-dimensional native electrophoresis. *Anal. Biochem.* **217:** 220–230.
34. He, C. H., L. X. Xie, C. M. Allan, U. C. Tran, and C. F. Clarke. 2014. Coenzyme Q supplementation or over-expression of the yeast Coq8 putative kinase stabilizes multi-subunit Coq polypeptide complexes in yeast *coq* null mutants. *Biochim. Biophys. Acta.* **1841:** 630–644.
35. Wittig, I., H. P. Braun, and H. Schagger. 2006. Blue native PAGE. *Nat. Protoc.* **1:** 418–428.
36. Marbois, B., L. X. Xie, S. Choi, K. Hirano, K. Hyman, and C. F. Clarke. 2010. *para*-Aminobenzoic acid is a precursor in coenzyme Q_6 biosynthesis in *Saccharomyces cerevisiae*. *J. Biol. Chem.* **285:** 27827–27838.
37. Buchan, D. W., F. Minneci, T. C. Nugent, K. Bryson, and D. T. Jones. 2013. Scalable web services for the PSIPRED Protein Analysis Workbench. *Nucleic Acids Res.* **41:** W349–W357.
38. Jones, D. T., and D. Cozzetto. 2015. DISOPRED3: precise disordered region predictions with annotated protein-binding activity. *Bioinformatics.* **31:** 857–863.
39. Waterhouse, A., M. Bertoni, S. Bienert, G. Studer, G. Tauriello, R. Gumienny, F. T. Heer, T. A. P. de Beer, C. Rempfer, L. Bordoli, et al. 2018. SWISS-MODEL: homology modelling of protein structures and complexes. *Nucleic Acids Res.* **46:** W296–W303.
40. Chaudhury, S., S. Lyskov, and J. J. Gray. 2010. PyRosetta: a script-based interface for implementing molecular modeling algorithms using Rosetta. *Bioinformatics.* **26:** 689–691.
41. Benkert, P., S. C. Tosatto, and D. Schomburg. 2008. QMEAN: a comprehensive scoring function for model quality assessment. *Proteins.* **71:** 261–277.
42. Lüthy, R., J. U. Bowie, and D. Eisenberg. 1992. Assessment of protein models with three-dimensional profiles. *Nature.* **356:** 83–85.
43. Colovos, C., and T. O. Yeates. 1993. Verification of protein structures: patterns of nonbonded atomic interactions. *Protein Sci.* **2:** 1511–1519.
44. Chen, V. B., W. B. Arendall 3rd, J. J. Headd, D. A. Keedy, R. M. Immormino, G. J. Kapral, L. W. Murray, J. S. Richardson, and D. C. Richardson. 2010. MolProbity: all-atom structure validation for macromolecular crystallography. *Acta Crystallogr. D Biol. Crystallogr.* **66:** 12–21.
45. Trott, O., and A. J. Olson. 2010. AutoDock Vina: improving the speed and accuracy of docking with a new scoring function, efficient optimization, and multithreading. *J. Comput. Chem.* **31:** 455–461.
46. Adams, P. D., P. V. Afonine, G. Bunkoczi, V. B. Chen, I. W. Davis, N. Echols, J. J. Headd, L. W. Hung, G. J. Kapral, R. W. Grosse-Kunstleve, et al. 2010. PHENIX: a comprehensive Python-based system for macromolecular structure solution. *Acta Crystallogr. D Biol. Crystallogr.* **66:** 213–221.
47. Gerlt, J. A., J. T. Bouvier, D. B. Davidson, H. J. Imker, B. Sadkhin, D. R. Slater, and K. L. Whalen. 2015. Enzyme Function Initiative-Enzyme Similarity Tool (EFI-EST): a web tool for generating protein sequence similarity networks. *Biochim. Biophys. Acta.* **1854:** 1019–1037.
48. Shannon, P., A. Markiel, O. Ozier, N. S. Baliga, J. T. Wang, D. Ramage, N. Amin, B. Schwikowski, and T. Ideker. 2003. Cytoscape: a software environment for integrated models of biomolecular interaction networks. *Genome Res.* **13:** 2498–2504.
49. UniProt Consortium T. 2018. UniProt: the universal protein knowledgebase. *Nucleic Acids Res.* **46:** 2699.
50. Katoh, K., and D. M. Standley. 2013. MAFFT multiple sequence alignment software version 7: improvements in performance and usability. *Mol. Biol. Evol.* **30:** 772–780.
51. Nguyen, L. T., H. A. Schmidt, A. von Haeseler, and B. Q. Minh. 2015. IQ-TREE: a fast and effective stochastic algorithm for

estimating maximum-likelihood phylogenies. *Mol. Biol. Evol.* **32:** 268–274.
52. Miller, M. A., T. Schwartz, B. E. Pickett, S. He, E. B. Klem, R. H. Scheuermann, M. Passarotti, S. Kaufman, and M. A. O'Leary. 2015. A RESTful API for access to phylogenetic tools via the CIPRES science gateway. *Evol. Bioinform. Online.* **11:** 43–48.
53. Miller, M. A., W. Pfeiffer, and T. Schwartz. 2010. Creating the CIPRES Science Gateway for inference of large phylogenetic trees. Gateway Computing Environments Workshop (GCE) in New Orleans, LA. November 14, 2010. 1–8.
54. Hoang, D. T., O. Chernomor, A. von Haeseler, B. Q. Minh, and L. S. Vinh. 2018. UFBoot2: improving the Ultrafast Bootstrap approximation. *Mol. Biol. Evol.* **35:** 518–522.
55. NCBI Resource Coordinators. 2018. Database resources of the National Center for Biotechnology Information. *Nucleic Acids Res.* **46:** D8–D13.
56. Vrablik, M., L. Zlatohlavek, T. Stulc, V. Adamkova, M. Prusikova, L. Schwarzova, J. A. Hubacek, and R. Ceska. 2014. Statin-associated myopathy: from genetic predisposition to clinical management. *Physiol. Res.* **63(Suppl 3):** S327–S334.
57. Peterson, T. A., A. Adadey, I. Santana-Cruz, Y. Sun, A. Winder, and M. G. Kann. 2010. DMDM: domain mapping of disease mutations. *Bioinformatics.* **26:** 2458–2459.
58. Abd, T. T., and T. A. Jacobson. 2011. Statin-induced myopathy: a review and update. *Expert Opin. Drug Saf.* **10:** 373–387.
59. Busso, C., L. Bleicher, J. R. Ferreira-Junior, and M. H. Barros. 2010. Site-directed mutagenesis and structural modeling of Coq10p indicate the presence of a tunnel for coenzyme Q_6 binding. *FEBS Lett.* **584:** 1609–1614.
60. Gatta, A. T., A. C. Sauerwein, A. Zhuravleva, T. P. Levine, and S. Matthews. 2018. Structural insights into a StART-like domain in Lam4 and its interaction with sterol ligands. *Biochem. Biophys. Res. Commun.* **495:** 2270–2274.
61. Horenkamp, F. A., D. P. Valverde, J. Nunnari, and K. M. Reinisch. 2018. Molecular basis for sterol transport by StART-like lipid transfer domains. *EMBO J.* **37:** e98002.
62. Jentsch, J. A., I. Kiburu, K. Pandey, M. Timme, T. Ramlall, B. Levkau, J. Wu, D. Eliezer, O. Boudker, and A. K. Menon. 2018. Structural basis of sterol binding and transport by a yeast StARkin domain. *J. Biol. Chem.* **293:** 5522–5531.
63. Hsieh, E. J., P. Gin, M. Gulmezian, U. C. Tran, R. Saiki, B. N. Marbois, and C. F. Clarke. 2007. *Saccharomyces cerevisiae* Coq9 polypeptide is a subunit of the mitochondrial coenzyme Q biosynthetic complex. *Arch. Biochem. Biophys.* **463:** 19–26.
64. Tauche, A., U. Krause-Buchholz, and G. Rodel. 2008. Ubiquinone biosynthesis in *Saccharomyces cerevisiae*: the molecular organization of O-methylase Coq3p depends on Abc1p/Coq8p. *FEMS Yeast Res.* **8:** 1263–1275.
65. Yin, H., L. Xu, and N. A. Porter. 2011. Free radical lipid peroxidation: mechanisms and analysis. *Chem. Rev.* **111:** 5944–5972.
66. Porter, N. A. 1986. Mechanisms for the autoxidation of polyunsaturated lipids. *Acc. Chem. Res.* **19:** 262–268.
67. Iyer, L. M., A. M. Burroughs, and L. Aravind. 2006. The prokaryotic antecedents of the ubiquitin-signaling system and the early evolution of ubiquitin-like beta-grasp domains. *Genome Biol.* **7:** R60.
68. Hudson, C. M., B. Y. Lau, and K. P. Williams. 2014. Ends of the line for tmRNA-SmpB. *Front. Microbiol.* **5:** 421.
69. Zhang, Y., and M. Inouye. 2011. RatA (YfjG), an *Escherichia coli* toxin, inhibits 70S ribosome association to block translation initiation. *Mol. Microbiol.* **79:** 1418–1429.
70. Karzai, A. W., M. M. Susskind, and R. T. Sauer. 1999. SmpB, a unique RNA-binding protein essential for the peptide-tagging activity of SsrA (tmRNA). *EMBO J.* **18:** 3793–3799.
71. Karzai, A. W., E. D. Roche, and R. T. Sauer. 2000. The SsrA-SmpB system for protein tagging, directed degradation and ribosome rescue. *Nat. Struct. Biol.* **7:** 449–455.
72. Jouanneau, Y., H. S. Jeong, N. Hugo, C. Meyer, and J. C. Willison. 1998. Overexpression in *Escherichia coli* of the *rnf* genes from *Rhodobacter capsulatus*–characterization of two membrane-bound iron-sulfur proteins. *Eur. J. Biochem.* **251:** 54–64.
73. Reyes-Prieto, A., B. Barquera, and O. Juarez. 2014. Origin and evolution of the sodium-pumping NADH: ubiquinone oxidoreductase. *PLoS One.* **9:** e96696.
74. Biegel, E., S. Schmidt, J. M. Gonzalez, and V. Muller. 2011. Biochemistry, evolution and physiological function of the Rnf complex, a novel ion-motive electron transport complex in prokaryotes. *Cell. Mol. Life Sci.* **68:** 613–634.
75. Okamura, Y., Y. Aoki, T. Obayashi, S. Tadaka, S. Ito, T. Narise, and K. Kinoshita. 2015. COXPRESdb in 2015: coexpression database for animal species by DNA-microarray and RNAseq-based expression data with multiple quality assessment systems. *Nucleic Acids Res.* **43:** D82–D86.
76. Murley, A., and J. Nunnari. 2016. The emerging network of mitochondria-organelle contacts. *Mol. Cell.* **61:** 648–653.
77. Kornmann, B., E. Currie, S. R. Collins, M. Schuldiner, J. Nunnari, J. S. Weissman, and P. Walter. 2009. An ER-mitochondria tethering complex revealed by a synthetic biology screen. *Science.* **325:** 477–481.
78. Allan, C. M., A. M. Awad, J. S. Johnson, D. I. Shirasaki, C. Wang, C. E. Blaby-Haas, S. S. Merchant, J. A. Loo, and C. F. Clarke. 2015. Identification of Coq11, a new coenzyme Q biosynthetic protein in the CoQ-synthome in *Saccharomyces cerevisiae*. *J. Biol. Chem.* **290:** 7517–7534.
79. Floyd, B. J., E. M. Wilkerson, M. T. Veling, C. E. Minogue, C. Xia, E. T. Beebe, R. L. Wrobel, H. Cho, L. S. Kremer, C. L. Alston, et al. 2016. Mitochondrial protein interaction mapping identifies regulators of respiratory chain function. *Mol. Cell.* **63:** 621–632.
80. Chatr-Aryamontri, A., R. Oughtred, L. Boucher, J. Rust, C. Chang, N. K. Kolas, L. O'Donnell, S. Oster, C. Theesfeld, A. Sellam, et al. 2017. The BioGRID interaction database: 2017 update. *Nucleic Acids Res.* **45:** D369–D379.
81. Zhu, Q., A. K. Wong, A. Krishnan, M. R. Aure, A. Tadych, R. Zhang, D. C. Corney, C. S. Greene, L. A. Bongo, V. N. Kristensen, et al. 2015. Targeted exploration and analysis of large cross-platform human transcriptomic compendia. *Nat. Methods.* **12:** 211–214.
82. Kovalyov, L. I., M. A. Kovalyova, P. L. Kovalyov, M. V. Serebryakova, S. A. Moshkovskii, and S. S. Shishkin. 2006. Polymorphism of delta3,5-delta2,4-dienoyl-coenzyme A isomerase (the *ECH1* gene product protein) in human striated muscle tissue. *Biochemistry (Mosc.).* **71:** 448–453.
83. Uhlén, M., L. Fagerberg, B. M. Hallström, C. Lindskog, P. Oksvold, A. Mardinoglu, A. Sivertsson, C. Kampf, E. Sjöstedt, A. Asplund, et al. 2015. Proteomics. Tissue-based map of the human proteome. *Science.* **347:** 1260419.
84. Fagerberg, L., B. M. Hallstrom, P. Oksvold, C. Kampf, D. Djureinovic, J. Odeberg, M. Habuka, S. Tahmasebpoor, A. Danielsson, K. Edlund, et al. 2014. Analysis of the human tissue-specific expression by genome-wide integration of transcriptomics and antibody-based proteomics. *Mol. Cell. Proteomics.* **13:** 397–406.
85. Subramanian, K., A. Jochem, M. Le Vasseur, S. Lewis, B. R. Paulson, T. R. Reddy, J. D. Russell, J. J. Coon, D. J. Pagliarini, and J. Nunnari. 2019. Coenzyme Q biosynthetic proteins assemble in a substrate-dependent manner into domains at ER-mitochondria contacts. *J. Cell Biol.* **218:** 1353–1369.
86. Clark, B. J. 2012. The mammalian START domain protein family in lipid transport in health and disease. *J. Endocrinol.* **212:** 257–275.
87. Alpy, F., C. Wendling, M. C. Rio, and C. Tomasetto. 2002. MENTHO, a MLN64 homologue devoid of the START domain. *J. Biol. Chem.* **277:** 50780–50787.
88. Alpy, F., and C. Tomasetto. 2006. MLN64 and MENTHO, two mediators of endosomal cholesterol transport. *Biochem. Soc. Trans.* **34:** 343–345.
89. Persson, B., and Y. Kallberg. 2013. Classification and nomenclature of the superfamily of short-chain dehydrogenases/reductases (SDRs). *Chem. Biol. Interact.* **202:** 111–115.
90. Baertling, F., L. Sanchez-Caballero, M. A. M. van den Brand, C. W. Fung, S. H. Chan, V. C. Wong, D. M. E. Hellebrekers, I. F. M. de Coo, J. A. M. Smeitink, R. J. T. Rodenburg, et al. 2018. *NDUFA9* point mutations cause a variable mitochondrial complex I assembly defect. *Clin. Genet.* **93:** 111–118.
91. Yamamoto, T., H. Tamaki, C. Katsuda, K. Nakatani, S. Terauchi, H. Terada, and Y. Shinohara. 2013. Molecular basis of interactions between mitochondrial proteins and hydroxyapatite in the presence of Triton X-100, as revealed by proteomic and recombinant techniques. *J. Chromatogr. A.* **1301:** 169–178.
92. Cronan, J. E. 2014. Biotin and lipoic acid: synthesis, attachment, and regulation. *Ecosal Plus.* **6:** doi:10.1128/ecosalplus.ESP-0001-2012.
93. Hiltunen, J. K., M. S. Schonauer, K. J. Autio, T. M. Mittelmeier, A. J. Kastaniotis, and C. L. Dieckmann. 2009. Mitochondrial fatty acid synthesis type II: more than just fatty acids. *J. Biol. Chem.* **284:** 9011–9015.
94. Hibbs, M. A., D. C. Hess, C. L. Myers, C. Huttenhower, K. Li, and O. G. Troyanskaya. 2007. Exploring the functional landscape of

gene expression: directed search of large microarray compendia. *Bioinformatics*. **23:** 2692–2699.
95. Eisenberg-Bord, M., H. S. Tsui, D. Antunes, L. Fernández-del-Río, M. C. Bradley, C. D. Dunn, T. P. T. Nguyen, D. Rapaport, C. F. Clarke, and M. Schuldiner. 2019. The endoplasmic reticulum-mitochondria encounter structure complex coordinates coenzyme Q biosynthesis. *Contact (Thousand Oaks)*. **2:** 2515256418825409.
96. Cohen, Y., Y. A. Klug, L. Dimitrov, Z. Erez, S. G. Chuartzman, D. Elinger, I. Yofe, K. Soliman, J. Gartner, S. Thoms, et al. 2014. Peroxisomes are juxtaposed to strategic sites on mitochondria. *Mol. Biosyst.* **10:** 1742–1748.
97. Merkwirth, C., and T. Langer. 2008. Mitofusin 2 builds a bridge between ER and mitochondria. *Cell.* **135:** 1165–1167.
98. Mourier, A., E. Motori, T. Brandt, M. Lagouge, I. Atanassov, A. Galinier, G. Rappl, S. Brodesser, K. Hultenby, C. Dieterich, et al. 2015. Mitofusin 2 is required to maintain mitochondrial coenzyme Q levels. *J. Cell Biol.* **208:** 429–442.
99. Gin, P., and C. F. Clarke. 2005. Genetic evidence for a multi-subunit complex in coenzyme Q biosynthesis in yeast and the role of the Coq1 hexaprenyl diphosphate synthase. *J. Biol. Chem.* **280:** 2676–2681.
100. Do, T. Q., J. R. Schultz, and C. F. Clarke. 1996. Enhanced sensitivity of ubiquinone-deficient mutants of *Saccharomyces cerevisiae* to products of autoxidized polyunsaturated fatty acids. *Proc. Natl. Acad. Sci. USA.* **93:** 7534–7539.
101. Hsu, A. Y., T. Q. Do, P. T. Lee, and C. F. Clarke. 2000. Genetic evidence for a multi-subunit complex in the O-methyltransferase steps of coenzyme Q biosynthesis. *Biochim. Biophys. Acta.* **1484:** 287–297.
102. Gin, P., A. Y. Hsu, S. C. Rothman, T. Jonassen, P. T. Lee, A. Tzagoloff, and C. F. Clarke. 2003. The *Saccharomyces cerevisiae* *COQ6* gene encodes a mitochondrial flavin-dependent monooxygenase required for coenzyme Q biosynthesis. *J. Biol. Chem.* **278:** 25308–25316.
103. Marbois, B. N., and C. F. Clarke. 1996. The *COQ7* gene encodes a protein in *Saccharomyces cerevisiae* necessary for ubiquinone biosynthesis. *J. Biol. Chem.* **271:** 2995–3004.
104. Johnson, A., P. Gin, B. N. Marbois, E. J. Hsieh, M. Wu, M. H. Barros, C. F. Clarke, and A. Tzagoloff. 2005. *COQ9*, a new gene required for the biosynthesis of coenzyme Q in *Saccharomyces cerevisiae*. *J. Biol. Chem.* **280:** 31397–31404.
105. Poon, W. W., R. J. Barkovich, A. Y. Hsu, A. Frankel, P. T. Lee, J. N. Shepherd, D. C. Myles, and C. F. Clarke. 1999. Yeast and rat Coq3 and *Escherichia coli* UbiG polypeptides catalyze both O-methyltransferase steps in coenzyme Q biosynthesis. *J. Biol. Chem.* **274:** 21665–21672.
106. Belogrudov, G. I., P. T. Lee, T. Jonassen, A. Y. Hsu, P. Gin, and C. F. Clarke. 2001. Yeast *COQ4* encodes a mitochondrial protein required for coenzyme Q synthesis. *Arch. Biochem. Biophys.* **392:** 48–58.
107. Baba, S. W., G. I. Belogrudov, J. C. Lee, P. T. Lee, J. Strahan, J. N. Shepherd, and C. F. Clarke. 2004. Yeast Coq5 C-methyltransferase is required for stability of other polypeptides involved in coenzyme Q biosynthesis. *J. Biol. Chem.* **279:** 10052–10059.
108. Tran, U. C., B. Marbois, P. Gin, M. Gulmezian, T. Jonassen, and C. F. Clarke. 2006. Complementation of *Saccharomyces cerevisiae coq7* mutants by mitochondrial targeting of the *Escherichia coli* UbiF polypeptide: two functions of yeast Coq7 polypeptide in coenzyme Q biosynthesis. *J. Biol. Chem.* **281:** 16401–16409.
109. Hsieh, E. J., J. B. Dinoso, and C. F. Clarke. 2004. A $tRNA^{TRP}$ gene mediates the suppression of *cbs2–223* previously attributed to *ABC1/COQ8*. *Biochem. Biophys. Res. Commun.* **317:** 648–653.

APPENDIX V

The Endoplasmic Reticulum-Mitochondria Encounter Structure Complex Coordinates Coenzyme Q Biosynthesis

Contact
Volume 2: 1–14
© The Author(s) 2019
Article reuse guidelines:
sagepub.com/journals-permissions
DOI: 10.1177/2515256418825409
journals.sagepub.com/home/ctc
SAGE

The Endoplasmic Reticulum-Mitochondria Encounter Structure Complex Coordinates Coenzyme Q Biosynthesis

Michal Eisenberg-Bord[1,#], Hui S. Tsui[2,#], Diana Antunes[3,#], Lucía Fernández-del-Río[2,#], Michelle C. Bradley[2], Cory D. Dunn[4,5], Theresa P. T. Nguyen[6], Doron Rapaport[3], Catherine F. Clarke[2], and Maya Schuldiner[1]

Abstract

Loss of the endoplasmic reticulum (ER)-mitochondria encounter structure (ERMES) complex that resides in contact sites between the yeast ER and mitochondria leads to impaired respiration; however, the reason for that is not clear. We find that in *ERMES* null mutants, there is an increase in the level of mRNAs encoding for biosynthetic enzymes of coenzyme Q_6 (CoQ_6), an essential electron carrier of the mitochondrial respiratory chain. We show that the mega complexes involved in CoQ_6 biosynthesis (CoQ synthomes) are destabilized in ERMES mutants. This, in turn, affects the level and distribution of CoQ_6 within the cell, resulting in reduced mitochondrial CoQ_6. We suggest that these outcomes contribute to the reduced respiration observed in ERMES mutants. Fluorescence microscopy experiments demonstrate close proximity between the CoQ synthome and ERMES, suggesting a spatial coordination. The involvement of the ER-mitochondria contact site in regulation of CoQ_6 biogenesis highlights an additional level of communication between these two organelles.

Keywords

coenzyme Q, endoplasmic reticulum, ER-mitochondrial encounter structure, mitochondrion (mitochondria)

Introduction

Over the past two decades, our initial conception of eukaryotic cell architecture has been gradually altered. The original idea of solitary organelles scattered sparsely in the cytosol has been replaced by an appreciation of the close cooperation that exists between organelles. Indeed, organelles are tightly packed together and are anything but solitary. All organelles appear to have the capacity to be tethered to one another by designated structures termed membrane contact sites, and these contact sites are generated by use of tethering molecules (Kakimoto et al., 2018; Shai et al., 2018; Valm et al., 2017). Such areas of close membrane apposition allow for the transfer of metabolites, lipids, and other molecules between the two organelles (Eisenberg-Bord, Shai, Schuldiner, & Bohnert, 2016). One of the most studied contact sites is formed between the endoplasmic reticulum (ER) and mitochondria. In the budding yeast *Saccharomyces cerevisiae* (hereafter termed yeast),

[1]Department of Molecular Genetics, Weizmann Institute of Science, Rehovot, Israel
[2]Department of Chemistry and Biochemistry and the Molecular Biology Institute, UCLA, Los Angeles, CA, USA
[3]Interfaculty Institute of Biochemistry, University of Tübingen, Tübingen, Germany
[4]Institute of Biotechnology, Helsinki Institute of Life Science, University of Helsinki, Helsinki, Finland
[5]Department of Molecular Biology and Genetics, Koç University, İstanbul, Turkey
[6]Department of Chemistry, Loyola University Maryland, Baltimore, MD, USA

[#]The first four authors contributed equally to this work.

Received July 29, 2018. Revised December 27, 2018. Accepted December 27, 2018.

Corresponding Authors:
Maya Schuldiner, Weizmann Institute, 234 Herzl St, Rehovot 7610001, Israel.
Email: maya.schuldiner@weizmann.ac.il
Catherine F. Clarke, Department of Chemistry and Biochemistry and the Molecular Biology Institute, UCLA, Los Angeles, CA, USA 90095-1569.
Email: cathy@chem.ucla.edu
Doron Rapaport, University of Tübingen Hoppe-Seyler-Str. 4 Tübingen, 72076 Germany.
Email: doron.rapaport@uni-tuebingen.de

a prominent complex promoting association of the ER and mitochondria is the ER-mitochondria encounter structure (ERMES; Kornmann et al., 2009). ERMES is composed of four subunits: two mitochondrial subunits (Mdm10 and Mdm34), an ER localized subunit (Mmm1), and a soluble subunit (Mdm12).

One of the most closely examined roles of ERMES is the transfer of phospholipids. As mitochondria cannot synthesize most of the lipids that they require, phospholipids, sterols, and ceramide/sphingolipids must be imported from the ER. Hence, ER-mitochondria contact sites accommodate many lipid transfer factors and proteins that are involved in lipid metabolism (Dimmer & Rapaport, 2017). Recently, it was shown that the Mmm1-Mdm12 complex can mediate phospholipid transfer *in vitro* and that mutations in *MMM1* or *MDM12* lead to impaired phospholipid transfer through the ERMES complex *in vivo* (Kawano et al., 2018). Surprisingly, ERMES mutants typically exhibit only a mild decrease in specific phospholipids at mitochondria due to the existence of compensatory mechanisms for phospholipid transfer (González Montoro et al., 2018; John Peter et al., 2017; Kojima, Endo, & Tamura, 2016; Lang, Peter, Walter, & Kornmann, 2015; Tan et al., 2013). Despite the moderate effects on lipid transfer between organelles, ERMES disruption leads to a wide array of cellular phenotypes, including loss of mitochondrial morphology, increased loss of mitochondrial DNA, and reduced respiratory capacity (Berger, Sogo, & Yaffe, 1997; Hobbs, Srinivasan, McCaffery, & Jensen, 2001; Kornmann et al., 2009; Youngman et al., 2004). Why loss of ERMES causes these adverse phenotypes, including respiratory deficiency, has not yet been fully elucidated. Hence, we have focused our attention on the role of ERMES in regulating respiration.

Here, we show that cells lacking ERMES components exhibit increased mRNA levels for proteins that participate in the coenzyme Q_6 (CoQ_6) biosynthetic pathway. CoQ_6 is a polyisoprenylated benzoquinone lipid that functions within the electron transport chain of the inner mitochondrial membrane of yeast. CoQ_6 can also act as a lipophilic antioxidant (Awad et al., 2018; Tran & Clarke, 2007). All of the steps required for the assembly of the polyisoprenoid diphosphate tail of CoQ, its ligation to aromatic ring precursors, and modification of the ring precursor are catalyzed by Coq enzymes associated with the matrix side of the mitochondrial inner membrane (Awad et al., 2018; Bentinger, Tekle, & Dallner, 2010). Many of the these Coq polypeptides (Coq3-Coq9 and Coq11) assemble within a mega complex termed the CoQ synthome (Allan et al., 2015; Belogrudov et al., 2001; He, Xie, Allan, Tran, & Clarke, 2014; Marbois et al., 2005; Marbois, Gin, Gulmezian, & Clarke, 2009). Synthesis of the polyisoprenoid tail of CoQ_6 originates from compounds that derive from the mevalonate pathway associated with the ER, suggesting that the ER-mitochondria contact site might promote movement of CoQ_6, or its biochemical intermediates and precursors, between these two organelles.

Indeed, we show that the CoQ synthome is destabilized in ERMES mutants, and this results in transcriptionally upregulated, yet inefficient, *de novo* CoQ_6 biosynthesis. Such compromised synthesis results in an increase of CoQ_6-intermediates as well as accumulation of CoQ_6 at non-mitochondrial cellular membranes. We further demonstrate that ERMES mutants harbor decreased steady-state levels of CoQ_6 and CoQ_6-intermediates within mitochondria. This reduced level may contribute to the respiratory deficiency. Furthermore, ERMES-mediated contacts seem to be located in proximity to specialized matrix niches where the CoQ synthome is enriched, suggesting a spatially regulated process. Our study provides new insights into the relevance of ER-mitochondria contacts to CoQ_6 homeostasis and, more broadly, to cellular respiration.

Materials and Methods

Strains and Plasmids

Saccharomyces cerevisiae strains and plasmids used in this study are listed in Table S1 and Table S2, respectively. Yeast strains were based on strains S288C (BY4741; Brachmann et al., 1998) or W303 (Thomas & Rothstein, 1989). Transformations of polymerase chain reaction (PCR) products into yeast cells were performed using the Li-acetate method (Gietz & Woods, 2006; Janke et al., 2004; Longtine et al., 1998). Primers were designed using Primers-4-Yeast: http://www.weizmann.ac.il/Primers-4-Yeast/ (Yofe & Schuldiner, 2014).

RNA-Sequencing

S288C (BY4741) cells were cultured overnight in a synthetic medium SD (2% [wt/vol] glucose, 0.67% [wt/vol] yeast nitrogen base with ammonium sulfate and amino acid supplements) at 30°C. W303 cells were cultured overnight in a synthetic medium SGly (3% [wt/vol] glycerol, 0.67% [wt/vol] yeast nitrogen base with ammonium sulfate and amino acid supplements) at 30°C. In the morning, cells were back-diluted to OD_{600}~ 0.01 and followed until reaching OD_{600}~ 0.2. Cells were centrifuged (3,000 *g*, 3 min), and the pellet was frozen in liquid nitrogen and stored at −80°C until further analysis.

For all samples, RNA was purified as described (Voichek, Bar-Ziv, and Barkai, 2016). Briefly, RNA was extracted according to a protocol of Nucleospin® 96 RNA Kit (Machery-Nagel) with two modifications: Lysis was performed by adding 450 µl of lysis buffer containing 1 M sorbitol, 100 mM EDTA, and 0.45 µl

lyticase (10 IU/µl) to cells in a 96 deep-well plate. The plate was then incubated for 30 min at 30°C, centrifuged (3,000 *g*, 10 min) and the supernatant was removed. In addition, dithiothreitol was used as a replacement for β-mercaptoethanol.

For S288C (BY4741) cells, RNA was fragmented, RNA molecules harboring a poly(A) were enriched, and this was followed by cDNA preparation, barcoding, and sequencing using Illumina HiSeq 2500, as described in Voichek et al. (2016). For W303 cells, RNA libraries were created by reverse transcription with a barcoded poly(T). DNA-RNA hybrids were pooled, followed by use of a hyperactive variant of the Tn5 transposase for fragmentation. SDS (0.2%) was used to strip Tn5 from DNA. Following SDS treatment, samples were purified using Solid Phase Reversible Immobilization (Beckman Coulter) Beads. cDNA was then amplified using PCR and sequenced using the Illumina NextSeq 500.

Single end reads were mapped to *S. cerevisiae* genome (R64 in SGD; Cherry et al., 2012) using bowtie (parameters: –best –a –m 2 –strata –5 10; Liu et al., 2005). Following alignment, reads mapped to rRNA were excluded. For S288C samples, reads were down sampled to 400,000 reads and normalized for PCR bias using the unique molecular identifier (Kivioja et al., 2012). For all samples, expression of each gene was the summary of reads aligned between 400 bp upstream and 200 bp downstream of the predicted open reading frame. The gene expression summary was normalized to be 1,000,000 and a gene with an expression below 10 was excluded from further analysis (Voichek et al., 2016). Each sample was analyzed twice, and values shown are typically the average of the two. However, if only one sample had a value, that value was utilized.

Mitochondrial Purification

Yeast wild-type and ERMES mutant cultures were cultured in YPGly (3% [wt/vol] glycerol, 1% [wt/vol] Bacto yeast extract, and 2% [wt/vol] Bacto peptone) at 30°C. Cells were harvested at $OD_{600} < 4.0$, and mitochondria were purified with discontinuous Nycodenz as described (Glick & Pon, 1995). Protease inhibitor mixture (Roche Complete EDTA-free), phosphatase inhibitor cocktail set II (EMD Millipore), and phosphatase inhibitor cocktail set 3 (Sigma-Aldrich) were added to the solutions. Gradient-purified mitochondria were frozen in liquid nitrogen and stored at −80°C until further analysis. Mitochondria from yeast Δ*coq* mutants were purified in the same manner from cultures expanded in YPGal medium (2% [wt/vol] galactose, 0.1% [wt/vol] dextrose, 1% [wt/vol] Bacto yeast extract, and 2% [wt/vol] Bacto peptone).

SDS-PAGE Analysis of Steady-State Levels of Coq Polypeptides

Purified mitochondria were resuspended in SDS sample buffer consisting of 50 mM Tris, pH 6.8, 10% glycerol, 2% SDS, 0.1% bromophenol blue, and 1.33% β-mercaptoethanol and proteins were separated by SDS-PAGE on 12% Tris-glycine polyacrylamide gels. An aliquot of 25 µg of purified mitochondria, as measured by the bicinchoninic acid assay standardized using bovine serum albumin, was loaded in each lane.

Two-Dimensional Blue Native- and SDS-PAGE Analysis of CoQ Synthome

Analyses of protein complexes by blue native (BN) gel electrophoresis were performed as previously described (Schagger, Cramer, & Vonjagow, 1994; Wittig, Braun, & Schägger, 2006). Briefly, an aliquot of 200 µg protein of purified mitochondria was pelleted by centrifugation (14,000 *g*, 10 min) and solubilized at a concentration of 4 mg protein/ml on ice for 1 h with BN solubilization buffer containing 11 mM HEPES, pH 7.4, 0.33 M sorbitol, 1× NativePAGE sample buffer (Thermo Fisher Scientific), 16 mg/ml digitonin (Biosynth), Roche Complete EDTA-free protease inhibitor mixture (Roche Complete EDTA-free), phosphatase inhibitor cocktail set II, and phosphatase inhibitor cocktail set 3. The soluble fraction was obtained by centrifugation (100,000 *g*, 10 min) and the protein concentration in the supernatant was determined by bicinchoninic acid assay. NativePAGE 5% G-250 sample additive (Thermo Fisher Scientific) was added to the supernatant to a final concentration of 0.25%. The first-dimension BN gel electrophoresis was performed using NativePAGE 4-16% Bis-Tris gel 1.0 mm x 10 wells (Thermo Fisher Scientific). First-dimension gel slices were soaked in hot SDS sample buffer for 15 min before loading them onto second dimension 12% Tris-glycine polyacrylamide gels. The high molecular weight standards for first-dimension BN gel electrophoresis were obtained from GE Healthcare (Sigma-Aldrich) and the molecular weight standards for the second dimension SDS-PAGE were obtained from Bio-Rad.

Immunoblot Analyses

Proteins were transferred onto 0.45 µm nitrocellulose membrane (Bio-Rad). Membranes were blocked in 0.5% bovine serum albumin, 0.1% Tween 20, 0.02% SDS in phosphate-buffered saline. Membranes were probed with primary antibodies in the same blocking buffer at the dilutions listed in Table S3. IRDye 680LT goat anti-rabbit IgG secondary antibody or IRDye 800CW goat anti-mouse IgG secondary antibody

(LiCOR) was used at 1:10,000 dilutions. Blot images were recorded using LiCOR Odyssey Infrared Scanner (LiCOR).

BN-PAGE and Analysis of ATP Synthase

Wild type and Δ*mdm10* of the W303 background were grown in SLac (2% [wt/vol] lactate, 0.67% [wt/vol] Bacto yeast nitrogen base without amino acids), harvested at $OD_{600} < 2.0$ and isolated by differential centrifugation as described (Daum, Bohni, and Schatz (1982). BN-PAGE was performed as described earlier (Schägger, 2002). Briefly, 100 µg mitochondria were lysed in 40 µl buffer containing digitonin (1% digitonin, 20 mM Tris-HCl, 0.1 mM EDTA, 50 mM NaCl, 10% [vol/vol] glycerol, 1 mM PMSF, pH 7.2). After incubation on ice for 15 min and a clarifying spin (30,000 *g*, 15 min, 2°C), 5 µl sample buffer (5% (w/v) Coomassie blue G, 500 mM 6-amino-N-caproic acid, 100 mM Bis-Tris, pH 7.0) was added. The native complexes were analyzed by electrophoresis in a 6–14% gradient of acrylamide blue native gel. Proteins were transferred to polyvinylidene fluoride membranes and proteins were further analyzed by immunodecoration.

Stable Isotope Labeling

Cells were shaken overnight at 30°C in 100 ml of YPGly and diluted the next morning to an OD_{600} ~0.1 with fresh YPGly. The cultures were incubated as before until they reached an OD_{600} of 0.6. Then ethanol (as vehicle control) or 8 µg/ml of the stable isotopes $^{13}C_6$-pABA or $^{13}C_6$-4HB were added, and the cultures were expanded for an additional 5 h. At each time point, triplicates of 10 ml culture were harvested by centrifugation (3,000 *g*, 5 min). Cell pellets were stored at −20°C.

Lipid Extractions and Analysis of CoQ_6 and CoQ_6 Intermediates

For lipid extractions, approximately 100 µg of purified mitochondria from each strain were prepared in triplicates. The same amount of internal standard CoQ_4 was added to all samples and standards, followed by the addition of 2 ml methanol. Lipids were extracted twice, each time with 2 ml petroleum ether. Extracted lipids were dried down with N_2 and stored at −20°C. Lipid extraction from isotopically labeled whole cell was performed in the same way from frozen cell pellets in triplicate.

For lipid analyses, dried lipids were reconstituted in 200 µl of 0.5 mg/ml benzoquinone in order to oxidize hydroquinones to quinones. An aliquot of 20 µl of each sample was injected into a 4000 QTRAP linear MS/MS spectrometer (Applied Biosystems). Applied Biosystems software, Analyst version 1.4.2, was used for data acquisition and processing. The chromatographic separation was carried out using a Luna 5 µm phenyl-hexyl column (100 × 4.6 mm, 5 µm; Phenomenex) and a mobile phase consisted of 95:5 methanol/isopropanol solution with 2.5 mM ammonium formate as solution A and 100% isopropanol solution with 2.5 mM ammonium formate as solution B. The percentage of solution B was increased linearly from 0 to 10% over 7 min, whereby the flow rate was increased from 650 to 800 µl/min. Each sample was analyzed using multiple reaction monitoring mode. The precursor-to-product ion transitions monitored for each sample are listed in Table S4. The area value of each peak, normalized with the correspondent standard curve and internal standard, was referred to the total mitochondrial protein present in the sample or total OD of cells in each cell pellet. Statistical analysis was performed with GraphPad Prism with one-way analysis of variance Bonferroni's multiple comparisons test, with the Greenhouse-Geisser correction for mitochondrial lipid analyses, and with two-way analysis of variance Dunnett's multiple comparisons test for whole cell lipid analyses.

Microscopy

Yeast were cultured overnight at 30°C in either SGly for W303 cells or SD for S288C strain. In the morning, cells were back-diluted to OD_{600}~0.2 and cultured until reaching mid-logarithmic phase. Cells were then moved to glass-bottom, 384-well microscope plates (Matrical Bioscience) coated with Concanavalin A. After 20 min incubation at room temperature to enable adherence of cells to the matrix, the wells were washed with medium. Cells were then imaged at room temperature using a 60× oil lens (NA 1.4) in the VisiScope Confocal Cell Explorer system, which is composed of a Zeiss Yokogawa spinning disk scanning unit (CSU-W1) coupled with an inverted IX83 microscope (Olympus). Single–focal-plane images were taken using a PCO-Edge sCMOS camera, controlled by VisiView software (GFP-488 nm, RFP-561 nm, or BFP-405 nm). Images were reviewed using ImageJ, where brightness adjustment and cropping were performed.

Results

Yeast Lacking ERMES Have Higher Levels of Transcripts for Coenzyme Q Biosynthesis Enzymes

To investigate how ERMES contributes to the respiratory capacity of yeast cells, we measured the transcriptional response prompted by deletion of genes encoding ERMES subunits. We performed RNA sequencing on ERMES mutants from two different yeast genetic backgrounds: W303 yeast that were cultured on medium

containing glycerol (a nonfermentable carbon source), to ensure preservation of their mitochondrial DNA (Hobbs et al., 2001), or S288C (BY4741) yeast, in which the ERMES mutants harbor reduced levels of mitochondrial DNA, and were therefore cultured on medium containing glucose to enable fermentation (the complete list of mRNA levels in ERMES mutants is in Table S5).

When surveying transcripts which are associated with mitochondrial respiration, we noticed that the mRNA levels of most *COQ* genes involved in the biosynthesis of CoQ_6 were elevated relative to those in the respective control, in both genetic backgrounds and irrespective of the medium used (Figure 1(a) for W303 and Figure S1(a) for S288C). Of note, the mRNA levels of genes encoding for subunits of the respiration complexes did not show a consistent trend of either up- or downregulation (Figure S1(b).

We therefore tested whether the higher mRNA levels of the *COQ* genes resulted in higher protein levels of those polypeptides, in mitochondria purified from W303 cells (Figure 1(b)). We examined the steady-state levels of Coq proteins that have previously been identified as members of the CoQ synthome, as well as Coq10, which is not part of the CoQ synthome but is thought to chaperone CoQ_6 from the synthome to sites of function (Allan et al., 2013; Barros et al., 2005). Surprisingly, we observed that the steady-state levels of all Coq proteins in the mutant cells were either similar, or even slightly reduced, relative to their amounts in control cells (Figure 1(b)).

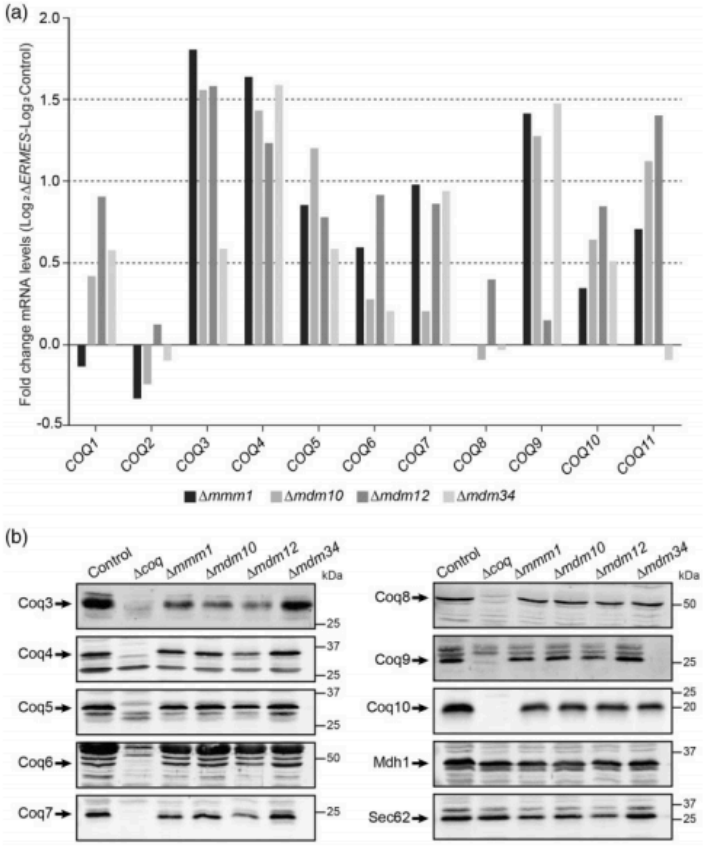

Figure 1. Cells lacking ERMES show higher levels of *COQ* mRNAs without alterations to Coq proteins. (a) Levels of mRNAs of the indicated *COQ* genes were measured in different W303-based strains deleted for ERMES subunits (Δ*mmm1*, Δ*mdm10*, Δ*mdm12* Δ*mdm34*), and a control strain, during growth in medium containing glycerol. The majority of *COQ* biosynthetic genes show higher mRNA levels compared to the control. Values are averages of two biological repeats. (b) Immunoblotting for steady-state levels of Coq polypeptides in purified mitochondria isolated from the indicated W303-based strains. Shown are mutants of the ERMES complex (Δ*mmm1*, Δ*mdm10*, Δ*mdm12*, and Δ*mdm34*), Δ*coq* (Δ*coq3*-Δ*coq10*) and a control, demonstrating that steady-state levels of the different Coq polypeptides were not dramatically altered in the ERMES deletion strains. Immunoblotting was performed with antisera against designated yeast Coq polypeptides (Coq3-Coq10), Mdh1 as a mitochondrial marker, and Sec62 as an ER marker. Arrows denote the corresponding protein in their respective blots. Images are representative gels from at least two biological replicates.

The CoQ Synthome Is Destabilized in the Absence of ERMES Subunits

As the overall mRNA levels of the *COQ* transcripts were higher in ERMES deletions, yet there was no major difference in protein levels, it seems that Coq proteins might be less stable in cells lacking the ERMES complex. Since most of the Coq polypeptides assemble in the CoQ synthome (Belogrudov et al., 2001; He et al., 2014; Marbois et al., 2005; Marbois et al., 2009) and proteins may become unstable when not assembled properly into their natural complexes, we examined the CoQ synthome by two-dimensional BN-PAGE (Figures 2 and S2(a)). Previously, the CoQ synthome was studied when galactose was used as a carbon source (He et al., 2014; Nguyen et al., 2014). However, to match the conditions we previously used for our assays, we followed Coq4, Coq5, and Coq9 in mitochondrial lysates from glycerol-cultured W303 cells. As expected, in control cells, the CoQ synthome was represented by high molecular weight signals, spanning a size range of 140 kDa to >1 MDa for both Coq4 and Coq9 (Figures 2(a) and (b) and S2(a)) and between 440 kDa to >1 MDa for Coq5 (Figure 2(b)). However, in the ERMES mutant strains, the majority of very large species (>MDa), representing the CoQ synthome, was replaced by subcomplexes with apparent migration equal to or less than ~440 kDa (Figures 2 and S2(a)), indicating that the CoQ synthome is indeed destabilized in the absence of the ERMES complex. This is not due to a general destabilization of mitochondrial complexes, as the ATP synthase (complex V) was not affected by the absence of the ERMES subunit Mdm10 (Figure S2(b)). Furthermore, previous work did not reveal any change in the migration behavior of porin oligomers and the Tim22 complex in Δ*mdm10* strains (Meisinger et al., 2004). Collectively, our current results, alongside previous observations, suggest that the effect of ERMES mutants on the CoQ synthome is specific.

ERMES Deletion Strains Show Elevated De Novo *Synthesis of CoQ_6 and Accumulate CoQ_6 and CoQ_6-Intermediates in Whole Cells*

To quantify how the biosynthesis of CoQ_6 is affected by destabilization of the CoQ synthome in ERMES mutants,

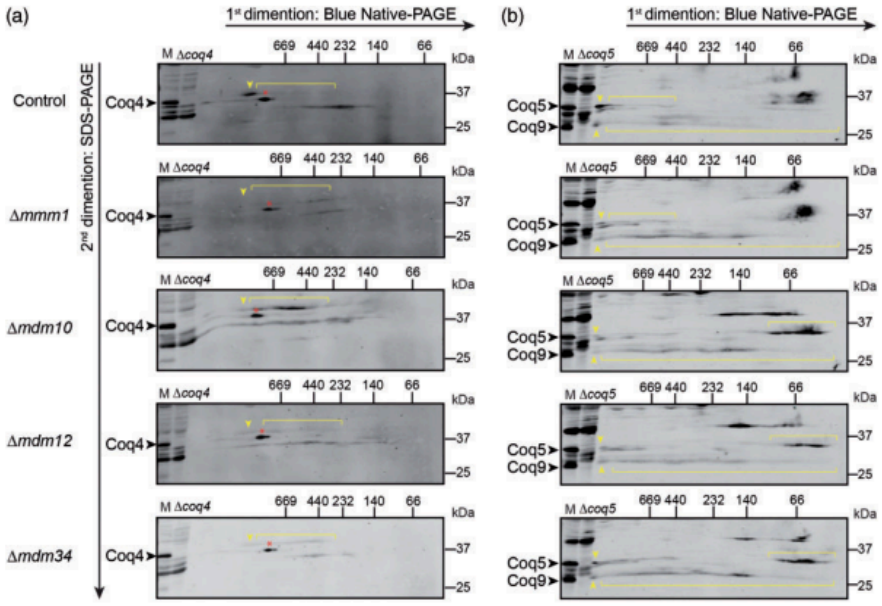

Figure 2. The CoQ synthome is destabilized in the absence of ERMES subunits. (a) Two-dimensional Blue Native-SDS-PAGE gel electrophoresis analysis of the CoQ synthome in mitochondria from ERMES mutants or from a wild-type (WT) control strain. Gels were immunoblotted against Coq4. In the control sample, the CoQ synthome appears as complexes ranging from 232 kDa to >1 MDa (the positions of the synthome is marked by the yellow arrow), while in the Δ*ERMES* strains, the high molecular weight signal is replaced by a signal dispersed over a range of smaller molecular weights (indicated by brackets). The relevant band was identified by comparing the bands in the WT and Δ*coq4* lanes. The red asterisk (*) indicates a discrete nonspecific signal observed with the antisera to Coq4. (b) Two-dimensional Blue Native-SDS-PAGE gel electrophoresis was performed as described in (a). Mitochondria from Δ*coq5* strain were used to identify specific bands (Coq9 is also destabilized and undetectable in the Δ*coq5* strain). Gels were immunoblotted against Coq5 and Coq9. The strong Coq5 and Coq9 bands in the higher molecular weight (>669 kDa) in the control sample (indicated by yellow arrows) are weaker in the Δ*ERMES* strains and are replaced by an additional diffuse signal in the lower molecular weights (indicated by brackets).

we measured *de novo* synthesis of CoQ_6 *in vivo*. Yeast cells may utilize either para-aminobenzoic acid (pABA) or 4-hydroxybenzoic acid (4HB) as ring precursors of CoQ_6 (Marbois et al., 2010; Pierrel et al., 2010). Early-stage intermediates, hexaprenyl-aminobenzoic acid (HAB) and hexaprenyl-hydroxybenzoic acid (HHB) are derived from prenylation of pABA or 4HB, respectively. Subsequent modifications of the aromatic ring produce late-stage intermediates such as demethyl-demethoxy-Q_6H_2 ($DDMQ_6$), and demethoxy-Q_6H_2 (DMQ_6), which eventually lead to production of Q_6H_2 (for a schematic of the pathway, see Figure 3(a)). The amino substituent on the pABA ring is removed by a combination of Arh1, Yah1, Coq6, and Coq9 (He et al., 2015; Ozeir et al., 2015) and 4-imino-demethyl-demethoxy-Q_6H_2 ($IDDMQ_6$) and 4-imino-demethoxy-Q_6H_2 ($IDMQ_6$) likely represent dead-end products.

To determine whether CoQ_6 production was altered in the ERMES deletion strains, we analyzed *de novo* biosynthesis of $^{13}C_6$-CoQ_6 with ^{13}C ring-labeled precursors, namely, $^{13}C_6$-pABA and $^{13}C_6$-4HB. Surprisingly,

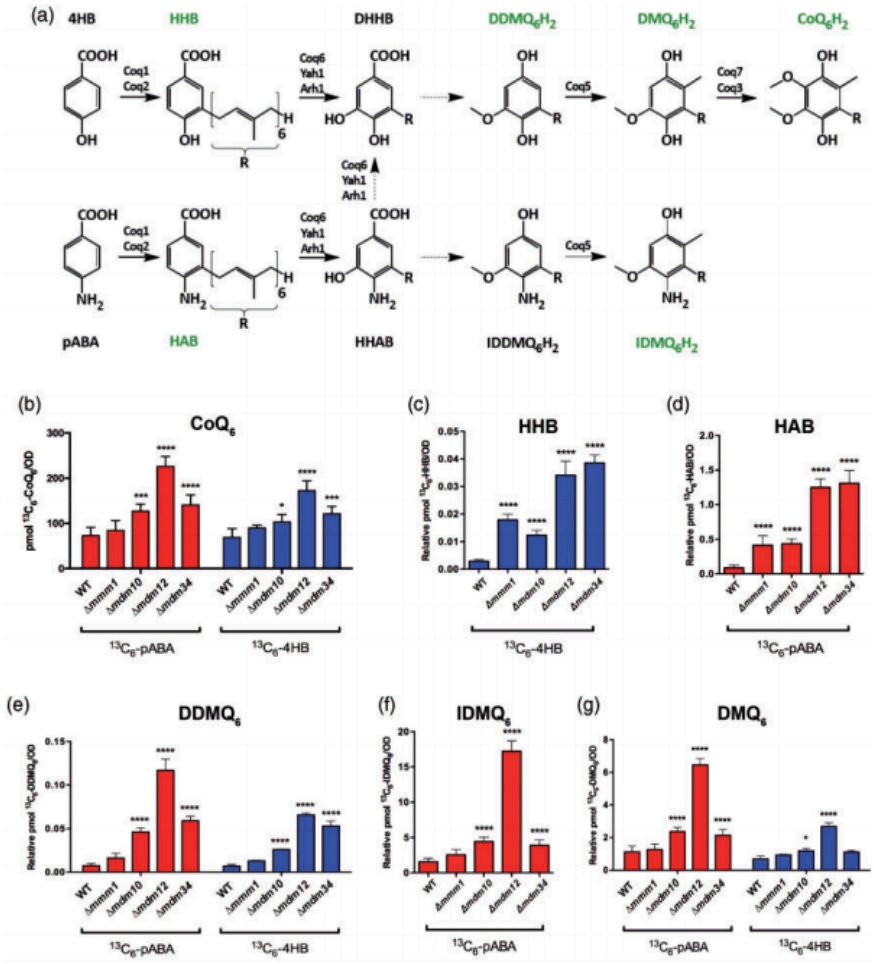

Figure 3. Biosynthesis of CoQ_6 and CoQ_6-intermediates is increased in cells lacking the ERMES complex. (a) Schematic representation of selected steps of the CoQ_6 biosynthesis pathway. CoQ_6-intermediates that were analyzed using mass spectrometry (MS) are indicated in green text. (b-g) MS-MS analysis for CoQ_6 and CoQ_6-intermediates in whole cell lipid extracts from W303 control, Δ*mmm1*, Δ*mdm10*, Δ*mdm12*, and Δ*mdm34* strains. $^{13}C_6$-CoQ_6 and $^{13}C_6$-CoQ_6-intermediates derived from $^{13}C_6$-pABA are depicted in red, while the $^{13}C_6$-CoQ_6 and $^{13}C_6$-CoQ_6-intermediates derived from $^{13}C_6$-4HB are depicted in blue. The biosynthesis of $^{13}C_6$-CoQ_6 (b) is increased in Δ*mdm10*, Δ*mdm12*, and Δ*mdm34* strains labeled with $^{13}C_6$-pABA or $^{13}C_6$-4HB. The biosynthesis of $^{13}C_6$-HHB (c) and $^{13}C_6$-HAB (d) is significantly higher in all the ERMES deletion strains. The *de novo* levels of demethyl-demethoxy-Q_6 ($^{13}C_6$-$DDMQ_6$) (e), 4-imino-DMQ_6 ($^{13}C_6$-$IDMQ_6$) (f), and demethoxy-Q_6 ($^{13}C_6$-DMQ_6) (g) are significantly increased in Δ*mdm10*, Δ*mdm12*, and Δ*mdm34* strains, with the exception of $^{13}C_6$-DMQ_6 in Δ*mdm34* that did not change after the labeling with $^{13}C_6$-4HB. Values are the mean of three repeats. The error bar indicates ±SD. Statistically significant differences between control (WT) and each of the ERMES mutants are represented by *, $p < .05$; **, $p < .01$; ***, $p < .001$, and ****, $p < .0005$. HHB = hexaprenyl-hydroxybenzoic acid; HAB = hexaprenyl-aminobenzoic acid; CoQ = Coenzyme Q; DDMQ = demethyl-demethoxy-Q; DMQ = demethoxy-Q; IDMQ = 4-imino-demethoxy-Q.

we saw that Δ*mdm10*, Δ*mdm12*, and Δ*mdm34* cells showed enhanced *de novo* synthesis of $^{13}C_6$-CoQ_6 (Figure 3(b)). These mutants also accumulated CoQ_6-intermediates emanating from $^{13}C_6$-pABA and $^{13}C_6$-4HB, whereas Δ*mmm1* cells only contained significantly higher amount of $^{13}C_6$-labeled HAB and HHB, but not the other intermediates (Figure 3(c) to (g)). We also measured the levels of unlabeled CoQ_6 (which correspond to the steady-state levels) in the same samples and observed an accumulation of unlabeled CoQ_6 and CoQ_6-intermediates in most of the ERMES deletion mutants, regardless of the presence or absence of ^{13}C-labeled precursor (Figure S3). The results suggest that the destabilized CoQ synthome in ERMES mutants results in an aberrant accumulation of CoQ_6 as well as CoQ_6-intermediates.

ERMES Deletion Strains Show Decreased Steady-State Levels of CoQ_6 and CoQ_6-Intermediates in Isolated Mitochondria

Although the biosynthesis of yeast CoQ_6 occurs exclusively within mitochondria, CoQ_6 is present in all cellular membranes (Bentinger et al., 2010). To focus on the status of CoQ_6 in mitochondria, we compared the steady-state content of CoQ_6 in mitochondria isolated from the ERMES deletion mutants to mitochondria obtained from a control strain. Although the overall cellular levels of CoQ_6 in these mutants were increased, the steady-state levels of CoQ_6 per unit of mitochondrial protein were significantly reduced in mitochondria isolated from Δ*mmm1*, Δ*mdm10*, or Δ*mdm12* strains (Figure 4(a)). Only strains lacking Mdm34 appeared to have nearly normal levels of CoQ_6. Isolated mitochondria from all of the ERMES deletion strains also contained lower levels of the late-stage intermediates $IDMQ_6$ and DMQ_6 (Figure 4(b) and (c), respectively). The levels of the late-stage intermediate $DDMQ_6$ were reduced in all strains, though the reduction was not statistically significant (Figure 4(d)). Our finding of decreased steady-state levels of CoQ_6 and its late intermediates in isolated mitochondria suggests that the accumulation of these molecules in whole cell lipid extracts (Figures 3 and S3) must reside in non-mitochondrial membranes. Moreover, reduced levels of pathway product in vicinity to the enzymes may reduce feedback

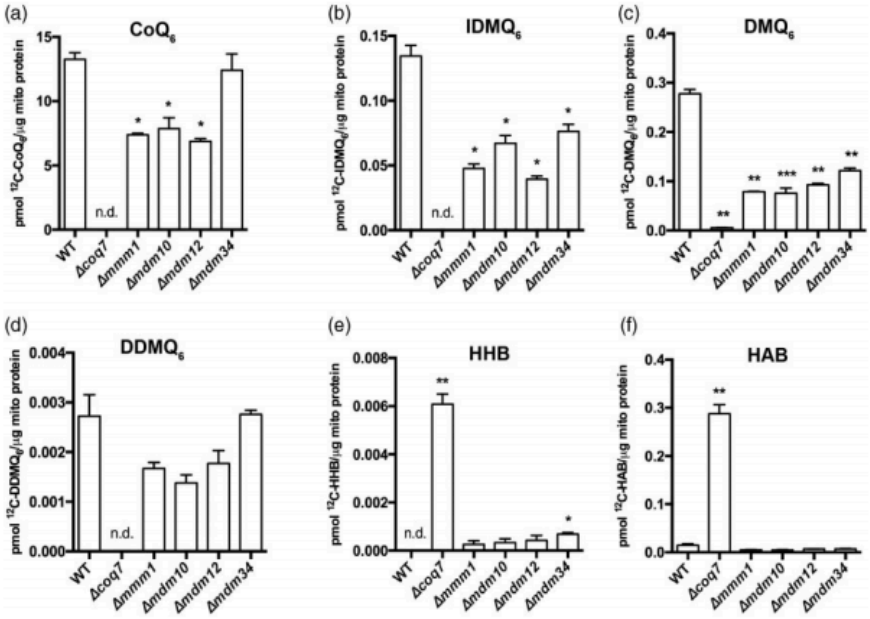

Figure 4. Mitochondria from ERMES mutants show less CoQ_6 and CoQ_6-intermediates. (a-f) Targeted MS-MS analyses for CoQ_6 and CoQ_6-intermediates from purified mitochondria from W303 wild-type (WT) control, ERMES mutants (Δ*mmm1*, Δ*mdm10*, Δ*mdm12*, and Δ*mdm34*) as well as Δ*coq7*, which was included as a negative control. Levels of (a) CoQ_6 were significantly reduced in all ERMES deletion strains except for Δ*mdm34*. Levels of (b) $IDMQ_6$ and (c) DMQ_6 were significantly reduced in all ERMES deletion strains. Levels of (d) $DDMQ_6$ were not significantly changed. Levels of (e) HHB and (f) HAB were significantly higher in the Δ*coq7* strain; however, ERMES deletion strains did not show an accumulation of either HHB or HAB (with the exception of Δ*mdm34* accumulating HHB). Values are means of three biological repeats. The error bar indicates ±SD. Statistically significant differences between the control and each of the ERMES mutants are represented by *, $p < .05$; **, $p < .01$; ***, $p < .001$; and ****, $p < .0005$. n.d. = not detected. HHB = hexaprenyl-hydroxybenzoic acid; HAB = hexaprenyl-aminobenzoic acid; CoQ = Coenzyme Q; DDMQ = demethyl-demethoxy-Q; DMQ = demethoxy-Q; IDMQ = 4-imino-demethoxy-Q.

inhibition (Berg, Tymoczko, & Stryer, 2002; Gehart & Pardee, 1962; Umbarger, 1961), providing an explanation for the increased rate of synthesis observed in ERMES mutants. However, feedback inhibition has not yet been reported for Coq enzymes.

In the complete absence of the CoQ synthome, strains fail to make CoQ_6 and can only carry out the first two steps of the biosynthetic pathway, producing HAB or HHB from the prenylation reaction of pABA or 4HB, respectively, using precursors derived from the mevalonate pathway in the ER (He et al., 2014). Indeed, deletion of the *COQ7* gene resulted in a dramatic accumulation of HHB and HAB (Figure 4(e) and (f)), as observed previously (Tran & Clarke, 2007). Interestingly, in the strains deleted for ERMES subunits, this accumulation of early CoQ_6-intemediates did not occur (with the exception of HHB slightly accumulating in the Δ*mdm34* strain (Figure 4(e))). The difference in the accumulation phenotypes between the ERMES-deletion strains and Δ*coq7* suggests that in addition to stabilizing the CoQ synthome, ERMES has a role at an earlier stage of the pathway.

The CoQ Synthome Resides in Specific Membrane Niches in Proximity to ERMES Contacts

Strains lacking ERMES subunits exhibit increased levels of cellular CoQ_6 and CoQ_6-intermediates, yet mitochondrial CoQ_6 and CoQ_6-intermediates are decreased and the CoQ synthome is destabilized. In addition, early pathway intermediates do not accumulate, suggesting a reduced flux of precursors from the ER. We wondered whether the ERMES complex may play a role in organizing the CoQ synthome and the trafficking of CoQ_6-related metabolites near ER-mitochondria contacts. As tagging Coq polypeptides with green fluorescent protein (GFP) does not impair their function (Figure S4(a)), we tagged Coq3, Coq4, Coq6, Coq9, and Coq11 with GFP and performed fluorescence microscopy. We noticed that these proteins are not distributed evenly throughout the mitochondrial matrix, but rather manifest a more punctate distribution (data not shown), suggesting that there might be discrete areas inside the mitochondrial matrix that are dedicated to the synthesis of CoQ_6. If the assembly of the CoQ synthome depends on ERMES, in a strain deleted for ERMES the punctate pattern of the GFP-tagged Coq polypeptide should disappear. Indeed, when we GFP-tagged Coq6 and Coq9 in a strain harboring a deletion for *MDM34*, the Coq-GFP punctate pattern was lost and the GFP signal was now spread throughout the entire mitochondrion (Figure S4(b)). However, as these mutants show dramatic alteration in mitochondrial morphology (Kornmann et al., 2009), it is hard to determine whether this effect is direct. To better understand the spatial relationship between ERMES and the CoQ synthome, we tagged Coq6 and Coq9 with GFP in a strain expressing Mdm34 fused to mCherry. Analyses of these cells revealed that more than 70% of the Mdm34-mCherry-marked contacts colocalized with Coq6-GFP or Coq9-GFP puncta (Figure 5(a) and quantification in Figure 5(b)). This colocalization was independent of genetic background and was also evident in a S288C background strain (Figure S4(c)). Our results strongly suggest that the localization of the CoQ synthome is coordinated with the position of the ER-mitochondria contact site.

Interestingly, in the yeast genome, the *COQ10* and *MDM12* genes are adjacent and likely to share a promoter (Cherry et al., 2012). Indeed, SPELL analysis of transcriptional co-regulation (Hibbs et al., 2007) demonstrates that these two genes are co-expressed. We therefore tested whether Coq10 is involved in the positioning of the CoQ synthome next to ERMES. To this end, we removed *COQ10*, then assessed colocalization between Coq6-GFP and Mdm34-mCherry. The Coq6-GFP signal was dramatically reduced upon *COQ10* deletion, consistent with previous findings (Hsieh et al., 2007). Nevertheless, several Coq6-GFP-containing puncta were observed. Quantification of the colocalization between these Coq6-GFP puncta and Mdm34-mCherry revealed that the positioning of the CoQ synthome next to the ERMES complex was reduced in the *coq10* null mutant (Figure 5(c) and quantification in Figure 5(d)). Our results suggest that the positioning of the CoQ synthome within mitochondria is a regulated process which depends upon the presence of Coq10.

Discussion

Contact sites play a critical role in shaping cellular architecture, and their facilitation of small molecule transfer between organelles enables tight regulation of biochemical pathways. In this study, we show that ERMES, an ER-mitochondria contact site tether, plays a key role in regulating CoQ_6 biosynthesis and distribution.

The ERMES complex appears to impact CoQ_6 synthesis on two levels. First, absence of the ERMES complex leads to destabilization of the CoQ synthome, perturbed CoQ_6 synthesis, and altered distribution of CoQ_6 and its precursors. Second, there is a clear spatial coordination of the ERMES complex with the CoQ synthome (Figure 5(e)). It is possible that ERMES may directly impact the CoQ synthome; however, there is no evidence showing direct interaction of ERMES subunits with known members of the CoQ synthome. We also note that the effects of ERMES disruption on the synthome and CoQ_6 biogenesis may be, at least in part, indirectly prompted by changes to phospholipid metabolism (Elbaz-Alon et al., 2014; Hönscher et al., 2014; Kawano et al., 2018; Lahiri et al., 2014) or by alteration

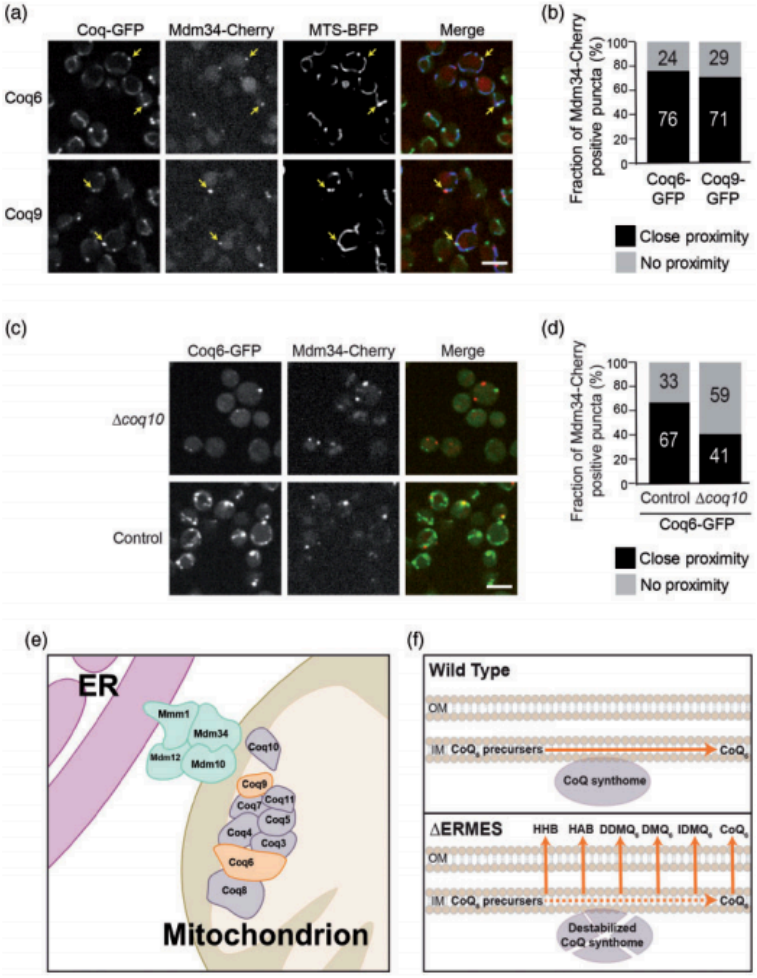

Figure 5. Members of the CoQ synthome reside in a matrix niche that underlies the ERMES complex. (a) Yeast cells expressing the indicated GFP-tagged Coq protein, the ERMES component Mdm34 tagged with mCherry, and a marker for the mitochondrial matrix (blue fluorescent protein [BFP] fused to a mitochondrial targeting sequence [MTS]) were imaged using fluorescence microscopy. Mitochondrial Coq foci that underlie ERMES are indicated by arrows. Scale bar = 5 μM. (b) Quantification of (a), for each cell, the Coq-GFP foci were identified. Then the proximity between each Mdm34-mCherry puncta and Coq-GFP was assessed. $n = 100$ Mdm34-mCherry puncta. (c) Yeast cells expressing Coq6-GFP, Mdm34-mCherry, and a MTS-BFP were imaged using fluorescence microscopy on either control or *Δcoq10* background. Scale bar = 5 μM. (d) Quantification of (c). The proximity between each Mdm34-mCherry puncta and the Coq6-GFP signal was examined. $n = 100$ Mdm34-mCherry puncta. (e) Schematic representation of the colocalization of ERMES and the CoQ synthome. Coq6 and Coq9, which were visualized in (a), are highlighted in orange. (f) A suggested model for the retention of CoQ_6 and CoQ_6-intermediates inside mitochondria: Under normal conditions, the CoQ synthome is well assembled and CoQ_6 biosynthesis (represented by the red arrow) occurs efficiently inside mitochondria. This catalytic efficiency ensures that early- and late-stage CoQ_6-intermediates do not accumulate, and optimal funneling through the pathway reduces loss across the mitochondrial outer membrane and into the rest of the cell. When the ERMES complex is absent, the stability of the CoQ synthome is compromised. A partially destabilized CoQ synthome underlies inefficient CoQ biosynthesis, leading to leakage of early- and late-stage CoQ_6-intermediates. OM = outer membrane, IM = inner membrane; GFP = green fluorescent protein; BFP = blue fluorescent protein; MTS = mitochondrial targeting sequence; ER = endoplasmic reticulum; ERMES = ER mitochondria encounter structure; HHB = hexaprenyl-hydroxybenzoic acid; HAB = hexaprenyl-aminobenzoic acid; CoQ = Coenzyme Q; DDMQ = demethyl-demethoxy-Q; DMQ = demethoxy-Q; IDMQ = 4-imino-demethoxy-Q.

of the shape and size of mitochondria (Hanekamp et al., 2002; Tan et al., 2013; Youngman et al., 2004).

We have shown that Coq10 is involved in the coordination of CoQ_6 synthesis across the ER-mitochondria interface (Figure 5(c) and (d)). *COQ10* encodes a membrane-spanning protein harboring a putative steroidogenic acute regulatory-related lipid transfer (StART) domain and a lipid-binding pocket for CoQ_6

and late-stage CoQ_6-intermediates (Allan et al., 2013) . Although Coq10 has not been shown to be part of the CoQ synthome, it is necessary for efficient *de novo* CoQ_6 biosynthesis and respiration (Allan et al., 2013). The co-expression of the *COQ10* and *MDM12* genes (Hibbs et al., 2007) might help coordinate the levels of Coq10 and ERMES to allow a better positioning of the CoQ synthome next to ER-mitochondria contact sites as they fluctuate in amount with changing cellular needs. Intriguingly, when overexpressed, Mdm12 is capable of entering the nucleus (Weill et al., 2018), raising the possibility of feedback control of the CoQ synthome-ERMES interaction. Moreover, the specific mechanism by which COQ genes are transcriptionally upregulated by ERMES disruption remains to be determined, but extensive communication exists between mitochondria and the nucleus (Eisenberg-Bord & Schuldiner, 2017), and at least one pathway by which CoQ biosynthesis can be upregulated by CoQ deficiency has been revealed in metazoans (Oks, Lewin, Goncalves, & Sapir, 2018).

How do CoQ_6 and CoQ_6-intermediates escape from mitochondria and accumulate in non-mitochondrial membranes in the ERMES deletion mutants? This might be due to a direct or indirect effect. Given that many Coq proteins of the CoQ synthome can bind to CoQ_6 or its biosynthetic intermediates, we propose that a destabilized CoQ synthome causes reduced sequestration of CoQ_6 within mitochondria (Figure 5(f)). In an alternative, yet not mutually exclusive model, disruption of ERMES mutants leads to reduced degradation of CoQ_6 outside of mitochondria. Although CoQ_6 degradation has not been studied extensively, it is believed that degradation of the polyisoprene tail of CoQ_6 may be carried out in peroxisomes via both α- and β-oxidation (Wanders, 2014). Indeed, we have previously shown that peroxisome-mitochondria (PERMIT) contact sites reside in proximity to ER-mitochondria contact sites (Cohen et al., 2014), raising the possibility that loss of ERMES may also affect the capacity to degrade escaped CoQ_6.

Excitingly, our findings are likely to have relevance to human health and disease. In mammals, the mitofusin 2 (MFN2) protein acts as a tether between the ER and mitochondria (de Brito & Scorrano, 2008), and conditional *MFN2* knock-out mice exhibit impaired respiration linked to a decrease in mitochondrial levels of the mammalian ubiquinones, CoQ_9 and CoQ_{10} (Mourier et al., 2015). It is hypothesized that this phenotype is not directly related to the role of MFN2 in mitochondrial fusion as the CoQ deficiency was not linked to the morphology of the mitochondrial network. These findings further suggest that a reduction in ER-mitochondria tethering can perturb CoQ biosynthesis, suggesting parallels between the yeast and mammalian cells.

Acknowledgments

We thank Rodney Rothstein for strains, we thank Christian Ungermann, Jodi Nunnari and Naama Barkai for plasmids, we thank Lee McAlister-Henn and David Meyer for antibodies, and we thank Ido Amit for the transposase required for the sequencing. We thank Yoav Voichek and Yulia Gordon for producing and analyzing the RNA-sequencing data. We thank Alexander Brandis and Tevi Mehlman from the Targeted Metabolomics unit of the Life Sciences Core Facilities of the Weizmann Institute for Mass-Spectrometry analysis.

Declaration of Conflicting Interests

The author(s) declared no potential conflicts of interest with respect to the research, authorship, and/or publication of this article.

Funding

The author(s) disclosed receipt of the following financial support for the research, authorship, and/or publication of this article: CDD acknowledges funding from an EMBO Installation Grant (2138) and from an European Research Council Starting Grant (RevMito 637649). MEB is grateful to the Azrieli Foundation for the award of an Azrieli Fellowship. This work was supported by the Deutsche Forschungsgemeinschaft (DIP to MS and DR), and the IMPRS "From Molecules to Organisms" (DA). Work in the Schuldiner lab is additionally supported by an SFB1190 from the DFG as well as a "Life" grant from the Volkswagen foundation. MS is an incumbent of the Dr. Gilbert Omenn and Martha Darling Professorial Chair in Molecular Genetics. This work is supported by the National Science Foundation Grant MCB-1330803 (to CFC) and by the National Institutes of Health Grant T32 GM 008496 to HST and MCB.

Supplemental material

Supplemental material for this article is available online.

References

Allan, C. M., Awad, A. M., Johnson, J. S., Shirasaki, D. I., Wang, C., Blaby-Haas, C. E., Clarke, C. F. (2015). Identification of Coq11, a new coenzyme Q biosynthetic protein in the CoQ-synthome in *Saccharomyces cerevisiae*. *Journal of Biological Chemistry*, *290*, 7517–7534.

Allan, C. M., Hill, S., Morvaridi, S., Saiki, R., Johnson, J. S., Liau, W. S., Clarke, C. F. (2013). A conserved START domain coenzyme Q-binding polypeptide is required for efficient Q biosynthesis, respiratory electron transport, and antioxidant function in *Saccharomyces cerevisiae*. *Biochimica et Biophysica Acta – Molecular and Cell Biology of Lipids*, *1831*, 776–791.

Awad, A. M., Bradley, M. C., Fernández-Del-Río, L., Nag, A., Tsui, H. S., & Clarke, C. F. (2018). Coenzyme Q10 deficiencies: Pathways in yeast and humans. *Essays in Biochemistry*, *62*, 361–376.

Barros, M. H., Johnson, A., Gin, P., Marbois, B. N., Clarke, C.F., & Tzagoloff, A. (2005). The *Saccharomyces cerevisiae COQ10* gene encodes a START domain protein required for function of coenzyme Q in respiration. *Journal of Biological Chemistry*, *280*, 42627–42635.

Belogrudov, G. I., Lee, P. T., Jonassen, T., Hsu, A. Y., Gin, P., & Clarke, C. F. (2001). Yeast *COQ4* encodes a mitochondrial protein required for coenzyme Q synthesis. *Archives of Biochemistry and Biophysics*, *392*, 48–58.

Bentinger, M., Tekle, M., & Dallner, G. (2010). Coenzyme Q – Biosynthesis and functions. *Biochemical and Biophysical Research Communication*, *396*, 74–79.

Berg, J. M., Tymoczko, J. L., & Stryer, L. (2002). *The biosynthesis of amino acids*. New York: W H Freeman.

Berger, K. H., Sogo, L. F., & Yaffe, M. P. (1997). Mdm12p, a component required for mitochondrial inheritance that is conserved between budding and fission yeast. *Journal of Cell Biology*, *136*, 545–553.

Brachmann, C. B., Davies, A., Cost, G. J., Caputo, E., Li, J., Hieter, P., & Boeke, J. D. (1998). Designer deletion strains derived from *Saccharomyces cerevisiae* S288C: A useful set of strains and plasmids for PCR-mediated gene disruption and other applications. *Yeast*, *14*, 115–132.

Cherry, J. M., Hong, E. L., Amundsen, C., Balakrishnan, R., Binkley, G., Chan, E. T., Wong, E. D. (2012). Saccharomyces Genome Database: The genomics resource of budding yeast. *Nucleic Acids Research*, *40*, D700–D705.

Cohen, Y., Klug, Y. A., Dimitrov, L., Erez, Z., Chuartzman, S. G., Elinger, D., Schuldiner, M. (2014). Peroxisomes are juxtaposed to strategic sites on mitochondria. *Molecular Biosystems*, *10*, 1742–1748.

Daum, G., Bohni, P. C., & Schatz, G. (1982). Import of proteins into mitochondria. *Journal of Biological Chemistry*, *257*, 13028–13033.

de Brito, O. M., & Scorrano, L. (2008). Mitofusin 2 tethers endoplasmic reticulum to mitochondria. *Nature*, *456*, 605–610.

Dimmer, K. S., & Rapaport, D. (2017). Mitochondrial contact sites as platforms for phospholipid exchange. *Biochimica et Biophysica Acta – Molecular and Cell Biology of Lipids*, *1862*, 69–80.

Eisenberg-Bord, M., & Schuldiner, M. (2017). Ground control to major TOM: Mitochondria-nucleus communication. *FEBS Journal*, *284*, 196–210.

Eisenberg-Bord, M., Shai, N., Schuldiner, M., & Bohnert, M. (2016). A tether is a tether is a tether: Tethering at membrane contact sites. *Developmental Cell*, *39*, 395–409.

Elbaz-Alon, Y., Rosenfeld-Gur, E., Shinder, V., Futerman, A. H., Geiger, T., & Schuldiner, M. (2014). A dynamic interface between vacuoles and mitochondria in yeast. *Developmental Cell*, *30*, 95–102.

Gehart, J. C., & Pardee, A. B. (1962). The enzymology of control by feedback inhibition. *Journal of Biological Chemistry*, *237*, 891–896.

Gietz, R. D., & Woods, R. A. (2006). Yeast transformation by the LiAc/SS Carrier DNA/PEG method. *Methods in Molecular Biology*, *313*, 107–120.

Glick, B. S., & Pon, L. A. (1995). Isolation of highly purified mitochondria from *Saccharomyces cerevisiae*. *Methods in Enzymology*, *260*, 213–223.

González Montoro, A., Auffarth, K., Hönscher, C., Bohnert, M., Becker, T., Warscheid, B., Ungermann, C. (2018). Vps39 interacts with Tom40 to establish one of two functionally distinct vacuole-mitochondria contact sites. *Developmental Cell*, *45*, 621.e7–636.e7.

Hanekamp, T., Thorsness, M. K., Rebbapragada, I., Fisher, E. M., Seebart, C., Darland, M. R., Thorsness, P. E. (2002). Maintenance of mitochondrial morphology is linked to maintenance of the mitochondrial genome in *Saccharomyces cerevisiae*. *Genetics*, *162*, 1147–1156.

He, C. H., Black, D. S., Nguyen, T. P. T., Wang, C., Srinivasan, C., & Clarke, C. F. (2015). Yeast Coq9 controls deamination of coenzyme Q intermediates that derive from para-aminobenzoic acid. *Biochimica et Biophysica Acta*, *1851*, 1227–1239.

He, C. H., Xie, L. X., Allan, C. M., Tran, U. C., & Clarke, C. F. (2014). Coenzyme Q supplementation or overexpression of the yeast Coq8 putative kinase stabilizes multi-subunit *Coq* polypeptide complexes in yeast coq null mutants. *Biochimica et Biophysica Acta – Molecular and Cell Biology of Lipids*, *1841*, 630–644.

Hibbs, M. A., Hess, D. C., Myers, C. L., Huttenhower, C., Li, K., & Troyanskaya, O. G. (2007). Exploring the functional landscape of gene expression: Directed search of large microarray compendia. *Bioinformatics*, *23*, 2692–2699.

Hobbs, A. E., Srinivasan, M., McCaffery, J. M., & Jensen, R. E. (2001). Mmm1p, a mitochondrial outer membrane protein, is connected to mitochondrial DNA (mtDNA) nucleoids and required for mtDNA stability. *Journal of Cell Biology*, *152*, 401–410.

Hönscher, C., Mari, M., Auffarth, K., Bohnert, M., Griffith, J., Geerts, W., Ungermann, C. (2014). Cellular metabolism regulates contact sites between vacuoles and mitochondria. *Developmental Cell*, *30*, 86–94.

Hsieh, E. J., Gin, P., Gulmezian, M., Tran, U. C., Saiki, R., Marbois, B. N., & Clarke, C. F. (2007). *Saccharomyces cerevisiae* Coq9 polypeptide is a subunit of the mitochondrial coenzyme Q biosynthetic complex. *Archives of Biochemistry and Biophysics*, *463*, 19–26.

Janke, C., Magiera, M. M., Rathfelder, N., Taxis, C., Reber, S., Maekawa, H., Knop, M. (2004). A versatile toolbox for PCR-based tagging of yeast genes: New fluorescent proteins, more markers and promoter substitution cassettes. *Yeast*, *21*, 947–962.

John Peter, A. T., Herrmann, B., Antunes, D., Rapaport, D., Dimmer, K. S., & Kornmann, B. (2017). Vps13-Mcp1 interact at vacuole-mitochondria interfaces and bypass ER-mitochondria contact sites. *Journal of Cell Biology*, *216*, 3219–3229.

Kakimoto, Y., Tashiro, S., Kojima, R., Morozumi, Y., Endo, T., & Tamura, Y. (2018). Visualizing multiple inter-organelle contact sites using the organelle-targeted split-GFP system. *Scientific Reports*, *8*, 6175.

Kawano, S., Tamura, Y., Kojima, R., Bala, S., Asai, E., Michel, A. H., Endo, T. (2018). Structure–function insights into direct lipid transfer between membranes by Mmm1–Mdm12 of ERMES. *Journal of Cell Biology*, *217*, 1–22.

Kivioja, T., Vähärautio, A., Karlsson, K., Bonke, M., Enge, M., Linnarsson, S., & Taipale, J. (2012). Counting absolute

numbers of molecules using unique molecular identifiers. *Nature Methods*, *9*, 72–74.

Kojima, R., Endo, T., & Tamura, Y. (2016). A phospholipid transfer function of ER-mitochondria encounter structure revealed *in vitro*. *Scientific Reports*, *6*, 30777.

Kornmann, B., Currie, E., Collins, S. R., Schuldiner, M., Nunnari, J., Weissman, J. S., & Walter, P. (2009). An ER-mitochondria tethering complex revealed by a synthetic biology screen. *Science*, *325*, 477–481.

Lahiri, S., Chao, J. T., Tavassoli, S., Wong, A. K. O., Choudhary, V., Young, B. P., Loewen, C. J., Prinz, W. A. (2014). A conserved endoplasmic reticulum membrane protein complex (EMC) facilitates phospholipid transfer from the ER to mitochondria. *PLoS Biology*, *12*, e1001969.

Lang, A. B., Peter, A. T. J., Walter, P., & Kornmann, B. (2015). ER-mitochondrial junctions can be bypassed by dominant mutations in the endosomal protein Vps13. *Journal of Cell Biology*, *210*, 883–890.

Liu, C. L., Kaplan, T., Kim, M., Buratowski, S., Schreiber, S. L., Friedman, N., & Rando, O. J. (2005). Single-nucleosome mapping of histone modifications in *S. cerevisiae*. *PLoS Biology*, *3*, e328.

Longtine, M. S., McKenzie, A., Demarini, D. J., Shah, N. G., Wach, A., Brachat, A. Philippsen, P., … Pringle, J. R. (1998). Additional modules for versatile and economical PCR-based gene deletion and modification in *Saccharomyces cerevisiae*. *Yeast*, *14*, 953–961.

Marbois, B., Gin, P., Faull, K. F., Poon, W. W., Lee, P. T., Strahan, J., Clarke, C. F. (2005). Coq3 and Coq4 define a polypeptide complex in yeast mitochondria for the biosynthesis of coenzyme Q. *Journal of Biological Chemistry*, *280*, 20231–20238.

Marbois, B., Gin, P., Gulmezian, M., … Clarke, C. F. (2009). The yeast Coq4 polypeptide organizes a mitochondrial protein complex essential for coenzyme Q biosynthesis. *Biochimica et Biophysica Acta – Molecular and Cell Biology of Lipids*, *1791*, 69–75.

Marbois, B., Xie, L. X., Choi, S., Hirano, K., Hyman, K., & Clarke, C. F. (2010). Para-aminobenzoic acid is a precursor in coenzyme Q6 biosynthesis in *Saccharomyces cerevisiae*. *Journal of Biological Chemistry*, *285*, 27827–27838.

Meisinger, C., Rissler, M., Chacinska, A., Szklarz, L. K. S., Milenkovic, D., Kozjak, V., Schonfisch, B., Lohaus, C., Meyer, H.E., Yaffe, M.P., Guiard, B., Wiedemann, N., Pfanner, N. (2004). The mitochondrial morphology protein Mdm10 functions in assembly of the preprotein translocase of the outer membrane. *Developmental Cell*, *7*, 61–71.

Mourier, A., Motori, E., Brandt, T., Lagouge, M., Atanassov, I., Galinier, A. Rappl, G., Brodesser, S., Hultenby, K., Dieterich, C. Larsson, N. G. (2015). Mitofusin 2 is required to maintain mitochondrial coenzyme Q levels. *Journal of Cell Biology*, *208*, 429–442.

Nguyen, T. P. T., Casarin, A., Desbats, M. A., Doimo, M., Trevisson, E., Santos-Ocaña, C., Salviati, L. (2014). Molecular characterization of the human COQ5 C-methyltransferase in coenzyme Q10 biosynthesis. *Biochimica et Biophysica Acta—Molecular and Cell Biology of Lipids*, *1841*, 1628–1638.

Oks, O., Lewin, S., Goncalves, I. L., & Sapir, A. (2018). The UPRmt protects *Caenorhabditis elegans* from mitochondrial dysfunction by upregulating specific enzymes of the mevalonate pathway. *Genetics*, *209*, 457–473.

Ozeir, M., Pelosi, L., Ismail, A., Mellot-Draznieks, C., Fontecave, M., & Pierrel, F. (2015). Coq6 is responsible for the C4-deamination reaction in coenzyme Q biosynthesis in *Saccharomyces cerevisiae*. *Journal of Biological Chemistry*, *290*, 24140–24151.

Pierrel, F., Hamelin, O., Douki, T., Kieffer-Jaquinod, S., Mühlenhoff, U., Ozeir, M., … Fontecave, M. (2010). Involvement of mitochondrial ferredoxin and para-aminobenzoic acid in yeast coenzyme Q biosynthesis. *Chemistry & Biology*, *17*, 449–459.

Schägger, H. (2002). Respiratory chain supercomplexes of mitochondria and bacteria. *Biochimica et Biophysica Acta—Bioenergetics*, *1555*, 154–159.

Schagger, H., Cramer, W. A., & Vonjagow, G. (1994). Analysis of molecular masses and oligomeric states of protein complexes by blue native electrophoresis and isolation of membrane protein complexes by two-dimensional native electrophoresis. *Analytical Biochemistry*, *217*, 220–230.

Shai, N., Yifrach, E., van Roermund, C. W. T., Cohen, N., Bibi, C., IJlst, L., Cavellini, L., Meurisse, J., Schuster, R., Zada, L., Mari, M.C., Reggiori, F.M., Hughes, A.L., Escobar-Henriques, M., Cohen, M.M., Waterham, H.R., Wanders, R.J.A., Schuldiner, M., … Zalckvar, E. (2018). Systematic mapping of contact sites reveals tethers and a function for the peroxisome-mitochondria contact. *Nature Communications*, *9*, 1761.

Tan, T., Ozbalci, C., Brügger, B., Rapaport, D., & Dimmer, K. S. (2013). Mcp1 and Mcp2, two novel proteins involved in mitochondrial lipid homeostasis. *Journal of Cell Science*, *126*, 3563–3574.

Thomas, B. J., & Rothstein, R. (1989). Elevated recombination rates in transcriptionally active DNA. *Cell*, *56*, 619–630.

Tran, U. C., & Clarke, C. F. (2007). Endogenous synthesis of coenzyme Q in eukaryotes. *Mitochondrion*, *7* Suppl, S62–S71.

Umbarger, H. E. (1961). Feedback control by endproduct inhibition. *Cold Spring Harbor Symposia on Quantitative Biology*, *26*, 301–312.

Valm, A. M., Cohen, S., Legant, W. R., Melunis, J., Hershberg, U., Wait, E., Cohen, A.R., Davidson, M.W., Betzig, E., Lippincott-Schwartz, J. (2017). Applying systems-level spectral imaging and analysis to reveal the organelle interactome. *Nature*, *546*, 162–167.

Voichek, Y., Bar-Ziv, R., & Barkai, N. (2016). Expression homeostasis during DNA replication. *Science*, *351*, 1087–1090.

Wanders, R. J. A. (2014). Metabolic functions of peroxisomes in health and disease. *Biochimie*, *98*, 36–44.

Weill, U., Yofe, I., Sass, E., Stynen, B., Davidi, D., Natarajan, J., Ben-Menachem, R., Avihou, Z., Goldman, O., Harpaz, N., Chuartzman, S., Kniazev, K., Knoblach, B., Laborenz, J., Boos, F., Kowarzyk, J., Ben-Dor, S., Zalckvar, E., Herrmann, J.M., Rachubinski, R.A., Pines, O., Rapaport, D., Michnick, S.W., Levy, E.D., Schuldiner, M. (2018).

Genome-wide SWAp-Tag yeast libraries for proteome exploration. *Nature Methods*, *15*, 617–622.

Wittig, I., Braun, H.-P., & Schägger, H. (2006). Blue native PAGE. *Nature Protocols*, *1*, 418–428.

Yofe, I., & Schuldiner, M. (2014). Primers-4-Yeast: A comprehensive web tool for planning primers for *Saccharomyces cerevisiae*. *Yeast*, *31*, 77–80.

Youngman, M. J., Hobbs, A. E. A., Burgess, S. M., Srinivasan, M., & Jensen, R. E. (2004). Mmm2p, a mitochondrial outer membrane protein required for yeast mitochondrial shape and maintenance of mtDNA nucleoids. *Journal of Cell Biology*, *164*, 677–688.

APPENDIX VI

Recombinant RquA catalyzes the *in vivo* conversion of ubiquinone to rhodoquinone in *Escherichia coli* and *Saccharomyces cerevisiae*

Contents lists available at ScienceDirect

BBA - Molecular and Cell Biology of Lipids

journal homepage: www.elsevier.com/locate/bbalip

Recombinant RquA catalyzes the *in vivo* conversion of ubiquinone to rhodoquinone in *Escherichia coli* and *Saccharomyces cerevisiae*

Ann C. Bernert[a], Evan J. Jacobs[b], Samantha R. Reinl[b], Christina C.Y. Choi[b], Paloma M. Roberts Buceta[b], John C. Culver[b], Carly R. Goodspeed[b], Michelle C. Bradley[c], Catherine F. Clarke[c], Gilles J. Basset[a], Jennifer N. Shepherd[b,*]

[a] Plant Molecular and Cellular Biology Program, University of Florida, Gainesville, FL, United States
[b] Department of Chemistry and Biochemistry, Gonzaga University, Spokane, WA, United States
[c] Department of Chemistry and Biochemistry, University of California Los Angeles, CA, United States

ARTICLE INFO

Keywords:
Rhodoquinone
Ubiquinone
Fumarate reduction
Anaerobic respiration
Biosynthesis

ABSTRACT

Terpenoid quinones are liposoluble redox-active compounds that serve as essential electron carriers and antioxidants. One such quinone, rhodoquinone (RQ), couples the respiratory electron transfer chain to the reduction of fumarate to facilitate anaerobic respiration. This mechanism allows RQ-synthesizing organisms to operate their respiratory chain using fumarate as a final electron acceptor. RQ biosynthesis is restricted to a handful of prokaryotic and eukaryotic organisms, and details of this biosynthetic pathway remain enigmatic. One gene, *rquA*, was discovered to be required for RQ biosynthesis in *Rhodospirillum rubrum*. However, the function of the gene product, RquA, has remained unclear. Here, using reverse genetics approaches, we demonstrate that RquA converts ubiquinone to RQ directly. We also demonstrate the first *in vivo* synthetic production of RQ in *Escherichia coli* and *Saccharomyces cerevisiae*, two organisms that do not natively produce RQ. These findings help clarify the complete RQ biosynthetic pathway in species which contain RquA homologs.

1. Introduction

Quinones serve as essential electron carriers in conserved, central metabolic processes such as respiration and photosynthesis. Ubiquinone (Coenzyme Q or Q, Fig. 1) is a core component of the electron transport chain in mitochondria. While Q is near ubiquitous in aerobic organisms, other, more exotic prenylated quinones facilitate energy production in facultative anaerobes [1]. Rhodoquinone (RQ, Fig. 1) is one of these rarer quinones and is a structural analog of Q. RQ has an amino group at C-2 position of the benzoquinone ring while Q has a methoxy group. This small structural change alters their respective midpoint redox potentials from +100 mV for Q to −63 mV for RQ [2]. With this lower midpoint redox potential, RQ can accept electrons from Complex I and the resulting RQH_2 donates electrons directly to fumarate reductase to maintain the chemiosmotic gradient needed for ATP generation in the absence of oxygen [3,4].

While RQ is an integral compound of core anaerobic bioenergetics, its complete biosynthesis is still not known. Rhodoquinone biosynthesis protein A (RquA) was discovered in a forward genetics screen of *Rhodospirillum rubrum* as a putative methyltransferase-like enzyme that contributes to RQ biosynthesis [5]. The *rquA* gene is required for anaerobic growth of *R. rubrum*, and the null mutant, Δ*rquA* is incapable of synthesizing RQ [5]. However, the exact function and substrate of the RquA gene product has remained elusive. Q has been hypothesized to be a precursor of RQ from radiolabeling assays [6] and artificial feeding experiments in *R. rubrum* [7], but no genetic evidence has been provided. Furthermore, it is unknown whether this conversion would occur in a single or multi-step process.

A recent phylogenetic analysis of *rquA*'s origin and distribution was reported by Stairs, et al. [4]. The authors found that *rquA* is extremely rare and sparingly distributed among the alphaproteobacteria, betaproteobacteria, and gammaproteobacteria classes of bacteria, and four of the five eukaryotic supergroups in which it is found [4]. It was proposed that RquA homologs likely evolved from the proteobacterial class I SAM-dependent methyltransferases [4]. The closest homologs of RquA are those used in Q biosynthesis: Coq3 and Coq5 in *Saccharomyces cerevisiae*, or UbiE and UbiG in *Escherichia coli* [5]. It is possible that RquA evolved from proteins that were capable of binding Q and later gained a new enzymatic function to facilitate RQ biosynthesis [4]. Homologs of *rquA* are also found in select eukaryotes that produce RQ

* Corresponding author at: Department of Chemistry and Biochemistry, Gonzaga University, 502 East Boone Avenue, Spokane, WA 99258, United States.
E-mail address: shepherd@gonzaga.edu (J.N. Shepherd).

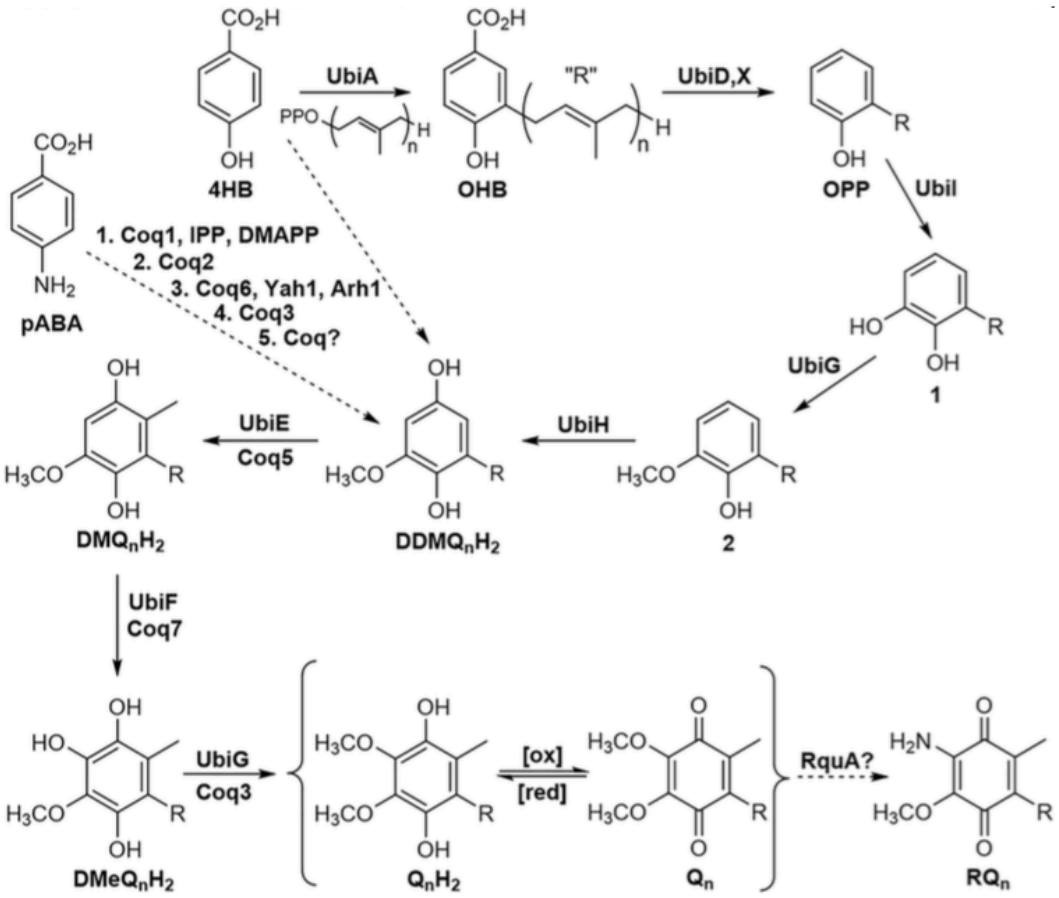

Fig. 1. The biosynthetic pathway of ubiquinone (Q) in *E. coli* (Ubi) and *S. cerevisiae* (Coq), as well as the proposed pathway to RQ biosynthesis in organisms with an RquA homolog. In *E. coli*, 4-hydroxybenzoic acid (4HB) is prenylated by UbiA to form 3-octaprenyl-4-hydroxybenzoate (OHB) which undergoes decarboxylation by UbiD and UbiX. Hydroxylation of the resulting product, 3-octaprenylphenol (OPP), is catalyzed by UbiI to form 3-octaprenyl catechol (compound 1). The first *O*-methylation is catalyzed by UbiG to convert compound 1 to 2-octaprenyl-6-methoxyphenol (compound 2). Hydroxylation of compound 2 with UbiH yields demethyldemethoxyubiquinol ($DDMQH_2$). The Q pathway in yeast can start from 4HB or *para*-aminobenzoic acid (pABA), and after multiple steps, catalyzed by Coq1, Coq2, Yah1, Arh1, Coq3 and other Coq polypeptides, results in the common intermediate, $DDMQH_2$. The *C*-methylation of $DDMQH_2$ with UbiE or Coq5 then produces demethoxyubiquinol ($DMQH_2$). A final hydroxylation of $DMQH_2$ by UbiF or Coq7 yields demethylubiquinol ($DMeQH_2$), which can then be methylated again by UbiG or Coq3 to produce ubiquinol (QH_2), the reduced form of Q. The *R. rubrum* protein, RquA, is proposed to convert Q to RQ. The number of isoprene units in the tail (R) is represented by the letter "n" and varies between species (*e.g.* in yeast $n = 6$, in *E. coli* $n = 8$, and in *R. rubrum* $n = 10$).

such as *Euglena gracilis* [4,8], and the protist, *Pygsuia biforma* [4]. It has been hypothesized that the *rquA* gene was transferred from prokaryotes to eukaryotes by multiple independent lateral gene transfer events after the development of mitochondria [4].

Some higher order eukaryotes such as the metazoans, *Caenorhabditis elegans* and *Ascaris suum*, also produce RQ [9,10]; however, they do not possess a *rquA* homolog in their genome [4]. The RQ biosynthetic pathway in species that do not have a gene encoding for RquA appears to differ from the pathway in *R. rubrum*; namely, Q is not a required precursor of RQ. For example, the *C. elegans clk-1* mutant, is deficient in Q_9 and builds up the demethoxyubiquinone-9 (DMQ_9) intermediate; however, the mutant can still produce RQ_9 [11,12]. These data suggest that these metazoans may have convergently evolved the ability to synthesize RQ in adaption to hypoxia and require different RQ biosynthetic intermediates and enzymes [4].

While RQ biosynthesis remains under-studied, Q biosynthesis in prokaryotes and yeast is better understood. Known steps in the Q biosynthetic pathway are outlined in Fig. 1. *E. coli ubi* null mutants have been used to elucidate the majority of intermediates and Ubi polypeptides required for Q biosynthesis [13]. Polypeptides of interest in this work include UbiG, which performs an *O*-methylation reaction of Compound 1 (Fig. 1), and the null mutant, Δ*ubiG*, accumulates OPP [14]. UbiH then facilitates a hydroxylation of Compound 2 (Fig. 1) to form $DDMQ_8H_2$, and the corresponding mutant, Δ*ubiH*, accumulates Compound 2, in addition to OPP [14]. The following *C*-methylation step is facilitated by UbiE. The Δ*ubiE* mutant thus accumulates $DDMQ_8H_2$ [15]. UbiF completes the last hydroxylation to produce $DMeQ_8H_2$, and the corresponding mutant, Δ*ubiF*, accumulates DMQ_8H_2 [16,17]. The final *O*-methylation of $DMeQ_8H_2$ to form Q_8H_2 also requires UbiG [18]. *E. coli* UbiE, UbiF, UbiG, UbiH, UbiI, UbiJ and UbiK polypeptides form a high molecular mass soluble metabolon responsible for the ring modification steps in synthesis of Q_8 [19].

The biosynthesis of Q in *S. cerevisiae* (yeast) is known to require a membrane bound complex of at least eight polypeptides, which are products of genes *COQ3–COQ9* and *COQ11* [20]. *COQ1* and *COQ2* gene products are required for assembly of the polyprenyldiphosphate tail and its attachment to the ring precursor [21,22]. Similar to *E. coli*, yeast do not produce or require RQ. The primary metabolic pathways used by

yeast are fermentation or respiration, the latter process requiring Q. Yeast can synthesize Q from either 4HB or pABA (Fig. 1) [23,24]. Deletion of any of the *COQ* genes results in defects in Q biosynthesis and growth on a non-fermentable carbon source [21,22]. Unlike in *E. coli*, the immediate Q biosynthetic precursors do not accumulate in the yeast null *coq* mutants. For example, the yeast mutant, *coq3*Δ, cannot produce Q_6 and is incapable of respiration; however, the only precursors detected in this mutant are the very early intermediates, 3-hexaprenyl-4-hydroxybenzoic acid (derived from 4HB) and 3-hexaprenyl-4-aminobenzoic acid (derived from pABA). These intermediates accumulate in most of the *coq3* to *coq9* null mutants, which is thought to be due to the required macromolecular protein complex required for Q biosynthesis [20]. However, it was demonstrated that the *E. coli* gene homolog, *ubiG*, can rescue respiration in the *coq3*Δ mutant and restore the ability to synthesize Q_6 [25].

Here, we investigate Q and these earlier Q biosynthetic intermediates as substrates for RquA. Using genetics and analytical biochemistry, we demonstrate that recombinant RquA requires the presence of Q to produce RQ in both a prokaryote and eukaryote model. This work has elucidated a complete pathway for RQ biosynthesis in *rquA*-producing species, a critical compound for anaerobic respiration.

2. Methods

2.1. Yeast and E. coli strains and plasmids

A complete list of yeast and *E. coli* strains with their genotypes, specifications, and sources are listed in Table 1. A full list of plasmids used in this study and their sources are given in Table 2.

2.2. Construction of pET303_RquA

The *rquA* gene [Rru_A3227] was amplified by PCR from chromosomal *R. rubrum* DNA using Pfu Ultra II Hotstart Master Mix (Agilent, La Jolla, CA) with a forward primer containing an *Xba*I restriction site, p303XbaI_F (5′-CAGTTCTAGAATGACTAAGCACCAAGGTGCGG TCC-3′) and a reverse primer with an *Xho*I cutsite, p303XhoI_R (5′-ACGTCTC GAGAGCGCG TCGCTCCGC-3′). The Champion™ pET303/CT-His vector (Invitrogen, Waltham, MA) and *rquA* amplicon were separately digested with XbaI and XhoI in NEBuffer 4 (NEB, Ipswich, MA) and cleaned with a DNA Clean and Concentrator-5 kit (Zymo Research, Irvine, CA). Ligation was achieved using T4 DNA ligase and T4 DNA Rapid Reaction Ligase Buffer (NEB, Ipswich, MA) with a 6:1 molar ratio of insert:vector. The ligation mixture was used to transform *E. coli* DH5α and XJb (DE3) autolysis Mix and Go! cells (Zymo Research, Irvine, CA), using ampicillin for selection. The plasmid sequence was verified by Sanger sequencing.

Table 2
Plasmids used.

Plasmids	Source
pET303_RquA	This work
pBAD24	[28]
pBAD24_RquA	This work
pQM	[25]
pQM_RquA	This work
pQMG	[25]
pRCM_RquA	This work
pRCM	[29]

2.3. Expression of RquA in E. coli BL21 (DE3) cells

pET303_RquA was transformed into *E. coli* BL21 (DE3) cells. Three colonies of this transformation were grown overnight in 2 mL culture of M9 minimal media amended with ampicillin. The next day, 500 µL of each of these cultures was added to 30 mL of M9 minimal media amended with ampicillin in 250 mL flasks. Cultures were then incubated at 37 °C with shaking at 250 rpm. Untransformed *E. coli* BL21 (DE3) cells were run in parallel without ampicillin. Once cultures reached an OD_{600} of 0.4 they were cooled to 25 °C and expression of RquA was induced using 100 µM of IPTG. Incubation continued at 25 °C for another 16 h, at which point 15 mL of each culture was harvested by centrifugation. Pellets were then resuspended in 1 mL of milli-Q sterile water and frozen at −80 °C for storage until lipid extraction.

2.4. Q_3 feeding assays in XJb (DE3) E. coli expressing RquA

A single colony of XJb::pET303_RquA was used to inoculate 5 mL of Luria-Bertani (LB) broth amended with ampicillin, and the culture was grown overnight at 37 °C with 250 rpm shaking. Outgrowth cultures (100 mL) were prepared from overnight culture in 500 mL flasks with LB amended with ampicillin and arabinose (3 mM final), at a starting OD_{600} of 0.01, and grown for 2.5 h to an OD_{600} of 0.4–0.6. Cultures were induced with 100 µM of IPTG and then divided into six 15-mL aliquots in 125 mL flasks before adding concentrated Q_3 substrate in ethanol (5 and 10 µM final). The Q_3 substrate was synthesized in two steps from 2,3-dimethoxy-5-methylbenzoquinone using previously published protocols [27]. Feeding cultures were grown for 18 h at 25 °C with shaking, and pellets were harvested from 5 mL of culture and frozen at −80 °C. Each condition was performed in triplicate, and controls without vectors were prepared without ampicillin, at the same Q_3 concentrations.

2.5. Expression of RquA in E. coli ubi knockouts

The *rquA* gene was subcloned from pET303_RquA into pBAD24 [28] using the following primers: forward (5′-CTAGCAGGAGGAATTCATGA

Table 1
Genotype and source of yeast and *E. coli* strains.

Strain designation	Genotype/specifications	Source
S. cerevisiae		
W303-1A	MAT α *ade2-1 his3-1,15 leu2-3,112 trp1-1 ura3-1*	R. Rothstein[a]
CC303	MAT α *ade2-1 his3-1,15 leu2-3,112 trp1-1 ura3-1 coq3::LEU2*	[26]
E. coli		
K12	Wild-type	
JW2875 Δ*ubiH*	F-, Δ(*araD-araB*)*567*, Δ*lacZ4787*(::rrnB-3), λ-, Δ*ubiH758*::*kan*, *rph-1*, Δ(*rhaD-rhaB*)*568*, *hsdR514*	CGSC Keio Collection
JW2226 Δ*ubiG*	F-, Δ(*araD-araB*)*567*, Δ*lacZ4787*(::rrnB-3), λ-, Δ*ubiG785*::*kan*, *rph-1*, Δ(*rhaD-rhaB*)*568*, *hsdR514*	CGSC Keio Collection
JW5581 Δ*ubiE*	F-, Δ(*araD-araB*)*567*, Δ*lacZ4787*(::rrnB-3), λ-, *rph-1*, Δ*ubiE778*::*kan*, Δ(*rhaD-rhaB*)*568*, *hsdR514*	CGSC Keio Collection
JW0659 Δ*ubiF*	F-, Δ(*araD-araB*)*567*, Δ*lacZ4787*(::rrnB-3), Δ*ubiF722*::*kan*, λ-, *rph-1*, Δ(*rhaD-rhaB*)*568*, *hsdR514*	CGSC Keio Collection
BL21	One Shot® BL21 Star™ DE3 pLysS cells	Invitrogen
XJb	BL21 (DE3) with chromosomally inserted λ lysozyme gene inducible by arabinose	Zymo Research

[a] Dr. Rodney Rothstein, Department of Human Genetics, Columbia University.

CTAAGCACCAAGGTGCGG-3′) and reverse (5′-GCAGGTCGACTCTAGA TTAAGCGCGTCGCTCCGC-3′) with *InFusion* cloning technology. An empty pBAD24 vector was used as a control. Expression of RquA was shown to be tightly controlled in the pBAD24 vector and could be expressed at low to high levels using arabinose concentrations ranging from 0.0002% to 0.2% w/v. Wild-type *E. coli* K12 and the Q biosynthetic knockout mutants, Δ*ubiG*, Δ*ubiH*, Δ*ubiE*, and Δ*ubiF* were transformed with pBAD24 and pBAD24_RquA. A 2 mL pre-culture was grown overnight with appropriate selection from individual colonies of each of the transformed mutant strains. Pre-cultures were used to inoculate 30 mL of LB broth amended with appropriate selection in 250 mL flasks. Cultures were incubated at 37 °C with shaking at 250 rpm. Expression was induced with 0.2% w/v (13,000 μM) arabinose when OD_{600} = 0.5. Cultures were then grown until they reached OD_{600} = 1, at which point they were harvested by centrifugation and resuspended in 1 mL of milliQ water. Resuspended pellets were then frozen at −80 °C for storage until lipid extraction and analysis.

2.6. Construction of pQM_RquA

The *rquA* gene was amplified from pET303_RquA using Q5® High Fidelity Master Mix (NEB, Ipswich, MA) with the forward primer, pQM*ClaI*_F (5′-CGAAGATCGATACTAAGCAC CAAGGTGCGGT-3′) and the reverse primer, pQM*KpnI*_R (5′-TGATCGGTACCTTAAGC GCGTCG CTCCGCGACGA-3′), containing ClaI and KpnI restriction sites, respectively. The pQM plasmid containing a *COQ3* mitochondrial leader sequence [25] and the *rquA* amplicon were double digested with ClaI and KpnI-HF in CutSmart® buffer (NEB, Ipswich, MA). The linear vector and insert were ligated using the same conditions as for pET303_RquA, and the ligation mixture was transformed into NEB® 5-alpha Competent *E. coli* (NEB, Ipswich, MA) using the Efficiency Transformation Protocol (C2987H/C2987I). The sequence of pQM_RquA was verified with Sanger sequencing.

2.7. Construction of pRCM_RquA

The *rquA* gene was amplified as described in Section 2.6 using the pQM*ClaI*_F primer and the reverse primer, pRCM*KpnI*His_R (5′-TGATC GGTACCTTAATGATGATGATGATGAT GAGCGCGTCGCTCCGCGA CGA-3′). The *rquA* amplicon, containing a C-terminal hexahistidine tag, and the multi-copy pRCM plasmid [29] were both double digested with ClaI and KpnI-HF as described above. The linear pRCM vector was purified by gel extraction using a Zymoclean® Gel DNA Recovery Kit (Zymo Research, Irvine, CA) prior to ligation with the *rquA*-his_6 insert. The sequence of pRCM_RquA was validated using Sanger sequencing.

2.8. Expression of RquA in S. cerevisiae

Growth media for *S. cerevisiae* were prepared as described [30] and included YPD (1% yeast extract, 2%, peptone, 2% dextrose), YPG (1% yeast extract, 2% peptone, 3% glycerol), SD complete and SD-Ura [0.18% yeast nitrogen base without amino acids, 2% dextrose, 0.14% NaH_2PO_4, 0.5% $(NH_4)_2SO_4$, and complete amino acid supplement lacking uracil]. Wild-type W303 yeast was transformed with single copy vectors pQM, pQM_RquA, and pQMG [25], and with multi-copy vectors pRCM and pRCM_RquA [29] using standard protocols [30], and selection was performed on SD-Ura plates. The pQMG vector harboring the *ubiG* gene was previously constructed from pQM, which contains a *COQ3* mitochondrial leader sequence [25]. The mutant W303::Δ*coq3* yeast [31] was similarly transformed with the three single copy vectors. Overnight cultures in SD-complete (no vector) or SD-Ura (with vector) of the ten strains were prepared from single colony scrapes and used to inoculate 15-mL cultures in 125 mL flasks. Cultures with no vector or single copy vectors were grown at 30 °C for 12 h with 250 rpm shaking, while cultures containing the multi-copy vector required a 24 h growth period to reach similar OD_{600} values [3–4]. Aliquots containing 5-mL of culture (15–20 OD_{600} units) were pelleted for lipid extraction and LC-MS analysis. Dilution assays were performed with 2 μL spots of yeast cells diluted in PBS buffer to OD_{600} 0.2, 0.04, 0.008, 0.0016, and 0.00032 on agar plates containing YPD, YPG, SD-complete or SD-Ura media with 2% bacto agar.

2.9. BL21 E. coli lipid extraction and HPLC analysis

Resuspended pellets were thawed at room temperature and transferred to 5 mL Pyrex tubes containing 500 μL of 0.1 mm zirconia/silica beads (BioSpec Products, Inc., Bartlesville, OK) and vortexed at full speed for 120 s. Next, 5 μmol Q_{10} internal standard and 2 mL 95% ethanol was added prior to another 120 s of vortexing. Tubes were then incubated at 70 °C for 15 min with intermitted mixing and then cooled to room temperature. Lipids were extracted twice with 5 mL hexane phase partitions. Hexane fractions were combined and evaporated to dryness under nitrogen gas. The dried lipid extract was then resuspended in 200 μL methanol:dichloromethane (10:1) and transferred to a 1.5 mL Eppendorf tube for centrifugation (21,000 × *g*; 5 min). From this centrifuged sample, 50 μL was injected on HPLC using a SUPELCO Discovery® C-18 column (25 cm × 4.6 mm × 5 μm) held at 30 °C with a flow rate of 1 mL per min of solvent methanol:hexane (90:10). Quinones were detected by diode array spectrophotometry (1260 DAD HS, Agilent Technologies, Germany).

2.10. Lipid extraction of XJb E. coli and S. cerevisiae for LC-MS quantitation

Cell pellets were thawed and 500 pmol Q_6 internal standard (for *E. coli*) or 1000 pmol Q_3 (for yeast) was added prior to lipid extraction, using methods previously reported for *R. rubrum* [7]. Dried lipid extracts were resuspended in 20 μL hexane and 955 μL ethanol, and 30 min prior to LC-MS injection, 25 μL of $FeCl_3$ (100 mM, 2.5 mM final) was added to ensure full oxidation of quinones. Standards were extracted using the same protocol at the following concentrations: For *E. coli*, standards contained Q_6 (5 pmol/10 μL injection), RQ_3 (1.5, 3.0, 4.5, 6.0, or 12 pmol/10 μL injection) and Q_3 (6.0, 12, 24, 36, or 48 pmol/10 μL injection); for yeast, standards contained Q_3 (10 pmol/μL injection) and Q_6 (0.3, 0.6, 1.2, 3.0, or 6.0 pmol/10 μL injection). The standards Q_3 and RQ_3 were synthesized at Gonzaga University using previously published procedures [27,32]. The Q_8 and RQ_8 standards were isolated from BL21::pET303_RquA extracts by preparative HPLC at the University of Florida, Gainesville. The Q_6 and Q_{10} standards were purchased from Sigma-Aldrich (St. Louis, MO). Since an RQ_6 standard was not available, the quantity of RQ_6 was determined using a pmol conversion from the Q_6 standard curve and applying a RQ/Q response correction factor of 2.45 (which was determined from RQ_8/Q_8 and RQ_3/Q_3 standards). The lipid extracts and standards were separated using high performance liquid chromatography (Waters Alliance 2795, Waters Corporation, Milford, MA) and quinones were quantified using a triple quadrupole mass spectrometer in positive electrospray mode (Waters Micromass Quattro Micro, Waters Corporation, Milford, MA). Chromatography was performed at 4 °C using a pentafluorophenyl propyl column (Luna PFP(2), 50 by 200 mm, 3 μm, 100 Å, Phenomenex, Torrance, CA) at a flow rate of 0.5 mL/min and injection volumes of 10 μL. Quinones were eluted between 1.7 and 6.6 min by using a gradient system containing water with 0.1% formic acid (buffer A) and acetonitrile with 0.1% formic acid (buffer B). The water and acetonitrile used were liquid chromatography-mass spectrometry (LC-MS)-grade Optima (Fisher Scientific, Pittsburgh, PA), and the formic acid was > 99% packaged in sealed 1-mL ampoules (Thermo-Scientific, Rockford, IL). The gradient (buffer A-buffer B) method used was as follows: 0 to 3.5 min (30:70), 3.50 to 3.75 min (30:70 to 2:98), 3.75 to 7.25 min (2:98), 7.25 to 7.5 min (2:98 to 30:70), and 7.50 to 9 min (30:70). Quantitation was accomplished using MRM of singly charged ions, and monitored for the mass transition from each quinone

Table 3
LC-MS parameters for each quinone.

MS parameter	Q_3	RQ_3	Q_6	RQ_6	Q_8	RQ_8
Dwell time (s)	0.1	0.1	0.1	0.1	0.1	0.1
Cone (V)	20	25	31	35	35	39
Collision (V)	20	20	28	28	30	30
Precursor mass $[M + H]^+$ (m/z)	387.2	372.2	591.4	576.4	727.6	712.6
Ion product mass $[M]^+$ (m/z)	197.2	182.2	197.2	182.2	197.2	182.2

precursor ion ($[M + H]^+$) to its respective tropylium product ion ($[M]^+$). Mass Lynx V. 4.1 software was used for data acquisition and processing. Linear slopes were calculated using peak areas with a bunching parameter of 3 and two smoothing functions. The following global conditions were used for MS/MS analysis of all compounds: Capillary voltage, 3.60 kV; Source temp, 120 °C; Desolvation temp, 400 °C; Desolvation N_2 gas flow, 800 L/h; and Cone N_2 gas flow, 100 L/h. Argon gas was used for the collision gas and was obtained from the boil-off from a bulk liquid argon storage tank. Additional quinone-specific parameters are listed in Table 3. Samples were analyzed in duplicate and the pmol quinone was determined from the standard curve and corrected for recovery of internal standard. Samples were then normalized by OD_{600} unit of original culture. Accurate mass determination of RQ was performed using a Waters LCT Premier XE time-of-flight mass spectrometer in positive electrospray mode using a Waters UPLC with the same chromatography conditions.

3. Results

3.1. RquA leads to the production of RQ_8 and a depletion of Q_8 in E. coli

To test if Q was a substrate of RquA, recombinant RquA was expressed in *E. coli*. Wild-type *E. coli* lipid extract profiles contain three major quinone peaks: ubiquinone-8 (Q_8), demethylmenaquinone-8 (DMK_8), and menaquinone-8 (MK_8) (Fig. 2A.I). When RquA was expressed in wild-type *E. coli*, a fourth peak accumulated, coinciding with a depletion of the native Q_8. This new peak eluted approximately 2 min prior to the native Q_8 peak (Fig. 2A.II). This peak had a maximum absorption spectrum identical to that of RQ at 283 nm (Fig. 2A.II) [6,33]. Time-of-flight (TOF) MS analysis provided an accurate mass determination of RQ_8, which was within 1 ppm of the calculated exact mass (Fig. 2B). In induced cultures of *E. coli* BL21::pET303_RquA, the quantity of RQ_8 averaged 250.6 ± 125.0 pmol RQ_8/OD_{600} unit, compared to only 19.3 ± 10.7 pmol Q_8/OD_{600} unit (Fig. 2C). In the BL21 control cells, there was an average of 203.2 ± 18.6 pmol Q_8/OD_{600} unit, and no RQ_8 was detected (Fig. 2C). The observation that Q_8 quantity is depleted, while RQ_8 is formed, suggests that RquA uses a substrate from the Q pool to form RQ.

3.2. Feeding of Q_3 to E. coli expressing RquA leads to formation of RQ_3

To test if Q could serve as a direct precursor, synthetic Q_3 was fed to induced cultures of *E. coli* XJb::pET303_RquA at 5 µM and 10 µM concentrations, the RQ_3 product was detected using LC-MS with MRM analysis, and validated with a synthetic standard (Fig. 3). RQ_3 was not found in the controls without vector (Fig. 3). The RQ_3 peak that elutes at 1.68 min corresponds to a 372.2 > 182.2 m/z mass transition, indicative of fragmentation of the molecular ion, $[RQ_3 + H]^+$, to form the RQ tropylium product ion (see Appendix A, Fig. A.1 for LC-MS chromatograms). The amount of RQ_3 product that accumulated from increasing concentrations of Q_3 (5 and 10 µM) was similarly proportional at 12.1 ± 0.4 and 25.0 ± 3.5 pmol RQ_3/OD_{600} unit, respectively (Fig. 3). RQ_8 was observed under these conditions at 6.40 min with a mass transition of 712.6 > 182.2 m/z at 494.3 ± 38.2 and 433.1 ± 69.2 pmol RQ_8/OD_{600} unit, respectively (Figs. 3 and A.1). These data help confirm that Q serves as the direct precursor of RQ.

3.3. RquA leads to accumulation of RQ_8 only in E. coli strains that produce Q_8

To further confirm if RquA uses Q directly as a substrate, or acts on an earlier Q intermediate, we expressed RquA in a series of Q biosynthetic knockout mutants in *E. coli*. These mutations each halt the production of Q at different enzymatic steps and the corresponding mutants accumulate the respective intermediate as described earlier. The Q biosynthetic enzymes targeted in this study were UbiG, UbiH, UbiE and UbiF. In this experiment, RquA was provided access to four Q biosynthetic intermediates which accumulate in the corresponding null mutants: *ΔubiG*, *ΔubiH*, *ΔubiE*, and *ΔubiF*. The respective intermediates tested as potential substrates for RQ biosynthesis were: OPP, 2-octaprenyl-6-methoxyphenol (Compound 2), $DDMQ_8$ and DMQ_8. We found that RquA was not able to produce RQ in any of these mutants (Fig. 4A). Again, we observed the formation of RQ with RquA in an *E. coli* strain that contained Q (Fig. 4A). It was also observed in this system that higher induction of expression of RquA in *E. coli* K12 pBAD24_RquA correlated with higher RQ_8 and lower Q_8 levels and that the depletion of Q_8 was found to be roughly proportional to the accumulation of RQ_8 in an approximate 1:1 mole ratio (Fig. 4B).

3.4. RquA expression in wild-type yeast leads to formation of RQ_6

W303 yeast transformed with the single copy vectors, pQM, pQM_RquA and pQMG, were capable of growth on YPD, YPG, SD complete and SD-Ura plates (Fig. 5A). The rich YPD and YPG media were used to compare growth on a fermentable carbon source (dextrose) *versus* a non-fermentable carbon source (glycerol). Yeast incapable of performing respiration (*i.e.* lacking Q) cannot grow on YPG. SD-complete and SD-minus uracil media were used to select for the pQM and pRCM plasmids. Only yeast transformed with these plasmids can grow without uracil. W303 transformed with the multi-copy vectors, pRCM and pRCM_RquA, also showed growth on the four media types (see Appendix A, Fig. A.2). LC-MS with MRM analysis revealed that yeast containing the pQM_RquA and pRCM_RquA vectors produced a new RQ_6 product at 5.85 min with mass transition of 576.4 > 182.2 m/z (see sample chromatograms in Appendix A, Fig. A.3). The accurate mass of RQ_6 was confirmed using LC-TOF-MS to within 1 ppm of the calculated exact mass (Fig. 5C). The average quantity of RQ_6 in the W303::pQM_RquA cultures was determined to be 12.9 ± 0.3 pmol/OD_{600} (Fig. 5D), while the amount of RQ_6 in W303::pRCM_RquA was 15.3 ± 1.5 pmol/OD_{600}. Overall, there was about 10–20 times less RQ_6 produced in yeast than RQ_8 produced in *E. coli* expressing RquA (Fig. 2C). These quantities are consistent with the proportions of native Q_6 and Q_8 recovered from yeast and *E. coli*, respectively, in the absence of RquA. This experiment demonstrates that RquA can convert Q to RQ in a eukaryote and that its activity is not restricted to prokaryotic lineages, consistent with the natural distribution of RquA homologs in the genomes of bacterial and eukaryotic species.

3.5. Expression of RquA in Δcoq3 yeast does not produce RQ or rescue respiration

The yeast *coq3Δ* null mutant cannot grow on glycerol (YPG) (Fig. 5B); however, transformation with pQMG, containing the *E. coli ubiG* gene, recovered the synthesis of Q_6 and restored respiration and the mutant's ability to grow on YPG [25] (Fig. 5B). Since RquA is annotated on NCBI as a methyltransferase, and shares sequence similarity to UbiG, we tested the *rquA* gene under the same experimental conditions. We found that the pQM_RquA vector did not rescue respiration in the *Δcoq3* yeast (Fig. 5B), nor was RQ_6 detected in the corresponding lipid extracts by LC-MS (Fig. A.3). LC-MS analysis confirmed that the only *Δcoq3* strain to produce Q_6 contained pQMG (Fig. A.3). This experiment demonstrates that RquA cannot functionally replace Coq3.

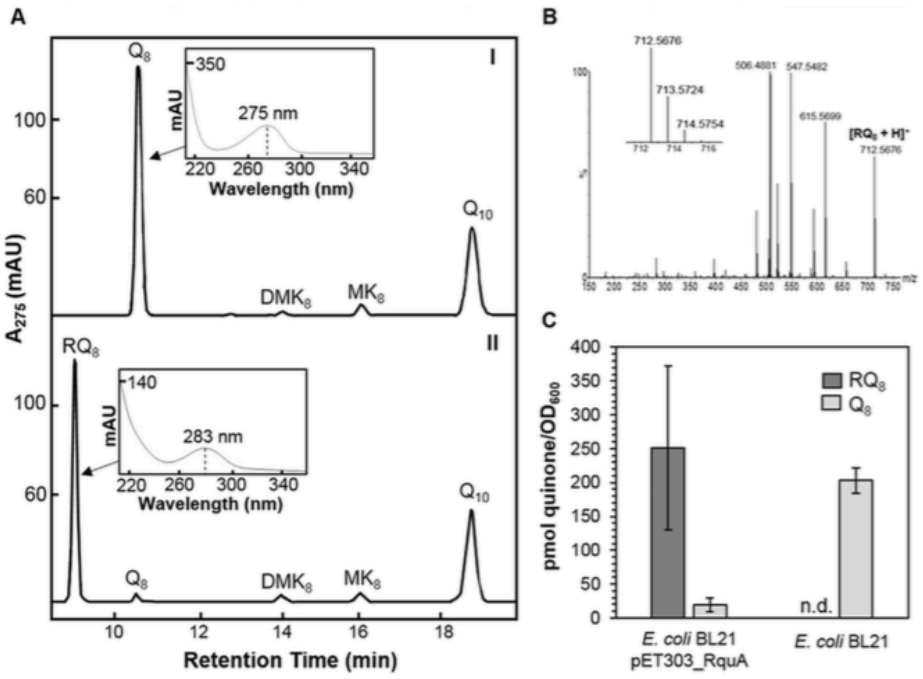

Fig. 2. Expression of RquA in *E. coli*. (A.I) HPLC chromatogram of lipid extracts from *E. coli* BL21 showing the three major lipid peaks: ubiquinone-8 (Q_8), demethylmenaquinone-8 (DMK_8), menaquinone-8 (MK_8) and the internal standard, ubiquinone-10 (Q_{10}); inset plot is the Q_8 absorption spectrum. (A.II) Chromatogram of lipid extracts of *E. coli* BL21::pET303_RquA cells where a new peak is formed with RquA expression; inset, RQ_8 absorption spectrum. (B) The mass spectrum of $[RQ_8 + H]^+$ obtained from an extracted ion chromatogram of *E. coli* BL21::pET303_RquA lipid extracts shows the molecular ion at 712.5676 *m/z* (exact mass of $C_{48}H_{74}NO_3$, 712.5669 amu). (C) Quantities of RQ and Q produced in *E. coli* BL21 cells with and without induced pET303_RquA.

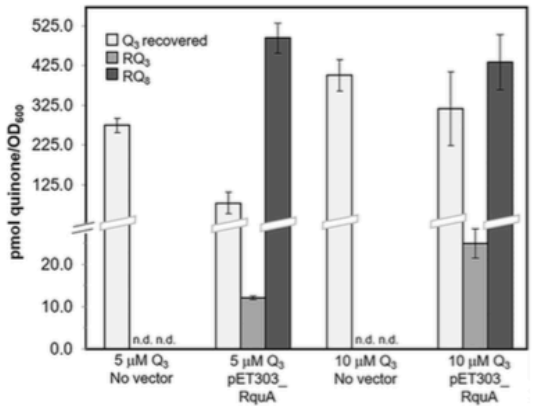

Fig. 3. Levels of RQ_3 (and RQ_8) produced and Q_3 recovered from XJb *E. coli* Q_3 feeding assays with and without the pET303_RquA vector. No RQ_3 or RQ_8 were detected in the absence of vector and the amounts of RQ_3 produced in the presence of the pET303_RquA vector were proportional to the amount of Q_3 added.

4. Discussion

Due to its central function in anaerobic bioenergetics, RQ is a molecule of high interest; yet, information on its biosynthetic pathway is limited. Understanding RQ biosynthesis is worthwhile as it has been cited as a possible target for control of helminth parasites [7]. While several recent discoveries have been made in *R. rubrum* [5,7,34], the complete pathway for RQ biosynthesis has not been reported. Prior to the work presented here, the enigma for RQ-producing species containing the *rquA* gene included whether Q was a substrate of RquA and whether RQ was a product of the RquA reaction.

In this work, we demonstrate that expression of RquA from *R. rubrum* yields RQ in two species that do not naturally produce RQ, *E. coli* and yeast. The RQ generated varied in tail length (RQ_3, RQ_6, and RQ_8) depending on the Q substrate available to RquA. RquA was unable to utilize any of the Q biosynthetic intermediates tested as substrates in *E. coli*. It was shown that in the absence of Q, no RQ was made in either *E. coli* or yeast. These results provide direct evidence that RquA is necessary and sufficient to convert Q to RQ.

The presence of RQ in yeast did not appear to decrease cell viability in plate dilution assays on the four different types of media. However, yeast transformed with the pRCM_RquA multi-copy vector required double the growth time to achieve the same cell density as cultures containing single-copy vectors. This could be due to Q-cycle bypass reactions that have been previously reported with addition of exogenous RQ to yeast [32], or to reduced levels of Q. Despite lower levels of Q_8 in *E. coli* expressing RquA, there was no effect on growth on plates or in liquid media. It is possible that RQ can act as a substitute for menaquinone, the low potential quinone found naturally in *E. coli* [35].

RquA shows sequence homology to class I *S*-adenosylmethionine (SAM)-dependent methyltransferase enzymes, such as Coq3 in yeast and UbiG in *E. coli* [7,18,25]. However, certain residues within the RquA SAM-binding motif differ from those observed in close homologs for which methyltransferase activity has been demonstrated [5]. There are several examples in the literature where methyltransferase-like proteins have alternate functions, and SAM is implicated as an electrostatic catalyst rather than as a methyl donor [36–38]. The data presented here do not support the role of RquA as a methyltransferase, and we propose that RquA may instead be catalyzing a transamination for the direct conversion Q to RQ.

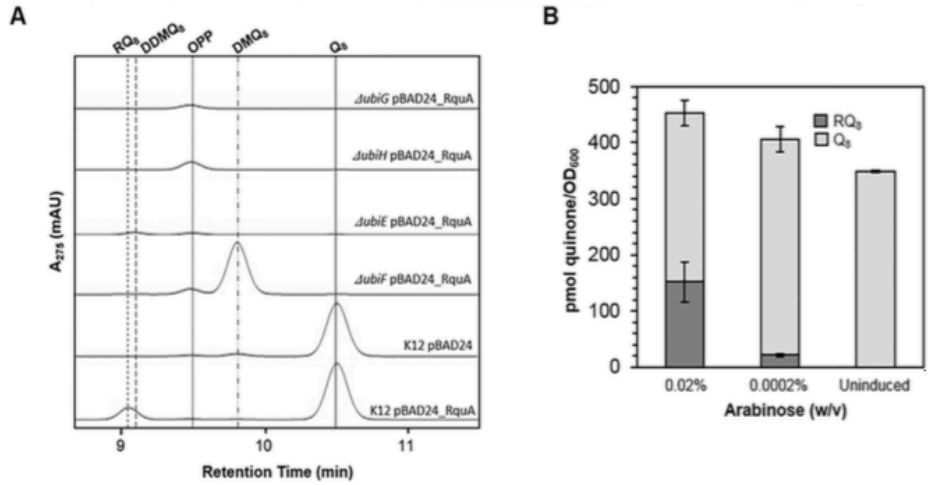

Fig. 4. Expression of RquA in *E. coli* Q biosynthetic knockout strains. (A) HPLC profiles of the lipid extracts of *E. coli* strains tested with and without RquA expressed show that RQ production occurs only in strains which produce Q. Lines mark the retention time of available Q biosynthetic intermediates in the *E. coli* strains tested (OPP, DDMQ and DMQ), as well as the Q and RQ products. (B) Levels of RQ_8 and Q_8 produced in *E. coli* K12 cells with pBAD24_RquA were quantified under high induction (0.02% arabinose), low induction (0.0002% arabinose), and uninduced conditions.

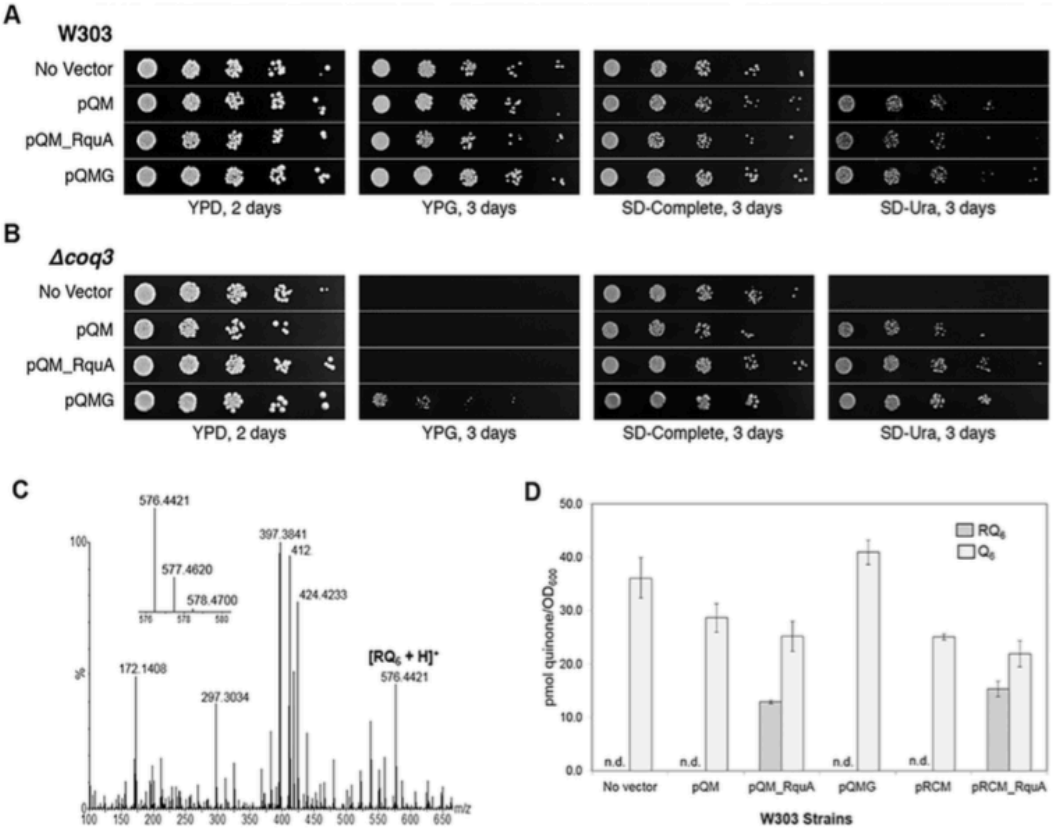

Fig. 5. Expression of RquA in yeast. Yeast dilution assays on YPD, YPG, SD-complete, or minus uracil (SD-Ura) plates: (A) Wild-type W303 yeast containing pQM, pQM_RquA, and pQMG vectors grow on all four media types. The W303 yeast control without a vector cannot grow on SD-Ura. Additional dilution assay plates for W303::pRCM and W303::pRCM_RquA are shown in Fig. A.2. (B) Mutant W303 Δ*coq3* yeast strains grown on the same media show survival on non-fermentable carbon (YPG) only in the presence of the pQMG vector containing the *ubiG* gene. (C) The mass spectrum of $[RQ_6 + H]^+$ from yeast W303::pQM_RquA lipid extracts shows the molecular ion at 576.4421 *m/z* (exact mass of $C_{38}H_{58}NO_3$, 576.4417 amu). (D) RQ_6 is produced only in W303 yeast transformed with the pQM_RquA and pRCM_RquA vectors.

A candidate gene approach was recently used in *R. rubrum* to screen for other genes that may be involved in RQ biosynthesis [34]. Gene targets were selected using transcriptome data obtained from RNA sequencing of aerobically and anaerobically grown *R. rubrum*, using *rquA* as a standard for comparison. Targets were further screened using comparative genomic data between *Rhodoferax ferrireducens* and *Rhodobacter sphaeroides*, a RQ-producing and non-RQ-producing species, respectively. Candidates were chosen that were differentially expressed under anaerobic conditions, and had homologs in the RQ-producing species, *R. ferrireducens*, but not in *R. sphaeroides*. Knockout mutants were generated for each new candidate, and RQ and Q levels were measured. No candidate was found to be as essential as *rquA* for RQ biosynthesis, though two genes were found to modulate Q biosynthesis in anoxic conditions, which had a direct effect on RQ levels (*e.g.* increased Q production yielded higher RQ levels). This work provides further evidence that Q is a required precursor to RQ, and RquA may be acting alone in this conversion.

5. Conclusion

Our findings have shed new light on the RQ biosynthetic pathway in species containing the *rquA* gene. Discovering that RquA uses Q as a substrate, and catalyzes the conversion of Q to RQ, was unexpected. The conversion of Q to RQ involves the addition of ammonia and elimination of methanol. This reaction has been observed non-enzymatically *in vitro* [39] supporting that it could also occur *in vivo*. The need to convert Q to RQ directly, despite the addition-elimination reaction required to do so, provides hints at the demand of RQ-synthesizing organisms to quickly convert the midpoint redox potential of their electron carrying quinones in changing environmental conditions. Future work in our laboratories will explore the mechanism of RquA and its regulation in changing oxygen environments.

Supplementary data to this article can be found online at https://doi.org/10.1016/j.bbalip.2019.05.007.

Transparency document

The Transparency document associated with this article can be found, in online version.

CRediT authorship contribution statement

Ann C. Bernert: Conceptualization, Investigation, Methodology, Formal analysis, Writing - original draft, Writing - review & editing. **Evan J. Jacobs:** Investigation, Methodology, Writing - original draft, Writing - review & editing. **Samantha R. Reinl:** Investigation, Methodology, Writing - review & editing. **Christina C.Y. Choi:** Investigation, Methodology, Writing - review & editing. **Paloma M. Roberts Buceta:** Investigation, Writing - review & editing. **John C. Culver:** Methodology. **Carly R. Goodspeed:** Investigation. **Michelle C. Bradley:** Methodology, Writing - review & editing. **Catherine F. Clarke:** Conceptualization, Funding acquisition, Resources, Supervision, Writing - review & editing. **Gilles J. Basset:** Conceptualization, Funding acquisition, Resources, Project administration, Supervision, Methodology, Formal analysis, Writing - review & editing. **Jennifer N. Shepherd:** Conceptualization, Funding acquisition, Resources, Project administration, Supervision, Investigation, Methodology, Formal analysis, Writing - original draft, Writing - review & editing.

Acknowledgements

This research was supported in part by a grant to Gonzaga University from the Howard Hughes Medical Institute through the Undergraduate Science Education Program, the Dr. Scholl Foundation (JNS), the Kay Nakamaye Research Award (EJJ), the National Science Foundation Grants MCB-1330803 (CFC), MCB-1712608 (GJB), GRFP DGE-1842473 (ACB), the National Institutes of Health Grant T32 GM 008496 (MCB), and the Ruth L. Kirschstein National Service Award GM-007185 (MCB). The authors would like to thank Dr. Kirk Anders at Gonzaga University for his donation of yeast media supplies and assistance with the growth and culturing of yeast, and Dr. Jeff Cronk for helpful discussion about methyltransferase enzyme structure and mechanism, and well as for proofreading early drafts of the manuscript. We thank Scott Economu for his assistance with the operation and maintenance of LC-MS instruments, and Angie Hinz for her assistance as the research coordinator for the science departments at Gonzaga University.

References

[1] M. Kawamukai, Biosynthesis and applications of prenylquinones, Biosci. Biotechnol. Biochem. 82 (2018) 963–977, https://doi.org/10.1080/09168451.2018.1433020.

[2] B.A.C. Ackrell, M.K. Johnson, R.P. Gunsalas, G. Cecchini, Structure and function of succinate dehydrogenase and fumarate reductase, p. 229–297, in: F. Muller (Ed.), Chemistry and Biochemistry of Flavoenzymes, vol. III, CRC Press, Inc., Boca Raton, FL, 1992.

[3] M. Muller, M. Mentel, J.J. van Hellemond, K. Henze, C. Woehle, S.B. Gould, R. Yu, M. van der Giezen, A.G.M. Tielens, W.F. Martin, Biochemistry and evolution of anaerobic energy metabolism in eukaryotes, Microbiol. Mol. Biol. Rev. 76 (2012) 444–495, https://doi.org/10.1128/MMBR.05024-11.

[4] C.W. Stairs, L. Eme, S.A. Muñoz-Gómez, A. Cohen, G. Dellaire, J.N. Shepherd, J.P. Fawcett, A.J. Roger, Microbial eukaryotes have adapted to hypoxia by horizontal acquisitions of a gene involved in rhodoquinone biosynthesis, eLife 7 (2018) e34292, , https://doi.org/10.7554/eLife.34292.

[5] Z.T. Lonjers, E.L. Dickson, T.P. Chu, J.E. Kreutz, F.A. Neacsu, K.R. Anders, J.N. Shepherd, Identification of a new gene required for the biosynthesis of rhodoquinone in *Rhodospirillum rubrum*, J. Bacteriol. 194 (2012) 965–971, https://doi.org/10.1128/JB.06319-11.

[6] W.W. Parson, H. Rudney, The biosynthesis of ubiquinone and rhodoquinone from p-hydroxybenzoate and p-hydroxybenzaldehyde in *Rhodospirillum rubrum*, J. Biol. Chem. 240 (1965) 1855–1863 (14285535).

[7] B.C. Brajcich, A.L. Iarocci, L.A.G. Johnstone, R.K. Morgan, Z.T. Lonjers, M.J. Hotchko, J.D. Muhs, A. Kieffer, B.J. Reynolds, S.M. Mandel, B.N. Marbois, C.F. Clarke, J.N. Shepherd, Evidence that ubiquinone is a required intermediate for rhodoquinone biosynthesis in *Rhodospirillum rubrum*, J. Bacteriol. 192 (2010) 436–445, https://doi.org/10.1128/JB.06319-11.

[8] M. Hoffmeister, A. van der Klei, C. Rotte, K.W.A. van Grinsven, J.J. van Hellemond, K. Henze, A.G.M. Tielens, W. Martin, Euglena gracilis rhodoquinone:ubiquinone ratio and mitochondrial proteome differ under aerobic and anaerobic conditions, J. Biol. Chem. 279 (2004) 22422–22429, https://doi.org/10.1074/jbc.M400913200.

[9] T. Yamashita, T. Ino, H. Miyoshi, K. Sakamoto, A. Osanai, E. Nakamaru-Ogiso, K. Kita, Rhodoquinone reaction site of mitochondrial complex I, in parasitic helminth, *Ascaris suum*, Biochim. Biophys. Acta 1608 (2004) 97–103, https://doi.org/10.1016/j.bbabio.2003.10.006.

[10] S. Takamiya, T. Matsui, H. Taka, K. Murayama, M. Matsuda, T. Aoki, Free-living nematodes *Caenorhabditis elegans* possess in their mitochondria an additional rhodoquinone, an essential component of the eukaryotic fumarate reductase system, Arch. Biochem. Biophys. 371 (1999) 284–289, https://doi.org/10.1006/abbi.1999.1465.

[11] T. Jonassen, P.L. Larsen, C.F. Clarke, A dietary source of coenzyme Q is essential for growth of long-lived *Caenorhabditis elegans clk-1* mutants, Proc. Natl. Acad. Sci. U. S. A. 98 (2001) 421–426, https://doi.org/10.1073/pnas.021337498.

[12] H. Miyadera, H. Amino, A. Hiraishi, H. Taka, K. Murayama, H. Miyoshi, K. Sakamoto, N. Ishii, S. Hekimi, K. Kita, Altered quinone biosynthesis in the long-lived *clk-1* mutants of *Caenorhabditis elegans*, J. Biol. Chem. 276 (2001) 7713–7716, https://doi.org/10.1074/jbc.C000889200.

[13] L. Aussel, F. Pierrel, L. Loiseau, M. Lombard, M. Fontecave, F. Barras, Biosynthesis and physiology of coenzyme Q in bacteria, Biochim. Biophys. Acta 1837 (2014) 1004–1011, https://doi.org/10.1016/j.bbabio.2014.01.015.

[14] I.G. Young, P. Stroobant, C.G. MacDonald, F. Gibson, Pathway for ubiquinone biosynthesis in *Escherichia coli* K-12: gene-enzyme relationship and intermediates, J. Bacteriol. 114 (1973) 42–52 4572721.

[15] P. Stroobant, I.G. Young, F. Gibson, Mutants of *Escherichia coli* K-12 blocked in the final reaction of ubiquinone biosynthesis: characterization and genetic analysis, J. Bacteriol. 109 (1972) 134–139 4333375.

[16] O. Kwon, A. Kotsakis, R. Meganathan, Ubiquinone (coenzyme Q) biosynthesis in *Escherichia coli*: identification of the *ubiF* gene, FEMS Microbiol. Lett. 186 (2000) 157–161, https://doi.org/10.1111/j.1574-6968.2000.tb09097.

[17] I.G. Young, L.M. McCann, P. Stroobant, F. Gibson, Characterization and genetic analysis of mutant strains of *Escherichia coli* K-12 accumulating the ubiquinone precursors 2-octaprenyl-6-methoxy-1,4-benzoquinone and 2-octaprenyl-3-methyl-6-methoxy-1,4-benzoquinone, J. Bacteriol. 105 (1971) 769–778 4323297.

[18] W.W. Poon, R.J. Barkovich, A.Y. Hsu, A. Frankel, P.T. Lee, J.N. Shepherd, D.C. Myles, C.F. Clarke, Yeast and rat Coq3 and *Escherichia coli* UbiG polypeptides catalyze both O-methyltransferase steps in coenzyme Q biosynthesis, J. Biol. Chem.

274 (1999) 21665–21672 10419476.
[19] Hajj Chehade, M., Pelosi, L., Rascalou, B., Kazemzadeh, K., Fyfe, C.D., Vo, C., Fontecave, M., Lombard, M., Loiseau, L., Aussel, L., Brugiere, S., Coute, Y., Ciccone, L., Barras, F., and Pierrel, F. (2018) A soluble metabolon synthesizes the isoprenoid lipid ubiquinone. Cell Chem Biol. Dec 17. pii: S2451-9456(18)30439-2. https://doi.org/10.1016/j.chembiol.2018.12.001
[20] C.M. Allan, A.M. Awad, J.S. Johnson, D.I. Shirasaki, C. Wang, C.E. Blaby-Haas, S.S. Merchant, J.A. Loo, C.F. Clarke, Identification of Coq11, a new coenzyme Q biosynthetic protein in the CoQ-synthome in *Saccharomyces cerevisiae*, J. Biol. Chem. 290 (2015) 7517–7534, https://doi.org/10.1074/jbc.M114.633131.
[21] J.A. Stefely, D.J. Pagliarini, Biochemistry of mitochondrial coenzyme Q biosynthesis, Trends Biochem. Sci. 42 (2017) 824–843, https://doi.org/10.1016/j.tibs.2017.06.008.
[22] A.M. Awad, M.C. Bradley, L. Fernandez-Del-Rio, A. Nag, H.S. Tsui, C.F. Clarke, Coenzyme Q10 deficiencies: pathways in yeast and humans, Essays Biochem. 62 (2018) 361–376, https://doi.org/10.1042/ebc20170106.
[23] B. Marbois, L.X. Xie, S. Choi, K. Hirano, K. Hyman, C.F. Clarke, para-Aminobenzoic acid is a precursor in coenzyme Q_6 biosynthesis in *Saccharomyces cerevisiae*, J. Biol. Chem. 285 (2010) 27827–27838, https://doi.org/10.1074/jbc.M110.151894.
[24] F. Pierrel, O. Hamelin, T. Douki, S. Kieffer-Jaquinod, U. Muehlenhoff, M. Ozeir, R. Lill, M. Fontecave, Involvement of mitochondrial ferredoxin and para-aminobenzoic acid in yeast coenzyme Q biosynthesis, Chem. Biol. 17 (2010) 449–459, https://doi.org/10.1016/j.chembiol.2010.03.014.
[25] A.Y. Hsu, W.W. Poon, J.A. Shepherd, D.C. Myles, C.F. Clarke, Complementation of *coq3* mutant yeast by mitochondrial targeting of the *Escherichia coli* UbiG polypeptide: evidence that UbiG catalyzes both O-methylation steps in ubiquinone biosynthesis, Biochemistry. 35 (1996) 9797–9806, https://doi.org/10.1021/bi9602932.
[26] T.Q. Do, J.R. Schultz, C.F. Clarke, Enhanced sensitivity of ubiquinone deficient mutants of *Saccharomyces cerevisiae* to products of autooxidized polyunsaturated fatty acid, Proc. Natl. Acad. Sci. 93 (1996) 7534–7539 8755509.
[27] N. Naruta, Regio- and stereoselective synthesis of coenzymes Q_n (n = 2-10), vitamin K, and related polyprenylquinones, J. Org. Chem. 45 (1980) 4097–4104, https://doi.org/10.1021/jo01309a006.
[28] L. Guzman, D. Belin, M.J. Carson, J. Beckwith, Tight regulation, modulation, and high-level expression by vectors containing the arabinose PBAD promoter, J. Bacteriol. 177 (1995) 4121–4130 7608087.
[29] C.M. Allan, S. Hill, S. Morvaridi, R. Saiki, J.S. Johnson, W. Liau, K. Hirano, T. Kawashima, Z. Ji, J.A. Loo, J.N. Shepherd, C.F. Clarke, A conserved START domain coenzyme Q-binding polypeptide is required for efficient Q biosynthesis, respiratory electron transport, and antioxidant function in *Saccharomyces cerevisiae*, Biochim. Biophys. Acta 1831 (2013) 776–791, https://doi.org/10.1016/j.bbalip.2012.12.007.
[30] D. Burke, D. Dawson, T. Stearns, Methods in Yeast Genetics. Cold Spring Harbor Laboratory Press, Plainview, NY, 2000.
[31] C.F. Clarke, W. Williams, J.H. Teruya, Ubiquinone biosynthesis in *Saccharomyces cerevisiae*: isolation and sequence of *COQ3*, the 3,4-dihydroxy-5-hexaprenylbenzoate methyltransferase gene, J. Biol. Chem. 266 (1991) 16636–16644 (1885593).
[32] J.L. Cape, J.R. Strahan, M.J. Lenaeus, B.A. Yuknis, T.T. Le, J.N. Shepherd, M.K. Bowman, D.M. Kramer, The respiratory substrate rhodoquinol induces Q-cycle bypass reactions in the yeast cytochrome bc_1 complex: mechanistic and physiological implications, J. Biol. Chem. 280 (2005) 34654–34660, https://doi.org/10.1074/jbc.M507616200.
[33] N. Castro-Guerrero, R. Jasso-Chávez, R. Moreno-Sánchez, Physiological role of rhodoquinone in *Euglena gracilis* mitochondria, Biochim. Biophys. Acta 1710 (2005) 113–121, https://doi.org/10.1016/j.bbabio.2005.10.002.
[34] A.R.M. Campbell, B.R. Titus, M.R. Kuenzi, F. Rodriguez-Perez, A.D.L. Brunsch, M.M. Schroll, M.C. Owen, J.D. Cronk, K.R. Anders, J.N. Shepherd, Investigation of candidate genes involved in the rhodoquinone biosynthetic pathway in *Rhodospirillum rubrum*, PLoS ONE 14 (2019) e0217281.
[35] B. Nowicka, J. Kruk, Occurrence, biosynthesis and function of isoprenoid quinones, Biochim. Biophys. Acta Bioenerg. 1797 (2010) 1587–1605, https://doi.org/10.1016/j.bbabio.2010.06.007.
[36] S. Korolev, Y. Ikeguchi, T. Skarina, S. Beasley, C. Arrowsmith, A. Edwards, A. Joachimiak, A.E. Pegg, A. Savchenko, The crystal structure of spermidine synthase with a multisubstrate adduct inhibitor, Nat. Struct. Biol. 9 (2002) 27–31, https://doi.org/10.1038/nsb737.
[37] A. Jansson, H. Koskiniemi, A. Erola, J. Wang, P. Mäntsälä, G. Schneider, J. Niemi, Aclacinomycin 10-hydroxylase is a novel substrate-assisted hydroxylase requiring S-adenosyl-L-methionine as cofactor, J. Biol. Chem. 280 (2005) 3636–3644, https://doi.org/10.1074/jbc.M412095200.
[38] M. Ohashi, F.L. Liu, Y. Hai, M. Chen, M. Tang, Z. Yang, M. Sato, K. Watanabe, K.N. Houk, Y. Tang, SAM-dependent enzyme-catalysed pericyclic reactions in natural product biosynthesis, Nature. 549 (2017) 502–518, https://doi.org/10.1038/nature23882.
[39] H.W. Moore, K. Folkers, Coenzyme Q. LXII. Structure and synthesis of rhodoquinone, a natural aminoquinone of the coenzyme Q group, J. Am. Chem. Soc. 87 (1965) 1409–1410 14293762.

APPENDIX VII

Chromatin-remodeling SWI/SNF complex regulates coenzyme Q_6 synthesis and a metabolic shift to respiration in yeast

JBC ARTICLE

Chromatin-remodeling SWI/SNF complex regulates coenzyme Q_6 synthesis and a metabolic shift to respiration in yeast

Received for publication, May 23, 2017, and in revised form, July 17, 2017 Published, Papers in Press, July 24, 2017, DOI 10.1074/jbc.M117.798397

Agape M. Awad[‡§1], Srivats Venkataramanan[§¶1], Anish Nag[‡§], Anoop Raj Galivanche[¶], Michelle C. Bradley[‡§], Lauren T. Neves[§¶], Stephen Douglass[¶], Catherine F. Clarke[‡§2], and Tracy L. Johnson[§¶3]

From the [‡]Department of Chemistry and Biochemistry, the [§]Molecular Biology Institute, and the [¶]Department of Molecular Cell and Developmental Biology, UCLA, Los Angeles, California 90095

Edited by Dennis R. Voelker

Despite its relatively streamlined genome, there are many important examples of regulated RNA splicing in *Saccharomyces cerevisiae*. Here, we report a role for the chromatin remodeler SWI/SNF in respiration, partially via the regulation of splicing. We find that a nutrient-dependent decrease in Snf2 leads to an increase in splicing of the *PTC7* transcript. The spliced *PTC7* transcript encodes a mitochondrial phosphatase regulator of biosynthesis of coenzyme Q_6 (ubiquinone or CoQ_6) and a mitochondrial redox-active lipid essential for electron and proton transport in respiration. Increased splicing of *PTC7* increases CoQ_6 levels. The increase in *PTC7* splicing occurs at least in part due to down-regulation of ribosomal protein gene expression, leading to the redistribution of spliceosomes from this abundant class of intron-containing RNAs to otherwise poorly spliced transcripts. In contrast, a protein encoded by the non-spliced isoform of *PTC7* represses CoQ_6 biosynthesis. Taken together, these findings uncover a link between Snf2 expression and the splicing of *PTC7* and establish a previously unknown role for the SWI/SNF complex in the transition of yeast cells from fermentative to respiratory modes of metabolism.

Similar to other eukaryotic genomes, genes in *Saccharomyces cerevisiae* may be interrupted by non-coding sequences, called introns. Introns are removed from the pre-mRNA through the action of the spliceosome, a macromolecular machine composed of five small nuclear ribonucleoproteins. The spliceosome recognizes consensus sequence signals on the pre-mRNA, termed splice sites, by which it subsequently binds to the intron and catalyzes its removal via two transesterification reactions (1). Pre-mRNA splicing is critical for accurate gene expression in all eukaryotes, and there is significant evidence that alterations in microenvironments, such as changes in the chromatin state or chromatin-modifying factors, can affect splicing outcomes (1). However, the mechanisms for how chromatin and chromatin factors influence splicing are not completely understood.

Although the genome of *S. cerevisiae* contains a smaller number of introns than metazoan genomes, there are, nonetheless, numerous examples of intron-dependent gene regulation (2). The largest functional class of intron-containing genes (ICGs)[4] in budding yeast is ribosomal protein genes (RPGs) that encode the protein components of the ribosome. Therefore, the energy-intensive process of translation is under the heavy regulatory control of the spliceosome, such that splicing of RPGs can be finely tuned to the cells' environmental conditions and to nutrient availability (3).

Interestingly, this enrichment of introns within RPGs impacts the splicing of, as well as provides an opportunity for the regulation of, other ICGs within the yeast genome. About a third of yeast introns occur in RPGs, and the high transcription levels of these genes means that about 90% of the intron load encountered by the spliceosome is from this one functional class of genes (4). Indeed, the prevalence of RPG introns functions to titrate spliceosomes away from other introns, especially those containing suboptimal splice sites. Conversely, down-regulating RPG expression promotes the splicing of transcripts harboring suboptimal splice sites. This effect is perhaps best described during the process of yeast meiosis. Under conditions of vegetative growth, a number of meiosis-specific ICGs are expressed, but they possess suboptimal splice sites and are therefore poorly recognized by the spliceosome and suboptimally spliced. However, upon the down-regulation of RPGs during meiosis, increased availability of the previously limiting pool of spliceosomes leads to improved splicing efficiency of introns in meiosis-specific transcripts (5, 6).

This work was supported by National Science Foundation Grants MCB-1330803 and 1518316, and by NIGMS, National Institutes of Health, Grant GM-085474; the Whitcome Pre-doctoral Fellowship in Molecular Biology (to S. V.); and Ruth L. Kirschstein National Service Award GM-007185 (to M. B). The authors declare that they have no conflicts of interest with the contents of this article. The content is solely the responsibility of the authors and does not necessarily represent the official views of the National Institutes of Health.

RNA-seq data are available in the Gene Expression Omnibus (GEO) under accession number GSE94404.

[1] Both authors contributed equally to this work.

[2] To whom correspondence may be addressed: UCLA Dept. of Chemistry and Biochemistry, 607 Charles E. Young Dr. E., Box 156905, Los Angeles, CA 90095. Tel. 310-825-0771; Fax: 310-206-5213; E-mail: cathy@chem.ucla.edu.

[3] To whom correspondence may be addressed: UCLA Dept. of Molecular Cell and Developmental Biology, 610 Charles E. Young Dr. S., Los Angeles, CA 90095. Tel.: 310-206-2416; E-mail: tljohnson@ucla.edu.

[4] The abbreviations used are: ICG, intron-containing gene; RPG, ribosomal protein gene; ns, non-spliced; s, spliced; CoQ, coenzyme Q; DMQ_6, 5-demethoxy-Q_6; 4HB, 4-hydroxybenzoic acid; HHB, 3-hexaprenyl-4-hydroxybenzoic acid; qPCR, quantitative PCR; TOR, target of rapamycin.

There are other important examples of intron-based regulation in *S. cerevisiae*, especially among ICGs with non-consensus splice sites (7, 8). One such gene is *PTC7*, which encodes a Mg^{2+}/Mn^{2+}-dependent, type 2C serine/threonine protein phosphatase (9). The intron within *PTC7* is particularly intriguing because it contains a non-consensus branch-point sequence, rendering its splicing relatively inefficient under logarithmic growth conditions. The *PTC7* intron lacks a premature termination codon and is translated in-frame. The longer, non-spliced (ns) form of the *PTC7* RNA encodes a longer protein ($Ptc7_{ns}$) that contains a single trans-membrane helix located near the N terminus but is otherwise identical to the protein isoform derived from the spliced *PTC7* RNA ($Ptc7_s$). The read-through nature of the *PTC7* intron is conserved across yeast species, indicating potential functionality for both $Ptc7_s$ and $Ptc7_{ns}$ protein isoforms (10). $Ptc7_{ns}$ has been localized to the nuclear membrane, whereas $Ptc7_s$ is located within mitochondria (10). $Ptc7_s$ has been implicated in regulation of coenzyme Q (also termed ubiquinone or CoQ) biosynthesis via its phosphatase activity (11, 12). However, mechanisms of regulation of Ptc7 itself and the role of the evolutionarily conserved $Ptc7_{ns}$ isoform remain outstanding questions.

CoQ is a redox-active lipid composed of a fully substituted benzoquinone ring and a polyisoprenoid tail and is required for mitochondrial electron transport. The length of the polyisoprenoid group is species-specific; humans produce CoQ_{10}, and *S. cerevisiae* produce CoQ_6, with 10 and 6 isoprene units, respectively. The primary role of CoQ in the inner mitochondrial membrane is to accept the electrons from complex I and complex II and pass those electrons to complex III. Several other metabolic pathways, such as pyrimidine synthesis, sulfide oxidation, and fatty acid β-oxidation, rely on CoQ as an electron carrier (13). CoQ is present in all intracellular membranes, where it may function as a lipid-soluble antioxidant. Several human syndromes, including encephalomyopathy, ataxia, cerebellar atrophy, myopathy, and steroid-resistant nephrotic syndrome, are linked to primary deficiencies in CoQ biosynthesis (14–17).

Mitochondrial proteins are responsible for facilitating the biosynthesis of CoQ_6 in *S. cerevisiae* and include Coq1–Coq11 (18). Many of the Coq proteins necessary for the biosynthesis of CoQ_6 associate in a high-molecular weight complex (termed the "CoQ-synthome"), a multisubunit complex that is peripherally associated with the inner mitochondrial membrane on the matrix side (18). $Ptc7_s$ has been shown to localize to the mitochondria, where it is thought to regulate the phosphorylation state of Coq7 (11) and/or influence mitochondrial respiratory metabolism (12). In the former case, Ptc7s is believed to control, at least in part, the phosphorylation state of the Coq7 polypeptide, which modulates its hydroxylase activity. Coq7 catalyzes the hydroxylation of 5-demethoxy-Q_6 (DMQ_6), the penultimate step in the biosynthesis of CoQ_6 in yeast (19, 20).

The conserved SWI/SNF complex utilizes ATP hydrolysis by Snf2, the catalytic subunit, to disrupt specific histone–DNA contacts, resulting in the sliding or eviction of nucleosomes from the locus. As a result, Snf2 activity contributes to transcriptional regulation (21, 22). The genome-wide distribution of SWI/SNF is responsive to conditions of stress, and the complex is required for transcription of a number of stress response genes (23, 24). We have previously reported that levels of Snf2 change in response to nutrient conditions. We have also reported that the change in Snf2 leads to changes in levels of RPG transcripts, thereby regulating splicing outcomes (6). Here, we show that changes in levels of Snf2 modulate the CoQ_6 biosynthetic pathway in *S. cerevisiae*. First, we show that deletion of Snf2 alters the relative levels of $Ptc7_s$ and $Ptc7_{ns}$ isoforms in yeast and increases both the rate of synthesis and steady-state levels of CoQ_6. This is due to down-regulation of RPG transcripts and an increase in the available pool of spliceosomes. Moreover, we find that the Snf2 protein is down-regulated over time under batch growth conditions and nutrient depletion, and together with a concomitant increase in the splicing of *PTC7*, this leads to higher CoQ_6 levels in preparation for the transition from a fermentative mode of metabolism to a respiratory mode. Furthermore, we show that the two Ptc7 isoforms have opposing effects on the CoQ_6 biosynthetic pathway, which may explain contradictory reports in the literature about the effects of Ptc7 on CoQ_6 levels (11, 12). Importantly, although Snf2 is down-regulated in response to nutrient-depleted conditions, it is nonetheless required for growth on nonfermentable carbon sources, suggesting that dynamic control of Snf2 levels is crucial for the transition from fermentation to respiration.

Results

Deletion of Snf2 leads to enhanced splicing of PTC7 and a shift in the ratios of Ptc7 protein isoforms

Previously published RNA sequencing data for yeast lacking Snf2, the core ATPase component of the SWI/SNF complex (GEO accession number GSE94404), revealed an increase in splicing of a number of introns (6). Satisfyingly, the greatest improvement in splicing upon deletion of Snf2 is experienced by *RPL22B*, via a previously described mechanism consistent with down-regulation of RPG expression (25). The next two largest improvements in splicing efficiency are experienced by *YBR062C* (an ORF of unknown function) and *PTC7*, a previously described type 2C serine-threonine mitochondrial phosphatase that contains all 11 canonical motifs of the PPM family (type 2C) protein phosphatases, previously reported to play a role in CoQ_6 biosynthesis in yeast (11) (Fig. 1*A*). This increase in splicing of *PTC7* RNA was verified by RT-PCR (Fig. 1*B*). In addition, the results from the RNA-seq and RT-PCR were also independently verified by qPCR (data not shown). It has previously been demonstrated that increased splicing of poorly recognized introns can be achieved by decreased expression of competing, highly expressed RPGs (5). Furthermore, we have shown that deletion of Snf2 causes *en masse* down-regulation of RPGs and consequent improvement in splicing of a large number of introns (6). RPG down-regulation in the absence of Snf2 was validated by RT-PCR analysis. For example, expression of RPS16A and RPL34B, two intron-containing RPGs, is down-regulated in *snf2*Δ yeast compared with WT (Fig. 1*C*).

The *PTC7* transcript makes two distinct protein isoforms, one from the nonspliced and one from the spliced RNA. The spliced isoform ($Ptc7_s$) localizes to the mitochondria, whereas

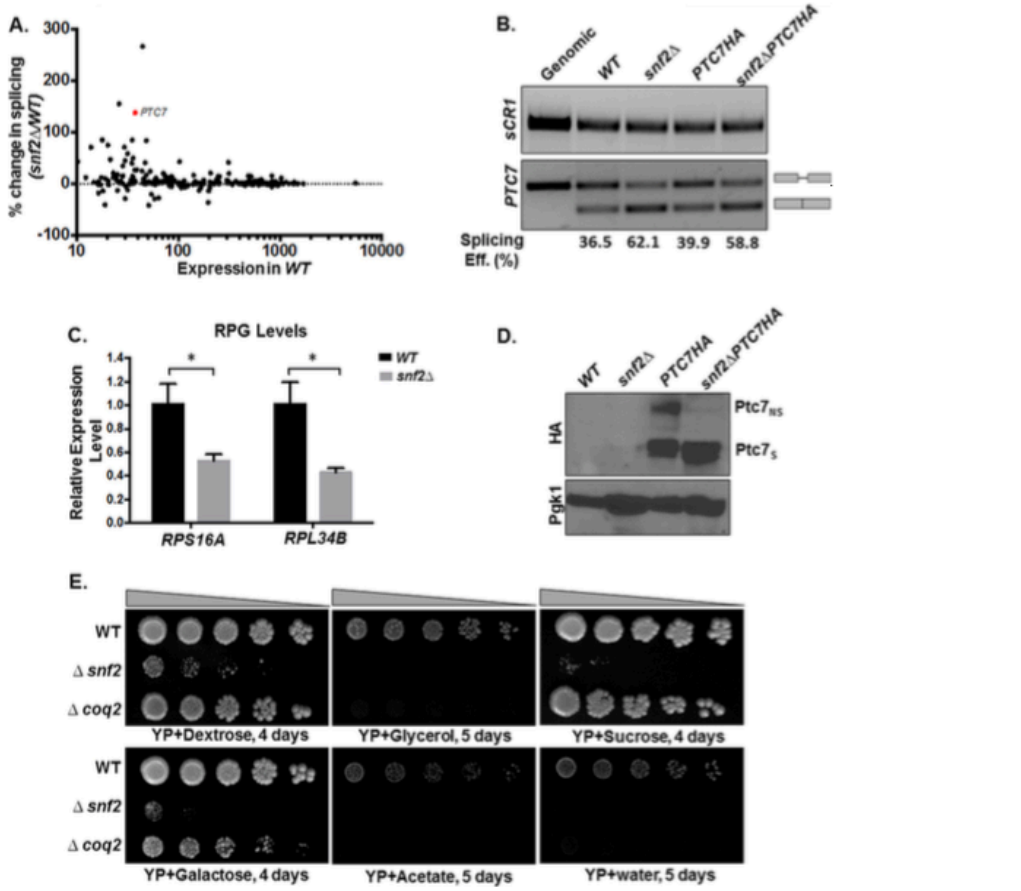

Figure 1. Deletion of *SNF2* enhances splicing of *PTC7* and the steady-state levels of the short Ptc7 protein isoform. *A*, deletion of *SNF2* enhances splicing of a subset of yeast RNAs, including *PTC7*. The scatter plot shows changes in splicing of individual introns in *snf2*Δ yeast over WT plotted against expression in WT. Percentage change in splicing is calculated as 100 × (S.E. in *snf2*Δ − S.E. in WT)/(S.E. in WT). *PTC7* is represented by the *red dot*. *B*, expression and splicing of *PTC7* in *WT* and *snf2*Δ yeast with HA-tagged and untagged Ptc7. Semiquantitative analysis of splicing efficiency of *PTC7* mRNA is indicated *below* each *lane*. *sCR1* served as an internal control. *Gray bars*, exons of the RNA; *thin gray line*, intron. *C*, RT-qPCR measurement of selected intron-containing RPG transcripts between WT and *snf2*Δ yeast strains. Shown is the mean of three biological replicates (unpaired Student's *t* test; *, $p < 0.05$). *Error bars*, S.D. *D*, deletion of *SNF2* affects steady-state levels of HA-tagged Ptc7 proteins. Proteins derived from the nonspliced and spliced forms of the *PTC7*-HA RNA are denoted as *Ptc7*$_{ns}$*HA* and *Ptc7*$_{s}$*HA*, respectively. Pgk1 (phosphoglycerate kinase 1) served as a loading control. *E*, serial dilutions (5-fold) of WT BY4741, *snf2*Δ, and *coq2*Δ (negative respiratory-deficient control; W303 background, because the deletion is unstable in the BY background) on YP agar plates with the indicated carbon sources.

the nonspliced isoform ($Ptc7_{ns}$) has been reported to localize to the nuclear envelope (10). The *PTC7* gene was endogenously HA-tagged, and Western blot analysis demonstrated that deletion of Snf2 leads to an increase in the levels of $Ptc7_{s}$ compared with $Ptc7_{ns}$ (Fig. 1*D*). It is noteworthy that the increase in the ratio of $Ptc7_{s}/Ptc7_{ns}$ polypeptides in the WT and *snf2*Δ cells appears to be greater than the increased ratio of spliced/unspliced RNA.

It has previously been demonstrated that yeast strains lacking Snf2 fail to grow on non-fermentable carbon sources, such as glycerol or acetate (26). However, *snf2*Δ mutants frequently incur secondary mutations, and the growth of such strains can resemble WT. Therefore, growth on fermentable and non-fermentable carbon sources was used as a quality control for the assessment of the *bona fide* phenotype (24) of *snf2*Δ prior to each experiment (Fig. 1*E*).

Deletion of Snf2 leads to increased CoQ_6 synthesis in yeast and improves the flux from DMQ_6 to CoQ_6

$Ptc7_{s}$ has previously been described as playing a role in regulating CoQ_6 synthesis in *S. cerevisiae* (11). A schematic of the entire CoQ_6 biosynthetic pathway with 4-hydroxybenzoic acid as the ring precursor and the role of Ptc7 is detailed in Fig. 2*A*. $Ptc7_{s}$ is thought to enhance CoQ_6 biosynthesis via its activation of Coq7 and subsequent catalysis of the hydroxylation of DMQ_6, the penultimate step of CoQ_6 biosynthesis (Fig. 2*B*) (11, 27).

$^{13}C_6$-Labeled 4-hydroxybenzoic acid ($^{13}C_6$-4HB), a ring precursor for Q biosynthesis, was used to determine the levels of $^{13}C_6$-CoQ_6 biosynthesis in WT *versus* *snf2*Δ yeast grown to similar culture densities. The absence of Snf2 causes increased steady-state levels of CoQ_6 and increased *de novo* biogenesis of $^{13}C_6$-CoQ_6 (Fig. 3*A*). Additionally, there are significant changes in the levels of *de novo* synthesized DMQ_6, as well as 3-hexa-

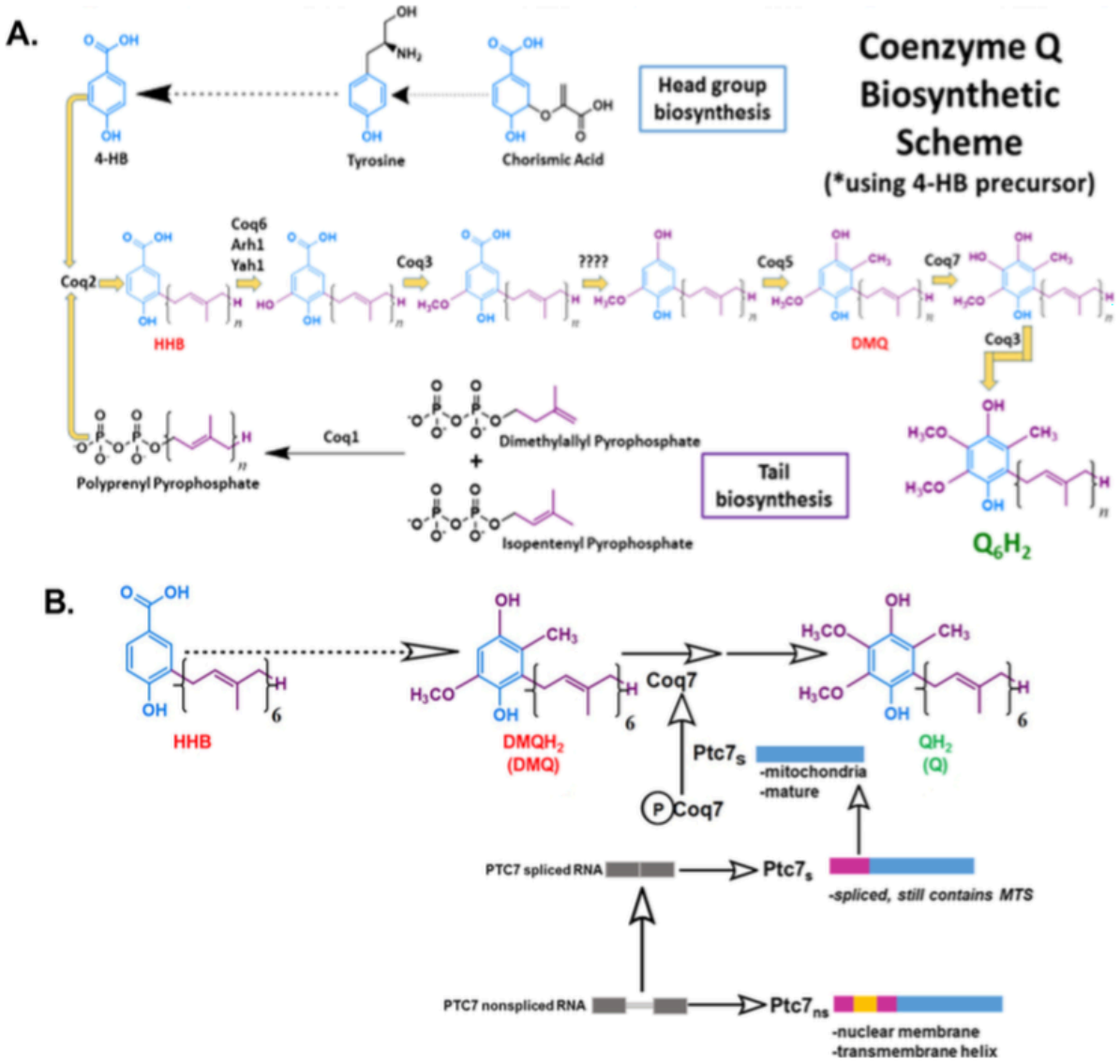

Figure 2. CoQ_6 biosynthetic pathway in *S. cerevisiae* and role of $Ptc7_s$ isoform on Coq7 phosphorylation and function. *A*, schematic of CoQ_6 biosynthetic pathway in yeast using 4HB as a ring precursor, ultimately forming the reduced CoQ_6H_2 product *in vivo*. The *question marks above* the decarboxylation and second hydroxylation steps denote that the enzyme(s) responsible is still unknown. *B*, schematic of the CoQ_6 biosynthetic pathway in yeast. The proposed function of $Ptc7_s$ as a mitochondrial phosphatase modulating Coq7 activity is indicated. $Ptc7_{ns}$ has been localized to nuclear membrane. The *gray bars* represent the exon regions of the RNA, and the *thin gray line* represents the intron region of the RNA. The *pink-colored regions* represent the predicted 38-amino acid mitochondrial targeting sequence (*MTS*) of the protein, the *yellow region* represents the 31-amino acid intron of the protein (which interrupts the MTS after amino acid 19, hence spanning from amino acid 20 to 50), and the *blue region* depicts the mature and spliced polypeptide, which spans from amino acid 51 to 374 (47).

prenyl-4-hydroxybenzoic acid (HHB), an early CoQ_6 biosynthetic intermediate (Fig. 3, *B* and *D*). Consistent with the increased synthesis of CoQ_6 being a consequence of Ptc7 action, the *snf2*Δ yeast show significantly lower ratios of $^{13}C_6$-DMQ_6 level to $^{13}C_6$-CoQ_6 content, indicating a significant increase in the efficiency of conversion of DMQ_6 to CoQ_6, namely the step catalyzed by Coq7, a target of $Ptc7_s$ (Fig. 3*C*) (11). Strikingly, we also observe that the levels of both steady-state and *de novo* synthesized HHB are significantly lower in *snf2*Δ than in the WT yeast (Fig. 3*D*). This suggests that the deletion of Snf2 not only causes higher CoQ_6 production by regulating catalysis from DMQ_6 but that it also funnels the early precursors more efficiently than WT, thus allowing a more streamlined conversion of intermediates of the pathway to the overall product of CoQ_6. This is reinforced by the observation that *snf2*Δ yeast show significantly lower ratios of $^{13}C_6$-HHB to $^{13}C_6$-CoQ_6 content (Fig. 3*E*).

Depletion of Snf2 during batch growth is associated with increased PTC7 splicing and increased CoQ_6 production

Because *snf2*Δ yeast have a significantly slower growth rate than WT, we considered the possibility that the increased CoQ_6

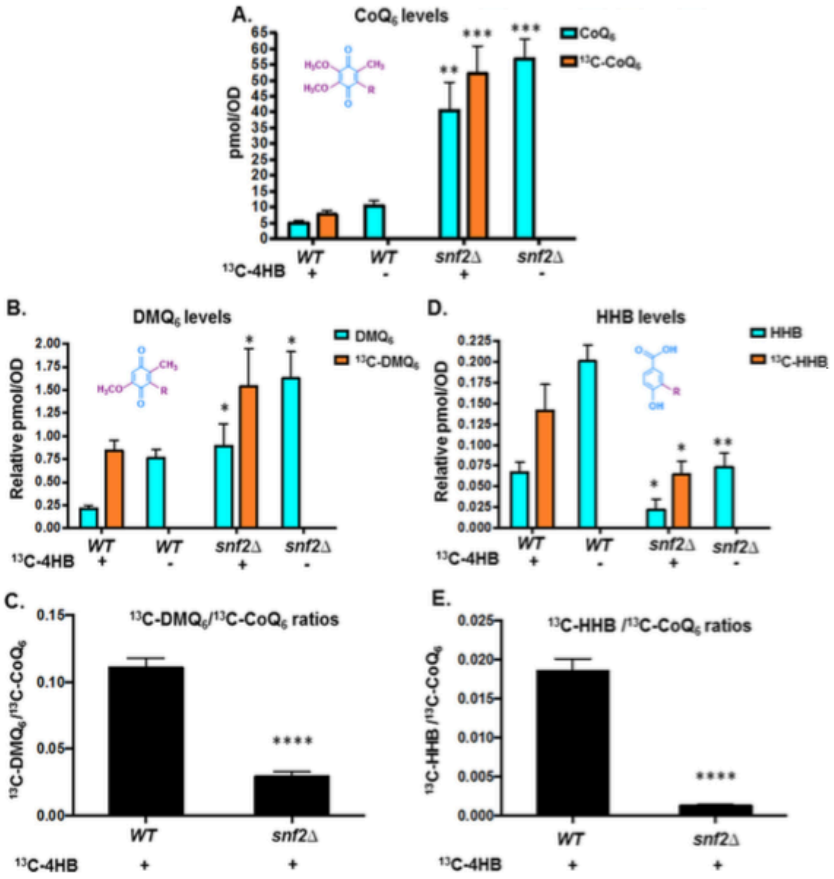

Figure 3. Deletion of *SNF2* leads to increased steady state levels and *de novo* CoQ_6 biosynthesis in yeast and improves the flux from DMQ_6 to CoQ_6. *A*, levels of steady-state CoQ_6 (^{12}C-CoQ_6, *blue bars*) and *de novo* synthesized CoQ_6 ($^{13}C_6$-CoQ_6, *orange bars*) were determined in WT and *snf2*Δ yeast. $^{13}C_6$-4HB was added during midlog phase (A_{600} = 0.5), and labeling was allowed to proceed until a cell density of A_{600} ~1.75 was reached by both strains. ^{12}C-CoQ_6 and $^{13}C_6$-CoQ_6 present in yeast cell pellets were quantified by HPLC-MS/MS, as described under "Experimental procedures." *Error bars*, S.D. of $n = 3$ biological replicates (unpaired Student's *t* test between *corresponding bars* for *snf2*Δ and WT; **, $p < 0.005$; ***, $p < 0.0005$). *B*, levels of steady-state (^{12}C-DMQ_6, *blue bars*) and *de novo* synthesized DMQ_6 ($^{13}C_6$-DMQ_6, *orange bars*) were determined in WT and *snf2*Δ yeast. DMQ_6 was determined from the same cultures as in *A*. *Error bars*, S.D. of $n = 3$ biological replicates (unpaired Student's *t* test between corresponding bars for *snf2*Δ and *WT*; *, $p < 0.05$). *C*, ratios of $^{13}C_6$-DMQ_6/$^{13}C_6$-CoQ_6 in WT and *snf2*Δ yeast, depicting flux of conversion of $^{13}C_6$-DMQ_6 to $^{13}C_6$-CoQ_6. *Error bars*, S.D. of $n = 3$ biological replicates (unpaired Student's *t* test between corresponding bars for *snf2*Δ and WT; ****, $p < 0.00005$). *D*, levels of steady-state HHB (^{12}C-HHB, *blue bars*) and *de novo* synthesized HHB ($^{13}C_6$-HHB, *orange bars*) were determined in WT and *snf2*Δ yeast. HHB was determined from the same cultures as in *A*. *Error bars*, S.D. of $n = 3$ biological replicates (unpaired Student's *t* test between *corresponding bars* for *snf2*Δ and WT; *, $p < 0.05$; **, $p < 0.005$). *E*, ratios of ^{13}C-HHB/^{13}C-CoQ_6 in WT and *snf2*Δ yeast, depicting flux of conversion of $^{13}C_6$-HHBto $^{13}C_6$-CoQ_6. *Error bars*, S.D. of $n = 3$ biological replicates (unpaired Student's *t* test between *corresponding bars* for *snf2*Δ and WT; ****, $p <$ 0.00005).

synthesis was a consequence of the increased time in culture required to achieve equal cell density. To address this, rates of CoQ_6 biosynthesis in WT and *snf2*Δ yeast were determined at timed intervals of culture. First, measurements of steady-state and *de novo* synthesis rates of CoQ_6 between 2 and 12 h of batch growth in YPD revealed that whereas there is indeed an increased rate of synthesis in the *snf2*Δ yeast strain, the steady-state levels of CoQ_6 plateau within 4–6 h of labeling (Fig. 4*A*). We also observe decreasing levels of Snf2 as the time course progresses and nutrients are depleted (Fig. 4*B*). Consistent with the role of Snf2 in RPG transcription, RPG levels decrease with time in batch cultures of yeast, in a manner that tracks well with decreasing levels of Snf2 (Fig. 4*C*). This decrease also coincides with a concomitant increase in the splicing of *PTC7* (Fig. 4, *D* and *E*). Notably, splicing of the *PTC7* transcript in *snf2*Δ yeast starts off higher than in WT yeast, but as Snf2 is depleted from the WT strain, splicing of the *PTC7* transcript approaches the levels of splicing in the *snf2*Δ strain (Fig. 4*F*).

To better understand the kinetics of CoQ_6 synthesis, a shorter time course was performed to capture points preceding the plateau, between 0 and 5 h of labeling. Within 4 h after labeling with ^{13}C-4HB precursor, significant down-regulation in the levels of Snf2 protein is evident (Fig. 5*A*). The decrease in the level of Snf2 protein is mirrored in the increase in splicing efficiency of *PTC7* transcript in the WT strain (Fig. 5, *B–E*). It is interesting to note that the *PTC7* transcript is initially better spliced in the *snf2*Δ strain than in WT, but as the levels of Snf2 in the WT yeast decrease, splicing improves to a degree comparable with the *snf2*Δ strain (Fig. 5, *D* and compare *C* and *F*).

Additionally, there is a striking increase in the overall CoQ_6 product and its *de novo* biosynthesis in the *snf2*Δ yeast within 0–5 h of labeling, as compared with CoQ_6 levels of the WT

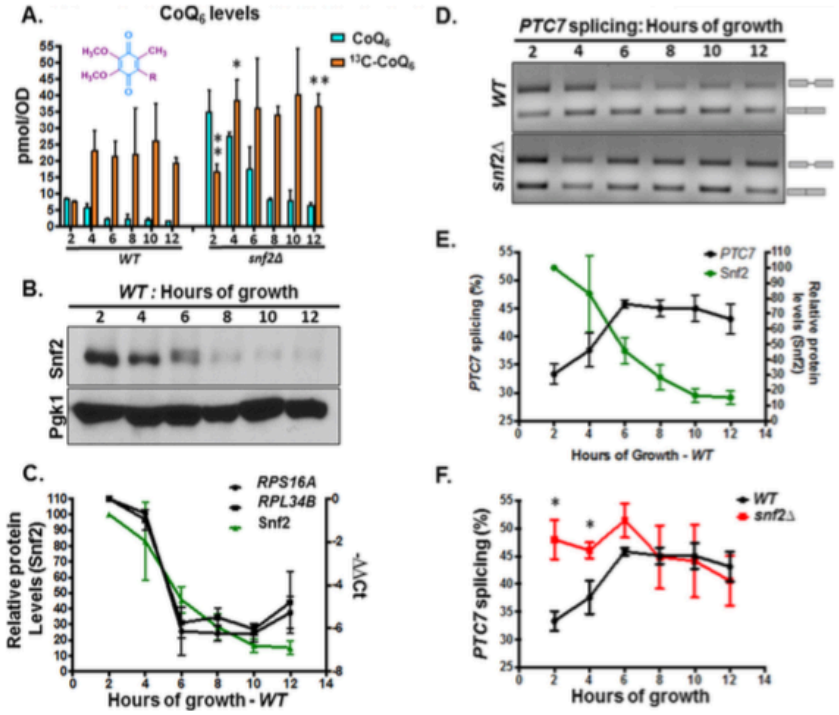

Figure 4. Snf2 levels decrease during batch growth, coinciding with increased *PTC7* splicing and increased CoQ_6 synthesis. *A*, levels of steady-state CoQ_6 (^{12}C-CoQ_6, *blue bars*) and *de novo* synthesized CoQ_6 ($^{13}C_6$-CoQ_6, *orange bars*) in WT and *snf2*Δ yeast were determined at the designated hours after labeling with $^{13}C_6$-4HB. *Error bars*, S.D. of $n = 3$ biological replicates (unpaired Student's *t* test between *corresponding bars* for *snf2*Δ and WT; *, $p < 0.05$; **, $p < 0.005$). *B*, steady-state levels of Snf2 protein in WT cells corresponding to samples from *A* were determined by immunoblot. Pgk1 served as a loading control. *C*, RT-qPCR measurement of selected intron-containing RPG transcripts (*black lines*) and Snf2 protein levels (*green line*) in WT yeast cells were determined at the designated hours after labeling with $^{13}C_6$-4HB as indicated in *A*. Shown is the mean of three biological replicates. *Error bars*, S.D. *D*, expression and splicing of *PTC7* in WT and *snf2*Δ yeast cells corresponding to samples from *A*. PCR products representing the spliced and nonspliced forms are indicated. *E*, quantification of splicing of *PTC7* transcript (*black line*) and Snf2 protein levels (*green line*) in WT yeast cells corresponding to samples from *D*. Snf2 protein levels were previously depicted in *C* and are shown here again for purposes of comparison. Shown is the mean of three biological replicates. *Error bars*, S.D. *F*, quantification of splicing of *PTC7* transcripts in WT and *snf2*Δ yeast cells corresponding to samples from *D*. The splicing of WT *PTC7* shown in *D* is depicted again here for purposes of comparison. Shown is the mean of three biological replicates. *Error bars*, S.D. (unpaired Student's *t* test; *, $p < 0.05$.

during the same time course (Fig. 6, compare *A* and *F*). Furthermore, the gradual increase in CoQ_6 biosynthesis observed in the WT strain plateaus at 3–4 h after labeling (Fig. 6*A*), by which point the significant down-regulation in the levels of Snf2 protein is also evident (Fig. 5*A*). The steady-state and *de novo* synthesized levels of DMQ_6 and HHB were also measured in the 5-h time course of WT and *snf2*Δ yeast (Fig. 6, *B*, *C*, *G*, and *H*). Strikingly, the conversion of *de novo* DMQ_6 to CoQ_6 increases (as shown by the decreased ratio of $^{13}C_6$-DMQ_6 to $^{13}C_6$-CoQ_6) in a manner concurrent with the decrease in Snf2 levels and increase in *PTC7* splicing in WT (compare Fig. 6*D* with Fig. 5 (*A* and *B*)). In fact, as the levels of Snf2 in WT yeast decrease, the conversion efficiency of DMQ_6 to CoQ_6 approaches the low ratio of DMQ_6 to CoQ_6 in *snf2*Δ yeast (Fig. 6, compare *D* and *I*). The role of $Ptc7_s$ in the increased synthesis of CoQ_6 in the absence of Snf2 can be inferred from the observation that whereas the conversion efficiency from DMQ_6 to CoQ_6 is higher in the absence of Snf2, the level of DMQ_6 itself does not change appreciably between WT and *snf2*Δ yeast over the 5-h time course (Fig. 6, compare *B* and *G*). However, the *snf2*Δ cells also show significantly lower rates of HHB synthesis (Fig. 6, compare *C* and *H*), as well as lower ratios of $^{13}C_6$-HHB to $^{13}C_6$-CoQ_6 content (Fig. 6, compare *E* and *J*), consistent with the observation that deletion of Snf2 markedly accelerates the synthesis of CoQ_6, presumably by expediting the conversion of these intermediates to the final product.

RPG down-regulation in general leads to increased PTC7 splicing

Our previous work showed that Snf2-dependent down-regulation of ribosomal protein genes enhances splicing, particularly of genes with nonconsensus splice sites. To determine whether the observed increase in *PTC7* splicing is a consequence of RPG down-regulation *per se*, rapamycin was used to inhibit target of rapamycin (TOR)-dependent RPG transcription in a Snf2-independent manner (28) (Fig. 7*A*). It has also been previously published that rapamycin mitigates certain mitochondrial disorders in *Drosophila* and improves lifespan in response to TOR inhibition, purportedly by modulating carbon metabolism (29). In our work, rapamycin treatment led to a significant increase in the splicing of the *PTC7* transcript (Fig. 7, *B* and *C*). As previously observed, the change in the ratio of $Ptc7_s$/$Ptc7_{ns}$ protein (Fig. 1*D*) is greater than the change in the ratio of spliced to nonspliced transcript upon the deletion of Snf2 (Fig. 1*B*). This suggests that whereas Snf2-dependent RPG down-regulation changes the splicing of the *PTC7* transcript,

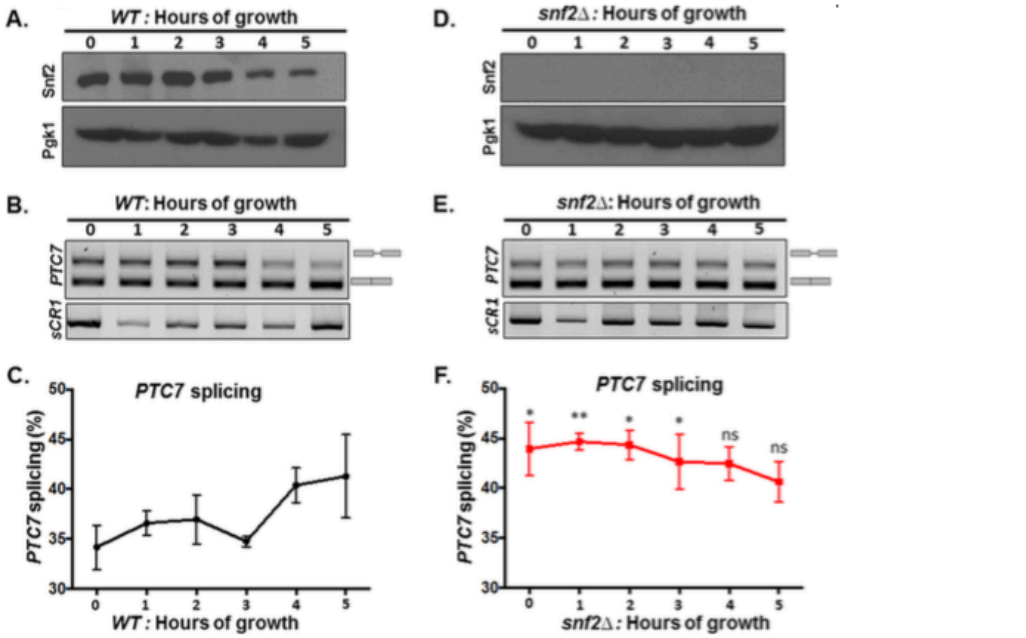

Figure 5. The decrease in Snf2 levels over time in batch cultures of WT yeast correlates with enhanced splicing of *PTC7* RNA. *A*, steady-state levels of Snf2 protein in WT cells corresponding to samples from indicated time points were determined by immunoblot. Pgk1 (phosphoglycerate kinase 1) served as a loading control. *B*, expression and splicing of *PTC7* in WT yeast cells corresponding to samples from *A*; PCR products represent the spliced and nonspliced forms, as indicated. *C*, quantification of splicing of *PTC7* transcript (*black line*) in WT yeast cells corresponding to samples from *B*. Shown is the mean of three biological replicates. *Error bars*, S.D. *D*, the Snf2 protein is absent in *snf2*Δ cells corresponding to samples from the indicated time points as determined by immunoblot. Pgk1 served as a loading control. *E*, expression and splicing of *PTC7* in *snf2*Δ yeast cells corresponding to samples from *D*; PCR products representing the spliced and nonspliced forms are indicated. *F*, quantification of splicing of *PTC7* transcript (*red line*) in *snf2*Δ yeast cells corresponding to samples from *E*. Shown is the mean of three biological replicates. *Error bars*, S.D. (unpaired Student's *t* test between *corresponding bars* for *snf2*Δ and WT in *C*; *, $p < 0.05$; **, $p < 0.005$).

there are probably additional layers of gene regulation that control the relative levels of the $Ptc7_s$ and $Ptc7_{ns}$ protein isoforms. Experiments probing these mechanisms are currently ongoing. Nonetheless, these results are consistent with a model whereby down-regulation of RPG expression redirects spliceosomes from these abundant transcripts to otherwise poorly spliced transcripts, such as *PTC7* (5, 6). In light of the role of Snf2 in RPG expression, changes in Snf2 levels allow fine-tuning of splicing in response to the cell's metabolic needs.

Ptc7 isoforms have differing and opposing effects on CoQ_6 synthesis

The predicted structures of the two isoforms of Ptc7, $Ptc7_s$ and $Ptc7_{ns}$, have been modeled (Fig. 8, *A* and *B*). In fact, the $Ptc7_{ns}$ contains a transmembrane helix, encoded for by the *PTC7* intron, which is capable of spanning the nuclear membrane. Overall, the presence of this transmembrane helix is not predicted to influence the folding of the rest of the protein, thus potentially retaining its phosphatase activity (Fig. 8).

To determine the effect of each Ptc7 isoform on CoQ_6 synthesis, we assayed CoQ_6 levels in cells expressing both forms of Ptc7, $Ptc7_s$ only, $Ptc7_{ns}$ only, or neither (*ptc7*Δ). As reported previously, there is no significant change in CoQ_6 synthesis levels in the *ptc7*Δ mutant (12, 30). However, exclusive expression of $Ptc7_s$ leads to an increase in CoQ_6 synthesis, whereas exclusive expression of $Ptc7_{ns}$ leads to a decrease in CoQ_6 synthesis (Fig. 9*A*). The relative RNA levels from each strain are shown (Fig. 9*B*). Moreover, there are no significant changes observed in the protein levels of Snf2 or Coq7, the target of Ptc7 activity (Fig. 9*C*), in these strains. Whereas each of these isoforms was expressed within the endogenous context and from the endogenous *PTC7* promoter, protein levels of the $Ptc7_{ns}$ appeared to be increased relative to the other isoforms (Fig. 9, *B* and *C*), perhaps due to a cellular feedback mechanism that increases expression or enhances stability of $Ptc7_{ns}$.

The steady-state and *de novo* synthesized levels of CoQ_6 were also measured in a 5-h time course with the yeast strains expressing either $Ptc7_{ns}$ or $Ptc7_s$. Both steady-state and *de novo* CoQ_6 biosynthesis are significantly lower in $Ptc7_{ns}$ strain than in the $Ptc7_s$ and in fact appear to be actively repressed, suggesting that the two isoforms of Ptc7 have differing and opposing effects on CoQ_6 biosynthesis (Fig. 9*D*). In addition, the exclusive presence of $Ptc7_s$ causes increased *de novo* biogenesis of ^{13}C-CoQ_6 as compared with the exclusive presence $Ptc7_{ns}$ (Fig. 9*D*). Whereas the positive effect of $Ptc7_s$ on CoQ_6 biosynthesis is consistent with the mechanisms of Ptc7 action described previously, it is clear that $Ptc7_{ns}$ has a repressive effect on CoQ_6 biosynthesis (compare $Ptc7_{ns}$ and *ptc7*Δ in Fig. 9*A*). To begin to elucidate the mechanism of this repression, we assayed the mRNA transcript levels of genes encoding components of the CoQ_6 biosynthetic complex (*viz. COQ1–11* and *PTC7*). On average, there is little change in the expression of the complex upon deletion of Snf2 (Fig. 9, *G* and *H*) or with the exclusive expression of $Ptc7_s$ or *ptc7*Δ. However, exclusive expression of $Ptc7_{ns}$ is associated with pronounced down-regulation of every

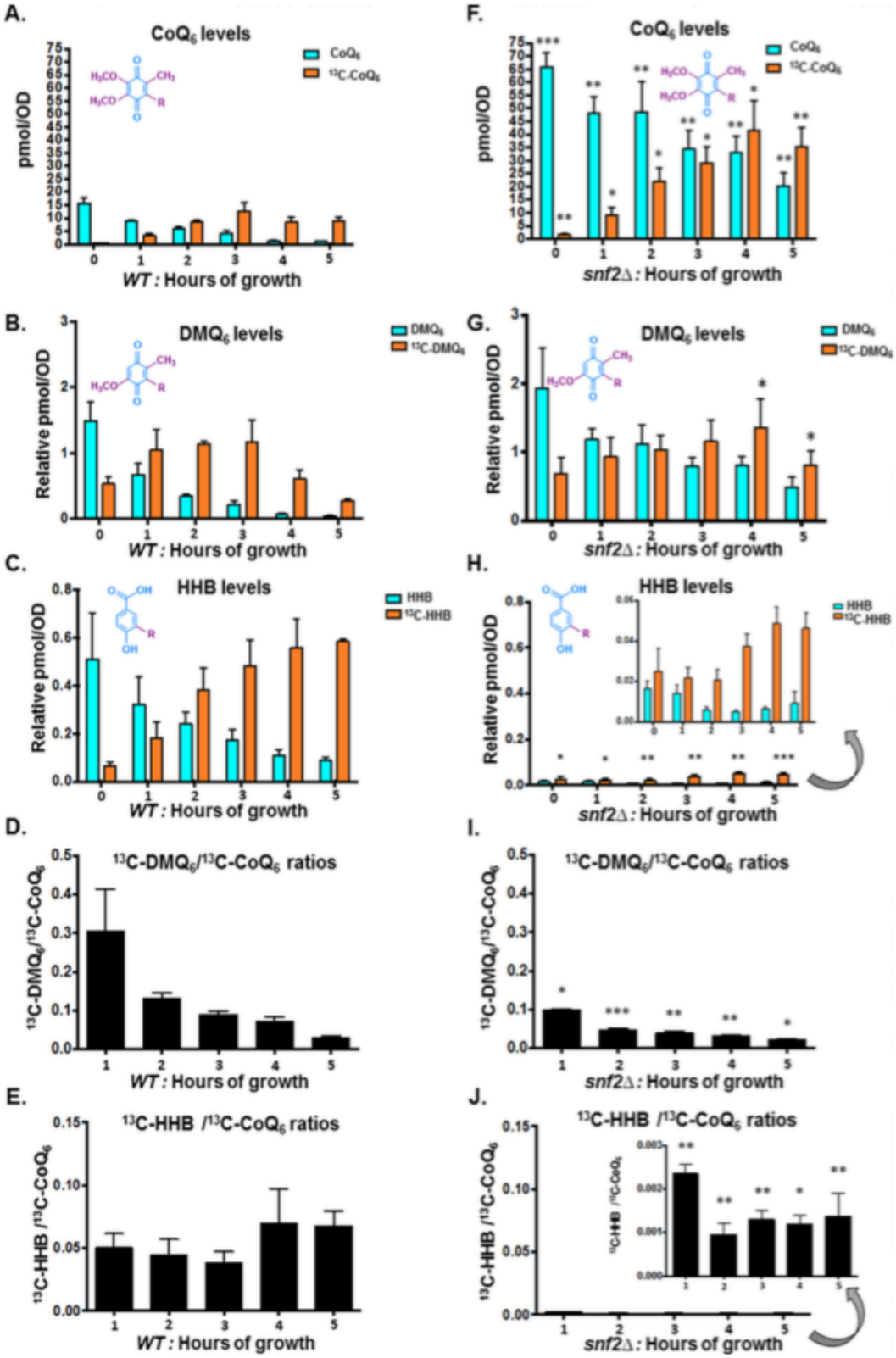
A.
CoQ6 levels
CoQ6
13C-CoQ6
pmol/OD
WT : Hours of growth
F.
CoQ6 levels
snf2Δ : Hours of growth
B.
DMQ6 levels
DMQ6
13C-DMQ6
Relative pmol/OD
WT : Hours of growth
G.
DMQ6 levels
snf2Δ : Hours of growth
C.
HHB levels
HHB
13C-HHB
Relative pmol/OD
WT : Hours of growth
H.
HHB levels
snf2Δ : Hours of growth
D.
13C-DMQ6/13C-CoQ6 ratios
WT : Hours of growth
I.
13C-DMQ6/13C-CoQ6 ratios
snf2Δ : Hours of growth
E.
13C-HHB /13C-CoQ6 ratios
WT : Hours of growth
J.
13C-HHB /13C-CoQ6 ratios
snf2Δ : Hours of growth

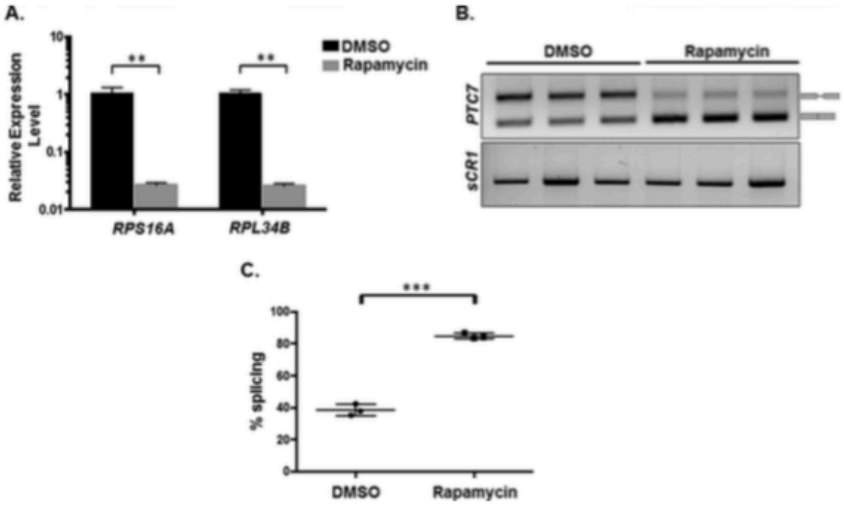

Figure 7. RPG down-regulation and redistribution of spliceosomes result in increased *PTC7* splicing. *A*, RT-qPCR measurement of selected intron-containing RPG transcripts between WT yeast treated with rapamycin and a vehicle control. Mean of three biological replicates (unpaired Student's *t* test, $^{**}p < 0.005$). *Error bars*, S.D. *B*, expression and splicing of *PTC7* in WT yeast treated with rapamycin and a vehicle control (DMSO). PCR products representing the spliced and nonspliced forms are indicated. *C*, quantification of three independent biological replicates of *B* (unpaired Student's *t* test; $^{***}p < 0.0005$). *Error bars*, S.D.

member of the CoQ-synthome (Fig. 9, *E* and *F*). Although the mechanism by which these components are down-regulated is unclear, it is interesting that $Ptc7_{ns}$ has previously been localized to the nuclear membrane (10), hinting at a novel role for this isoform in expression of the RNAs encoding the CoQ-synthome. Two possible mechanisms by which nucleus-localized $Ptc7_{ns}$ may affect synthesis of the CoQ-synthome are via direct action on nucleus-localized Coq7 or via indirect effects on gene expression. It is important to mention here that to the best of our knowledge, no reports have demonstrated nuclear localization of, or a nuclear role for, Coq7 in *S. cerevisiae*.

Interestingly, yeast strains engineered to express either $Ptc7_s$ or $Ptc7_{ns}$ still retain the ability to grow on medium containing a non-fermentable carbon source, as do *ptc7*Δ null mutants (data not shown). This is consistent with our prior observations that ~1–10% of CoQ_6 levels are sufficient for comparable growth on medium containing a nonfermentable carbon source. It has been postulated that residual CoQ_6 levels are observed due to the overlapping activities of Ptc5 and/or Ptc6, and in fact the *ptc5*Δ*ptc7*Δ double null mutant has impaired growth under conditions of temperature stress (11, 31). It is also worth noting that unlike the deletion of *SNF2*, the conversion efficiencies or ratios between the early components of the pathway (DMQ_6 or HHB) and CoQ_6 do not vary between strains exclusively expressing either Ptc7 isoform (Fig. 10, *C* and *D*). This is because although there are significant changes in the levels of *de novo* synthesized DMQ_6 as well as HHB when comparing $Ptc7_s$ to $Ptc7_{ns}$ (Fig. 10, *A* and *B*), $Ptc7_s$ is synthesizing higher levels of *de novo* CoQ_6, DMQ_6, and HHB, compared with overall lower levels of these same lipids in $Ptc7_{ns}$ (Fig. 10, *C* and *D*). Thus, the overall conversion efficiencies (ratios) between both isoforms are comparable (Fig. 10, *C* and *D*). This is consistent with our interpretation that the absence of Snf2 contributes to the metabolic state of the cell in other ways in addition to its role in regulation of the Ptc7 isoforms.

Figure 6. Overall conversion efficiency of the CoQ_6 biosynthetic pathway increases upon depletion of Snf2, with increased conversions of both DMQ_6 to Q_6 and HHB to Q_6. *A*, levels of steady-state CoQ_6 (^{12}C-CoQ_6, *blue bars*) and *de novo* synthesized CoQ_6 ($^{13}C_6$-CoQ_6, *orange bars*) in WT yeast cells were determined at the designated hours after labeling with $^{13}C_6$-4HB. *Error bars*, S.D. of $n = 3$ biological replicates. *B*, levels of steady-state DMQ_6 (^{12}C-DMQ_6, *blue bars*) and *de novo* synthesized DMQ_6 ($^{13}C_6$-DMQ_6, *orange bars*) in WT yeast were determined at the designated hours after labeling with $^{13}C_6$-4HB. *Error bars*, S.D. of $n = 3$ biological replicates. *C*, levels of steady-state HHB (^{12}C-HHB, *blue bars*) and *de novo* synthesized ($^{13}C_6$-HHB, *orange bars*) in WT and *snf2*Δ yeast were determined at the designated hours after labeling with $^{13}C_6$-4HB. *Error bars*, S.D. of $n = 3$ biological replicates. *D*, the ratio of $^{13}C_6$-DMQ_6/$^{13}C_6$-CoQ_6 in WT yeast was determined at the designated hours after labeling with $^{13}C_6$-4HB. *Error bars*, S.D. of $n = 3$ biological replicates. The 0-h time point is excluded, because the ratio is not indicative of pathway conversion. *E*, the ratio of $^{13}C_6$-HHB/$^{13}C_6$-CoQ_6 in WT yeast was determined at the designated hours after labeling with $^{13}C_6$-4HB. *Error bars*, S.D. of $n = 3$ biological replicates. The 0-h time point is excluded, because the ratio is not indicative of pathway conversion. *F*, levels of steady-state CoQ_6 (^{12}C-CoQ_6, *blue bars*) and *de novo* synthesized ($^{13}C_6$-CoQ_6, *orange bars*) in *snf2*Δ yeast cells were determined at the designated hours after labeling with $^{13}C_6$-4HB. *Error bars*, S.D. of $n = 3$ biological replicates (unpaired Student's *t* test between *corresponding bars* for *snf2*Δ and WT in *A*; $^{*}p < 0.05$; $^{**}p < 0.005$; $^{***}p < 0.0005$). *G*, levels of steady-state DMQ_6 (^{12}C-DMQ_6, *blue bars*) and *de novo* synthesized DMQ_6 ($^{13}C_6$-DMQ_6, *orange bars*) in *snf2*Δ yeast were determined at the designated hours after labeling with $^{13}C_6$-4HB. *Error bars*, S.D. of $n = 3$ biological replicates. (unpaired Student's *t* test between *corresponding bars* for *snf2*Δ and WT in *B*; $^{*}p < 0.05$). *H*, levels of steady-state HHB (^{12}C-HHB, *blue bars*) and *de novo* synthesized HHB ($^{13}C_6$-HHB, *orange bars*) in *snf2*Δ yeast were determined at the designated hours after labeling with ^{13}C-4HB. *Error bars*, S.D. of $n = 3$ biological replicates (unpaired Student's *t* test between corresponding bars for *snf2*Δ and WT in *C*; $^{*}p < 0.05$; $^{**}p < 0.005$; $^{***}p < 0.0005$). *I*, the ratio of $^{13}C_6$-DMQ_6/$^{13}C_6$-CoQ_6 in *snf2*Δ yeast cells was determined at the designated hours after labeling with $^{13}C_6$-4HB. *Error bars*, S.D. of $n = 3$ biological replicates (unpaired Student's *t* test between corresponding bars for *snf2*Δ and WT in *D*; $^{*}p < 0.05$; $^{**}p < 0.005$; $^{***}p < 0.0005$). The 0-h time point is excluded, because the ratio is not indicative of pathway conversion. *J*, the ratio of $^{13}C_6$-HHB/$^{13}C_6$-CoQ_6 in *snf2*Δ yeast cells was determined at the designated hours after labeling with $^{13}C_6$-4HB. *Error bars*, S.D. of $n = 3$ biological replicates (unpaired Student's *t* test between *corresponding bars* for *snf2*Δ and WT in *E*; $^{*}p < 0.05$; $^{**}p < 0.005$). The 0-h time point is excluded, because the ratio is not indicative of pathway conversion.

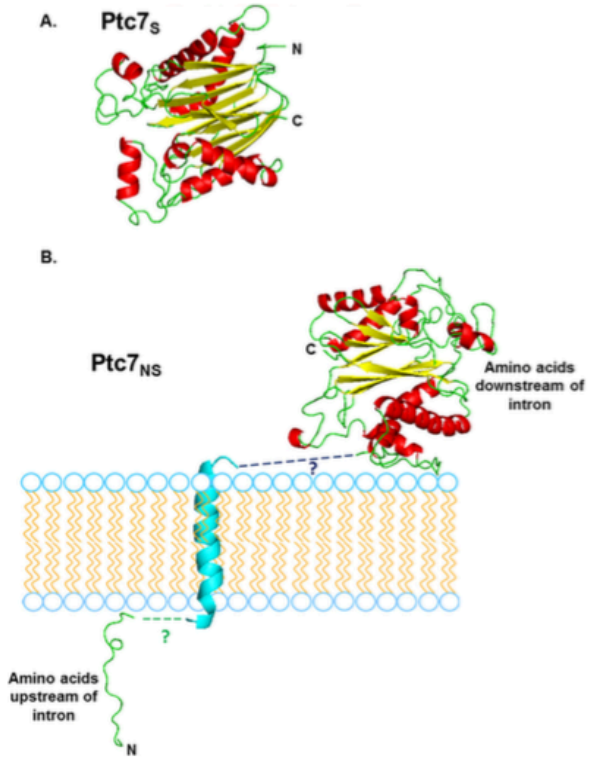

Figure 8. Structural predictions of mitochondrial Ptc7$_s$ and nuclear membrane traversing Ptc7$_{ns}$. *A*, PHYRE2 homology modeling of mature mitochondrial Ptc7$_s$, which is experimentally determined to start at amino acid Gly[39] (46). 85% of residues modeled at >90% confidence (15% of residues modeled *ab initio*). The N terminus and C terminus of the protein are shown. *B*, PHYRE2 homology modeling of nuclear membrane Ptc7$_{ns}$. The predicted trans-membrane helix encoded by the intron is shown in *cyan*. 86% of residues modeled at >90% confidence (14% of residues modeled *ab initio*. To show the interaction with the nuclear membrane, the N-terminal loop residing on the one side of the nuclear membrane is proposed to be linked to the modeled transmembrane helix, which is then proposed to be linked to the rest of the Ptc7 protein that is predicted to reside on the alternate side of the nuclear membrane. The *nine black dashes* connecting the helix to the larger portion of the protein represent nine amino acids in the intron that were in an unmodeled region.

These data reveal a novel role for Snf2 in respiration and specifically in the transition from a largely fermentative mode of metabolism to a largely respiratory one in *S. cerevisiae*, as shown by the model in Fig. 11. Under conditions of high nutrient availability, Snf2-dependent transcription of intron-rich RPGs sequesters spliceosomes away from transcripts with weak splice sites, such as *PTC7*. As a consequence, both isoforms of the Ptc7 protein are expressed at appreciable levels, and their opposing effects on CoQ_6 synthesis ensure that CoQ_6 is maintained at a relatively low level. As the nutrients in the medium are depleted, the levels of Snf2 and, consequently, RPG transcripts, decrease concurrently, freeing up spliceosomes to act on *PTC7*. This leads to better splicing of *PTC7* and a shift in the relative abundances of the two protein isoforms, which eventually leads to an increase in CoQ_6 synthesis.

Discussion

Whereas it has been broadly acknowledged that chromatin states and chromatin factors influence splicing outcomes in various organisms, identifying the functional importance of such regulation under biologically relevant conditions remains a challenge. We have shown previously that down-regulation of Snf2, the core ATPase component of the SWI/SNF chromatin-remodeling complex, in response to nutrient depletion leads to a change in cellular splicing outcomes due to down-regulation of RPGs and subsequent redistribution of spliceosomes (5, 6). We show here that Snf2-dependent changes in splicing of *PTC7* during yeast growth, combined with the general conditions in the cell in the absence of Snf2, causes a shift in the ratio of two distinct isoforms of the Ptc7 protein that have distinct and opposing effects on CoQ_6 biosynthesis. This change in the ratio of the isoforms is concomitant with an increase in CoQ_6 levels in the cell, preparing for the transition from a largely fermentative to a respiratory mode of metabolism.

Previous studies have presented contradictory evidence regarding the involvement of *PTC7* in CoQ_6 biosynthesis. Ptc7 is required for the dephosphorylation of Coq7, thus transitioning Coq7 to its "active" form, which is able to catalyze the penultimate step of the CoQ_6 pathway. This led to the prediction that the *ptc7*Δ strain would demonstrate decreased CoQ_6 synthesis, as assayed by quantification of lipids from purified mitochondria (11). Surprisingly, although Ptc7 supports general respiratory function, the absence of *PTC7* does not lead to a deficiency in CoQ_6 levels, as assayed in lipid extracts of whole cells (12) (Fig. 9*A*). The studies here help to resolve this apparent contradiction. Studies with the *ptc7*Δ cells fail to address the opposing roles that the two Ptc7 isoforms have in the cell under WT conditions. Only cells with the capacity to express both Ptc7$_s$ and Ptc7$_{ns}$ can accurately reflect the full extent of Ptc7 function. We demonstrate that exclusive expression of Ptc7$_{ns}$ has a significant repressive effect on CoQ_6 biosynthesis (Fig. 9, *A* and *D*). Notably, the rates of conversions from precursors in the pathway to the final product remained unchanged, indicating down-regulation of the entire pathway (Fig. 10, *C* and *D*). Consistent with this, we observe down-regulation of almost all of the components of the CoQ_6 biosynthetic complex upon exclusive expression of Ptc7$_{ns}$ (Fig. 9*F*). The mechanism by which Ptc7$_{ns}$ affects RNA expression is as yet unknown, and investigations to understand the same are ongoing.

PTC7 is not the only known example of a gene in *S. cerevisiae* encoding functional proteins from both the nonspliced pre-mRNA as well as the "mature" spliced mRNA (10). We recently reported translation of unspliced *GCR1* pre-mRNA leading to a functional Gcr1 protein, although in this case, translation starts from within the retained intron (7). Whereas the read-through nature of the intron is conserved across most *Saccharomycetaceae* species, the intron is excised in the same species (analysis of publicly available RNA-seq data sets; data not shown), rendering it likely that both forms of the protein are necessary and functional. This is illustrated in the case of *Tetrapisispora blattae*, which, like *S. cerevisiae*, underwent a whole genome duplication event; but unlike *S. cerevisiae*, which lost the duplications of most of its genes, *T. blattae* retains two copies of the *PTC7* gene. Interestingly, the two *PTC7* genes in *T. blattae* subfunctionalized into a gene that encodes a mitochondrial PP2C (Ptc7$_b$, from a spliced transcript of *PTC7b* con-

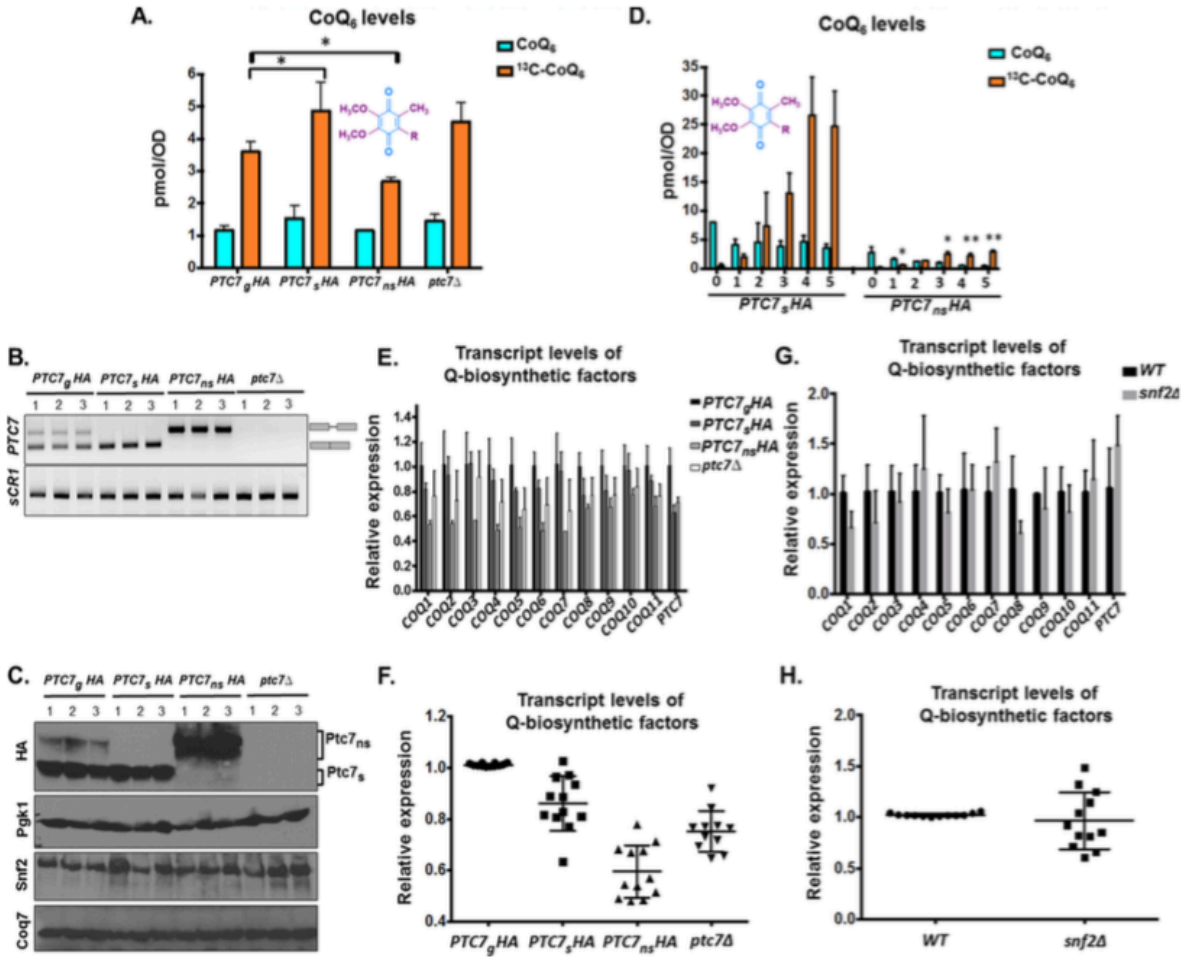

Figure 9. Ptc7 isoforms have differing and opposing effects on CoQ_6 synthesis. *A*, levels of steady-state CoQ_6 (^{12}C-CoQ_6, *blue bars*) and *de novo* synthesized CoQ_6 ($^{13}C_6$-CoQ_6, *orange bars*) in strains expressing distinct Ptc7 isoforms (*$PTC7_gHA$*, genomic, both isoforms expressed; *$PTC7_sHA$*, exclusively expresses the isoform from spliced mRNA; *$PTC7_{ns}HA$*, exclusively expresses the isoform from nonspliced pre-mRNA) and *ptc7Δ*. Labeling with $^{13}C_6$-4HB was allowed to proceed for 3 h. *Error bars*, S.D. of $n = 3$ biological replicates (unpaired Student's *t* test; *, $p < 0.05$). *B*, expression and splicing of *PTC7* for samples corresponding to *A*. PCR products representing the spliced and nonspliced forms are indicated. *C*, steady-state levels of HA-tagged Ptc7 proteins were determined by immunoblotting for samples corresponding to *A*. Proteins derived from the nonspliced and spliced forms of the *PTC7* RNA are denoted as $Ptc7_{ns}$ and $Ptc7_s$, respectively. Pgk1 (phosphoglycerate kinase 1) served as a loading control. Immunoblots for Snf2 and Coq7 are also included. *D*, levels of steady-state (^{12}C-CoQ_6, *blue bars*) and *de novo* synthesized ($^{13}C_6$-CoQ_6, *orange bars*) CoQ_6 in *$PTC7_sHA$* and *$PTC7_{ns}HA$* yeast cells were determined at the designated hours after labeling with $^{13}C_6$-4HB. *Error bars*, S.D. of $n = 3$ biological replicates (unpaired Student's *t* test between corresponding bars for *$PTC7_sHA$* and *$PTC7_{ns}HA$*; *, $p < 0.05$; **, $p < 0.005$). *E*, RT-qPCR measurement of *COQ1–COQ11* and *PTC7* transcript levels between strains expressing different Ptc7 isoforms (*$PTC7_gHA$*, genomic, both isoforms expressed; *$PTC7_sHA$*, exclusively expresses the isoform from spliced mRNA; *$PTC7_{ns}HA$*, exclusively expresses the isoform from nonspliced pre-mRNA) and *ptc7Δ*. Shown is the mean of three biological replicates. *Error bars*, S.D. *F*, summary analysis of transcript levels of Q-biosynthetic factors from *E*. *G*, RT-qPCR measurement of *COQ1-COQ11* and *PTC7* transcript levels between WT and *snf2Δ* yeast. Shown is the mean of three biological replicates. *Error bars*, S.D. *H*, summary analysis of transcript levels of Q-biosynthetic factors from *G*.

taining a stop codon within its intron) and a second gene encoding a PP2C predicted to localize to the nuclear envelope ($Ptc7_a$, from an nonspliced transcript of *PTC7a* (32). This conservation further suggests that both protein isoforms derived from the *PTC7* transcript in *S. cerevisiae* are functional. Cells lacking $Ptc7_{ns}$ show increased sensitivity to latrunculin A treatment, compared with strains expressing both isoforms of Ptc7 or lacking $Ptc7_s$ (10). Such sensitivity might suggest a distinct role for $Ptc7_{ns}$ in actin filament formation.

It is noteworthy that nuclear roles for numerous metabolic enzymes have been described previously. The ability of metabolic enzymes to "moonlight" in the nucleus, affecting gene regulation at various steps, appears to be crucial for the ability of cells to sense and adapt to their potentially distinct nutrient environments (33). Numerous mitochondrial enzymes, such as succinate dehydrogenase, fumarase, aconitase, and malate dehydrogenase (all components of the Krebs cycle), have been shown to have significant nuclear roles in the regulation of gene expression (34–38). In some of these cases, enzymatic activity of these enzymes has been shown to be crucial to their nuclear roles (39). This precedence, combined with the evolutionarily conserved presence of an isoform of Ptc7 in the nuclear membrane, raises the possibility that a nucleus-localized phosphatase is crucial to regulation of components of the CoQ_6 biosyn-

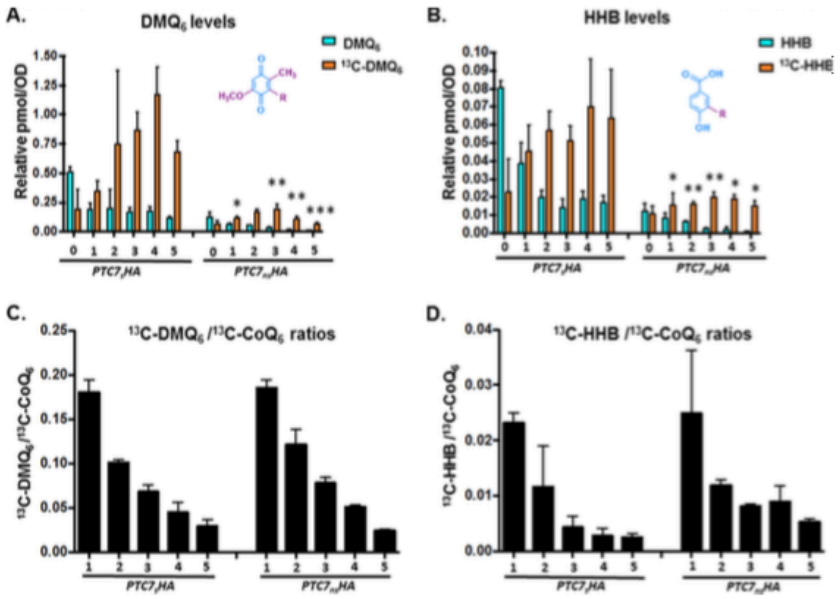

Figure 10. Exclusive expression of Ptc7 isoforms dramatically alters levels of CoQ_6 biosynthetic pathway intermediates DMQ_6 and HHB, yet overall conversion efficiency between both isoforms is comparable. *A*, levels of steady-state DMQ_6 (^{12}C-DMQ_6, *blue bars*) and *de novo* synthesized DMQ_6 ($^{13}C_6$-DMQ_6, *orange bars*) in *PTC7*$_s$*HA* and *PTC7*$_{ns}$*HA* yeast cells were determined at the designated hours after labeling with $^{13}C_6$-4HB. *Error bars*, S.D. of $n = 3$ biological replicates (unpaired Student's *t* test between *corresponding bars* for *PTC7*$_s$*HA* and *PTC7*$_{ns}$*HA*; *, $p < 0.05$; **, $p < 0.005$; ***, $p < 0.0005$). *B*, levels of steady-state HHB (^{12}C-HHB, *blue bars*) and *de novo* synthesized HHB ($^{13}C_6$-HHB, *orange bars*) in *PTC7*$_s$*HA* and *PTC7*$_{ns}$*HA* yeast cells were determined at the designated hours after labeling with $^{13}C_6$-4HB. *Error bars*, S.D. of $n = 3$ biological replicates (unpaired Student's *t* test between *corresponding bars* for *PTC7*$_s$*HA* and *PTC7*$_{ns}$*HA*; *, $p < 0.05$; **, $p < 0.005$). *C*, ratio of $^{13}C_6$-DMQ_6/$^{13}C_6$-CoQ_6 in *PTC7*$_s$*HA* and *PTC7*$_{ns}$*HA* yeast cells were determined at the designated hours after labeling with $^{13}C_6$-4HB. Ratios were derived from levels of $^{13}C_6$-CoQ_6, as shown in Fig. 7*D*. *Error bars*, S.D. of $n = 3$ biological replicates. The 0-h time point is excluded, because the ratio is not indicative of pathway conversion. *D*, ratio of $^{13}C_6$-HHB/$^{13}C_6$-CoQ_6 in *PTC7*$_s$*HA* and *PTC7*$_{ns}$*HA* yeast cells were determined at the designated hours after labeling with $^{13}C_6$-4HB. Ratios were derived from levels of $^{13}C_6$-CoQ_6, as shown in Fig. 7*D*. *Error bars*, S.D. of $n = 3$ biological replicates. The 0-h time point is excluded, because the ratio is not indicative of pathway conversion.

thetic pathway. Intriguingly, CLK-1 and COQ7, the *C. elegans* and human homologs of Coq7, which is a target for Ptc7 in *S. cerevisiae* (11), have been demonstrated to localize to the nucleus and are postulated to have roles independent of CoQ biosynthesis (40). COQ7 has also been shown to associate with chromatin in HeLa cells (40), although recently this has been attributed to a transformed cell phenomenon (41). Whereas nuclear localization of Coq7 in *S. cerevisiae* has not been demonstrated, we suggest a potential role in nuclear gene regulation for Ptc7 via phosphatase activity on Coq7 or other unidentified targets, including conventionally nuclear and other "moonlighting" mitochondrial enzymes.

It is also possible that Ptc7 has a substrate other than Coq7 that affects expression of the CoQ_6-synthome. In fact, a recent study identified with high confidence numerous differentially phosphorylated proteins in a *ptc7*Δ strain (12). Notably, this proteomic analysis does not distinguish between the potential effects of the two Ptc7 isoforms globally. In fact, rescue using plasmid-based expression of *PTC7* (full-length) does not restore dephosphorylation levels for a number of nuclear proteins, although the increased phosphorylation of mitochondrial proteins upon deletion of *PTC7* is almost completely reversed by exogenous expression of Ptc7 (12). Furthermore, it is possible that the mitochondrial role for $Ptc7_s$ is in fact covered by multiple redundancies. Ptc5 and Ptc6, two other PP2C protein phosphatases, also localize to the mitochondrial membrane, and *PTC5* demonstrates a negative genetic interaction with *PTC7*, indicating the possibility of overlapping functions (11, 31).

Interestingly, the effect of Snf2 deletion on CoQ_6 biosynthesis does not perfectly mirror the exclusive expression of $Ptc7_s$. We postulate that this is partially due to the Snf2 affecting the flux of the entire CoQ_6 biosynthetic pathway, as demonstrated by the increased conversion of early precursors. Whereas deletion of Snf2 does not, on average, change the expression of the components of the CoQ_6-synthome (Fig. 9, *G* and *H*), it is possible the Snf2 may have other effects of CoQ_6 flux. We are exploring these possibilities.

Intriguingly, although the absence of Snf2 enhances levels of CoQ_6, yeast strains lacking Snf2 have a severe growth defect on non-fermentable carbon sources, such as glycerol or acetate (26) (Fig. 1*E*). However, Snf2 protein is undetectable by immunoblotting during growth in medium containing glycerol or acetate as the only carbon source (data not shown). This leads us to hypothesize that before Snf2 protein is down-regulated in response to glucose depletion, it is required for the transition from a fermentative metabolic state to one that is predominantly respiratory in nature. The molecular details of the requirement for Snf2 in this transition are the subject of ongoing investigation. However, it is probably at least in part due to its reported role in the activation (de-repression) of genes whose transcription had previously been subject to glucose-mediated catabolite repression. This activation occurs once the glucose has been depleted or the yeast have been shifted to a

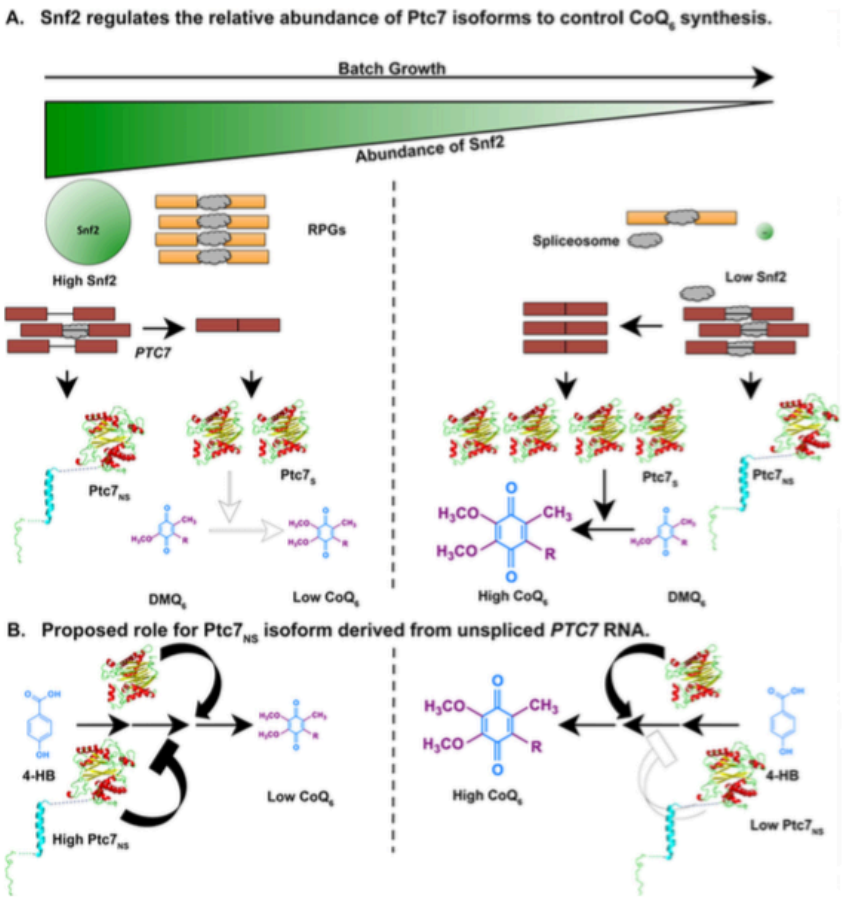

Figure 11. Model for a novel role for Snf2 in respiration, and in the transition from a primarily fermentative mode of metabolism to a primarily respiratory mode of metabolism. *A*, during *S. cerevisiae* batch growth, the abundance of Snf2 decreases in conjunction with depletion of nutrients in the medium. RPGs under the control of Snf2 are down-regulated, allowing redistribution of spliceosomes to other poorly spliced transcripts. Splicing of the *PTC7* transcript increases, enhancing the ratio of $Ptc7_s$/$Ptc7_{ns}$ and overall levels of $Ptc7_s$. These changes in Ptc7 isoform levels lead to increased conversion of DMQ_6 and increased synthesis of CoQ_6. The *darker arrow* represents a greater effect or reaction conversion, whereas a *lighter arrow* represents a smaller effect or reaction conversion. *B*, $Ptc7_{ns}$ has a repressive effect on CoQ_6 biosynthesis. CoQ_6 levels are low or high, depending on the levels of the $Ptc7_{ns}$ isoform relative to $Ptc7_s$. Similar to *A*, *darker arrows* and *bars* denote a larger effect, whereas *lighter arrows* and *bars* denote a smaller effect.

different, non-fermentable carbon source (26). We postulate that once the gene expression profile required for adaptation to the new nutrient environment has been initiated and/or established, the requirement for Snf2 is relieved, and in fact, the down-regulation of Snf2 enhances splicing of *PTC7*. This transient requirement for Snf2 bears striking similarities to a previous report detailing the role of Snf2 in reversing Ume6-mediated repression at certain meiotic genes early in meiosis, before it is itself down-regulated to enable splicing of meiotic transcripts (6).

This work reveals a mechanism by which SWI/SNF acts as a nexus point in the fermentation–respiratory transition in *S. cerevisiae*. We also demonstrate opposing effects of isoforms of a single gene, *PTC7*, on the process of CoQ_6 biosynthesis, via distinct mechanisms. Numerous aspects of these mechanisms remain to be studied, as well as their potential roles in the gene regulation response to other physiological conditions that yeast might experience.

Experimental procedures

Yeast strains and culture conditions

The yeast strains used in this study are listed in Table 1. All strains except W303Δcoq2 are derived from the BY background. Yeast strains were grown in YPD (1% yeast extract, 2% peptone, 2% dextrose) medium at 30 °C. Snf2 and Ptc7 null strains were maintained with a backup expression plasmid (pRS316 backbone harboring either *SNF2* or *PTC7*). The plasmid was shuffled out by growth on 5-fluoroorotic acid before using the strains in experiments. Strains with tagged isoforms of Ptc7 were a kind gift from Dr. Ron Davis (10). These strains were back-crossed against WT or *snf2*Δ strains, and daughter strains used for this study are listed in Table 1. The *snf2*Δ strain was observed to spontaneously mutate if grown on YPD for longer than 7–8 days, acquiring suppressor mutations that made it difficult to distinguish from WT. Hence, for all experiments with *snf2*Δ, the plasmid contain-

Table 1
Genotype and source of yeast strains

Strain number	Name	Genotype	Source/reference
TJY6724	WT	*MATa his3Δ leu2Δ LYS2 met15Δ ura3Δ*	Ref. 6
TJY6727	*snf2Δ*	*MATα his3Δ leu2Δ ura3Δ snf2Δ::NatMX*	Ref. 6
TJY7114	*PTC7-HA*	*MATa his3Δ leu2Δ ura3Δ PTC7-HA:KanMX*	This study
TJY7115	*snf2ΔPTC7-HA*	*MATa his3Δ leu2Δ ura3Δ snf2Δ::NatMX PTC7-HA:KanMX*	This study
W303Δ*coq2*	*coq2Δ*	*MATa ade2-1 his3-1,15 leu2-3,112 trp1-1 ura3-1 coq2::HIS3*	Ref. 47
TJY7116	*PTC7-HA*	*MATa his3Δ leu2Δ ura3Δ PTC7-HA:KanMX*	This study
TJY7118	*PTC7$_m$-HA*	*MATa his3Δ leu2Δ ura3Δ PTC7$_m$-HA:KanMX*	This study
TJY7142	*ptc7Δ*	*MATa his3Δ leu2Δ ura3Δ ptc7Δ:KanMX*	This study
BY4741Δ*coq9*	*coq9Δ*	*MATα his3Δ0 leu2Δ0 met15Δ0 ura3Δ0 coq9::KANMX4*	Ref. 48

ing *SNF2* was shuffled out prior to each experiment, allowing a fresh *snf2Δ* strain with each experiment, to avoid these suppressor mutants. We found that this was absolutely instrumental to observe the proper phenotype and behavior of the *snf2Δ* strain.

RNA-sequencing analyses

The RNA-sequencing data reported in this study were generated previously (6). Briefly, RNA sequencing libraries were prepared using the Illumina Truseq® V3 kit and ribosomal RNA depletion (Ribo-Zero, Illumina). Single-end, 50-nucleotide sequence reads (HiSeq 2000) were aligned to SacCer3 and spliced transcripts from the Ares Lab Yeast Intron Database version 3 (42) in a single step using STAR (43). Only the highest scoring alignments for each read were kept, allowing for at most a single tie. Reads/kb/million were computed for each gene by dividing the total number of reads that aligned entirely within the gene's exon boundaries by the gene's total exon length in kilobase pairs per million mapped reads. Reads within ICGs were categorized as exonic, spliced, or unspliced. Exonic reads map entirely within an exon, as defined by the Ares Lab Yeast Intron Database. Introns with annotated small nucleolar RNAs within the defined intron boundaries were disregarded in this analysis. Spliced reads are those that align with a gap that corresponds to an annotated intron, and unspliced reads map partially within an exon and partially within an intron with no gap. Spliced and unspliced read counts were normalized by dividing total spliced counts by the number of potential unique alignment positions that contribute to the total. For spliced reads, this is read length minus one for every intron. For unspliced read counts, this is the length of the intron plus the read length minus one. Splicing efficiency for each intron was calculated as normalized spliced counts divided by the sum of the normalized spliced and normalized unspliced counts. Changes in splicing efficiency were calculated as percentage difference over WT efficiency and plotted against expression levels (reads/kb/million) in WT. Data are available under GEO accession number GSE94404, and detailed methods were described previously (6).

RT-PCR and real-time PCR analysis

RNA was isolated from a 5-ml aliquot of cell culture corresponding to time points described in each experiment. After DNase treatment (Roche Applied Science), equal quantities of total RNA from each sample were used to make cDNA using a cDNA synthesis kit (Fermentas). To detect *PTC7* splicing isoforms, primers flanking the intronic sequences were used for PCR using 1 μl of cDNA diluted 1:20. PCR products were then separated on a 2% agarose gel and imaged. RT-qPCR was done in a 10-μl reaction volume with gene-specific primers using 1 μl of cDNA diluted 1:20 using Perfecta SYBR Green Fastmix (Quanta Biosciences) and a CFX96 Touch System (Bio-Rad). All samples were analyzed in triplicate for each independent experiment. RT-qPCR was also performed for the *scR1* (cytoplasmic signal recognition particle RNA subunit) RNA from each cDNA sample. Gene expression analysis was done by $2^{-\Delta Ct}$ methods using *scR1* as a reference. -Fold expression of mRNA was measured compared with WT by $2^{-\Delta\Delta Ct}$ methods (44).

Immunoblots

Protein was isolated from cell pellets with FA-1 lysis buffer (50 mM HEPES, pH 7.5, 150 mM NaCl, 1 mM EDTA, 1% Triton X-100, 0.1% sodium deoxycholate, 1 mM PMSF, and protease inhibitors) with bead beating. The buffer was supplemented with protease inhibitor mixture tablet (Roche Applied Science). Total protein was resolved by SDS-PAGE. The gel was transferred to PVDF membrane, and proteins were detected with the following antibodies at the stated dilutions: anti-SNF2 antibody (yN-20, Santa Cruz Biotechnology) at a 1:200 dilution in 2% milk, anti-HA antibody (901514, BioLegend) at a 1:2000 dilution in 5% milk, anti-Pgk1 antibody (459250, Invitrogen) at a 1:3000 dilution in 5% milk, or anti-Coq7 antibody (described previously (16) at a 1:2000 dilution in 3% milk. Signal was detected with enhanced chemiluminescence (Thermo Scientific) as described by the manufacturer.

Metabolic labeling of CoQ_6 with $^{13}C_6$-labeled precursors

Yeast strains were grown overnight in 25 ml of YPD in a shaking incubator (30 °C, 250 rpm) and diluted to an A_{600} of 0.1 in 60 ml of fresh YPD the next morning. The cultures were incubated as before to an A_{600} of 0.5 (midlog phase) and subsequently treated with $^{13}C_6$-4HB at 10 μg/ml (600 μg total) or ethanol vehicle control (0.015%, v/v). At designated time periods, cells were harvested by centrifugation at 3000 × *g* for 5 min, from 50-ml aliquots (used for lipid extraction) or 10-ml aliquots (used for RNA and protein analysis). Cell pellets were stored at −20 °C.

Analysis of CoQ_6 and CoQ_6 intermediates

Lipid extraction of cell pellets was conducted as described (18) with methanol and petroleum ether and CoQ_4 as the internal standard. Lipid measurements were performed by HPLC-

MS/MS and normalized to total OD. Prior to mass spectrometry analysis, all samples were treated with 1.0 mg/ml benzoquinone to oxidize hydroquinones to quinones. Mass spectrometry analyses utilized a 4000 QTRAP linear MS/MS spectrometer (Applied Biosystems), and data were acquired and analyzed using Analyst version 1.4.2 and 1.5.2 software (Applied Biosystems). Separation of lipid quinones was performed with a binary HPLC delivery system and a Luna 5μ phenyl-hexyl column (100 × 4.6 mm, 5 μm; Phenomenex). The mobile phase consisted of a 95:5 methanol/isopropyl alcohol solution with 2.5 mM ammonium formate as solution A and a 100% isopropyl alcohol solution with 2.5 mM ammonium formate as solution B. The percentage of solution B was increased linearly from 0 to 5% over 6 min, whereby the flow rate was increased from 600 to 800 μl. Initial flow rate and mobile phase conditions were changed back to initial phase conditions linearly over 3.5 min. Each sample was analyzed using multiple-reaction monitoring mode. The following precursor-to-product ion transitions were detected as well as the +17 *m/z* ammoniated adducts for each of the metabolic products: $^{13}C_6$-HHB *m/z* 553.4/157.0 (ammoniated: 570.4/157.0), ^{12}C-HHB *m/z* 547.4/151.0 (ammoniated: 564.4/151.0), $^{13}C_6$-DMQ_6 *m/z* 567.6/173.0 (ammoniated: 584.6/173.0), ^{12}C-DMQ_6 *m/z* 561.6/167.0 (ammoniated: 578.6/167.0), $^{13}C_6$-CoQ_6 *m/z* 597.4/203.1 (ammoniated: 614.4/203.1), ^{12}C-CoQ_6 *m/z* 591.4/197.1 (ammoniated: 608.4/197.1), and ^{12}C-CoQ_4 *m/z* 455.4/197.0 (ammoniated: 472.4/197.0).

Plate dilution assays

Strains were grown overnight in 5 ml of YPD and diluted to an A_{600} of 0.2 in sterile PBS. A 5-fold serial dilution in PBS was performed, after which 2 μl of each dilution (1×, 5×, 25×, 125×, and 625×) were spotted onto the designated carbon sources. The final A_{600} of the aforementioned dilution series are 0.2, 0.04, 0.008, 0.0016, and 0.00032, respectively.

PHYRE homology modeling

Phyre2 is a modeling program designed to analyze protein structure, function, and mutations (45). It is used to analyze the primary sequence of a protein and, with homology detection methods, constructs a structure that compares the protein of interest with other proteins (or motifs of proteins) with known structure. In regard to Ptc7, the full nonspliced version of the protein ($Ptc7_{ns}$), which is composed of 374 amino acids and retains its 31-amino acid intron (amino acids 19–50), was analyzed. The resulting structure and alignment coverage contained 86% of residues modeled at >90% confidence, with 14% of residues modeled *ab initio*. Additionally, the spliced isoform of Ptc7 ($Ptc7_s$), which is localized and processed in the mitochondria, comprised of 305 amino acids, resulting from the removal of the 31-amino acid intron and the excision of the predicted mitochondrial targeting sequence (the 38 N-terminal amino acids of $Ptc7_s$) (46), was also modeled using the PHYRE2 intensive modeling mode. The resulting structure and alignment coverage contains 85% of residues modeled at >90% confidence, with 15% of residues modeled *ab initio*.

Author contributions—A. M. A. and S. V. contributed equally to this work (both conducted the majority of the experiments, analyzed the results, and wrote the paper together). A. N. and M. C. B. assisted A. M. A. in conducting experiments; A. N. assisted A. M. A. in analyzing mass spectrometry results. A. R. G. and L. N. assisted S. V. in experiments, with A. R. G. also having assisted in the background research relating to PTC7 differential splicing in the snf2Δ strain shown in Fig. 1*A*. S. D. aligned the RNA-sequencing data and calculated splicing efficiencies. M. C. B. and L. N. thoroughly read and edited the working draft of the paper. C. F. C. and T. L. J. oversaw all details related to the project and provided guidance on experiments, data analysis, and the writing of this paper.

Acknowledgments—We thank Dr. James Bowie (UCLA) for advice and guidance in generating the PHYRE models and in the depiction of the spliced and nonspliced versions of Ptc7. We acknowledge the UCLA Molecular Instrumentation Core proteomics facility for the use of the QTRAP4000. We thank the laboratory of Dr. Ronald W. Davis (Stanford) for generously providing the Ptc7 spliced and nonspliced isoforms.

References

1. Naftelberg, S., Schor, I. E., Ast, G., and Kornblihtt, A. R. (2015) Regulation of alternative splicing through coupling with transcription and chromatin structure. *Annu. Rev. Biochem.* **84,** 165–198
2. Johnson, T. L., and Vilardell, J. (2012) Regulated pre-mRNA splicing: the ghostwriter of the eukaryotic genome. *Biochim. Biophys. Acta* **1819,** 538–545
3. Pleiss, J. A., Whitworth, G. B., Bergkessel, M., and Guthrie, C. (2007) Rapid, transcript-specific changes in splicing in response to environmental stress. *Mol. Cell* **27,** 928–937
4. Ares, M., Jr., Grate, L., and Pauling, M. H. (1999) An handful of intron-containing genes produces the lion's share of yeast mRNA. *RNA* **5,** 1138–1139
5. Munding, E. M., Shiue, L., Katzman, S., Donohue, J. P., and Ares, M., Jr. (2013) Competition between pre-mRNAs for the splicing machinery drives global regulation of splicing. *Mol. Cell* **51,** 338–348
6. Venkataramanan, S., Douglass, S., Galivanche, A. R., and Johnson, T. L. (2017) The chromatin remodeling complex Swi/Snf regulates splicing of meiotic transcripts in *Saccharomyces cerevisiae*. *Nucleic Acids Res.* 10.1093/nar/gkx373
7. Hossain, M. A., Claggett, J. M., Edwards, S. R., Shi, A., Pennebaker, S. L., Cheng, M. Y., Hasty, J., and Johnson, T. L. (2016) Posttranscriptional regulation of Gcr1 expression and activity is crucial for metabolic adjustment in response to glucose availability. *Mol. Cell* **62,** 346–358
8. Hossain, M. A., Rodriguez, C. M., and Johnson, T. L. (2011) Key features of the two-intron *Saccharomyces cerevisiae* gene *SUS1* contribute to its alternative splicing. *Nucleic Acids Res.* **39,** 8612–8627
9. Jiang, L., Whiteway, M., Ramos, C. W., Rodriguez-Medina, J. R., and Shen, S.-H. (2002) The YHR076W gene encodes a type 2C protein phosphatase and represents the seventh PP2C gene in budding yeast. *FEBS Lett.* **527,** 323–325
10. Juneau, K., Nislow, C., and Davis, R. W. (2009) Alternative splicing of *PTC7* in *Saccharomyces cerevisiae* determines protein localization. *Genetics* **183,** 185–194
11. Martín-Montalvo, A., González-Mariscal, I., Pomares-Viciana, T., Padilla-López, S., Ballesteros, M., Vazquez-Fonseca, L., Gandolfo, P., Brautigan, D. L., Navas, P., and Santos-Ocaña, C. (2013) The phosphatase Ptc7 induces coenzyme Q biosynthesis by activating the hydroxylase Coq7 in yeast. *J. Biol. Chem.* **288,** 28126–28137
12. Guo, X., Niemi, N. M., Hutchins, P. D., Condon, S. G., Jochem, A., Ulbrich, A., Higbee, A. J., Russell, J. D., Senes, A., Coon, J. J., and Pagliarini, D. J. (2017) Ptc7p dephosphorylates select mitochondrial proteins to enhance metabolic function. *Cell Rep.* **18,** 307–313

13. Turunen, M., Olsson, J., and Dallner, G. (2004) Metabolism and function of coenzyme Q. *Biochim. Biophys. Acta* **1660,** 171–199
14. Doimo, M., Desbats, M. A., Cerqua, C., Cassina, M., Trevisson, E., and Salviati, L. (2014) Genetics of coenzyme Q10 deficiency. *Mol. Syndromol.* **5,** 156–162
15. Quinzii, C. M., Emmanuele, V., and Hirano, M. (2014) Clinical presentations of coenzyme Q10 deficiency syndrome. *Mol. Syndromol.* **5,** 141–146
16. Tran, U. C., and Clarke, C. F. (2007) Endogenous synthesis of coenzyme Q in eukaryotes. *Mitochondrion* **7,** S62–S71
17. González-Mariscal, I., García-Testón, E., Padilla, S., Martín-Montalvo, A., Pomares Viciana, T., Vazquez-Fonseca, L., Gandolfo Domínguez, P., and Santos-Ocaña, C. (2014) The regulation of coenzyme Q biosynthesis in eukaryotic cells: all that yeast can tell us. *Mol. Syndromol.* **5,** 107–118
18. Allan, C. M., Awad, A. M., Johnson, J. S., Shirasaki, D. I., Wang, C., Blaby-Haas, C. E., Merchant, S. S., Loo, J. A., and Clarke, C. F. (2015) Identification of Coq11, a new coenzyme Q biosynthetic protein in the CoQ-synthome in *Saccharomyces cerevisiae*. *J. Biol. Chem.* **290,** 7517–7534
19. Padilla, S., Jonassen, T., Jiménez-Hidalgo, M. A., Fernández-Ayala, D. J., López-Lluch, G., Marbois, B., Navas, P., Clarke, C. F., and Santos-Ocaña, C. (2004) Demethoxy-Q, an intermediate of coenzyme Q biosynthesis, fails to support respiration in Saccharomyces cerevisiae and lacks antioxidant activity. *J. Biol. Chem.* **279,** 25995–26004
20. Padilla, S., Tran, U. C., Jiménez-Hidalgo, M., López-Martín, J. M., Martín-Montalvo, A., Clarke, C. F., Navas, P., and Santos-Ocaña, C. (2009) Hydroxylation of demethoxy-Q6 constitutes a control point in yeast coenzyme Q6 biosynthesis. *Cell Mol. Life Sci.* **66,** 173–186
21. Whitehouse, I., Flaus, A., Cairns, B. R., White, M. F., Workman, J. L., and Owen-Hughes, T. (1999) Nucleosome mobilization catalysed by the yeast SWI/SNF complex. *Nature* **400,** 784–787
22. Liu, X., Li, M., Xia, X., Li, X., and Chen, Z. (2017) Mechanism of chromatin remodelling revealed by the Snf2-nucleosome structure. *Nature* **544,** 440–445
23. Dutta, A., Gogol, M., Kim, J. H., Smolle, M., Venkatesh, S., Gilmore, J., Florens, L., Washburn, M. P., and Workman, J. L. (2014) Swi/Snf dynamics on stress-responsive genes is governed by competitive bromodomain interactions. *Genes Dev.* **28,** 2314–2330
24. Dutta, A., Sardiu, M., Gogol, M., Gilmore, J., Zhang, D., Florens, L., Abmayr, S. M., Washburn, M. P., and Workman, J. L. (2017) Composition and function of mutant Swi/Snf complexes. *Cell Rep.* **18,** 2124–2134
25. Gabunilas, J., and Chanfreau, G. (2016) Splicing-mediated autoregulation modulates Rpl22p expression in *Saccharomyces cerevisiae*. *PLoS Genet.* **12,** e1005999
26. Neigeborn, L., and Carlson, M. (1984) Genes affecting the regulation of SUC2 gene expression by glucose repression in *Saccharomyces cerevisiae*. *Genetics* **108,** 845–858
27. Martín-Montalvo, A., González-Mariscal, I., Padilla, S., Ballesteros, M., Brautigan, D. L., Navas, P., and Santos-Ocaña, C. (2011) Respiratory-induced coenzyme Q biosynthesis is regulated by a phosphorylation cycle of Cat5p/Coq7p. *Biochem. J.* **440,** 107–114
28. Martin, D. E., Soulard, A., and Hall, M. N. (2004) TOR regulates ribosomal protein gene expression via PKA and the Forkhead transcription factor FHL1. *Cell* **119,** 969–979
29. Wang, A., Mouser, J., Pitt, J., Promislow, D., and Kaeberlein, M. (2016) Rapamycin enhances survival in a *Drosophila* model of mitochondrial disease. *Oncotarget* **7,** 80131–80139
30. González-Mariscal, I., Martín-Montalvo, A., Ojeda-González, C., Rodríguez-Eguren, A., Gutiérrez-Rios, P., Navas, P., and Santos-Ocaña, C. (2017) Balanced CoQ6 biosynthesis is required for lifespan and mitophagy in yeast. *Microb. Cell* **4,** 38–51
31. Sharmin, D., Sasano, Y., Sugiyama, M., and Harashima, S. (2014) Effects of deletion of different PP2C protein phosphatase genes on stress responses in *Saccharomyces cerevisiae*. *Yeast* **31,** 393–409
32. Marshall, A. N., Montealegre, M. C., Jiménez-Lopez, C., Lorenz, M. C., and van Hoof, A. (2013) Alternative splicing and subfunctionalization generates functional diversity in fungal proteomes. *PLoS Genet.* **9,** e1003376
33. Boukouris, A. E., Zervopoulos, S. D., and Michelakis, E. D. (2016) Metabolic enzymes moonlighting in the nucleus: metabolic regulation of gene transcription. *Trends Biochem. Sci.* **41,** 712–730
34. De, P., and Chatterjee, R. (1962) Evidence of nucleolar succinic dehydrogenase activity. *Exp. Cell Res.* **27,** 172–173
35. De, P., and Chatterjee, R. (1962) Nucleolar localization of succinic dehydrogenase in human malignant cells with MTT. *Experientia* **18,** 562
36. Yogev, O., Yogev, O., Singer, E., Shaulian, E., Goldberg, M., Fox, T. D., and Pines, O. (2010) Fumarase: a mitochondrial metabolic enzyme and a cytosolic/nuclear component of the DNA damage response. *PLoS Biol.* **8,** e1000328
37. Jung, S. J., Seo, Y., Lee, K. C., Lee, D., and Roe, J. H. (2015) Essential function of Aco2, a fusion protein of aconitase and mitochondrial ribosomal protein bL21, in mitochondrial translation in fission yeast. *FEBS Lett.* **589,** 822–828
38. Lee, S. M., Kim, J. H., Cho, E. J., and Youn, H. D. (2009) A nucleocytoplasmic malate dehydrogenase regulates p53 transcriptional activity in response to metabolic stress. *Cell Death Differ.* **16,** 738–748
39. McEwen, B. S., Allfrey, V. G., and Mirsky, A. E. (1963) Studies on energy-yielding reactions in thymus nuclei. *J. Biol. Chem.* **238,** 2571–2578
40. Monaghan, R. M., Barnes, R. G., Fisher, K., Andreou, T., Rooney, N., Poulin, G. B., and Whitmarsh, A. J. (2015) A nuclear role for the respiratory enzyme CLK-1 in regulating mitochondrial stress responses and longevity. *Nat Cell Biol.* **17,** 782–792
41. Liu, J. L., Yee, C., Wang, Y., and Hekimi, S. (2017) A single biochemical activity underlies the pleiotropy of the aging-related protein CLK-1. *Sci. Rep.* **7,** 859
42. Grate, L., and Ares, M., Jr. (2002) Searching yeast intron data at Ares lab Web site. *Methods Enzymol.* **350,** 380–392
43. Dobin, A., Davis, C. A., Schlesinger, F., Drenkow, J., Zaleski, C., Jha, S., Batut, P., Chaisson, M., and Gingeras, T. R. (2013) STAR: ultrafast universal RNA-seq aligner. *Bioinformatics* **29,** 15–21
44. Livak, K. J., and Schmittgen, T. D. (2001) Analysis of relative gene expression data using real-time quantitative PCR and the $2(-\Delta\Delta C(T))$ method. *Methods* **25,** 402–408
45. Kelley, L. A., Mezulis, S., Yates, C. M., Wass, M. N., and Sternberg, M. J. (2015) The Phyre2 web portal for protein modeling, prediction and analysis. *Nat. Protoc.* **10,** 845–858
46. Vögtle, F. N., Wortelkamp, S., Zahedi, R. P., Becker, D., Leidhold, C., Gevaert, K., Kellermann, J., Voos, W., Sickmann, A., Pfanner, N., and Meisinger, C. (2009) Global analysis of the mitochondrial N-proteome identifies a processing peptidase critical for protein stability. *Cell* **139,** 428–439
47. Ashby, M. N., Kutsunai, S. Y., Ackerman, S., Tzagoloff, A., and Edwards, P. A. (1992) COQ2 is a candidate for the structural gene encoding para-hydroxybenzoate:polyprenyltransferase. *J. Biol. Chem.* **267,** 4128–4136
48. Winzeler, E. A., Shoemaker, D. D., Astromoff, A., Liang, H., Anderson, K., Andre, B., Bangham, R., Benito, R., Boeke, J. D., Bussey, H., Chu, A. M., Connelly, C., Davis, K., Dietrich, F., Dow, S. W., *et al.* (1999) Functional characterization of the *S. cerevisiae* genome by gene deletion and parallel analysis. *Science* **285,** 901–906

APPENDIX VIII

Inducible LAP-tagged Stable Cell Lines for Investigating Protein Function, Spatiotemporal Localization and Protein Interaction Networks

Video Article

Inducible LAP-tagged Stable Cell Lines for Investigating Protein Function, Spatiotemporal Localization and Protein Interaction Networks

Michelle Bradley[1], Ivan Ramirez[1], Keith Cheung[1], Ankur A. Gholkar[1], Jorge Z. Torres[1,2,3]

[1]Department of Chemistry and Biochemistry, University of California, Los Angeles

[2]Molecular Biology Institute, University of California, Los Angeles

[3]Jonsson Comprehensive Cancer Center, University of California, Los Angeles

Correspondence to: Jorge Z. Torres at torres@chem.ucla.edu

URL: http://www.jove.com/video/54870
DOI: doi:10.3791/54870

Keywords: Molecular Biology, Issue 118, TAP-tag, LAP-tag, Epitope-tag, Biochemical purifications, Affinity proteomics, Protein-protein interactions, Interactome, Protein interaction network, Protein localization

Date Published: 12/24/2016

Citation: Bradley, M., Ramirez, I., Cheung, K., Gholkar, A.A., Torres, J.Z. Inducible LAP-tagged Stable Cell Lines for Investigating Protein Function, Spatiotemporal Localization and Protein Interaction Networks. *J. Vis. Exp.* (118), e54870, doi:10.3791/54870 (2016).

Abstract

Multi-protein complexes, rather than single proteins acting in isolation, often govern molecular pathways regulating cellular homeostasis. Based on this principle, the purification of critical proteins required for the functioning of these pathways along with their native interacting partners has not only allowed the mapping of the protein constituents of these pathways, but has also provided a deeper understanding of how these proteins coordinate to regulate these pathways. Within this context, understanding a protein's spatiotemporal localization and its protein-protein interaction network can aid in defining its role within a pathway, as well as how its misregulation may lead to disease pathogenesis. To address this need, several approaches for protein purification such as tandem affinity purification (TAP) and localization and affinity purification (LAP) have been designed and used successfully. Nevertheless, in order to apply these approaches to pathway-scale proteomic analyses, these strategies must be supplemented with modern technological developments in cloning and mammalian stable cell line generation. Here, we describe a method for generating LAP-tagged human inducible stable cell lines for investigating protein subcellular localization and protein-protein interaction networks. This approach has been successfully applied to the dissection of multiple cellular pathways including cell division and is compatible with high-throughput proteomic analyses.

Video Link

The video component of this article can be found at http://www.jove.com/video/54870/

Introduction

To investigate the cellular function of an uncharacterized protein it is important to determine its *in vivo* spatiotemporal subcellular localization and its interacting protein partners. Traditionally, single and tandem epitope tags fused to the N or C-terminus of a protein of interest have been used to facilitate protein localization and protein interaction studies. For example, the tandem affinity purification (TAP) technology has enabled the isolation of native protein complexes, even those that are in low abundance, in both yeast and mammalian cell lines[1,2]. The localization and affinity purification (LAP) technology, is a more recent development that modifies the TAP procedure to include a localization component through the introduction of the green fluorescent protein (GFP) as one of the epitope tags[3]. This approach has given researchers a deeper understanding of a protein's subcellular localization in living cells while also retaining the ability to perform TAP complex purifications to map protein-protein interaction networks.

However, there are many issues associated with the use of TAP/LAP technologies that has hampered their widespread use in mammalian cells. For example, the length of time that is necessary to generate a stable cell line expressing a TAP/LAP tagged protein of interest; which typically relies on cloning the gene of interest into a viral vector and selecting single cell stable integrants with the desired expression level. Additionally, many cellular pathways are sensitive to constitutive protein overexpression (even at low levels) and can arrest cells or trigger cell death over time making the generation of a TAP/LAP stable cell line impossible. These and other constraints have impeded LAP/TAP methodologies from becoming high-throughput systems for protein localization and protein complex elucidation. Therefore, there has been considerable interest in the development of an inducible high-throughput LAP-tagging system for mammalian cells that takes advantage of current innovations in cloning and cell line technologies.

Here we present a protocol for generating stable cell lines with Doxycycline/Tetracycline (Dox/Tet) inducible LAP-tagged proteins of interest that applies advances in both cloning and mammalian cell line technologies. This approach streamlines the acquisition of data with regards to LAP-tagged protein subcellular localization, protein complex purification and identification of interacting proteins[4]. Although affinity proteomics utilizes a wide range of techniques for protein complex elucidation[5], our approach is beneficial for expediting the identification of these complexes and their native interaction networks and is amenable to high-throughput protein tagging that is necessary to investigate complex biological pathways that contain a multitude of protein constituents. Key to this approach are advancements in cloning strategies that enable high fidelity and expedited cloning of target genes into an array of vectors for gene expression *in vitro*, in various organisms like bacteria and baculovirus,

and in mammalian cells[6,7]. Additionally, the ORFeome collaboration has cloned thousands of sequence validated open reading frames in vectors that incorporate these advances in cloning, which are available to the scientific community[8-11]. In our system, the pGLAP1 LAP-tagging vector enables the simultaneous cloning of a large number of clones, which facilitates high-throughput LAP-tagging. This expedited cloning procedure is coupled to a streamlined approach for generating cell lines with LAP-tagged genes of interest inserted at a single pre-determined genomic locus. This makes use of cell lines that contain a single flippase recognition target (FRT) site within their genome, which is the site of integration for LAP-tagged genes. These cell lines also express the tetracycline repressor (TetR) that binds to Tet operators ($TetO_2$) upstream of the LAP-tagged genes and silences their expression in the absence of Dox/Tet. This allows for Dox/Tet inducible expression of the LAP-tagged protein at any given time. Having the capability of inducible LAP-tagged protein expression is critical, since many cellular pathways are sensitive to the levels of critical proteins governing the pathway and can arrest cell growth or trigger cell death when these proteins are constitutively overexpressed, even at low levels, making the generation of non-inducible LAP-tagged stable cell lines impossible[12].

Protocol

NOTE: An overview of the generation of inducible LAP-tagged stable cell lines for any protein of interest is illustrated in **Figure 1** and the overview of LAP-tagged protein expression, purification and preparation for mass proteomic analyses is illustrated in **Figure 3**.

1. Cloning the Open Reading Frame (ORF) of the Gene of Interest into the LAP-tag Vector

1. Cloning the ORF of the Gene of Interest into the Shuttle Vector.
    1. Use polymerase chain reaction (PCR) to amplify the ORF of interest with the appropriate attB1 and attB2 sites within the primers for either N-terminal fusion or C-terminal fusion. See **Table 1** for primer sequences and **Table 2** for PCR conditions.
    2. Gel purify the PCR products by resolving them on a 1% agarose gel. Excise the amplified band that is the correct size from the gel and extract it from the gel slice using a DNA gel extraction kit as per manufacturer's instructions.
    3. Incubate the purified attB containing PCR products with an attP containing shuttle vector and the recombinase that allows the PCR products to recombine into the vector as per manufacturer's instructions (see **Materials Table**).
    NOTE: Empty shuttle vectors and LAP-tagging vectors contain the *ccd*B gene and have to be propagated in *ccd*B resistant bacterial cells (see **Materials Table**). However the *ccdB* gene is recombined out when an ORF is inserted into these vectors, hence use standard DH5α *E. coli* cells when propagating vectors with cloned ORFs.
    4. Transform DH5α *E. coli* cells with 1 µl of the reaction product and plate the transformed cells onto a Luria broth (LB) agar plate with 50 mg/ml Kanamycin[13].
    5. Select the Kanamycin resistant colonies.
    6. Grow the selected colonies in LB media with 50 mg/ml Kanamycin, make a DNA mini-prep and confirm gene integration by DNA sequencing using the sequencing primers listed in **Table 3**.

2. Transferring the Gene of Interest from the Shuttle Vector into the LAP-tag Vector.
    1. Incubate the shuttle vector containing the sequence verified gene of interest ORF with the LAP-tag vector (pGLAP1 for N-terminal fusion) and the recombinase that mediates the transfer of the gene of interest from the shuttle vector into the LAP-tag vector as per manufacturer's instructions (see Materials).
    NOTE: A series of LAP/TAP vectors that can be used based on the desired promoter, epitope-tag, and N or C-terminal tagging can be found in **Table 4**.
    2. Transform DH5α *E. coli* cells with 1 µl of the reaction product and plate the transformed cells onto an LB agar plate with 100 mg/ml Ampicillin[13].
    3. Select the Ampicillin resistant colonies.
    4. Grow the selected colonies in LB media with 100 mg/ml Ampicillin, make a DNA mini-prep, and confirm gene integration by DNA sequencing using the sequencing primers listed in **Table 5**.

2. Generation of an Inducible Stable Cell Line that Expresses the LAP-tagged Gene of Interest

1. Select the cell line best suited for the project of interest. Alternatively, create a host cell line from any existing cell line that constitutively expresses the TetR and contains a FRT site that allows the LAP-tagged gene of interest to be stably integrated into the genome (see Materials).
NOTE: This protocol uses a HEK293 cell line that contains the TetR and an FRT site, which is grown in -Tet DMEM/F12 media [made with 10% fetal bovine serum (FBS) that is devoid of Tetracycline (-Tet)][4].
2. Determine the minimum concentration of Hygromycin required to kill the host cell line within 1 to 2 weeks after drug addition. The concentration can vary between host cell lines, with most ranging between 100 µg/ml and 800 µg/ml.
NOTE: HEK293 cells grown in -Tet DMEM/F12 media with 100 µg/ml Hygromycin at 37 °C and 5% CO_2 will die within 1-2 weeks.
3. Co-transfect the vector that expresses the flippase recombinase (mediates the integration of the LAP-tagged gene of interest into the FRT site within the genome of the cell) with the LAP-tagged vector into HEK293 cells using a transfection reagent as per manufacturer's instructions. Use a ratio of 4:1 of recombinase vector to LAP vector[14].
NOTE: The optimal ratio is dependent on the host cell line and method of transfection, and may require a titration. A ratio of 4:1 works well for most cell lines. Include a mock-transfected plate as a negative control.
4. One day post-transfection, replace the -Tet DMEM/F12 media with fresh media.
5. Two days post-transfection, split cells to 25% confluence. Allow cells ~5 hr to attach, then add Hygromycin-containing -Tet DMEM/F12 media at the concentration predetermined in step 2.2. For HEK293 cells use 100 µg/ml Hygromycin.

NOTE: The FRT containing HEK293 cell line also contains the TetR that is associated with Blasticidin resistance, therefore 5 µg/ml Blasticidin is used during the stable cell line selection process to select for the TetR and to minimize leaky expression.

6. Replace Hygromycin-containing -Tet DMEM/F12 media as needed until distinct cell foci appear that resemble opaque spots against the transparent plate.
7. Add 20 µl of trypsin on top of each cell foci and pipet up and down 2 times with a 200 µl pipet tip. Place cells in a 24 well plate and expand the cells by continual growth in Hygromycin-containing -Tet DMEM/F12 media.
8. Screen cells for inducible LAP-tagged protein expression by fixed-cell or live-cell fluorescence microscopy and/or Western blotting for the GFP tag within the LAP-tag[15].

3. Purification of LAP-tagged Protein Complexes

NOTE: The following LAP-tagged protein purification protocol details recommendations on conditions and volumes used for a typical LAP-tagged protein purification based on previous experience. However, caution should be exercised to ensure that empirical optimization is carried out for any protein complex and protein expression level of interest to provide the best results.

1. Cell Growth and Cell Harvesting.
    1. Expand the validated LAP-tagged cell line for TAP isolation of protein complexes, by continually passaging all HEK293 cells into larger plates and/or roller bottles in -Tet DMEM/F12 media at 37 °C and 5% CO_2.
    2. For Tet/Dox inducible cell lines, induce for 10-15 hr at a concentration of 0.2 µg/ml Tet/Dox when the cells reach ~70% confluency, before harvesting cells.
    NOTE: The concentration and induction time should be determined for each protein, a titration of 0.1-1 µg/ml Tet/Dox for 10-15 hr is recommended.
    3. Harvest cells by agitation or trypsinization and pellet cells at 875 x g for 5-10 min.

2. Coupling Anti-GFP Antibody to Protein A Beads
    1. Use 40 µg of antibody for immunoprecipitation from a lysate prepared from a 0.5 ml cell pellet, packed cell volume (PCV).
    NOTE: The amount of antibody needed will depend on the abundance of the LAP-tagged protein, among other factors, and will require optimization. A titration of 10-40 µg is recommended.
    2. Equilibrate 160 µl packed volume (PV) Protein A beads into PBST (PBS + 0.1% Tween-20) in a 1.5 ml tube. Wash 3 times with 1 ml of PBST.
    NOTE: All washes herein are carried out by centrifuging the beads at 5,000 x g for 10 sec.
    3. Resuspend beads in 500 µl PBST and add 80 µg of affinity-purified rabbit anti-GFP antibody to each tube of 160 µl beads. Mix for 1 hr at room temperature (RT).
    4. Wash beads 2 times with 1 ml of PBST. Then, wash beads 2 times with 1 ml of 0.2 M sodium borate, pH 9 (20 ml 0.2 M sodium borate + 15 ml 0.2 M boric acid). After the final wash, add 900 µl of the 0.2 M sodium borate, pH 9 to bring the final volume to 1 ml.
    5. Add 100 µl of 220 mM dimethylpimelimidate (DMP) to a final concentration of 20 mM. Rotate the tubes gently at RT for 30 min. For 220 mM DMP, resuspend contents of one 50 mg bottle in 877 µl of 0.2 M sodium borate, pH 9 and add immediately to the bead suspension.
    6. After incubation with DMP, wash beads 1 time with 1 ml of 0.2 M ethanolamine, 0.2 M NaCl pH 8.5 to inactivate the residual crosslinker. Resuspend beads in 1 ml of the same buffer and rotate for 1 hr at RT. Pellet beads and resuspend beads in 500 µl of 0.2 M ethanolamine, 0.2 M NaCl pH 8.5. Beads are stable for several months at 4 °C.

3. Preparation of Buffers for Cell Lysis and Complex Purification
    1. Prepare LAPX buffers (where X is the desired salt concentration [mM KCl] of the LAP buffer; 300 mM for cell lysis, 200 mM for most bead washes, and 100 mM for washing beads prior to eluting proteins) by making a pH 7.4 solution containing 50 mM 4-(2-hydroxyethyl)-1-piperazineethanesulfonic acid (HEPES), X mM KCl, 1 mM ethylene glycol tetraacetic acid (EGTA), 1 mM $MgCl_2$, and 10% glycerol.
    NOTE: The components of this buffer are used to approximate the environment in living cells. HEPES is used as a buffer in the pH rage of 7.2-8.2. KCl is a salt used to maintain the ionic strength of the buffer. EGTA is a chelating agent that binds calcium ions to reduce the levels of calcium compared to magnesium. Glycerol and $MgCl_2$ are used to improve the stability of proteins.
    2. Prepare $LAPX^N$ buffer by adding 0.05% nonyl phenoxypolyethoxylethanol to the LAPX buffer.
    NOTE: Nonyl phenoxypolyethoxylethanol is a mild detergent that solubilizes proteins, but preserves protein-protein interactions, thus a higher concentration is used during the extraction process and it is then lowered during the binding and washing steps.

4. Preparation of Cell Lysates
    1. Resuspend 500 µl of PCV into 2.5 ml of LAP300 with 0.5 mM dithiothreitol (DTT) and protease inhibitors. Add 90 µl of 10% nonyl phenoxypolyethoxylethanol (0.3% final) and mix by inversion.
    2. Place on ice for 10 min. Centrifuge at 21,000 x g for 10 min. Collect this low speed supernatant (LSS). Take a 10 µl sample of the LSS for gel analysis.
    3. Transfer LSS to a TLA100.3 tube and spin at 100,000 x g for 1 hr at 4 °C. Collect this high speed supernatant (HSS), in a tube and place on ice. Take a 10 µl sample of the HSS for gel analysis.
    NOTE: Avoid taking the top most lipid layer and the bottom most cell debris layer. The lipid layer should be removed by vacuum aspiration prior to collecting the HSS.

5. First Affinity Capture: Binding to Anti-GFP Beads
    1. Pre-elute antibody coupled beads (use 160 µl of beads per 0.5 ml cell pellet (PCV)) by washing them 3 times with 1 ml of elution buffer [3.5 M $MgCl_2$ with 20 mM Tris, pH 7.4] to get rid of uncoupled antibodies and reduce background. Do quickly. Do not leave beads in high salt for a long time.
    2. Wash beads 3 times with 1 ml of $LAP200^N$. Mix HSS extract with antibody beads for 1 hr at 4 °C. Centrifuge at 21,000 x g for 10 min. Take a 10 µl sample of the supernatant (*i.e.*, the flow through (FT)) for gel analysis.

3. Wash beads 3 times with 1 ml of LAP200^N with 0.5 mM DTT and protease inhibitors. Wash beads 2 times (5 min each) with 1 ml of LAP200^N with 0.5 mM DTT and protease inhibitors. Wash quickly 2 times with 1 ml of LAP200^N with 0.5 mM DTT and no protease inhibitors before adding the tobacco etch virus (TEV) protease.

6. TEV Cleavage
   1. Dilute 10 µg TEV protease in 1 ml of LAP200^N and rotate tubes at 4 °C overnight.
      NOTE: This step can be optimized for any LAP-tagged protein to be completed in a few hours by adjusting the concentration of TEV protease, which can aid the preservation of LAP-tagged protein complexes.
   2. Pellet beads and transfer supernatant to a fresh tube. Rinse beads twice with 160 µl LAP200^N with 0.5 mM DTT and protease inhibitors (triple concentration) to remove any residual protein. Take a 10 µl sample of the supernatant for gel analysis.

7. Second Affinity Capture: Binding to S Protein Agarose
   1. Wash 1 tube of 80 µl S protein agarose slurry (40 µl packed resin) 3 times with 1 ml of LAP200^N.
      NOTE: S protein binding to the S-tag will reconstitute an active RNase and an alternative second epitope tag should be considered for RNA containing protein complexes.
   2. Add TEV eluted supernatant to S protein agarose beads and rock for 3 hr at 4 °C. Pellet beads and wash 3 times with 1 ml of LAP200^N with 0.5 mM DTT and protease inhibitors. Wash beads 2 times with 1 ml of LAP100.

8. Protein Elution
   1. Elute proteins off S protein agarose by adding 50 µl of 4x Laemmli sample buffer and heat at 97 °C for 10 min.
      NOTE: Proteins can also be eluted from the beads with elution buffer (3.5 M $MgCl_2$ with 20 mM Tris, pH 7.4).

4. Identify Interacting Proteins by Mass Spectrometry Analysis

1. Test the quality of the purification by analyzing the collected samples by sodium dodecyl sulfate polyacrylamide gel electrophoresis (SDS-PAGE), silver staining the gel (see **Materials Table**) and by immunoblotting the eluates and probing with anti-GFP antibodies to ensure that the LAP-tagged purification worked[16], see **Figure 4**.
2. To identify stoichiometric and substoichiometric co-purifying species, take the final elution sample and separate it by SDS-PAGE. Stain the gel with a mass spectrometry compatible protein stain. Excise the most prominent bands and the space in between them from the gel and process them for analysis by mass spectrometry separately[16].
   NOTE: There are numerous approaches for separating the final purification eluates and preparing them for mass spectrometry[5]. For example, LAP-purified complexes can be eluted from S-protein beads by using high salt (3.5 M $MgCl_2$) and the entire protein population en masse can be analyzed by mass spectrometry[17]. Alternatively, final eluates can be separated for 1 mm by SDS-PAGE and a single 1 mm band can be excised and analyzed. This clears the complex mixture of any beads or particulate matter that will interfere with the analysis.

Representative Results

To highlight the utility of this system, the open reading frame (ORF) of the Tau microtubule binding protein was cloned into the shuttle vector by amplifying the Tau ORF with primers containing attB1 and attB2 sites (**Table 1**) and incubating the PCR products with the shuttle vector and a recombinase that mediates the insertion of the PCR products into the shuttle vector. The reaction products were used to transform DH5α bacteria[13] and plasmid DNA from Kanamycin resistant colonies was sequenced to ensure Tau insertion. A sequence validated shuttle-Tau vector was then used to transfer the Tau ORF into the pGLAP1 vector, which fused Tau in frame with the LAP (EGFP-TEV-S-Protein) tag, by incubating the shuttle-Tau vector with the pGLAP1 vector and the recombinase that mediates the transfer of the ORF from the shuttle vector to pGLAP1. The reaction products were used to transform DH5α bacteria[13] and plasmid DNA from Ampicillin resistant colonies was sequenced to ensure that the LAP-Tau fusion was in frame. Sequence validated pGLAP1-LAP-Tau was then co-transfected with a vector that expresses the flippase recombination enzyme into HEK293 cells that contained a single flippase recognition target (FRT) site within their genome, which is the site of integration for LAP-tagged genes[14]. This cell line also expressed the TetR that binds to Tet operators upstream of the LAP-tagged genes and silences their expression in the absence of Tet/Dox. Stable integrants were selected with -Tet DMEM/F12 media with 100 µg/ml Hygromycin for 5 days. Individual Hygromycin resistant cell foci were harvested by adding 20 µl of trypsin on top and pipetting up and down 2 times. Cells were placed in a 24 well plate and expanded by continual growth in -Tet DMEM/F12 media.

To verify that the Hygromycin resistant cells were capable of expressing LAP-Tau, HEK293 LAP-Tau cells were induced with 0.1 µg/ml Dox for 15 hr and protein extracts were prepared from non-induced and Dox-induced cells. These extracts were separated by SDS-PAGE, transferred to a PVDF membrane, and immunoblotted for GFP and Tubulin as loading control. As seen in **Figure 4A**, LAP-Tau (visualized with anti-GFP antibodies) was only expressed in the presence of Dox. To validate that LAP-Tau was properly localized to the mitotic microtubule spindle during mitosis, as had been previously shown for endogenous Tau[18], HEK293 LAP-Tau cells were induced with 0.1 µg/ml Dox for 15 hr and cells were fixed with 4% paraformaldehyde and co-stained for DNA (Hoechst 33342) and microtubules (anti-Tubulin antibodies). Consistently, LAP-Tau was localized to the mitotic spindle during metaphase of mitosis (**Figure 4B**). To verify that LAP-Tau and its interacting proteins could be purified with this system, HEK293 LAP-Tau cells were grown in roller bottles to ~70% confluency, induced with 0.1 µg/ml Dox for 15 hr, harvested by agitation, lysed with LAP300 buffer, and LAP-Tau was purified using the above protocol. Eluates from the LAP-Tau purification were resolved by SDS-PAGE and the gel was silver stained. **Figure 4C** shows the LAP-Tau purification, marked with an asterisk is LAP-Tau and several other bands indicative of Tau interacting proteins can be seen.

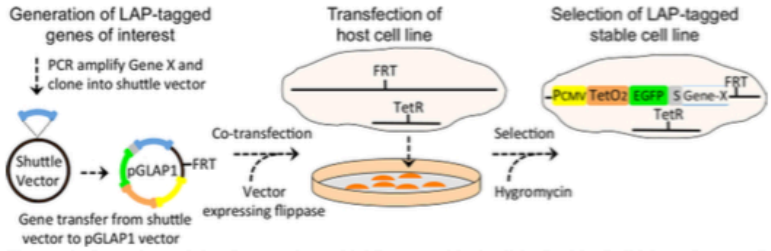

Figure 1: Overview of the Generation of LAP-tagged Inducible Stable Cell Lines for any Protein of Interest. The open reading frame (ORF) of genes of interest are amplified with attB1 and attB2 sites flanking the 5' and 3' end sequences, respectively (primer sequences are given in **Table 1**) and cloned into the shuttle vector. Sequence verified shuttle vectors with the gene of interest are then used to transfer the gene of interest into the pGLAP1 vector. The sequence verified pGLAP1 vector with the gene of interest is then co-transfected with the vector containing the flippase recombinase into the desired cell line that contains a single flippase recognition target (FRT) site within their genome, which is the site of integration for LAP-tagged genes. These cell lines also express the Tet repressor (TetR) that binds to Tet operators ($TetO_2$) upstream of the LAP-tagged genes and silences their expression in the absence of Tet/Dox. The LAP-tagged gene of interest is then recombined into the FRT site and stable integrants are selected with Hygromycin. Please click here to view a larger version of this figure.

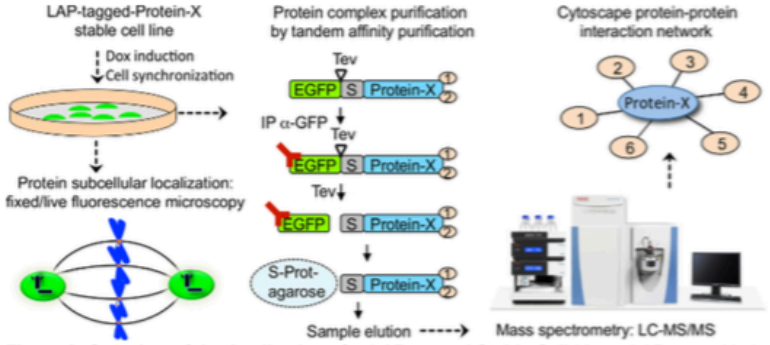

Figure 2: Overview of the Applications for LAP-tagged Stable Cell Lines. LAP-tagged inducible stable cell lines are induced to express the LAP-tagged protein of interest by Dox addition and can be synchronized at various stages of the cell cycle or can be stimulated with chemicals or ligands to activate any desired signaling pathway. The subcellular localization of the LAP-tagged protein of interest can be analyzed by live cell or fixed cell imaging. LAP-tagged proteins can also be tandem affinity purified and their interacting proteins can be identified by liquid chromatography tandem mass spectrometry (LC-MS/MS). Finally, Cytoscape can be used to generate a protein-protein interaction network of the bait protein. Dox indicates Doxycycline, IP indicates immunoprecipitate, EGFP indicates enhanced green fluorescent protein, Tev indicates TEV protease cleavage site, and S indicates S-tag. Please click here to view a larger version of this figure.

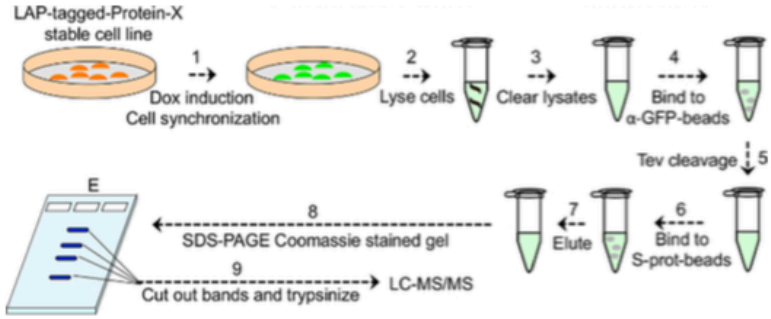

Figure 3: Overview of LAP-tagged Protein Expression, Purification and Preparation for Mass Spectrometry. The protocol has 9 steps: 1) growth and induction of LAP-tagged protein expression, 2) cell harvesting and lysis, 3) the preparation of lysates, 4) the binding of lysates to anti-GFP beads, 5) TEV protease cleavage of the GFP-tag, 6) the binding of lysates to S-protein beads, 7) the elution of the bait protein and interacting proteins, and 8-9) the preparation of samples for mass spectrometry-based proteomic analyses. Please click here to view a larger version of this figure.

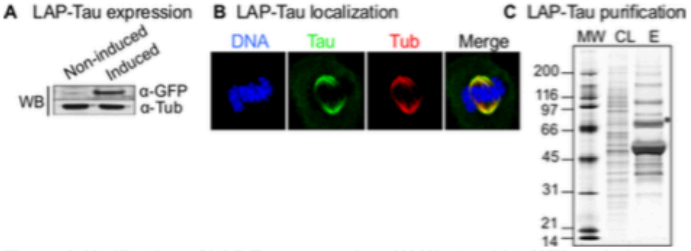

Figure 4: Verification of LAP-Tau expression. (**A**) Western blot (WB) analysis of protein samples from non-induced and Dox induced LAP-Tau HEK293 cells probed with anti-GFP and anti-Tubulin antibodies to detect the LAP-tagged Tau protein and the Tubulin loading control, respectively. Note that LAP-Tau is only expressed when the cells are induced with Dox. (**B**) Mitotic cells expressing LAP-Tau were fixed and co-stained for DNA (Hoechst 33342) and Tubulin (Tub) with anti-tubulin antibodies and the subcellular localization of LAP-tau was analyzed by fluorescence microcopy. Note that LAP-Tau localizes to the mitotic spindle and spindle poles during mitosis. (**C**) Silver stained gel of the LAP-Tau purification. MW indicates molecular weight, CL indicates cleared lysates, and E indicates final eluates. Samples were run on a 4-20% SDS-PAGE and the gel was silver stained to visualize the purified proteins. Note that a band corresponding to LAP-Tau is marked with an asterisk and several other bands corresponding to co-purifying proteins can be seen. Please click here to view a larger version of this figure.

N-terminal fusion	
Forward	5'-**GGGGACAAGT TTGTACAAAAAAGCAGGCT**TCATG-(>18gsn)-3'
Reverse	5'-**GGGGACCACTTTGTACAAGAAAGCTGGGTT** TTATCA-(>18gsn)-3'
C-terminal fusion	
Forward	5'-**GGGGACAAGTTTGTACAAAAAAGCAGGCT**TCACC-(>18gsn)-3'
Reverse	5'-**GGGGACCACTTTGTACAAGAAAGCTGGGT**G-(>18gsn)-3'

Table 1: Forward and Reverse Primers for Amplifying ORFs or Interest for Insertion into the Shuttle Vector. The attB sites are highlighted in bold letters, gsn denotes that more than 18 gene specific nucleotides are added to the primer.

Step		**Temperature**	**Time**
Initial denaturation		94 °C	2 min
PCR Amplification Cycles (35)	Denature	94 °C	30 sec
	Anneal	55 °C (depending on the primer Tm)	30 sec
	Extend	72 °C	1 min/kb
Hold		4 °C	indefinitely

Table 2: PCR Conditions for Amplification of the ORFs of Interest.

Vector	**Forward Sequencing Primer**	**Reverse Sequencing Primer**
Shuttle Vector	5'-TGTAAAACGACGGCCAGT-3'	5'-CAGGAAACAGCTATGAC-3'

Table 3: Forward and Reverse Sequencing Primers for the Shuttle Vector.

ID	Structure	Parental	Promoter	Bac Res	Mam Res	Tet reg?
pGLAP1	N-term EGFP-TEV-S peptide	pcDNA5/FRT/TO	CMV	Amp	Hyg	Yes
pGLAP2	N-term Flag-TEV-S peptide	pcDNA5/FRT/TO	CMV	Amp	Hyg	Yes
pGLAP3	N-term EGFP-TEV-S peptide; C-term V5	pEF5/FRT-V5	EF1a	Amp	Hyg	No
pGLAP4	N-term Flag-TEV-S peptide; ; C-term V5	pEF5/FRT-V5	EF1a	Amp	Hyg	No
pGLAP5	C-term S peptide-PreProt x2-EGFP	pEF5/FRT-V5	EF1a	Amp	Hyg	No

Table 4: List of Available LAP/TAP Vectors with Variable Promoters, Epitope-tags, and Dox Inducible Expression Capabilities for N or C-terminal Protein Tagging. Vectors are commercially available. Bac Res indicates bacterial resistance marker, Mam Res indicates mammalian cell resistance marker, Tet reg? indicates whether expression is Tet/Dox regulatable.

Vector	Forward Sequencing Primer	Reverse Sequencing Primer
pGLAP1	5'-ATCACTCTCGGCATGGACGAGCTGTACAAG-3'	5'-TGGCTGGCAACTAGAAGGCACAGTCGAGGC-3'
pGLAP2	5'-CGAACGCCAGCACATGGACAGGG-3'	5'-TGGCTGGCAACTAGAAGGCACAGTCGAGGC-3'
pGLAP3	5'-AGAAACCGCTGCTGCTAA-3'	5'-TAGAAGGCACAGTCGAGG-3'
pGLAP4	5'-AGACCCAAGCTGGCTAGGTAAGC-3'	5'-TAGAAGGCACAGTCGAGG-3'
pGLAP5	5'-CGTAATACGACTCACTATAG-3'	5'-TCCAGGGTCAAGGAAGGCACGG-3'

Table 5: Forward and Reverse Sequencing Primers for pGLAP Vectors.

Discussion

The outlined protocol describes the cloning of genes of interest into the LAP-tagging vector, the generation of inducible LAP-tagged stable cell lines, and the purification of LAP-tagged protein complexes for proteomic analyses. With respect to other LAP/TAP-tagging approaches, this protocol has been streamlined to be compatible with high-throughput approaches to map protein localization and protein-protein interactions within any cellular pathway. This approach has been widely applied to the functional characterization of proteins critical for cell cycle progression, mitotic spindle assembly, spindle pole homeostasis, and ciliogenesis to name a few and has aided the understanding of how misregulation of these proteins can lead to human diseases[15,16,19,20]. For example, our group recently utilized this system to define the function and regulation of the STARD9 mitotic kinesin (a candidate cancer target) in spindle assembly[15,21], to define a new molecular link between the Tctex1d2 dynein light chain and short rib polydactyly syndromes (SRPS)[19], and to define a new molecular link to understanding how mutation of the Mid2 ubiquitin ligase can lead to X-linked intellectual disabilities[16]. Other laboratories have also successfully applied this method, including one that determined that Tctn1, a regulator of mouse Hedgehog signaling, was a part of a ciliopathy-associated protein complex that regulated ciliary membrane composition and ciliogenesis in a tissue-dependent manner[22,23]. Therefore, this protocol can be broadly applied to the dissection of any cellular pathway.

A critical step in this protocol is the selection of LAP-tagged stable cell lines that are Hygromycin resistant. Special care should be taken to ensure that all cells in the control plate are dead before selecting foci in the experimental plate for amplification. Hygromycin can also be added during routine cell culturing of LAP-tagged stable cell lines to further ensure that all cells maintain the LAP-tagged gene of interest at the FRT site. We caution that not all LAP-tagged proteins will be functional and that it is important to have assays in place that can be used to test protein function. Examples of assays used to test protein function include the rescue of siRNA-induced phenotypes and *in vitro* activity assays. To address any potential problems with the addition of a large LAP-tag, we have previously generated TAP-tag vectors compatible with this system that contain smaller tags, like FLAG, which are less likely to inhibit the function and localization of the protein of interest[4]. In addition, LAP-tagging vectors exist for generating C-terminal LAP-tagged proteins or C-terminal TAP-tagged proteins that are compatible with this system, which can be used in cases where a LAP/TAP tag is not tolerated at the N-terminus of a protein. Additionally, the salt and detergent concentrations of the purification buffers ($LAPX^N$) can be modified to increase or decrease the purification stringency if none or too many interactions are observed. Similarly, the tandem affinity purification procedure is more stringent than single purification procedures and weak interactors may be lost, thus a single purification scheme can be used when few or no interactors are identified.

It is important to note that other GFP epitope tagging approaches exist that allow large scale GFP protein tagging for protein localization and purification studies[24,25]. These include the BAC TransgenOmics approach that utilizes bacterial artificial chromosomes to express GFP-tagged genes of interest from their native environment that contains all the regulatory elements, which mimics endogenous gene expression[24]. More recently, CAS9/single-guided RNA (sgRNA) ribonucleoprotein complexes (RNPs) have been used to endogenously tag genes of interest with a split-GFP system that allows the expression of GFP-tagged genes from their endogenous genomic loci[25]. Although both of these approaches enable the expression of tagged proteins under endogenous conditions, compared to the LAP-tagging protocol described here, they do not allow for inducible and tunable expression of the tagged genes of interest. Additionally, they have yet to be applied to tandem epitope tagging for TAP.

It is also important to note that other tagging systems can also be modified to become compatible with the system described here for generating inducible epitope-tagged stable cell lines. For example, proximity-dependent biotin identification (BioID) has garnered considerable attention due to its ability to define spatial and temporal relationships among interacting proteins[26]. This technique exploits protein fusions to a promiscuous strain of the *Escherichia coli* biotin ligase BirA, which biotinylates any protein within a ~10 nm radius of the enzyme. The biotinylated proteins are then affinity purified using biotin-affinity capture and analyzed for composition by mass spectrometry. BirA will biotinylate any protein in close proximity, even transiently, which makes it especially suited for detecting weaker interacting partners within a complex[27]. Additionally, the purification scheme does not necessitate that endogenous protein-protein interactions remain intact and can be carried out under denaturing conditions, thus reducing the rate of false positives. Within our current protocol, the substitution of the pGLAP1 vector by a BirA-tagging vector could transform this system from identifying protein-protein interactions based on affinity to detecting them based on proximity. Such a system would be highly advantageous for detecting transient protein interactions as is the case between many enzyme-substrate interactions and for mapping the spatiotemporal protein-protein interactions within defined structures as has been carried out for the centrosome and cilia[26,28].

Disclosures

The authors have nothing to disclose.

Acknowledgements

This work was supported by a National Science Foundation Grant NSF-MCB1243645 (JZT), any opinions, findings, and conclusions or recommendations expressed in this material are those of the authors and do not necessarily reflect the views of the National Science Foundation. The funders had no role in study design, data collection and analysis, decision to publish, or preparation of the manuscript.

References

1. Rigaut, G. *et al.* A generic protein purification method for protein complex characterization and proteome exploration. *Nat Biotechnol.* **17**, 1030-1032 (1999).
2. Puig, O. *et al.* The tandem affinity purification (TAP) method: a general procedure of protein complex purification. *Methods.* **24**, 218-229 (2001).
3. Cheeseman, I. M., & Desai, A. A combined approach for the localization and tandem affinity purification of protein complexes from metazoans. *Sci STKE.* **2005**, pl1 (2005).
4. Torres, J. Z., Miller, J. J., & Jackson, P. K. High-throughput generation of tagged stable cell lines for proteomic analysis. *Proteomics.* **9**, 2888-2891 (2009).
5. LaCava, J. *et al.* Affinity proteomics to study endogenous protein complexes: pointers, pitfalls, preferences and perspectives. *Biotechniques.* **58**, 103-119 (2015).
6. Landy, A. Dynamic, structural, and regulatory aspects of lambda site-specific recombination. *Annu Rev Biochem.* **58**, 913-949 (1989).
7. Hartley, J. L., Temple, G. F., & Brasch, M. A. DNA cloning using in vitro site-specific recombination. *Genome Res.* **10**, 1788-1795 (2000).
8. The ORFeome Collaboration: a genome-scale human ORF-clone resource. *Nat Methods.* **13**, 191-192 (2016).
9. Brasch, M. A., Hartley, J. L., & Vidal, M. ORFeome cloning and systems biology: standardized mass production of the parts from the parts-list. *Genome Res.* **14**, 2001-2009 (2004).
10. Lamesch, P. *et al.* hORFeome v3.1: a resource of human open reading frames representing over 10,000 human genes. *Genomics.* **89**, 307-315 (2007).
11. Rual, J. F. *et al.* Human ORFeome version 1.1: a platform for reverse proteomics. *Genome Res.* **14**, 2128-2135 (2004).
12. Fiering, S., Kim, C. G., Epner, E. M., & Groudine, M. An "in-out" strategy using gene targeting and FLP recombinase for the functional dissection of complex DNA regulatory elements: analysis of the beta-globin locus control region. *Proc Natl Acad Sci U S A.* **90**, 8469-8473 (1993).
13. Sambrook, J., Fritsch, E. F., & Maniatis, T. *Molecular cloning : a laboratory manual.* 2nd ed. edn, Cold Spring Harbor Laboratory, (1989).
14. Uyttersprot, N., Costagliola, S., & Miot, F. A new tool for efficient transfection of dog and human thyrocytes in primary culture. *Mol Cell Endocrinol.* **142**, 35-39 (1998).
15. Senese, S. *et al.* A unique insertion in STARD9's motor domain regulates its stability. *Mol Biol Cell.* **26**, 440-452 (2015).
16. Gholkar, A. A. *et al.* The X-Linked-Intellectual-Disability-Associated Ubiquitin Ligase Mid2 Interacts with Astrin and Regulates Astrin Levels to Promote Cell Division. *Cell Rep.* **14**, 180-188 (2016).
17. Graumann, J. *et al.* Applicability of tandem affinity purification MudPIT to pathway proteomics in yeast. *Mol Cell Proteomics.* **3**, 226-237 (2004).
18. Connolly, J. A., Kalnins, V. I., Cleveland, D. W., & Kirschner, M. W. Immunoflourescent staining of cytoplasmic and spindle microtubules in mouse fibroblasts with antibody to tau protein. *Proc Natl Acad Sci U S A.* **74**, 2437-2440 (1977).
19. Gholkar, A. A. *et al.* Tctex1d2 associates with short-rib polydactyly syndrome proteins and is required for ciliogenesis. *Cell Cycle.* **14**, 1116-1125 (2015).
20. Cheung, K. *et al.* Proteomic Analysis of the Mammalian Katanin Family of Microtubule-severing Enzymes Defines Katanin p80 subunit B-like 1 (KATNBL1) as a Regulator of Mammalian Katanin Microtubule-severing. *Mol Cell Proteomics.* **15**, 1658-1669 (2016).
21. Torres, J. Z. *et al.* The STARD9/Kif16a Kinesin Associates with Mitotic Microtubules and Regulates Spindle Pole Assembly. *Cell.* **147**, 1309-1323 (2011).
22. Garcia-Gonzalo, F. R. *et al.* A transition zone complex regulates mammalian ciliogenesis and ciliary membrane composition. *Nat Genet.* **43**, 776-784 (2011).
23. Chih, B. *et al.* A ciliopathy complex at the transition zone protects the cilia as a privileged membrane domain. *Nat Cell Biol.* **14**, 61-72 (2012).
24. Leonetti, M. D., Sekine, S., Kamiyama, D., Weissman, J. S., & Huang, B. A scalable strategy for high-throughput GFP tagging of endogenous human proteins. *Proc Natl Acad Sci U S A.* **113**, E3501-3508 (2016).

25. Poser, I. *et al.* BAC TransgeneOmics: a high-throughput method for exploration of protein function in mammals. *Nat Methods.* **5**, 409-415 (2008).
26. Firat-Karalar, E. N., & Stearns, T. Probing mammalian centrosome structure using BioID proximity-dependent biotinylation. *Methods Cell Biol.* **129**, 153-170 (2015).
27. Roux, K. J., Kim, D. I., & Burke, B. BioID: a screen for protein-protein interactions. *Curr Protoc Protein Sci.* **74**, Unit 19 23 (2013).
28. Gupta, G. D. *et al.* A Dynamic Protein Interaction Landscape of the Human Centrosome-Cilium Interface. *Cell.* **163**, 1484-1499 (2015).